Government of Western Australia

Department of
Mines and Petroleum

REPORT
171

THE VOLCANOLOGY, PETROGENESIS, AND ECONOMIC POTENTIAL OF THE MESOPROTEROZOIC SHALLOW-WATER, INTRA-CALDERA, LAVA-LIKE RHEOMORPHIC KATHLEEN IGNIMBRITE, WEST MUSGRAVE PROVINCE, CENTRAL AUSTRALIA

by CC Medlin

MONASH University

NGAANYATJARRA COUNCIL Aboriginal Corporation

Geological Survey of Western Australia

Government of **Western Australia**
Department of **Mines and Petroleum**

REPORT 171

THE VOLCANOLOGY, PETROGENESIS, AND ECONOMIC POTENTIAL OF THE MESOPROTEROZOIC SHALLOW-WATER, INTRA-CALDERA, LAVA-LIKE RHEOMORPHIC KATHLEEN IGNIMBRITE, WEST MUSGRAVE PROVINCE, CENTRAL AUSTRALIA

by
CC Medlin

School of Geosciences, Monash University, Melbourne, Australia

Perth 2017

Geological Survey of Western Australia

MINISTER FOR MINES AND PETROLEUM
Hon Bill Johnston MLA

ACTING DIRECTOR GENERAL, DEPARTMENT OF MINES AND PETROLEUM
David Smith

EXECUTIVE DIRECTOR, GEOLOGICAL SURVEY OF WESTERN AUSTRALIA
Rick Rogerson

REFERENCE
The recommended reference for this publication is:
Medlin, CC 2017, The volcanology, petrogenesis, and economic potential of the Mesoproterozoic shallow-water, intra-caldera, lava-like rheomorphic Kathleen Ignimbrite, west Musgrave Province, central Australia: Geological Survey of Western Australia, Report 171, 294p.

National Library of Australia Cataloguing-in-Publication entry

Creator:	Medlin, C. C., author.
Title:	The volcanology, petrogenesis, and economic potential of the Mesoproterozoic shallow-water, intra-caldera, lava-like rheomorphic Kathleen Ignimbrite, West Musgrave Province, central Australia / CC Medlin.
ISBN:	9781741687521 (ebook)
Subjects:	Geology--Australia, Central--West Musgrave Province Geology, Stratigraphic. Volcanology--Australia, Petrogenesis--Australia, Ignimbrite. West Musgrave Ranges Region (W.A.)
Other Authors/Contributors:	Geological Survey of Western Australia, issuing body.

Grid references in this publication refer to the Australia Geodetic Datum 1984 (AGD84). Locations mentioned in the text are referenced using Australian Map Grid (AMG) coordinates, Zone 52. All locations are quoted to at least the nearest 100 m.

Notice to the reader
This Report is an accepted PhD research thesis submitted by the author to the School of Geosciences, Monash University, Melbourne, and was partially funded by the Geological Survey of Western Australia (GSWA). The scientific content of the Report, and the drafting of figures, has been the responsibility of the author and has not been modified by GSWA. All work carried out in the west Musgrave region was done so within the framework of a collaborative project involving GSWA, the traditional owners of the region and the Ngaanyatjarra Council. The considerable efforts of the traditional owners and of the Ngaanyatjarra Council in facilitating this work, is gratefully acknowledged.

Permission statement

Permission was granted from Oxford University Press to republish the following article in Chapter 3:

Medlin, CC, Jowitt, SM, Cas, RAF, Smithies, RH, Kirkland, CL, Maas, RA, Raveggi, M, Howard, HM, Wingate, MTD 2015, Petrogenesis of the A-type, Mesoproterozoic Intra-caldera Rheomorphic Kathleen Ignimbrite and Comagmatic Rowland Suite Intrusions, West Musgrave Province, Central Australia: Products of Extreme Fractional Crystallization in a Failed Rift Setting, Journal of Petrology, 56 (3): 493–525, doi.org/10.1093/petrology/egv007.

Permission was granted from Elsevier to republish the following article in Chapter 5:

Jowitt, SM, Medlin, CC, Cas, RAF 2017, The Rare Earth Element (REE) mineralisation potential of highly fractionated rhyolites: a potential low-grade, bulk tonnage source of critical metals, Ore Geology Reviews, 86, 548–562, doi.org/10.1016/j.oregeorev.2017.02.027.

Published 2017 by Geological Survey of Western Australia
This Report is published in digital format (PDF) and is available online at <www.dmp.wa.gov.au/GSWApublications>.

Further details of geological publications and maps produced by the Geological Survey of Western Australia are available from:
Information Centre
Department of Mines and Petroleum
100 Plain Street | EAST PERTH WESTERN AUSTRALIA 6004
Telephone: +61 8 9222 3459 Facsimile: +61 8 9222 3444
www.dmp.wa.gov.au/GSWApublications

Cover photograph: View of the north side of the Kathleen Ignimbrite at Mount Glyde

The volcanology, petrogenesis, and economic potential of the Mesoproterozoic shallow-water, intra-caldera, lava-like rheomorphic Kathleen Ignimbrite, west Musgrave Province, central Australia

by

Christopher Cleghorne Medlin

A thesis in submission for the degree of
Doctor of Philosophy

Monash University
School of Geosciences
Melbourne, Australia

April 2014

I certify that I have made all reasonable efforts to secure copyright permissions for third-party content included in this thesis and have not knowingly added copyright content to my work without the owner's permission.

Errata and Addendum

Chapter 2.

Errata

p. 43 line 30: Replace 'The only phenocrysts within this facies are' with 'The dominant phenocryst within this facies is'. Add at the end of the sentence 'Feldspar phenocrysts do occur in this facies, however they are rare.'.

p. 58 line 23: 'Tambora (Indonesia)' should be replaced with 'Kikai-Akaboya (Japan)'.

Addendum

p. 43 line 03: Insert '*aphyric**' in the title of this facies and a footnote at the bottom of the page which states the following: 'Aphyric* – In this instance and throughout the text aphyric has been used to describe the texture in this facies even though there are phenocrysts present, as they are notably rare to absent and constitute <5 vol. % of the matrix.'.

p. 50 line 19: Insert citation after 'hot deformation of lava autobreccias (Manley and Fink, 1987)'.

Additional references to be added to the end of this chapter

Manley, C.R. and Fink, J.H., 1987. Internal textures of rhyolite flows as revealed by research drilling. Geology, 15(6), 549-552.

Chapter 3.

Errata

p. 107 line 24: Replace the existing third paragraph with the following paragraph: 'The experimental research into the partial melting of basaltic and andesitic greenstones and amphibolites generated partial melts that are superficially similar (e.g., lowest H_2O melting experiments by Thy *et al*., 1990) in that they produced melts with SiO_2 and Al_2O_3 concentrations similar to the Pussy Cat Group rhyolites, and water-saturated melting experiments of both Beard and Lofgren (1991) and Thy *et al*. (1990) yielded melts with FeO and SiO_2 concentrations that overlap with Pussy Cat Group compositions, but the overall compositions of both water-saturated and undersaturated melts produced during this previous research are dissimilar (e.g., in terms of K_2O and CaO) to the compositions of all samples analysed during this study. These isotopic and whole-rock geochemical dissimilarities strongly suggest that another process must have been responsible for the generation of the Pussy Cat Group magmas.'.

p. 107 line 39: Replace the existing fourth paragraph with the following paragraph: 'It is still possible that partial melting played a small role in the formation of the Pussy Cat Group rhyolites and cannot definitively be ruled out, but it is extremely unlikely that this process was the dominant control on the formation of these magmas. This corroborates the findings of Smithies *et al*. (2013) and Kirkland *et al*. (2012), who both argue against the genesis of silicic magmas in the West Musgrave Province by partial melting of continental crustal material.'.

p. 114 line 21: Replace the existing second paragraph with the following paragraph: 'The samples have high Y/Nb ratios and are therefore classified within the A_2 group of magmas (Fig. 3.6b), although this classification implies an origin and tectonic setting that sharply contrasts with those discussed in the previous sections of this paper. This is the result of the fact that these discrimination diagrams are dependent on Y/Nb and Y/Ta ratios being constant, whereas, and as stated by Eby (1990; 1992), the crystallisation of certain minor phases such as allanite and zircon can lead to an increase in Y/Nb ratios and the erroneous classification of A_1 group samples as A_2. This change in Y/Nb ratios is related to changes in compatibility during the fractional crystallisation of highly evolved rhyolites (Miller and Mittlefehldt, 1982; Eby, 1990), and such changes in compatibility have been demonstrated to occur during the fractionation of the Pussy Cat Group rhyolites (Fig. 3.6b), indicating that these rhyolites most probably have higher Y/Nb ratios that those expected for the majority of rhyolites that formed in this setting (i.e., suggests misclassification of the Pussy Cat Group units as A_2 rather than A_1). This potential misclassification is acknowledged by Eby (1992), who states that it is not possible on the basis of trace element data to rule out a subcontinental mantle source and concedes that some A_2 magmas can have mantle-derived origins.'.

p. 115 line 28: Replace the last sentence with this 'Although many authors agree that the Snake River Plain rhyolites are derived through crustal melting (e.g., Bindeman *et al*., 2007, Watts *et al.*, 2011, Boroughs *et al*., 2005, Ellis *et al*., 2013), some A-type Snake River Plain rhyolites have been shown to form through fractional crystallisation (e.g., Leeman *et al*., 2008; McCurry *et al*., 2008; Christiansen and McCurry 2008; Christiansen, 2005), and in this situation a crustal density filter serves to suppress the intermediate composition magmas, creating the characteristic bimodal associations inherent with A-type rhyolites.'.

p. 118, line 34: Replace point 4) with this: 'Some form of trigger mechanism, for example cryptic silicic magma recharge (de Silva *et al*., 2008), would have caused this magma chamber to erupt and empty out (e.g., Ammonia Tanks Tuff; Deering *et al*., 2011).'.

Addendum

p. 115 line 37: This is supported 'through' research by 'Tuttle and Bowen (1958)' and Gualda and Ghiorso (2013).

p. 116 line 05: high temperature'*' with a footnote at the bottom of the page stating the following: '* – A review paper on rhyolite volcanism in the central SRP (see Ellis *et al*., 2013) stated that the high temperature rhyolites in the Snake River Plain are >850°C with Honjo *et al*. (1992) defining a range from 850–1000°C. However, Branney *et al*. (2008), Christiansen (2005) and Christiansen and McCurry (2007) all noted a broader range from 830–1050°C, with Cathey and Nash (2004) noting a range from 800–1000°C. Based on these overlaps in magmatic temperatures, the Pussy Cat Group rhyolites are considered to fall within the temperature ranges defined for high-temperature rhyolites of the SRP.'.

Additional references to be added to the end of this chapter

Bindeman, I.N., Watts, K.E., Schmitt, A.K., Morgan, L.A. and Shanks, P.W., 2007. Voluminous low δ 18O magmas in the late Miocene Heise volcanic field, Idaho: Implications for the fate of Yellowstone hotspot calderas. Geology, 35(11): 1019-1022.

Boroughs, S., Wolff, J., Bonnichsen, B., Godchaux, M. and Larson, P., 2005. Large-volume, low- δ 18O rhyolites of the central Snake River Plain, Idaho, USA. Geology, 33(10): 821-824.

Cathey, H.E. and Nash, B.P., 2004. The Cougar Point Tuff: implications for thermochemical zonation and longevity of high-temperature, large-volume silicic magmas of the Miocene Yellowstone hotspot. Journal of Petrology, 45(1): 27-58.

Ellis, B.S., Wolff, J.A., Boroughs, S., Mark, D.F., Starkel, W.A. and Bonnichsen, B., 2013. Rhyolitic volcanism of the central Snake River Plain: a review. Bulletin of Volcanology, 75(8): 1-19.

Honjo, N., Bonnichsen, B., Leeman, W.P. and Stormer Jr, J.C., 1992. Mineralogy and geothermometry of high-temperature rhyolites from the central and western Snake River Plain. Bulletin of Volcanology, 54(3): 220-237.

Leeman, W.P., Annen, C. and Dufek, J., 2008. Snake River Plain–Yellowstone silicic volcanism: implications for magma genesis and magma fluxes. Geological Society, London, Special Publications, 304(1): 235-259.

Tuttle, O.F. and Bowen, N.L., 1958. Origin of granite in the light of experimental studies in the system $NaAlSi_3O_8$–$KAlSi_3O_8$–SiO_2–H_2O. Geological Society of America Memoirs, 74: 1-146.

Watts, K.E., Bindeman, I.N. and Schmitt, A.K., 2011. Large-volume rhyolite genesis in caldera complexes of the Snake River Plain: insights from the Kilgore Tuff of the Heise Volcanic Field, Idaho, with comparison to Yellowstone and Bruneau–Jarbidge rhyolites. Journal of Petrology, 52(5): 857-890.

Chapter 4.

Addendum

p. 134 line 12: Add the following citations at the end of the first sentence ('Rittmann, 1958; Wolff and Wright, 1981;' Branney *et al*., 2004).

Table of Contents

List of Appendices

List of Figures

List of Tables

Abstract

The rhyolitic 1071 ± 5 Ma Kathleen Ignimbrite (Formation) forms part of a ~1 km thick, volcanic-sedimentary rock succession at the base of the Talbot Sub-basin and Pussy Cat Group. This group is one of many thick and extensive bimodal volcanic-sedimentary successions within the failed intra-cratonic rift-dominated Bentley Supergroup, located in the remote Musgrave region of central Australia. The ancient Kathleen Ignimbrite (KI) represents an intra-caldera fill-sequence that resulted from a very large explosive caldera-forming eruption during the Mesoproterozoic evolution of the west Musgrave Province. The Kathleen caldera has an estimated minimum intra-caldera volume of ~190 km^3 and could even represent a Volcanic Explosivity Index (VEI) 7 or greater magnitude explosive eruption.

The KI is remarkably well-preserved and exhibits well-defined volcanic textures, such as two distinct eutaxitic fiamme populations, one crystal-rich, the other crystal-poor or aphyric, remnants of devitrified glass shards, autobreccia, hyaloclastite and peperite, as well as prominent planar to folded laminations and flow-banding, interpreted to have formed during rheomorphism. Much of the up to 640 m thick deposit is welded and, in particular, the basal 50 m is extremely welded and lava-like in nature and shows evidence of having behaved rheomorphically. The high grades of welding in this deposit have obliterated many of the original vitriclastic textures, but this study demonstrates that the deposit is indeed ignimbritic and constitutes an intra-caldera eruption fill-sequence. The KI constitutes three members: the lower ignimbritic Kurrparu Member consists of a basal, crystal-poor, lava-like rheomorphic facies with a quench-fragmented bottom contact with wet underlying sediments that grades up into a thick poorly-sorted crystal-rich to crystal-poor matrix supported lapilli tuff facies with unequivocal vitriclastic textures, followed by a gradational change to a eutaxitic to upper crystal-poor facies. Overlying the Kurrparu Member are thin interbedded breccias and crystal-rich to crystal-poor, eutaxitic to non-eutaxitic vitriclastic ignimbrites and breccias of the Karlaya Member, which in turn is overlain by the reworked shallow-water turbiditic volcaniclastic upper Kilykilykarri Member.

The KI was emplaced in an initial shallow-water *marine shelf-type* or *large lake-type* palaeodepositional environment. Large volumes of magma were emplaced as slightly less evolved, coeval and cogenetic, syn-sedimentary, crystal-rich, porphyritic rhyolite intrusions into the sedimentary rocks that host the KI sequence, representing magmatism from a shared, compositionally zoned magma chamber that was contemporaneous with the caldera eruption. The rhyolitic Pussy Cat Group magmas that formed the high-silica KI and its associated intrusions were evolved, anhydrous, and metaluminous (to slightly peraluminous) A-type magmas that were enriched in the rare earth elements (REE; up to 794 ppm total REE) and fluorine (≤0.8 wt%) and are similar to topaz rhyolites of the

central western USA. These rhyolitic magmas originated from a common source and were generated by extended fractionation of basaltic magmas.

The crude vertical stratification within the KI varies between crystal-rich to crystal-poor and has the two pumice populations in addition to geochemical and textural differences in the eruption sequence. This suggests two possible eruption model scenarios, both of which fit the results: one involving the tapping of an evolved melt-rich aphyric cap of a shallow-level zoned magma chamber with the later extraction and mixing of a more primitive crystal-rich basal cumulate, the other requiring silicic magma recharge from a hotter, more buoyant, aphyric silicic magma originating from a common deeper-seated magma reservoir that triggered the eruption and subsequent mixing of the upper-crustal zoned magma chamber.

The physical volcanology, palaeoenvironment and geochemistry (barring higher fluorine concentrations) of the KI are similar to ignimbrites of the Snake River Plain of the central USA, suggesting a new locality for Snake River (SR)-type volcanism. Despite these similarities the KI has lower magmatic crystallisation temperatures (~830°C), lower eruption and deposition temperatures, and lower viscosity values ($10^{8.16}$ Pa.s) than the extremely welded SR-type rheomorphic ignimbrites. The lava-like rheomorphism seen in the KI deposit does not appear to be related to one single factor, but instead appears to be related to a combination of rheomorphism-controlling factors that are to date unique to the KI. In addition, the extreme fractionation and associated heavy REE enrichment associated with the formation of evolved, high-silica rhyolite magmas such as those that formed the KI means these types of deposits may be future low-grade, bulk-tonnage REE mineral deposits.

This research highlights the high volumes of coeval and cogenetic juvenile mantle-derived felsic magmatism that affected this area and validates the intra-cratonic instabilities suggested for current tectonic setting of west Musgrave Province during the Giles Event and Ngaanyatjarra Rift. It provides additional evidence for the recognition of a large silicic component associated with a likely large igneous province (LIP) within the Talbot Sub-basin of the west Musgrave Province and supports the presence of possible supervolcanos and likely supereruptions in central Australia during the Mesoproterozoic.

Monash University

Declaration for thesis based or partially based on conjointly published or unpublished work

General Declaration

In accordance with Monash University Doctorate Regulation 17.2 Doctor of Philosophy and Research Master's regulations the following declarations are made:

I hereby declare that this thesis contains no material which has been accepted for the award of any other degree or diploma at any university or equivalent institution and that, to the best of my knowledge and belief, this thesis contains no material previously published or written by another person, except where due reference is made in the text of the thesis.

This thesis includes 4 unpublished papers. The core theme of the thesis is the volcanology, petrogenesis, and economic potential of a rheomorphic ignimbrite deposit in central Australia. The ideas, development and writing up of all the papers in the thesis were the principal responsibility of myself, the candidate, working within the School of Geosciences, Monash University under the supervision of Prof. Ray Cas and Dr. Simon Jowitt, and also under the supervision of Dr Hugh Smithies (Geological Survery of Western Australia) and Dr Mario Werner (Geological Survey of South Australia).

The inclusion of co-authors reflects the fact that the work came from active collaboration between researchers and acknowledges input into team-based research.

In the case of Chapters 2, 3, 4 and 5 my contribution to the work involved the following:

Thesis chapter	Publication title	Publication status	Nature and extent of candidate's contribution
2	Eruption and emplacement of the oldest subaqueous intra-caldera lava-like rheomorphic ignimbrite: The Mesoproterozoic 1071 ± 5 Ma Kathleen Ignimbrite, west Musgrave Province, central Australia	Ready for submission	80%: development of ideas, data collection, interpretation, compilation, and write-up
3	Petrogenesis of the A-type, Mesoproterozoic intra-caldera rheomorphic Kathleen Ignimbrite and co-magmatic Rowland Suite intrusions, west Musgrave Province, central Australia: products of extreme fractional crystallisation in a failed rift setting	Submitted, reviewed and ready for re-submission	80%: development of ideas, data collection, interpretation, compilation, and write-up
4	Determining the controls on rheomorphism of a Mesoproterozoic lava-like ignimbrite in the subaqueously emplaced, intra-caldera, high-silica Kathleen Ignimbrite, west Musgrave Province, central Australia	Ready for submission	90%: development of ideas, data collection, interpretation, compilation, and write-up
5	Rare Earth Element (REE) mineralisation within highly fractionated rhyolites: the equivalent of low-grade porphyry deposits in the REE world?	Ready for submission	90%: development of ideas, sample preparation, data interpretation, compilation, and write-up

I have renumbered sections of submitted or published papers in order to generate a consistent presentation within the thesis.

Signed: _____

Date: _____

Chapter 1

Introduction

1.1 Introductory statement

Large volume felsic systems, including silicic large igneous province (SLIP; Bryan, 2007; Bryan and Ferrari, 2013) events, occur throughout the world and a large part of the geological rock record (e.g., Mesoproterozoic Gawler Range Volcanics, South Australia; Jurassic Chon Aike, Patagonia; Early Cretaceous Parana-Etendeka, South America-Africa; Eocene Sierra Madre Occidental, Mexico; Miocene to Quaternary Snake River Plain Volcanic Province, Idaho-Wyoming, USA; Pliocene to Quaternary Taupo Volcanic Zone; Bryan, 2007; Pankhurst *et al*., 2011). Although the volcanic style of these systems varies from effusive to explosive, caldera volcanoes and their associated welded to rheomorphic ignimbrite deposits are important features within these large volume felsic systems (Bryan *et al*., 2002; 2010; e.g., multiple calderas in the Sierra Madre Occidental, Mexico, Aguirre-Díaz *et al*., 2008; Yellowstone caldera and others in the Snake River Plain, Idaho-Wyoming, USA, Christiansen, 2001; Watts *et al*., 2011; Taupo, Okataina, Rotorua and other calderas in the Taupo Volcanic Zone, Spinks *et al*., 2005). These caldera systems and their related successions (Fig. 1.1) form through very large explosive eruptions, often at supereruption scale (>450 km^3 of erupted magma or >1000 km^3 of erupted pyroclastic deposits; Sparks *et al*., 2005; Self, 2006), and are relatively poorly documented and understood, despite the fact that these events have catastrophic and far-reaching events and produce deposits that occur frequently throughout the geological record (Lipman, 2000; Mason *et al*., 2004). Such eruptions will be major environmental, socio-economic and anthropological catastrophes, not if, but when they occur in the present day (Self, 2006; Self and Blake, 2008).

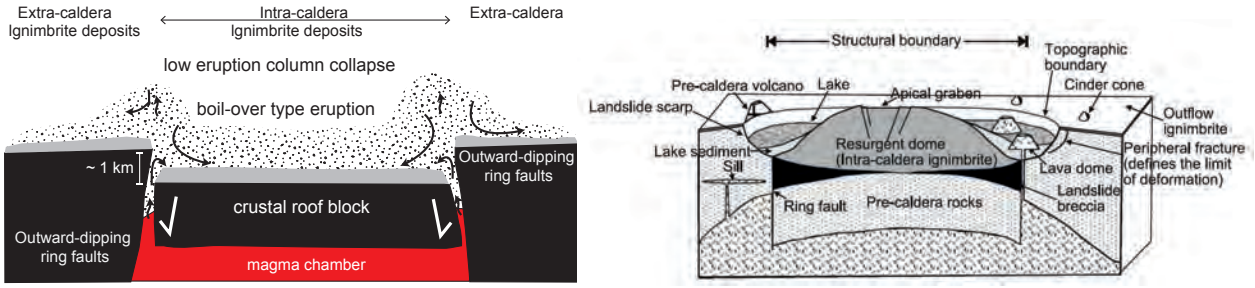

Figure 1.1: Schematic anatomy of an explosive caldera during formation, with collapse along outward-dipping ring faults, intra- and extra-caldera ignimbrite deposits and structures related to caldera systems (adapted from Willcock, 2013; Lipman, 2000).

Studies on modern caldera systems include research on the Taupo Volcanic Zone of New Zealand, (Wilson *et al*., 1995), calderas of the San Juan Volcanic Field, Colorado, (Lipman, 1976, Lipman, 1984, Bachmann *et al*., 2002, Lipman and McIntosh, 2008), the Timber Mountain-Oasis Valley Caldera Complex, (Byers, 1976, Christiansen *et al*., 1977, Broxton *et al*., 1989), and the Cerro Galan caldera, NW Argentina, Sparks *et al*., 1985, Folkes *et al*., 2011, Cas *et al*., 2011). These studies provide useful analogues for the ancient caldera systems and their successions, although these modern successions often have poorly or incompletely exposed caldera fill successions, primarily as a result of caldera collapse. In comparison, the exhumation and erosion of the successions associated with ancient felsic systems often provide good opportunities to study intra-caldera fill sequences in their entirety (e.g., the Permian Ora caldera; Willcock *et al*., 2013).

The Mesoproterozoic, ca. 1071 Ma Kathleen Ignimbrite (Formation) (KI) of the Pussy Cat Group in the remote west Musgrave region of central Australia forms part of a ~1 km thick, rhyolitic volcanic-sedimentary rock succession with a preserved outcrop of ~40 km^2. It is dominated by eutaxitically textured ignimbritic rocks that provide evidence of a very large explosive caldera-forming eruption at ca. 1071 Ma. This eruption sequence is fully exposed from its base upwards, and the KI locally reaches over 640 m in thickness. The top of the sequence is cross-cut by younger, porphyritic rhyolitic intrusions. There is no correlated preserved extra-caldera outcrop, but the available limited geometrical information indicates a calculated minimum intra-caldera volume of ~190 km^3 for the intra-caldera pyroclastic deposits of Kathleen caldera, with an extrapolated minimum total eruption volume of ~380 km^3, using an intra- to extra-caldera relationship of 1:1 (Lipman, 1984; Mason *et al*., 2004). The volume of erupted pyroclastic deposits would rank this volcano as a very large explosive eruption with a magnitude (Mason *et al*., 2004) or volcanic explosivity index (VEI; Self, 2006) of 7, similar to the Campanian Tuff (Italy; Pappalardo *et al*., 2008), Kikai-Akahoya (Japan; Self, 2006) or the 1815 A.D. Tambora (Indonesia; Self *et al*., 1984; de Silva, 2008) eruptions.

Despite its age and the numerous regional tectonic events that have affected the west Musgrave Province, the KI eruption sequence is well preserved and exhibits volcanic textures, such as well-defined eutaxitic fiamme populations and remnants of devitrified glass shards. The basal 50 m is lava-like and is marked by prominent planar to folded laminations and flow-banding that also includes a basal flow banded clast breccia.

Stratigraphic relationships with both underlying and overlying sedimentary successions such as intruding clastic dykes, magma-wet sediment mixing interactions, and the presence of sedimentary structures such as hummocky cross stratification, have allowed for constraints to be placed on the possible palaeodepositional environment. It is

proposed that the deposition and emplacement of the KI took place in an initial shallow-water *marine shelf-type* or *large lake-type* setting. Large volume, syn-sedimentary, porphyritic rhyolite intrusions are also emplaced into these sedimentary successions, and these may be genetically related to the KI.

The well-preserved textural features and physical volcanology of this volcanic-sedimentary rock succession, combined with the exposed vertical thickness, lateral extent, and subaqueous palaeodepositional setting, provide a natural laboratory to study felsic volcanic intra-caldera fill sequences. In addition, the lava-like nature of the base of the KI is indicative of rheomorphic behaviour within an intra-caldera setting and provides an opportunity to comprehensively assess the various factors and conditions that led to rheomorphism in the deposit. Not only is the physical volcanology worthy of further study, but the preservation of this succession allows the geochemical determination of the petrogenesis of the coeval magmas that formed this succession. Moreover, understanding how this system formed provides an opportunity to assess the economic potential for these high silicate rhyolites to be low grade, bulk tonnage sources of the heavy rare earth elements. For these reasons this succession forms the basis for an excellent research topic.

1.2. Specific aims

This research will address the following principal aims:

- To evaluate if the KI sequence represents an explosive caldera-forming eruption sequence that was deposited within an intra-caldera setting.
- To establish the palaeoenvironmental depositional setting of the volcanic-succession through an analysis of the sediments that host the sequence.
- To reconstruct an eruption, transportation and emplacement model for the KI sequence.
- To determine the petrogenesis of the KI and its associated magmas.
- To constrain the age of eruption and timing of events in the volcanic-sedimentary succession.
- To determine what the link is (if any) between the KI and associated voluminous intruding porphyritic rhyolites.
- To explore the contentious issue of subaqueous pyroclastic flows.
- To investigate rheomorphism in extremely welded ignimbrites, determine the controls of rheomorphism, and establish the factors that caused the KI to behave rheomorphically.
- To determine whether the KI has any potential economic interest.
- To use the outcomes of this research to improve the broader tectonic understanding of the Musgrave region and in doing so contribute to a better understanding of the

palaeotectonic setting, evolution and formation of Proterozoic Australia.

1.3 Background on the research area

The Musgrave region is covered by the Bentley, Scott, Talbot, and Cooper International Series of 1:250 000 Sheet areas in Western Australia and bounded by 25° and 27° lines of latitude S and 126° and 129° lines of longitude W (Fig. 1.2a). The research area falls within the traditional lands of the Ngaanyatjarra people and forms part of the Ngaanyatjarraku Shire (Fig. 1.2b), an Aboriginal Native Title land. This area was first mapped in detail by the Geological Survey of Western Australia in 1966–1970 (first published in Daniels, 1974), but due to the remoteness of the area and Aboriginal Native Title land rights, was not investigated again from a systematic regional geological perspective until 1987–1995, when Geoscience Australia undertook a regional mapping program (Glikson *et al*., 1995; 1996). From 2004 until present, the Geological Survey of Western Australia (GSWA) has been given permission to geologically investigate the area in detail and produce regional 1:100 000 scale geological map sheets of the area, supported by geophysical, geochronological, geochemical, and structural data interpretations (Smithies *et al*., 2009). Mineral exploration work is currently being conducted in the area by various mining companies, with some positive results to date. Before I continue to present this research, I would like to acknowledge and pay respect to the traditional owners of the ancestral land on which this study was conducted, the Ngaanyatjarra people. As I share my own knowledge and research of this area may I also pay respect to the knowledge embedded forever within the Aboriginal Custodianship of Country.

1.4 Regional geology

This section provides a brief introduction of the Musgrave region, with a specific focus on the west Musgrave Province, the Giles Event and the Bentley Supergroup. For a more comprehensive overview of the regional geology and tectonic setting of the Musgrave region please refer to Appendix A.

1.4.1 The Musgrave region and west Musgrave Province

The Musgrave region of central Australia (Fig. 1.3) consists of two essential geological components, the 1.60–1.15 Ga Musgrave Province and rocks formed during the 1085–1040 Ma Giles Event. Together these cover an area that extends across the borders between the Northern Territory, South Australia and Western Australia (Smithies *et al*., 2013; 2014). The Musgrave Province is defined as a WNW-ESE orientated belt of high-grade metamorphic rocks that is up to 800 km long and 350 km wide and is bound by Neoproterozoic to Mesozoic sedimentary basins. These basins formed before the

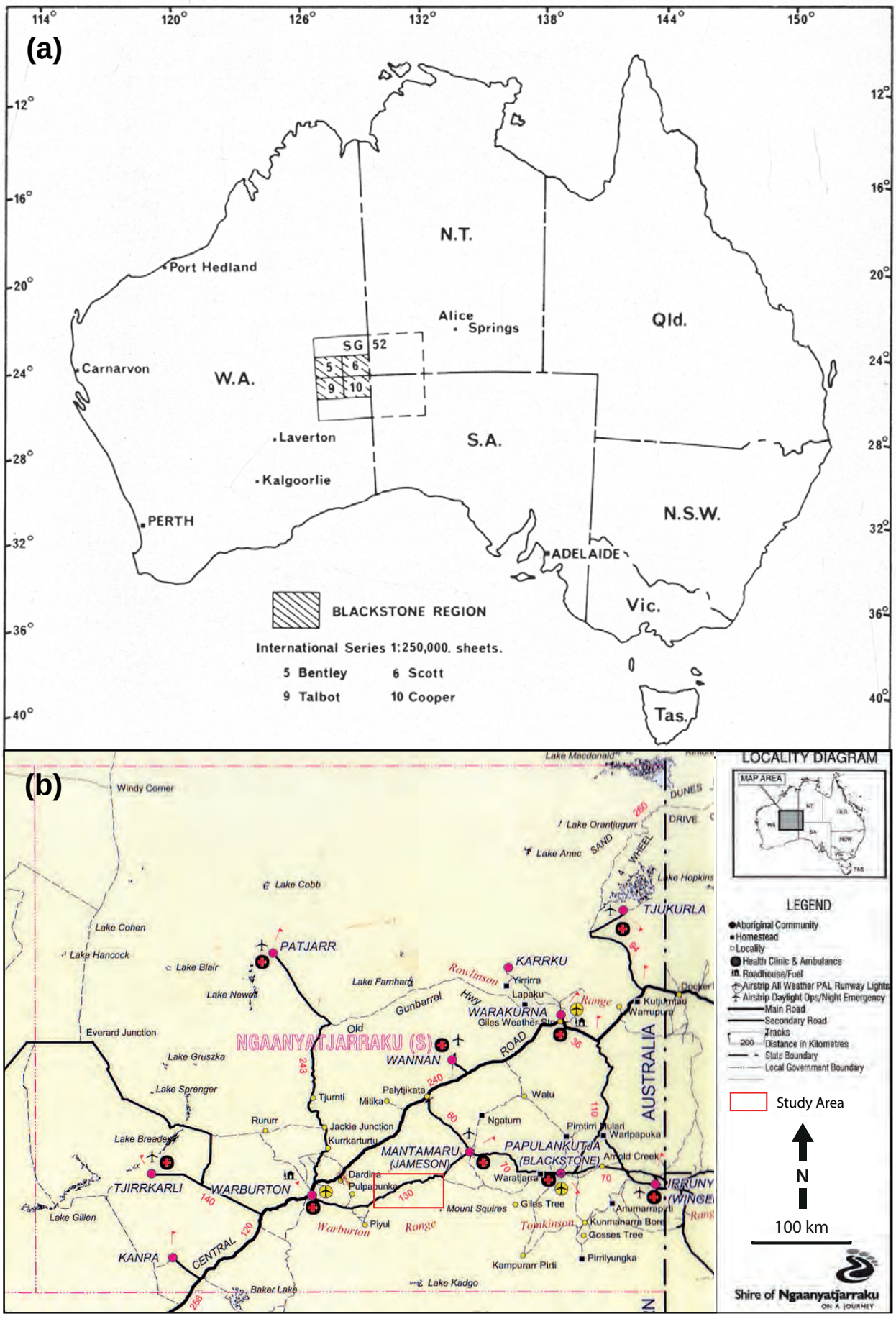

Figure 1.2: a) The Blackstone Region of Western Australia (adapted from Daniels, 1974). b) The Ngaanyatjarraku Shire and Aboriginal Communities within the area. Research area highlighted in red (adapted from Sinclair Knight Merz, 2001). North is upwards, to the top for all geographical maps.

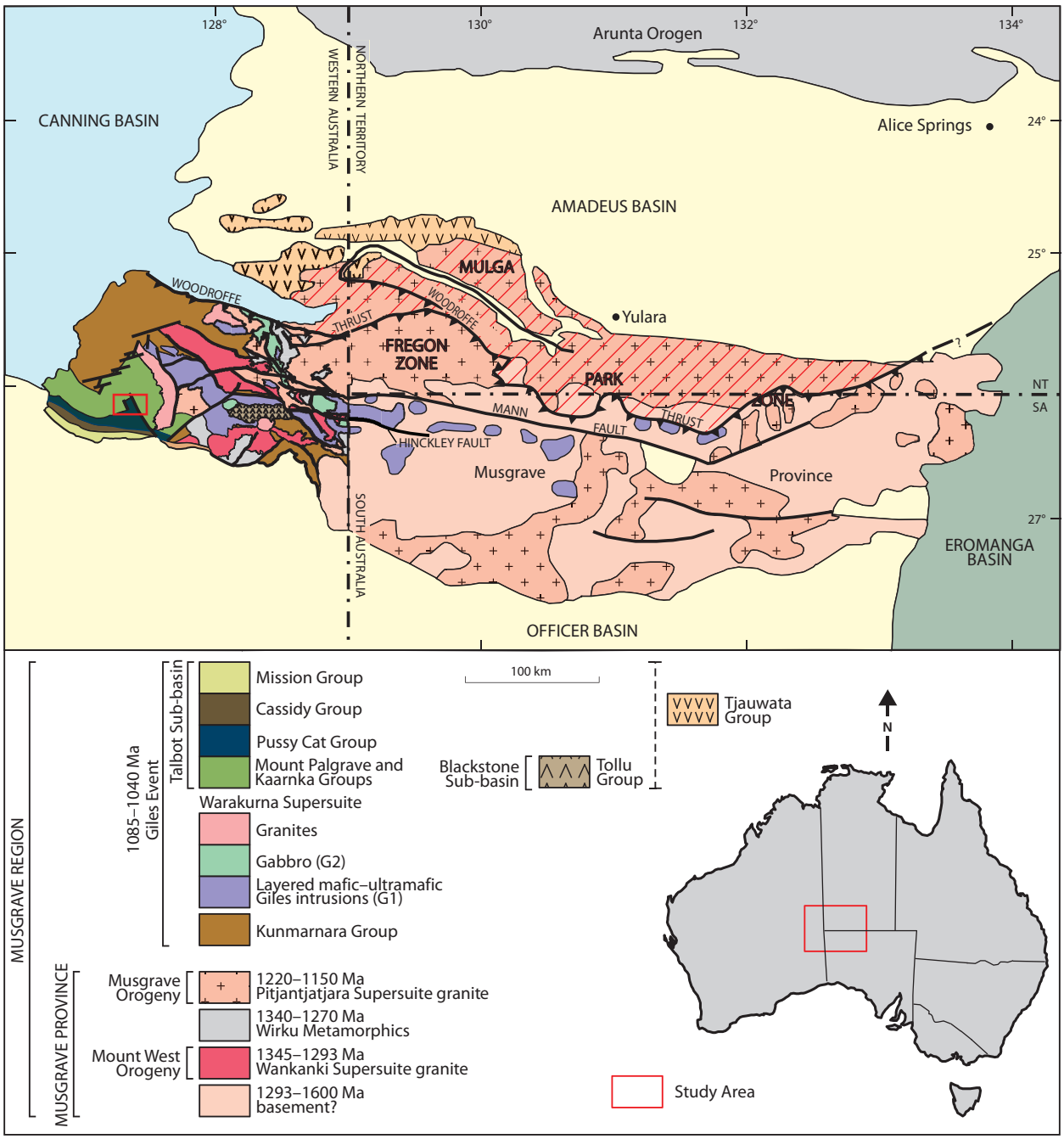

Figure 1.3: The Musgrave region and Musgrave Province (adapted from Glikson *et al*., 1996; Edgoose *et al*., 2004; Howard *et al*., 2011; Smithies *et al*., 2013).

end of the 1220–1150 Ma Musgrave Orogeny and consist of a poorly defined basement, Wankanki Supersuite, the Wirku Metamorphics and the Pitjantjatjara Supersuite (Fig. 1.3; Howard *et al*., 2011; Wade *et al*., 2008; Smithies *et al*., 2009; 2014). Younger rocks related to the 1085–1040 Ma Giles Event include the Bentley Supergroup and the Warakurna Supersuite (Wade *et al*., 2008; Smithies *et al*., 2009; 2013; 2014). The west Musgrave Province (Fig. 1.4) refers to the western half of the Musgrave Province (i.e. within Western Australia) and the rocks related to the Giles Event. In broad lithological terms, the Musgrave Province consists of high-grade metamorphic basement rocks (amphibolite to granulite facies), with overlying voluminous volcanic and lesser sedimentary rocks (Conor, 1987; Scrimgeour *et al*., 1999; Wade *et al*., 2006; Smithies *et al*., 2014), both of

which are both intruded by a number of younger granitoids, mafic-ultramafic layered and massive intrusions, and mafic and felsic dykes (Wade *et al*., 2006).

1.4.2 Tectonic evolution of the Musgrave Region and west Musgrave Province

The Musgrave Province lies at the convergence of the Proterozoic amalgamation of the North, West and South Australian Cratons (Fig. 1.5) and has undergone a number of deformational events that are summarised in detail by Wade *et al*. (2008). It also records a large part of the Australian continent's evolution (Aitken and Betts, 2009), starting with early Mesoproterozoic (ca. 1600 Ma) continental growth (Gray, 1978; Camacho and Fanning, 1995; Wade *et al*., 2006), the mid-to-late Mesoproterozoic (ca. 1.30–1.1 Ga) assembly

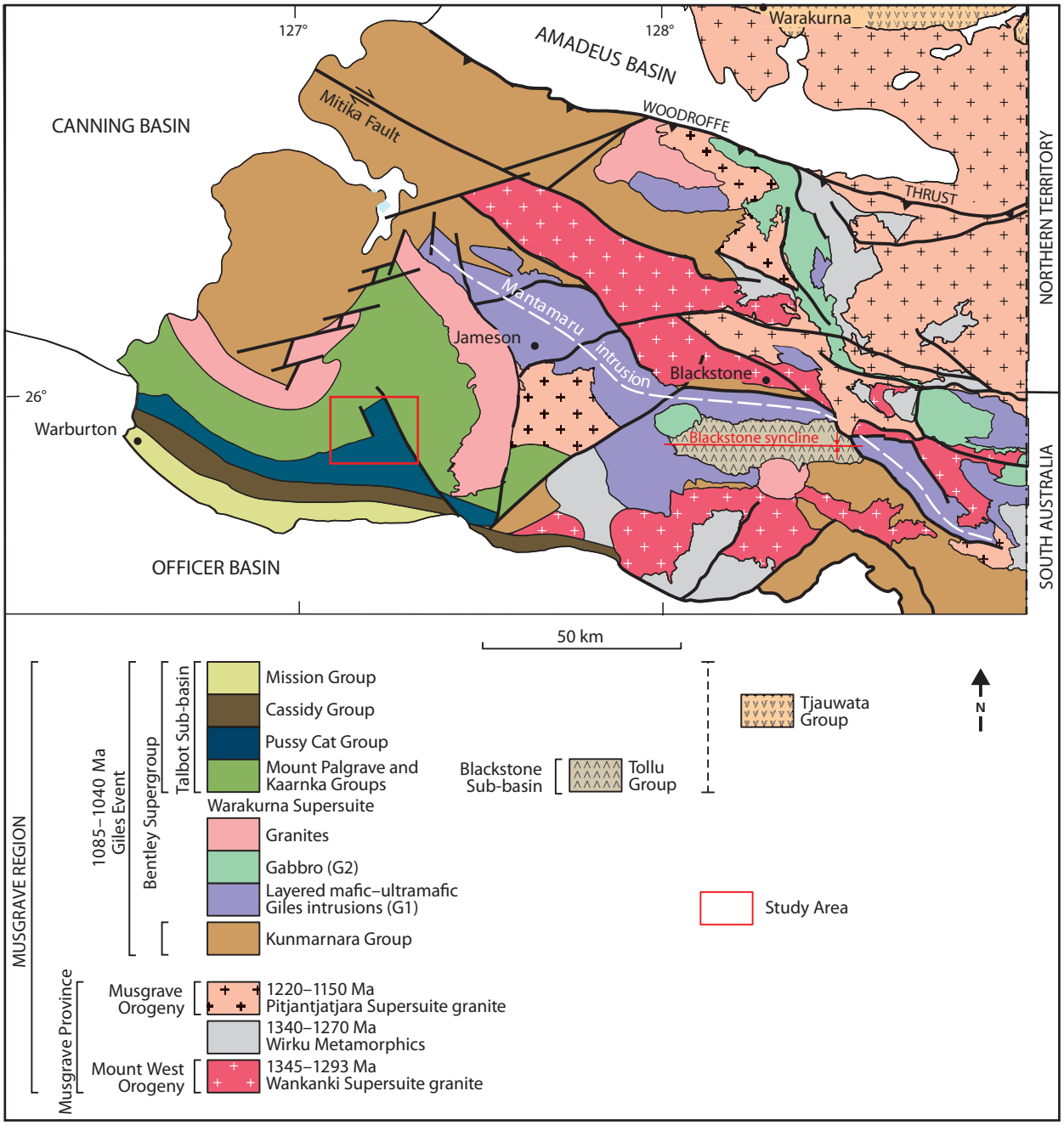

Figure 1.4: The west Musgrave Province and detailed stratigraphy (adapted from Smithies *et al*., 2013).

of Rodinia (Maboko *et al*., 1992; Glikson *et al*., 1995; Camacho *et al*., 1997; Edgoose *et al*., 2004; Wade *et al*., 2008), the mid-Neoproterozoic (ca. 800 Ma) breakup of Rodinia (Zhao and McCulloch, 1993; Wade *et al*., 2008) and the late Neoproterozoic to early Cambrian (ca. 600–500 Ma) assembly of Gondwana (Maboko *et al*., 1991; Camacho and McDougal, 2000; Wade *et al*., 2005). This indicates that an improved understanding of the tectonic setting of the Musgrave Province will in turn lead to improved reconstructions of the early Australian continent. The research presented in this thesis focuses on felsic magmatism related to the tectonic setting of the west Musgrave Province between the 1220–1150 Ma Musgrave Orogeny and the 1085–1040 Ma Giles Event. A suggestion by Smithies *et al*. (2014) is that these two events potentially be seen as a continuum of the anomalous crustal heat, which characterised the Musgrave Province during this time.

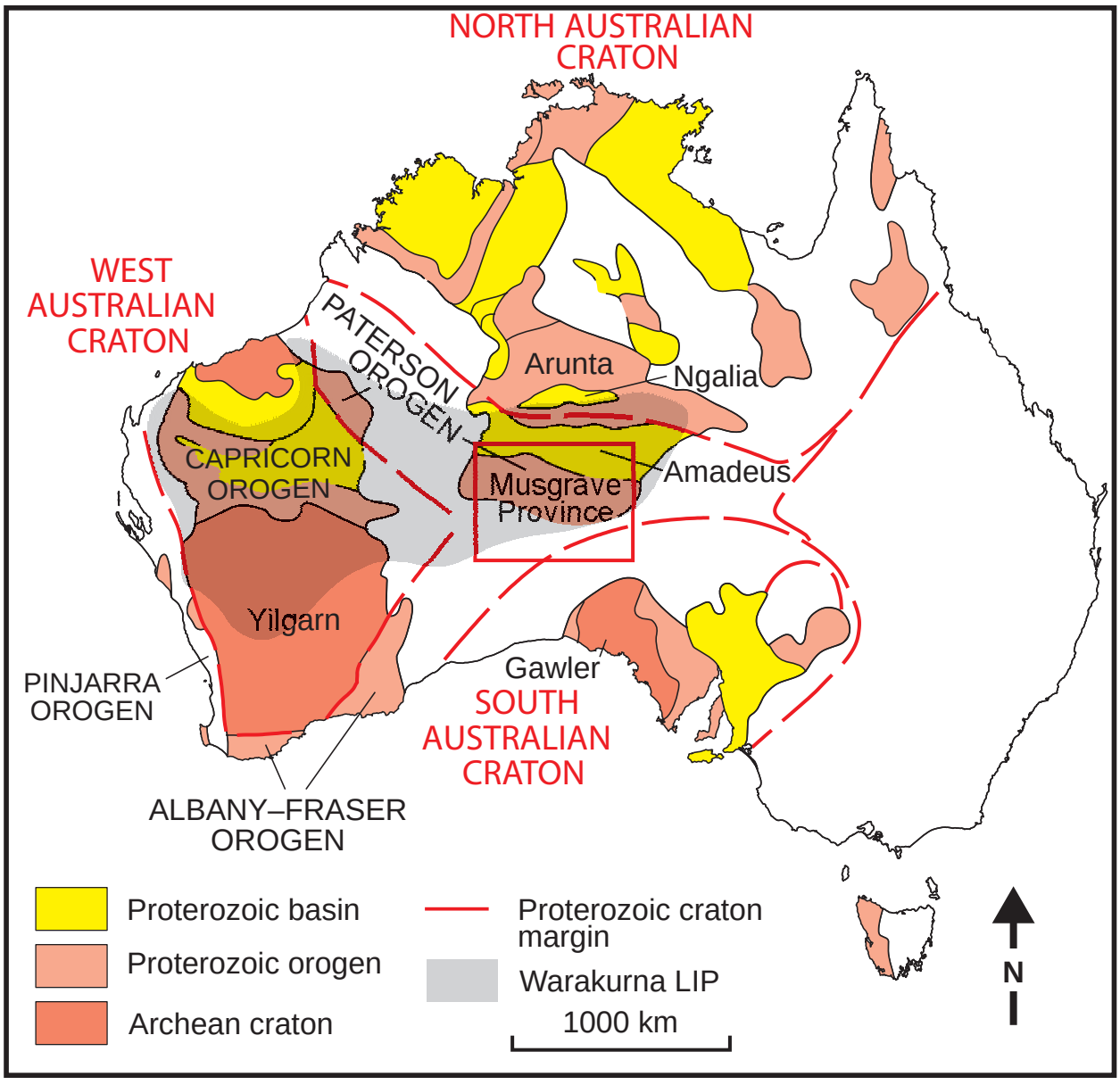

Figure 1.5: Location of the Musgrave Province in terms of the tectonic framework of Proterozoic Australia, and the extent of the Warakurna LIP (adapted from Myers *et al*., 1996; Smithies *et al*., 2013).

The Musgrave Orogeny affected the entirety of the Musgrave Province and involved intense mylonitic deformation with widespread amphibolite- to granulite-facies metamorphism and the generation of the voluminous, Pitjantjatjara Supersuite granites in a suggested intra-plate setting (Edgoose *et al*., 2004; Wade *et al*., 2008; Howard *et al*., 2011; Smithies *et al*., 2011). This event represents an unusually long period of ultra-high temperature metamorphism (Kelsey *et al*., 2009; 2010) and continuous lower crustal thinning in an extensional intracontinental setting developed within a suture zone between three older cratonic blocks (Smithies *et al*., 2010; 2014; Howard *et al*., 2011). Smithies *et al*. (2011; 2014) therefore propose that the continental crust beneath the Musgrave region was thinner than in the surrounding North, West and South Australian cratons, allowing it to act as an asthenospheric heat-sink for a long period of time. By the end of the Musgrave Orogeny and the start of the Giles Event, the Musgrave region had experienced at least 100 Ma of high to ultra-high crustal temperatures in either an intracontinental or distal backarc environment (Kirkland *et al*., 2013; Smithies *et al*., 2011; 2014).

The Musgrave Orogeny was followed by the emplacement of large volumes of mantle-derived mafic to felsic magmas into and onto the Musgrave Province during the Giles Event, which coincided with the assembly of Rodinia (Cawood, 2005). This event has been interpreted to be the result of a deep mantle plume (Zhao and McCulloch, 1993; Wingate *et al*., 2004; Morris and Pirajno, 2005; Godel *et al*., 2011; Pirajno and Hoatson, 2012). However, the almost continuous (>30 Ma) continental mafic and felsic magmatism in this area suggests a more complex intra-plate geodynamic setting for this event (Smithies *et al*., 2011, 2014). The heat responsible for this magmatism involved conductive heat (including a large radiogenic component), residual heat from under- and intra-plating of mantle-derived melts during the Musgrave Orogeny, and advective heat resulting from a continuation of this process during the Giles Event (Smithies *et al*., 2011; 2014; Kirkland *et al*., 2013). It is thought that movement along the Mundrabilla Shear Zone, a prominent south-north trending, continent-scale basement structural lineament that intersects the west Musgrave Province (Aitken *et al*., 2012), could have catastrophically disrupted the long-term regional Musgrave thermal anomaly (still present after the Musgrave Orogeny) by juxtaposing lithospheric material with contrasting thermal and physical properties, causing major asthenospheric upwellings that provided a source of heat for the Giles Event (Smithies *et al*., 2014). The primitive mafic Alcurra Dolerite (Suite) crosscuts and dissects most of the Musgrave Province, and may represent the feeder dykes to the Giles intrusions (Zhao and McCulloch, 1993; Zhao *et al*., 1994; Glikson *et al*., 1996; Scrimgeour *et al*., 1999; Wade *et al*., 2008).

1.4.3 The Giles Event

The Giles Event is associated with the formation of variably deformed mafic-

ultramafic layered and massive intrusions (Giles intrusions), voluminous bimodal volcanics (Bentley Supergroup), granitic intrusions, massive gabbros mixed and intermingled with the granites, felsic and mafic dykes and a supracrustal rift-related succession (Glikson *et al*., 1995; 1996; Sun *et al*., 1996; Close *et al*., 2003; Edgoose *et al*., 2004; Wade *et al*., 2008; Howard *et al*., 2011). All igneous rocks related to this event have been assigned to the Warakurna Supersuite, which outcrops across ~1.5 million km^2 of central and western Australia; this includes the ca. 1078–1073 Ma Warakurna Large Igneous Province (LIP) although future reclassification may assign all of this to a single long-lived LIP event (Fig. 1.1.5; Wingate *et al*., 2004; Morris and Pirajno, 2005; Howard *et al*., 2011). The structural expression of the Giles Event is the long-lived failed intra-plate Ngaanyatjarra Rift, which formed the Bentley Basin (Evins *et al*., 2010) into which the Bentley Supergoup (Daniels, 1974) is deposited.

1.4.3.1 The Bentley Supergroup

The Bentley Supergroup hosts all of the bimodal volcanic rocks of the Warakurna Supersuite and Ngaanyatjarra Rift-related successions. It is only preserved in the 'upper-crustal' west Musgrave Province, and consists of felsic and mafic volcanics, volcaniclastic rocks and interlayered sedimentary rocks (Daniels, 1974; Smithies *et al*., 2009; 2014). The volcanic rocks associated with the Bentley Supergroup are thought to be comagmatic with the layered mafic-ultramafic Giles intrusions and coeval granites (Compston and Nesbitt, 1967; Daniels, 1974; Glikson *et al*., 1995; 1996).

The outcrop of the Bentley Supergoup defines the preserved extent of the Bentley Basin, which is subdivided into the three sub-basins, namely the Talbot, Blackstone and Finlayson Sub-basins (Fig. 1.6; Howard *et al*., 2011; Smithies *et al*., 2014). The Talbot Sub-basin lies to the west of the Jamieson Community (Fig. 1.2b), it is the main preserved depositional basin in this area, and contains the largest amount of the Bentley Supergroup rocks, with the thickest preserved continuous stratigraphic column measuring some ~12 km (Smithies *et al*., 2013). It consists of a series of thick and regionally continuous layers of rhyolitic ignimbrites, rheomorphic ignimbrites and lava flows that are interlayered with basaltic lava flows and siliciclastic rocks (Howard *et al*., 2011; Smithies *et al*., 2014).

The Talbot Sub-basin is largely undeformed barring local deformation adjacent to shears and faults, although most of the rocks have undergone greenschist facies metamorphism (Smithies *et al*., 2013). The stratigraphic base of this group is represented by the effusive and ignimbritic rocks of the Mount Palgrave Group, a west- to southwest-younging succession of dacitic to rhyolitic volcanic and pyroclastic rocks that are intercalated with minor amounts of basalt and sedimentary rocks (Howard *et al*., 2011). The eastern margin of the Palgrave area is intruded by the syn-volcanic Winburn granite,

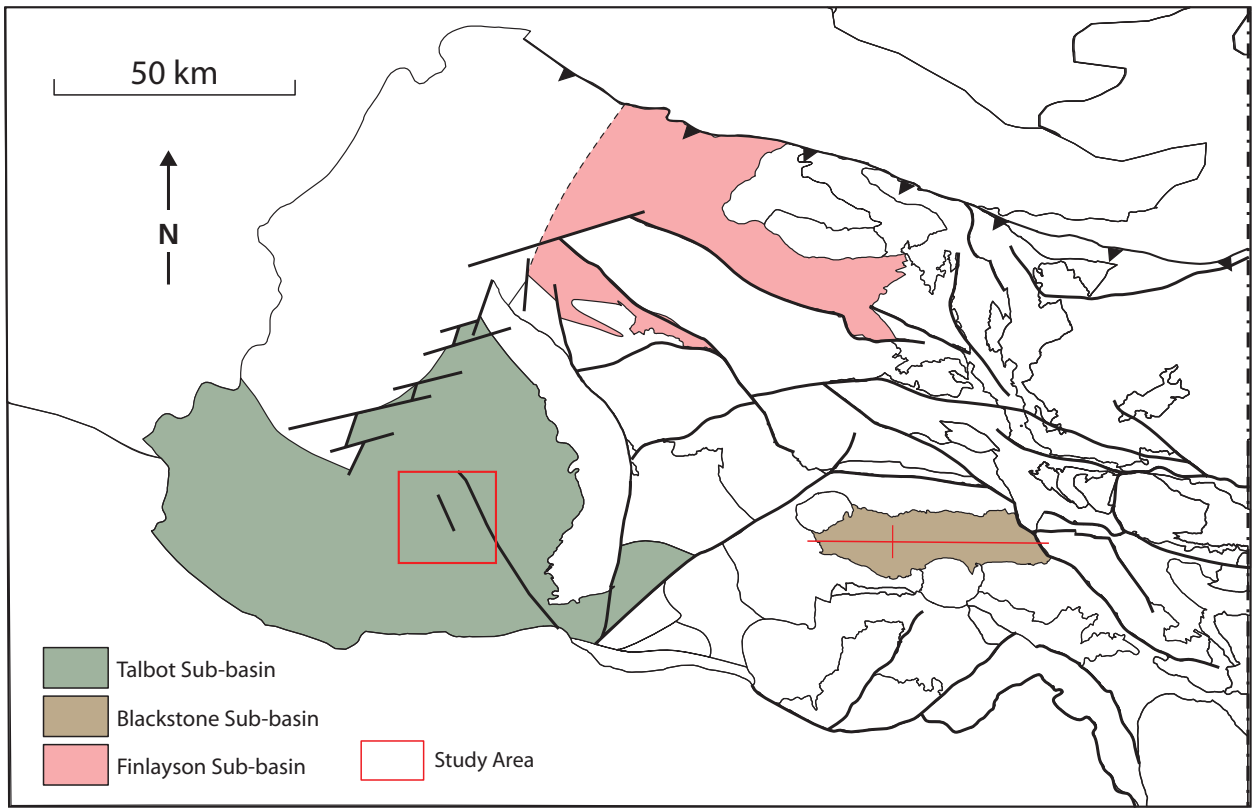

Figure 1.6: Various sub-basins of the Bentley Basin and Bentley Supergroup discussed in the text (adapted from Smithies *et al*., 2014).

a suite of monzogranitic to alkali-feldspar granites and quartz-alkali feldspar syenites that removed the base of the thick volcanic succession that makes up the Mount Palgrave Group (Smithies *et al*., 2013; 2014). The Mount Palgrave Group as a whole reflects a series of voluminous, highly-evolved, rhyolitic magmas and lesser tholeiitic mafic magmas and represent the products of a series of high-energy and violent eruptions (Smithies *et al*., 2013).

The Mount Palgrave Group is overlain by the Kaarnka Group, which represents a discrete north-northwest trending oval-shaped basin that is up to 27 km wide and 46 km long and is thought to represent a caldera cluster (Daniels, 1974; Smithies *et al*., 2013). Daniels (1974) originally interpreted three areas in west Musgrave Province to represent discreet fault-bounded cauldrons (an eroded caldera complex; Fig. 1.7), although Smithies *et al*. (2013) only recognise one of these areas, now termed the Kaarnka caldera cluster, and modified the original postulated extent of these calderas. This group is characterised by massive to flow-banded rhyolite with intercalated ignimbrites and lesser amounts of siliciclastic sedimentary rocks and basalts (Smithies *et al*., 2013). This group is thought to host the Talbot Sub-basin supervolcano and reflects a supereruption event in the west Musgrave Province (Smithies *et al*., 2013; 2014).

The Mount Palgrave and Kaarnka groups in the southern part of the Talbot Sub-basin are directly overlain, in an apparently conformable manner, by the Pussy Cat Group,

which in turn is overlain by the Cassidy and Mission groups. These groups constitute volcanic-sedimentary successions and form a stratigraphically continuous, bow-shaped, W to NW–E to SE-trending package that is south-dipping and -younging, and attains a cumulative thickness of several kilometres (Howard *et al*., 2011). Units within the Cassidy Group are also considered to be the result of single voluminous supereruptions (erupted volumes >450 km^3; Sparks *et al*., 2005; Self, 2006; Smithies *et al*., 2014).

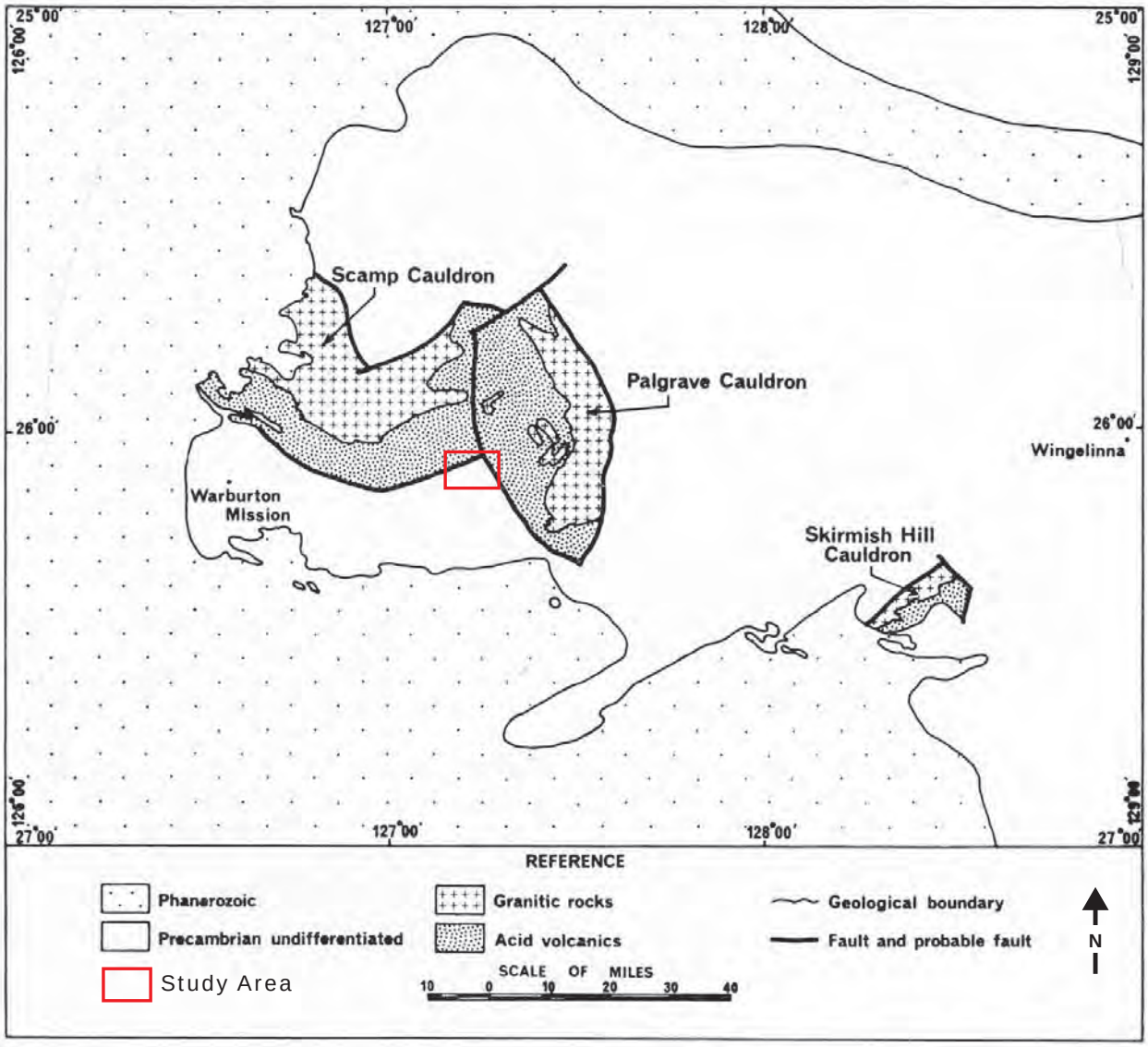

Figure 1.7: The three possible calderas complexes (referred to as cauldrons) identified by Daniels (1974) and the relative positions of the previous Scamp and Palgrave volcanic associations (the area within the cauldrons) (adapted from Daniels, 1974). Note the research study area located within the red square outline.

1.5 Methods

Specific methods are summarised in each chapter, but briefly the main methods used in this research are initial fieldwork involving geological field mapping, volcanic facies analysis, stratigraphic logging, sampling, and laboratory-based research involving petrography, geochemistry (including radiogenic isotopes), geochronology, geothermometry and geochemical modelling (including viscosity calculations) techniques.

Details of the specific methods used for each chapter are summarised in the individual chapters.

1.6 Outline of thesis structure

This thesis is structured as a series of publishable papers that are bookended by this introductory chapter (Chapter 1) and a conclusion and discussion chapter (Chapter 6). This structure is according to and compliant with the rules of Monash University and represents a thesis-by-publication. This format does lead to minor repetition of some background material or cross-referencing between chapters, as each research chapter is considered to be a stand-alone manuscript or journal article. This enables each chapter to focus on the research aims of the thesis.

- Chapter 1 is an introductory chapter that presents the contextual background and the specific aims of this research, as well as the concise regional geology and tectonic setting of the area.
- Chapter 2 addresses the physical volcanology of the Kathleen Ignimbrite, presents the facies and stratigraphic architecture of the volcanic-sedimentary sequence that hosts the Kathleen Ignimbrite and interpretations of the volcanology and palaeodepositional environment, and discusses the rheomorphism of the KI, the presence of subaqueous pyroclastic flows and proposes an eruption model. This will be submitted to Journal of Volcanology and Geothermal Research.
- Chapter 3 discusses the petrogenesis of the rhyolites of the Pussy Cat Group, with specific focus on the petrography, geochemistry, and geochronology of these rhyolites. The petrogenesis is supported by geochemical data and modelling, with an origin through extended fractional crystallisation being proposed for the Kathleen Ignimbrite and its associated magmas. This chapter has been submitted to Journal of Petrology and has been reviewed, revised and resubmitted for consideration for publication.
- Chapter 4 links the physical volcanology, petrography and the geochemistry of the Kathleen Ignimbrite and investigates the factors that caused the Kathleen Ignimbrite to behave rheomorphically. A comprehensive overview of rheomorphism and rheomorphic ignimbrites is also provided in this chapter. This chapter will be submitted to Bulletin of Volcanology.
- Chapter 5 explores the economic potential of these highly evolved rhyolites through the petrogenetic processes discussed in Chapter 3 and proposes that they be seen as the porphyry deposits of the rare earth element world. This chapter will be submitted to either Economic Geology or Mineralium Deposita.
- Chapter 6 is a summary of all the results achieved through this research, followed by a discussion of the broader implications of this study.

1.7 References

Aguirre-Díaz, G.J., Labarthe-Hernández, G., Tristán-González, M., Nieto-Obregón, J. and Gutiérrez-Palomares, I., 2008. The ignimbrite flare-up and graben calderas of the Sierra Madre Occidental, México. Developments in Volcanology, 10: 143-180.

Aitken, A.R.A. and Betts, P.G., 2009. Constraints on the Proterozoic supercontinent cycle from the structural evolution of the south-central Musgrave Province, central Australia. Precambrian Research, 168(3-4): 284-300.

Aitken, A.R.A., Smithies, R.H., Dentith, M.C., Joly, A., Evans, S. and Howard, H.M., 2012. Magmatism-dominated intracontinental rifting in the Mesoproterozoic: The Ngaanyatjarra Rift, central Australia. Gondwana Research.

Bachmann, O., Dungan, M.A. and Lipman, P.W., 2002. The Fish Canyon magma body, San Juan volcanic field, Colorado: rejuvenation and eruption of an upper-crustal batholith. Journal of Petrology, 43(8): 1469-1503.

Broxton, D.E., Warren, R.G., Byers, F.M. and Scott, R.B., 1989. Chemical and mineralogic trends within the Timber Mountain-Oasis Valley Caldera Complex, Nevada: Evidence for multiple cycles of chemical evolution in a long-lived silicic magma system. Journal of Geophysical Research: Solid Earth (1978–2012), 94(B5): 5961-5985.

Bryan, S.E., 2007. Silicic large igneous provinces. Episodes, 30(1): 20-31.

Bryan, S.E. and Ferrari, L., 2013. Large igneous provinces and silicic large igneous provinces; progress in our understanding over the last 25 years. Geological Society of America Bulletin, Pre-Issue Publication.

Bryan, S.E., Peate, I.U., Peate, D.W., Self, S., Jerram, D.A., Mawby, M.R., Marsh, J. and Miller, J.A., 2010. The largest volcanic eruptions on Earth. Earth-Science Reviews, 102(3): 207-229.

Byers, F.M., 1976. Volcanic suites and related cauldrons of Timber Mountain-Oasis Valley caldera complex, southern Nevada. U.S. Geol. Surv. Prof. Pap.: 70.

Camacho, A., Compston, W., McCulloch, M. and McDoucall, I., 1997. Timing and exhumation of eclogite facies shear zones, Musgrave Block, central Australia. Journal of Metamorphic Geology, 15(6): 735-751.

Camacho, A. and Fanning, C.M., 1995. Some isotopic constraints on the evolution of the granulite and upper amphibolite facies terranes in the eastern Musgrave Block, central Australia. Precambrian Research, 71(1-4): 155-181.

Camacho, A. and McDougal, I., 2000. Intracratonic, strike-slip partitioned transpression and the formation and exhumation of eclogite facies rocks: An example from the Musgrave Block, central Australia. Tectonics, 19(5): 978-996.

Cashman, K. and Cas, R., 2011. Introduction to the Special Issue of Bulletin of Volcanology,“The Cerro Galan Ignimbrite and Caldera: characteristics and origins of a very large volume ignimbrite and its magma system”. Bulletin of Volcanology,

73(10): 1425-1426.

Cawood, P.A., 2005. Terra Australis Orogen; Rodinia breakup and development of the Pacific and Iapetus margins of Gondwana during the Neoproterozoic and Paleozoic. Earth-Science Reviews, 69(3-4): 249-279.

Christiansen, R.L., 2001. The Quaternary and pliocene Yellowstone plateau volcanic field of Wyoming, Idaho, and Montana.

Christiansen, R.L., Lipman, P.W., Carr, W., Byers, F., Orkild, P.P. and Sargent, K., 1977. Timber Mountain–Oasis Valley caldera complex of southern Nevada. Geological Society of America Bulletin, 88(7): 943-959.

Close, D.F., Edgoose, C.J. and Scrimgeour, I.R., 2003. Hull and Bloods Range Special, Northern Territory. 1:100000 Geological Map Series Explanatory Notes, Northern Territory Geological Survey, Darwin.

Compston, W. and Nesbitt, R.W., 1967. Isotopic age of the Tollu volcanics, W. A. Journal of the Geological Society of Australia, 14, Part 2: 235-238.

Conor, C.H.H., 1987. The geology of the Eateringinna 1:100000 sheet area eastern Musgrave Block, South Australia. M.Sc Thesis, University of Adelaide, Adelaide.

Daniels, J.L., 1974. The geology of the Blackstone region, Western Australia. Bulletin - Geological Survey of Western Australia, 123: 257.

de Silva, S., Salas, G. and Schubring, S., 2008. Triggering explosive eruptions-The case for silicic magma recharge at Huaynaputina, southern Peru. Geology, 36(5): 387-390.

Edgoose, C.J., Scrimgeour, I.R. and Close, D.F., 2004. Geology of the Musgrave Block, Northern Territory. Northern Territory Geological Survey, Report 15.

Evins, P.M., Smithies, R.H., Howard, H.M., Kirkland, C.L., Wingate, M.T.D. and Bodorkos, S., 2010. Devil in the detail; the 1150-1000 Ma magmatic and structural evolution of the Ngaanyatjarra Rift, west Musgrave Province, central Australia. Precambrian Research, 183(3): 572-588.

Folkes, C.B., Wright, H.M., Cas, R.A., de Silva, S.L., Lesti, C. and Viramonte, J.G., 2011. A re-appraisal of the stratigraphy and volcanology of the Cerro Galán volcanic system, NW Argentina. Bulletin of volcanology, 73(10): 1427-1454.

Glikson, A.Y., Ballhaus, C.G., Clarke, G.L., Sheraton, J.W., Stewart, A.J. and Sun, S.S., 1995. Geological framework and crustal evolution of the Giles mafic- ultramafic complex and environs, western Musgrave Block, central Australia. AGSO Journal of Australian Geology & Geophysics, 16(1-2): 41-67.

Glikson, A.Y., Stewart, A.J., Ballhaus, C.G., Clarke, G.L., Feeken, E.H.J., Leven, J.H., Sheraton, J.W. and Sun, S.S., 1996. Geology of the western Musgrave Block, central Australia, with particular reference to the mafic-ultramafic Giles Complex. Bulletin - Australian Geological Survey Organisation, 239.

Godel, B., Seat, Z., Maier, W.D. and Barnes, S.-J., 2011. The Nebo-Babel Ni-Cu-PGE sulfide deposit (West Musgrave Block, Australia): Pt. 2. Constraints on parental

magma and processes, with implications for mineral exploration. Economic Geology, 106(4): 557-584.

Gray, C.M., 1978. Geochronology of granulite-facies gneisses in the western Musgrave Block, central Australia. J. Geol. Soc. Aust., 25: 403-414.

Howard, H.M., Werner, M., Smithies, R.H., Evins, P.M., Kirkland, C.L., Kelsey, D.E., Hand, M., Collins, A.S., Pirajno, F., Wingate, M.T.D., Maier, W.D. and Raimondo, T., 2011. The geology of the west Musgrave Province and the Bentley Supergroup -- a field guide. Record - Geological Survey of Western Australia, Perth, Australia, 2011/14: 125 pp.

Kelsey, D.E, Hand, M., Smithies, R.H., Evins, P., Clark, C. and Kirkland, C.L, 2009. High-temperature, high geothermal gradient metamorphism in the Musgrave Province, central Australia; potential constraints on tectonic setting. Biennial Conference of the Specialist Group for Geochemistry, Mineralogy and Petrology, Kangaroo Island, November 2009. Geological Society of Australia Abstracts, 28 pp.

Kelsey, D.E., Smithies, R.H., Hand, M., Evins, P.M., Clark, C. and Kirkland, C.L., 2010. What is the tectonic setting of long-lived Grenvillian-aged ultrahigh temperature, high geothermal gradient metamorphism in the Musgrave Province, central Australia, Geological Society of America, Abstracts with Programs, Denver Colorado, 42:5.

Kirkland, C.L., Smithies, R.H., Woodhouse, A.J., Howard, H.M., Wingate, M.T.D., Belousova, E.A., Cliff, J., Murphy, R. and Spaggiari, C.V., 2013. Constraints and deception in the isotopic record; the crustal evolution of the west Musgrave Province, central Australia. Gondwana Research, 23: 759-781.

Lipman, P.W., 1976. Caldera-collapse breccias in the western San Juan Mountains, Colorado. Geological Society of America Bulletin, 87(10): 1397-1410.

Lipman, P.W., 1984. The roots of ash flow calderas in western North America; windows into the tops of granitic batholiths. Journal of Geophysical Research, 89(B10): 8801-8841.

Lipman, P.W., 2000. Calderas. In: H. Sigurdsson (Editor), Encyclopedia of Volcanoes. Academic Press, San Francisco.

Lipman, P.W. and McIntosh, W.C., 2008. Eruptive and noneruptive calderas, northeastern San Juan Mountains, Colorado; where did the ignimbrites come from? Geological Society of America Bulletin, 120(7-8): 771-795.

Maboko, M.A.H., McDougall, I., Zeitler, P.K. and Williams, I.S., 1992. Geochronological evidence for ~530-550 Ma juxtaposition of two Proterozoic metamorphic terranes in the Musgrave Ranges, central Australia. Australian Journal of Earth Sciences, 39(4): 457-471.

Maboko, M.A.H., Williams, I.S. and Compston, W., 1991. Zircon U-Pb chronometry of the pressure and temperature history of granulites in the Musgrave Ranges, central Australia. Journal of Geology, 99(5): 675-697.

Mason, B.G., Pyle, D.M. and Oppenheimer, C., 2004. The size and frequency of the

largest explosive eruptions on Earth. Bulletin of Volcanology, 66(8): 735-748.

Morris, P.A. and Pirajno, F., 2005. Mesoproterozoic sill complexes in the Bangemall Supergroup, Western Australia; geology, geochemistry, and mineralization potential. Report - Geological Survey of Western Australia. Perth, Australia, 99: 83 pp.

Myers, J.S., Shaw, R.D. and Tyler, I.M., 1996. Tectonic evolution of Proterozoic Australia. Tectonics, 15(6): 1431-1446.

Pankhurst, M., Schaefer, B. and Betts, P., 2011. Geodynamics of rapid voluminous felsic magmatism through time. Lithos, 123(1): 92-101.

Pappalardo, L., Ottolini, L. and Mastrolorenzo, G., 2008. The Campanian Ignimbrite (southern Italy) geochemical zoning: insight on the generation of a super-eruption from catastrophic differentiation and fast withdrawal. Contributions to Mineralogy and Petrology, 156(1): 1-26.

Pirajno, F. and Hoatson, D.M., 2012. A review of Australia's Large Igneous Provinces and associated mineral systems: Implications for mantle dynamics through geological time. Ore Geology Reviews, 48: 2-54.

Scrimgeour, I.R., Close, D.F. and Edgoose, C.J., 1999. Petermann Ranges, N.T. 1:250000 Geological Series Explanatory Notes SG52-7, Department of Mines and Energy, Northern Territory Geological Survey.

Self, S., 2006. The effects and consequences of very large explosive volcanic eruptions. Philosophical Transactions of the Royal Society A: Mathematical, Physical and Engineering Sciences, 364(1845): 2073-2097.

Self, S. and Blake, S., 2008. Consequences of explosive supereruptions. Elements, 4(1): 41-46.

Self, S., Rampino, M., Newton, M. and Wolff, J., 1984. Volcanological study of the great Tambora eruption of 1815. Geology, 12(11): 659-663.

Smithies, R.H., Howard, H.M., Evins, P.M., Kirkland, C.L., Bordorkos, S. and Wingate, M.T.D., 2009. The west Musgrave Complex - new geological insights from recent mapping, geochronology, and geochemical studies. Record - Geological Survey of Western Australia, Perth, Australia, 2008/19: 20.

Smithies, R.H., Howard, H.M., Evins, P.M., Kirkland, C.L., Kelsey, D.E., Hand, M., Wingate, M.T.D., Collins, A.S. and Belousova, E., 2011. High-temperature granite magmatism, crust-mantle interaction and the Mesoproterozoic intracontinental evolution of the Musgrave Province, central Australia. Journal of Petrology, 52(5): 931-958.

Smithies, R.H., Howard, H.M., Evins, P.M., Kirkland, C.L., Kelsey, D.E., Hand, M., Wingate, M.T.D., Collins, A.S., Belousova, E.A. and Allchurch, S., 2010. Geochemistry, geochronology and petrogenesis of Mesoproterozoic felsic rocks in the west Musgrave Province, Central Australia, and implications for the Mesoproterozoic tectonic evolution of the region. Record - Geological Survey of Western Australia,

Perth, Australia, 106: 82.

Smithies, R.H., Howard, H.M., Kirkland, C.L., Werner, M., Medlin, C.C., Wingate, M.T.D. and Cliff, J.B., 2013. Geochemical evolution of rhyolites of the Talbot Sub-basin and associated felsic units of the Warakurna Supersuite Report - Geological Survey of Western Australia, Perth, Australia, 118: 74 pp.

Smithies, R., Kirkland, C., Korhonen, F., Aitken, A., Howard, H., Maier, W., Wingate, M., Quentin de Gromard, R. and Gessner, K., 2014. The Mesoproterozoic thermal evolution of the Musgrave Province in central Australia–plume vs. the geological record. Gondwana Research.

Sparks, R.S.J., Francis, P.W., Hamer, R.D., Pankhurst, R.J., O'Callaghan, L.O., Thorpe, R.S. and Page, R., 1985. Ignimbrites of the Cerro Galan Caldera, NW Argentina. Journal of Volcanology and Geothermal Research, 24(3-4): 205-248.

Sparks, R.S.J., Self, S., Grattan, J.P., Oppenheimer, C., Pyle, D.M. and Rymer, H., 2005. Super-eruptions: global effects and future threats, London, UK.

Spinks, K.D., Acocella, V., Cole, J.W. and Bassett, K.N., 2005. Structural control of volcanism and caldera development in the transtensional Taupo Volcanic Zone, New Zealand. Journal of Volcanology and Geothermal Research, 144(1): 7-22.

Sun, S.S., Sheraton, J.W., Glikson, A.Y. and Stewart, A.J., 1996. A major magmatic event during 1050-1080 Ma in central Australia, and emplacement age for the Giles Complex. AGSO Research Newsletter, 24: 13-15.

Wade, B.P., Barovich, K.M., Hand, M., Scrimgeour, I.R. and Close, D.F., 2006. Evidence for early Mesoproterozoic arc magmatism in the Musgrave Block, central Australia; implications for Proterozoic crustal growth and tectonic reconstructions of Australia. Journal of Geology, 114(1): 43-63.

Wade, B.P., Hand, M. and Barovich, K.M., 2005. Nd isotopic and geochemical constraints on provenance of sedimentary rocks in the eastern Officer Basin, Australia: Implications for the duration of the intracratonic Petermann Orogeny. Journal of the Geological Society, 162(3): 513-530.

Wade, B.P., Kelsey, D.E., Hand, M. and Barovich, K.M., 2008. The Musgrave Province; stitching north, west and south Australia. Precambrian Research, 166(1-4): 370-386.

Watts, K.E., Bindeman, I.N. and Schmitt, A.K., 2011. Large-volume rhyolite genesis in caldera complexes of the Snake River Plain: insights from the Kilgore Tuff of the Heise Volcanic Field, Idaho, with comparison to Yellowstone and Bruneau–Jarbidge rhyolites. Journal of Petrology, 52(5): 857-890.

Willcock, M.A.W., 2013. Understanding large caldera in-filling processes: the facies, stratigraphic architecture and volcanology of the Permian Ora Formation and caldera super-eruption, northern Italy., Monash University, http://arrow.monash.edu.au/hdl/1959.1/897291.

Willcock, M.A.W., Cas, R.A.F., Giordano, G. and Morelli, C., 2013. The eruption, pyroclastic

flow behaviour, and caldera in-filling processes of the extremely large volume (1290 km^3), intra- to extra-caldera, Permian Ora (ignimbrite) Formation, southern Alps, Italy. Journal of Volcanology and Geothermal Research, 265: 102-126.

Wilson, C., Houghton, B., McWilliams, M., Lanphere, M., Weaver, S. and Briggs, R., 1995. Volcanic and structural evolution of Taupo Volcanic Zone, New Zealand: a review. Journal of volcanology and geothermal research, 68(1): 1-28.

Wingate, M.T.D., Pirajno, F. and Morris, P.A., 2004. Warakurna large igneous province: A new Mesoproterozoic large igneous province in west-central Australia. Geology, 32(2): 105-108.

Zhao, J.-x. and McCulloch, M.T., 1993. Melting of a subduction-modified continental lithospheric mantle: evidence from late Proterozoic mafic dike swarms in central Australia. Geology, 21(5): 463-466.

Zhao, J.-x., McCulloch, M.T. and Korsch, R.J., 1994. Characterisation of a plume-related ~ 800 Ma magmatic event and its implications for basin formation in central-southern Australia. Earth and Planetary Science Letters, 121(3-4): 349-367.

Eruption and emplacement of the oldest subaqueous intra-caldera lava-like rheomorphic ignimbrite: The Mesoproterozoic 1071 ± 5 Ma Kathleen Ignimbrite, west Musgrave Province, central Australia

C.C. Medlin[1], R.A.F. Cas[1], M. Werner[2] and R.H. Smithies[3]

[1]School of Geosciences, Monash University, Wellington Road, Clayton, Victoria, 3800, Australia
[2]Geological Survey of South Australia, GPO Box 1264, Adelaide, South Australia, 5001, Australia.
[3]Geological Survey of Western Australia, 100 Plain Street, East Perth, Western Australia, 6004, Australia.

Keywords: rheomorphic ignimbrite, caldera, shallow-water, turbidite, subaqueous volcanism, central Australia, Mesoproterozoic

Abstract

The 1071 ± 5 Ma rhyolitic Kathleen Ignimbrite (Formation) is part of a ~1 km thick, felsic, volcanic-sedimentary succession that represents a likely subaqueous explosive caldera system. This system erupted in the west Musgrave Province of central Australia, a WNW–ESE-orientated belt of high-grade metamorphic rocks that are overlain by voluminous volcanic and sedimentary rocks, all of which are intruded by granitic plutons, mafic-ultramafic layered and massive intrusions, and mafic and felsic dykes.

The Kathleen Ignimbrite consists of three facies associations: a thick, basal, intra-caldera, rheomorphic ignimbrite, the Kurrparu Member, interpreted as a simple single cooling unit of ≤500 m thickness. It has well-preserved volcanic textures, including columnar jointing, eutaxitic fiamme, autobreccia, hyaloclastite, peperite, and characteristic flow-bands and flow-folds that are particularly prominent in the basal 50 m. These define an apparently coherent lava-like facies indicative of extremely high-grade welding and intense rheomorphic flow conditions. The Kurrparu Member is overlain by the Karlaya Member, which consists of multiple, thin, eutaxitically textured welded ignimbrites with plastically deformed and devitrified shard textures. Above this is the Kilykilykarri Member, a stratified volcaniclastic turbidite and debris flow deposit. This caldera-filling volcanic succession conformably overlies shallow-water shelf-type or large lake-type setting storm turbidite and mudstone deposits and lesser basal mafic volcanic rocks. The sediments host

a subvolcanic, syn-sedimentary, porphyritic rhyolite sill, which is coeval and comagmatic with the caldera-forming Kathleen Ignimbrite and is likely related to magma resurgence beneath the interpreted Kathleen caldera.

The textures and facies documented in this combined volcanic-sedimentary succession indicate an eruptive model and palaeoenvironment that involved: 1) a large stratified upper crustal magma chamber, 2) an explosive caldera-forming eruption of at least two high-temperature, low-viscosity, rhyolite magmas, one aphyric to crystal-poor, the other crystal-rich; 3) a shallow, subaqueous depositional environment; 4) a low unstable continuously collapsing eruption column, 5) a sustained, high mass flux pyroclastic flow system; 6) formation of a volcanotectonic depression or caldera; 7) conditions that facilitated heat retention and high-degrees of welding; and 8) a slope. The Kathleen Ignimbrite represents the oldest documented case of an intra-caldera, lava-like rheomorphic ignimbrite that was initially emplaced in a subaqueous environment.

2.1 Introduction and Aims

Large-volume felsic explosive eruptions can have devastating effects on Earth's climate and environment (Sparks *et al*., 2005; Self, 2006; Miller and Wark, 2008). The deposits formed during these events are the only evidence we have to understand the nature of these eruptions and the dynamics or processes involved (Wilson, 2008). These eruptions commonly result in large volume pyroclastic flow deposits or ignimbrites, erupted from large, explosive caldera volcanoes. Caldera forming ignimbrites are deposited in two settings, the intra-caldera setting, and the surrounding extra-caldera setting. The inward and downward collapse of the roof block of a subsurface magma chamber produces a syn-eruptive, deepening caldera depression, in which very thick intra-caldera ignimbrites pond. Outside the caldera potentially far flowing pyroclastic flows deposit much thinner extra-caldera ignimbrites. Both the intra-caldera and extra-caldera ignimbrites range from non-welded to welded in character (Branney and Kokelaar, 2002). Sometimes, welded ignimbrites may still be hot and plastic enough when deposited that they can flow secondarily as lavas, and are called rheomorphic ignimbrites. Rheomorphic ignimbrites are the high-temperature, low-viscosity end-members of the spectrum of ignimbrites, and may preserve characteristics that are hybrid between welded ignimbrites and lava flows (Branney and Kokelaar, 1992).

In modern environments, usually only the extra-caldera ignimbrites are exposed, whereas in older settings, much of these may be eroded and erosional incision has exposed the intra-caldera successions. It is therefore usually only in such older settings that the geology of intra-caldera successions and the nature of caldera filling processes can be determined. However, there are relatively few detailed studies of intra-caldera

ignimbrite successions and how they formed (e.g., Willcock *et al*., 2013).

In this study, detailed volcanic facies analysis is used alongside geological mapping and petrography to investigate the palaeoenvironmental setting, eruption style and emplacement processes involved in the formation of the extremely thick (>500 m thick) intra-caldera rheomorphic 1071 ± 5 Ma Kathleen Ignimbrite (Formation), exposed in the west Musgrave region of central Australia. With nearly continuous exposure this study affords an opportunity to contribute further to understanding caldera forming and infilling processes, and presents a unique opportunity to assess the role of ignimbrite rheomorphism in intra-caldera settings, which has rarely been addressed.

2.2 Regional geological setting and previous work

2.2.1 The Musgrave Region and west Musgrave Province

The 1.60–1.15 Ga Musgrave Province (Fig; 1a) of central Australia is an 800 km long and 350 km wide, ESE–WSW-trending belt of high-grade amphibolite to granulite facies metamorphic rocks, which is bound by Neoproterozoic to Mesozoic sedimentary basins and lies at the convergence of the Proterozoic amalgamation of the North, West and South Australian Cratons, all of which played a significant role in the magmatism of the area (Fig. 2.1b; Daniels, 1974; Wade *et al*., 2008; Smithies *et al*., 2009; 2011; 2014; Howard *et al*., 2011). In the western half of the province, in the state of Western Australia, the high grade metamorphic rocks are overlain by widespread rhyolitic and basaltic volcanic rocks and variably deformed and lower grade metamorphosed sedimentary rocks that are intruded by granitic plutons, mafic-ultramafic layered and massive intrusions, and numerous mafic and felsic dykes (Daniels, 1974; Smithies *et al*., 2009; 2010; Evins *et al*., 2010; Kirkland *et al*. 2013).

Although the Musgrave region (i.e. Musgrave Province and younger successions/ events) has a long tectonic history, this paper focuses on part of the rock succession produced during the 1085–1040 Ma Giles Event (Wade *et al*., 2008; Smithies *et al*., 2009; 2010; 2011 Howard *et al*., 2011) that resulted in a long-lived, failed intra-continental rift, known as the Ngaanyatjarra Rift (Evins *et al*., 2010). All the volcanic and sedimentary components associated with this rift were deposited in the Bentley Basin and are assigned to the Bentley Supergoup (Daniels, 1974; Howard *et al*., 2011). The volume of contemporaneous felsic igneous rocks associated with this event (~22 000 km^3), is consistent with this being the silicic component of a likely large igneous province that occurred within the west Musgrave Province; of which the already recognised Warakurna Large Igneous Province (LIP) is a short-lived, but voluminous part thereof (Fig. 2.1b; Wingate *et al*., 2004; Morris and Pirajno, 2005; Howard *et al*., 2011; Smithies *et al*., 2013; 2014).

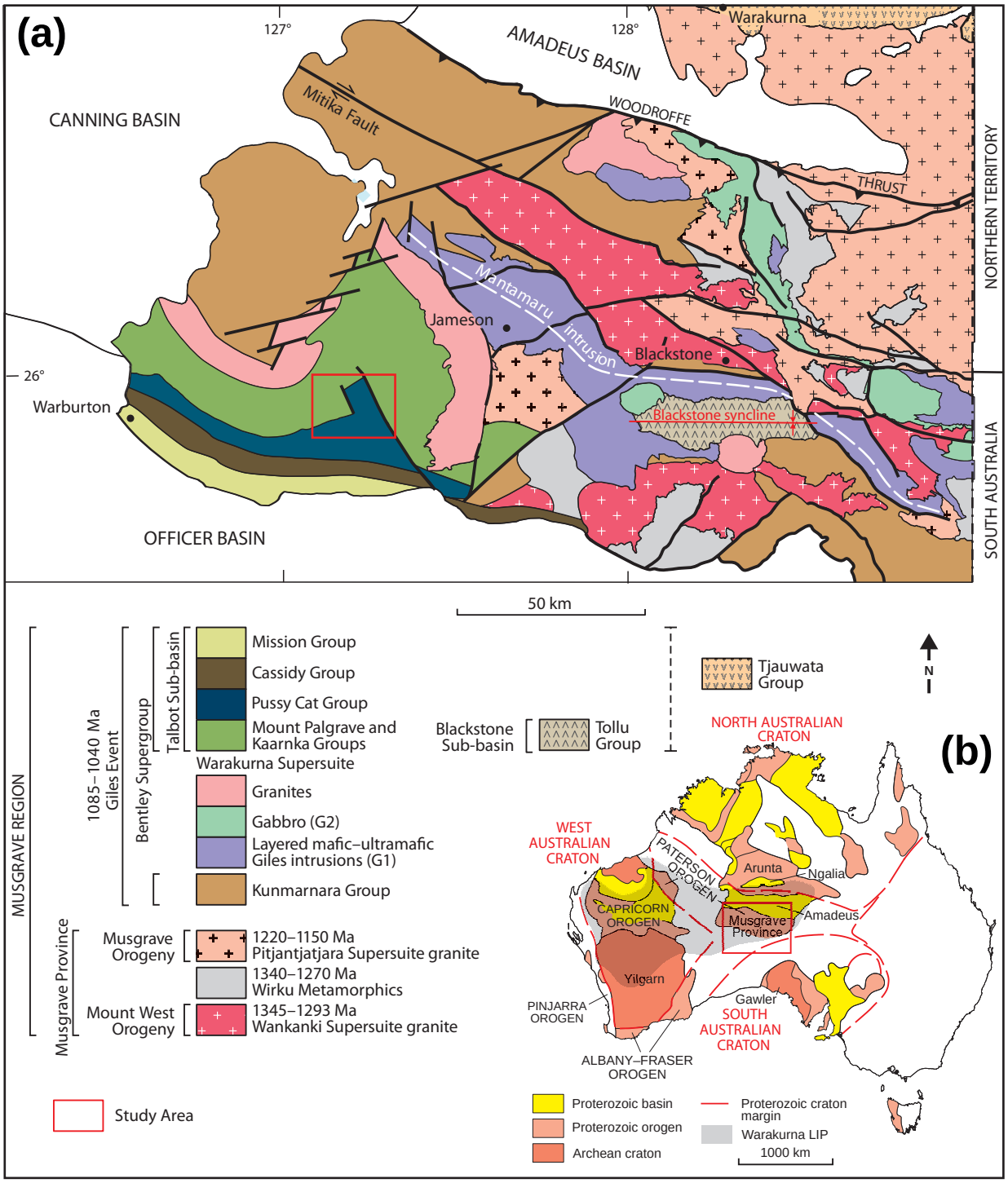

Figure 2.1: a) Location of the west Musgrave Province and surrounding regional geology (adapted from Glikson *et al*., 1996; Edgoose *et al*., 2004; Howard *et al*., 2011; Smithies *et al*., 2013). b) Location of the Musgrave Province in terms of the tectonic framework of Proterozoic Australia, and the extent of the Warakurna LIP (adapted from Myers *et al*., 1996; Smithies *et al*., 2013). Location of study area highlighted in red, and expanded on in Fig. 2.2.

The Talbot Sub-basin of the 1085–1040 Ma Bentley Supergroup, formed during a failed intra-plate extensional rifting event, much like the present-day East African Rift. It is similar to the bimodal, rhyolite-dominated Snake River Plain of southern Idaho and northern Nevada, USA, in that it contains thick rhyolitic lava and ignimbrite sheets (e.g., Branney *et al*., 2006; 2008; Ellis *et al*., 2013). Many of the thick, large volume rhyolitic volcanic units found in this basin have been interpreted as ignimbrites (Howard *et al*.,

2011; Werner *et al*., 2012; Smithies *et al*., 2013) with Daniels (1974) mapping one of these units, the Kathleen Ignimbrite (Formation) of the Pussy Cat Group, as a possible 'rheoignimbrite' and interpreting it as a simple single unit.

2.2.2 The Bentley Basin, Talbot Sub-basin and Pussy Cat Group stratigraphy

The Bentley Basin formed between 1085 and 1040 Ma as part of the Ngaanyatjarra Rift (Evins *et al*., 2010; Smithies *et al*., 2013). The Talbot Sub-basin (Fig. 2.2; Table 2.1) is one of several sub-basins within the Bentley Basin and consists of the basal Mount Palgrave Group of effusive rhyolite lavas and ignimbrites, which is overlain by the rhyolitic ignimbrite-dominated Kaarnka Group, the southward dipping and younging bimodal and volcano-sedimentary Pussy Cat and Cassidy groups, and the uppermost basaltic and sedimentary Mission Group (Daniels, 1974; Howard *et al*., 2011; Smithies *et al*., 2013).

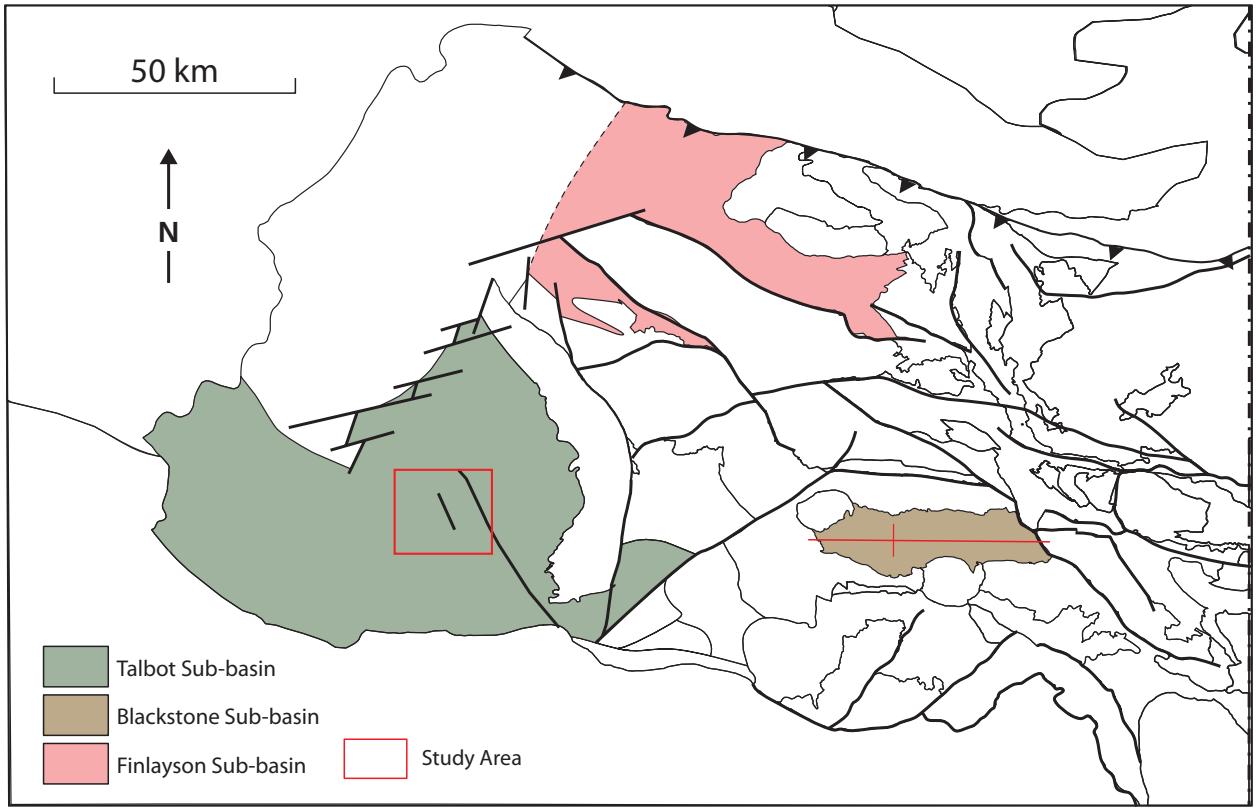

Figure 2.2: Location of the Talbot Sub-basin and other sub-basins of the Bentley Supergroup (adapted from Smithies et al., 2013).

A part of the Pussy Cat Group (PCG), outcropping in the Whitby Range, is the focus of this study. The Whitby Range can be structurally subdivided into five main domains by dominant NNW-SSE striking faults (Fig. 2.3); a fairly deformed and sheared western section (A), a low-relief middle section (B), a well-preserved and relatively undeformed eastern section (C) which is where most of the observations come from, a fault-offset northeast section (D), and an unconfirmed faulted and displaced southeast section (E). The group outcrops across the central-southern part of the Talbot Sub-basin

Table 2.1: Summarised stratigraphy of the Talbot Sub-basin (adapted from Daniels, 1974, Howard *et al*., 2011, Smithies *et al*., 2013).

<table>
<tr><th>Age</th><th>Events</th><th colspan="7">Stratigraphy</th></tr>
<tr><td>550 Ma</td><td>Petermann Orogeny</td><td colspan="7"></td></tr>
<tr><td rowspan="4">1085–1040 Ma</td><td rowspan="4">Giles Event and Ngaanyatjarra Rift</td><td rowspan="3">Bentley Supergroup</td><td rowspan="3">Talbot Sub-basin</td><td colspan="5">Mission Group</td></tr>
<tr><td colspan="5">Cassidy Group</td></tr>
<tr><td rowspan="2">Kaarnka Group</td><td rowspan="2">Pussy Cat Group</td><td colspan="2">Glyde Formation</td><td rowspan="2">Rowland Suite</td></tr>
<tr><td rowspan="2">Kathleen Ignimbrite (Formation)</td><td>Kilykilykarri Member</td></tr>
<tr><td>Karlaya Member</td><td>Kurrparu Member</td></tr>
<tr><td></td><td></td><td></td><td colspan="2">Cleghorne Formation</td><td></td></tr>
<tr><td></td><td></td><td></td><td colspan="4">Mount Palgrave Group</td></tr>
<tr><td></td><td></td><td>Warakurna Supersuite</td><td colspan="5">Giles Complex – layered mafic-ultramafic intrusions and Alcurra Dolerite (Suite)</td></tr>
<tr><td>1220–1150 Ma</td><td>Musgrave Orogeny</td><td colspan="7"></td></tr>
</table>

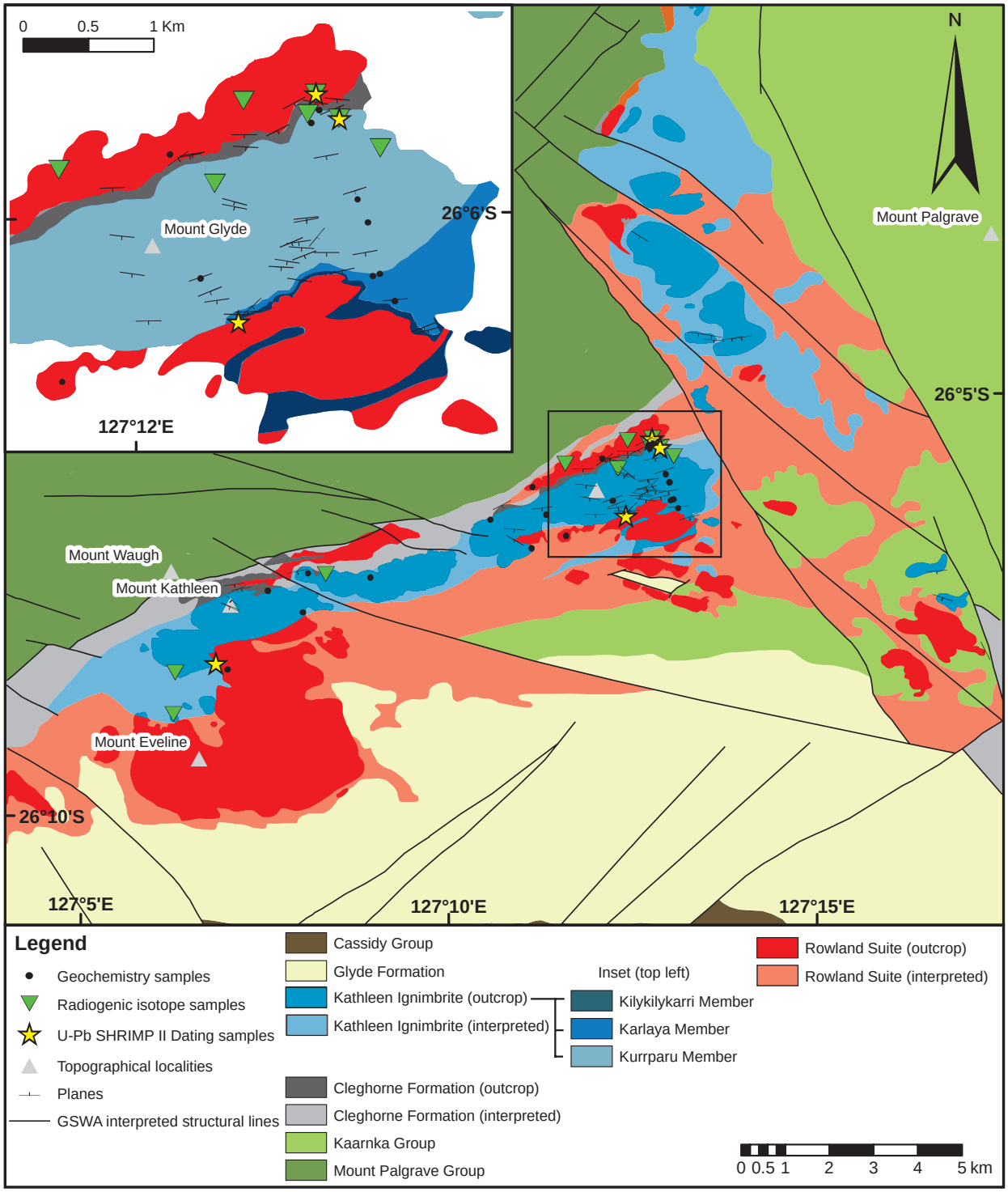

Figure 2.3: Geological map of the study area. Dark colours indicate exposures, whereas lighter shades of the same colour indicates interpreted bedrock. Geochemical sample locations are indicated by yellow stars. Structural sections A, B, C, D and E are indicated on the map (adapted from Werner *et al*., 2012).

and detailed descriptions of the all the stratigraphic units can be found in Howard *et al*. (2011). Our study area (red box – Figs. 2.1a and 2.3) consists of a previously unnamed basal, volcaniclastic-sedimentary formation forming the base of the PCG, here named the Cleghorne Formation (CF), which is underlain by the Mount Palgrave Group, overlain by the felsic volcanic Kathleen Ignimbrite (KI) and, higher up, by the mafic volcano-sedimentary Glyde Formation (Fig. 2.3). A suite of sub-volcanic porphyritic rhyolites,

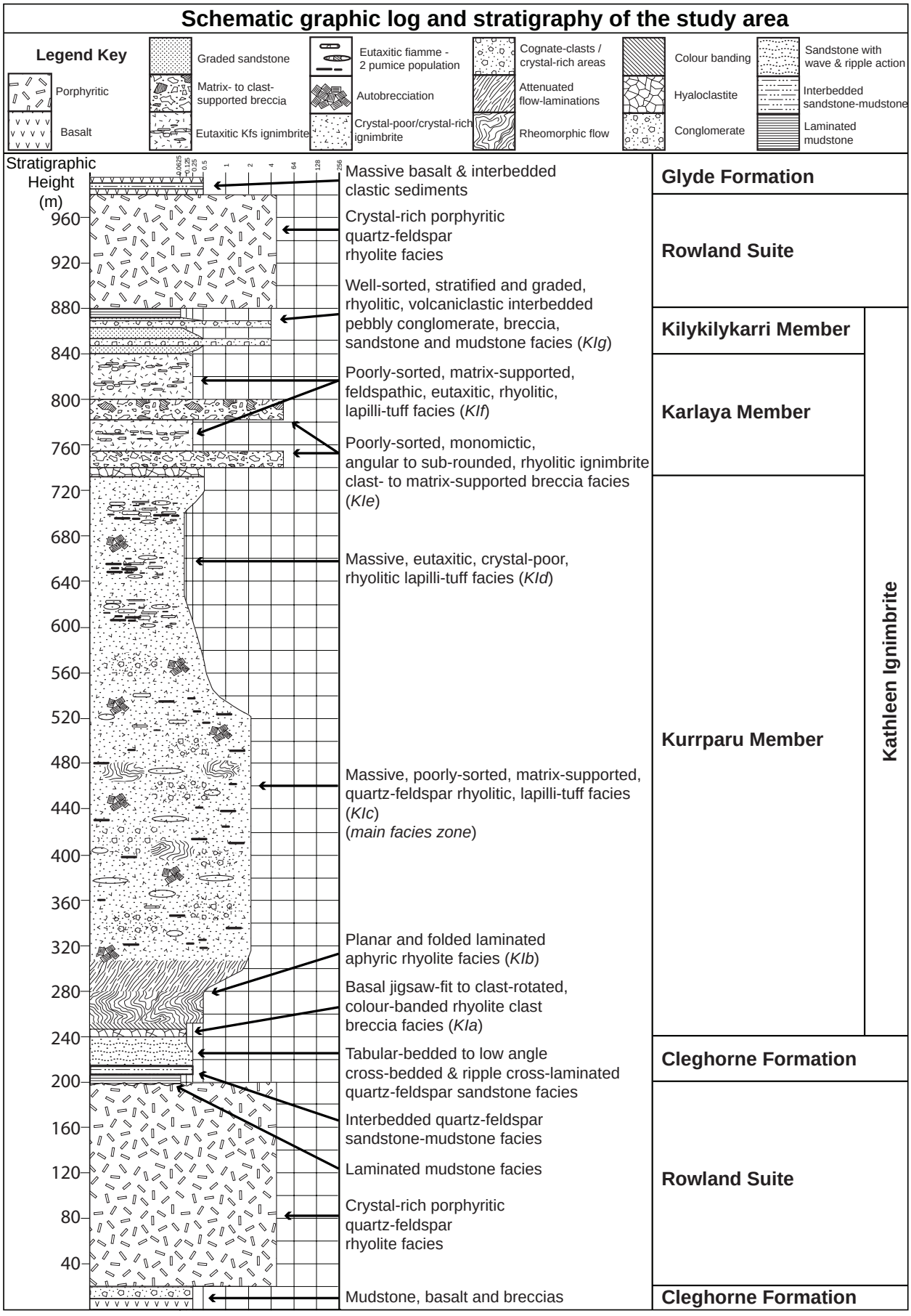

Figure 2.4: Schematic graphic log of the stratigraphy in the study area. Observations predominantly from the eastern section (C; Fig. 2.2), as this section offers the best exposure, least deformation, and most continuous outcrop. This log is representative of the whole formation, with similar facies and textures were observed in the other sections. The true vertical thickness is plotted on the left hand column, calculated using an average dip for the entire succession of 25°.

here named the Rowland Suite (RS), form voluminous intrusions within the volcano-sedimentary succession of the lower PCG (Fig. 2.3). In the study area the package dips at 20°–30° to the south-southeast and outcrops over a minimum strike length of ~22 km before being covered by Quaternary sands. Fig. 2.4 shows the detailed stratigraphy of the study area as a composite graphic log. The KI has a maximum preserved stratigraphic thickness of ~650 m, while the accumulated thickness of the CF is in the order of ~100 m. Stratiform rhyolites of the RS, underlying the KI, reach a maximum thickness of ~250 m.

The upper CF consists of a basal laminated mudstone facies, an interbedded quartz-feldspar sandstone-mudstone facies and a tabular-bedded to low-angle cross-bedded and ripple cross-laminated quartz-feldspar sandstone facies. The KI consists of the basal Kurrparu, intermediate Karlaya and upper Kilykilykarri members. These members are made up of various facies, which are described in detail below.

2.3 Facies descriptions and interpretations

Detailed mapping and sampling at regularly spaced intervals during traverses over the ~1 km thick volcano-sedimentary succession helped define the various lithofacies of the sequence (Fig. 2.4; Table 2.2). Here, each of the lithofacies units are described, from the lowermost CF sedimentary succession, to the uppermost Kilykilykarri Member of the KI.

2.3.1 Facies of the Cleghorne Formation (CF)

Only the upper portion of the sedimentary-volcanic CF will be considered and used to determine the palaeoenvironmental setting as its stratigraphic context is well constrained in our study area. The lower portion of the CF constitutes a basal succession of mud-rich breccias, conglomerates, pebbly sandstones, and intercalated mudstones, overlain by an interval of extrusive basaltic lavas. These basalts are in turn overlain by an upward fining succession of mud-dominated sedimentary rocks leading into the upper CF. The upper portion of the CF, described below, is dominated by an association of three sedimentary lithofacies that are variously cut by intrusive rhyolites of the RS.

Description of facies association:

2.3.1.1 Laminated mudstone facies

A very fine-grained, grey, laminated, mudstone interval with planar to wavy, contorted laminations (Fig. 2.5a) reaches a thickness of 10–20 m, with a lateral exposed extent of ~200 m and forms the ‘basal unit’ for the CF in the main study area (C, Fig. 2.3). Locally this facies contact with the RS is irregular and discordant, with these laminations

Table 2.2: Stratigraphy of the Pussy Cat Group, indicating relationships between the Cleghorne Formation (CF), Rowland Suite (RS), and Kathleen Ignimbrite (KI), as well as their respective sub-members (adapted from Daniels, 1974, Howard *et al*., 2011, Smithies *et al*., 2013).

Pussy Cat Group (PCG)			
Formations	**Lithofacies Associations and lithofacies**		**Age**
Glyde Formation	Massive basalt interbedded with clastic sediments		
Rowland suite (RS)	Crystal-rich, porphyritic, quartz-feldspar rhyolite facies		Sample 195058 1076 ± 5 Sample 195031 1078 ± 5 Ma
Kathleen Ignimbrite (Formation) (KI)	Kilykilykarri Member	Well-sorted, stratified and graded, rhyolitic, volcaniclastic, interbedded pebbly conglomerate, breccia, sandstone and mudstone facies (*Klg*)	
	Karlaya Member	Poorly-sorted, matrix-supported, feldspathic, eutaxitic, rhyolitic lapilli-tuff facies (*Klf*)	
		Poorly-sorted, monomictic, angular to sub-rounded, rhyolitic ignimbrite clast- to matrix-supported breccia facies (*Kle*)	
	Kurrparu Member	Massive, eutaxitic, crystal-poor, rhyolitic lapilli-tuff facies (*Kld*)	
		Massive, poorly-sorted, matrix-supported, quartz-feldspar, rhyolitic lapilli-tuff facies (*main facies zone/Klc*)	Sample 195723 1071 ± 5 Ma
		Planar and folded laminated aphyric rhyolite facies (*Klb*)	
		Basal jigsaw-fit to clast-rotated, colour-banded, rhyolite clast breccia facies (*Kla*)	
Upper Cleghorne Formation (CF)	Tabular-bedded to low-angle cross-bedded and ripple cross-laminated quartz-feldspar sandstone facies		
	Interbedded quartz-feldspar sandstone-mudstone facies		
	Laminated mudstone facies		
Rowland Suite (RS)	Crystal-rich, porphyritic, quartz-feldspar rhyolite facies		Sample 195001 1062 ± 8 Ma
Lower Cleghorne Formation	Breccias, mudstones and basalt		

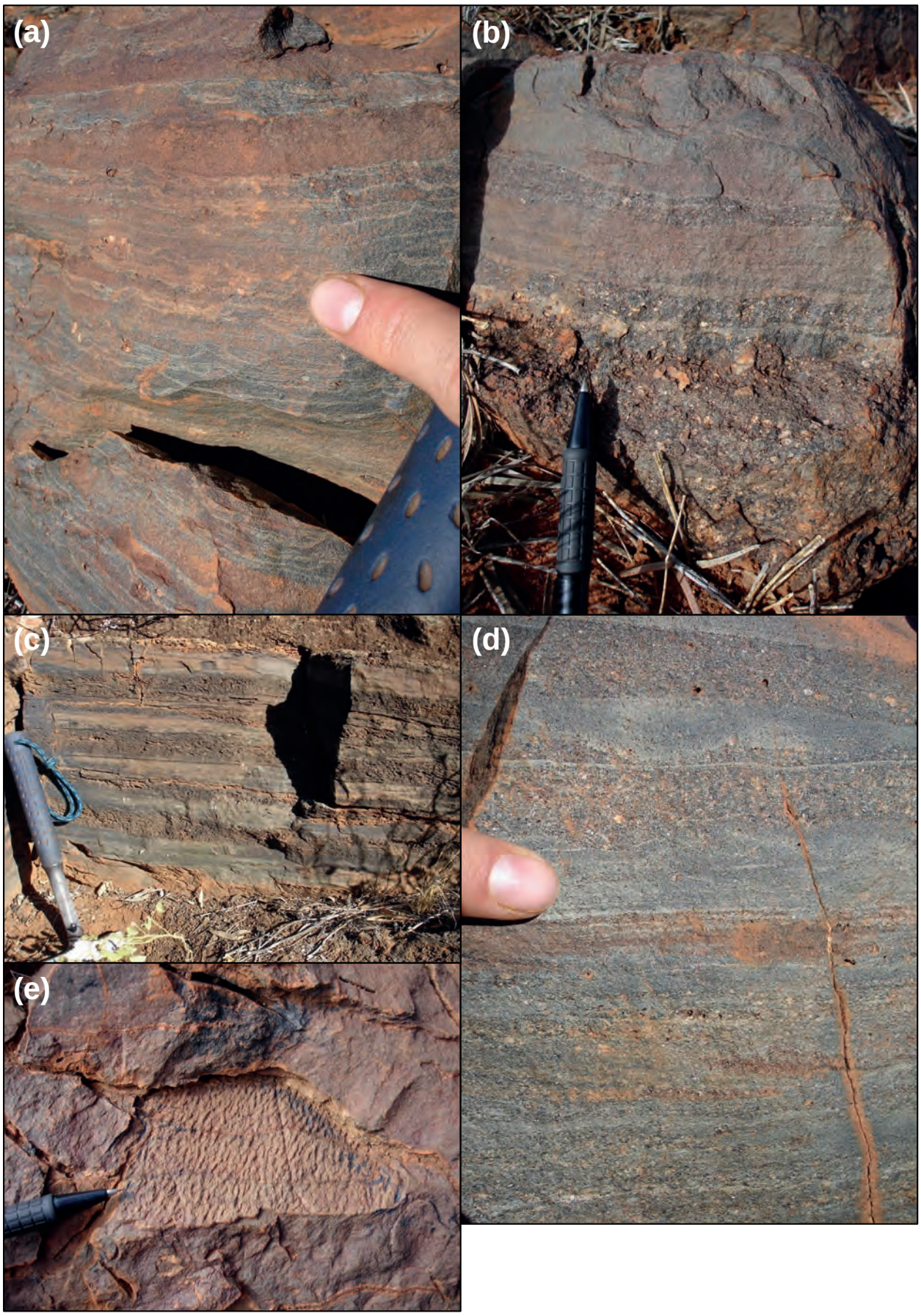

Figure 2.5: Upper Cleghorne Formation. a) Laminated mudstone facies with thin, planar to wavy, contorted laminations (ripple marks or dish structures?) in the Cleghorne Formation. b) The interbedded quartz-feldspar sandstone-mudstone facies (top half) showing an irregular contact with the porphyritic rhyolite Rowland Suite intrusion (bottom half). c) Interbedded quartz-feldspar sandstone-mudstone facies that is diffusely planar bedded. d) Sandstone beds exhibit grading and downward scouring into the laminated mudstone horizons. e) Symmetrical small wave ripples on a bedding plane.

appearing disturbed by porphyritic rhyolite apophyses, as described below (*Section 2.3.2*).

2.3.1.2 Interbedded quartz-feldspar sandstone-mudstone facies

Overlying the *laminated mudstone facies* is a graded-bedded, upward-fining succession that outcrops in both the eastern and western sections of the study area and in places has an irregular contact with the intrusive RS (Fig. 2.5b) that varies from highly irregular (fluidal), to local mixed clast breccias, to sharp. This facies consists of dark-brown, interbedded sandstones and laminated mudstones that are diffusely planar bedded (Fig. 2.5c), and contain large (up to 3 mm) volcanic quartz and feldspar crystal fragments. Individual sandstone beds are up to 10 cm thick and laminated mudstones are up to 3 cm thick, with the whole interval attaining a thickness of approximately 10 m. The sandstone beds are graded, and both the sandstones and mudstones contain scour structures (Fig. 2.5d). Small, symmetrical ripples are also present in this facies (Fig. 2.5e).

2.3.1.3 Tabular-bedded to low angle cross-bedded and ripple cross-laminated quartz-feldspar sandstone facies

Above the *interbedded quartz-feldspar sandstone-mudstone facies* is a thick (~50 m) dark-brown, well-sorted, graded and upward fining bedded sandstone facies (Fig. 2.6) that has an along strike extent of 22 km. It is the dominant uppermost facies within the upper CF. The basal section of the facies is characterised by thick (~30–40 m) tabular massive sandstone beds (Fig. 2.6a) that transition upwards into thinner low angle cross-bedded to planar-bedded sandstones (Fig. 2.6b) that are less than 10 m thick and contain individual beds less than 1 cm thick. These sandstones contain low-angle planar cross-bedding (Fig. 2.6c) and long (Fig. 2.6d) to short (Fig. 2.6e) wavelength (1.5 to 0.7 m amplitude) upward convex and concave stratification, as well as symmetrical ripple mark horizons. Slumping or soft sediment deformation and fluid-escape features (Fig. 2.6f; convolute bedding) are also present in the basal thicker sandstone beds. The sediments are volcanogenic and contain a visually estimated ~30% volcanic quartz and ~30% feldspar modal abundance.

Interpretation of facies association:

The facies that make up this association represent a volcaniclastic sedimentary succession that contains primary felsic volcanic clastic components. The lowermost *laminated mudstone facies* was deposited in a sub-wave base, low energy, suspension settling dominated environment, resulting from hemi-pelagic suspension sedimentation of clay and silt particles (Henrich and Huneke, 2011). The graded beds within the *tabular-bedded to low-angle cross-bedded and ripple cross-laminated quartz-feldspar sandstone facies* and the *interbedded quartz-feldspar sandstone-mudstone facies* are typical

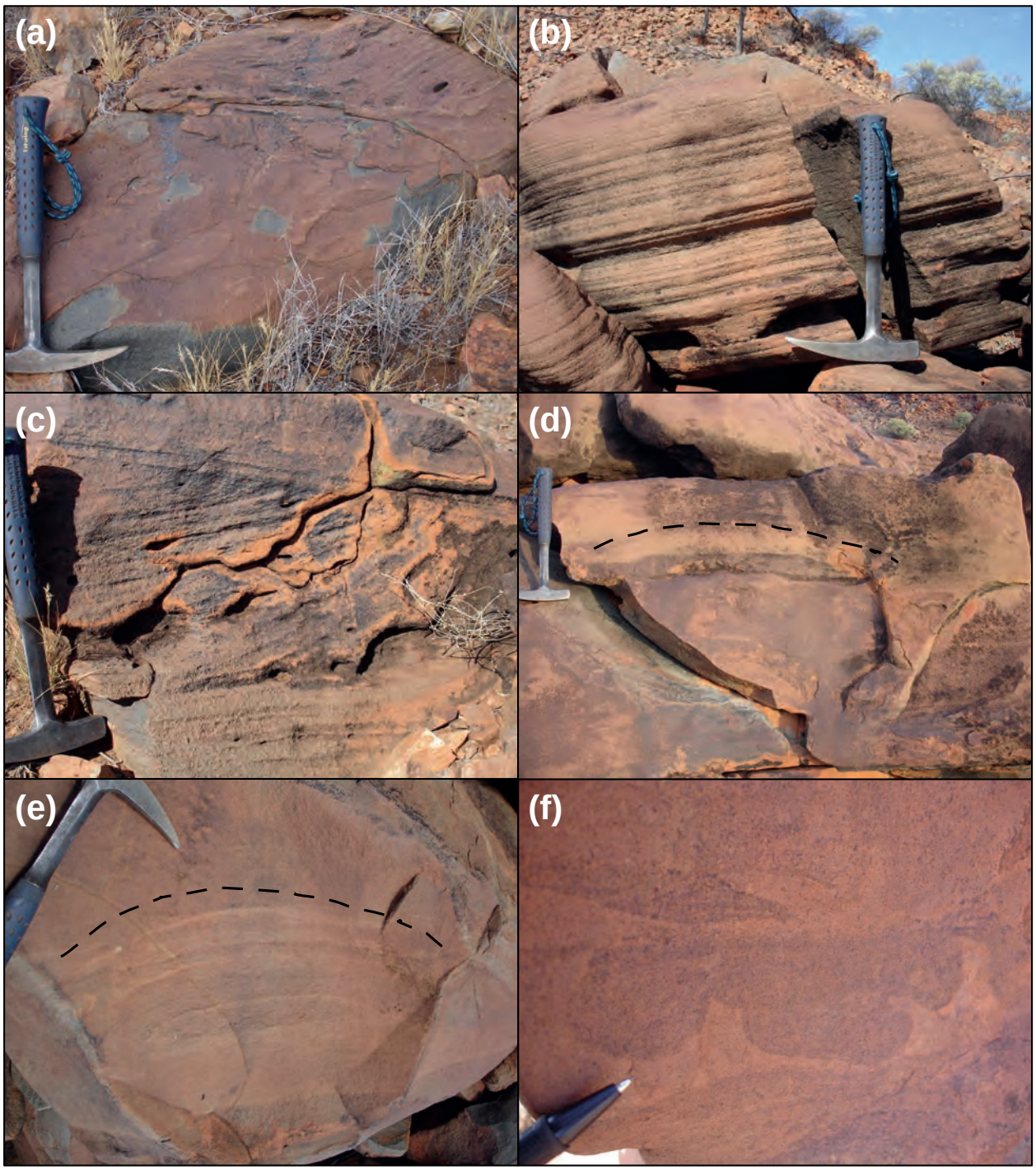

Figure 2.6: Upper Cleghorne Formation - tabular-bedded to low-angle cross-bedded and ripple cross-laminated quartz-feldspar sandstone facies. a) Tabular cross-bedding (top) above a planar erosional contact overlying a thick, fairly structureless and massive sandstone bed (bottom). b) Tabular bedding at the top of the facies. c) Low-angle planar cross-stratification below the upper tabular beds. Hummocky cross-stratification, both longer (~1.5 m; d) and shorter (~70 cm; e) wavelengths. f) Load-cast structures indicating dewatering of the thicker basal sandstone beds.

normally-graded, upward-fining Bouma sequences (Bouma, 1962; Shanmugam, 1997) that are indicative of deposition by high-density turbidity currents (Lowe, 1982; Boggs, 1987; Nichols, 2009). This indicates that the 30–50 m thick sequence containing both of these facies represents a series of cyclical turbidite beds, deposited at water depths below the fair weather wave-base and were not reworked by waves, tides, or longshore currents (Fritz and Howells, 1991). The tabular-bedded sandstones represent upper flow-regime

conditions characteristic of wave swash in shallow foreshore water depths (Clifton, 1988; Fritz *et al*., 1990; Fritz and Howells, 1991). Alternatively, the tabular-bedded sandstones represent part of a tempestite deposit caused by storm processes again within a shallow-water setting (Aigner, 1985).

The low angle cross-bedding seen in the *tabular-bedded to low angle cross-bedded and ripple cross-laminated quartz-feldspar sandstone facies* is interpreted as hummocky and swaley cross-bedding that was produced by storm-wave base reworking of off-shore turbidity current deposits (Harms *et al*., 1975; Leckie and Walker, 1982; Dumas and Arnott, 2006). The presence of hummocky and swaley cross-stratification in the *tabular-bedded to low angle cross-bedded and ripple cross-laminated quartz-feldspar sandstone facies* is indicative of shallow-marine conditions (Harms *et al*., 1975; Leckie and Walker, 1982; Dumas and Arnott, 2006), and more specifically deposition in the offshore transition zone of a storm-affected shelf between fair-weather and storm-wave bases, where sands are resedimented by storm wave action to form very characteristic bed-forms and structures (Dott and Bourgeois, 1982; Leckie and Walker, 1982; Duke, 1985; Dumas and Arnott, 2006; Nichols, 2009). Storm conditions can affect sedimentation at tens of meters of water depth, indicating that these structures are characteristic of shallow-water sandy shelf conditions found just above the storm wave base, although the presence of preserved swales suggests these formed in shallower waters (Dumas and Arnott, 2006; Nichols, 2009). In the absence of clear Proterozoic fossils, it is unclear whether it was a shallow-marine or shallow-lacustrine environment, but the magnitude of the hummocky cross stratification suggests a large fetch distance for storm waves and therefore a very large body of water.

The symmetrical ripples represent either waning storm wave generated small hummocky bed-forms, or fair-weather, shallow-water, wave-generated symmetrical ripples. The secondary depositional structures such as the convolute bedding or soft sediment deformational features within the *tabular-bedded to low angle cross-bedded and ripple cross-laminated quartz-feldspar sandstone facies* are indicative of rapid sedimentation and instability with localised small-scale liquefaction (dewatering) of recently deposited material, most probably caused by mass flow deposition on a slope or by the induction of shear stress by a flow of overlying fluid above the sediment (Boggs, 1987; Nichols, 2009).

The depositional basin appears to have shallowed from deeper water, low-energy regime mudstones to shallow-water, high-energy event sandstones, with a further restriction to water depths at or above the storm wave base indicated by the presence of hummocky cross-stratification with maximum water depths up to 50 m (Bourgeois, 1980; Hunter and Clifton, 1982), but most likely between 13 and 50 m (Dumas and Arnott, 2006). Additionally the upper flow-regime tabular-bedded sandstones are characteristic

of wave swash in shallow foreshore water depths. These changes are indicative of a proximal offshore to lower shoreface to lower foreshore transitional environment (Howard and Reineck, 1981). This indicates that the CF was deposited in a shallow sub-tidal palaeoenvironment affected by periodic storm events, similar to the depositional environment of the Lower Rhyolitic Tuff Formation and the Garth Tuff of north Wales, UK (Howells *et al*., 1986; Fritz and Howells, 1991).

2.3.2 Rowland Suite (RS)

2.3.2.1 Crystal-rich porphyritic quartz-feldspar rhyolite facies

Figure 2.7: Rowland Suite. a) Crystal-rich porphyritic rhyolite texture of the Rowland Suite. b) Clastic dyke intrusion (dark fine-grained material) of Cleghorne Formation sediment into the Rowland Suite rhyolite along the contact margin. c) Upper contact of Rowland Suite with the Cleghorne Formation, showing intermingling relationship with an apophysis of rhyolite (left) intruding into the dark matrix of sediment, disturbing bedding (right). d) Blocky and fluidal peperite textures on the contact. e) Photomicrograph of the microscopic groundmass texture of the Rowland Suite (XPL).

Description:

Interleaved with the sediments of the upper CF and sitting below the volcanic succession of the KI (Formation), there is an up to ~250 m thick, coherent, massive, homogenous, grey, medium-grained, crystal-rich (~40 vol. %), porphyritic quartz-feldspar rhyolite facies that thins to the west (Fig. 2.7a). This facies outcrops along almost the entire strike length of the KI and occurs as a laterally semi-continuous, fairly stratiform unit within the upper CF. The upper contact of this facies with, interbedded sandstones and mudstones of the CF, is highly irregular, with intermingling of sediment and porphyritic rhyolite indicated by mm-to-cm scale apophyses and rhyolite clast breccia with a sedimentary matrix. The apophyses have both irregular and planar margins with fine-grained, dark coloured, matrix-supported sediment with dispersed larger quartz and feldspar crystal fragments (Fig. 2.7b). Coarse-grained porphyritic rhyolite appears to have squeezed and deformed finer-grained, layered sedimentary horizons as suggested by soft-state deformation features in the sediment at the contact in places (Fig. 2.7c). Clusters of rhyolite clasts with jigsaw-fit textures are also present and are entirely surrounded by sedimentary material; these clasts have either planar to curviplanar edges or wispy and necked margins (Fig. 2.7d). There are slight crystal size variations on the contact of this facies and the contact is not strictly stratiform with the overlying sedimentary succession but cross-cuts the various facies described above. The lower contact does not crop out, but sedimentary strata underlie the rhyolite regionally.

Primary igneous minerals in the rhyolite (Fig. 2.7e) ~25% K-feldspar (comprising microperthite and microcline), ~10% plagioclase, ~35% quartz ~10% biotite and ~10% Fe–Ti oxides. The secondary minerals constitute ~5% muscovite and ~3% carbonate. The K-feldspar and plagioclase phenocrysts are pink and white respectively, euhedral to subhedral and <13 mm in size. The quartz phenocrysts are rounded to subhedral, frequently embayed, plutonic in shape and <9 mm in size. These phenocrysts are set in a coherent, microcrystalline and microgranular intergrown quartz-feldspar mosaic groundmass with an almost granoblastic texture. The groundmass contains ~5% primary accessory minerals, which include fluorite, zircon, titanite and apatite. Glomerocrysts of biotite, titanite and Fe–Ti oxides occur in the groundmass.

Interpretation:

The upper contact is interpreted to represent intrusive inter-fingering of the porphyritic rhyolite into the overlying CF sediments while they were still weakly consolidated and water-saturated (Fig. 2.7c). In-situ, blocky, rhyolite breccia with jigsaw-fit blocky to fluidal clast shapes, is suggestive of autoclastic brecciation of the porphyritic rhyolite. This most probably occurred as a result of interaction between wet, weakly consolidated sediments and a hot rhyolitic magma, causing instantaneous cooling of the magma by pore waters in the sediment and in-situ quench fragmentation through cooling, contraction, and

granulation that produced a jigsaw-fit hyaloclastite breccia (Pichler, 1965; Kokelaar, 1982; Cas, 1992) at the margins of the magmatic body. The intense heating and convection of interstitial pore water within the sediment by the rhyolite, caused fluidisation of the wet sediments, and injection of a slurry of watery sediment into the cracks between hyaloclasts and mixing of the two forming blocky to fluidal peperite (Rittmann, 1962; Pichler, 1965; Schmincke, 1967; Kokelaar, 1982; Busby-Spera and White, 1987; Cas *et al*., 1990; Skilling *et al*., 2002).

The contact relationships discussed above combined with the geometry of the unit and the homogenous, coherent to marginal brecciated texture of the facies indicates that the RS is a sub-volcanic high-level syn-depositional sill that intruded into the upper CF sediments whilst they were still wet and weakly consolidated. The granoblastic groundmass texture is due to devitrification and recrystallisation of the original primary glass.

2.3.3 Kathleen Ignimbrite (KI)

The KI (Formation) contains seven volcanic lithofacies that have a total preserved thickness of ≤650 m; this volcanic succession forms a prominent topographic feature known as the Whitby Range, with the two most distinctive topographic features named Mount Kathleen (in the west; A; Fig. 2.3) and Mount Glyde (in the east; C; Fig. 2.3).

The seven volcanic lithofacies are (from bottom to top):

a. Basal jigsaw-fit to clast-rotated, colour-banded, rhyolite clast breccia (*KIa*);
b. Planar and folded laminated aphyric rhyolite facies (*KIb*);
c. Massive, poorly-sorted, matrix-supported, quartz-feldspar rhyolitic, lapilli-tuff facies (*main facies* zone/*KIc*);
d. Massive, eutaxitic, crystal-poor, rhyolitic lapilli-tuff facies (*KId*);
e. Poorly-sorted, monomictic, angular to sub-rounded, rhyolitic ignimbrite clast- to matrix-supported breccia facies (*KIe*);
f. Poorly-sorted, matrix-supported, feldspathic, eutaxitic, rhyolitic lapilli-tuff facies (*KIf*);
g. Well-sorted, stratified and graded, rhyolitic, volcaniclastic, interbedded pebbly conglomerate, breccia, sandstone and mudstone facies (*KIg*).

These lithofacies are grouped into three separate stratigraphic subdivisions from bottom to top (see Fig. 2.4; Table 2.2):

i. The Kurrparu Member, containing four facies (a–d) that formed during a single significant depositional and volcanic event of sustained duration.
ii. The Karlaya Member (e–f), containing two repeating facies (e) that mark a change in depositional conditions from the Kurrparu Member and reflect a reoccurring series of

similar volcanic events.

iii. The Kilykilykarri Member, containing one distinct facies (g) that is markedly different to the underlying Kurrparu and Karlaya members.

2.3.3.1 The Kurrparu Member

2.3.3.1.1 Massive, poorly-sorted, matrix-supported, quartz-feldspar rhyolitic, lapilli-tuff facies (*KIc*)

Description:

The Kurrparu Member is dominated by an up to 350 m thick, *massive, poorly-sorted, matrix-supported, quartz-feldspar rhyolitic, lapilli-tuff facies (KIc*) that is hereafter referred to as the *main facies zone* of the Kurrparu Member. This facies is grey to blue-grey coloured, contains fine-grained, black micaceous lithic clasts, most likely of sedimentary origin, and coarse-grained, crystal-rich, phaneritic quartz-feldspar dominated clasts (Fig. 2.8a) that vary from spheroidal (10–25 cm in size) to distinctly flattened, irregular and fiamme-like (up to 30 cm in length; Fig. 2.8b), containing bi-pyramidal, resorbed volcanic quartz and euhedral to subhedral K-feldspar and plagioclase phenocrysts (Fig. 2.8c). In some cases these clasts, appear to be attenuated, much like fiamme, and have irregular edges that are associated with quartz and feldspar crystal, similar in morphology trails that lead away from clast edges (Fig. 2.8d). Some aphyric fiamme-like clasts also occur in this facies, which are thin, highly irregular and wispy shaped, but they are not abundant. A crude alignment of both clast-types defines a planar fabric in the otherwise massive deposit that is consistent with the dip of the package. In contrast to these aligned clasts, isolated and discrete clast-rotated breccia zones are also present, but are not laterally continuous. The blocky brecciated clasts (~5 cm) within these zones preserve evidence of rotational movement indicated by randomly oriented laminated lapilli-tuff clasts (Fig. 2.8f).

The poorly-sorted, matrix-supported texture (Fig. 2.8d) that characterises this facies is defined by the phaneritic clasts dispersed in a fine matrix of crystal fragments and finer original vitric ash matrix, a heterogeneous distribution of quartz and feldspar macrocrysts into crystal-poor areas (<5 vol.% macrocrysts), and irregular patches, discontinuous layers, or lenses with high concentrations of quartz and feldspar (up to 50 vol.%) that have faint boundaries, defined by slight grain-size variations and colour contrasts to the surrounding crystal-poor matrix (Fig. 2.8c).

Crystals and crystal fragments constitute up to 40% in the matrix of this facies, consisting of ~30% volcanic quartz, ~25% mesoperthitic K-feldspar, ~20% plagioclase, ~10% biotite and ~5% oxides, occurring as primary igneous constituents, together with ~5%

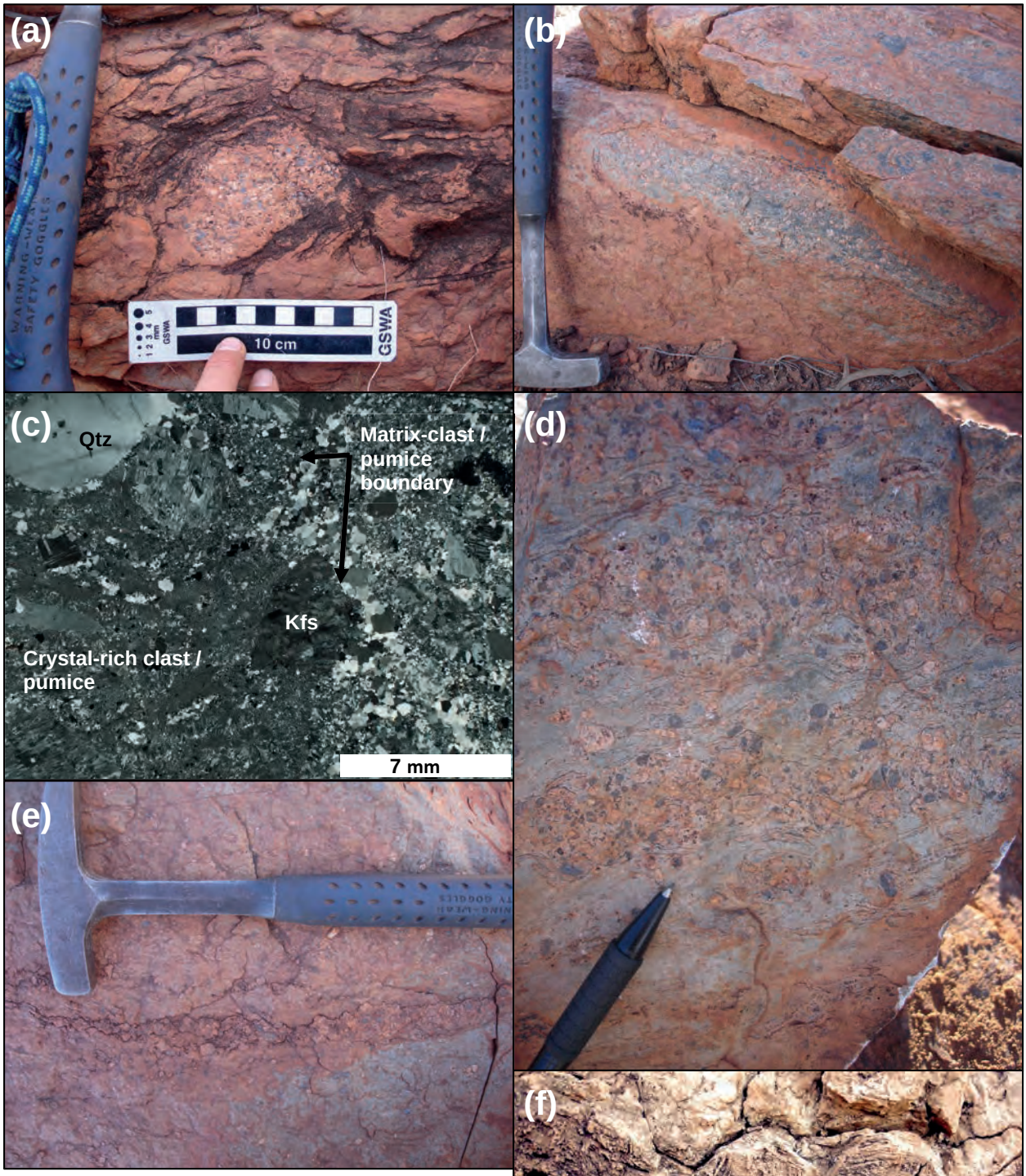

Figure 2.8: Kurrparu Member - massive, poorly-sorted, matrix-supported, quartz-feldspar rhyolitic, lapilli-tuff facies or *main facies zone* (*KIc*).
a) A coherent coarse-grained porphyritic rhyolite lithic clast within the facies matrix, showing rotational movement to left. b) Variably squashed, coarse-grained, crystal-rich pumice/cognate clast. c) Photomicrograph showing the boundary between the clasts/pumice (left) and the ignimbrite matrix (right; XPL). d) The ` distribution of crystals in the facies demonstrating poor sorting, and the arrangement of crystal-rich and -poor areas defining a planar fabric. e) Attenuated and flattened, coarse-grained, crystal-rich pumice/ cognate clast. f) Clast-rotated autoclastic rhyolitic breccia, showing jig-saw fit rotated monomictic clasts (autobreccia).

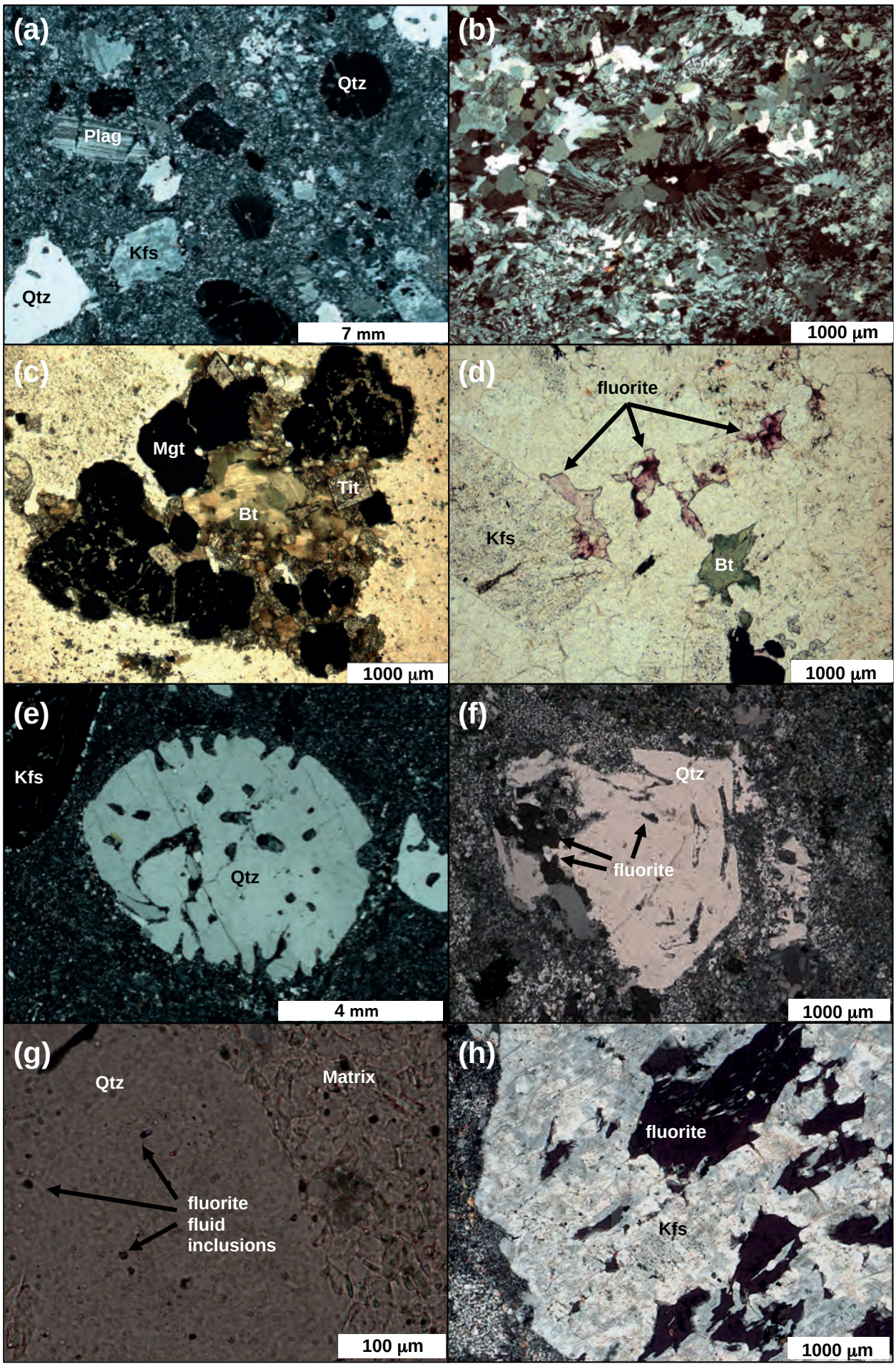
(a)
Qtz
Plag
Kfs
Qtz
7 mm
(b)
1000 μm
(c)
Mgt
Tit
Bt
1000 μm
(d)
fluorite
Kfs
Bt
1000 μm
(e)
Kfs
Qtz
4 mm
(f)
Qtz
fluorite
1000 μm
(g)
Qtz
Matrix
fluorite
fluid
inclusions
100 μm
(h)
fluorite
Kfs
1000 μm

Figure 2.9 (oppposite page): Photomicrographs of the *main facies zone* (*KIc*). a) Typical texture, with a devitrified granophyric quartz-feldspar matrix containing fragmental quartz, K-feldspar and plagioclase phenocrysts (XPL). b) Aphyric pumice with a fine-grained granophyric quartz-feldspar groundmass containing spherulites (the radial, fibrous quartz crystallites emanating from an isotropic fluorite crystal core in the centre of the picture; XPL). c) A large glomerocryst of biotite, titanite and Fe-Ti oxides found throughout the matrix (PPL). d) Purple fluorite crystals within the matrix (PPL). e) A large, embayed quartz phenocryst (XPL). f) Typical bi-pyramidal volcanic quartz with fluorite inclusions. g) Tiny fluorite fluid inclusions within phenocrystic quartz (PPL). h) Unaltered K-feldspar phenocryst containing small isotropic fluorite inclusions (XPL).

primary minor accessory minerals such as fluorite, apatite, zircon, titanite and garnet (Fig. 2.9a). Interstitial chlorite, carbonate and muscovite constitute secondary mineral phases (<5%). Pyrite and chalcopyrite have also been noted. The remaining >60% of the matrix is a very fine-grained devitrified microgranular quartz-feldspar mosaic (Fig. 2.9b). Crystals within this mosaic range in size from 0.1–0.05 mm, with some granoblastic regions (>1 mm). Biotite, titanite and Fe–Ti oxide glomerocrysts (mm scale) are present in the matrix (Fig. 2.9c), and green biotite crystal fragments are present as large clusters or individual crystals up to 0.2 mm in size. Purple fluorite is also present in the matrix as individual isolated crystals (0.1–1 mm) or within clusters that are up to 2 cm in size (Fig. 2.9d). This facies contains abundant large (mm to cm scale) feldspar and quartz macrocrysts; quartz macrocrysts are euhedral to angular, broken and irregular in shape, range from 0.2–9 mm in size, are commonly embayed (Fig. 2.9e) to bi-pyramidal in shape, and contain fluorite inclusions (Fig. 2.9f) and fluid inclusions (Fig. 2.9g). Feldspar crystal fragments vary from euhedral to anhedral, angular and broken, and are dominantly mesoperthitic alkali feldspar with lesser plagioclase. The mesoperthitic alkali feldspars are coarse-grained, subhedral and are up to 24 mm in size, and contain albite lamellae that form large stringer domains or entire crystals and create coarse internal patchwork patterns. These mesoperthitic alkali feldspars contain large fluorite inclusions (Fig. 2.9h) and in some cases show a slight alteration with secondary carbonate, green mica and chlorite, as well as fine-grained granoblastic quartz rims. Plagioclase crystals have polysynthetic twinning, are anhedral to rarely subhedral, are up to 4 mm in size, and show instances of sericite alteration, giving a speckled appearance. Compared with the crystals in the clasts, the crystals in the matrix are more fragmented and contain few glomerocrysts.

Macroscopic oval to round siliceous nodules that are up to 30 mm in size are present in the western section of the *main facies zone* (A; Fig. 2.3). Thin section petrography indicates that these are spherulites that are composed of radial quartz fibres (Fig. 2.9b), and occur laterally across the facies.

Interpretation:

The angular and frequently broken nature of crystals within this facies is characteristic of a fragmental volcaniclastic rock. The crystal population is monomictic, juvenile and consistent with a rhyolitic volcanic source, and, barring the possible rounding of a few porphyry clasts; no components within the up to 350 m thick facies preserve any

evidence of sedimentary reworking. Even the rounded clasts could be result of vent milling and not surface process related rounding. The massive, poorly-sorted, matrix-supported texture and the wide range of fragment sizes, with large clasts and crystals dispersed in the dominant fine matrix, together with the fiamme-like fragments is consistent with a pyroclastic flow deposit origin (Smith, 1960a; Sparks *et al*., 1973; Wright *et al*., 1981; Wilson and Walker, 1982; Cas and Wright, 1987; Branney and Kokelaar, 2002). Glass shards have not been recognised in this facies, but the texture of the facies is similar to *Facies* (*KI*g) described in the Karlaya Member (*Section 2.3.3.2.1*), in which welded glass shard textures are visible. The microgranular, granophyric, quartz-feldspar mosaic texture seen in the matrix of this facies appears to be a devitrification texture commonly associated with ancient volcanic deposits (Lofgren, 1971; McPhie *et al*., 1993) but could in part at least, also represent post-depositional silicification (Gifkens *et al*., 2005). As a result, only limited observation of the original fine matrix component is possible. The poor sorting of the facies probably relates to high-density particle concentration during emplacement (Cas, 1978). The irregular patches, discontinuous layers, or lenses containing high concentrations of quartz and feldspar crystals (Fig. 2.8d) are interpreted to be large (>1 m), squashed and flattened pumice clasts or fiamme; the planar fabric alignment of these is consistent with a eutaxitic fiamme texture. These characteristics suggest that this facies is a welded pyroclastic ash-flow tuff or ignimbrite deposit. The spherulites in this facies are similar to those in the welded, Ordovician, Garth Tuff ignimbrite of North Wales, UK (McArthur *et al*., 1998).

There are three possible origins for the large quartz and feldspar macrocrysts identified in the matrix, including:

a) Crystals liberated from the magma during an explosive eruption (i.e. juvenile magmatic phenocrysts).
b) Crystals separated from the juvenile magmatic clasts (pumice or cognate) during transport and deposition.
c) Xenocrysts of country rock with a similar composition and mineralogy to the ignimbrite (i.e. the coarse grained porphyritic rhyolite underlying the KI; see RS, above, for facies description and interpretation).

It is possible that all three scenarios could be correct and that the large crystals within this facies have three different sources. However, the crystal population in the matrix is identical to the crystal population in the fiamme, indicating that the majority of the crystals are juvenile magmatic crystals. The crystal-rich fiamme indicate eruption of a sub-liquidus temperature, crystal-rich magma. The aphyric fiamme indicate contemporaneous eruption of a near liquidus to supra-liquidus temperature magma. The different crystal sizes could indicate pulsating eruption events with different magma batches, although as there is no record or evidence to support a significant time break in this facies, it is

interpreted to be a continuous on-going event.

2.3.3.1.2 Planar and folded laminated aphyric rhyolite facies (*KIb*)

Description:

The *main facies zone* of the Kurrparu Member grades downwards into the *planar and folded laminated aphyric rhyolite facies* (*KIb*), a 30 to 50 m thick, crystal- and lithic-poor, fine-grained, matrix-supported facies that contains laterally continuous layering or laminations (Fig. 2.10a) that are planar towards the base, but become folded (Fig. 2.10b) and more intensely convoluted and contorted with chaotic fold patterns in the upper levels of this facies (Fig. 2.10c). This change from planar to folded is marked by both transitional and sharp contacts between planar and convoluted fold laminations. Certain areas within the previously described *main facies zone (KIc)* also contain similar laminations, although they occur in discrete zones, are not laterally continuous, and grade into non-laminated *main facies zone (KIc).*

The banding is defined by alternating matrix grainsizes that have diffuse boundaries, representing slight variations in the overall facies rather than an entirely new facies. The laminations (Fig. 2.10d) are ≤1 cm thick and have an aphanitic, microcrystalline, granophyric quartz-feldspar texture. Interspersed with these “normal” layers or laminations are thin (2–5 mm) concordant, laterally planar and continuous ‘vein-like’ features that are defined by granoblastic recrystallized quartz (Fig. 2.10e) and tiny radiating elongate marginal quartz crystallites (Fig. 2.10f). These features can also be discontinuous and truncated, with boundaries that range from sharp to diffuse. Fluorite crystals (0.1–1 mm) and fluorite inclusions within quartz, Fe–Ti oxides, green to brown biotite, and carbonates are also present throughout these vein-like features. There is a strong fabric defined by microgranular quartz-feldspar crystals that are either parallel with or at a slight angle to the bands and ‘vein-like’ features described above.

The only phenocrysts within this facies are subhedral volcanic bi-pyramidal to rounded and strongly embayed quartz and fragmented quartz crystals (0.5–1.1 mm), with an overall crystal abundance of <5%. Dark coloured, fine-grained micaceous lithic clasts that closely resemble sediments from the CF and coarse-grained quartz–feldspar-phyric rhyolite clasts that closely resemble the RS are dispersed with a low abundance of <10%. The laterally continuous layers become frequently truncated and discontinuous towards the top of this facies. The folding of the laminations occurs at both meso- (a few cm) and macro (a few metres to tens of metres) scales, and the chaotic geometry and random orientations of these folds indicates they are ptygmatic. Along the base of this facies is a thin zone (<20 cm thick) of alternating light and dark colour-banded aphanitic rhyolite. These alternating bands are about 1 cm thick and have ptygmatic folds in some areas.

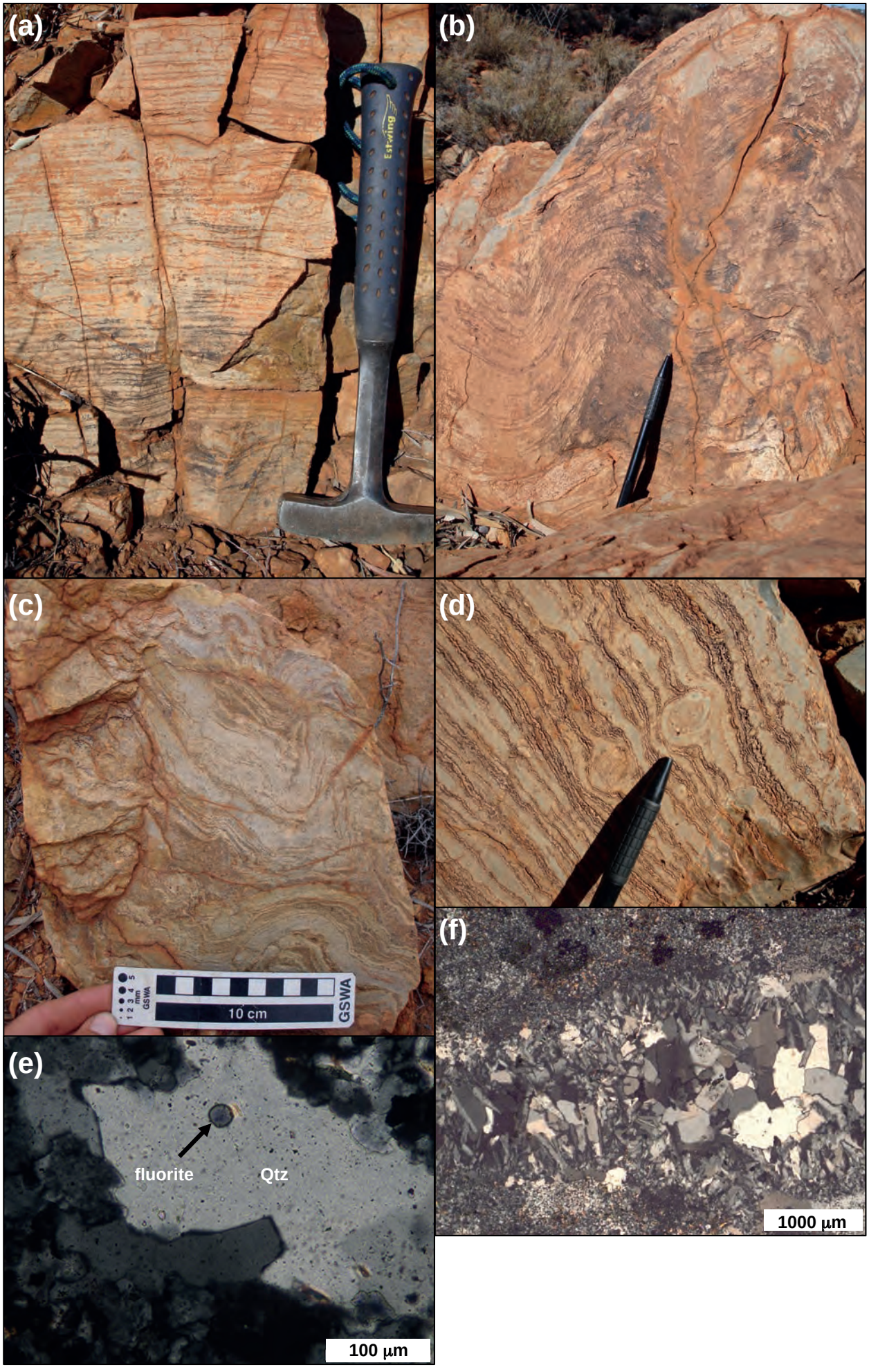
(a)
(b)
(c)
10 cm
GSWA
(d)
(e)
fluorite
Qtz
100 µm
(f)
1000 µm

Figure 2.10 (opposite page): Kurrparu Member - planar and folded laminated aphyric rhyolite facies (KIb) demonstrating rheomorphism and lava-like welding. a) Basal planar laminations or flow bands from rheomorphic flow. b) Gentle open isoclinal folded flow laminations. c) Chaotic ptygmatic folding of the laminations with refolded folds. d) Pervasive lineations along gas-driven shear partings with rounded spherulite clast development. e) Photomicrograph of fluorite fluid inclusion (top centre) within vapour phase quartz found within shear partings (XPL). f) Photomicrograph of the typical texture of shear partings or lineations defined by devitirified granoblastic quartz (in the centre), K-feldspar and tiny quartz crystallites (on the edges) and isotropic fluorite inclusions throughout (XPL).

Large-scale (tens of metres) columnar jointing is also present towards the base of this facies in the eastern section (C: Fig. 2.3). The gradational upper transition into the ignimbritic *main zone facies* (*KIc*) is marked by a gradual increase in the phenocryst content, the appearance of feldspars (generally previously absent) and the occurrence of the two-types of fiamme and a decrease in the laterally continuous laminations with frequent truncation.

Interpretation:

The layering or laminations within this facies are similar to flow-laminations or banding that are common in coherent rhyolitic lavas and intrusions (Benson and Kittleman, 1968; Fink and Manley, 1987). The absence of visible vitriclastic textures, including fiamme at the mesoscopic scale suggest that this is a coherent silicic lava facies. However, the lack of a continuous basal autobreccia, almost always associated with unambiguous silicic lava-flows (Cas and Wright, 1987; Fink and Manley, 1987), and the upward gradational facies change into the unequivocal upper ignimbritic *main zone facies* suggests that this facies was also vitriclastic and is therefore a part of the Kathleen Ignimbrite, rather than a separate coherent silicic lava facies.

This apparently coherent facies with planar and folded laminations is therefore interpreted to be a rheomorphic ‘lava-like’ ignimbrite, which is an intensely welded, extremely high-grade form of ignimbrite that underwent gravity-and load-driven mass flowage during and after deposition and welding as a pyroclastic flow deposit. Remobilisation of the still hot, plastic, welded deposit produced hot-state ductile shear deformation producing rheomorphic flow banding and flow folding (Schmincke and Swanson, 1967; Chapin and Lowell, 1979a; Wolff and Wright, 1981; Walker, 1983; Ekren *et al*., 1984; Branney *et al*., 1992; Branney and Kokelaar, 1992; Leat and Schmincke, 1993; Kobberger and Schmincke, 1999b; Kokelaar and Koeniger, 2000; Branney and Kokelaar, 2002; Sumner and Branney, 2002).

During welding of a particulate pyroclastic flow deposit, viscous particles, including both pumice and matrix coalescence and agglutinate to form a non-particulate, dense, fluidal viscous deposit domain within the pyroclastic flow deposit. As long as this dense, plastic magmatic mass retains a sufficiently high temperature, and has low enough yield strength and viscosity it can undergo laminar flow or viscous shearing in response to gravitational potential, or perhaps even to the shearing effect of an overlying particulate

pyroclastic flow (Branney *et al*., 1992; Branney and Kokelaar, 1992; Stevenson *et al*., 1993; Kobberger and Schmincke, 1999a; Gottsmann and Dingwell, 2001; Gottsmann and Dingwell, 2002; Soriano *et al*., 2002; Gonnermann and Manga, 2005). Rheomorphic remobilisation requires either syn- or post-depositional gravitational potential, perhaps provided by some form of slope inducing laminar shear. This process can attenuate pumiceous clasts (fiamme) to form agglutinated fluidal non-particulate flow-laminations (Schmincke, 1975; Chapin and Lowell, 1979b; Reedman *et al*., 1987b).

Flow laminations or banding result during pyroclastic flow emplacement due to differences in viscosities. Gases and volatiles accumulate along these viscosity incompetencies and can accommodate shearing. Actual partings or vugs (i.e. open spacings) can also develop by the separation of adjacent flow laminae during laminar flow shearing of these gas-rich layers, termed 'planar exsolution partings' (Andrews and Branney, 2011) or 'shear partings'. Such partings can then be filled in by secondary minerals precipitated from exsolved magmatic volatiles during vapour-phase alteration and degassing of an ignimbrite pile (Cas and Wright, 1987; Branney *et al*., 1992), forming vein-like, quartz-filled laminations. Although these features can closely resemble vein quartz (Adams, 1920), the diffuse boundaries and lack of continuity of these vein-like features do not support a tectonically-induced hydrothermal origin.

The sharp contact between areas of planar flow and folded flow banding is caused by differences in viscosity and cooling rates in the deposit, producing heterogeneous intra-formational deformation along some horizons, with the chaotic ptygmatic folding of flow-laminations indicative of the extremely plastic state of the ignimbrite during rheomorphic remobilisation. Columnar jointing towards the base of the facies is characteristic of both densely welded ignimbrites and lavas, but implies that this facies was emplaced while hot and dense (Cas and Wright, 1987). The colour banding at the base of this facies is most likely a devitrification effect as indicated by the textural variations described above; it is unlikely that this represents a welded, ash-sized, fall-out tuff deposit as this type of deposit would be well-sorted and successive layers would likely show some variations in grain size (Wolff and Wright, 1981; Cas and Wright, 1987), neither of which are observed.

Rheomorphism is indicative of an extreme grade of welding that involves the gravity-driven flow of a fused fragmental rock during and after compaction of either fall or flow pyroclastic deposits (Wolff and Wright, 1981; Branney *et al*., 1992; Branney and Kokelaar, 1992; Bachmann *et al*., 2000b; Pioli and Rosi, 2005; Lavallee *et al*., 2008; Andrews and Branney, 2011). Rheomorphic ignimbrites are deposited by very hot pyroclastic density currents that contain a fused sheet of hot volcanic glass and ash, which spreads and flows downslope over weeks to months prior to cooling and passing through the brittle–ductile transition (Schmincke and Swanson, 1967; Andrews and Branney, 2011).

The flow banding, folding, and internal discordances or detachments in this facies record both plastic and brittle-ductile deformation, primarily as a result of heterogeneous strain rates within the deposit. This is primarily the result of varying rates of cooling below the glass transition temperature within the facies; this created viscosity contrasts, which in turn produced strain boundaries that localised deformation (Benson and Kittleman, 1968; Gonnermann and Manga, 2005).

Although no specific structural measurements and analysis of the folds and flow banding were taken, the deformation in this facies shows remarkable similarities to the pervasive planar foliation, elongation lineation, recumbent isoclinal folds, sheath folds and refolded folds (Chapter 4) described by Andrews *et al*., (2011) for the lava-like rheomorphic Grey's Landing ignimbrite, southern Idaho, USA, interpreted to represent a thin, ductile, intense, upward migrating, non-coaxial shear zone (Branney and Kokelaar, 1992), with a basal flat domain (e.g., the planar flow domain described above) and an upper contorted band (e.g., the folded flow banding described above) with its larger scale folds, representing an increase in the thickness of the rheomorphic shear zone (Andrews and Branney, 2011). The aphyric nature of this facies indicates that the primary magma was erupted at a near liquidus temperature, which would have facilitated intense welding and rheomorphism.

2.3.3.1.3 Basal jigsaw-fit to clast-rotated, colour-banded rhyolite clast breccia facies (*KIa*)

Description:

The *planar and folded laminated aphyric rhyolite facies* (*KIb*) grades downwards into a variably thick (<20 cm) *basal jigsaw-fit to clast-rotated, colour-banded rhyolite clast breccia facies* (*KIa;* Fig. 2.11a) that is pervasive across the base of the succession. This facies has a generally sharp contact with underlying CF sediments, but in places this contact is irregular and is marked by domains of mixed sediment and rhyolite clasts. The clasts are angular, autoclastic, flow-banded and microcrystalline rhyolite fragments that are arranged in a jigsaw fit pattern. They vary in size on a mm to cm scale and in places are supported by a fine-grained matrix that closely resembles the underlying sedimentary facies and contains quartz and feldspar fragments with abundant mica. There are also areas in this facies where the underlying sediment cross-cuts upwards into facies *KIa* and *KIb* in seams that are up over 50 m long and up to 5 m wide (Fig. 2.11b).

Interpretation:

This facies is interpreted as a quench-fragmented hyaloclastite and peperite at the base of the *planar and folded laminated aphyric rhyolite facies (KIb)* and marks the contact between the KI and the CF sediments. A quench fragmented hyaloclastite origin is supported by the fact that all clasts within this facies are lithologically identical, the same

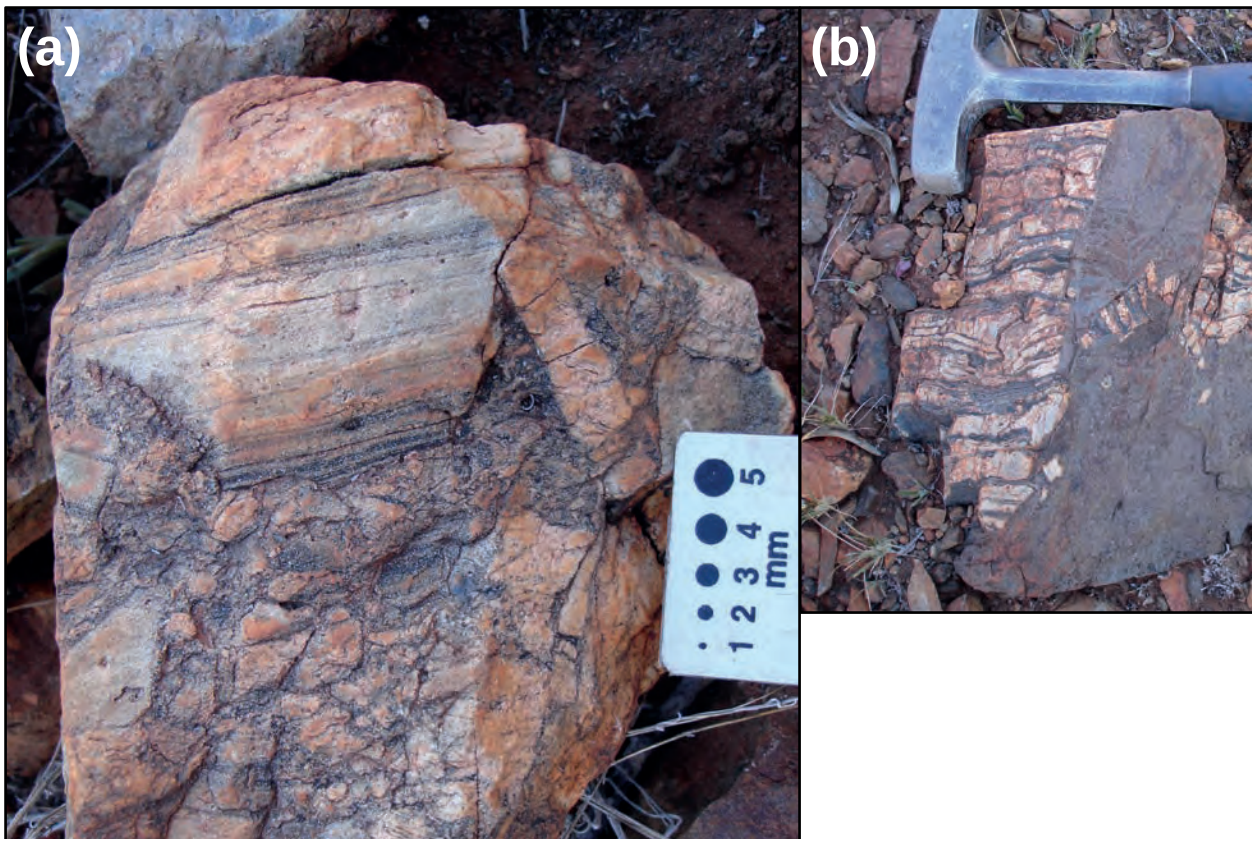

Figure 2.11: Kurrparu Member – basal jigsaw-fit to clast-rotated, colour-banded, rhyolite clast breccia facies (KIa) seen all along the basal contact of the Kathleen Ignimbrite. a) Hyaloclastite b) A clastic dyke (right) emanating from the underlying Upper Cleghorne Formation, cross cuts the basal colour bands of the Kathleen Ignimbrite (left).

as the rhyolite facies, and have a jigsaw-fit texture. The facies therefore formed by in-situ brecciation, and define a texture that is similar, if not more pronounced, to that found at the upper contact of the RS with the CF, as described and interpreted above in *Section 2.3.2.1*. The rhyolite clast-sediment mixtures are also interpreted as peperite, as for the equivalent breccias at the top of the RS. In addition, the fact that the substrate (i.e. the CF sediments) was wet during deposition of the KI, as evidenced by the peperitic mixing at the base of the KI, indicates that ignimbrite and turbidite deposition was contemporaneous. The cross-cutting seams of sediment into the overlying ignimbritic facies is interpreted to represent clastic dyke intrusions from the fluidisation of wet sediments (Kokelaar, 1982; Jolly and Lonergan, 2002).

2.3.3.1.4 Massive, eutaxitic, crystal-poor, rhyolitic lapilli-tuff facies (*KId*)

Description:

The upper part of the *main facies zone* (*KIc*) is associated with a gradual decrease in the size and overall crystal abundance of the matrix to sparse macrocrystic quartz crystals <6 mm in size and with abundances <5%. This change is also associated with more abundant, well-defined, irregular, wispy, lensoidal, cigar-shaped fiamme-like clasts (up to 15 cm), with low aspect ratios, that are frequently aligned to produce a strong

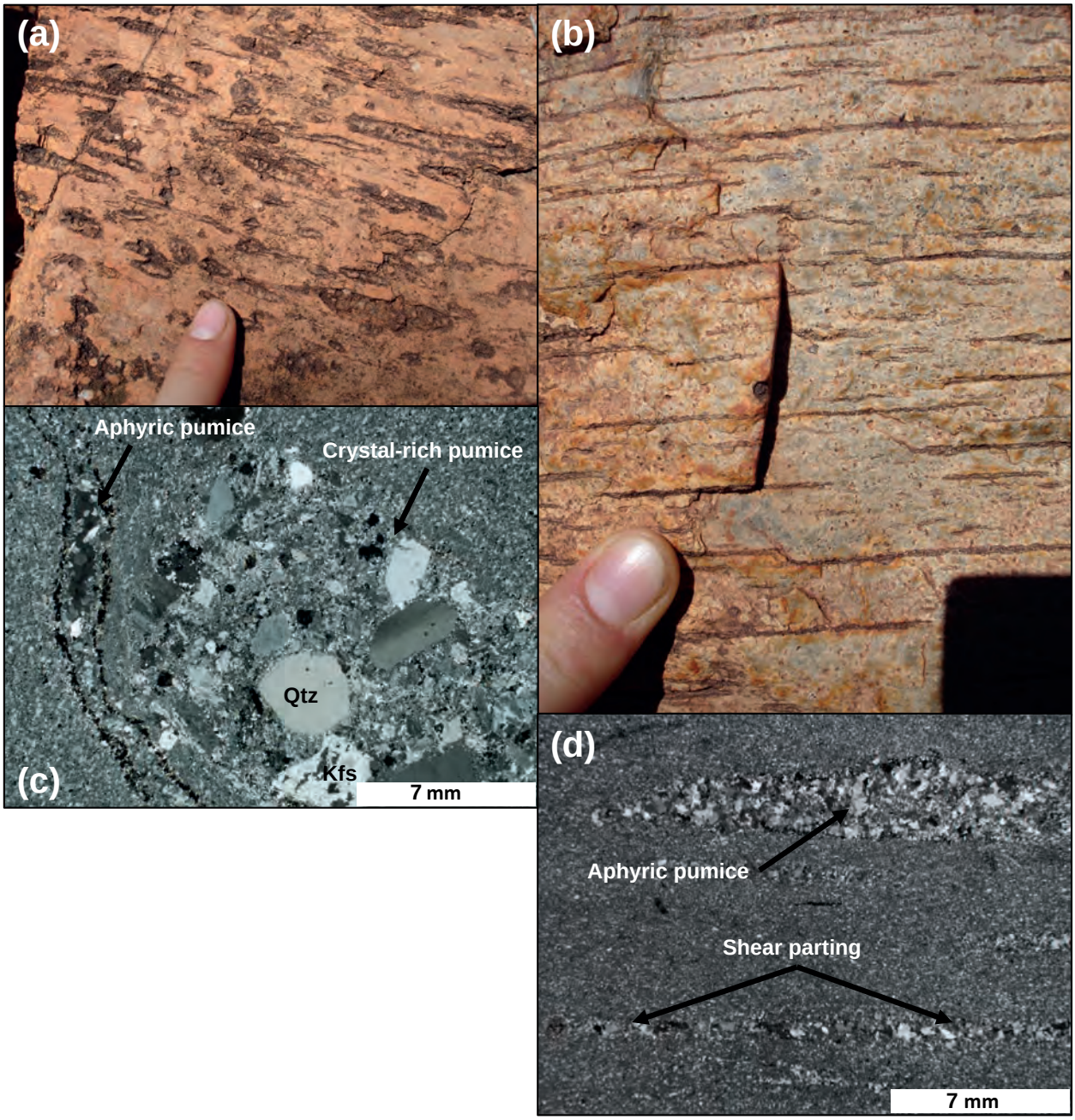

Figure 2.12: Kurrparu Member - massive, eutaxitic, crystal-poor, rhyolitic lapilli-tuff facies (*KId*) with two distinct eutaxitic fiamme populations. a) The coarse-grained, crystal-rich fiamme population, b) The fine-grained, crystal-poor or aphyric fiamme population. c) Photomicrograph of the two pumice populations side by side, aphyric pumice (left), crystal-rich pumice (right; XPL). d) Aphyric fiamme (top) and thin laterally continuous lineation defining a shear parting(bottom; XPL).

planar fabric (i.e. eutaxitic; Figs. 2.12a and 2.12b). This marks the start of a new 50 to 100 m thick *massive, eutaxitic, crystal-poor, rhyolitic lapilli-tuff facies* (*KId*) that extends across the entire strike length of the KI. This facies is also poorly-sorted, with a matrix supported texture of dispersed fiamme-like clasts in a fine, ash size matrix. There are two distinct populations of fiamme-like clasts (Fig. 2.12c); a coarse-grained and crystal-rich population (Fig. 2.12a) that is comprised of quartz and feldspar phenocrysts set within a granophyric quartz-feldspar groundmass, and a fine-grained aphyric population (Fig. 2.12b) that contains no phenocrysts and consists of a microgranular quartz groundmass with feldspar crystallites and fluorite crystals (Fig. 2.12c). The coarse-grained and crystal-

rich fiamme-like clasts are remarkably similar to squashed pumice clasts within the *main facies zone* (*KIc*). The other aphyric population is significantly different in that it consists of thin, lenticular, highly irregular, wispy and 'vein-like' pumice shapes that are often rimmed by Fe–Ti oxides, biotite, and fluorite. Both pumice populations occur at the base of this facies, but only the fine-grained and aphyric pumice are present towards the top of the facies, and the upper 10 to 20 m lacks any pumice or fabric, and is characterised by the presence of a few small quartz phenocrysts dispersed throughout the microgranular matrix.

Interpretation:

The presence of abundant fiamme, a eutaxitic texture, a massive, matrix-supported, poorly sorted texture, and a pervasive planar fabric defined by aligned fiamme-like clasts are all indicative of welded ignimbrite (Smith, 1960a; 1960b; Ross and Smith, 1961; Cas and Wright, 1987; Quane and Russell, 2005). This, combined with the fact that this facies is gradational with the ignimbritic *main zone facies* (*KIc*), means that this facies forms part of the KI. Branney and Kokelaar (2002) suggest that the presence of eutaxitic fabrics in rocks is indicative of hot welding deformation of pyroclasts, although these textures may not be associated with welding and can form during cold burial-compaction associated with diagenesis (e.g., Branney and Sparks, 1990), hot deformation of lava autobreccias, or tectonic deformation. The distinct lack of any evidence of these alternatives suggests that this texture was most likely formed by welding. In addition, the presence of two distinct pumice populations in this facies suggests that at least two different batches of magma were involved in the formation of the KI, one sub-liquidus the other at liquidus to supra-liquidus temperature, while the overall low crystal content in this facies indicates eruption of the source magma at or near liquidus temperature.

2.3.3.2 The Karlaya Member

2.3.3.2.1 Poorly-sorted, monomictic, angular to sub-rounded, rhyolitic ignimbrite clast- to matrix-supported breccia facies (*KIe*)

Description:

The upper *massive, eutaxitic, crystal-poor, rhyolitic lapilli-tuff facies* (*KId*) of the KI has either a sharp (Fig. 2.13a) or gradational contact with an overlying *poorly-sorted, monomictic, angular to sub-rounded, clast- to matrix-supported breccia facies* (*KIe*; Fig. 2.13b). The thickness of this facies varies between tens of centimetres to a few metres (<5 m) and is laterally discontinuous, but is present in both eastern and western sections of the KI (C; A; Fig. 2.3). The facies appears to be massive, fairly sorted and lensoidal in geometry due to the discontinuity across strike, with an overall absence of grading and fiamme. In places the facies contains horizons where there is an increase in clasts,

clast reworking and the development of a clast-supported framework. This facies is interbedded with facies (*KId*) in the eastern section (C; Fig. 2.3) and is also present as isolated outcrops within the western section. Lapilli-sized, angular to sub-rounded clasts

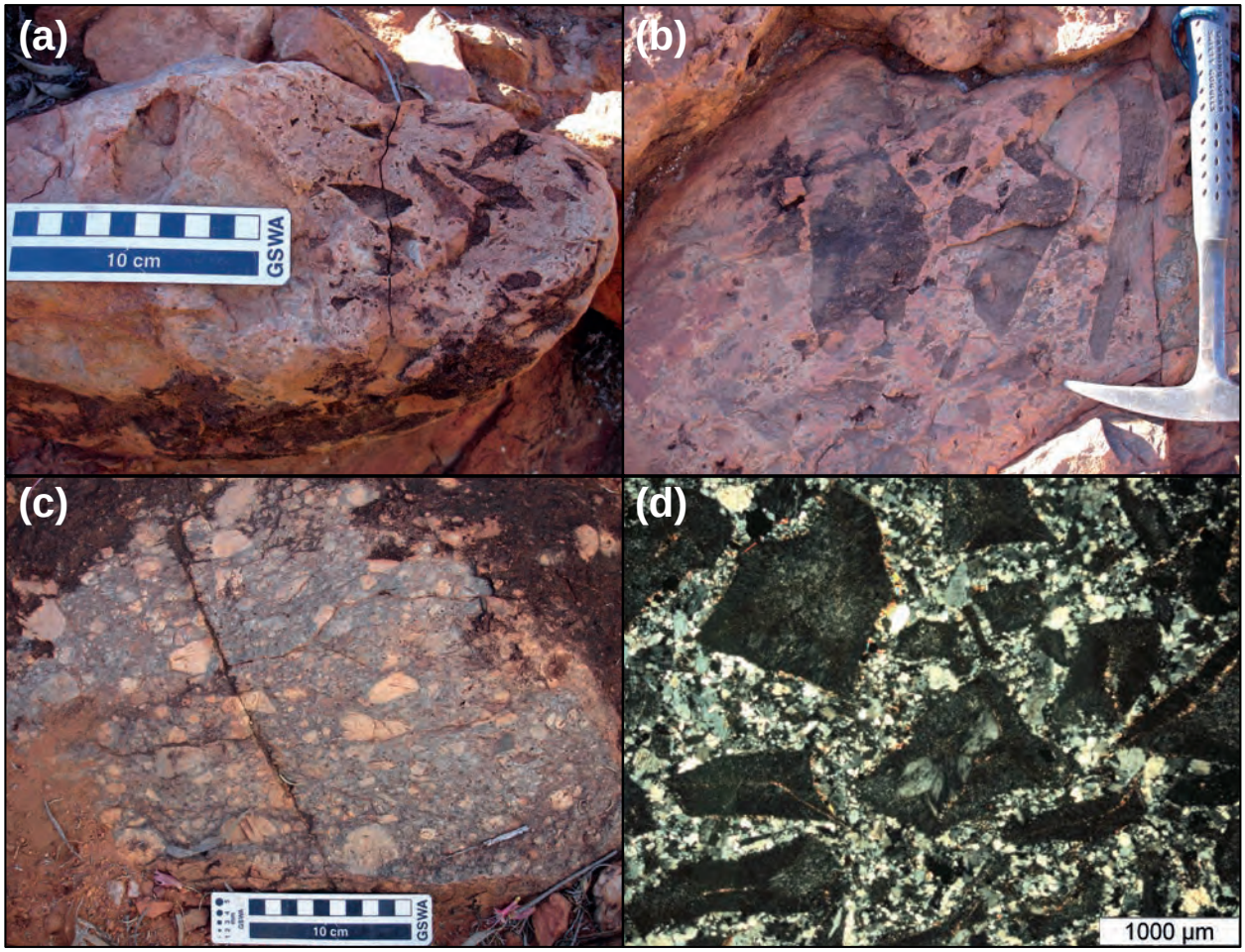

Figure 2.13: Karlaya Member - poorly-sorted, monomictic, angular to sub-rounded rhyolitic clast- to matrix-supported breccia facies (KIe). a) Sharp contact of facies (KIe; right) with the upper Kurrparu facies (KId; left). b) Angular rhyolitic ignimbrite clasts within a matrix-supported breccia. e) Breccia with sub-rounded to angular clasts of fine-grained weathered ignimbrite and feldspathic ignimbrite. f) Photomicrograph of the blocky, relict glass shards with curviplanar margins (XPL).

of fine-grained rhyolitic ignimbrite are present, one light coloured, the other dark and containing K-feldspar macrocrysts and appears to be a welded ignimbrite (Fig. 2.13c). The microtexture in the matrix consists of fragments which look like altered, devitrified, blocky glass shards with curviplanar margins (Fig. 2.13d) set in a devitrified granophyric, probably originally ashy matrix.

Interpretation:

This facies represents the first abrupt change in deposition of the Kurrparu Member and therefore marks the start of the Karlaya Member. The clasts in this breccia are similar to the underlying *massive, eutaxitic, crystal-poor, rhyolitic lapilli-tuff facies (KId)* as well as containing clasts similar to the overlying *poorly-sorted, matrix-supported, feldspathic, eutaxitic, rhyolitic, lapilli-tuff facies (KIf*), suggesting that this breccia indicates

local reworking of the upper part of the Kurrparu Member. Lack of evidence of tractional structures and pervasive rounding of the clasts indicates little tractional reworking or that in-situ reworking has occurred. The blocky glass shard fragments may possibly be of phreatomagmatic origin, given the initial subaqueous depositional environment, such an origin cannot be excluded. This means the facies can be interpreted as either a mass flow deposit; a small volume, primary non-welded pyroclastic flow deposit (still part of the Kurrparu event, but representing waning phase activity); or a secondary debris flow deposit, pene-contemporaneous with the KI deposition with the possible interaction of water. The relationships with the next overlying facies (*KIf*) suggests this facies (*KIe*) could be a co-ignimbrite breccia facies to facies (*KIf*) as described in Cas and Wright (1987), with Druitt and Sparks (1984) suggesting the appearance of such localised breccias between normal ignimbrites indicates caldera collapse.

2.3.3.2.2 Poorly-sorted, matrix-supported, feldspathic, eutaxitic, rhyolitic, lapilli-tuff facies (*KIf*)

Description:

The Karlaya Member is dominated by a *poorly-sorted, matrix-supported, feldspathic, eutaxitic, rhyolitic, lapilli-tuff facies* (*KIf*) that is interbedded with intervals of the *poorly-sorted, monomictic, angular to sub-rounded, rhyolitic clast- to matrix-supported breccia facies* (*KIe*). This facies appears to be bedded and up to 100 metres thick, being present in the eastern, western, and northern sections of the study area (C; A; D; Fig. 2.3). It has a dark black to blue very fine-grained matrix that contains abundant (25 vol. %) K-feldspar macrocrysts (up to 5cm) that are subhedral, elongate to oblate, and have long axes that are aligned parallel to bedding (Fig. 2.14a). Rounded quartz phenocrysts are also present in this facies, although far less (5–10 vol. %) than in the Kurrparu Member. The matrix contains small, fine-grained, wispy-shaped clasts with rare quartz and feldspar phenocrysts (Fig. 2.14b) and larger, crystal-rich, coarse-grained cigar-shaped quartz and feldspar phenocryst-bearing clasts (Fig. 2.14c), both of which closely resemble fiamme and define an apparent eutaxitic foliation. This facies is less welded than facies in the Kurrparu Member, with the fiamme less flattened and attenuated than those in facies *KIc* and *KId*. The upper and lower portions of this facies are crystal-poor and lack fiamme, and the facies contains thin bubble-walled cuspate and platey, relict glass shard textures (Figs. 2.13d and 2.13e) that have undergone some plastic deformation. These shard textures were found in samples from both the eastern and western sections (C, A; Fig. 2.2) of the formation, however the samples from the western section may actually belong to the Kurrparu Member, based on a spatial association with the shard-bearing samples from the eastern section. This is because it is difficult to distinguish the contact between the two members in the western section due to deformation.

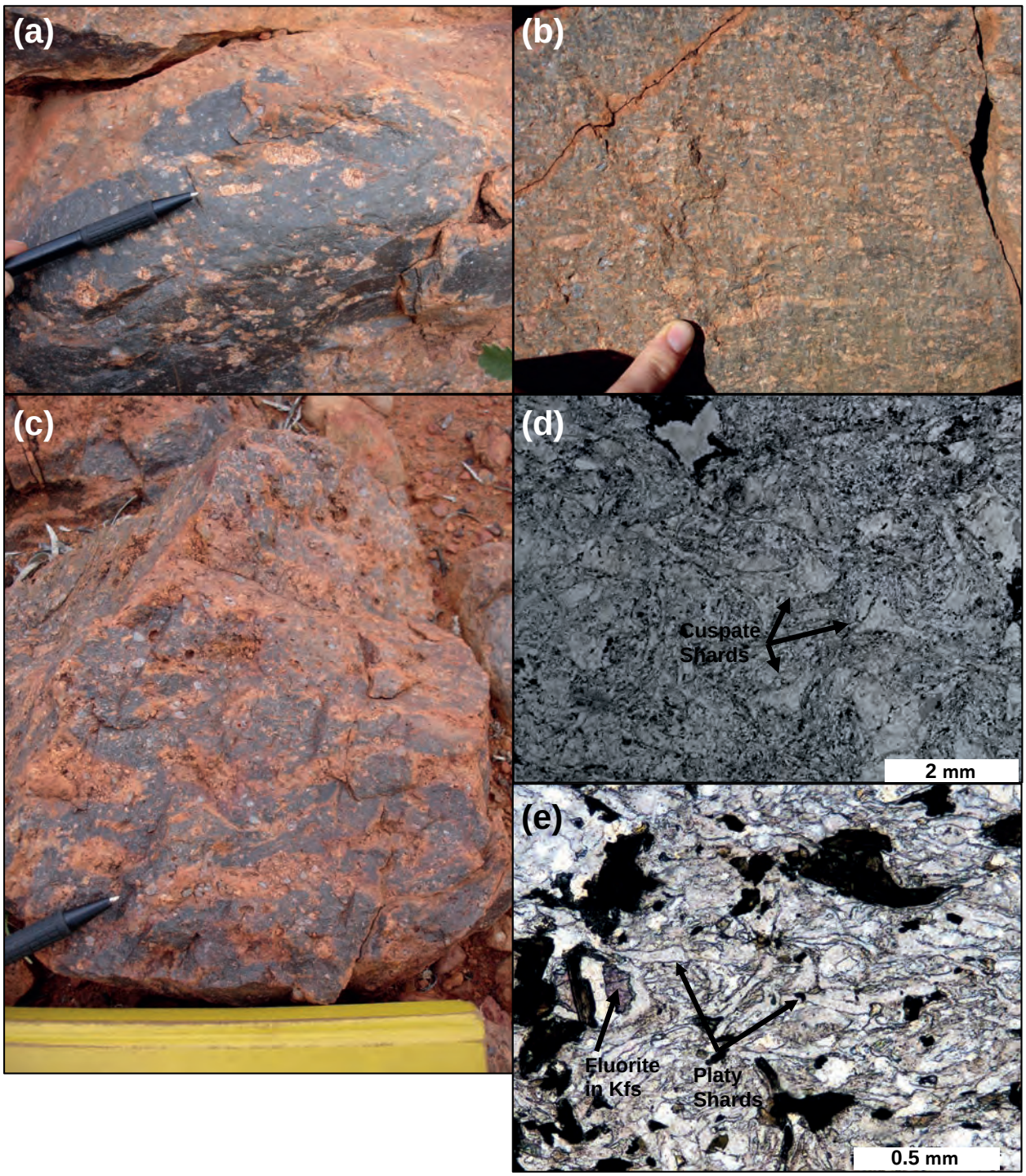

Figure 2.14: Karlaya Member - poorly-sorted, matrix-supported, feldspathic, eutaxitic, rhyolitic lapilli-tuff facies (KIf). a) Poorly-sorted K-feldspar-rich nature of the facies showing a planar fabric. b) Eutaxitic aphyric, flattened cigar-shaped fiamme. c) Wispy, relatively undeformed, crystal-rich fiamme, not seen in the underlying Kurrparu Member. Photomicrographs of vitriclastic shard textures, both cuspate, bubble-wall (d) and platy (e) plastically deformed clasts, as well a purple fluorite inclusion within a K-feldspar phenocryst.

Interpretation:

The much darker matrix, a relative increase in the abundance of K-feldspar macrocrysts and decrease in quartz phenocrysts, the more clearly defined individual fiamme shapes and an absence of the *planar and folded laminated aphyric rhyolite facies* (*KIb*) facies distinguishes this facies from the Kurrparu Member. The poor sorting and thick massive nature of the facies, the presence of fiamme in a fine-grained matrix,

and the preferred alignment of K-feldspar macrocrysts and fiamme all suggest that this facies is a pyroclastic flow deposit. In addition, the distinct differences between this facies and the Kurrparu Member indicates that these separate ignimbrite facies most probably originated from different pyroclastic flow-forming eruption events. The fact that this facies is interbedded with intervals of the *poorly-sorted, monomictic, angular to sub-rounded, clast- to matrix-supported breccia facies* (*KIe*) also suggests that at least two different pyroclastic flow deposits, and possibly more, were deposited above the thick Kurrparu Member.

Again the occurrence of both crystal-rich and crystal-poor or aphyric fiamme indicates contemporaneous eruption of two magmas, one sub-liquidus temperature and the other near liquidus temperature.

2.3.3.3 The Kilykilykarri Member

2.3.3.3.1 Well-sorted, stratified and graded, rhyolitic, volcaniclastic interbedded pebbly conglomerate, breccia, sandstone and mudstone facies (*KIg*)

Description:

Overlying the *poorly-sorted, matrix-supported, feldspathic, eutaxitic, rhyolitic, lapilli-tuff facies* (*KIf*), is a *well-sorted, stratified and graded, rhyolitic, volcaniclastic interbedded pebbly conglomerate, breccia, sandstone and mudstone facies* (*KIg*) that comprises the bulk of the Kilykilykarri Member. The contact between the Karlaya and Kilykilykarri members does not outcrop, although the abrupt change in facies between the members and the proximity to each other suggests little loss of stratigraphic continuity, and therefore a sharp contact can be inferred. This facies is restricted to the eastern section (C; Fig. 2.3) of the KI, although it most likely originally outcropped across the strike length of the formation, but was truncated by the intrusion of numerous, younger, cross-cutting porphyritic rhyolites that overlie the KI. The overall thickness of this facies interval is ≤50 m and the preserved lateral extent is at least 500 m. It is well-bedded and sorted, containing fragments of angular or broken quartz and feldspar crystals in a stratified succession with beds that range in thickness from a few mm (in the upper fine ash-mudstone beds) to 50–60 cm (in the conglomerate, breccia and coarse sandstone beds). The sandstone beds (Fig. 2.15a) are graded, showing both reverse-grading and upward fining, are well-sorted, exhibit downward-scouring and alternate between thicker (5–7 cm) coarse- and thinner (2–5 cm) slightly finer-grained beds and show load cast (Fig. 2.15b) and convolute structures, truncated bedding, ripple cross lamination and small amplitude (30 cm λ) convex-up stratification similar to the hummocky cross stratification seen in the *tabular-bedded to low-angle cross-bedded and ripple cross-laminated quartz-feldspar sandstone facies* of the CF. Intercalations of matrix- to clast-supported pebbly

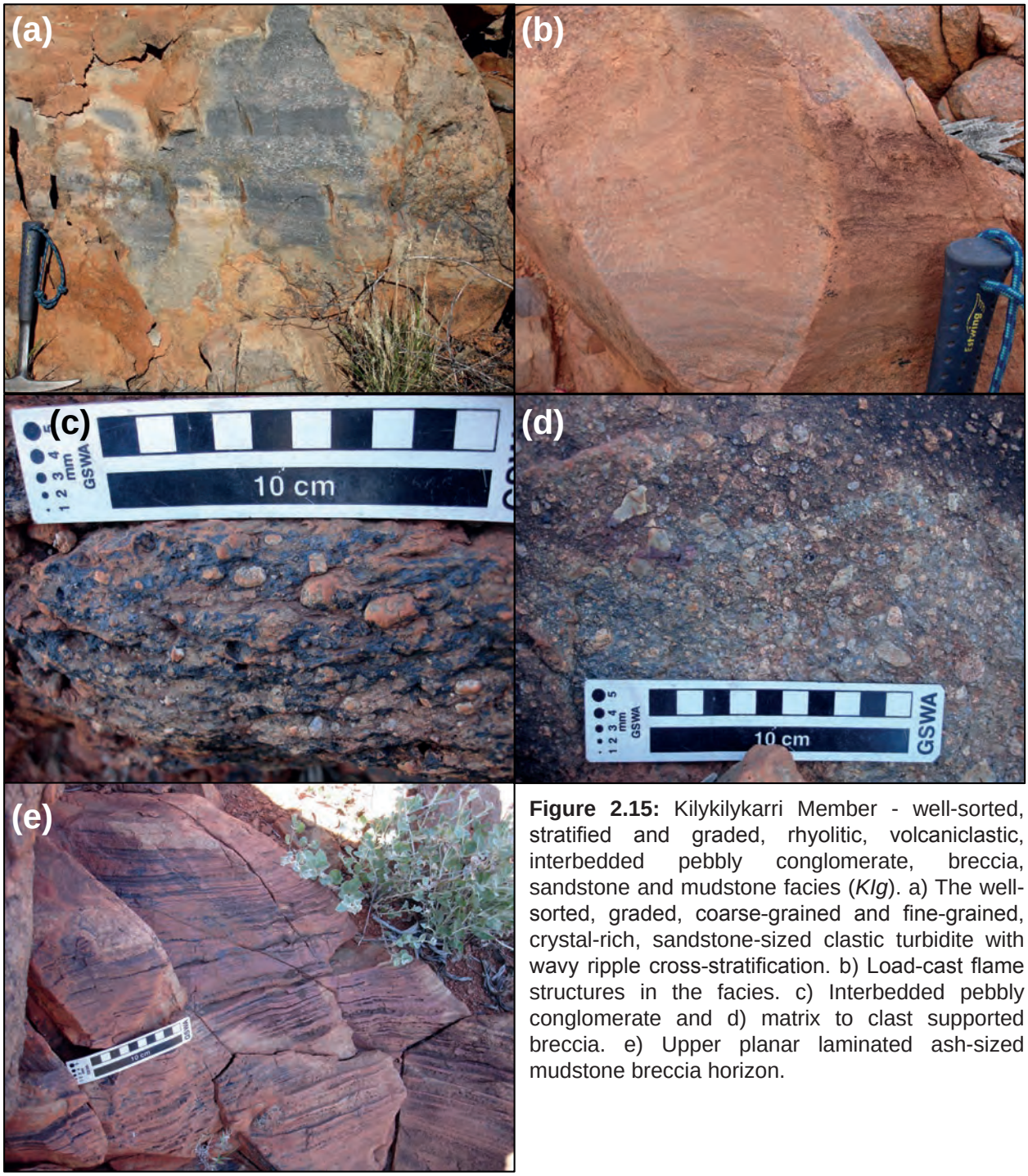

Figure 2.15: Kilykilykarri Member - well-sorted, stratified and graded, rhyolitic, volcaniclastic, interbedded pebbly conglomerate, breccia, sandstone and mudstone facies (*Klg*). a) The well-sorted, graded, coarse-grained and fine-grained, crystal-rich, sandstone-sized clastic turbidite with wavy ripple cross-stratification. b) Load-cast flame structures in the facies. c) Interbedded pebbly conglomerate and d) matrix to clast supported breccia. e) Upper planar laminated ash-sized mudstone breccia horizon.

conglomerates (Fig. 2.15c) and breccias (Fig. 2.15d) with sub-angular to rounded clasts of feldspar and quartz are frequent. Planar laminated mudstone intervals (up to 40 cm thick) occur towards the top of the facies (Fig. 2.15e).

This facies is capped by an approximately 50 m thick stratiform porphyritic rhyolite facies that extends laterally for approximately 2 km and is very similar to the *quartz-feldspar porphyritic rhyolite facies* of the RS. The contact with the underlying *well-sorted, stratified and graded, rhyolitic, volcaniclastic interbedded pebbly breccia, sandstone and mudstone facies* (*Klg*), although highly weathered and altered, is sharp and irregular, and appears to be stratiform to cross-cutting in places.

Interpretation:

The rounding of clasts, bedded nature, sorting and graded nature of the intervals within this facies is characteristic of a sedimentary deposit. The clastic quartz-feldspar detrital composition is most likely sourced from the underlying ignimbrites, making this facies a stratified volcaniclastic deposit, possibly of an epiclastic nature. The presence of graded bedding, load-cast and flame structures, convolute bedding and the well-sorted nature of the horizons are all consistent with deposition in a subaqueous environment by turbidity currents (Boggs, 1987; Nichols, 2009). This is supported by the alternating succession of graded coarse- to fine-grained sandstone intervals present throughout the facies (Fig. 2.15a), typical of a series of upward-fining Bouma sequences consistent with clastic turbidite deposition (Bouma, 1962; Shanmugam, 1997). The presence of convex-up stratifications, interpreted to be hummocky cross-stratification, is again indicative of relatively shallow-water conditions and deposition below the fair-weather wave base, as discussed in the interpretation of the *tabular-bedded to low-angle cross-bedded and ripple cross-laminated quartz-feldspar sandstone facies* in the CF (*Section 2.3.1.3*) The alternating coarse- and fine-grained intervals, intercalated pebbly conglomerates and breccias and fine-grained planar laminated intervals, indicate a succession of constantly changing energy events into a normally low-energy ambient environment, as represented by ash-mudstone intercalations. The pebbly conglomerates and breccias were formed by debris or high-concentration turbidity flows that transported volcaniclastic material derived from a shoreline to a relatively shallow-water offshore shelf-type setting, represented by the turbidite beds, whereas the upper planar laminated mudstone-ash horizons represent deeper water. This suggests that this facies represents a series of subaqueous volcaniclastic turbidites of ash-to-lapilli sized fragments with interbedded debris flow deposits and provides evidence of transgression and a deepening shallow-water environment, after the deposition of the KI, such as a shallow offshore environment, with nearby unstable slopes, such as those surrounding caldera walls, where instability and failure causes the formation of the interbedded conglomerate and breccia horizons.

This facies is similar to a subaqueous ash-turbidites deposited in the Onikobe caldera lake, Japan (Yamada, 1973), parts of the volcaniclastic sediments of the Ordovician Lower Rhyolitic Tuff, Garth Tuff and Pitts Head Tuff formations, North Wales, U.K. (Fritz *et al*., 1990; Fritz and Howells, 1991; Kokelaar and Koeniger, 2000); and thin bedded facies of the Mineral King caldera-complex, Sierra Nevada (Busby-Spera, 1986).

The stratiform coherent porphyritic rhyolite facies that caps these volcaniclastic sediments is mineralogically and texturally similar to the intrusive porphyritic rhyolite facies of the RS (described above), suggesting a link between the two. There is no evidence of sediment fluidisation and/or quench fragmentation on the basal contact of this facies with the underlying sediments, suggesting that the intrusion is much younger

than the Kilykilykarri Member, supported by a cross-cutting relationship. In Chapter 3 it was demonstrated that the numerous porphyritic rhyolites, which intrude into the PCG, are geochemically identical to one another, as well as being cogenetic with the magmas of the KI, therefore this facies is part of the same RS underlying the KI and has intruded into the sediments of Kilykilykarri Member.

2.4. Discussion

2.4.1 The Kathleen caldera and its caldera-filling succession

The four facies that make up the Kurrparu Member all have gradational contacts, meaning the ignimbritic *main facies zone* (*KIc*) is genetically related to other facies. This, coupled with the lack of any clear depositional breaks until the start of the Karlaya Member, means that all four facies define a single ignimbrite deposit with a combined minimum thickness of approximately 500 m. Such a thick, large volume ignimbrite deposit is usually sourced from an explosive caldera-forming eruption (Williams, 1941; Gorshkov, 1963; Cas and Wright, 1987). Ignimbrites are thought to originate along continuous ring fissures that bound these caldera structures (Cas and Wright, 1987; Lipman, 2000a) and ignimbrites are either deposited as thick, ponded, intra-caldera deposits bound by outward-dipping ring faults within the caldera, or as thinner, outward radiating extra-caldera outflow sheets on the flanks of the caldera. The key criteria in establishing whether or not an ignimbrite deposit represents intra- or extra-caldera deposits in the absence of a clearly defined caldera structure, are the thickness and welding intensity of the deposit (Lipman, 1984). Extra-caldera outflow sheets rarely attain a thickness in excess of 200 m (Cas and Wright, 1987), whereas the syn-eruptive subsidence of the caldera floor facilitates ponding of pyroclastic flows in the confined space of the collapsing caldera depression, meaning that intra-caldera ignimbrite deposits can attain thicknesses in excess of hundreds of metres to kilometres in thickness (Lipman, 1984; Cas and Wright, 1987; Branney and Kokelaar, 2002). Intra-caldera ignimbrites are often characterised by densely welded basal sections (Lipman, 1984), and the significant thickness and extremely high-grade of welding of the Kurrparu Member is consistent with an intra-caldera ignimbrite deposit. U-Pb SHRIMP dating on zircons from the *main facies zone* (*KIc*) yielded an age of 1071 ± 5 Ma (Chapter 3) for this ignimbrite deposit, indicating that at least one explosive caldera forming eruption took place ca. 1070 Ma during the deposition of the PCG. The interpreted caldera is hereafter referred to as the Kathleen caldera.

Calderas tend not to form in isolation but as parts of more extensive provinces dominated by numerous nested caldera structures, such as the Yellowstone Caldera Complex (Girard and Stix, 2009c; Yates and Ellis, 2012), the San Juan caldera system (Lipman, 2000b; Lipman and McIntosh, 2008), and the Taupo Volcanic Zone, New

Zealand caldera complex (Wilson *et al*., 1995). The Kathleen caldera could therefore provide evidence for a larger explosive caldera system within the Bentley Supergroup during the Giles and Ngaanyatjarra Rift events.

2.4.1.1 Volume estimates

The absence of 3-dimensional spatial information for the Kathleen caldera means that it is difficult to estimate the volume of erupted material from the Kathleen caldera, although the known dimensions of just the Kurrparu Member (thickness of >500 m, lateral extent of >22 km) yields a minimum intra-caldera volume of 190 km^3, based on the assumption that the third dimension was the same as the preserved lateral dimension. This calculation assumes a roughly circular caldera structure with a diameter of 22 kilometres. The lack of preservation of any extra-caldera outflow or ash fall-out deposits that would have been associated with the caldera-forming Kathleen eruption means that it is not possible to accurately estimate the total volume of erupted material from the eruption. It has been suggested that intra-caldera volumes are roughly equal to extra-caldera volumes and extra-caldera volumes are approximately equal to some ash fall-out volumes (Sparks and Walker, 1977; Lipman, 1984; Mason, *et al*., 2004), giving a proposed minimum total volume of erupted material for the Kathleen eruption of ~380 km^3 (excluding any possible ash fall-out volumes due to inferred eruption style). This defines a very large volcanic eruption with a magnitude (Mason *et al*., 2004) or VEI (Volcanic Explosivity Index; Newhall and Self, 1982) of 7 or greater, similar to that of Campanian Tuff (Italy) or Tambora (Indonesia) eruptions (Self, 2006). Smithies *et al*., 2014 has suggested that the KI represents a super-eruption (>450 km^3 erupted material) type deposit, which is quite possible if an associated ash fall-out volume for the eruption is also assumed.

2.4.2 The Kathleen Ignimbrite: a rheomorphic lava-like intra-caldera succession

Ignimbrites can be welded or non-welded and can exhibit varying degrees of welding within a single deposit (Smith, 1960a; 1960b; Ross and Smith, 1961; Briggs, 1976; Duffield and Dalrymple, 1990; Sparks *et al*., 1999; Carey and Sigurdsson, 2007). A sustained explosive event produces multiple pyroclastic flows that progressively aggrade (Branney and Kokelaar, 1992; 2002) to form a continuous succession of rapidly stacked isothermal sheets that form a single simple cooling unit (Smith, 1960b; Ross and Smith, 1961; Riehle, 1973; Riehle *et al*., 1995; 2010), where the differing degrees of welding intensity define distinct facies or vertical variations within a single pyroclastic flow deposit.

The changes in crystal content, mineralogy, and texture of the KI up through the sequence define a crude vertical stratification that starts with the crystal-poor base, mixed crystal-rich and -poor *main facies zone* (*KIc*) and a crystal-poor upper facies of

the Kurrparu Member. This is overlain by the multiply stacked, K-feldspar-rich ignimbrites of the Karlaya Member and the uppermost stratified volcaniclastic Kilykilykarri Member, supporting the progressive or incremental aggradation model of ignimbrite deposition for this succession (Branney and Kokelaar, 1992; 2002) and can be interpreted as a single simple cooling unit.

The ignimbrite classification scheme of Branney and Kokelaar (1992); modified from Walker, (1983) is based on the proportion and the intensity of welding within particular ignimbrite deposits, and has classes that range from non-welded through to rheomorphic lava-like ignimbrites. The KI is clearly welded, as evidenced by the abundant fiamme, the presence of eutaxitic textures and the pervasive planar fabric within the formation. In addition, the presence of a basal, lava-like, rheomorphic ignimbrite facies (*KIb*) within the Kurrparu Member suggests that this deposit underwent the highest degree and grade of welding-compaction. This involves the coalescence of ash particles and pumice clasts, the obliteration of any pyroclast outlines and the development of an apparent coherent texture within the originally fragmental lithofacies (Branney and Kokelaar, 2002). This therefore indicates that the KI is an '*extremely high-grade*' ignimbrite within the classification of Branney and Kokelaar (1992) and is therefore classified as a lava-like rheomorphic ignimbrite deposit. Other examples of facies associations that exhibit an extremely high-grade, lava-like rheomorphic facies, include the Trans-Pecos Volcanic Field in Texas (Henry *et al*., 1988), Airy's Bridge Formation in the Lake District, UK (Branney *et al*., 1992), and the Snake River Plain volcanic province of southwestern Idaho (Ekren *et al*., 1984; Bonnichsen and Kauffman, 1987; Branney *et al*., 1992; Andrews and Branney, 2011).

2.4.3 Rheomorphism: the deceptive phenomenon of imparting an apparent coherent rock texture in a pyroclastic rock

There has been much discussion in the literature regarding lava-like silicic facies in volcanic fields and their origins, including whether or not these represent true lavas or extremely high-grade rheomorphic ignimbrites in the absence of clear vitriclastic textures (see. Cas, 1978; Cleverly and Bristow, 1982; Ekren *et al*., 1984; Branney *et al*., 1986; Hausback, 1987; Henry *et al*., 1988; Milner *et al*., 1992; Manley, 1995; 1996; Kirstein *et al*., 2001; Andrews and Branney, 2011). Rheomorphism is particularly deceptive in that it obliterates primary vitriclastic textures imparting an apparent coherent (i.e. lava-like) texture making it in some instances, virtually impossible to distinguish between the two (Branney *et al*., 1992).

In the case of the Kurrparu member of the KI, it was not possible to identify all of the key criteria used to distinguish between silicic lavas and rheomorphic ignimbrites (see

Bonnichsen and Kauffman 1987; Henry and Wolff 1992; Andrews and Branney, 2011), as either they were not present, not preserved, or not applicable. Arguments for a silicic lava interpretation for the Kurrparu member is the lack of pervasive relict shard textures, the basal lava-like facies, and the pervasive presence of autoclastic breccia along the basal contact of the member, as these features are commonly associated with and considered diagnostic of silicic lavas. However it has been shown, that the basal autoclastic breccia is actually hyaloclastite and the lava-like facies is ignimbritic through association with the *main facies* zone (*KIc*) (see *Section 2.3.3.1.1*). The lack of pervasive relict shard textures remains a problem, however our interpretation is that the high degree of welding and subsequent devitrification and recrystallization of the deposit destroyed any delicate primary glass shard textures that may have been present in the Kurrparu Member, and that the unequivocal vitriclastic, shard textures, found in the western section of the Karlaya Member, may indeed be part of the underlying Kurrparu Member, as it is quite difficult to distinguish the two members apart from one another in the western section. On balance, the preserved characteristics thereby support a fragmental pyroclastic flow origin for the entire KI (including the Kurrparu Member), despite the misleading apparently coherent textures imparted by rheomorphism on some of its facies.

2.4.4 Palaeoenvironmental setting of the Kathleen Ignimbrite

The CF formed in a shallow-water setting within a proximal offshore to lower foreshore to shoreface type transitional basin or depositional environment, similar to that of the Ordovician Lower Rhyolitic Tuff Formation, Pitts Head Tuff Formation, and Garth Tuff Formation of North Wales, UK (Reedman *et al*., 1987a; Fritz *et al*., 1990; Fritz and Howells, 1991). The *tabular-bedded to low-angle cross-bedded and ripple cross-laminated quartz-feldspar sandstone facies* directly underlying the KI formed in shallow water (<50 m). The contact between the top of the CF and the KI appears to be conformable as the underlying CF sediments were wet and weakly consolidated during ignimbrite deposition, as evidenced by the quench fragmented hyaloclastite and peperitic base of the Kathleen Ignimbrite. The fluidisation of wet sediments is also supported by the presence of intrusive clastic dykes and dykelets (Kokelaar, 1982) along the base of the KI that extend upwards into the volcanic succession. This suggests that the initial thick intra-caldera pyroclastic flows were emplaced contemporaneously with the sedimentary rocks of the CF, and therefore the base of the ignimbrite was emplaced in a shallow-water setting. Given that the inferred water depth was <50 m and the ignimbrite is >500 m thick, much of the ignimbrite may not have “seen” water during emplacement. However, the stratified volcaniclastic sediments of the Kilykilykarri Member, which overlies the Kurrparu and Karlaya ignimbrites, represent volcaniclastic turbidite, debris flow, and pebble breccia deposits that were deposited within an offshore shallow-water environment, most likely originating from failure or instability of the Kathleen caldera rim during late-stage caldera collapse.

The existence of subaqueous depositional environments in the lower parts of the Talbot Sub-basin prior to the deposition of the CF is supported by drilling from a site to the east of the study area in the underlying upper Mount Palgrave Group. This drilling intersected pillow basalts associated with sedimentary rocks very similar to those of the CF. Contemporaneous deposition of the KI and the CF in a relatively shallow-water setting indicates that the initial emplacement of the thick intra-caldera rheomorphic Kurrparu Member of the Kathleen Ignimbrite Formation took place in a subaqueous environment; in comparison, the upper surface of the formation was probably subaerially exposed, as the ~500 m thick ignimbrite would have displaced the inferred shallow water (<50 m deep) shoreline, unless the rate of caldera subsidence exceeded the accumulation rate of the ignimbrite. Evidence for a delayed shoreline transgression (i.e. post deposition and cooling) is provided by subaqueous deposition of the overlying stratified volcaniclastic sediments of the Kilykilykarri Member and the lack of quench fragmented facies in the uppermost parts of the Kurrparu and Karlaya ignimbrites.

2.4.5 Subaqueous rheomorphism: A rare phenomenon

Subaqueous pyroclastic flows and the effect of water on welding in these ignimbrites remains a contentious topic (e.g., Yamada, 1973; Sparks *et al*., 1980a; 1980b; 1999; Howells *et al*., 1986; Orton *et al*., 1987; Reedman *et al*., 1987a; Whitham, 1989; Cas *et al*., 1990; Sigurdsson *et al*., 1990; Cas and Wright, 1991; Kokelaar and Busby, 1992; Fritz and Stillman, 1996; Kokelaar and Koeniger, 2000; Legros and Druitt, 2000; Freundt, 2003; Keating, 2005; Trofimovs *et al*., 2006; 2008). It is argued that the majority of pyroclastic flows in subaqueous settings do not actually support hot emplacement and a subaqueous depositional environment involving the entire ignimbrite being totally submerged at the time of deposition, with the only examples to date being the Ordovician shallow-marine ignimbrites of Ireland and Wales, and the Miocene ignimbrites of southwest Japan, both of which formed from subaerially erupted pyroclastic flows that moved into shallow water (Cas and Wright, 1991). Santorini provides a modern example of caldera-forming ignimbrites being erupted in subaqueous environments, although the majority of research into the volcanism on Santorini has focused on subaerial deposits, with little research on subaqueous deposits, and none specifically addressing the welding of subaqueous pyroclastic flows (Friedrich *et al*., 1988; Druitt *et al*., 1997; 1999; Carey and Sigurdsson, 2007).

Very little research has been undertaken on rheomorphic ignimbrites in subaqueous environments, leading to a commonly held notion that it is not possible to maintain the heat required for a pyroclastic deposit to undergo the high grades of welding associated with rheomorphism in a subaqueous setting. Sparks *et al*. (1980a; 1980b) identified subaqueous welding in a modern welded tuff off Dominca, in the Lesser Antilles, and

proposed that subaqueous environments may be more favourable to welding than many subaerial environments, primarily as a result of the reduction of viscosity by the dissolution of steam into rhyolitic glass (Kokelaar 1982), although it should be noted that Cas and Wright (1991) disputed the hot state of emplacement and type of deposit for this Dominican tuff. If Sparks *et al*. (1980a; 1980b) were correct it is likely that more cases of subaqueous intensely welded, extremely high-grade ignimbrites (i.e. rheomorphic ignimbrites) would have been recorded. This is not the case, as the single documented example of a subaqueous rheomorphic ignimbrite is the Pitts Head Tuff of North Wales, UK (Kokelaar and Koeniger, 2000), where an extra-caldera ignimbrite outflow sheet was erupted subaerially and flowed into a shallow sea for about 3–4 km, displacing the original shoreline, progressively aggrading and in places undergoing rheomorphic welding, the majority of which initially took place under water.

The KI satisfies some of the criteria for subaqueous pyroclastic flows of Cas and Wright (1991), undergoing hot emplacement, as evidenced by the extremely high degree of welding in the deposit, although it is likely that the ignimbrite was not completely submerged as only the initial emplacement of the intra-caldera ignimbrite records evidence of contact with a subaqueous environment. The KI represents the oldest documented case, thus far, of a *lava-like* rheomorphic *intra-caldera* ignimbrite and the first documented case of emplaced within an initially subaqueous environment. This is unlike both the Ordovician Pitts Head Tuff, which is an *extra-caldera* ignimbrite and not as intensely rheomorphic, and the *subaerially emplaced* intra-caldera lava-like rheomorphic Ordovician Bad Step Tuff, Lake District, UK (Branney *et al*., 1992).

2.4.6 The relationship between the Rowland Suite and the Kathleen Ignimbrite

This study has shown that the Rowland Suite intruded contemporaneously with deposition of the CF and eruption of the KI, so the question is what is the relationship, other than spatial, between the RS and the KI, if any? Numerous examples can be found where the emplacement of comagmatic rhyolites are associated with caldera formation and the resurgence of an underlying magma chamber is an accepted part of numerous caldera formation models (e.g., Lipman, 1984; Sparks *et al*., 1985; Campbell *et al*., 1987; Cas and Wright, 1987). Campbell *et al*. (1987) document rhyolitic deep-seated dykes, sills and shallow-level intrusive domes that are intimately associated with the formation and evolution of the Lower Rhyolitic Tuff Formation Caldera, North Wales, UK. These intrusions either preceded caldera eruption, were intruded during caldera resurgence, or were associated with the final stages of caldera evolution. One possible model for the rhyolite intrusion below the Kathleen caldera is provided by Sparks *et al*. (1985), who document the impeding of a resurgent magma beneath a thick intra-caldera ignimbrite at Cerro Galan, Chile, which lead to the formation of a shallow-level intrusion directly beneath

the caldera. Such a model can explain the relationships seen within the Kathleen caldera and the intra-caldera KI sequence, where contemporaneous local rhyolite intrusions from the RS, that are both mineralogically and compositionally similar to the rhyolitic KI and shown to have been derived through a process of extended fractional crystallisation from a common shared recharging magma chamber or reservoir to that of the ignimbrites (Chapter 3), may also be intimately associated with the evolution of the Kathleen caldera during possible late-stage resurgent activity in the underlying caldera magma chamber. Through this coeval, comagmatic and cogenetic relationship (Chapter 3) it is possible to constrain a Kathleen caldera forming eruption age to somewhere between 1070 and 1066 Ma and further extended this relationship to include all the porphyritic rhyolite intrusions in the PCG.

The fact that intrusive RS underlying the KI did not pass through a few tens of metres of the overlying CF sediments suggests that the intrusion had reached its neutral buoyancy level within the relatively weakly consolidated sedimentary pile of the CF. This is consistent with a post-KI emplacement for the underlying RS intrusion.

2.4.7 Snake-River type volcanism in the west Musgrave Province

Branney *et al*. (2008) proposed a very specific type of continental rhyolitic volcanism known as Snake-River (SR)-type volcanism, based on the Central Snake River Plain Volcanic Province of central-westernern America. SR-type volcanism is similar to the volcanism recorded by the Pussy Cat Group succession in that both include large-volume, lithic-poor rhyolitic ignimbrites, intense, high-grade welding, including rheomorphism, the widespread development of rheomorphic lava-like facies within ignimbrites (i.e. the *planar and fold laminated rhyolite facies* of the Kurrparu Member), extensive, fines-rich ash deposits (i.e. the Kilykilykarri Member) and emplacement in subaqueous (lacustrine to alluvial) environments (i.e. palaeoenvironments of the CF and Kilykilykarri Member). In addition, Andrews *et al*. (2008) state that SR-type rheomorphic ignimbrites exhibit common diagnostic features including dense welding with little remnant porosity, sparse post-welding vesiculation, curvilinear rheomorphic folds, well-developed flow-banding or laminations, intense elongation lineations, and upper and lower vitrophyres and spherulitic zones that overlie parallel-laminated, partially fused, ash-fall tuffs; they lack basal autobreccias but have locally autobrecciated upper surfaces. Although the KI is significantly older than the SR volcanism, and is devitrified and slightly metamorphosed, it still exhibits all of the above characteristics barring the underlying parallel-laminated, partially fused, ash-fall tuffs. This strongly suggests that the PCG succession closely resembles SR-type volcanism, and could represent another type locality for this type of magmatism. This is corroborated by Smithies *et al*. (2013), who have expanded this interpretation to include all felsic volcanism within the Talbot Sub-basin of the west

Musgrave Province, demonstrating the existence of widespread Mesoproterozoic SR-type volcanism.

2.5 Emplacement history and eruption model for the caldera-forming Kathleen Ignimbrite sequence

This emplacement history for the KI sequence is based on the descriptions and interpretations of the various facies shown on the schematic log shown in Fig. 2.4 and demonstrated on the eruption model shown in Fig. 2.16:

(1) The KI was emplaced in a subaqueous shallow-water environment contemporaneous with deposition of the underlying CF and the overlying volcaniclastic sediments. This most likely occurred in a shallow-water shelf- or large lake-type setting, even possibly a large pre-existing caldera-lake or rift-lake type palaeoenvironment.

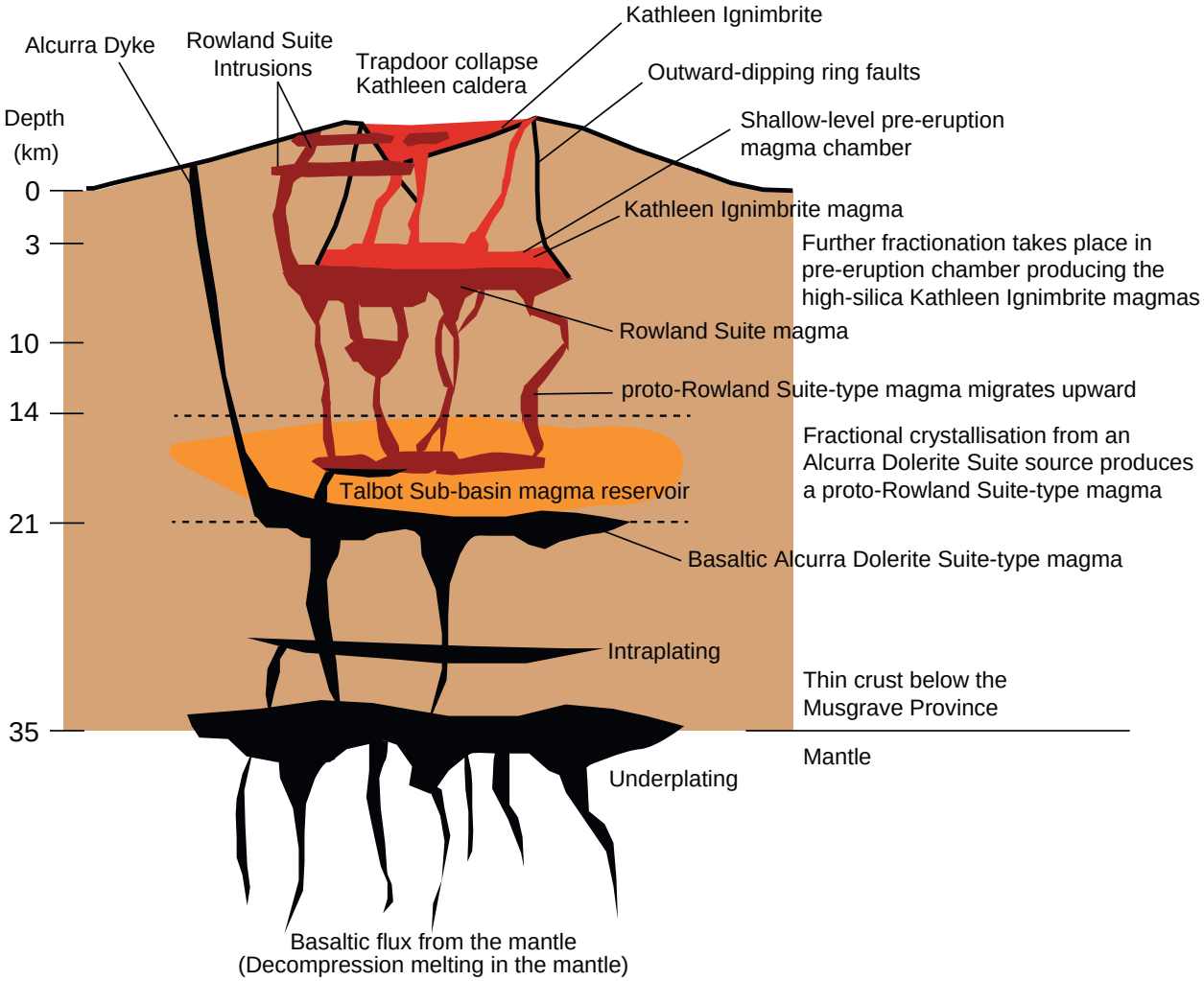

Figure 2.16: A schematic diagram illustrating the emplacement model for the rhyolites of the Pussy Cat Group, showing the Talbot Sub-basin magma reservoir at mid-crustal depths, feeding the shallow upper-crustal magma chamber, underlying the Kathleen caldera, from which the evolved and differentiated Pussy Cat Group rhyolites erupt (adapted from de Silva *et al*., 2006, Folkes *et al*., 2011).

(2) A caldera by definition requires a shallow sub-volcanic magma chamber with a minimum size that is at least the volume of extruded pyroclastic material and at least the preserved dimension of the Kathleen caldera. This suggests the existence of a shallow (~3–10 km; (Chapter 3)) magma chamber ≥22 km in diameter (≥390 km^3 in volume) below the Kathleen caldera prior to eruption of the KI and intrusion of the RS.

(3) The presence of both crystal-rich and aphyric fiamme at varying levels of the stratigraphy within the KI indicates the contemporaneous existence and eruption of two separate cogenetic rhyolitic magmas (Chapter 3). It can be speculated that the injection of a higher-temperature, aphyric magma (at or near liquidus temperature) into a magma chamber containing already cooled and highly crystallised magma (>30% crystals and below liquidus temperature) may have either triggered the Kathleen eruption (de Silva *et al*., 2008; Gerard and Stix, 2009a; 2009b; Wright *et al*., 2011) or primed the magma chamber to erupt, pending an external trigger, such as a tectonic earthquake or faulting during the extensional Ngaanyatjarra rifting. The heat of the near-liquidus temperature magma intruding the sub-liquidus temperature crystallised magma may have initiated volatile exsolution in the latter, in addition to any new volatiles the former may have introduced to the chamber. The crystal-rich magma may already have been close to volatile saturation due its high degree of crystallisation. Such contemporaneous dual magma batches have been documented in other caldera forming systems (e.g., Bachmann *et al*., 2000a; 2005; Bachmann and Bergantz, 2004; de Silva *et al*., 2008) including suggestions that the hotter recharge magma could have catalysed eruption of the cooler crystallised magma. Alternatively the aphyric magmas could represent tapping of a more evolved, fractionated, low-density melt-rich cap, while the crystal-rich magmas, have tapped a deeper basal, more primitive, high-density crystal-mush cumulate; both or which are cogenetic and originate from within a common stratified magma chamber as invoked by Deering *et al*. (2011) for the Ammonia Tanks Tuff, southwest Nevada, and shown in Chapter 3 to be a viable model for this system.

(4) Over-pressuring of the magma chamber combined with a trigger mechanism caused instantaneous depressurisation of the large rhyolitic magma chamber resulting in a very large explosive, caldera-forming eruption of at least a magnitude or VEI of 7.

(5) The lack of an apparent basal ash fall-out deposit meant that this eruption most likely involved immediate low pyroclastic fountaining without the development of a high eruption column from the start of the eruption, in a ‘boil-over’ eruption (Cas and Wright, 1987; Branney and Kokelaar, 2002). This is similar to the eruption style proposed for the rheomorphic ignimbrites of the Snake River Plain Volcanic Province of southern Idaho and northern Nevada, USA (e.g., Andrews and Branney, 2011), and would have generated a very hot, sustained quasi-steady

pyroclastic density current associated with a continuously collapsing, low and unsteady eruption column (Sparks and Wilson, 1976; Sparks *et al*., 1978; Branney and Kokelaar, 2002; Andrews and Branney, 2011).

(6) The initial magma to erupt was the near-liquidus temperature, aphyric magma (facies *KIa* and *KIb*). This originated either from the low-density melt-rich cap or a recharge magma coming from a deeper reservoir than the Kathleen magma chamber, and because of its higher temperature and buoyancy, it was able to ascend quicker and erupt first. The passage of a hot, recharging, buoyant aphyric magma through the crystal-rich cumulate magma, or the tapping of a hotter aphyric melt-rich cap, would both have destabilised the zoned magma chamber, ensuring mixing and forcing "draw-up" of the initially denser, vesiculating crystal-rich magma cumulate into the eruption conduit and vent system. The later part of the eruption involved simultaneous eruption of both magmas (facies *KIc*), followed by the eruption of the aphyric magma again (facies *KId*) and finally eruption and intrusion of the more crystal-rich magma cumulate (facies *KIf* and the RS).

(7) The ensuing collapse of the roof block of the caldera into the underlying magma chamber along outward-dipping ring dykes either during trap-door or hinged downsag style collapse (Lipman, 1984; 1997; 2000a), provided the slope that was essential for rheomorphic flow, as well as a volcano-tectonic depression that allowed the sustained pyroclastic density currents to pool, pond and progressively aggrade forming a thick stack of flows.

(8) Initial emplacement of the thick Kurrparu Member pyroclastic flows into the shallow-water (13–50 m deep) setting of CF is associated with little disruption of the underlying wet sediments and no evidence for phreatic explosions. This could be due to film boiling, where fairly stable boundary conditions are created by the formation of a sheath-like film or carapace of water vapour (Leidenfrost effect; Walker, 1977; Mills, 1984; Howells *et al*., 1985), that insulates the hot, gas-supported, high-particle concentration pyroclastic flow to a certain degree, allowing very little mixing and ingestion of water. Alternatively both welding and rheomorphism could have already taken place prior to contact with the water, creating a denser, less impermeable ignimbrite that then entered the shallow-water environment with little ingestion of water upon contact (Sparks *et al*., 1980b; Mcleod *et al*., 1999). Caldera subsidence was most likely coincident with or slightly behind the rate of ignimbrite deposition or the eruption mass discharge rate, causing shoreline displacement (Legros and Druitt, 2000) as a result of an initial water depth of <50 m and an intra-caldera ignimbrite thickness of at least 500 m. This suggests that the upper parts of the KI were probably subaerially exposed until deposition of the Kilykilykarri Member.

(9) Progressive and rapid aggradation of the intra-caldera pyroclastic flow deposits would have caused the deposits to retain sufficient heat to allow welding and

agglutination of the ignimbrite deposit into a non-particulate state. This would have occurred both during and after-emplacement, with ponding and pooling of the ignimbrite within the caldera, greatly aiding in retaining heat. This period of eruption also generated quench fragmented hyaloclastites along the base of the ignimbrite deposit during rheomorphic flow over the wet substrate.

(10) The deposition of the welded eutaxitic but not rheomorphic Karlaya Member ignimbrites above the Kurrparu Member indicate on-going caldera collapse and volcano-tectonic instability with their associated co-ignimbrite lag breccia deposits and may signal a slight change in the eruption style of the Kathleen caldera due to the difference in welded grade. It is also possible that these thinner pyroclastic flows may represent outflows from an adjacent nested caldera-forming eruption as does commonly occur in caldera systems or complexes (Lipman, 2000a; Cole *et al*., 2005).

(11) The shallow-water setting of upper Kilykilykarri Member records transgression of a shoreline after cooling of the underlying ignimbrites and final subsidence of the caldera, which could have occurred after the end of the eruption. These volcaniclastic turbidites and debris flows were formed during subaqueous resedimentation of proximally sourced pyroclastic material, most likely derived from the Kathleen caldera rim walls.

(12) Possible late-stage resurgent activity in the magma chamber below the Kathleen caldera resulted in the intrusion of the coeval and comagmatic, crystal-rich RS rhyolite intrusions from the same magma chamber as the KI magmas, as it has been shown that these are the cogenetic products of extended fractional crystallisation (Chapter 3).

It is unclear whether the Kathleen caldera eruption was fully subaqueous or largely subaerial, although the basal section of the KI was emplaced subaqueously. This is similar to the model of Cas and Wright (1987; 1991), who proposed that subaqueous emplacement of a pyroclastic flow may be the result of subaqueous explosive eruption of vesiculating rhyolitic magma at shallow water depths (<1 km) associated with high eruption rates, syn-eruption basement subsidence (i.e. caldera formation) and the ponding of an intra-caldera ignimbrite.

In summary, the KI sequence records the oldest documented case of an intra-caldera, lava-like rheomorphic ignimbrite and the first-documented case of an intra-caldera lava-like rheomorphic ignimbrite that was initially emplaced in a subaqueous environment. The volcanic setting in which the formation occurs, and the ignimbrites themselves, are similar to the Snake River (SR)-type volcanism and related ignimbrites of central-western America.

2.6 Conclusions

- The KI is part of a Mesoproterozoic ~1 km thick, rhyolitic, ignimbrite-dominated volcanic-sedimentary succession that formed during a very large, explosive, caldera-forming, felsic eruption at ca. 1070 Ma in central Australia.
- It is dominated by the ~500 m thick (minimum), intra-caldera, lava-like rheomorphic to normally welded Kurrparu Member. This member represents a simple, single cooling unit with multiple facies that range from intensely high-grade lava-like rheomorphic welding to normal eutaxitic welding conditions.
- The KI volcanic succession conformably overlies shallow-water (<50 m), volcaniclastic-sedimentary, turbidite shelf-type or large lake-type sediments of the upper CF. The initial emplacement of the KI and possibly the initial eruption of the Kathleen caldera, was within this shallow-water subaqueous palaeoenvironment. The upper parts of the thick intra-caldera Kurrparu Member were subaerially exposed as a result of shoreline displacement/regression, and the overlying Kilykilykarri Member records shoreline transgression and the inundation of caldera with the return of a shallow-water palaeoenvironment.
- The coeval and comagmatic RS intrusion underlying the KI may represent late-stage resurgent activity in the magma chamber below the Kathleen caldera.
- The formation and emplacement of such a highly welded (i.e. lava-like rheomorphic) pyroclastic flow in subaqueous conditions is highly unusual, making the KI a rare example of a subaqueous pyroclastic flow deposit that has unequivocal pyroclastic characteristics and records a hot state of emplacement and rheomorphism, within an initially subaqueous depositional environment.
- The KI eruption was a high-temperature, felsic, explosive, caldera-forming boil-over type eruption, characterised by a sustained, low, continuously collapsing, ignimbrite-forming, eruption column, and the deposition of a thick, high-temperature, low-viscosity, progressively aggrading, pyroclastic flow.
- The eruption involved at least two types of magmas, represented by the two pumice populations (i.e. crystal-rich and aphyric), the two crystal-poor basal facies, the mixed crystal-rich and -poor *main facies zone*, the upper crystal-poor facies of the Kurrparu Member, the eutaxitic, two pumice bearing crystal-rich ignimbrite facies of the Karlaya Member and lastly the underlying coeval and comagmatic, crystal-rich RS rhyolite intrusion. These facies define a crude vertical stratification within KI and are interpreted to be cogenetic and to have come from a stratified common magma chamber or reservoir, with the aphyric magma either a melt-rich cap or a hot silicic recharge magma and the crystal-rich magma representing the cumulate portion.
- A continuously subsiding, sloped, volcano-tectonic depression allowed progressive aggradation of the pyroclastic flows and ponding. This was an ideal environment for

a thick, heat-retaining intra-caldera ignimbrite deposit to develop non-particulate flow conditions and lava-like rheomorphism.

- The Kathleen caldera provides unequivocal evidence for at least one very large caldera-forming eruption in the west Musgrave Province with a minimum diameter of ~22 km and intra-caldera volume of 190 km^3 and it is likely that the Kathleen caldera was part of a once even larger, nested caldera complex in the Talbot Sub-basin of the west Musgrave Province, with a high-likelihood of a supereruption or supervolcano. This coupled with evidence for more widespread and long-lived (>30 Ma) felsic magmatism in the Talbot Sub-basin, supports the recognition of a large silicic igneous volcanic province in the west Musgrave Province, much like the Yellowstone Caldera-Complex and Snake River Plain volcanic province of central-western America.
- When comparing the KI to other known and documented ignimbrite deposits, it shares similar palaeoenvironmental settings to the Ordovician *intra-caldera* Lower Rhyolitic Tuff, Garth Tuff, Capel Curig formations and one of the *extra-caldera* rheomorphic outflow sheets of the Pitts Head Tuff, North Wales, UK, as well as the Mineral King Monarch Tuff, Sierra Nevada, USA. It also shares many of the characteristics of other lava-like, rheomorphic ignimbrites such as the intra-caldera Bad Step Tuff Formation, English Lake District, UK and the extra-caldera Grey's Landing ignimbrite, southern Idaho, USA.

2.7 Acknowledgements

I acknowledge the Geological Survey of Western Australia (GSWA) for their funding, resources and logistical support to make this research project possible; the Ngaanyatjarra Council and their people for the privilege and unique opportunity to conduct this research on their traditional lands; various GSWA field assistants; and Monash Volcanology Research Group (MonVolc) for support and additional research funding.

2.8 References

Adams, S.F., 1920. A microscopic study of vein quartz. Economic Geology and the Bulletin of the Society of Economic Geologists, 15(8): 623-664.

Aigner, T., 1985. Storm depositional systems; dynamic stratigraphy in modern and ancient shallow-marine sequences. Springer Verlag, Berlin, Federal Republic of Germany, 174 pp.

Andrews, G.D.M. and Branney, M.J., 2011. Emplacement and rheomorphic deformation of a large, lava-like rhyolitic ignimbrite; Grey's Landing, southern Idaho. Geological Society of America Bulletin, 123(3-4): 725-743.

Bachmann, O. and Bergantz, G.W., 2004. On the origin of crystal-pore rhyolites; extracted

from batholithic crystal mushes. Journal of Petrology, 45(8): 1565-1582.

Bachmann, O., Dungan, M. and Bussy, F., 2005. Insights into shallow magmatic processes in large silicic magma bodies: the trace element record in the Fish Canyon magma body, Colorado. Contributions to Mineralogy and Petrology, 149(3): 338-349.

Bachmann, O., Dungan, M. and Lipman, P., 2000. Voluminous lava-like precursor to a major ash-flow tuff: low-column pyroclastic eruption of the Pagosa Peak Dacite, San Juan volcanic field, Colorado. Journal of Volcanology and Geothermal Research, 98(1): 153-171.

Benson, G.T. and Kittleman, L.R., 1968. Geometry of flow layering in silicic lavas. American Journal of Science, 266(4): 265-276.

Boggs, S., Jr., 1987. Principles of sedimentology and stratigraphy. Merrill Publ. Co., Columbus, OH, United States, 784 pp.

Bonnichsen, B. and Kauffman, D.F., 1987. Physical features of rhyolite lava flows in the Snake River plain volcanic province, southwestern Idaho. Special Paper - Geological Society of America, 212: 119-145.

Bouma, A.H., 1962. Sedimentology of some Flysch deposits; a graphic approach to facies interpretation. Elsevier, Amsterdam, 168 pp.

Bourgeois, J., 1980. A transgressive shelf sequence exhibiting hummocky stratification; the Cape Sebastian Sandstone (Upper Cretaceous), southwestern Oregon. Journal of Sedimentary Petrology, 50(3): 681-702.

Branney, M., Bonnichsen, B., Andrews, G., Barry, T., Ellis, B. and McCurry, M., 2006. A new type of voluminous silicic volcanism, "Snake River (SR)-type volcanism"; evidence from southern Idaho and northern Nevada, USA. Abstracts with Programs - Geological Society of America, 38(6): 4.

Branney, M.J., Bonnichsen, B., Andrews, G.D.M., Ellis, B., Barry, T.L. and McCurry, M., 2008. 'Snake River (SR)-type' volcanism at the Yellowstone hotspot track; distinctive products from unusual, high-temperature silicic super-eruptions. Bulletin of Volcanology, 70(3): 293-314.

Branney, M.J. and Kokelaar, B.P., 2002. Pyroclastic density currents and the sedimentation of ignimbrites. Geological Society Publishing House, Bath, United Kingdom, 143 pp.

Branney, M.J., Kokelaar, B.P. and McConnell, B.J., 1992. The Bad Step Tuff; a lava-like rheomorphic ignimbrite in a calc-alkaline piecemeal caldera, English Lake District. Bulletin of Volcanology, 54(3): 187-199.

Branney, M.J. and Kokelaar, P., 1992. A reappraisal of ignimbrite emplacement: progressive aggradation and changes from particulate to non-particulate flow during emplacement of high-grade ignimbrite. Bulletin of Volcanology, 54(6): 504-520.

Branney, M.J., Millward, D. and Lawrence, D.J.D., 1986. The Stockdale (Yarlside) Rhyolite, a rheomorphic ignimbrite?; discussion and reply. Proceedings of the Yorkshire

Geological Society, 46(1): 80-82.

Branney, M.J. and Sparks, R.S.J., 1990. Fiamme formed by diagenesis and burial-compaction in soils and subaqueous sediments. Journal of the Geological Society of London, 147(6): 919-922.

Briggs, N.D., 1976. Welding and crystallisation zonation in Whakamaru Ignimbrite, central North Island, New Zealand. New Zealand Journal of Geology and Geophysics, 19(2): 189-212.

Busby-Spera, C.J., 1986. Depositional features of rhyolitic and andesitic volcaniclastic rocks of the Mineral King submarine caldera complex, Sierra Nevada, California. Journal of Volcanology and Geothermal Research, 27(1-2): 43-76.

Busby-Spera, C.J. and White, J.D.L., 1987. Variation in peperite textures associated with differing host-sediment properties. Bulletin of Volcanology, 49(6): 765-776.

Campbell, S.D.G., Reedman, A.J., Howells, M.F. and Mann, A.C., 1987. The emplacement of geochemically distinct groups of rhyolites during the evolution of the lower rhyolitic tuff formation caldera (Ordovician), North Wales, U.K. Geological Magazine, 124(6): 501-511.

Carey, S. and Sigurdsson, H., 2007. Exploring submarine arc volcanoes. Oceanography, 20(4): 80-89.

Cas, R.A.F., 1978. Silicic lavas in Paleozoic flyschlike deposits in New South Wales, Australia; behavior of deep subaqueous silicic flows. Geological Society of America Bulletin, 89(12): 1708-1714.

Cas, R.A.F., 1992. Submarine volcanism; eruption styles, products, and relevance to understanding the host-rock successions to volcanic-hosted massive sulfide deposits. Economic Geology, 87(3): 511-541.

Cas, R.A.F., Allen, R.L., Bull, S.W., Clifford, B.A. and Wright, J.V., 1990. Subaqueous, rhyolitic dome-tome tuff cones; a model based on the Devonian Bunga Beds, southeastern Australia and a modern analogue. Bulletin of Volcanology, 52(3): 159-174.

Cas, R.A.F. and Wright, J.V., 1987. Volcanic successions: modern and ancient. A geological approach to processes, products and successions. Allen & Unwin, London, UK, 528 pp.

Cas, R.A.F. and Wright, J.V., 1991. Subaqueous pyroclastic flows and ignimbrites: an assessment. Bulletin of Volcanology, 53(5): 357-380.

Chapin, C.E. and Lowell, G.R., 1979. Primary and secondary flow structures in ash-flow tuffs of the Gribbles Run paleovalley, central Colorado. Special Paper - Geological Society of America(180): 137-154.

Cleverly, R.W. and Bristow, J.W., 1982. Flow-banded and contorted tuffs; examples from southern Africa (Lebombo Province) and western North America. Abstracts with Programs - Geological Society of America, 14(7): 464.

Clifton, H.E., 1988. Sedimentologic approaches to paleobathymetry, with applications to

the Merced Formation of Central California. Palaios, 3(5): 507-522.

Cole, J.W., Milner, D.M. and Spinks, K.D., 2005. Calderas and caldera structures; a review. Earth-Science Reviews, 69(1-2): 1-26.

Daniels, J.L., 1974. The geology of the Blackstone region, Western Australia. Bulletin - Geological Survey of Western Australia, 123: 257.

de Silva, S., Salas, G. and Schubring, S., 2008. Triggering explosive eruptions-The case for silicic magma recharge at Huaynaputina, southern Peru. Geology, 36(5): 387-390.

de Silva, S., Zandt, G., Trumbull, R., Viramonte, J.G., Salas, G. and Jimenez, N., 2006. Large ignimbrite eruptions and volcano-tectonic depressions in the Central Andes; a thermomechanical perspective. Geological Society Special Publications, 269: 47-63.

Deering, C.D., Bachmann, O. and Vogel, T.A., 2011. The Ammonia Tanks Tuff; erupting a melt-rich rhyolite cap and its remobilized crystal cumulate. Earth and Planetary Science Letters, 310(3-4): 518-525.

Dott, R.H., Jr. and Bourgeois, J., 1982. Hummocky stratification; significance of its variable bedding sequences. Geological Society of America Bulletin, 93(8): 663-680.

Druitt, T.H., Davies, M. and Lanphere, M., 1997. Evolution of Santorini Caldera.

Druitt, T.H., Edwards, L.E., Mellors, R.M., Pyle, D.M., Sparks, R.S.J., Lanphere, M.A., Davies, M. and B., B., 1999. Santorini Volcano. Geological Society Publishing House, Bath, United Kingdom, 165 pp.

Druitt, T.H. and Sparks, R.S.J., 1984. On the formation of calderas during ignimbrite eruptions. Nature (London), 310(5979): 679-681.

Duffield, W.A. and Dalrymple, G.B., 1990. The Taylor Creek Rhyolite of New Mexico: a rapidly emplaced field of lava domes and flows. Bulletin of Volcanology, 52(6): 475-487.

Duke, W.L., 1985. Hummocky cross-stratification, tropical hurricanes, and intense winter storms. Sedimentology, 32(2): 167-194.

Dumas, S. and Arnott, R.W.C., 2006. Origin of hummocky and swaley cross-stratification; the controlling influence of unidirectional current strength and aggradation rate. Geology (Boulder), 34(12): 1073-1076.

Edgoose, C.J., Scrimgeour, I.R. and Close, D.F., 2004. Geology of the Musgrave Block, Northern Territory. Northern Territory Geological Survey, Report 15.

Ekren, E.B., McIntyre, D.H. and Bennett, E.H., 1984. High-temperature, large-volume, lavalike ash-flow tuffs without calderas in southwestern Idaho. U. S. Geological Survey, Reston, VA, United States, 76 pp.

Ellis, B., Wolff, J.V.,, Boroughs, S., Mark, D., Starkel, W. and Bonnichsen, B., 2013. Rhyolitic volcanism of the central Snake River Plain: a review. Bulletin of Volcanology, 75(8): 1-19.

Evins, P.M., Smithies, R.H., Howard, H.M., Kirkland, C.L., Wingate, M.T.D. and Bodorkos,

S., 2010. Devil in the detail; the 1150-1000 Ma magmatic and structural evolution of the Ngaanyatjarra Rift, west Musgrave Province, central Australia. Precambrian Research, 183(3): 572-588.

Fink, J.H. and Manley, C.R., 1987. Origin of pumiceous and glassy textures in rhyolite flows and domes. Special Paper - Geological Society of America, 212: 77-88.

Folkes, C.B., de Silva, S.L., Wright, H.M. and Cas, R.A., 2011. Geochemical homogeneity of a long-lived, large silicic system; evidence from the Cerro Galan caldera, NW Argentina. Bulletin of volcanology, 73(10): 1455-1486.

Freundt, A., 2003. Entrance of hot pyroclastic flows into the sea: experimental observations. Bulletin of Volcanology, 65(2-3): 144-164.

Friedrich, W.L., Eriksen, U., Tauber, H., Heinemeier, J., Rud, N., Thomsen, M.S. and Buchardt, B., 1988. Existence of a water-filled caldera prior to the Minoan eruption of Santorini, Greece. Naturwissenschaften, 75(11): 567-569.

Fritz, W.J. and Howells, M.F., 1991. A shallow marine volcaniclastic facies model: an example from sedimentary rocks bounding the subaqueously welded Ordovician Garth Tuff, North Wales, U.K. Sedimentary Geology, 74(1-4): 217-240.

Fritz, W.J., Howells, M.F., Reedman, A.J. and Campbell, S.D.G., 1990. Volcaniclastic sedimentation in and around an Ordovician subaqueous caldera, Lower Rhyolitic Tuff Formation, North Wales. Geological Society of America Bulletin, 102(9): 1246-1256.

Fritz, W.J. and Stillman, C.J., 1996. A subaqueous welded tuff from the Ordovician of County Waterford, Ireland. Journal of Volcanology and Geothermal Research, 70(1-2): 91-106.

Gifkens, K., Hermann, W. and Large, R., 2005. Altered Volcanic Rocks: A guide to description and intrepretation. Centre for Ore Deposit Research, University of Tasmania.

Girard, G. and Stix, J., 2009a. Buoyant replenishment in silicic magma reservoirs: Experimental approach and implications for magma dynamics, crystal mush remobilization, and eruption. Journal of Geophysical Research B: Solid Earth, 114(8).

Girard, G. and Stix, J., 2009b. Magma recharge and crystal mush rejuvenation associated with early post-collapse upper basin member rhyolites, Yellowstone Caldera, Wyoming. Journal of Petrology, 50(11): 2095-2125.

Girard, G. and Stix, J., 2009c. The future of volcanism at Yellowstone Caldera. Eos, Transactions, American Geophysical Union, 90(52, Suppl.).

Glikson, A.Y., Stewart, A.J., Ballhaus, C.G., Clarke, G.L., Feeken, E.H.J., Leven, J.H., Sheraton, J.W. and Sun, S.S., 1996. Geology of the western Musgrave Block, central Australia, with particular reference to the mafic-ultramafic Giles Complex. Bulletin - Australian Geological Survey Organisation, 239.

Gonnermann, H.M. and Manga, M., 2005. Flow banding in obsidian: A record of evolving

textural heterogeneity during magma deformation. Earth and Planetary Science Letters, 236(1-2): 135-147.

Gorshkov, G.S., 1963. On the origin of ignimbrites in relation to the study of recent eruptions. Bulletin of Volcanology, 25: 33-37.

Gottsmann, J. and Dingwell, D.B., 2001. Journal of Volcanology and Geothermal Research, 105(4): 323-342.

Gottsmann, J. and Dingwell, D.B., 2002. Bulletin of Volcanology, 64(6): 410-422.

Harms, J.C., Southard, J.B., Spearing, D.R. and Walker, R.G., 1975. Depositional environments as interpreted from primary sedimentary structures and stratification sequences. Society of Sedimentary Geology, Tulsa, OK, United States, 161 pp.

Hausback, B.P., 1987. An extensive, hot, vapor-charged rhyodacite flow, Baja California, Mexico. Special Paper - Geological Society of America, 212: 111-118.

Henrich, R. and Huneke, H., 2011. Hemipelagic advection and periplatform sedimentation. Deep-Sea Sediments. Developments in Sedimentology, Elsevier, Amsterdam, 63: 353-396.

Henry, C.D., Price, J.G., Rubin, J.N., Parker, D.F., Wolff, J.A., Self, S., Franklin, R. and Barker, D.S., 1988. Widespread, lavalike silicic volcanic rocks of Trans-Pecos Texas. Geology (Boulder), 16(6): 509-512.

Henry, C.D. and Wolff, J.A., 1992. Distinguishing strongly rheomorphic tuffs from extensive silicic lavas. Bulletin of Volcanology, 54(3): 171-186.

Howard, H.M., Werner, M., Smithies, R.H., Evins, P.M., Kirkland, C.L., Kelsey, D.E., Hand, M., Collins, A.S., Pirajno, F., Wingate, M.T.D., Maier, W.D. and Raimondo, T., 2011. The geology of the west Musgrave Province and the Bentley Supergroup -- a field guide. Record - Geological Survey of Western Australia, Perth, Australia, 2011/14: 125 pp.

Howard, J.D. and Reineck, H.-E., 1981. Depositional facies of high-energy beach-to-offshore sequence; comparison with low-energy sequence. AAPG Bulletin, 65(5): 807-830.

Howells, M.F., Campbell, S.D.G. and Reedman, A.J., 1985. Isolated pods of subaqueous welded ash-flow tuff; a distal facies of the Capel Curig Volcanic Formation (Ordovician), North Wales. Geological Magazine, 122(2): 175-180.

Howells, M.F., Reedman, A.J. and Campbell, S.D.G., 1986. The submarine eruption and emplacement of the Lower Rhyolitic Tuff Formation (Ordovician), N Wales. Journal of the Geological Society of London, 143, Part 3: 411-423.

Hunter, R.E. and Clifton, E.H., 1982. Cyclic deposits and hummocky cross-stratification of probable storm origin in Upper Cretaceous rocks of the Cape Sebastian area, southwestern Oregon. Journal of Sedimentary Petrology, 52(1): 127-143.

Jolly, R.J.H. and Lonergan, L., 2002. Mechanisms and controls on the formation of sand intrusions. Journal of the Geological Society of London, 159, Part 5: 605-617.

Keating, G.N., 2005. The role of water in cooling ignimbrites. Journal of volcanology and

geothermal research, 142(1): 145-171.

Kirkland, C.L., Smithies, R.H., Woodhouse, A.J., Howard, H.M., Wingate, M.T.D., Belousova, E.A., Cliff, J., Murphy, R. and Spaggiari, C.V., 2013. Constraints and deception in the isotopic record; the crustal evolution of the west Musgrave Province, central Australia. Gondwana Research, 23: 759-781.

Kirstein, L.A., Hawkesworth, C.J. and Garland, F.G., 2001. Felsic lavas or rheomorphic ignimbrites; is there a chemical distinction? Contributions to Mineralogy and Petrology, 142(3): 309-322.

Kobberger, G. and Schmincke, H.U., 1999a. Bulletin of Volcanology, 60(6): 465-485.

Kobberger, G. and Schmincke, H.U., 1999b. Deposition of rheomorphic ignimbrite D (Mogan Formation), Gran Canaria, Canary Islands, Spain. Bulletin of Volcanology, 60(6): 465-485.

Kokelaar, B.P., 1982. Fluidization of wet sediments during the emplacement and cooling of various igneous bodies. Journal of the Geological Society of London, 139, Part 1: 21-33.

Kokelaar, P. and Busby, C., 1992. Subaqueous explosive eruption and welding of pyroclastic deposits. Science, 257(5067): 196-201.

Kokelaar, P. and Koeniger, S., 2000. Marine emplacement of welded ignimbrite; the Ordovician Pitts Head Tuff, North Wales. Journal of the Geological Society of London, 157, Part 3: 517-536.

Lavallee, Y., Dingwell, D.B., Hess, K., Andrews, G., Branney, M., Quane, S. and Russell, K.J., 2008. Absolute healing of pyroclasts during welding of a rheomorphic ignimbrite. Eos, Transactions, American Geophysical Union, 89(53, Suppl.).

Leat, P.T. and Schmincke, H.-U., 1993. Large-scale rheomorphic shear deformation in Miocene peralkaline ignimbrite E, Gran Canaria. Bulletin of Volcanology, 55(3): 155-165.

Leckie, D.A. and Walker, R.G., 1982. Storm- and tide-dominated shorelines in Cretaceous Moosebar-lower Gates interval; outcrop equivalents of Deep Basin gas trap in Western Canada. AAPG Bulletin, 66(2): 138-157.

Legros, F. and Druitt, T.H., 2000. On the emplacement of ignimbrite in shallow-marine environments. Journal of Volcanology and Geothermal Research, 95(1,Äì4): 9-22.

Lipman, P.W., 1984. The roots of ash flow calderas in western North America; windows into the tops of granitic batholiths. Journal of Geophysical Research, 89(B10): 8801-8841.

Lipman, P.W., 1997. Subsidence of ash-flow calderas; relation to caldera size and magma-chamber geometry. Bulletin of Volcanology, 59(3): 198-218.

Lipman, P.W., 2000a. Calderas. In: H. Sigurdsson (Editor), Encyclopedia of Volcanoes. Academic Press, San Francisco.

Lipman, P.W., 2000b. The central San Juan caldera cluster: regional volcanic framework. Ancient Lake Creede: Its Volcanotectonic Setting, History and Sedimentation and

Relation to Mineralization in the Creede Mining District. Geol. Soc. Am. Spec.Publ.

Lipman, P.W. and McIntosh, W.C., 2008. Eruptive and noneruptive calderas, northeastern San Juan Mountains, Colorado; where did the ignimbrites come from? Geological Society of America Bulletin, 120(7-8): 771-795.

Lofgren, G., 1971. Experimentally produced devitrification textures in natural rhyolitic glass. Geological Society of America Bulletin, 82(1): 111-124.

Lowe, D.R., 1982. Sediment gravity flows; II, Depositional models with special reference to the deposits of high-density turbidity currents. Journal of Sedimentary Petrology, 52(1): 279-297.

Manley, C.R., 1995. How voluminous rhyolite lavas mimic rheomorphic ignimbrites; eruptive style, emplacement conditions, and formation of tuff-like textures. Geology (Boulder), 23(4): 349-352.

Manley, C.R., 1996. In situ formation of welded tuff-like textures in the carapace of a voluminous silicic lava flow, Owyhee Country, SW Idaho. Bulletin of Volcanology, 57(8): 672-686.

Mason, B.G., Pyle, D.M. and Oppenheimer, C., 2004. The size and frequency of the largest explosive eruptions on Earth. Bulletin of Volcanology, 66(8): 735-748.

McArthur, A., Cas, R. and Orton, G., 1998. Distribution and significance of crystalline, perlitic and vesicular textures in the Ordovician Garth Tuff (Wales). Bulletin of Volcanology, 60(4): 260-285.

Mcleod, P., Carey, S. and Sparks, R.S.J., 1999. Behaviour of particle-laden flows into the ocean: experimental simulation and geological implications. Sedimentology, 46(3): 523-536.

McPhie, J., Doyle, M. and Allen, R., 1993. Volcanic Textures: A guide to the intrepretation of textures in volcanic rocks. Centre for Ore Deposit Research, University of Tasmania.

Miller, C.F. and Wark, D.A., 2008. Supervolcanoes and their explosive supereruptions. Elements, 4(1): 11-15.

Mills, A.A., 1984. Pillow lavas and the Leidenfrost effect. Journal of the Geological Society of London, 141(1): 183-186.

Milner, S.C., Duncan, A.R. and Ewart, A., 1992. Quartz latite rheoignimbrite flows of the Etendeka Formation, north-western Namibia. Bulletin of Volcanology, 54(3): 200-219.

Morris, P.A. and Pirajno, F., 2005. Mesoproterozoic sill complexes in the Bangemall Supergroup, Western Australia; geology, geochemistry, and mineralization potential. Report - Geological Survey of Western Australia, Perth, Australia, 99: 75 pp.

Myers, J.S., Shaw, R.D. and Tyler, I.M., 1996. Tectonic evolution of Proterozoic Australia. Tectonics, 15(6): 1431-1446.

Newhall, C.G. and Self, S., 1982. The Volcanic Explosivity Index (VEI) An Estimate of

Explosive Magnitude for Historical Volcanism. Journal of Geophysical Research, 87(C2): 1231-1238.

Nichols, G., 2009. Sedimentology and stratigraphy. Wiley-Blackwell.

Orton, G., Howells, M.F., Reedman, A.J. and Campbell, S.D.G., 1987. Discussion on the submarine eruption and emplacement of the Lower Rhyolitic Tuff Formation (Ordovician), North Wales. Journal of the Geological Society of London, 144(3): 523-525.

Pichler, H., 1965. Acid hyaloclastites. Bulletin of Volcanology, 28: 293-310.

Pioli, L. and Rosi, M., 2005. Rheomorphic structures in a high-grade ignimbrite: the Nuraxi tuff, Sulcis volcanic district (SW Sardinia, Italy). Journal of Volcanology and Geothermal Research, 142(1): 11-28.

Quane, S.L. and Russell, J.K., 2005. Ranking welding intensity in pyroclastic deposits. Bulletin of Volcanology, 67(2): 129-143.

Reedman, A.J., Howells, M.F., Orton, G. and Campbell, S.D.G., 1987a. The Pitts Head Tuff Formation; a subaerial to submarine welded ash-flow tuff of Ordovician age, North Wales. Geological Magazine, 124(5): 427-439.

Reedman, A.J., Park, K.H., Merriman, R.J. and Kim, S.E., 1987b. Welded tuff infilling a volcanic vent at Weolseong, Republic of Korea. Bulletin of Volcanology, 49(3): 541-546.

Riehle, J.R., 1973. Calculated Compaction Profiles of Rhyolitic Ash-Flow Tuffs. Geological Society of America Bulletin, 84(7): 2193-2216.

Riehle, J.R., Miller, T.F. and Bailey, R.A., 1995. Cooling, degassing and compaction of rhyolitic ash flow tuffs: a computational model. Bulletin of Volcanology, 57(5): 319-336.

Riehle, J.R., Miller, T.F. and Paquereau-Lebti, P., 2010. Compaction profiles of ash-flow tuffs; modeling versus reality. Journal of Volcanology and Geothermal Research, 195(2-4): 106-120.

Rittmann, A., 1962. Volcanoes and their activity. Wiley, New York, 305 pp.

Ross, C.S. and Smith, R.L., 1961. Ash-flow tuffs: Their origin, geologic relations and identification. U.S. Geol. Surv. Prof. Pap., 366(366): 1-81.

Schmincke, H.-U., 1967. Fused tuff and peperites in south-central Washington. Geological Society of America Bulletin, 78(3): 319-330.

Schmincke, H.U., 1975. Volcanological aspects of peralkaline silicic welded ash-flow tuffs. Bulletin Volcanologique, 38, (1974)(3): 594-636.

Schmincke, H.U. and Swanson, D.A., 1967. Laminar viscous flowage structures in ash-flow tuffs from Gran Canaria, Canary islands. Journal of Geology, 75(6): 641-664.

Self, S., 2006. The effects and consequences of very large explosive volcanic eruptions. Philosophical Transactions of the Royal Society A: Mathematical, Physical and Engineering Sciences, 364(1845): 2073-2097.

Shanmugam, G., 1997. The Bouma Sequence and the turbidite mind set. Earth-Science

Reviews, 42(4): 201-229.

Sigurdsson, H., Carey, S., Mandeville, C. and Bronto, S., 1990. Subaqueous pyroclastic flow deposits from the 1883 eruption of Krakatau Volcano, Indonesia. Eos, Transactions, American Geophysical Union, 71(43): 1721.

Skilling, I., White, J. and McPhie, J., 2002. Peperite: a review of magma–sediment mingling. Journal of Volcanology and Geothermal Research, 114(1): 1-17.

Smith, R.L., 1960a. Ash flows. Geological Society of America Bulletin, 71(6): 795-841.

Smith, R.L., 1960b. Zones and zonal variations in welded ash flows. U. S. Geological Survey Professional Paper: 149-159.

Smithies, R.H., Howard, H.M., Evins, P.M., Kirkland, C.L., Bordorkos, S. and Wingate, M.T.D., 2009. The west Musgrave Complex - new geological insights from recent mapping, geochronology, and geochemical studies. Record - Geological Survey of Western Australia, Perth, Australia, 2008/19: 20 pp.

Smithies, R.H., Howard, H.M., Evins, P.M., Kirkland, C.L., Kelsey, D.E., Hand, M., Wingate, M.T.D., Collins, A.S. and Belousova, E., 2011. High-temperature granite magmatism, crust-mantle interaction and the Mesoproterozoic intracontinental evolution of the Musgrave Province, central Australia. Journal of Petrology, 52(5): 931-958.

Smithies, R.H., Howard, H.M., Evins, P.M., Kirkland, C.L., Kelsey, D.E., Hand, M., Wingate, M.T.D., Collins, A.S., Belousova, E.A. and Allchurch, S., 2010. Geochemistry, geochronology and petrogenesis of Mesoproterozoic felsic rocks in the west Musgrave Province, Central Australia, and implications for the Mesoproterozoic tectonic evolution of the region. Record - Geological Survey of Western Australia, Perth, Australia,106: 82 pp.

Smithies, R.H., Howard, H.M., Kirkland, C.L., Werner, M., Medlin, C.C., Wingate, M.T.D. and Cliff, J.B., 2013. Geochemical evolution of rhyolites of the Talbot Sub-basin and associated felsic units of the Warakurna Supersuite. Report - Geological Survey of Western Australia, Perth, Australia, 118: 74 pp.

Smithies, R.H., Kirkland, C.L., Korhonen, F.J., Aitken, A.R.A., Howard, H.M., Maier, W.D., Wingate, M.T.D., Quentin de Gromard, R. and Gessner, K., 2014. The Mesoproterozoic thermal evolution of the Musgrave Province in central Australia–plume vs. the geological record. Gondwana Research.

Soriano, C., Zafrilla, S., Martí, J., Bryan, S., Cas, R. and Ablay, G., 2002. Bulletin of the Geological Society of America, 114(7): 883-895.

Sparks, R.S.J., and Walker, G., 1977. The significance of vitric-enriched air-fall ashes associated with crystal-enriched ignimbrites. Journal of Volcanology and Geothermal Research, 2(4): 329-341.

Sparks, R.S.J., Francis, P.W., Hamer, R.D., Pankhurst, R.J., O'Callaghan, L.O., Thorpe, R.S. and Page, R., 1985. Ignimbrites of the Cerro Galan Caldera, NW Argentina. Journal of Volcanology and Geothermal Research, 24(3-4): 205-248.

Sparks, R.S.J., Self, S. and Walker, G.P.L., 1973. Products of Ignimbrite Eruptions. Geology (Boulder), 1(3): 115-118.

Sparks, R.S.J., Sigurdsson, H. and Carey, S.N., 1980a. The entrance of pyroclastic flows into the sea; I, Oceanographic and geologic evidence from Dominica, Lesser Antilles. Journal of Volcanology and Geothermal Research, 7(1-2): 87-96.

Sparks, R.S.J., Sigurdsson, H. and Carey, S.N., 1980b. The entrance of pyroclastic flows into the sea; II, Theoretical considerations on subaqueous emplacement and welding. Journal of Volcanology and Geothermal Research, 7(1-2): 97-105.

Sparks, R.S.J., Tait, S.R. and Yanev, Y., 1999. Dense welding caused by volatile resorption. Journal of the Geological Society of London, 156, Part 2: 217-225.

Sparks, R.S.J. and Wilson, L., 1976. A model for the formation of ignimbrite by gravitational column collapse. Journal of the Geological Society of London, 132, Part 4: 441-451.

Sparks, R.S.J., Wilson, L. and Hulme, G., 1978. Theoretical modeling of the generation, movement, and emplacement of pyroclastic flows by column collapse. Journal of Geophysical Research, 83(B4): 1727-1739.

Sparks, R.S.J., Self, S., Grattan, J.P., Oppenheimer, C., Pyle, D.M. and Rymer, H., 2005. Super-eruptions: global effects and future threats, London, UK.

Stevenson, R.J., Briggs, R.M. and Hodder, A.P.W., 1993. Journal of Volcanology and Geothermal Research, 57(1-2): 39-56.

Sumner, J.M. and Branney, M.J., 2002. The emplacement history of a remarkable heterogeneous, chemically zoned, rheomorphic and locally lava-like ignimbrite; "TL" on Gran Canaria. Journal of Volcanology and Geothermal Research, 115(1-2): 109-138.

Trofimovs, J., Amy, L., Boudon, G., Deplus, C., Doyle, E., Fournier, N., Hart, M.B., Komorowski, J.C., Le Friant, A., Lock, E.J., Pudsey, C., Ryan, G., Sparks, R.S.J. and Talling, P.J., 2006. Submarine pyroclastic deposits formed at the Soufriere Hills Volcano, Montserrat (1995-2003); what happens when pyroclastic flows enter the ocean? Geology (Boulder), 34(7): 549-552.

Trofimovs, J.R., Sparks, S.J. and Talling, P.J., 2008. Anatomy of a submarine pyroclastic flow and associated turbidity current; July 2003 dome collapse, Soufriere Hills Volcano, Montserrat, West Indies. Sedimentology, 55(3): 617-634.

Wade, B.P., Kelsey, D.E., Hand, M. and Barovich, K.M., 2008. The Musgrave Province; stitching north, west and south Australia. Precambrian Research, 166(1-4): 370-386.

Walker, G.P.L., 1983. Ignimbrite types and ignimbrite problems. Journal of Volcanology and Geothermal Research, 17(1-4): 65-88.

Walker, J., 1977. Water on a hot skillet. Scientific American, 237(2): 126-130.

Werner, M., Howard, H.M. and Smithies, R.H., 2012. Mount Eveline, WA Sheet 4345 1:100 000 Geological Series Maps. Geological Survey of Western Australia. Perth,

Australia.

Whitham, A.G., 1989. The behaviour of subaerially produced pyroclastic flows in a subaqueous environment; evidence from the Roseau eruption, Dominica, West Indies. Marine Geology, 86(1): 27-40.

Willcock, M.A.W., Cas, R.A.F., Giordano, G. and Morelli, C., 2013. The eruption, pyroclastic flow behaviour, and caldera in-filling processes of the extremely large volume (1290 km^3), intra- to extra-caldera, Permian Ora (ignimbrite) Formation, southern Alps, Italy. Journal of Volcanology and Geothermal Research, 265: 102-126.

Williams, H., 1941. Calderas and their origin. University of California Publications in Geological Sciences, 25(6): 239-346.

Wilson, C., Houghton, B., McWilliams, M., Lanphere, M., Weaver, S. and Briggs, R., 1995. Volcanic and structural evolution of Taupo Volcanic Zone, New Zealand: a review. Journal of volcanology and geothermal research, 68(1): 1-28.

Wilson, C.J., 2008. Supereruptions and supervolcanoes: processes and products. Elements, 4(1): 29-34.

Wilson, C.J.N. and Walker, G.P.L., 1982. Ignimbrite depositional facies; the anatomy of a pyroclastic flow. Journal of the Geological Society of London, 139, Part 5: 581-592.

Wingate, M.T.D., Pirajno, F. and Morris, P.A., 2004. Warakurna large igneous province: A new Mesoproterozoic large igneous province in west-central Australia. Geology, 32(2): 105-108.

Wolff, J.A. and Wright, J.V., 1981. Rheomorphism of welded tuffs. Journal of Volcanology and Geothermal Research, 10(1-3): 13-34.

Wright, H.M., Folkes, C.B., Cas, R.A. and Cashman, K.V., 2011. Heterogeneous pumice populations in the 2.08-Ma Cerro Galán Ignimbrite: implications for magma recharge and ascent preceding a large-volume silicic eruption. Bulletin of volcanology, 73(10): 1513-1533

Wright, J.V., Self, S. and Fisher, R.V., 1981. Towards a facies model for ignimbrite-forming eruptions. In: S. Self and R.S.J. Sparks (Editors), Tephra studies; proceedings of the NATO Advanced Study Institute "Tephra studies as a tool in Quaternary research". D. Reidel Publ. Co., Dordrecht, Netherlands, pp. 433-439.

Yamada, E., 1973. Subaqueous pumice flow deposits in the Onikobe Caldera, Miyagi Prefecture, Japan. Journal of the Geological Society of Japan, 79(9): 585-597.

Yates, E.A. and Ellis, M.A., 2012. Locating the next Yellowstone Caldera. Northwest Geology, 41: 1-10.

Chapter 3

Petrogenesis of the A-type, Mesoproterozoic intra-caldera rheomorphic Kathleen Ignimbrite and co-magmatic Rowland Suite intrusions, west Musgrave Province, central Australia: products of extreme fractional crystallisation in a failed rift setting

C.C. Medlin[1*], S.M. Jowitt[1], R.A.F. Cas[1], R.H. Smithies[2], C.L. Kirkland[2], R.A. Maas[3], M. Raveggi[1], H.M. Howard[2] and M.T.D. Wingate[2]

[1]School of Geosciences, Monash University, Clayton, Victoria, 3800, Australia
[2]Geological Survey of Western Australia, 100 Plain Street, East Perth, Western Australia, 6004, Australia
[3]School of Earth Sciences, University of Melbourne, Parkville, Victoria, 3010, Australia

Keywords: A-type, geochemistry, geochronology, radiogenic isotopes, rhyolite, rheomorphic ignimbrite, west Musgrave Province, Mesoproterozoic

ABSTRACT

The Pussy Cat Group rhyolites of the Mesoproterozoic west Musgrave Province of central Australia, forming part of the Bentley Supergroup, were deposited during the ca. 1085–1040 Ma Ngaanyatjarra Rift and Giles events, and are related to the Warakurna Large Igneous Province. This study focuses on the two silicic components of the Pussy Cat Group, the Kathleen Ignimbrite (Formation) and the Rowland Suite. These silicic rocks are A-type, metaluminous (to slightly peraluminous) rhyolites and are enriched in the rare earth elements (REE) relative to average crustal abundances. The rhyolitic Kathleen Ignimbrite (Formation) records an explosive caldera fill-sequence and contains, amongst others, a thick (≤500 m), initially subaqueously emplaced, rheomorphic, intra-caldera ignimbrite unit, whereas the Rowland Suite consists of a number of mineralogically- and geochemically-related intrusive porphyritic rhyolites that intrude throughout the Pussy Cat Group. Whole-rock geochemistry, Rb-Sr, Sm-Nd and in-situ zircon Lu-Hf isotope data are indicative of a dominantly mantle-derived source for the magmas that formed the Pussy Cat Group rhyolites. SHRIMP U-Pb dating of these units indicate ages of 1062 ± 8, 1071 ± 5, 1076 ± 5, and 1078 ± 5 Ma. The magmas that formed these units were formed from extreme fractional crystallisation of a mantle-derived basaltic magma with minimal crustal contamination during a failed intra-plate extensional rift. This involved three main stages of fractional crystallisation, namely early fractionation of plagioclase, olivine, clinopyroxene and magnetite from a basaltic magma to reach an intermediate composition, which was followed by fractionation of plagioclase, K-feldspar and quartz to form a proto-Rowland Suite-type magma at mid-upper crustal

levels that then migrated into the shallow upper crust, forming a magma chamber and fractionating quartz, K-feldspar, plagioclase, magnetite and biotite ± minor REE-enriched accessory phases from the Rowland Suite magma to form the final stage, evolved Kathleen Ignimbrite magmas. This final fractionation phase generated the most evolved silicic rock suite identified to date within the entire west Musgrave Province. The new geochronological, geochemical, and isotopic data presented within this study indicate that these two units are coeval and comagmatic, suggesting a common source for the Kathleen Ignimbrite and the entire Rowland Suite. In addition, these data suggest that the porphyritic rhyolite intrusions represent the primitive, crystal-rich, cumulate end-member of the magmatic system, whereas the Kathleen Ignimbrite represents the most evolved end-member of the system and formed the crystal-poor to crystal-rich ignimbrite sequence from the most fractionated melts in the system; demonstrating thorough evacuation of a shared or at least partly linked, compositionally zoned and differentiated source magma chamber or chambers.

3.1 Introduction and specific aims of this study

Highly evolved rhyolites are frequently invoked in large explosive eruptions and catastrophic supereruptions (e.g., Yellowstone Caldera; Girard & Stix, 2012) that can have far-reaching environmental, climactic and biological impacts (Sparks *et al.*, 2005, Self, 2006, Miller & Wark, 2008); however, the petrogenesis of these rhyolites is still contentious and problematic (e.g., Hildreth, 1981, Bryan *et al.*, 2002, Bachmann & Bergantz, 2004), with numerous models proposed over the past few decades (see recent review by Dall'Agnol *et al.*, 2012). This paper focuses on the ca. 1070 Ma Kathleen Ignimbrite (Formation) and Rowland Suite units of the Pussy Cat Group in the west Musgrave Province of central Australia; these units provide a natural laboratory to investigate the petrogenesis of highly evolved rhyolites and enables comparison between these products of Mesoproterozoic volcanism and more modern day examples.

The Mesoproterozoic west Musgrave Province of central Australia consists of a series of bimodal silicic and basaltic volcanic rocks, granitic and mafic intrusions, and variably deformed and metamorphosed sediments (Howard *et al.*, 2011). The volcanic rocks in this area include very thick, large volume rhyolite units that Daniels (1974) interpreted to be ignimbrites. These units include the 1071 ± 5 Ma Kathleen Ignimbrite (Formation), an intra-caldera eruption fill-sequence that contains, amongst other units, a single ≤500 m thick, welded unit that contains well-defined fiamme, eutaxitic textures and a well-developed rheomorphic lava-like basal facies. This unit is the oldest documented initially subaqueously-emplaced, intra-caldera, lava-like rheomorphic ignimbrite yet discovered. The Kathleen Ignimbrite (Formation) is hosted by a ~1 km thick well-preserved volcanic–sedimentary succession that covers an area of ~40 km^2. It is associated with

large volume coeval and potentially comagmatic, subvolcanic rhyolitic intrusions and is both under- and overlain by shallow-water turbiditic sediments. A detailed description of the field relationships, physical volcanology and palaeoenvironmental setting of these units is provided in Chapter 2 of this thesis.

The volcanic rocks of the Pussy Cat Group represent a small part of more voluminous (22,000 km^3) and widespread (5,200 km^2) silicic magmatism preserved within the Talbot sub-basin of the Bentley Supergroup (Smithies *et al.*, 2013; 2014). This magmatism is thought to have occurred over a period of >30 Ma, and represents the silicic component of a large igneous province in the Musgrave Province that potentially redefines the recognised, shorter duration (1078–1073 Ma) Warakurna Large Igneous Province (LIP) event (Wingate *et al*., 2004; Smithies *et al.*, 2014).

This study uses new whole-rock and radiogenic isotope geochemical and secondary ion mass spectrometry (SIMS) U-Pb geochronological data to investigate the eruption and formation of the intra-caldera rheomorphic Kathleen Ignimbrite (Formation). This paper discusses the petrogenesis of this ignimbrite-dominated formation and that of the coeval, subvolcanic porphyritic rhyolite intrusions of the Rowland Suite. It also discusses the processes that generated the magmas that formed these differing but comagmatic units, including a model for their emplacement, which encompasses the tectonic setting and source model for the Mesoproterozoic silicic magmatism in this area.

3.2 Regional geological setting and previous work

3.2.1 The west Musgrave Province

The 1.60–1.15 Ga Musgrave Province is an 800 km long, 350 km wide ESE-WSW trending belt of amphibolite to granulite facies metamorphic rocks that is bounded by mid-Neoproterozoic to Mesozoic sedimentary basins in central-southern Australia (Fig. 3.1a; Wade *et al.*, 2008; Smithies *et al.*, 2009). It lies at the convergence of three important Australian Proterozoic structural trends that formed after the amalgamation of the North, West and South Australian cratons (Fig. 3.1b; Wade *et al.*, 2008; Howard *et al.*, 2011). The west Musgrave Province forms the extension of the Musgrave region and Musgrave Ranges into Western Australia. This western extension contains variably deformed and metamorphosed sediments that are overlain by rhyolitic and basaltic volcanic rocks interbedded with minor sedimentary rocks that are intruded by granitic plutons, mafic-ultramafic layered intrusions, and numerous mafic and silicic dykes (Daniels, 1974).

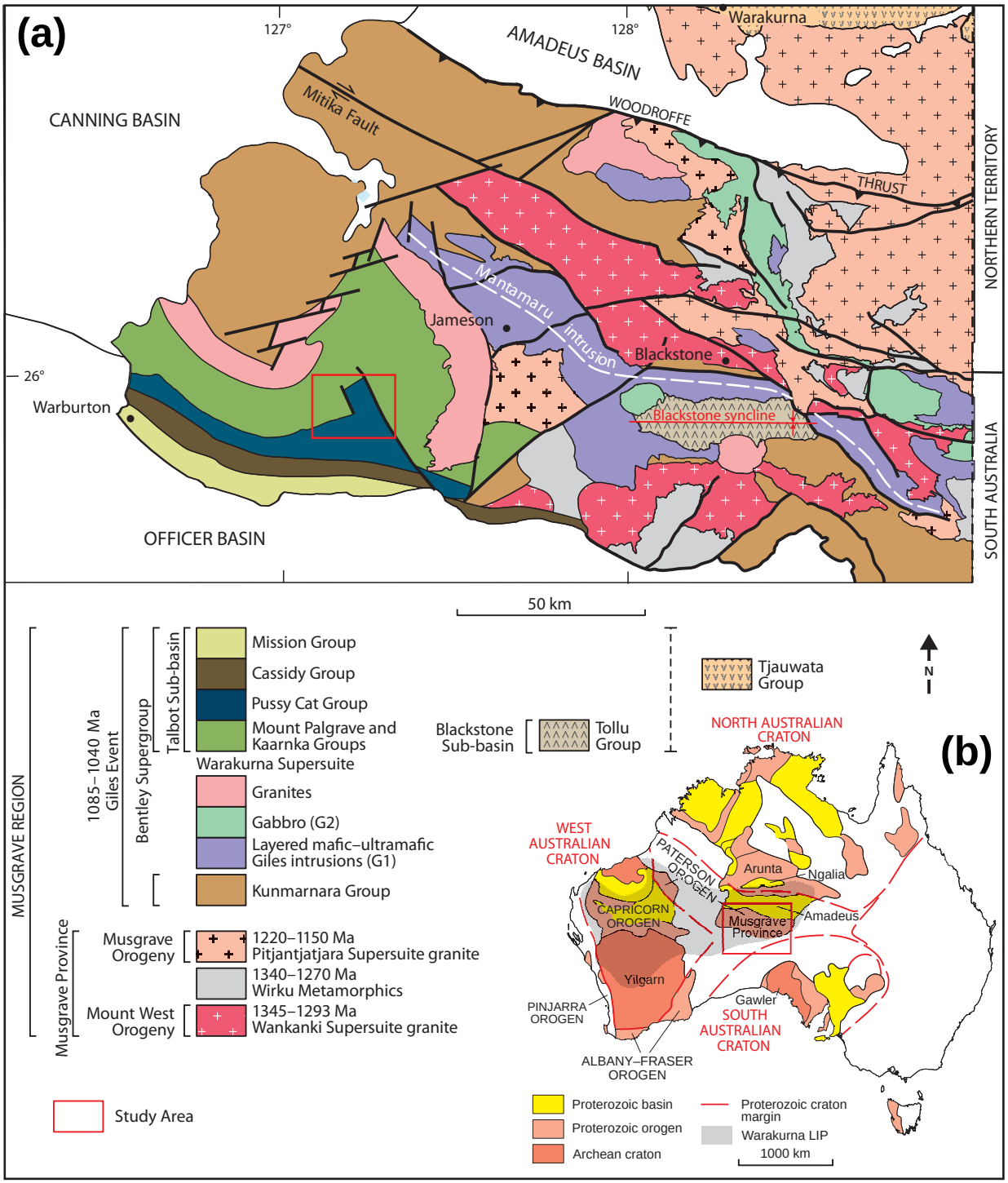

Figure 3.1: a) Location of the west Musgrave Province and surrounding regional geology (adapted from Glikson *et al*., 1996; Edgoose *et al*., 2004; Howard *et al*., 2011; Smithies *et al*., 2013). b) Location of the Musgrave Province in terms of the tectonic framework of Proterozoic Australia, and the extent of the Warakurna LIP (adapted from Myers *et al*., 1996; Smithies *et al*., 2013). Location of study area highlighted in red, and expanded on in Fig. 3.2.

3.2.2 The Giles Event

Although the Musgrave region has a long tectonic history, this paper focuses on the 1085–1040 Ma Giles Event (Wade *et al.*, 2008, Howard *et al.*, 2011). This extensional intra-plate event (Evins *et al*., 2010) involved an anomalous thermal perturbation that was caused by magma-focussing lithospheric architecture and large-scale tectonic movements,

which resulted in the addition of large volumes of mantle-derived silicic and mafic magma to the crust beneath the Musgrave Province over a period >30 Ma (Smithies *et al*., 2014). The Giles Event was contemporaneous with a long-lived but failed intra-plate rift, known as the Ngaanyatjarra Rift (Evins *et al.*, 2010), and it is recorded through the formation of mafic-ultramafic layered intrusions (Giles intrusions), voluminous bimodal volcanic rocks and granitic intrusions that are mixed and intermingled with massive gabbros, silicic and mafic dykes and a supracrustal rift-related succession (Glikson *et al.*, 1995, 1996, Sun *et al.*, 1996, Close *et al.*, 2003, Edgoose *et al.*, 2004, Wade *et al.*, 2008, Howard *et al.*, 2011). The parental magmas to these Giles intrusions are believed to be significantly juvenile, mantle-derived basaltic magmas that formed during regional underplating associated with the Giles Event and underwent minimal crustal contamination; these magmas are represented by the Alcurra Dolerite Suite dykes that cross-cut the Musgrave Province (Glikson *et al.*, 1996, Howard *et al.*, 2009; Smithies 2013; 2014). All of the volcanic and sedimentary components that formed during this failed rifting event were deposited in the Bentley Basin, and as such are assigned to the Bentley Supergoup (Howard *et al.*, 2011). The igneous rocks that formed during the Giles Event are part of the much larger Warakurna Supersuite, which also includes the Warakurna LIP that outcrops across ~1.5 million km^2 of central and western Australia (Wingate *et al.*, 2004, Morris & Pirajno, 2005, Howard *et al.*, 2011).

3.2.3 Tectonic setting during the Giles Event

The almost continuous (>30 Ma) continental mafic and silicic magmatism in the Musgrave region during the Giles Event suggests a more complex intra-plate geodynamic setting for this event (Smithies et al., 2011, 2014). Prior to the Giles Event, the 1220–1150 Ma Musgrave Orogeny created an unusually long period of ultra-high temperature metamorphism (Kelsey *et al*., 2009; 2010) and continuous lower crustal thinning in an extensional intracontinental setting that developed within a suture zone between three older cratonic blocks (Smithies *et al*., 2010; 2014; Howard et al., 2011). Smithies *et al*. (2011; 2014) therefore propose that the continental crust beneath the Musgrave region was thinner than in the surrounding North, West and South Australian cratons, allowing it to act as an asthenospheric melt-trap for a long period of time. By the end of the Musgrave Orogeny and the start of the Giles Event, the Musgrave region had experienced at least 100 Ma of high to ultra-high crustal temperatures in either intracontinental or distal backarc environments (Kirkland *et al*., 2013; Smithies *et al*., 2011; 2014). This heat provided the driving force behind the magmatism that occurred during the Giles Event, and this model contrasts with previous suggestions that the magmatism in this area was mantle plume-related (e.g., Wingate *et al.*, 2004, Morris & Pirajno, 2005). Kirkland *et al*. (2013) suggested that prior to the Giles Event, the lower crustal component of the Musgrave Province was a homogenised, anhydrous and refractory mixture of mantle-derived mafic

material and intermediate Proterozoic basement that was the result of two crust forming events at ca. 1900 and 1650–1550 Ma.

3.3 Bentley Basin, Talbot Sub-basin and Pussy Cat Group stratigraphy

The Bentley Basin formed between 1085 and 1040 Ma (Howard *et al.*, 2011, Smithies *et al.*, 2013). It contains the Talbot Sub-basin that contains a basal group of rhyolite lavas and ignimbrites of the Mount Palgrave Group, which are overlain by the rhyolitic ignimbrite-dominated Kaarnka Group, the southward dipping and younging, bimodal, volcanic-sedimentary Pussy Cat and Cassidy groups, and the uppermost basaltic and sedimentary Mission Group (Daniels, 1974, Howard *et al.*, 2011; Chapter 2).

The Pussy Cat Group outcrops in the southwestern part of the Talbot Sub-basin and is structurally subdivided into five main domains, compartmentalised by dominant NNW-SSE striking faults, namely a deformed and sheared western section (A), a low-relief middle section (B), a well-preserved and relatively undeformed eastern section (C), and faulted northeast (D) and southeast sections (E; Fig. 3.2). This group is split into the lowermost Cleghorne Formation (conformably overlying the Mount Palgrave Group), the overlying silicic Kathleen Ignimbrite (Formation), and the uppermost mafic volcanic-sedimentary Glyde Formation. Porphyritic rhyolite intrusions of the Rowland Suite cross-cut this volcanic-sedimentary succession (Fig. 3.2). The Kathleen Ignimbrite (Formation) and Rowland Suite intrusions form the focus of this study.

The ≤650 m thick Kathleen Ignimbrite (Formation) is a rhyolitic, ignimbrite-dominated volcanic sequence that is hosted within a shallow-water, volcaniclastic-sedimentary, shelf-type or large lake-type storm turbidite succession. This ignimbritic sequence was generated during a large, Late Mesoproterozoic, explosive, caldera-forming silicic eruption of at least magnitude or Volcanic Explosivity Index (VEI) 7 (Mason, 2004; Self, 2006; Chapter 2). The main Kathleen Ignimbrite (Formation) unit, the basal Kurrparu Member ignimbrite, is a single ≤500 m thick, lava-like rheomorphic to eutaxitically textured intra-caldera, cooling unit that was initially emplaced in a subaqueous palaeodepositional environment (Chapter 2). Conformably overlying the Kurrparu Member is the thinner interbedded breccia and ignimbrite dominated Karlaya Member, which is in turn overlain by the upper volcaniclastic turbiditic Kilykilykarri Member (Chapter 2). In comparison, the Rowland Suite consists of a number of porphyritic, crystal-rich, rhyolitic intrusions that are syn-sedimentary, sub-volcanic, and cross-cut the formations within the Pussy Cat Group; underlying, overlying, and intruding into the Kathleen Ignimbrite (Formation; Chapter 2). Both the Rowland Suite and Kathleen Ignimbrite outcrop over a minimum strike length of ~22 km before being covered by Quaternary sands, with the entire package dipping at 20°–30° to the southeast (Fig. 3.2).

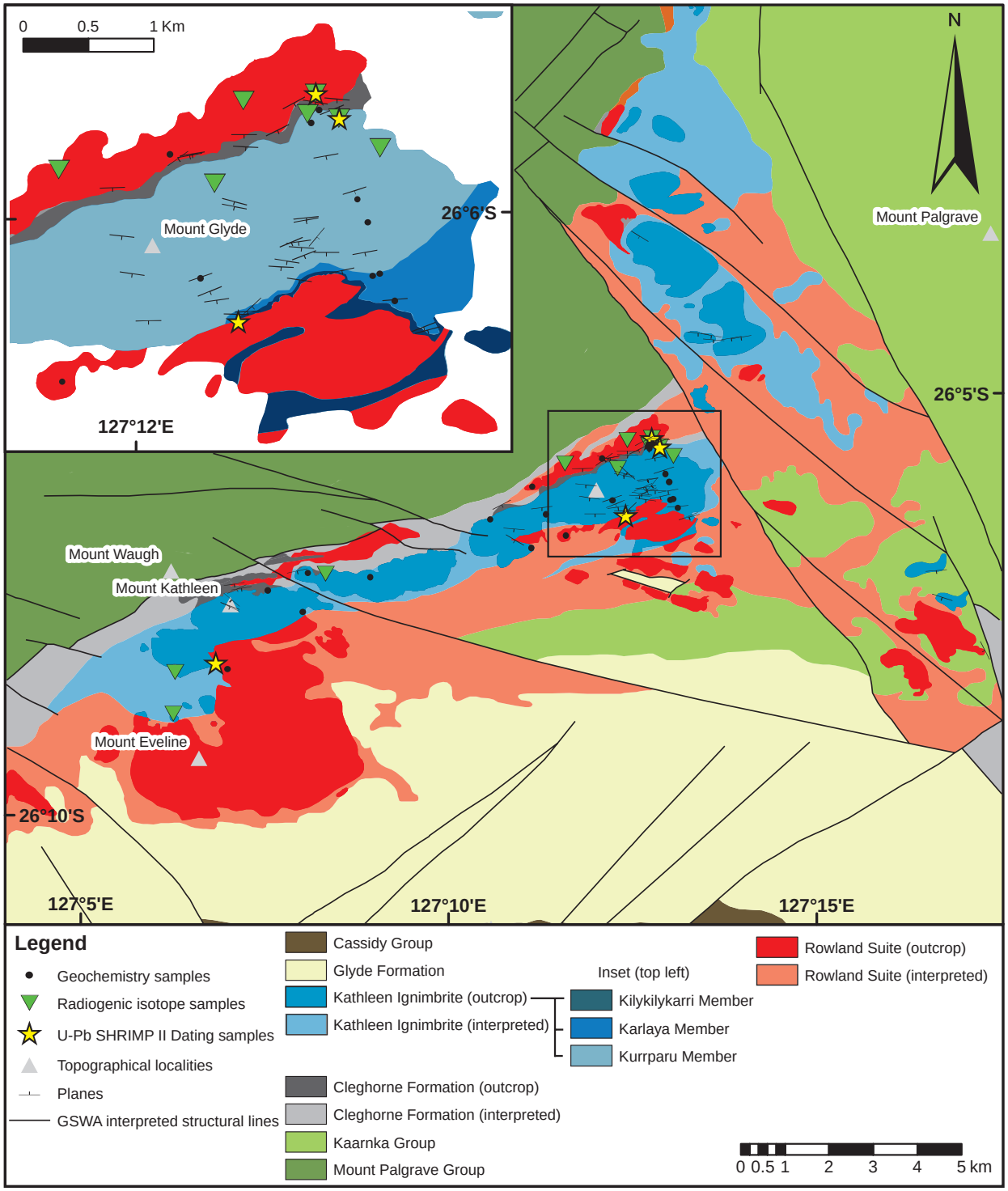

Figure 3.2: Geological map of the study area. Dark colours indicate exposures, whereas lighter shades of the same colour indicates interpreted bedrock. Geochemical sample locations are indicated by yellow stars. Structural sections A, B, C, D and E are indicated on the map (adapted from Werner *et al*., 2012).

3.4 Sampling

Field mapping and sampling were undertaken as part of an ongoing regional Geological Survey of Western Australia (GSWA) mapping program; samples were collected at regular intervals along traverses with the majority of sampling from the undeformed eastern section of the study area (section C; Fig. 3.2). Petrological descriptions are based on hand specimens and representative thin sections, and samples for U-Pb geochronology

from both the Rowland Suite and Kathleen Ignimbrite (Formation) were selected in order to provide stratigraphic age constraints.

3.5 Petrography

3.5.1 Kathleen Ignimbrite

The Kathleen Ignimbrite (Formation) consists of variably welded ignimbrites and some reworked and resedimented volcaniclastic deposits, although this paper focuses exclusively on the ignimbrites. The Kurrparu and Karlaya member ignimbrites are hereafter collectively referred to as the Kathleen Ignimbrite, as both members formed during the same continuous eruptive event that created the Kathleen caldera and subsequently in-fill this caldera. A number of distinct macroscopic lithofacies occur throughout the Kathleen Ignimbrite; the ignimbrites within this unit contain well-preserved volcanic features, such as columnar jointing, eutaxitic fiamme, autobreccias, peperite and hyaloclastites. Flow-laminations and flow-folds are present throughout, although they are particularly prominent in the basal 50 m, defining an apparently coherent lava-like facies. This facies is indicative of extremely high-grade welding and intense rheomorphic conditions.

The ignimbrites (Fig. 3.3a) contain a visually estimated modal abundance of a primary igneous mineral assemblage that is dominated by ~30% volcanic quartz, ~25% mesoperthitic K-feldspar, ~20% plagioclase, 10% biotite and ~5% Fe-Ti oxides, together with ~5% minor accessory minerals such as fluorite, apatite, zircon, titanite and garnet (Fig. 3.3b). The unit is almost all fresh, with very minor alteration represented by <5% secondary mineral phases, such as interstitial chlorite, carbonate, muscovite, pyrite and chalcopyrite. Phenocrysts and crystal fragments constitute up to 40% of the ignimbrites, with the remaining >60% present as a very fine-grained (0.1–0.5 mm, with some regions >1 mm) microgranular quartz-feldspar mosaic matrix (Fig. 3.3b). Glomerocrysts (mm-scale) of biotite, titanite and Fe-Ti oxides are also present in the matrix. Green biotite is abundant throughout the matrix within large clusters or as individual crystals (<0.2 mm). Individual isolated crystals (0.1–1 mm) or clusters (up to 2 cm in size) of purple fluorite are present throughout the matrix. Abundant large (mm- to cm-scale) feldspar and

Figure 3.3 (opposite page): Photos of macroscopic textural features in hand-samples and photomicrographs of microscopic textures seen in thin sections from the Pussy Cat Group rhyolites. a) Hand-sample of the Kathleen Ignimbrite showing the heterogeneous crystal distribution (i.e. mingling of the crystal-rich cumulate and crystal-poor melt-rich magmas). b) Typical matrix of the Kathleen Ignimbrite with embayed volcanic quartz, K-feldspar and plagioclase phenocrysts, sitting within a very fine-grained matrix, composed primarily of a quartz-feldspar mosaic (XPL). c) Hand-sample of the Rowland Suite showing the crystal-rich, coarse-grained nature of the intrusive suite. d) Typical groundmass texture of the Rowland Suite (XPL). e) Large glomerocryst of biotite, titanite and oxides occurring within both the matrix of the Kathleen Ignimbrite and groundmass of the Rowland Suite (PPL). f) CL image of representative zircons from sample 195001 (Rowland Suite) with numbered circles indicating the approximate positions of analysis sites, black crystals are not zircons. g) Coarse-grained, crystal-rich pumice population in the Kathleen Ignimbrite. h) Aphyric pumice population in the Kathleen Ignimbrite.

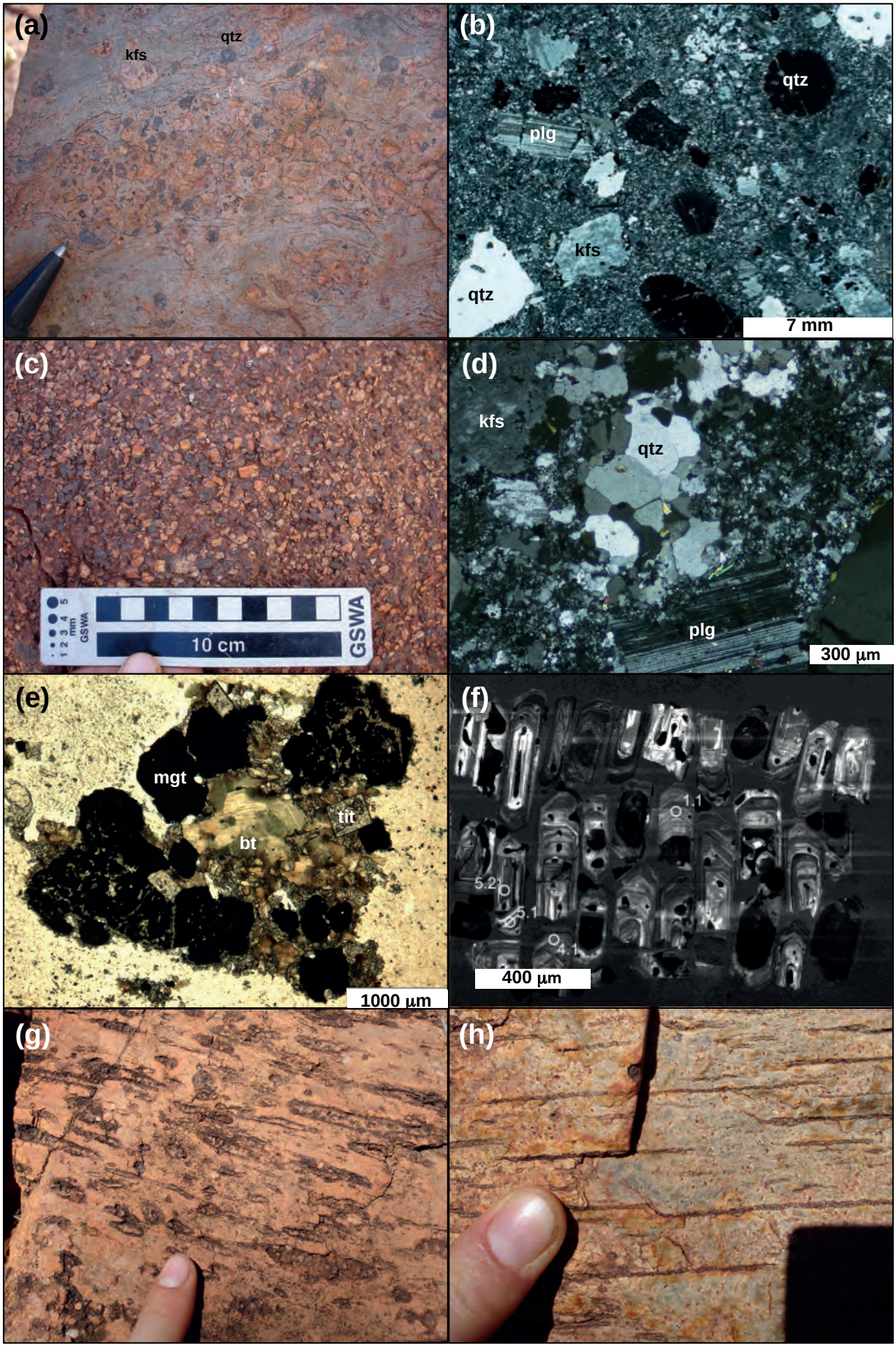
(a)
kfs
qtz
(b)
qtz
plg
kfs
qtz
7 mm
(c)
10 cm
GSWA
(d)
kfs
qtz
plg
300 µm
(e)
mgt
tit
bt
1000 µm
(f)
1.1
5.2
5.1
4.1
400 µm
(g)
(h)

quartz macrocrysts occur throughout the ignimbrite; the latter are euhedral (bi-pyramidal) to angular, broken and irregular in shape, range from 0.2–9 mm in size, commonly have embayed margins and contain fluorite inclusions. Mesoperthitic alkali feldspar macrocrysts are <24 mm in size and contain albite stringer domains and individual crystals that define a coarse internal patchwork pattern. The majority of unaltered feldspars phenocrysts host fluorite inclusions, while some feldspar phenocrysts are very slightly altered, with minor secondary carbonate, mica, and chlorite replacement and the development of fine-grained rims of granophyric quartz. Plagioclase is anhedral to rarely subhedral, angular, fractured, <4 mm in size, and some phenocrysts have slight sericite alteration that creates a speckled appearance. The matrix texture is interpreted to be the result of devitrification and recrystallisation of original primary fragmental glass.

The Kathleen Ignimbrite eruption sequence exhibits a crude stratification that demonstrates both variations in welding intensity and crystal content from the base to the top of the sequence (Chapter 2). The basal section is generally crystal-poor (<5 vol.%), with crystal abundances gradually increasing upwards and peaking in the middle of the sequence (15–25 vol.%), before gradually decreasing to a crystal-poor (<5 vol.%) facies, followed by an increase again in crystal abundance in the upper facies (10–20 vol.%). Overall the deposit is texturally heterogeneous, with coarse-grained, crystal-rich patches forming discontinuous layers or lenses with faint boundaries marked by changes in matrix texture, enclosed in crystal-poor domains (Fig. 3.3a). Crystal-rich areas have larger crystal grainsizes more abundant quartz and feldspar phenocrysts, and most likely represent juvenile pyroclasts, whereas crystal-poor areas are aphanitic and lack feldspar (<5 vol. % small quartz phenocrysts). In addition to the textural heterogeneity, there are two clearly distinguishable pumice populations; one is coarse grained and crystal-rich, the other is fine-grained and aphyric. Such features indicate the presence of two contemporaneous silicic magmas during the ignimbrite-forming eruption: a crystal-poor, near liquidus to supra-liquidus temperature magma that contained rare feldspar phenocrysts, and the other a crystal-rich, feldspar and quartz phenocryst dominated, sub-liquidus temperature magma (Chapter 2).

3.5.2 Rowland Suite

The Rowland Suite intrusions are grey to blue-grey, phaneritic, crystal-rich (15-40 vol. %) and porphyritic (Fig. 3.3c). Primary igneous minerals include ~20% to 25% microperthite and microcline K-feldspar, ~10% plagioclase, ~35% quartz, ~10% biotite, ~10% Fe–Ti oxides, and ~5% primary accessory minerals that include fluorite, zircon, titanite and apatite (Fig. 3.3d). Secondary mineral phases include <5% muscovite and <3% carbonate. K-feldspar and plagioclase phenocrysts are pink and white respectively, are euhedral to subhedral, and are <13 mm. Quartz phenocrysts are rounded to subhedral,

frequently embayed and <9 mm in size. The groundmass is a coherent, microcrystalline and microgranular intergrown quartz-feldspar mosaic that contains glomerocrysts of biotite, titanite and Fe–Ti oxides (Fig. 3.3e). The texture of the groundmass is interpreted to be the result of devitrification and recrystallisation of original primary coherent glass.

3.6 Analytical methods

All samples were cut, crushed, and milled using a diamond saw, ceramic hydraulic press, ceramic jaw-crusher, and tungsten-carbide mill at the School of Geosciences, Monash University and the Earth Sciences Department, Melbourne University, Melbourne, Australia.

Major element, F and Cl concentrations were determined using X-Ray Fluorescence (XRF) spectrometry and a Bruker-AXS S4 Pioneer XRF Spectrometer at the Advanced Analytical Centre, James Cook University, Townsville, Australia. Prior to major element analysis ~2 g of each sample was ignited in a muffle furnace at 1000°C to determine loss on ignition (LOI) values before 1 g of ignited sample was fused with 8 g of lithium tetraborate flux in Pt crucibles for 12 minutes at 1100°C, producing homogeneous glass fusion beads that were used during analysis. F and Cl analysis was undertaken on pressed pellets formed by mixing milled sample powders with binding agents and pressing the mixture into aluminium cups. The precision for major element results are better than ±1% (1 sd). Ferric and ferrous iron are reported as total Fe_2O_3.

Trace and rare earth element (REE) concentrations were determined by inductively coupled plasma-mass spectrometry (ICP-MS) and a Thermo Finnigan X series II quadrupole instrument at the School of Geosciences, Monash University. Prior to analysis, approximately 50 mg of milled sample powder was digested using a high pressure mixed HF-HNO_3-HCl acid attack in sealed Savillex Teflon vials in a hot plate at 150°C for approximately 48 hours. Subsequently the samples were dried down and taken back into solution using 3% HNO_3 for final presentation to the mass spectrometer. ICP-MS count rates were externally standardised using recommended values for the Sco 1 certified reference material, and drift corrections were applied using In and Bi as internal standards and by repeat analysis of dummy standards. The precision of the ICP-MS analysis undertaken during this study was assessed by repeat analyses and is generally better than 7.5%. The accuracy determined though repeat analysis of standards and individual samples indicate negligible contamination from sample preparation and a acceptable level of accuracy (Table 3.1 – Appendix B).

Zircon separation was undertaken at the Earth Sciences Department, University of Melbourne and the School of Geosciences, Monash University, Melbourne, Australia,

using crushing, sieving, heavy-liquid and magnetic separation before hand-picking under a binocular microscope. Zircon U-Pb dating was undertaken at the John de Laeter Centre for Isotope Research at Curtin University, Perth, Australia, using a Sensitive High Resolution Ion MicroProbe (SHRIMP II) instrument. Sample zircons and standards OG1 and BR266 (Stern, 2001a, 2001b, Stern *et al.*, 2009) were mounted in epoxy resin and polished to approximately half-grain thickness to expose grain centres. The zircons were imaged using transmitted and reflected light. Mounts were gold coated and imaged in a Phillips XL-30 SEM equipped with a cathodoluminescence (CL) detector (Fig. 3.3f).

Specific details of operating procedures for U, Th, and Pb measurements are given in Wingate and Kirkland (2013). The BR266 zircon standard (559 Ma, 903 ppm ^{238}U; Stern, 2001a) was used to calibrate U/Pb ratios and uranium concentrations. Fractionation of ^{207}Pb*/^{206}Pb* was monitored during each session by analysis of the 3465 Ma OG1 zircon standard (Stern *et al.*, 2009). No correction for ^{207}Pb*/^{206}Pb* fractionation was deemed necessary. The results of SHRIMP analysis are given in Table 3.2 – Appendix B and all uncertainties are stated as 2σ values. During all analytical sessions the BR266 standard indicated an external spot-to-spot uncertainty of less than 1.25% and a ^{238}U/^{206}Pb* calibration uncertainty of less than 0.6%. The calibration uncertainty, added in quadrature, is included in the uncertainties of ^{238}U/^{206}Pb* ratios and dates listed in Table 3.2 – Appendix B. Common Pb corrections were applied to all analyses using measured ^{204}Pb and the contemporaneous isotopic compositions of Stacey and Kramers (1975). However, owing to the low levels of common Pb in most analyses and the near-concordance of data, neither the type (e.g., 204-correction, 207-correction) nor application of common Pb corrections makes a significant difference to the calculated ages.

Zircon Lu-Hf isotope analysis was undertaken by laser ablation multicollector ICP-MS (LA-MC-ICP-MS) using a HelEx laser ablation system coupled to a Nu Plasma MC-ICP-MS (Woodhead *et al.*, 2004). The HelEx system is based on a Lambda Physik (Germany) 193 nm ArF excimer laser interfaced with a fast-washout two-volume ablation chamber (Eggins *et al.*, 1998). Polished zircon mounts, extracted from the same separates used for the U-Pb dating by ion microprobe, were placed in the ablation chamber with mounts containing reference material. Zircons were ablated in a helium atmosphere to minimise condensation of the ejecta plume, using a 55 μm laser spot with a 5 Hz repetition rate and a power density on sample <5 J/cm^2, resulting in a drill rate of 0.1-0.2 μm/pulse. Total Hf signals obtained for standard zircons (91500, QGNG, Plesovice, Temora-2) varied from 4-15 V for standards and unknowns. Mass bias for Hf isotopes was corrected by internal normalisation (^{179}Hf/^{177}Hf = 0.7325) using the exponential law. Correction of isobaric interference from ^{176}Yb on ^{176}Hf (typically 10-20%, up to 50% in rare cases) was constrained using the Yb mass bias determined by comparing the ^{173}Yb/^{173}Yb ratio measured during the analysis and the ratio recommended in Chu *et*

al. (2002). Interference from ^{176}Lu was monitored at ^{175}Lu, was typically <1%, and was corrected using measured Yb. ^{176}Hf/^{177}Hf ratios (corrected for gas blank, mass bias and interferences) for standard and unknowns had typical within-run precisions of ±0.000045-0.000070 (2se). Measured ^{176}Hf/^{177}Hf (±2sd) for Temora-2 (0.282670 ±44, n = 5; 0.282676 ±72, n = 12), Plesovice (0.282499 ±26, n = 4; 0.282493 ±30, n = 6), 91500 (0.282292 ±48, n = 8) and QGNG (0.281631 ±27, n = 3) are within error of solution determined reference values (Sláma *et al.*, 2008, Woodhead & Hergt, 2005); no bias corrections were therefore applied to the West Musgrave zircon data. Based on the results for standard zircons, external precision is estimated to be similar to internal precision of single spots, or ±2.5 εHf units. Lu/Hf ratios were calculated from count rates. Initial εHf values for unknowns were calculated relative to the average chondrite reference values (^{176}Lu/^{177}Hf = 0.0332, ^{176}Hf/^{177}Hf = 0.282772) of Blichert-Toft & Albarede (1997). Lu-Hf model ages (2-stage, T_{DM}^{2}) were calculated for a 4.56 Ga depleted mantle model with a present-day composition of ^{176}Lu/^{177}Hf = 0.0383, ^{176}Hf/^{177}Hf = 0.283225 (equivalent to εHf = +16) and a default crustal ^{176}Lu/^{177}Hf = 0.015 for the older stage (Griffin *et al.*, 2002, 2004, Kirkland *et al.*, 2013, Smithies *et al.*, 2013). The decay constant for ^{176}Lu is 1.867 x 10^{-11}/y (Scherer *et al.*, 2001, Söderlund *et al.*, 2004).

Radiogenic isotope analysis was undertaken in the VIEPS facilities at the University of Melbourne. Whole-rock Sm-Nd and Rb-Sr isotope analyses were undertaken by isotope dilution using ~60 mg of rock powder spiked with ^{85}Rb-^{84}Sr and ^{149}Sm-^{150}Nd tracers and dissolved at high pressure (Maas *et al.*, 2005). Sr, Sm and Nd were extracted using a combination of EICHROM Sr-, RE- and LN-resin, with Rb purified using conventional cation exchange chemistry. Total analytical blanks were <100 pg and negligible. All isotopic analyses were carried out on a Nu Plasma multi-collector ICP-MS coupled to a CETAC Aridus low-uptake desolvating nebuliser. Instrumental mass bias was corrected by normalising to ^{88}Sr/^{86}Sr = 8.37521 and ^{146}Nd/^{145}Nd = 2.0719425 (equivalent to ^{146}Nd/^{144}Nd = 0.7219; Vance & Thirlwall, 2002), using the exponential law as part of an on-line iterative spike-stripping/internal normalization procedure. Data are reported relative to SRM987 ^{88}Sr/^{86}Sr = 0.710230 and La Jolla ^{143}Nd/^{144}Nd = 0.511860. Typical in-run precisions (2se) are ±0.000020 (Sr) and ±0.000010 (Nd), with external precision (reproducibility, 2sd) of ±0.000040 (Sr) and ±0.000020 (Nd). External precisions for ^{87}Rb/^{86}Sr and ^{147}Sm/^{144}Nd obtained by isotope dilution are ±0.5% and ±0.2%, respectively. Results for international rock and solution standards (see Table 3.3 – Appendix B) agree with TIMS reference values (e.g., Raczek *et al.*, 2003). Modern CHUR has ^{147}Sm/^{144}Nd = 0.1967, ^{143}Nd/^{144}Nd = 0.512638. Sm-Nd model ages (T_{DM}^{2}) are 2-stage model ages relative to a model modern depleted mantle with ^{147}Sm/^{144}Nd = 0.2136, ^{143}Nd/^{144}Nd = 0.513151 and a crustal average ^{147}Sm/^{144}Nd ratio of 0.1100 for the older stage. Age-corrected initial εNd values have a propagated precision of ±0.5 units; the propagated precision for initial ^{87}Sr/^{86}Sr ratios is strongly influenced by the Rb/Sr ratio and ranges from ±0.0001 to ±0.0092 for the data

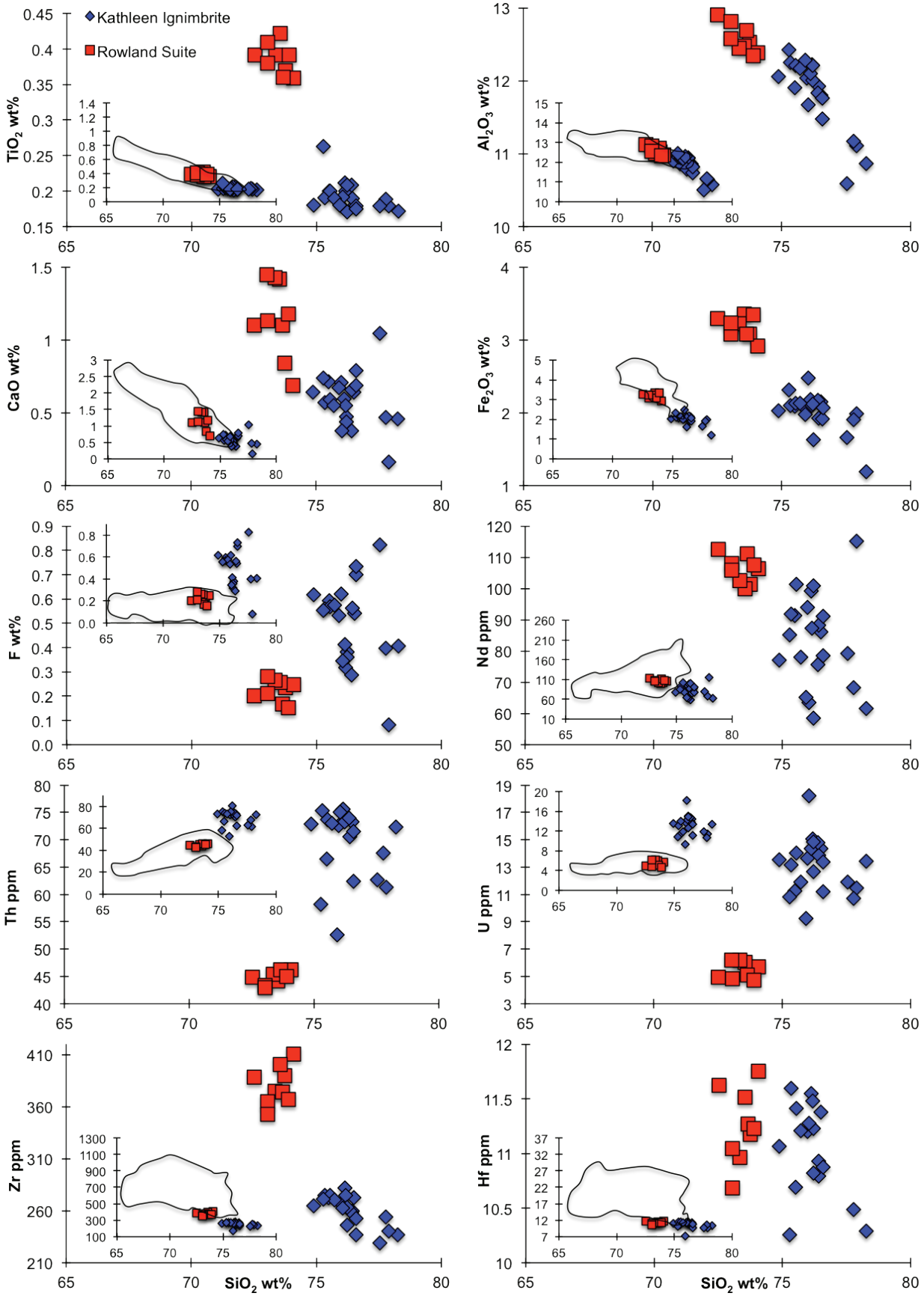

Figure 3.4: Harker diagrams for the Pussy Cat Group rhyolites and published west Musgrave silicic geochemical data for the Talbot Sub-basin (Inset; Smithies *et al*., 2013) showing SiO_2 variation *vs*. selected major and trace elements. Rowland Suite (red squares), Kathleen Ignimbrite (blue diamonds), Talbot Sub-basin rhyolites (black line field).

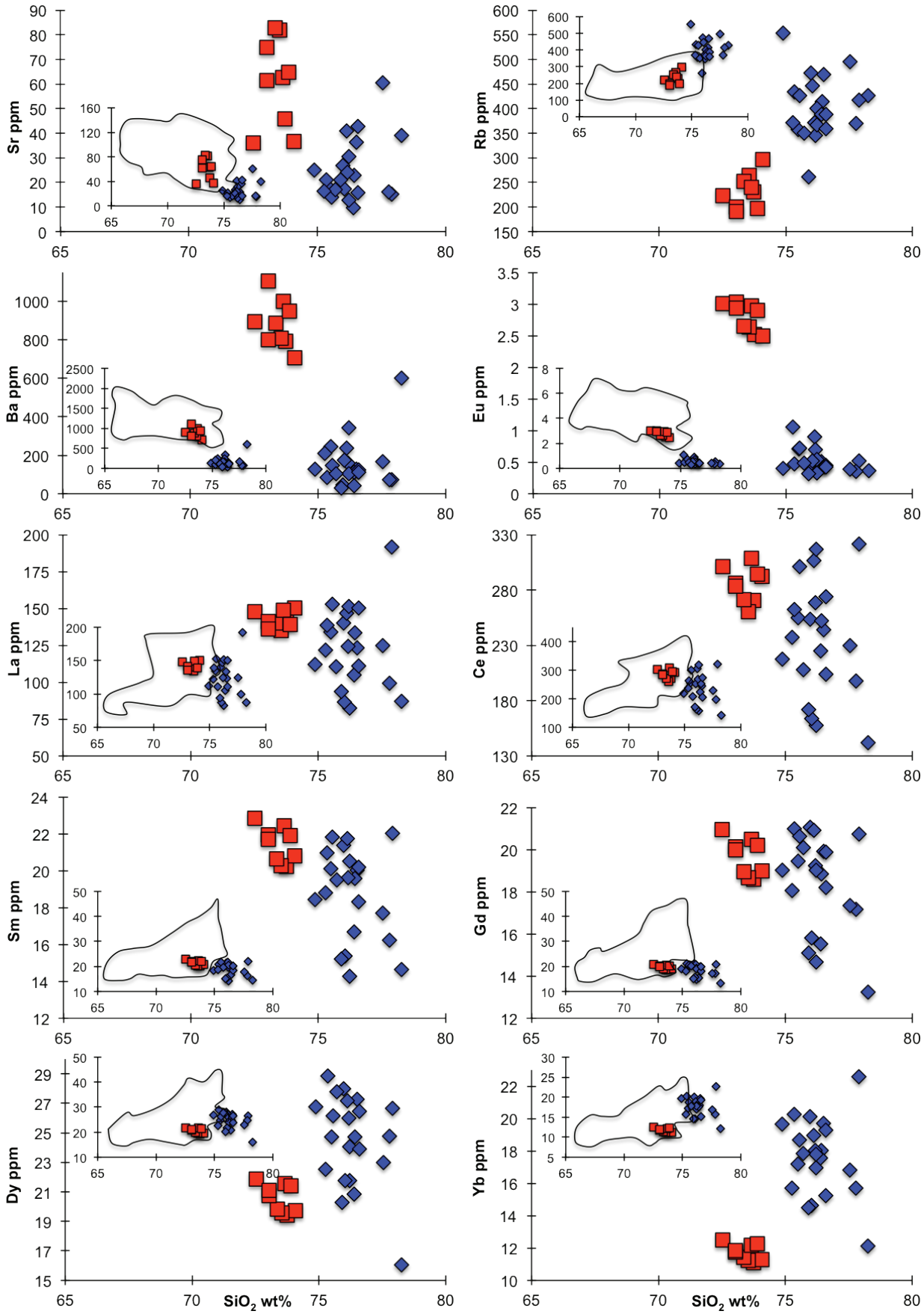

Figure 3.4 (continued).

presented here. Decay constants are: ^{87}Rb 1.42 10^{-11}/a; ^{147}Sm 6.54 10^{-12}/a; further details are given in Table 3.3 – Appendix B.

3.7 Results

3.7.1 Whole-rock geochemistry

All whole-rock compositions (excluding F and Cl) were normalised to 100% anhydrous before interpretation and iron concentrations are provided as total Fe_2O_3 (Table 3.1 – Appendix B). All samples analysed during this study contain moderate to high concentrations of SiO_2 (71–78 wt%), although the Kathleen Ignimbrite samples have higher and more variable SiO_2 concentrations than the Rowland Suite (Table 3.1 – Appendix B). Kathleen ignimbrite samples have Al_2O_3, CaO, Fe_2O_3, Zn, Hf, Nd and Zr concentrations that negatively correlate with SiO_2, whereas Sr and U concentrations positively correlate with SiO_2 (Fig. 3.4). In comparison, Rowland Suite samples have TiO_2, Al_2O_3, Fe_2O_3, CaO, Sr, Cd, Ba, and all rare earth elements (REE) except La concentrations that negatively correlate with SiO_2, whereas Be, Zr, Hf, and Nb have positive correlations in Harker diagrams (Fig. 3.4). There is a distinct change in the behaviour of the REE with the concentration of the heavy (HREE) in the Rowland Suite much lower than within the Kathleen Ignimbrite, and as evidenced by La and Dy concentrations (Fig. 3.4), the opposite is true of the light (LREE), suggesting a change in compatibility of the REE related to the differing fractionation of the two suites. The negative correlation for both Zr and Hf concentrations with SiO_2 for the Kathleen Ignimbrite and the fact that the Zr/Hf ratios decrease with decreasing Zr concentrations (Fig. 3.5a), are both indicative of zircon fractionation, and suggests that this suite was zircon saturated (Linnen and Keppler, 2002; Thomas *et al*., 2002; Agangi *et al.*, 2012). Although these rocks are Mesoproterozoic in age, they do retain igneous characteristics (e.g., Rb is fairly immobile in both units; Fig. 3.4). All of these Pussy Cat Group samples contain high concentrations of fluorine (0.2–0.8 wt%) relative to average crustal abundances (e.g., Rudnick and Gao, 2003). These samples are classified using the total alkali (K_2O+Na_2O) vs. SiO_2 TAS diagram of Le Maitre *et al*. (1989, 2002), which indicates that all samples are rhyolitic. Samples from both suites plot along or below the alkaline dividing line of Irvine and Baragar (1971), indicating they are generally subalkaline (Fig. 3.5b), and the majority of these samples have aluminium saturation index (ASI or A/CNK, namely the molar ratio of Al_2O_3 to CaO + K_2O + Na_2O; Frost & Frost, 2008, Zen, 1988) values that indicate they are metaluminous (ASI = 0.91–1.09), with a few samples classified as peraluminous (ASI >1.0; Frost *et al.*, 2001).

All samples have FeO* (FeO/FeO+MgO; Frost & Frost, 2008) values of 0.86–0.97 with modified alkali-lime index (MALI; Frost and Frost, 2008) values of 6.58–9.25,

classifying them as intermediate between alkali-calcic and calc-alkalic. In addition, all samples are A-type (Loiselle & Wones, 1979, Collins *et al.*, 1982, White & Chappell, 1983) and plot within the anorogenic granite field of Whalen *et al*. (1987) or the *within-plate* fields of the tectonic discrimination diagrams of Pearce *et al*. (1984; Fig. 3.6a), Whalen *et al.* (1987; Fig. 3.6b), Eby (1992; Fig. 3.6b) and Verma *et al*. (2013). All samples are therefore classified as A-type, alkali-calcic to calc-alkalic metaluminous to slightly peraluminous rhyolites that were generated during magmatism in an anorogenic intra-plate extensional tectonic setting, such as a rift or oceanic basin (Whalen *et al.*, 1987, Eby, 1990, Shellnutt & Zhou, 2007).

Kathleen Ignimbrite samples are LREE-enriched but have flat to slightly enriched HREE patterns on chondrite-normalised REE diagrams (La_N/Sm_N = ~4.1, Fig. 3.7a, where N denotes normalisation to chondrite values of Sun and McDonough, 1989), whereas

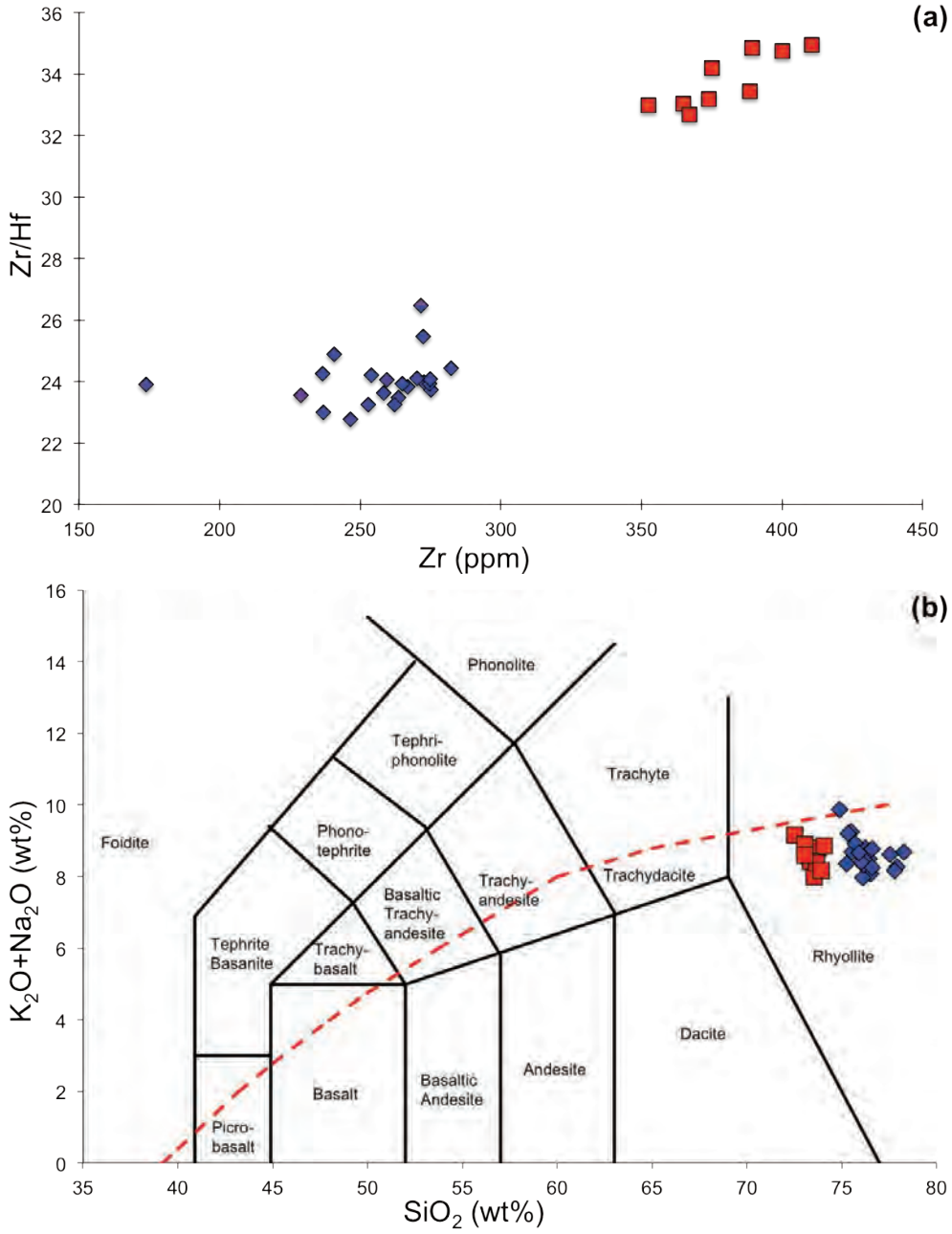

Figure 3.5:
a) Zr/Hf *vs*. Zr showing zircon saturation is reached in both units.
b) TAS Classification diagram with samples plotting below the alkaline dividing line of Irvine and Baragar (1971).

Rowland Suite samples contain higher LREE concentrations, albeit with similar La_N/Sm_N ratios (~4.2), but are comparatively HREE-depleted (Gd_N/Yb_N for the Kathleen Ignimbrite of ~0.9 vs. Gd/Yb_N for the Rowland Suite of ~1.4). Both suites have significant negative Eu anomalies (Eu/Eu*, where $Eu/Eu^* = Eu_N/\sqrt{Sm_N.Gd_N}$; Taylor & McLennan, 1985) with Kathleen Ignimbrite samples having lower values (average = 0.1) than Rowland Suite samples (average = 0.4). Both suites show negative anomalies with respect to primitive mantle (Sun and McDonough, 1989; Fig. 3.7b) for Ba, Ta, Sr and Ti, and are enriched in Rb, Th, and U, with the Kathleen Ignimbrite containing extremely high concentrations of Rb, Th and U compared to both the Rowland Suite and published average values for many other rhyolites (Mernagh & Miezitis, 2008). These rhyolites are compositionally similar to topaz rhyolites of central-western USA (e.g., Burt *et al*., 1982; Christiansen *et al*., 1986; 2007), which are also REE-enriched and have high F concentrations (>0.2 wt%).

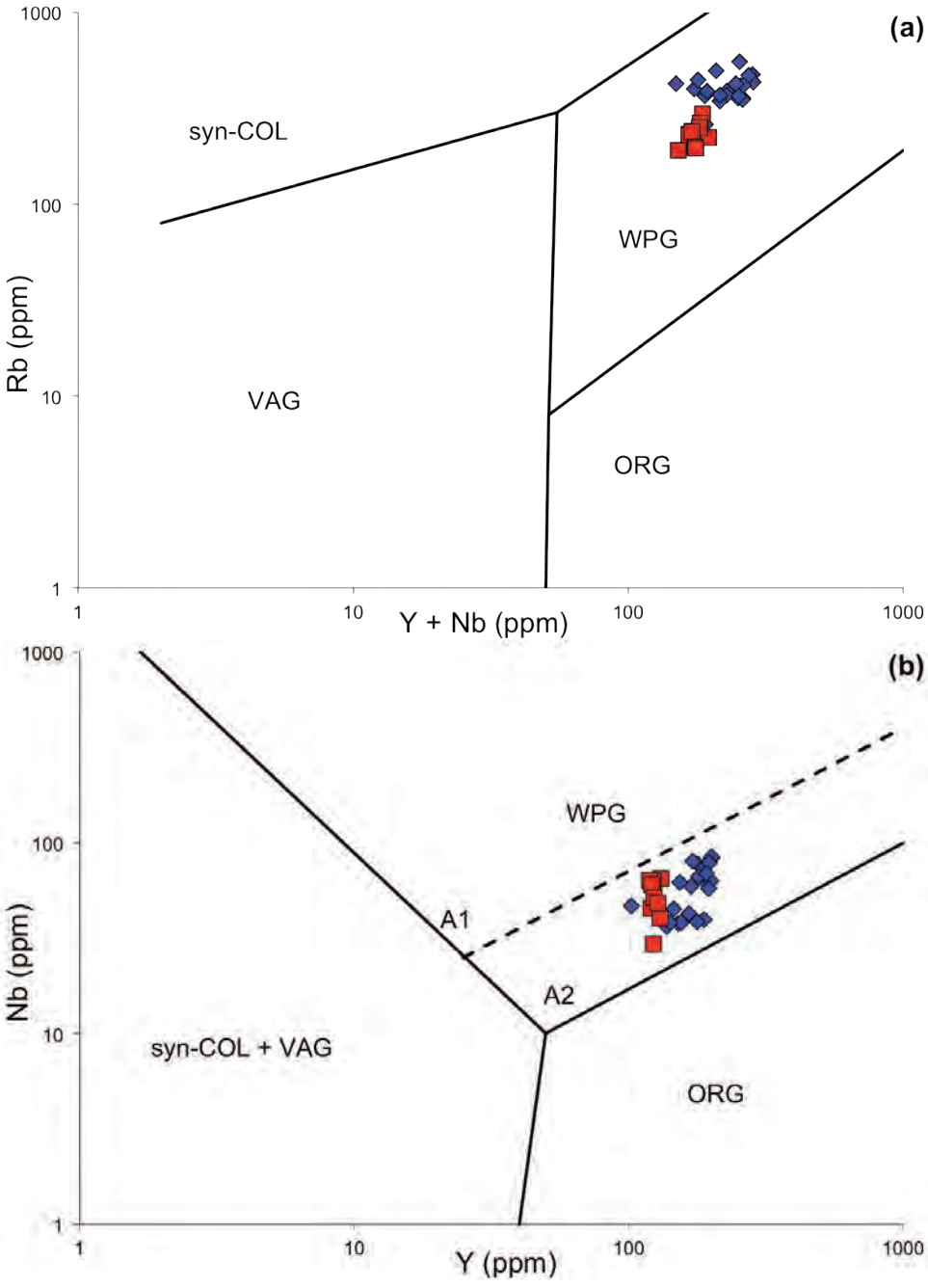

Figure 3.6: a) Typical anorogenic, A-type, within-plate signature of samples after Pearce *et al*. (1984).(WPG: within-plate granites, ORG: ocean-ridge granites, VAG: volcanic-arc granites, syn-COL: syn-collisional granites). b) Y-Nb diagram (Whalen *et al*., 1987) used for A-type classification, indicating A1 and A2 groups (Eby, 1990; 1992). The A1 group (Y/Nb ratios <1.2) are derived from mantle differentiates similar to sources for oceanic island, intraplate and rift-zone magmas, and the A2 group (Y/Nb ratios >1.2) are derived from processes that form continental crust and island-arc basalts. See discussion for further explanation on possible misinterpretation. Also note the two distinct clusters within the Kathleen Ignimbrite and the overlap between the two units.

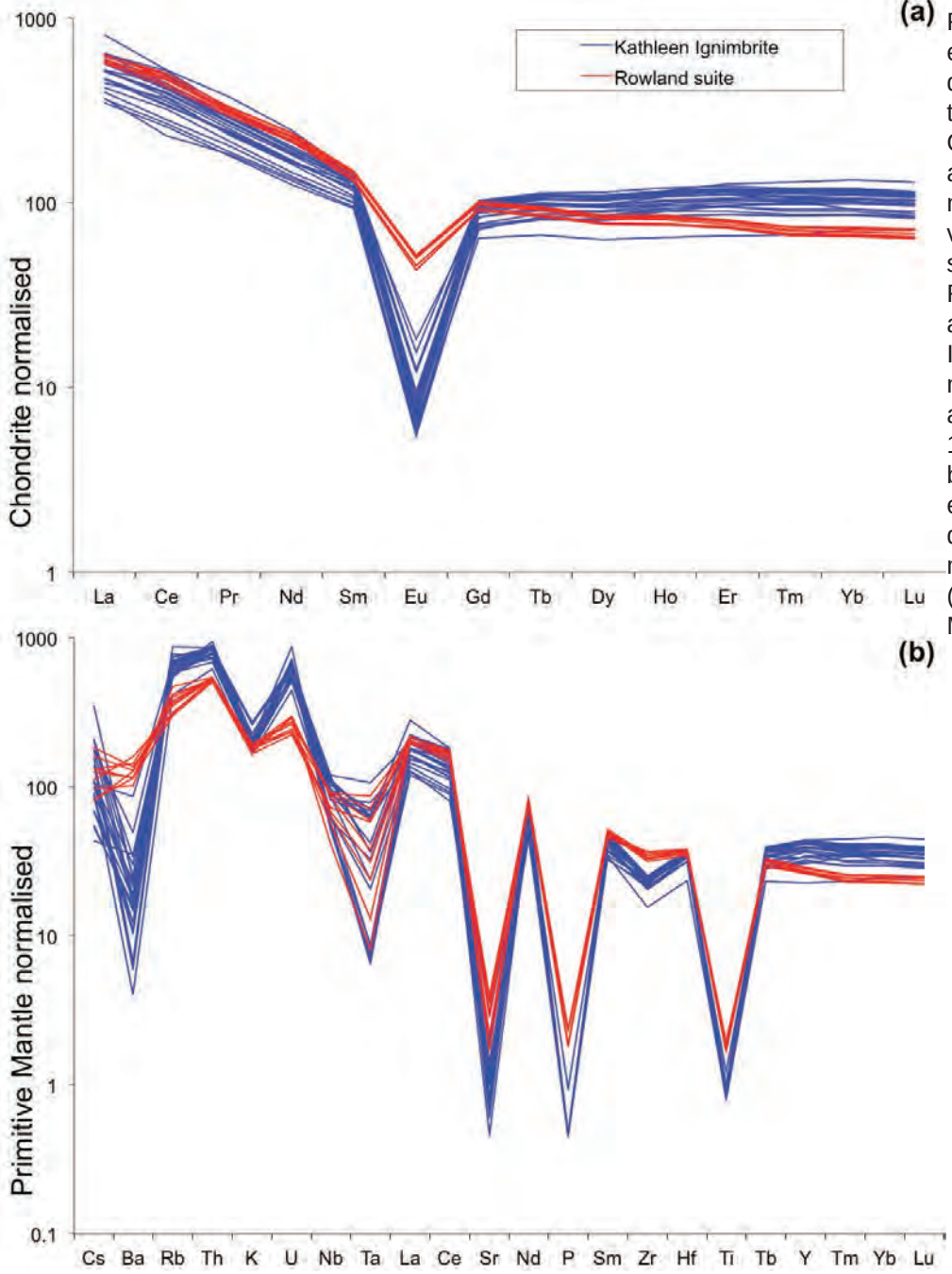

Figure 3.7: REE and multi-element variation diagrams for the Pussy Cat Group rhyolites: a) Chondrite normalised REE variation diagram showing both the Rowland Suite and the Kathleen Ignimbrite, chondrite normalised (Sun and McDonough, 1989). b) Extended trace element variation diagram, primitive mantle normalised (Sun and McDonough, 1989).

3.7.2 Geochronology

The zircons analysed during this study were euhedral, prismatic, colourless to pale brown, and up to 400 µm long. Cathodoluminescence (CL) imaging (Fig. 3.3f) indicates that the majority of these zircons are oscillatory zoned with many containing textural discordances indicating the presence of either xenocrysts or antecrysts. Many zircons with textural discordances have partially to nearly completely reabsorbed cores overgrown by oscillatory zoned zircon, although both cores and rims yield ages that are identical within uncertainty. Cores have lower CL emissions (consistent with higher uranium contents) than the oscillatory zoned overgrowths. A combined concordia diagram for four samples is shown in Fig. 3.8.

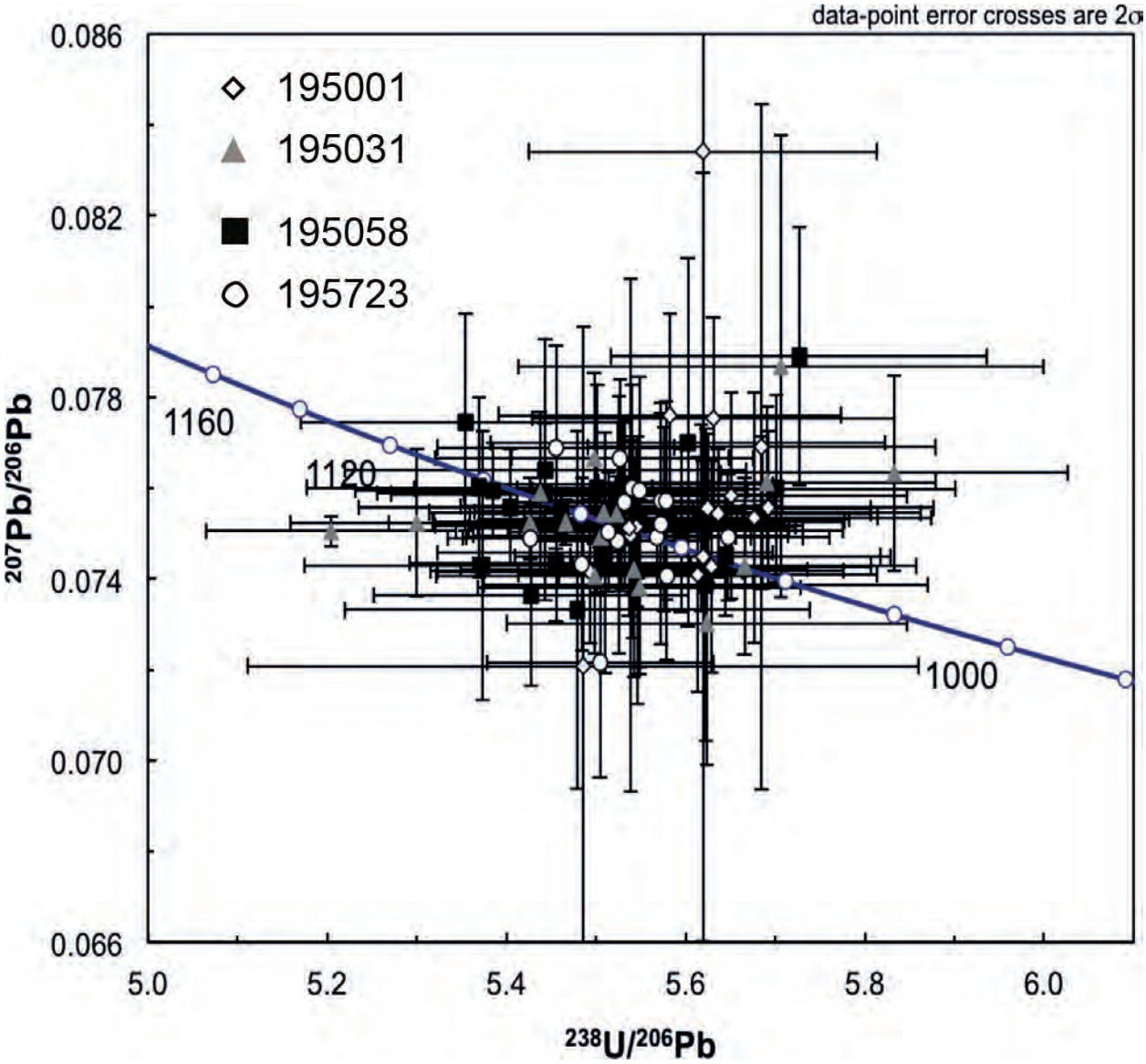

Figure 3.8: U–Pb analytical data on a combined concordia plot for Rowland Suite and Kathleen Ignimbrite samples analysed and used during this study: Rowland Suite (195001–diamond; 195031–triangle; 195058–square); Kathleen Ignimbrite (195723–circle); error bars show 2σ uncertainty; see Fig. 3.2 for sample locations.

Three Rowland Suite samples were dated (195001, 195031, and 195058); Sample 195001 is from a syn-sedimentary, sub-volcanic porphyritic rhyolite intrusion that underlies the Kathleen Ignimbrite in the east of the study area (Fig. 3.2). A total of 17 analyses were undertaken on 15 zircons during this study; 5 analyses are >5% discordant and are not considered further. A coherent group of 12 analyses (Fig. 3.8) yield a concordia age of 1062 ± 8 Ma (mean square weighted deviation (MSWD = 0.47; mean square of weighted deviates, York, 1966).

Sample 195031 is from a porphyritic rhyolite intrusion of the Rowland Suite that intrudes into the upper Kilykilykarri Member of the Kathleen Ignimbrite (Formation) in the east of the study area (Fig. 3.2). A total of 17 analyses were undertaken on 14 zircons, four of which are >5% discordant. Thirteen concordant analyses (Fig. 3.8) yield a concordia age of 1076 ± 5 Ma (MSWD = 0.96), identical to the lower intercept date of 1076 ± 8 Ma

(MSWD = 1.5) calculated from a common-Pb regression through all but two analyses. The two analyses excluded from the regression show evidence of either minor radiogenic-Pb loss (analysis 8.2; Table 3.2 – Appendix B) or the presence of an antecrystic component (analysis 8.1; Table 3.2 – Appendix B).

Sample 195058 is from a Rowland Suite porphyritic rhyolite intrusion that cross-cuts the Kathleen Ignimbrite in the western part of the study area (Fig. 3.2); a total of 30 analyses were undertaken on 25 zircons from this sample. Four analyses are >5% discordant and are excluded from further consideration. The remaining 26 analyses (Fig. 3.8) yield a concordia age of 1078 ± 5 Ma (MSWD = 0.84), within uncertainty of the age of the Rowland Suite rhyolite that overlies the Kathleen Ignimbrite in the eastern part of the study area (sample 195031).

Sample 195723 is from the Kathleen Ignimbrite in the east of the study area (Fig. 3.2) and a total of 16 analyses of 16 zircons from this sample were undertaken during this study. One analysis is >5% discordant and is excluded from further consideration. Fifteen analyses (Fig. 3.8) of zircon crystals from this sample yield a concordia age of 1071 ± 5 Ma (MSWD = 0.90), within the uncertainty of the ages of the underlying, overlying and cross-cutting Rowland Suite units.

3.7.3 Radiogenic Isotopes

Measured and age corrected $^{87}Sr/^{86}Sr$, $^{143}Nd/^{144}Nd$, and $^{176}Hf/^{177}Hf$ ratios are listed in Table 3.3 (Appendix B) and all initial isotopic ratios were corrected to a common crystallisation age of 1070 Ma (T); this approach was used as a simplification given the tight overlapping in ages of these units and is an average of the ages from the geochronology data.

3.7.3.1 Whole-Rock Sm-Nd and Rb-Sr isotopes

The whole-rock Sm-Nd and Rb-Sr isotope compositions of nine samples were determined during this study (Table 3.3 – Appendix B). All nine of these samples have Sm/Nd ratios close to average crust ($^{147}Sm/^{144}Nd$ 0.1155-0.1343; Table 3.3 – Appendix B), with homogenous and slightly positive initial εNd values (at 1070 Ma; +0.5 to +1.0; Fig. 3.9c), yielding Nd model ages (T_{DM}^{2}) that average 1.60 ± 0.02 Ga (1sd). These samples also have a Sm-Nd isochron age of 1050 ± 96 Ma.

In contrast, the Rb-Sr radiogenic systematics of these samples are clearly disturbed (Rb/Sr 3-31, Sr 16-77 ppm, Table 3.3 – Appendix B). Various combinations of data points yield similar regression results, all with large errors, and none are considered

reliable. Age correction of individual samples to a nominal age of 1070 Ma yields initial $^{87}Sr/^{86}Sr$ values <0.700 for all but 2 samples (199254: 0.7057±20; 205320: 0.7019±8). Although these two samples have among the highest Sr concentrations of any of the samples analysed during this study (63, 77 ppm), their Rb-Sr systems are unlikely to be undisturbed. These two samples yield an isochron age of ca. 1089 Ma, although this should not be considered robust.

3.7.3.2 In-situ zircon Lu-Hf isotopes

In-situ Lu-Hf isotope data (Table 3.4 – Appendix B) were obtained using zircon separates from seven of the nine samples above, some of which had previously been dated by SHRIMP II ion microprobe. A minimum of 20 zircons from each of the seven samples were analysed during this study. Measured Hf isotope ratios are very homogeneous, both within and between samples, with average age-corrected $^{176}Hf/^{177}Hf_{1070Ma}$ values of 0.28224-0.28227 (εHf +5.0 to +5.8; Table 3.4 – Appendix B), although zircons from

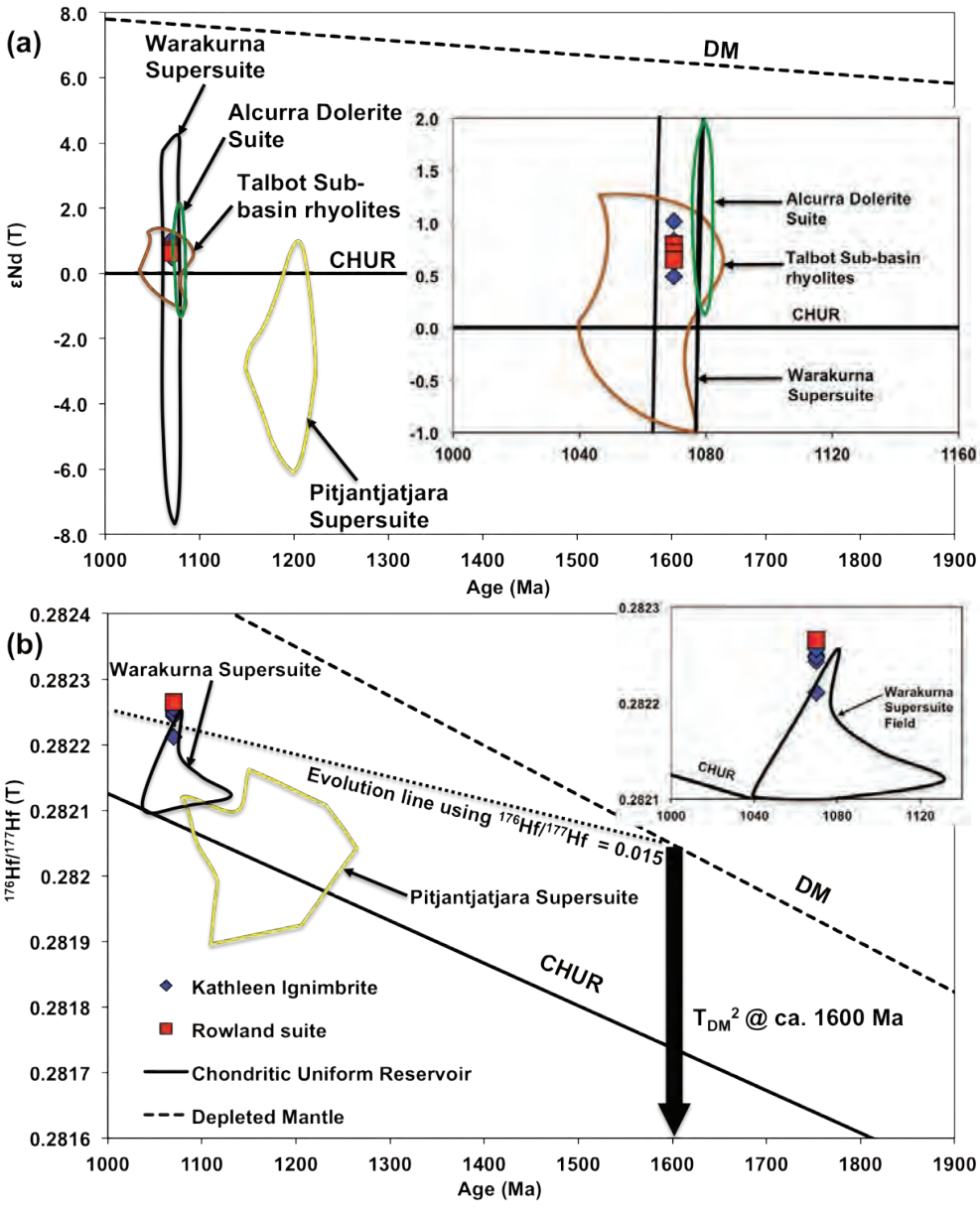

Figure 3.9: Diagrams showing isotopic variations within the Pussy Cat Group rhyolites compared to other units within the west Musgrave Province (Zhao and McCulloch 1993, Kirkland *et al*. 2013, Smithies *et al*. 2013); a) εNd *vs*. crystallisation age. b) Initial $^{176}Hf/^{177}Hf$ *vs*. crystallisation age. Plots indicate a similar radiogenic source region for the Rowland Suite and Kathleen Ignimbrite; a strong mantle origin with little to no crustal contamination for the Pussy Cat Group rhyolites; Nd isotopic similarity with the Alcurra Dolerite Suite; and a Hf two-stage model age of ca. 1600 Ma using a reference evolution line for $^{176}Hf/^{177}Hf$ = 0.015 (adapted from Kirkland *et al*., 2013).

sample 199254 are slightly less radiogenic (0.28221, εHf =+3.9 ±2.3). Average 2-stage Lu-Hf model ages (T_{DM}^{2}) for the zircon populations vary from 1.49 ±0.14 (2 sd) to 1.61 ±0.15 Ga (Fig. 3.9b; Table 3.4 – Appendix B). Only one inherited zircon was identified during analysis; this zircon has a distinctly evolved Hf isotope signature (measured $^{176}Hf/^{177}Hf$ = 0.28132 ±5, εHf = -51.3; versus all other zircons with εHf ~-14 to -19, n = 176). Kathleen Ignimbrite zircons (n = 153) have a mean εHf of +5.3 (+2.3 to +8.2) whereas Rowland Suite zircons (n = 24) have a mean εHf of +5.8 (+3.4 to +7.9). The mean 2-stage model age for all zircons analysed during this study is ca. 1.58 Ga (Scherer *et al*., 2001).

3.8 Discussion

3.8.1 Geochronology

There are no significant or systematic differences in age between zircon cores and rims. However, internal textural relationships, including rounding of zircon cores, discordant contacts with overgrowths, and contorted textures within some cores, are consistent with prolonged zircon growth. This suggests that the cores of these zircons have been partially to completely resorbed, potentially several times, prior to rim formation within the same, long-lived magma system, indicating that the zircons within both the Kathleen Ignimbrite and the Rowland Suite likely contain significant amounts of antecrysts (e.g., Charlier *et al.*, 2005, Miller *et al.*, 2007, Smithies *et al.*, 2013). In addition, two of the samples (195031 and 195058) are taken from Rowland Suite units that intrude into the upper member of, and cross-cut, the Kathleen Ignimbrite (Formation; i.e. are stratigraphically younger), both of which yielded slightly older mean crystallisation ages. These results are consistent with a larger dataset (n = 19) published by Smithies et al., (2013; 2014) for the silicic magmatism of the Talbot Sub-basin, where a large mid-crustal (14–21 km) magma reservoir source, the Talbot Sub-basin magma reservoir, is invoked for the continuous >30 Ma duration of silicic magmatism in the region and is evidenced by extensive overlap in the geochronology of silicic suites within this sub-basin, the presence of complex regrowth or multiple dissolution textures and little evidence for breaks in magmatic activity. Such magma reservoirs are considered critical components of large volume, long-lived silicic systems (e.g., Bachman and Bergantz, 2008; Reid, 2008; Gelman *et al*., 2013).

Based on this, the data presented here likely suggests that the magmas that formed the Pussy Cat Group resided within a common magma reservoir or even an upper level magma chamber (although given the uncertainty on the ages this may be too long for a single chamber) prior to emplacement or eruption, creating a single zircon population. This is also consistent with radiogenic isotope data discussed in the next section. A number of analyses from all four samples yield concordant zircon ages between 1044 Ma and 1049 Ma (Table 3.2 – Appendix B) that are interpreted to represent the youngest possible

age and timing of magmatism that formed Pussy Cat Group rhyolites. It is still possible given the uncertainty on the ages that the Kathleen Ignimbrite and Rowland Suite originated from two distinct sources; this highlights the need for a thorough testing of a common source hypothesis before such an alternative origin can be ruled out.

3.8.2 Radiogenic Isotopes

Whole-rock Nd and zircon Hf isotope systematics are remarkably homogeneous for the volcanic units and are suggestive of mantle-derived magma sources with positive εHf and εNd (Fig. 3.9a), as well as a possible common source region. Positive εNd(T) values imply that a relatively depleted mantle (DM) source may have been involved in the petrogenesis of these rocks (e.g., Zindler & Hart, 1986). The same is true of the $^{176}Hf/^{177}Hf$ values (Fig. 3.9b). Even though the Sr isotope systematics of these samples are disturbed, the comparatively low initial $^{87}Sr/^{86}Sr$ values also supports derivation or influence of a DM source. The data does not show an apparent crustal reworking trend during the 1085–1040 Ma magmatism in the area, corroborating the findings of Kirkland *et al*. (2013), as the data lie above the crustal Hf isotope evolution trend defined by older Musgrave Province zircon crystals (Fig. 3.9b). These compositions require significant renewed mantle-derived input that is consistent with the Giles Event age input of mantle-derived material directly into the crust (Wade *et al.*, 2006; Kirkland *et al.*, 2013).

The 1067 ± 8 Ma (Kirkland *et al*., 2009) Alcurra Dolerite Suite cross-cuts and dissects most of the Musgrave Province and is thought to represent the parental magmas that formed the mafic-ultramafic Giles intrusions. These intrusions are comagmatic with the silicic magmatism during the intra-plate extensional Giles Event (Glikson *et al.*, 1996, Howard *et al.*, 2009; Smithies 2013; 2014) and are therefore a potential source of mantle-derived magmas for the Pussy Cat Group rhyolites (Smithies *et al*., 2013). The Pussy Cat Group rhyolites lie on a horizontal line extending from Alcurra Dolerite Suite compositions on a plot of εNd *vs*. 1/Nd (Fig. 3.10), indicating that these rhyolites could possibly be generated by pure fractional crystallisation from a basaltic mantle-derived magma such as the Alcurra Dolerite Suite. The samples do not lie on the path of the dashed line indicated in Fig. 3.10 that shows a hypothetical crustal contamination trend from a primitive Alcurra Dolerite Suite source, which instead passes through the mixed (<25% by volume) lower crustal partial melt and (>50% by volume) juvenile mantle-derived granites of the 1220–1150 Ma Pitjantjatjara Supersuite (Smithies *et al.*, 2011). Furthermore, the Pussy Cat Group rhyolites are isotopically indistinct from the mantle-derived Alcurra Dolerite Suite, and notably isotopically different to the crustal contaminated Pitjantjatjara Supersuite (Smithies *et al.*, 2011). This potentially indicates an origin for the Pussy Cat Group rhyolites that favours fractional crystallisation from a basaltic mantle-derived magma and evolution within a closed magmatic system, with little crustal contamination, similar to that of some

rhyolites from Snake River Plain (e.g., McCurry *et al*., 2008). It should be noted that this isotopic data does not exclude derivation from an open source system (e.g., Fish Canyon Tuff; Bachman *et al*., 2002; Charlier *et al*., 2007) and as such, testing of a common source origin hypothesis for the Pussy Cat Group rhyolites needs to be undertaken.

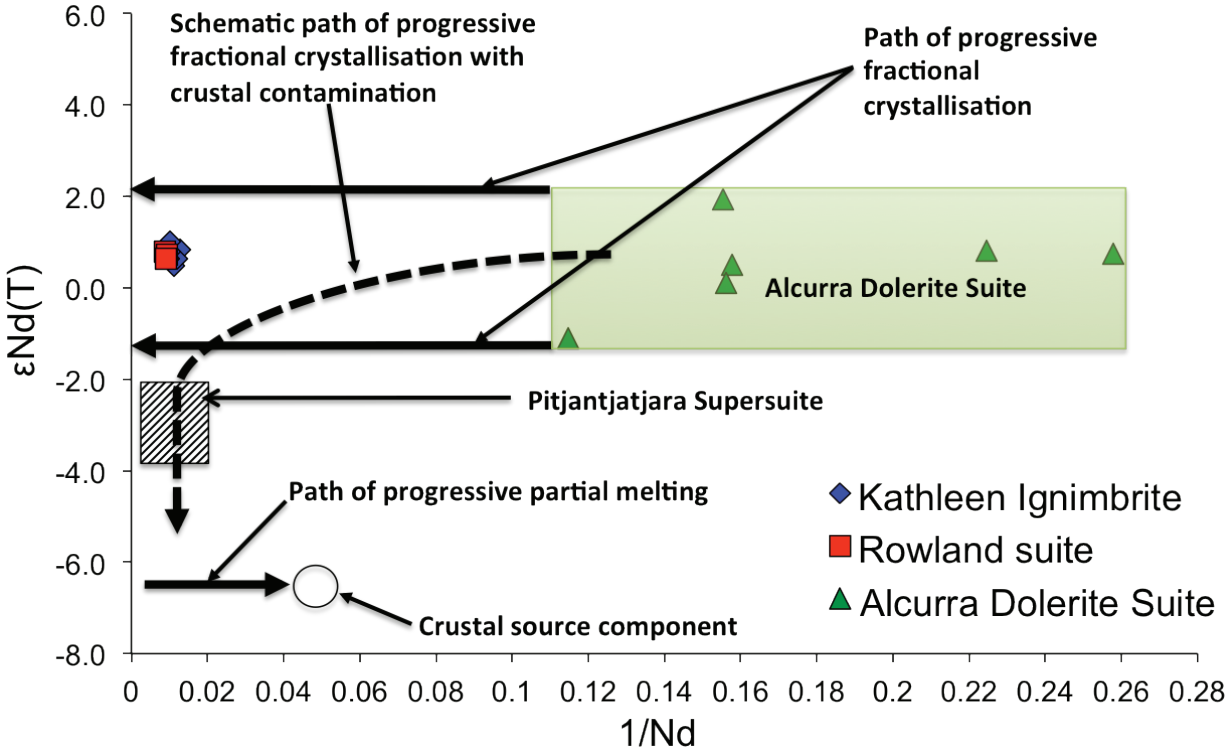

Figure 3.10: Plot of εNd *vs*. 1/Nd showing paths taken by an Alcurra Dolerite-type magma composition during pure fractional crystallisation (right to left solid arrow), partial melting (left to right solid arrow) and crustal contamination (curved dashed arrow) adapted from Smithies *et al*. (2011). Alcurra Dolerite Suite field is between εNd of ~+2 to -1, over a range of Nd concentrations, using uncontaminated data from Zhao and McCulloch (1993), and the crustal source component is the west Musgrave basement Wirku Metamorphics from Smithies *et al*. (2011).

3.8.3 Petrogenesis of the Pussy Cat Group rhyolites

The genesis of specific A-type silicic magmas, such as those that formed the Pussy Cat Group rhyolites, is controversial (e.g., Frost & Frost, 2011), with a number of models being proposed (e.g., Barker *et al.*, 1975, Loiselle & Wones, 1979, Collins *et al.*, 1982, Anderson, 1983, Anderson & Bender, 1989, Eby, 1990, 1992, Creaser *et al.*, 1991). These models and their processes were grouped by Frost and Frost (2011) into three main categories that cover the genesis of silicic A-type magmas: 1) partial melting of quartzofeldspathic crustal rocks (e.g., Thy *et al.*, 1990, Gunnarsson *et al.*, 1998); 2) differentiation through fractional crystallisation of basaltic magmas (e.g., Carmichael, 1964, Ritchey, 1980, MacDonald *et al.*, 1987, Furman *et al.*, 1992, Turner *et al.*, 1992a, Peccerillo *et al.*, 2003); 3) a combination of the first two models, whereby differentiating basaltic magmas assimilate crustal material (i.e. crustal contamination; e.g., Dungan *et al.*, 1986, Davidson & Wilson, 1989, Caffe *et al.*, 2002, Shellnutt & Dostal, 2012).

The geochronological, isotopic, petrological and field evidence discussed in the sections above indicates that the Rowland Suite and Kathleen Ignimbrite units are: a) both temporally and spatially related (corroborating the findings in Chapter 2), b) are mineralogically similar, c) have somewhat similar trace element ratios (Fig. 3.7; Table 3.1 – Appendix B), and d) are isotopically similar (Figs. 3.9 and 3.10). This provides a basis for testing a possible petrogenetic link between these two units. As such this section will examine the processes involved in the genesis of the magmas that formed the Pussy Cat Group rhyolites and try to define the links between these two units; using previously published natural melt and modelled experimental liquid compositions and new major and trace element geochemical modelling.

3.8.3.1 Petrogenesis through the interaction of mantle-derived melts with crustal materials

This model for the generation of silicic melts involves the assimilation of crustal components (i.e. crustal contamination) during either partial melting or fractional crystallisation. A minor amount of crustal contamination is indicated by the model ages being older than the crystallisation ages, and the presence of a single inherited zircon (as evidenced by a differing εHf isotope composition, and out of 177 total analyses); however, the radiogenic isotopic data discussed above (Fig. 3.8), suggests a dominant mantle-derived component for the origin of the Pussy Cat Group rhyolite magmas. This suggests that although the magmas most probably underwent crustal contamination during magma migration and/or during residency in mid- to upper crustal levels, any significant involvement of crustal material, either during contamination or by partial melting, can most likely be ruled out. This is further corroborated by the fact that the average Nb/Ta ratios for each suite are close to the ratios of typical mantle-derived melts (17.5 ± 2.0; Green, 1995, Kamber & Collerson, 2000), suggesting that these magmas have undergone little crustal contamination prior to eruption or emplacement, unless of course they assimilated crustal material with similar Nb/Ta values to that of mantle-derived melts.

3.8.3.2 Partial melting of crustal material

Another possible process that can form highly evolved silicic magmas such as those that formed the Pussy Cat Group rhyolites, is by small degree, but widespread partial melting of evolved continental crustal basement material, a process that can produce melts that are enriched in the LREE and other incompatible elements (e.g., Turner *et al.*, 1992b; Watt & Harley, 1993, Beard *et al.*, 1994, Ayres & Harris, 1997; Christiansen *et al*., 2007). Partial melting of granulitic basic lower crustal material within the west Musgrave Province contributed significantly to the generation of metaluminous and calc-alkaline halogen-, high field strength elements (HFSE)-, and Fe-enriched magmas (e.g., Pitjantjatjara Supersuite; Howard *et al.*, 2011, Smithies *et al.*, 2011), and the fact that the

Pussy Cat Group rhyolites are also halogen, HFSE and Fe-enriched indicates that this process may also be a viable way of generating these highly evolved melts. However, the significant isotopic differences (Fig. 3.9) between the Pitjantjatjara Supersuite magmas and the Pussy Cat Group rhyolites (see *Section 3.8.2*), precludes this, with the former plotting much closer to the CHUR line (i.e. much more crustal-dominated composition) on Fig. 3.9 than the Pussy Cat Group rhyolites. Although the Pitjantjatjara Supersuite magmas were derived through partial melting of crustal material, they still contain a dominant (>50% by volume) mantle-derived component and a lesser (<25% by volume) partial melting of crustal material component (Smithies *et al*., 2011). This suggests that the positive Nd compositions of the Pussy Cat Group rhyolites is indicative of a significantly higher percentage component of mantle-derived magma and significantly smaller component of crustal material than the Pitjantjatjara Supersuite magmas, again supporting volumetrically insignificant crustal contamination.

A non-crustal origin for the Pussy Cat Group rhyolites is also supported by the Nd isotopic composition of basement material within the west Musgrave Province; this basement has significantly negative εNd(T) values (Kirkland *et al.*, 2013), indicating that that the positive εNd(T) values of the Pussy Cat Group rhyolites cannot be derived by recycling of this ancient basement material. In addition, the partial melting of underplated young basaltic crust to form LREE-enriched peralkaline silicic magmas within the central Ethiopian Rift, a setting somewhat similar to the Mesoproterozoic Musgrave Province, did not yield compositions similar to the Pussy Cat Group rhyolites (Peccerillo *et al.*, 2003).

Finally, experimental research into the partial melting of basaltic and andesitic greenstones and amphibolites also produced melts that were significantly compositionally different to the Pussy Cat Group magmas (Thy *et al.*, 1990, Beard & Lofgren, 1991), again suggesting that a partial melting-related genesis for the Pussy Cat Group magmas is not likely. The partial melts generated during these studies are superficially similar (e.g., lowest H_2O melting experiments by Thy *et al*., 1990) in that they producing melts with SiO_2 and Al_2O_3 concentrations similar to the Pussy Cat Group rhyolites, and water-saturated melting experiments of both Beard and Lofgren (1991) and Thy *et al*. (1990) yielding melts with FeO and SiO_2 concentrations that overlap with Pussy Cat Group compositions, but the overall compositions of both water-saturated and undersaturated melts produced during this previous research are dissimilar to the compositions of all samples analysed during this study. These isotopic and whole-rock geochemical dissimilarities strongly suggest that another process must have been responsible for the generation of the Pussy Cat Group magmas.

It is still possible that partial melting played a small role in the formation of the Pussy Cat Group rhyolites and cannot definitively be ruled out, but it is extremely unlikely

that this process was instrumental in the formation of these magmas. This corroborates the findings of Smithies *et al*. (2013) and Kirkland *et al*. (2012), who both argue against the genesis of silicic magmas in the West Musgrave Province by partial melting of continental crustal material.

3.8.3.3 Fractional crystallisation

The other main process that can generate highly evolved silicic magmas is fractional crystallisation of mantle-derived (i.e. basaltic) magmas. However, rather than assuming that this is the case, this hypothesis needs to be robustly tested to determine whether fractional crystallisation could have formed the rhyolitic Pussy Cat Group magmas.

3.8.4 Trace element modelling

Trace element modelling was undertaken to assess the petrogenesis of the Pussy Cat Group rhyolites and to more robustly test our hypotheses of a cogenetic and fractionation-dominated origin for both Rowland Suite and Kathleen Ignimbrite units.

3.8.4.1 Trace element partitioning

Both Rowland Suite and Kathleen Ignimbrite units have significantly negative Sr, Eu and Ba anomalies that are indicative of substantial removal of alkali-feldspar (e.g., Christiansen *et al.*, 1986; Eby, 1990), and suggest that alkali-feldspar fractionation, rather than plagioclase, dominates the magmatic differentiation of both units, similar to rhyolites from the Emeishan LIP in SW China (Xu *et al.*, 2010). The distribution of Ba and Sr during

Figure 3.11:
Mineral vector diagram showing modelled fractional crystallisation vectors for the Pussy Cat Group rhyolite samples in terms of the variation of,
a) log Ba *vs*. log Sr
b) log Ba *vs*. log Eu/Eu*
c) log Rb *vs*. Log Sr.
These diagrams show that sample compositions can be explained through varying degrees of fractional crystallisation and indicate the cogenetic nature of the Pussy Cat Groups rhyolites, an intermediate suite (the Hogarth Formation) and the Alcurra Dolerite Suite (e.g., Eby 1990; Halliday e*t al*., 1991; Ayalew *et al*., 2002), as well as the fractionating mineral assemblages and proportions of minerals during each stage of fractionation. The direction of the vector line shows the compositional change in residual liquid when the vector-representing phase is progressively removed during fractional crystallisation of indicated mineral. The crosses on the fractionation vectors indicate progressive % fractional crystallisation (F) in odd numbers starting from 0% (i.e. 0, 10, 30, 50, 70, 90% F). A primitive Alcurra Dolerite Suite sample was chosen as the source composition for fractionation modelling from the Alcurra Dolerite Suite (solid green line field). First stage of fractionation of plag-olv-cpx-mgt (53:35:10:2) reaches the intermediate Hogarth Formation (purple field). Fractionation of plag-Kfs-qtz (65:20:15) links the Rowland Suite with the Hogarth Formation (stage 2). Further fractionation of qtz-Kfs-plag-mgt-bt ~(30:30:20:10:10) links the Kathleen Ignimbrite (stage 3). Abbreviations used: plag = plagioclase, Kfs = K-feldspar, olv = olivine, mgt= magnetite, cpx = clinopyroxene, tit = titanite, qtz = quartz, bt = biotite. Partition coefficient (D) values from www.earthref.org/GERM (19/04/2014) and Ayalew *et al*. (2002; Table 3.5). Alcurra Dolerite Suite and Hogarth Formation data from the GSWA WACHEM database <geochem.dmp.wa.gov.au/geochem/>.

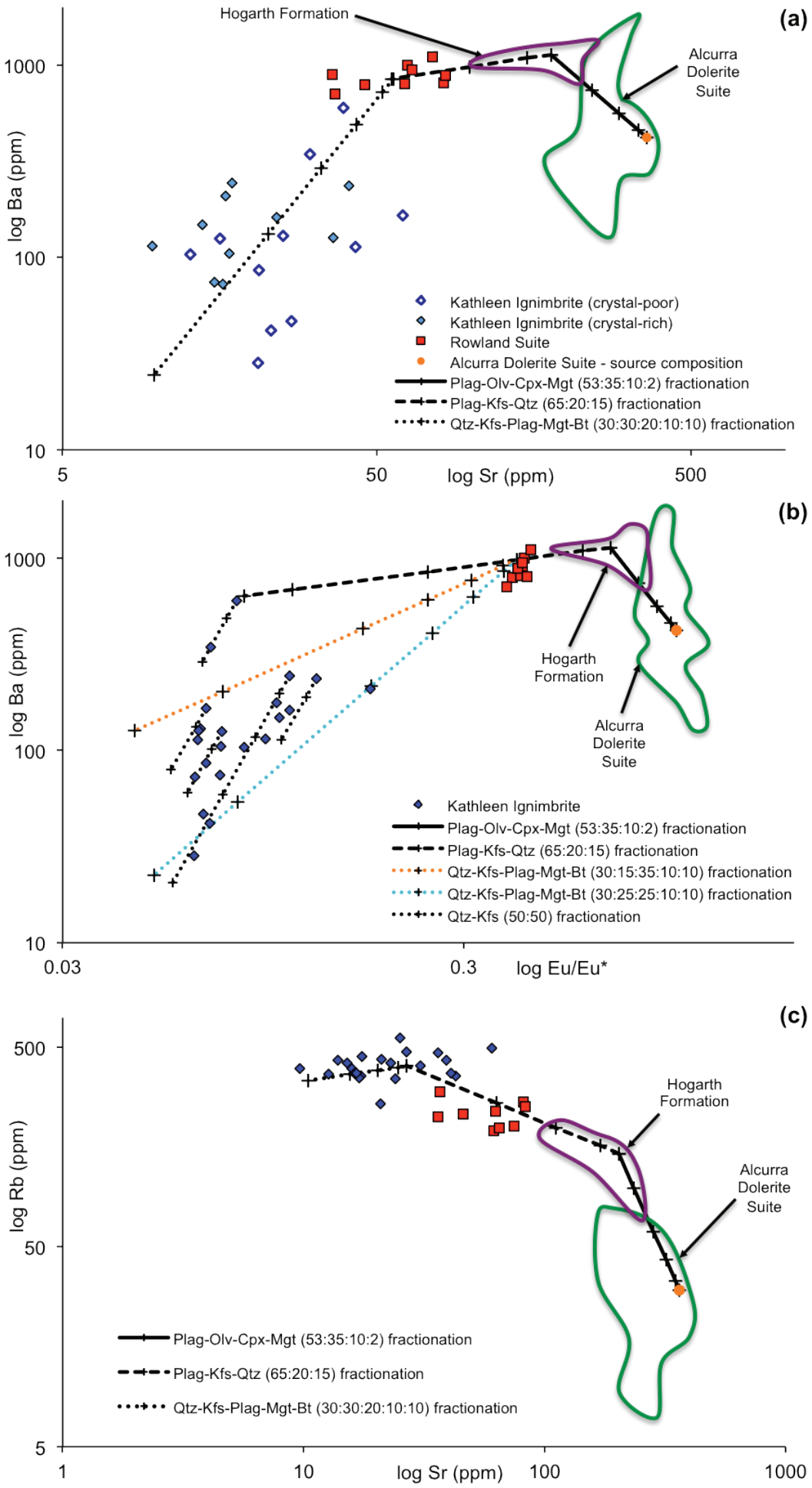
(a)
Hogarth Formation
Alcurra Dolerite Suite
log Ba (ppm)
1000
100
10
5
50
500
log Sr (ppm)
Kathleen Ignimbrite (crystal-poor)
Kathleen Ignimbrite (crystal-rich)
Rowland Suite
Alcurra Dolerite Suite - source composition
Plag-Olv-Cpx-Mgt (53:35:10:2) fractionation
Plag-Kfs-Qtz (65:20:15) fractionation
Qtz-Kfs-Plag-Mgt-Bt (30:30:20:10:10) fractionation
(b)
log Ba (ppm)
1000
100
10
0.03
0.3
log Eu/Eu*
Hogarth Formation
Alcurra Dolerite Suite
Kathleen Ignimbrite
Plag-Olv-Cpx-Mgt (53:35:10:2) fractionation
Plag-Kfs-Qtz (65:20:15) fractionation
Qtz-Kfs-Plag-Mgt-Bt (30:15:35:10:10) fractionation
Qtz-Kfs-Plag-Mgt-Bt (30:25:25:10:10) fractionation
Qtz-Kfs (50:50) fractionation
(c)
log Rb (ppm)
500
50
5
1
10
100
1000
log Sr (ppm)
Hogarth Formation
Alcurra Dolerite Suite
Plag-Olv-Cpx-Mgt (53:35:10:2) fractionation
Plag-Kfs-Qtz (65:20:15) fractionation
Qtz-Kfs-Plag-Mgt-Bt (30:30:20:10:10) fractionation

the fractionation of plagioclase and K-feldspar, two important minerals within both of the Pussy Cat Group rhyolite suites, and the extent of fractional crystallisation was modelled using Rayleigh fractionation modelling (equation 1; Fig. 3.11a):

$$C_L/C_O=F^{(D-1)} \quad (1)$$

where D is the bulk partition coefficient ($D=\Sigma X_i D_i$), X_i is the modal fraction of the given mineral phase, and D_i is the partition coefficient for element i (Rollinson, 1993). A primitive basaltic Alcurra Dolerite Suite composition was used as a parental liquid and fractionation vectors were calculated using appropriate partition coefficients for Ba and Sr into dominant fractionating mineral phases with bulk D values calculated for mixtures of these phases (Table 3.5). The fractionation modelling (Figs. 3.11a, 3.11b and 3.11c) incorporates the fractionation of Alcurra Dolerite Suite magmas and assumes that the Rowland Suite samples represent liquid compositions (rather than cumulates), using modal mineralogies for all three suites based on field and thin section observations and calculated CIPW norm values. The modelling in Fig. 3.11a indicates that the compositional changes between a basaltic Alcurra Dolerite Suite composition and the Rowland Suite samples can be explained by fractionation of a plagioclase-olivine-clinopyroxene-magnetite (53:35:10:2) mineral assemblage to reach intermediate composition magmas, with further fractionation of plagioclase-K-feldspar-quartz (65:20:15) from this intermediate composition to reach

Table 3.5: Partition coefficient (D) values used in trace element modelling taken from www.earthref.org/GERM (19/04/2014) and Ayalew *et al*. (2002).

		D values						
Rock Type	Mineral Element	Olv	Bt	Qtz	Mgt	Plag	Kfs	Cpx
Basalt	Ba	0.03			0.028	0.3		0.04
	Sr	0.02			0.077	2.94		0.16
	Rb	0.03			0	0.016	0.44	0.03
	Eu	0.001			0.062	0.7		0.458
	Sm	0.0011			0.074	0.11		0.3
	Gd	0.0029			0.0055	0.066		0.8
Dacite	Ba			0		0.3	6.12	
	Sr			0		2.94	3.87	
	Rb			0		0.0479	0.659	
	Eu			0		2.11	1.13	
	Sm			0		0.12	0.02	
	Gd			0		0.12	0.011	
Rhyolite	Ba		6.36	0	0.1	0.3	6.12	
	Sr		0.12	0	0.01	2.94	3.87	
	Rb		9.6	0	0	0.3	0.4	
	Eu		0.5	0	0.91	2	1.13	
	Sm		0.39	0	1.2	0.12	0.018	
	Gd		0.353	0	0.0055	0.9	0.011	

the Rowland Suite. The Rowland Suite and Kathleen Ignimbrite units can be linked by K-feldspar-quartz-plagioclase-biotite-magnetite (30:30:20:10:10) fractionation or slight variations thereof. Crystal-poor and -rich sections of the Kathleen ignimbrite define multiple but individual fractionation trends emanating from the Rowland Suite, suggesting that multiple or cyclic fractionation events may have occurred within a single magma chamber prior to eruption, and suggesting effective evacuation and separation of a liquid melt (producing a crystal-poor ignimbrite) from a feldspar-rich residue (i.e. a cumulate). This modelling suggests that all three suites are linked by fractional crystallisation and accumulation of silicate phases that are consistent with field and petrographic observations and CIPW norm calculations.

Another approach to mineral vector modelling was outlined by Eby (1992), who suggested that the effects of feldspar fractionation on the evolution of A-type magmas could be monitored using a Eu/Eu* vs. Ba diagram (Fig. 3.11b). This diagram indicates the relative importance of plagioclase versus K-feldspar in a fractionation trend between or within suites, and indicates once again that the Rowland Suite can be linked with the Alcurra Dolerite Suite by initial fractionation of plagioclase-olivine-clinopyroxene-magnetite (53:35:10:2) to reach an intermediate composition, with further fractionation of plagioclase-K-feldspar-quartz (65:20:15) to reach the Rowland Suite. The Rowland Suite and Kathleen Ignimbrite units can be linked by quartz-K-feldspar-plagioclase-magnetite-biotite fractionation at ratios of this assemblage that vary between (30:15:35:10:10) and (30:25:25:10:10). This modelling provides further evidence of feldspar crystallisation during the formation of these suites. More evolved K-feldspar-quartz fractionation (50:50) links samples within the Rowland Suite and within the Kathleen Ignimbrite, where near-vertical trends defines subsets of both suites that have fairly constant Eu anomalies with decreasing Ba concentrations. This is also evident in Fig. 3.11a, where Kathleen Ignimbrite samples lie along fractionation trends from multiple origins/sources within the Rowland Suite. These multiple fractionation trends are consistent with the modelling described above and again may indicate multiple or cyclic fractionation of trapped melts within a magma chamber prior to eruption.

Further evidence of a cogenetic fractional crystallisation relationship between the parental Alcurra Dolerite Suite and the Pussy Cat Group rhyolites is shown in Fig. 3.11c. All three suites in this diagram are linked in a characteristic inverted “L” or recumbent “V” shape that is indicative of fractional crystallisation (e.g., Ayalew *et al.*, 2002, Halliday *et al.*, 1991), with Rb concentrations increasing during plagioclase fractionation and the slight negative to horizontal trends defined by the evolved Pussy Cat Group rhyolites indicative of Sr depletion during fractional crystallisation of K-feldspar and/or biotite (Hanson, 1978). Similarly Fig. 3.12a indicates that a Rayleigh fractional crystallisation trend is able to link the Pussy Cat Group rhyolites, an intermediate composition suite,

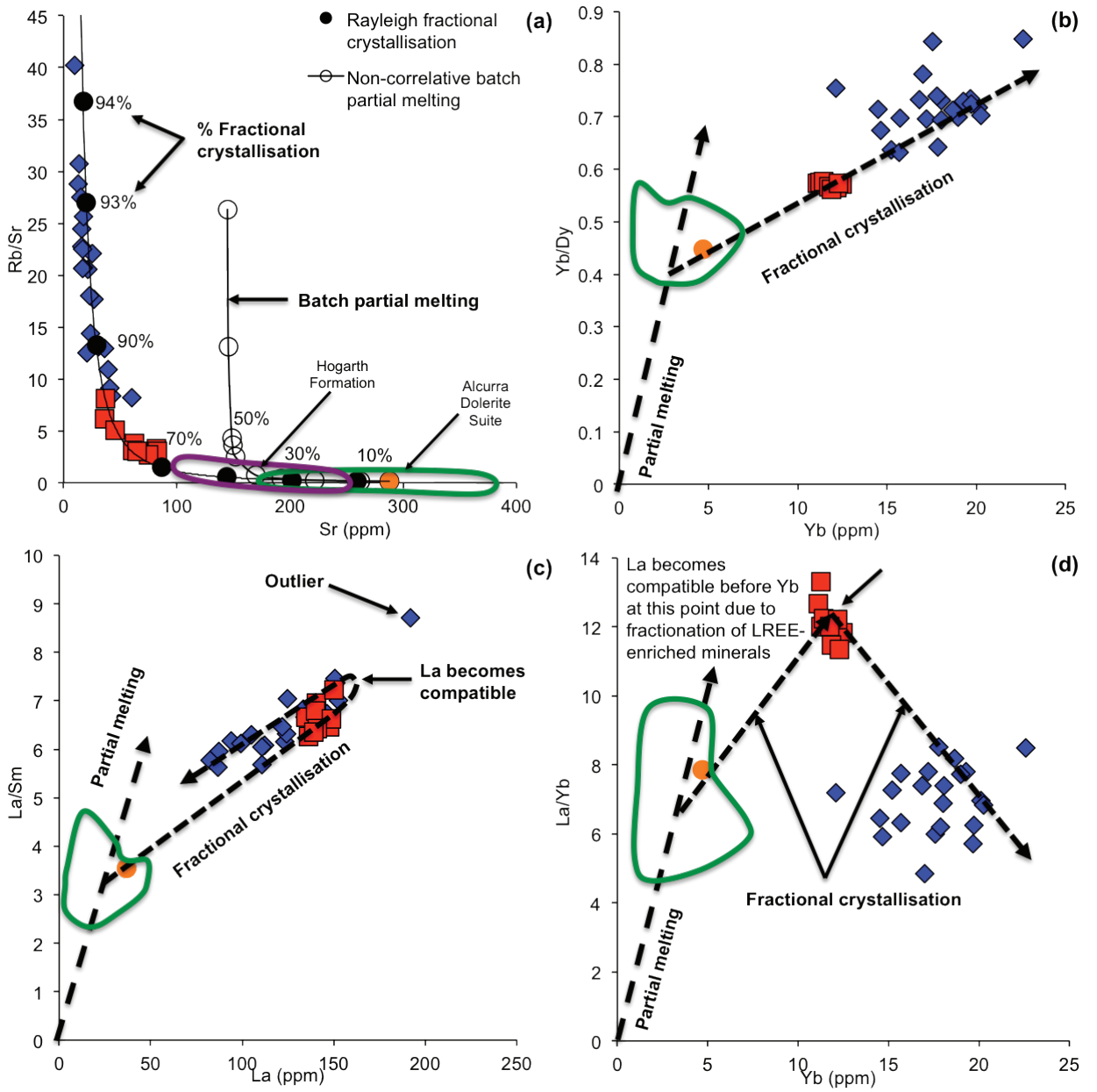

Figure 3.12: a) Rb/Sr *vs*. Sr diagram for the Pussy Cat Group rhyolites; the power law hyperbolic curve that connects the Alcurra Dolerite Suite, Hogarth Formation, Rowland Suite and Kathleen Ignimbrite is indicative of Rayleigh fractional crystallisation between these suites; a curve indicative of a partial melting relationship, not applicable in this case, is also shown, adapted from Halliday *et al*. (1991). b) Yb/Dy *vs*. Yb diagram indicating partial melting and dominant fractional crystallisation trends within the Alcurra Dolerite Suite; Rowland Suite and Kathleen Ignimbrite samples lie on a fractional crystallisation trend emanating from the Alcurra Dolerite Suite. c) La/Sm *vs*. La diagram showing Rowland Suite and Kathleen Ignimbrite samples plotting along on a fractional crystallisation trend derived from the Alcurra Dolerite Suite, but also showing the change in compatibility of La during fractionation of LREE-enriched minerals, such as allanite. The Kathleen Ignimbrite sample with an anomalously high La concentration is not considered representative of melt compositions. d) La/Yb *vs*. Yb diagram showing the change in compatibility of La with fractionation, as explained in Fig. 3.12c and seen again in Fig. 3.13b. Partial melting and fractional crystallisation paths on diagrams taken from Schiano *et al*. (2010).

and the Alcurra Dolerite Suite, through very high degrees of fractional crystallisation (up to 93%). A similar shaped curve would be defined on this diagram if the suites were linked by differential degrees of batch partial melting, however such modelling indicates samples would have to contain elevated Rb concentrations and would reach maximum Rb/Sr ratios at much higher concentrations of Sr (~50 ppm), clearly inconsistent with the very low

Sr concentrations found within the Pussy Cat Group rhyolites. Previous research (e.g., Sparks *et al.*, 1990, Halliday *et al.*, 1991, Ayalew *et al.*, 2002) indicates that a single stage partial melting model cannot generate rocks with Sr concentrations <100 ppm coincident with high Rb concentrations, suggesting that fractional crystallisation is probably the only closed system model capable of generating the Rb-Sr characteristics of the Pussy Cat Group rhyolites. A closed system is supported by the isotope signatures, the consistent high Rb/Sr characteristics, and the mineral fractionation vector modelling outlined above, indicating that these rhyolites most likely formed in a voluminous but closed crustal magma chamber that was present at the time of eruption and/or emplacement of these magmas.

3.8.4.2 Trace element compatibility during fractionation

Fractional crystallisation and batch partial melting processes can be identified using incompatible trace elements with different bulk solid/melt partition coefficients within C^H/C^M *vs.* C^H graphs, where C is the measured concentration of a trace element in the liquid, and *H* and *M* are two incompatible elements, with *H* being more incompatible than *M* (e.g., Schiano *et al.*, 2010). Samples linked by batch partial melting define straight lines on these graphs, whereas sub-horizontal trends are indicative of fractional crystallisation. Two end-member mixing and partial melting trends can also be identified, using this approach, with both processes defining hyperbolic curves at different points within the graph. Using Yb as a highly incompatible element and Dy as a moderately compatible element (Fig. 3.4), the Alcurra Dolerite Suite samples lie at the start of a fractionation trend that links the Rowland Suite and Kathleen Ignimbrite in a Yb/Dy *vs*. Yb diagram (Fig. 3.12b). Usually La is regarded as highly incompatible in magmatic systems, however in a La/Sm *vs*. La diagram (Fig. 3.12c), a single fractionation trend from the Alcurra Dolerite Suite only intersects some of the Rowland Suite and Kathleen Ignimbrite samples. This can be explained by the changing compatibility of the LREE within the Pussy Cat Group system, with La becoming compatible within these highly evolved magmas as a result of the precipitation of LREE-bearing elements such as allanite, monazite and fluorite (Miller and Mittlefehldt, 1982), with the now compatible La defining another fractionation trend but with decreasing La concentrations and La/Sm ratios. This has been observed in several other highly evolved rhyolite systems such as the Cenozoic topaz rhyolites of western USA (Christiansen *et al.*, 1983), and their rapakivi textured granite equivalents (Christiansen *et al.*, 2007), where small amounts of allanite crystallisation caused a decrease in the concentrations of the LREE in more evolved magmas (Mahood & Hildreth, 1983, Christiansen *et al.*, 1986, Eby, 1990). This effect is clearly evident in a La/Yb *vs*. Yb diagram (Fig. 3.12d), where a change in the fractionation trend emanating from the mantle partial melting trend that the Alcurra Dolerite samples lie on is caused by La becoming compatible during fractionation, explaining the changing behaviour of the LREE and HREE in Fig. 3.4 and Fig. 3.7. This also indicates that the HREE remained incompatible during the magmatism that formed these rhyolites.

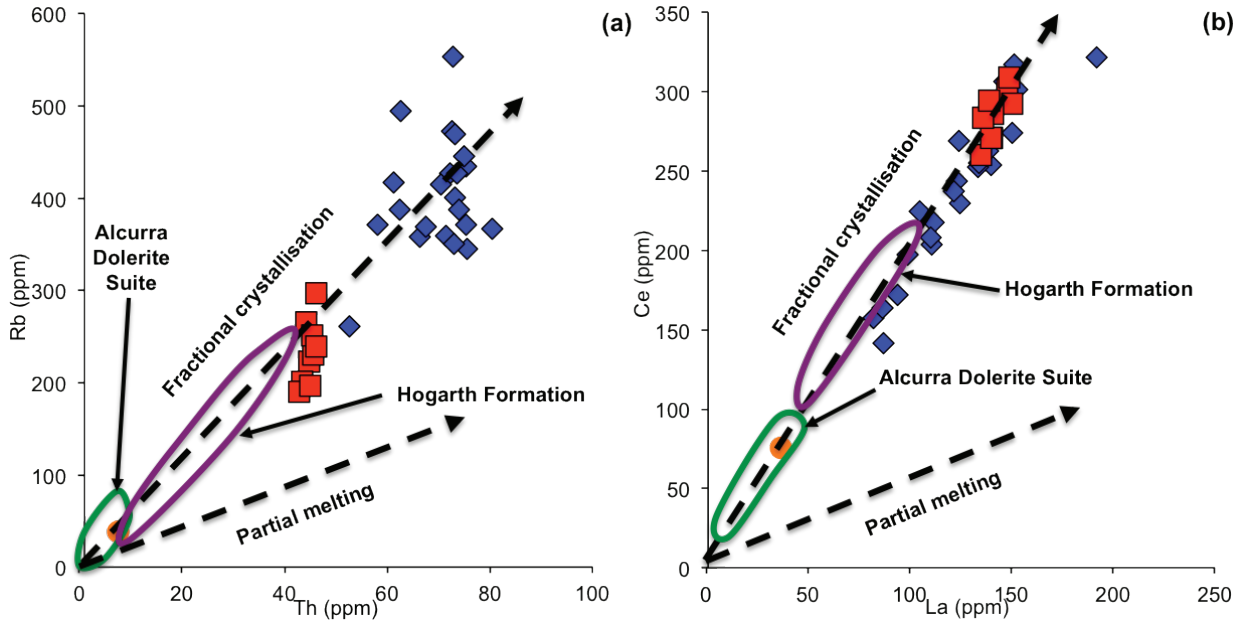

Figure 3.13: a) Rb *vs*. Th diagram, showing relative incompatibility of these two elements in both suites and a cogenetic fractional crystallisation relationship between the Pussy Cat rhyolites and the Alcurra Dolerite Suite and Hogarth Formation. b) Ce *vs*. La diagram indicating the cogenetic nature of the Alcurra Dolerite, Hogarth Formation, Rowland Suite and Kathleen Ignimbrite, with the lower concentrations of La and Ce within the more evolved Kathleen Ignimbrite indicating the change in compatibility (from incompatible to compatible) with ongoing fractionation and the precipitation of LREE-bearing minerals.

A similar approach is used in C^{H1} *vs.* C^{H2} diagrams, where *H1* and *H2* are two highly incompatible elements (e.g., Schiano *et al.*, 2010). Samples related by fractional crystallisation define straight lines on these graphs, whereas partial melting-related samples define hyperbolic curves and mixing-related samples define linear trends that deviate from the straight-line trends indicative of fractional crystallisation (Schiano *et al.*, 2010). Good linear correlations are observed for incompatible elements Th-Rb (Fig. 3.13a), Th-U, and Th-Yb at constant ratios, supporting a cogenetic fractional crystallisation relationship between these suites. To assess the effect of changing compatibility of the LREE in highly evolved rhyolites as outlined above, La was plotted on a C^{H1} *vs.* C^{H2} diagrams and defines good linear correlations with Ce, Pr, Nd, Sm, Gd and Hf at constant ratios for all three suites (see for example, La *vs*. Ce plot; Fig. 3.13b). The change in compatibility of the LREE from incompatible to compatible is demonstrated on this figure by the plotting of the more evolved Kathleen Ignimbrite samples closer to the origin than the less evolved Rowland Suite samples, as a result of the ongoing fractionation of the former and the decreasing of La concentrations relating to the changing compatibility of the LREE; this has also been described in other highly evolved silicic systems (e.g., Miller & Mittlefehldt, 1982, Christiansen *et al.*, 1986).

3.8.5 A petrogenetic emplacement model for the Pussy Cat Group rhyolites

Eby (1990, 1992) proposed that A-type magmas can be subdivided into two chemical groups on the basis of Y/Nb ratios, namely an A_1 group (Y/Nb ratios <1.2) derived from

sources like oceanic island basalts and emplaced in continental rifts or during intra-plate magmatism, and an A_2 group (Y/Nb ratios >1.2) derived from sources such as continental crust or underplated crust that has been through a cycle of continent-continent collision or island arc magmatism and emplaced in a variety of tectonic settings, which include postcollisional and anorogenic settings. Our samples have high Y/Nb ratios and are therefore classified within the A_2 group of magmas (Fig. 3.6b); however, this classification implies an origin and tectonic setting of this that sharply contrasts with those discussed in the previous sections. This is the result of the fact that these discrimination diagrams are dependent on the constant character of Y/Nb and Y/Ta; however, Eby (1990; 1992) states that the crystallisation of certain minor phases such as allanite and zircon can lead to an increase in Y/Nb ratios and the erroneous classification of A_1 group samples as A_2. The change in Y/Nb ratios is related to changes in compatibility during the fractional crystallisation of highly evolved rhyolites (Miller and Mittlefehldt, 1982; Eby, 1990). We have demonstrated that changes in compatibility occur during the fractionation of the Pussy Cat Group rhyolites (Fig. 3.13b), indicating that these rhyolites most probably have higher Y/Nb ratios that those expected for the majority of rhyolites. Eby (1992) also says that it is not possible on the basis of trace element data to rule out a subcontinental mantle source and concedes that some A_2 magmas can have mantle-derived origins.

One question that remains is the lack of intermediate volcanic compositions that bridge the gap between the Alcurra Dolerite Suite and Pussy Cat Group rhyolites. There is a distinct lack of intermediate composition volcanic rocks within the entire Talbot Sub-basin, although Smithies *et al*. (2013) indicate that the relatively minor dacitic Hogarth Formation of the Bentley Supergroup may represent an intermediate between the Alcurra and Pussy Cat units. Dufek and Bachmann (2010) suggest that these compositional “Daly” gaps are common and can be explained by the separation of crystals and liquids during the intermediate stages of fractionation, leading to a distinct lack of intermediate composition magmas within bimodal volcanic associations linked by fractional crystallisation. Some A-type Snake River Plain rhyolites can be formed by extreme fractional crystallisation of mantle-derived basaltic magma during continental rifting (e.g., McCurry *et al*. 2008; Christiansen and McCurry 2008), and in this situation a crustal density filter serves to suppress the intermediate composition magmas, creating the characteristic bimodal associations inherent with A-type rhyolites. For this to work, the intermediate magmas have to be Fe-rich and denser than the mafic or silicic magmas.

If these Pussy Cat Group rhyolites formed through fractional crystallisation, final fractionation most likely occurred within the shallow regions of the upper crust. This is supported by research by Gualda and Ghiorso (2013), who documented that high-silica rhyolites, such as the Kathleen Ignimbrite, can only form in the upper crust at low pressures between 1-3 kbar, and that high-silica melts originate from deeper cumulates in a silicic

magma system. These silicic magma systems are polybaric, crystallising over a large range of pressures, from the middle to the shallow upper crust, with silica concentration indirectly proportional to depth (Gualda and Ghiorso, 2013). The Pussy Cat Group rhyolites are also geochemically similar to the FIIIb-type rhyolites of Hart *et al*. (2004) and Lesher *et al*. (1986), who demonstrated that these rhyolites were generated through high temperature (830–850°C using the Zr saturation thermometer of Watson and Harrison, 1983; Chapter 4) and low pressure fractionation at shallow source depths (<10 km), most likely in high-level magma chambers. Hart *et al*. (2004) concluded that these silicic volcanic rocks and their comagmatic subvolcanic intrusions typify magmatism in rift environments with anomalously high heat flow, associated with the upwelling of hot mantle, thin crusts, and ascending pockets of magma. In addition, Bonin (2007) effectively demonstrated that A-type magmas are usually emplaced at shallow depths, and Smithies *et al*., (2013) suggested the presence of a mid-crustal (21–14 km) magma reservoir underneath the Talbot Sub-basin; this reservoir was the common source for all of the silicic magmatism in the region, but is too deep for the fractionation of the high-silica rhyolites of the Kathleen Ignimbrite. This, together with direct petrographic evidence (e.g., porphyritic textures and intrusive relationships), suggests that the Kathleen Ignimbrite magmas were fractionated from the Rowland Suite magmas in a shallow level, upper crustal magma chamber, after possible migration of a proto-Rowland Suite-type composition magma from a mid-crustal magma reservoir to this upper crustal chamber. Therefore it is proposed here that a high-level, pre-eruption staging magma chamber (10–3 km) formed directly beneath the Kathleen Caldera and had a plumbing system that tapped into the larger, deeper-seated Talbot Sub-basin magma reservoir proposed by Smithies *et al*. (2013) at a depth of 14–21 km below the west Musgrave Province.

The modelling discussed in *Section 3.8.4* favours the formation of the Pussy Cat Group rhyolites through extensive fractional crystallisation of a basaltic mantle-derived magma. An origin through the partial melting of crustal material cannot unequivocally be excluded, although the clear fractionation crystallisation trend, the almost identical isotopic compositions and the overlapping ages of the Rowland Suite and Kathleen Ignimbrite units is indicative of a comagmatic relationship between the two. In Chapter 2, it is suggested that the Kathleen Ignimbrite represents an intra-caldera fill within the Kathleen caldera and is associated with a voluminous (>380 km^3) magma chamber that acted as the single common source for the erupted material due to the continuous nature of eruption sequence and no evidence for significant time breaks. The presence of two petrologically distinct pumice populations in the Kathleen Ignimbrite (Chapter 2; also see *Section 3.5.1*), the crude stratigraphic layering seen in the Kathleen Ignimbrite succession that gradationally varies from crystal-poor at the base to mixed crystal-rich to -poor in the middle parts of the eruption sequence and an upper crystal-poor facies that then abruptly changes to a mixed facies again, and the two distinct clusters of trace and REE data within the Kathleen

Ignimbrite (Fig. 3.6b) suggests at least two types of chemically indistinct silicic magmas were involved during the caldera-forming eruption of the Kathleen Ignimbrite. None of the trace element trends indicate the introduction of new or foreign magmas, suggesting that these texturally distinct magmas were cogenetic, with one magma being crystal-rich and at sub-liquidus temperatures, whereas the other was crystal-poor and at or near liquidus temperatures. This is similar to the La Pacana caldera system of the central Andes, Chile (Lindsay *et al.*, 2001). Such textural heterogeneity in a deposit originating from a single magma chamber could be explained through a chemically zoned, stratified and differentiated magma chamber (e.g., Deering *et al*., 2011), which gave rise to the formation of the evolved, crystal-poor to crystal-rich Kathleen Ignimbrite and the less evolved crystal-rich Rowland Suite. The majority of evidence presented here suggests little crustal involvement in the petrogenesis of the Pussy Cat Group rhyolites, indicating that these magmas evolved through shallow closed-system fractional crystallisation of mantle-derived basaltic magmas, similar to rhyolites from the Eastern Snake River Plain (McCurry *et al.*, 2008).

A similar situation is presented by Deering *et al*. (2011), who modelled the Ammonia Tanks Tuff deposit, southwest Nevada, USA, a chemically zoned ignimbrite resulting from a super-volcanic eruption that also displays changes in crystal contents that are similar to the two pumice population and crude stratigraphic textural variations seen in the Kathleen Ignimbrite. They and suggested that a melt-rich, crystal-poor rhyolite cap and its differentiated cumulate mush can erupt simultaneously from a chemically and thermally zoned shallow magma chamber (Deering *et al*., 2011). This suggests that the crystal-rich juvenile pumice and crystal-rich zones found within the Kathleen Ignimbrite may represent tapped parts of the original semi-solid crystal mushes from within a common magma reservoir as observed elsewhere (e.g., Bachmann & Bergantz, 2004, Hildreth, 2004, Lindsay *et al.*, 2001). In addition, Christiansen (2005) suggested the magmas that form strongly fractionated, high-temperature, low-viscosity ignimbrites undergo efficient crystal-liquid separation and can become vertically zoned within large sill-like magma chambers. This suggests that the intrusive Rowland Suite represents the crystal-rich, cumulate end-member of the fractionation series, whereas the crystal-poor parts of the Kathleen Ignimbrite represent the highly evolved liquid melt end-member extracted from the Rowland Suite, and the crystal-rich parts of the Kathleen Ignimbrite, represent the dynamic mingling of the evolved crystal-poor interstitial melt with the crystal-rich Rowland Suite-type cognate material (Fig. 3.4d) in a shared, compositionally zoned magma chamber. One alternative explanation is that crystal-poor pumice population could be the result of silicic magma recharge (de Silva *et al.*, 2008) from the deeper Talbot Sub-basin by a hotter aphyric magma that is compositionally indistinct from the shallow-level magmas. Cryptic silicic magma is an effective trigger mechanism for large explosive eruptions and the eruption and evacuation of relatively immobile, viscous crystal mushes from magma

chambers (e.g., de Silva *et al.*, 2008; Deering *et al.*, 2011); this type of recharge is difficult to identify geochemically, but evidence in favour of it is provided for by the presence of the very fine-grained, crystal-poor pumice population and the crystal-poor, lava-like rheomorphic base of the intra-caldera Kathleen Ignimbrite deposit (Chapter 2).

For this study the proposed model (Fig. 3.14) for the emplacement of the Pussy Cat rhyolites is as follows:

1) Primitive mafic Alcurra Dolerite Suite parental magmas were generated by melting of the mantle during the Giles Event (Zhao & McCulloch, 1993, Glikson *et al.*, 1996, Godel *et al.*, 2011, Smithies *et al.*, 2013) before ascending to the base of the lower crust (~35 km), where they stalled and both under- and intra-plated the existing crust below the Musgrave Province (Smithies *et al.*, 2013).

2) Pockets of these mantle-derived magmas ascended through the lower crust and pooled in the mid- to upper-crust (Hildreth & Moorbath, 1988, Smithies *et al.*, 2013) at depths of 4–6 kbar (~14–21 km), forming the large homogenous Talbot Sub-basin magma reservoir (Annen *et al.*, 2006, Smithies *et al.*, 2013, Solano *et al.*, 2012).

3) Incomplete fractional crystallisation in the magma reservoir resulted in the formation of crystal mushes and intermediate composition magmas (e.g., Bachmann & Bergantz, 2004, Hildreth, 2004). These mushes (melts and crystal cumulates) detached from the reservoir and moved to upper-crustal levels where they stalled and accumulated in shallow magma chambers (Annen *et al.*, 2006). The melts within the top of this mid-crustal magma reservoir formed from fractionation of the basaltic Alcurra Dolerite Suite-type magmas, generation intermediate composition magmas that further fractionated to form proto-Rowland Suite-type magma compositions. As the generation of high-silica rhyolites (i.e. the Kathleen Ignimbrite) is confined to the shallow upper crust (e.g., Gualda & Ghiorso, 2013), these proto-Rowland Suite-type magmas must then have migrated to a shallower upper-crustal magma chamber at a depth of ~3–10 km, before further quartz-K-feldspar-plagioclase dominated fractionation of the cumulate Rowland Suite magmas formed a cap of extremely evolved melt-rich Kathleen Ignimbrite magmas in a similar manner to that envisioned by Deering *et al*. (2011) for the Ammonia Tanks Tuff. This created a voluminous (>380 km^3) stratified magma chamber located directly beneath the Kathleen Caldera.

4) A trigger mechanism, such as cryptic silicic recharge (de Silva *et al.*, 2008), caused this magma chamber to erupt and empty out (e.g., Deering *et al*., 2011).

5) Initial eruption of the Kathleen Ignimbrite would have been dominated by the extraction of the highly evolved crystal-poor melt-rich cap from the chamber, with subsequent depressurisation of the magma chamber causing mingling between crystal-rich cumulate and crystal-poor melt portions; this mingling formed eruption products that contained mixed populations of crystal-rich pumice clasts, cognate clasts, and crystal-

poor melt. The final waning eruption phase was dominated by extraction of only the crystal-poor melt-rich magma portion, forming a crude three-tiered stratification within the intra-caldera Kathleen Ignimbrite deposit (Chapter 2).

This emplacement model can explain the absence of evidence of significant crustal contamination within the Pussy Cat Group rhyolites, as discussed above. Evidence pointing towards a common source reservoir or magma chamber for the Pussy Cat Group rhyolites, and potentially for all silicic magmas in the study area (Smithies *et al*., 2013) is supported by the overlapping and tight clustering of zircon crystallisation ages, a lack of inheritance, the fact that the stratigraphically younger Rowland Suite intrusions cross-cut the stratigraphy of the study area but have slightly older crystallisation ages, similar isotopic signatures, and a distinctive overlap of the geochemistry with other silicic units from within the Talbot Sub-basin (Smithies *et al*., 2013).

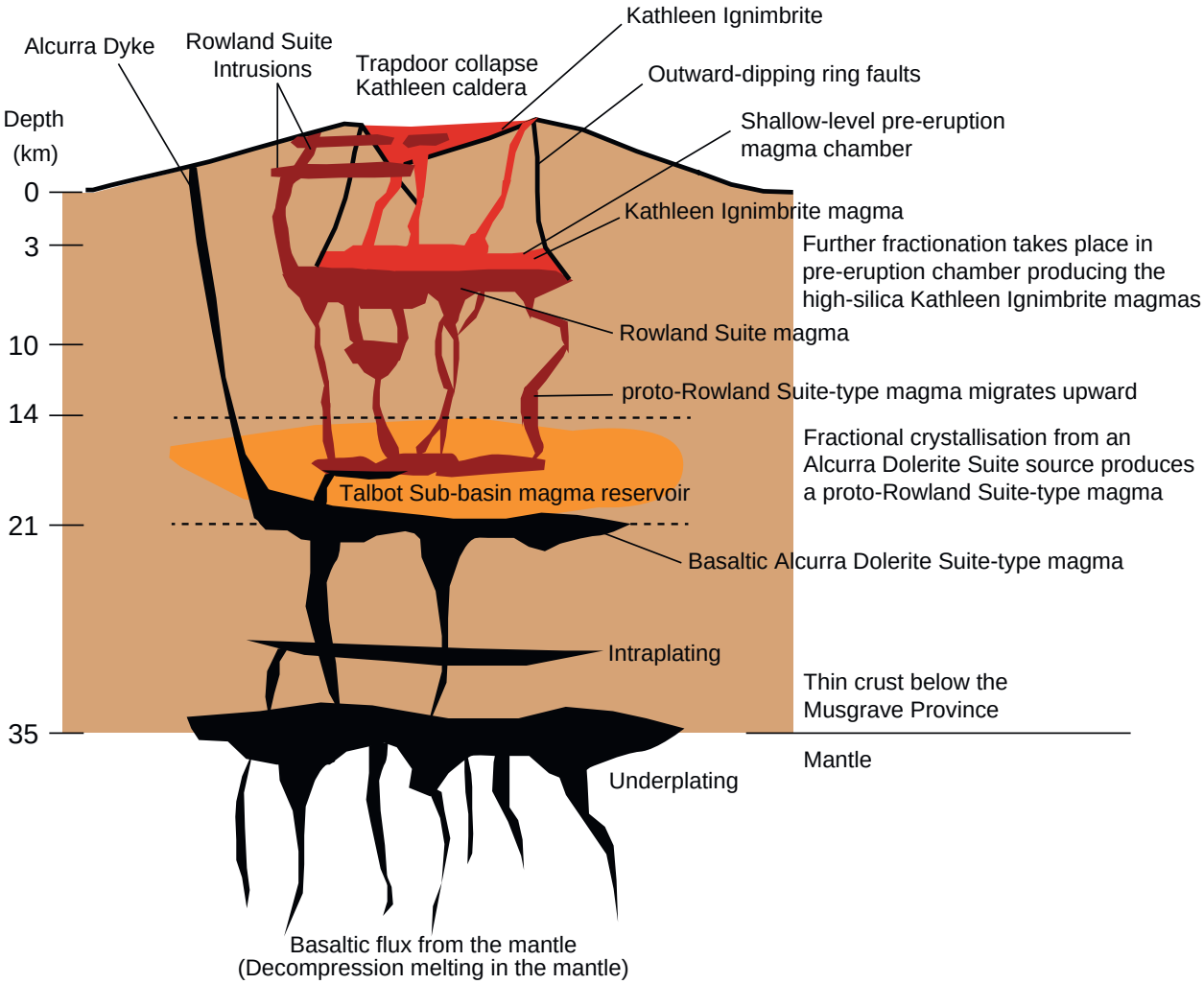

Figure 3.14: A schematic diagram illustrating the emplacement model for the rhyolites of the Pussy Cat Group, showing the Talbot Sub-basin magma reservoir at mid-crustal depths, feeding the shallow upper-crustal magma chamber, underlying the Kathleen caldera, from which the evolved and differentiated Pussy Cat Group rhyolites erupt (adapted from de Silva *et al*., 2006, Folkes *et al*., 2011).

3.9 Conclusions

This study provides an overview of the formation of highly evolved rhyolites during extreme fractional crystallisation of mantle-derived basaltic magmas. The Pussy Cat Group rhyolites show typical *within-plate* geochemical affiliations, are considered A-type, metaluminous and REE-enriched, and can be split into the cogenetic and comagmatic Kathleen Ignimbrite and Rowland Suite units. Both units are formed and linked through fractional crystallisation with minimal crustal contamination. The Rowland Suite is a more primitive, crystal-rich cumulate end-member, whereas the Kathleen Ignimbrite represents a more evolved, high-silica, crystal-poor, melt-rich end-member of the Pussy Cat Group rhyolites, albeit an end-member that contains Rowland Suite-like crystal-rich regions. These regions represent more cumulate-rich sections of a pre-eruption crystal mush within the Kathleen magma chamber. Our model for the petrogenesis of the Pussy Cat Group rhyolites involves a minimum of three stages of fractionation, with initial fractionation from a basaltic magma through an intermediate composition magma to form the partly crystallised Rowland Suite magma, which was followed by further fractionation that formed an evolved HFSE- and melt-rich cap of Kathleen Ignimbrite composition within a differentiated and stratified magma chamber. Polybaric fractionation from the primitive basaltic Alcurra Dolerite Suite magmas through the Rowland Suite to the evolved Kathleen Ignimbrite magmas was associated with the initial formation of proto-Rowland Suite-type magmas in a mid-crustal Talbot Sub-basin magma reservoir, before these magmas ascended to an upper-crustal magma chamber where further fractionation formed the Kathleen Ignimbrite magmas. This silicic magmatism represents a significant mantle-derived contribution to the magmatism associated with the Giles Event, and is consistent with the known magmatic history of the west Musgrave Province, where a common large-scale mid-crustal magma reservoir below the Talbot Sub-basin acted as a common source for all silicic magmatism during this period. The recognition of the large volume Kathleen Ignimbrite as a significant explosive caldera-forming event at ca. 1070 Ma, the cogenetic nature of this unit with the intrusive Rowland Suite and parental magmas to the Giles intrusions, and further evidence for more voluminous, widespread and long-lived (>30 Ma) comagmatic silicic magmatism and explosive caldera formation within the Talbot Sub-basin during the Giles Event and the Ngaanyatjarra Rift suggests that these Pussy Cat Group rhyolites represent part of the silicic component of a large igneous province in the west Musgrave Province that possibly redefines the Warakurna LIP.

3.10 Acknowledgements

I would like to acknowledge the Geological Survey of Western Australia for their logistical support and resources to help make this research project possible, the

Ngaanyatjarra Council and their people for the privilege and unique opportunity to conduct this research in their shire, and our various field assistants for help during fieldwork. We also thank the Monash Volcanology Research Group (MonVolc) for ongoing support during this study, and laboratory staff at Monash University and The University of Melbourne for assistance during analysis. Thank you to Eric Christiansen and two anonymous reviewers for constructive comments that helped improve the manuscript and Richard Price for editorial handling.

3.11 References

Agangi, A., Kamenetsky, V.S. and McPhie, J., 2012. Evolution and emplacement of high fluorine rhyolites in the Mesoproterozoic Gawler silicic large igneous province, South Australia. Precambrian Research, 208-211: 124-144.

Anderson, J.L., 1983. Proterozoic anorogenic granite plutonism of North America. Memoir - Geological Society of America, 161: 133-154.

Anderson, J.L. and Bender, E.E., 1989. Nature and origin of Proterozoic A-type granitic magmatism in the Southwestern United States of America. Lithos, 23(1-2): 19-52.

Annen, C., Blundy, J.D. and Sparks, R.S.J., 2006. The genesis of intermediate and silicic magmas in deep crustal hot zones. Journal of Petrology, 47(3): 505-539.

Arth, J.G., 1976. Behavior of trace elements during magmatic processes—a summary of theoretical models and their applications. J. Res. US Geol. Surv, 4: 41-47.

Ayalew, D., Barbey, P., Marty, B., Reisberg, L., Yirgu, G. and Pik, R., 2002. Source, genesis, and timing of giant ignimbrite deposits associated with Ethiopian continental flood basalts. Geochimica et Cosmochimica Acta, 66(8): 1429-1448.

Ayres, M. and Harris, N., 1997. REE fractionation and Nd-isotope disequilibrium during crustal anatexis: constraints from Himalayan leucogranites. Chemical Geology, 139(1): 249-269.

Bachmann, O., Dungan, M.A. and Lipman, P.W., 2002. The Fish Canyon magma body, San Juan volcanic field, Colorado: rejuvenation and eruption of an upper-crustal batholith. Journal of Petrology, 43: 1469-1503.

Bachmann, O. and Bergantz, G.W., 2004. On the origin of crystal-pore rhyolites; extracted from batholithic crystal mushes. Journal of Petrology, 45(8): 1565-1582.

Bachmann, O. and Bergantz, G.W., 2008. Rhyolites and their source mushes across tectonic settings. Journal of Petrology, 49: 2277-2285.

Barker, F., Wones, D.R., Sharp, W.N. and Desborough, G.A., 1975. The Pikes Peak Batholith, Colorado Front Range, and a model for the origin of the gabbro-anorthosite-syenite-potassic granite suite. Precambrian Research, 2(2): 97-160.

Beard, J.S. and Lofgren, G.E., 1991. Dehydration melting and water-saturated melting of basaltic and andesitic greenstones and amphibolites at 1, 3 and 6.9 kb. Journal of Petrology, 32(2): 365-401.

Beard, J.S., Lofgren, G.E., Sinha, A.K. and Tollo, R.P., 1994. Partial melting of apatite-bearing charnockite, granulite, and diorite: melt compositions, restite mineralogy, and petrologic implications. Journal of Geophysical Research, 99(B11): 21591-21521,21603.

Blichert-Toft, J. and Albarede, F., 1997. The Lu-Hf isotope geochemistry of chondrites and the evolution of the mantle-crust system. Earth and Planetary Science Letters, 148(1-2): 243-258.

Bonin, B., 2007. A-type granites and related rocks: evolution of a concept, problems and prospects. Lithos, 97(1): 1-29.

Bryan, S.E., Riley, T.R., Jerram, D.A., Stephens, C.J. and Leat, P.T., 2002. Silicic volcanism; an undervalued component of large igneous provinces and volcanic rifted margins. Special Paper - Geological Society of America, 362: 97-118.

Burt, D.M., Sheridan, M.F., Bikun, J.V. and Christiansen, E.H., 1982. Topaz rhyolites; distribution, origin, and significance for exploration. Economic Geology and the Bulletin of the Society of Economic Geologists, 77(8): 1818-1836.

Caffe, P.J., Trumbull, R.B., Coira, B.L. and Romer, R.L., 2002. Petrogenesis of early Neogene magmatism in the northern Puna; implications for magma genesis and crustal processes in the Central Andean Plateau. Journal of Petrology, 43(5): 907-942.

Carmichael, I.S.E., 1964. The petrology of Thingmuli, a Tertiary volcano in eastern Iceland. Journal of Petrology, 5(3): 435-460.

Charlier, B., Bachmann, O., Davidson, J., Dungan, M. and Morgan, D., 2007. The upper crustal evolution of a large silicic magma body: Evidence from crystal-scale Rb–Sr isotopic heterogeneities in the Fish Canyon magmatic system, Colorado. Journal of Petrology, 48(10): 1875-1894.

Charlier, B.L.A., Wilson, C.J.N., Lowenstern, J.B., Blake, S., van Calsteren, P.W. and Davidson, J.P., 2005. Magma generation at a large, hyperactive silicic volcano (Taupo, New Zealand) revealed by U-Th and U-Pb systematics in zircons. Journal of Petrology, 46(1): 3-32.

Christiansen, E.H., 2005. Contrasting processes in silicic magma chambers; evidence from very large volume ignimbrites. Geological Magazine, 142(6): 669-681.

Christiansen, E.H., Burt, D.M., Sheridan, M.F. and Wilson, R.T., 1983. The petrogenesis of topaz rhyolites from the Western United States. Contributions to Mineralogy and Petrology, 83(1-2): 16-30.

Christiansen, E.H., Sheridan, M.F. and Burt, D.M., 1986. The geology and geochemistry of Cenozoic topaz rhyolites from the Western United States. Geological Society of America (GSA), Boulder, CO, United States, 82 pp.

Christiansen, E.H., Haapala, I. and Hart, G.L., 2007. Are Cenozoic topaz rhyolites the erupted equivalents of Proterozoic rapakivi granites? Examples from the Western United States and Finland. Lithos, 97(1-2): 219-246.

Christiansen, E.H. and McCurry, M., 2008. Contrasting origins of Cenozoic silicic volcanic rocks from the western Cordillera of the United States. Bulletin of Volcanology, 70(3): 251-267.

Chu, N.-C., Taylor, R.N., Chavagnac, V., Nesbitt, R.W., Boella, R.M., Milton, J.A., German, C.J., Bayon, G. and Burton, K., 2002. Hf isotope ratio analysis using multi-collector inductively coupled plasma mass spectrometry: an evaluation of isobaric interference corrections. Journal of Analytical and Atomic Spectrometry, 17: 1567-1574.

Close, D.F., Edgoose, C.J. and Scrimgeour, I.R., 2003. Hull and Bloods Range Special, Northern Territory. 1:100000 Geological Map Series Explanatory Notes, Northern Territory Geological Survey, Darwin.

Collins, W.J., Beams, S.D., White, A.J.R. and Chappell, B.W., 1982. Nature and origin of A-type granites with particular reference to southeastern Australia. Contributions to Mineralogy and Petrology, 80(2): 189-200.

Creaser, R.A., Price, R.C. and Wormald, R.J., 1991. A-type granites revisited; assessment of a residual-source model. Geology (Boulder), 19(2): 163-166.

Dall'Agnol, R., Frost, C.D. and Rämö, O.T., 2012. IGCP Project 510 “A-type Granites and Related Rocks through Time”: Project vita, results, and contribution to granite research. Lithos, 151(0): 1-16.

Daniels, J.L., 1974. The geology of the Blackstone region, Western Australia. Bulletin - Geological Survey of Western Australia, 123: 257.

Davidson, J.P. and Wilson, I.R., 1989. Evolution of an alkali basalt-trachyte suite from Jebel Marra Volcano, Sudan, through assimilation and fractional crystallization. Earth and Planetary Science Letters, 95(1-2): 141-160.

de Silva, S., Salas, G. and Schubring, S., 2008. Triggering explosive eruptions-The case for silicic magma recharge at Huaynaputina, southern Peru. Geology, 36(5): 387-390.

de Silva, S., Zandt, G., Trumbull, R., Viramonte, J.G., Salas, G. and Jimenez, N., 2006. Large ignimbrite eruptions and volcano-tectonic depressions in the Central Andes; a thermomechanical perspective. Geological Society Special Publications, 269: 47-63.

Deering, C.D., Bachmann, O. and Vogel, T.A., 2011. The Ammonia Tanks Tuff; erupting a melt-rich rhyolite cap and its remobilized crystal cumulate. Earth and Planetary Science Letters, 310(3-4): 518-525.

Dufek, J. and Bachmann, O., 2010. Quantum magmatism; magmatic compositional gaps generated by melt-crystal dynamics. Geology (Boulder), 38(8): 687-690.

Dungan, M.A., Lindstrom, M.M., McMillan, N.J., Moorbath, S., Hoefs, J. and Haskin, L.A., 1986. Open system magmatic evolution of the Taos Plateau volcanic field, northern New Mexico; 1, The petrology and geochemistry of the Servilleta Basalt. Journal of Geophysical Research, 91(B6): 5999-6028.

Eby, G.N., 1990. The A-type granitoids; a review of their occurrence and chemical characteristics and speculations on their petrogenesis. Lithos, 26(1-2): 115-134.

Eby, G.N., 1992. Chemical subdivision of the A-type granitoids; petrogenetic and tectonic implications. Geology (Boulder), 20(7): 641-644.

Edgoose, C.J., Scrimgeour, I.R. and Close, D.F., 2004. Geology of the Musgrave Block, Northern Territory. Northern Territory Geological Survey, Report 15.

Eggins, S.M., Kinsley, L.K. and Shelley, J.M.G., 1998. Deposition and element fractionation processes occurring during athmospheric pressure laser sampling for analysis by ICPMS. Applied Surface Science, 127-129: 278-286.

Evins, P.M., Smithies, R.H., Howard, H.M., Kirkland, C.L., Wingate, M.T.D. and Bodorkos, S., 2010. Devil in the detail; the 1150-1000 Ma magmatic and structural evolution of the Ngaanyatjarra Rift, west Musgrave Province, central Australia. Precambrian Research, 183(3): 572-588.

Folkes, C.B., de Silva, S.L., Wright, H.M. and Cas, R.A., 2011. Geochemical homogeneity of a long-lived, large silicic system; evidence from the Cerro Galan caldera, NW Argentina. Bulletin of volcanology, 73(10): 1455-1486.

Frost, B.R., Barnes, C.G., Collins, W.J., Arculus, R.J., Ellis, D.J. and Frost, C.D., 2001. A geochemical classification for granitic rocks. Journal of Petrology, 42(11): 2033-2048.

Frost, B.R. and Frost, C.D., 2008. A geochemical classification for feldspathic igneous rocks. Journal of Petrology, 49(11): 1955-1969.

Frost, C.D. and Frost, R., 2011. On ferroran (A-type) granitoids; their compositional variability and modes of origin. Journal of Petrology, 52(1): 39-53.

Furman, T., Frey, F.A. and Meyer, P.S., 1992. Petrogenesis of evolved basalts and rhyolites at Austurhorn, southeastern Iceland; the role of fractional crystallization. Journal of Petrology, 33(6): 1405-1445.

Gelman, S.E., Gutiérrez, F.J. and Bachmann, O., 2013. On the longevity of large upper crustal silicic magma reservoirs. Geology, 41: 759-762.

Giles, D., Betts, P. and Lister, G., 2002. Far-field continental backarc setting for the 1.80-1.67 Ga basins of northeastern Australia. Geology (Boulder), 30(9): 823-826.

Girard, G. and Stix, J., 2012. Future volcanism at Yellowstone caldera: Insights from geochemistry of young volcanic units and monitoring of volcanic unrest. GSA Today, 22(9).

Glikson, A.Y., Ballhaus, C.G., Clarke, G.L., Sheraton, J.W., Stewart, A.J. and Sun, S.S., 1995. Geological framework and crustal evolution of the Giles mafic- ultramafic complex and environs, western Musgrave Block, central Australia. AGSO Journal of Australian Geology & Geophysics, 16(1-2): 41-67.

Glikson, A.Y., Stewart, A.J., Ballhaus, C.G., Clarke, G.L., Feeken, E.H.J., Leven, J.H., Sheraton, J.W. and Sun, S.S., 1996. Geology of the western Musgrave Block, central Australia, with particular reference to the mafic-ultramafic Giles Complex.

Bulletin - Australian Geological Survey Organisation, 239.

Godel, B., Seat, Z., Maier, W.D. and Barnes, S.-J., 2011. The Nebo-Babel Ni-Cu-PGE sulfide deposit (West Musgrave Block, Australia): Pt. 2. Constraints on parental magma and processes, with implications for mineral exploration. Economic Geology, 106(4): 557-584.

Green, T.H., 1995. Significance of Nb/Ta as an indicator of geochemical processes in the crust-mantle system. Chemical Geology, 120(3-4): 347-359.

Griffin, W.L., Belousova, E.A., Shee, S.R., Pearson, N.J. and O'Reilly, S.Y., 2004. Archean crustal evolution in the northern Yilgarn Craton; U-Pb and Hf-isotope evidence from detrital zircons. Precambrian Research, 131(3-4): 231-282.

Griffin, W.L., Wang, X., Jackson, S.E., Pearson, N.J., O'Reilly, S.Y., Xu, X. and Zhou, X., 2002. Zircon chemistry and magma mixing, SE China; in-situ analysis of Hf isotopes, Tonglu and Pingtan igneous complexes. Lithos, 61(3-4): 237-269.

Gualda, G.A. and Ghiorso, M.S., 2013. Low-Pressure Origin of High-Silica Rhyolites and Granites. The Journal of Geology, 121(5): 537-545.

Gunnarsson, B., Marsh, B.D. and Taylor, H.P., Jr., 1998. Generation of Icelandic rhyolites; silicic lavas from the Torfajokull central volcano. Journal of Volcanology and Geothermal Research, 83(1-2): 1-45.

Halliday, A.N., Davidson, J.P., Hildreth, W. and Holden, P., 1991. Modelling the petrogenesis of high Rb/Sr silicic magmas. Chemical Geology, 92(1-3): 107-114.

Hanson, G.N., 1978. The application of trace elements to the petrogenesis of igneous rocks of granitic composition. Earth and Planetary Science Letters, 38(1): 26-43.

Hart, T.R., Gibson, H.L. and Lesher, C.M., 2004. Trace element geochemistry and petrogenesis of felsic volcanic rocks associated with volcanogenic massive Cu-Zn-Pb sulfide deposits. Economic Geology and the Bulletin of the Society of Economic Geologists, 99(5): 1003-1013.

Hildreth, W., 1981. Gradients in silicic magma chambers: implications for lithospheric magmatism. Journal of Geophysical Research: Solid Earth (1978–2012), 86(B11): 10153-10192.

Hildreth, W., 2004. Volcanological perspectives on Long Valley, Mammoth Mountain, and Mono Craters; several contiguous but discrete systems. Journal of Volcanology and Geothermal Research, 136(3-4): 169-198.

Hildreth, W. and Moorbath, S., 1988. Crustal contributions to arc magmatism in the Andes of central Chile. Contributions to Mineralogy and Petrology, 98(4): 455-489.

Howard, H.M., Smithies, R.H., Kirkland, C.L., Evins, P.M. and Wingate, M.T.D., 2009. Age and geochemistry of the Alcurra Suite in the west Musgrave Province and implications for orthomagmatic Ni-Cu-PGE mineralization during the Giles Event. Record - Geological Survey of Western Australia, Perth, Australia, 2009(16): 16 pp.

Howard, H.M., Werner, M., Smithies, R.H., Evins, P.M., Kirkland, C.L., Kelsey, D.E., Hand,

M., Collins, A.S., Pirajno, F., Wingate, M.T.D., Maier, W.D. and Raimondo, T., 2011. The geology of the west Musgrave Province and the Bentley Supergroup -- a field guide. Record - Geological Survey of Western Australia, Perth, Australia, 2011/14: 125 pp.

Irvine, T.N. and Baragar, W.R.A., 1971. A guide to the chemical classification of the common volcanic rocks. Canadian Journal of Earth Sciences = Journal Canadien des Sciences de la Terre, 8(5): 523-548.

Kamber, B.S. and Collerson, K.D., 2000. Role of "hidden" deeply subducted slabs in mantle depletion. Chemical Geology, 166(3-4): 241-254.

Kelsey, D.E, Hand, M., Smithies, R.H., Evins, P., Clark, C. and Kirkland, C.L, 2009. High-temperature, high geothermal gradient metamorphism in the Musgrave Province, central Australia: potential constraints on tectonic setting. Biennial Conference of the Specialist Group for Geochemistry, Mineralogy and Petrology, Kangaroo Island, November 2009. Geological Society of Australia Abstracts, 28 pp.

Kelsey, D.E., Smithies, R.H., Hand, M., Evins, P.M., Clark, C. and Kirkland, C.L., 2010. What is the tectonic setting of long-lived Grenvillian-aged ultrahigh temperature, high geothermal gradient metamorphism in the Musgrave Province, central Australia, Geological Society of America, Abstracts with Programs, Denver Colorado, 42: 5 pp.

Kirkland, C.L., Wingate, M.T.D., Evins, P.M., Howard, H.M. and Smithies, R. H., 2009. 194354: gabbro dyke , Doymeyer Hill. Geochronology Record - Geological Survey of Western Australia. Perth, Australia, 799: 4 pp.

Kirkland, C.L., Smithies, R.H., Woodhouse, A., Wingate, M.T.D., Howard, H.M., Cliff, J. and Belousova, E.A., 2012. A multi-isotopic approach to the crustal evolution of the west Musgrave Province. Report - Geological Survey of Western Australia, Perth, Australia, 115: 48.

Kirkland, C.L., Smithies, R.H., Woodhouse, A.J., Howard, H.M., Wingate, M.T.D., Belousova, E.A., Cliff, J., Murphy, R. and Spaggiari, C.V., 2013. Constraints and deception in the isotopic record; the crustal evolution of the west Musgrave Province, central Australia. Gondwana Research, 23: 759-781.

Le Maitre, R.W., Bateman, P., Dudek, A., Keller, J., Lameyre, J., Le Bas, M.J., Sabine, P.A., Schmid, R., Sorensen, H., Streckeisen, A., Woolley, A.R. and Zanettin, B., 1989. A classification of igneous rocks and glossary of terms. Blackwell Sci. Publ., Oxford, United Kingdom, 193 pp.

Le Maitre, R.W., Streckeisen, A., Zanettin, B., Le Bas, M.J., Bonin, B., Bateman, P., Bellieni, G., Dudek, A., Efremova, S., Keller, J., Lameyre, J., Sabine, P.A., Schmid, R., Sorensen, H. and Woolley, A.R., 2002. Igneous rocks; a classification and glossary of terms; recommendations of the International Union of Geological Sciences Subcommission on the Systematics of Igneous Rocks. Cambridge University Press, Cambridge, United Kingdom, 236 pp.

Lesher, C.M., Goodwin, A.M., Campbell, I.H. and Gorton, M.P., 1986. Trace-element geochemistry of ore-associated and barren, felsic metavolcanic rocks in the Superior Province, Canada. Canadian Journal of Earth Sciences = Journal Canadien des Sciences de la Terre, 23(2): 222-237.

Lindsay, J., Schmitt, A., Trumbull, R., De Silva, S., Siebel, W. and Emmermann, R., 2001. Magmatic evolution of the La Pacana caldera system, Central Andes, Chile: compositional variation of two cogenetic, large-volume felsic ignimbrites. Journal of Petrology, 42(3): 459-486.

Linnen, R.L. and Keppler, H., 2002. Melt composition control of Zr/Hf fractionation in magmatic processes. Geochimica et Cosmochimica Acta, 66(18): 3293-3301.

Loiselle, M.C. and Wones, D.R., 1979. Characteristics and origin of anorogenic granites. Abstracts with Programs - Geological Society of America, 11(7): 468.

Maas, R., Kamenetsky, M.B., Sobolev, A.V., Kamenetsky, V.S. and Sobolev, N.V., 2005. Sr, Nd, and Pb isotope evidence for a mantle origin of alkali chlorides and carbonates in the Udachnaya Kimberlite, Siberia. Geology (Boulder), 33(7): 549-552.

MacDonald, R., Davies, G.R., Bliss, C.M., Leat, P.T., Bailey, D.K. and Smith, R.L., 1987. Geochemistry of high-silica peralkaline rhyolites, Naivasha Kenya rift valley. Journal of Petrology, 28(6): 979-1008.

Mahood, G. and Hildreth, W., 1983. Large partition coefficients for trace elements in high-silica rhyolites. Geochimica et Cosmochimica Acta, 47(1): 11-30.

Mason, B.G., Pyle, D.M. and Oppenheimer, C., 2004. The size and frequency of the largest explosive eruptions on Earth. Bulletin of Volcanology, 66(8): 735-748.

McBirney, A.R., 1980. Mixing and unmixing of magmas. Journal of Volcanology and Geothermal Research, 7(3): 357-371.

McCurry, M., Hayden, K.P., Morse, L.H. and Mertzman, S., 2008. Genesis of post-hotspot, A-type rhyolite of the eastern Snake River Plain volcanic field by extreme fractional crystallization of olivine tholeiite. Bulletin of Volcanology, 70(3): 361-383.

Mernagh, T.P. and Miezitis, Y., 2008. A Review of the Geochemical Processes Controlling the Distribution of Thorium in the Earth's Crust and Australia's Thorium Resources. Record - Geoscience Australia: 60.

Miller, C.F. and Mittlefehldt, D.W., 1982. Depletion of light rare-earth elements in felsic magmas. Geology (Boulder), 10(3): 129-133.

Miller, C.F. and Wark, D.A., 2008. Supervolcanoes and their explosive supereruptions. Elements, 4(1): 11-15.

Miller, J.S., Matzel, J.E., Miller, C.F., Burgess, S.D. and Miller, R.B., 2007. Zircon growth and recycling during the assembly of large, composite arc plutons. Journal of Volcanology and Geothermal Research, 167(1): 282-299.

Morgavi, D., Perugini, D., De Campos, C.P., Ertel-Ingrisch, W. and Dingwell, D.B., 2013. Time evolution of chemical exchanges during mixing of rhyolitic and basaltic melts. Contributions to Mineralogy and Petrology, 166: 615-638.

Morris, P.A. and Pirajno, F., 2005. Mesoproterozoic sill complexes in the Bangemall Supergroup, Western Australia; geology, geochemistry, and mineralization potential. Report - Geological Survey of Western Australia. Perth, Australia, 99: 83 pp.

Myers, J.S., Shaw, R.D. and Tyler, I.M., 1996. Tectonic evolution of Proterozoic Australia. Tectonics, 15(6): 1431-1446.

Nash, W.P. and Crecraft, H.R., 1985. Partition coefficients for trace elements in silicic magmas. Geochimica et Cosmochimica Acta, 49(11): 2309-2322.

Pearce, J.A., Harris, N.B.W. and Tindle, A.G., 1984. Trace element discrimination diagrams for the tectonic interpretation of granitic rocks. Journal of Petrology, 25(4): 956-983.

Peccerillo, A., Barberio, M.R., Yirgu, G., Ayalew, D., Barbieri, M. and Wu, T.W., 2003. Relationships between mafic and peralkaline silicic magmatism in continental rift settings; a petrological, geochemical and isotopic study of the Gedemsa Volcano, central Ethiopian Rift. Journal of Petrology, 44(11): 2003-2032.

Raczek, I., Jochum, K.P. and Hofmann, A.W., 2003. Neodymium and Strontium Isotope Data for USGS Reference Materials BCR-1, BCR-2, BHVO-1, BHVO-2, AGV-1, AGV-2, GSP-1, GSP-2 and Eight MPI-DING Reference Glasses. Geostandards Newsletter, 27: 173-179.

Reid, M.R., 2008. How long does it take to supersize an eruption? Elements, 4: 23-28.

Ritchey, J.L., 1980. Divergent magmas at Crater Lake, Oregon: products of fractional crystallization and vertical zoning in a shallow, water-undersaturated chamber. Journal of Volcanology and Geothermal Research, 7(3): 373-386.

Rollinson, H.R., 1993. Using geochemical data: evaluation, presentation, interpretation. Pearson Education Ltd., Longman Group, United Kingdom, 352 pp.

Rudnick, R. and Gao, S., 2003. Composition of the continental crust. Treatise on geochemistry, 3: 1-64.

Scherer, E., Muenker, C. and Mezger, K., 2001. Calibration of the lutetium-hafnium clock. Science, 293(5530): 683-687.

Schiano, P., Monzier, M., Eissen, J.P., Martin, H. and Koga, K.T., 2010. Simple mixing as the major control of the evolution of volcanic suites in the Ecuadorian Andes. Contributions to Mineralogy and Petrology, 160(2): 297-312.

Self, S., 2006. The effects and consequences of very large explosive volcanic eruptions. Philosophical Transactions of the Royal Society A: Mathematical, Physical and Engineering Sciences, 364(1845): 2073-2097.

Shellnutt, J.G. and Dostal, J., 2012. An evaluation of crustal assimilation within the Late Devonian South Mountain Batholith, SW Nova Scotia. Geological Magazine, 149(3): 353-365.

Shellnutt, J.G. and Zhou, M.-F., 2007. Permian peralkaline, peraluminous and metaluminous A-type granites in the Panxi district, SW China; their relationship to the Emeishan mantle plume. Chemical Geology, 243(3-4): 286-316.

Sláma, J., Kosler, J., Condon, D.J., Crowley, J.L., Gerdes, A., Hanchar, J.M., Horstwood,

M.S.A., Morris, G.A., Nasdala, L., Norberg, N., Schaltegger, U., Schoene, B., Tubrett, M.N. and Whitehouse, M.J., 2008. Plesovice zircon; a new natural reference material for U/Pb and Hf isotopic microanalysis. Chemical Geology, 249(1-2): 1-35.

Smithies, R.H., Howard, H.M., Evins, P.M., Kirkland, C.L., Bordorkos, S. and Wingate, M.T.D., 2009. The west Musgrave Complex - new geological insights from recent mapping, geochronology, and geochemical studies. Record - Geological Survey of Western Australia, Perth, Australia, 2008/19: 20 pp.

Smithies, R.H., Howard, H.M., Evins, P.M., Kirkland, C.L., Kelsey, D.E., Hand, M., Wingate, M.T.D., Collins, A.S. and Belousova, E., 2011. High-temperature granite magmatism, crust-mantle interaction and the Mesoproterozoic intracontinental evolution of the Musgrave Province, central Australia. Journal of Petrology, 52(5): 931-958.

Smithies, R.H., Howard, H.M., Evins, P.M., Kirkland, C.L., Kelsey, D.E., Hand, M., Wingate, M.T.D., Collins, A.S., Belousova, E.A. and Allchurch, S., 2010. Geochemistry, geochronology and petrogenesis of Mesoproterozoic felsic rocks in the west Musgrave Province, Central Australia, and implications for the Mesoproterozoic tectonic evolution of the region. Record - Geological Survey of Western Australia, Perth, Australia, 106: 82 pp.

Smithies, R.H., Howard, H.M., Kirkland, C.L., Werner, M., Medlin, C.C., Wingate, M.T.D. and Cliff, J.B., 2013. Geochemical evolution of rhyolites of the Talbot Sub-basin and associated felsic units of the Warakurna Supersuite, Report - Geological Survey of Western Australia, Perth, Australia, 118: 74 pp.

Smithies, R., Kirkland, C., Korhonen, F., Aitken, A., Howard, H., Maier, W., Wingate, M., Quentin de Gromard, R. and Gessner, K., 2014. The Mesoproterozoic thermal evolution of the Musgrave Province in central Australia–plume vs. the geological record. Gondwana Research.

Söderlund, U., Patchett, P.J., Vervoort, J.D. and Isachsen, C.E., 2004. The Lu-176 decay constant determined by Lu–Hf and U–Pb isotope systematics of Precambrian mafic intrusions. Earth and Planetary Science Letters, 219(3): 311-324.

Solano, J.M.S., Jackson, M.D., Sparks, R.S.J., Blundy, J.D. and Annen, C., 2012. Melt segregation in deep crustal hot zones; a mechanism for chemical differentiation, crustal assimilation and the formation of evolved magmas. Journal of Petrology, 53(10): 1999-2026.

Sparks, R.S.J., Huppert, H.E., Wilson, C.J.N., Halliday, A.N. and Mahood, G.A., 1990. Evidence for long residence times of rhyolitic magma in the Long Valley magmatic system; the isotopic record in precaldera lavas of Glass Mountain; discussion and replies. Earth and Planetary Science Letters, 99(4): 387-399.

Sparks, R.S.J., Self, S., Grattan, J.P., Oppenheimer, C., Pyle, D.M. and Rymer, H., 2005. Super-eruptions: global effects and future threats. Report of a Geological Society

of London working group. London, UK, 24 pp.

Stacey, J.S. and Kramers, J.D., 1975. Approximation of terrestrial lead isotope evolution by a two-stage model. Earth and Planetary Science Letters, 26(2): 207-221.

Stern, R.A., 2001a. A new isotopic and trace-element standard for the ion microprobe; preliminary thermal ionization mass spectrometry (TIMS) U-PB and electron-microprobe data; Radiogenic age and isotopic studies, Current Research - Geological Survey of Canada, Ottawa, ON, Canada, 10 pp.

Stern, R.A., 2001b. A new isotopic and trace-element standard for the ion microprobe: preliminary thermal ionization mass spectrometry (TIMS) U-Pb and electron-microprobe data. Geological Survey of Canada Report: 11 pp.

Stern, R.A., Bodorkos, S., Kamo, S.L., Hickman, A.H. and Corfu, F., 2009. Measurement of SIMS instrumental mass fractionation of Pb isotopes during zircon dating. Geostandards and Geoanalytical Research, 33(2): 145-168.

Sun, S.S. and McDonough, W.F., 1989. Chemical and isotopic systematics of oceanic basalts; implications for mantle composition and processes. Geological Society Special Publications, 42: 313-345.

Sun, S.S., Sheraton, J.W., Glikson, A.Y. and Stewart, A.J., 1996. A major magmatic event during 1050-1080 Ma in central Australia, and emplacement age for the Giles Complex. AGSO Research Newsletter, 24: 13-15.

Taylor, S.R. and McLennan, S.M., 1985. The continental crust: its composition and evolution. Blackwell, Oxford.

Thomas, J., Bodnar, R., Shimizu, N. and Sinha, A., 2002. Determination of zircon/melt trace element partition coefficients from SIMS analysis of melt inclusions in zircon. Geochimica et Cosmochimica Acta, 66(16): 2887-2901.

Thy, P., Beard, J.S. and Lofgren, G.E., 1990. Experimental constraints on the origin of Icelandic rhyolites. Journal of Geology, 98(3): 417-421.

Turner, S., Foden, J. and Morrison, R., 1992a. Derivation of some A-type magmas by fractionation of basaltic magma: an example from the Padthaway Ridge, South Australia. Lithos, 28(2): 151-179.

Turner, S., Sandiford, M. and Foden, J., 1992b. Some geodynamic and compositional constraints on" postorogenic" magmatism. Geology, 20(10): 931-934.

Vance, D. and Thirlwall, M., 2002. An assessment of mass discrimination in MC-ICPMS using Nd isotopes. Chemical Geology, 185: 227-240.

Verma, S.P., Pandarinath, K., Verma, S.K. and Agrawal, S., 2013. Fifteen new discriminant-function-based multi-dimensional robust diagrams for acid rocks and their application to Precambrian rocks. Lithos, 168–169(0): 113-123.

Wade, B.P., Barovich, K.M., Hand, M., Scrimgeour, I.R. and Close, D.F., 2006. Evidence for early Mesoproterozoic arc magmatism in the Musgrave Block, central Australia; implications for Proterozoic crustal growth and tectonic reconstructions of Australia. Journal of Geology, 114(1): 43-63.

Wade, B.P., Kelsey, D.E., Hand, M. and Barovich, K.M., 2008. The Musgrave Province;

stitching north, west and south Australia. Precambrian Research, 166(1-4): 370-386.

Watson, E.B. and Harrison, T.M., 1983. Zircon saturation revisited; temperature and composition effects in a variety of crustal magma types. Earth and Planetary Science Letters, 64(2): 295-304.

Watt, G. and Harley, S., 1993. Accessory phase controls on the geochemistry of crustal melts and restites produced during water-undersaturated partial melting. Contributions to Mineralogy and Petrology, 114(4): 550-566.

Werner, M., Howard, H.M. and Smithies, R.H., 2012. Mount Eveline, WA Sheet 4345 1:100 000 Geological Series Maps. Geological Survey of Western Australia. Perth, Australia.

Whalen, J.B., Currie, K.L. and Chappell, B.W., 1987. A-type granites; geochemical characteristics, discrimination and petrogenesis. Contributions to Mineralogy and Petrology, 95(4): 407-419.

White, A.J.R. and Chappell, B.W., 1983. Granitoid types and their distribution in the Lachlan fold belt, southeastern Australia. Memoir - Geological Society of America, 159: 21-34.

Wingate, M.T.D. and Kirkland, C.L., 2013. Introduction to geochronology information released in 2010. Report - Geological Survey of Western Australia. Perth, Australia, 5 pp.

Wingate, M.T.D., Pirajno, F. and Morris, P.A., 2004. Warakurna large igneous province: A new Mesoproterozoic large igneous province in west-central Australia. Geology, 32(2): 105-108.

Woodhead, J.D. and Hergt, J.M., 2005. A preliminary appraisal of seven natural zircon reference materials for in situ Hf isotope determination. Geostandards and Geoanalytical Research, 29(2): 183-195.

Woodhead, J.D., Hergt, J.M., Shelley, M., Eggins, S. and Kemp, R., 2004. Zircon Hf-isotope analysis with an excimer laser, depth profiling, ablation of complex geometries, and concomitant age estimation. Chemical Geology, 209(1-2): 121-135.

Xu, Y., Chung, S.-L., Shao, H. and He, B., 2010. Silicic magmas from the Emeishan large igneous province, southwest China; petrogenesis and their link with the end-Guadalupian biological crisis. Lithos (Oslo), 119(1-2): 47-60.

York, D., 1966. Least-squares fitting of a straight line. Canadian Journal of Physics, 44(5): 1079-1086.

Zen, E.A., 1988. Phase relations of peraluminous granitic rocks and their petrogenetic implications. Annual Review of Earth and Planetary Sciences, 16: 21-51.

Zhao, J.-x. and McCulloch, M.T., 1993. Melting of a subduction-modified continental lithospheric mantle: evidence from late Proterozoic mafic dike swarms in central Australia. Geology, 21(5): 463-466.

Zindler, A. and Hart, S., 1986. Chemical geodynamics. Annual Review of Earth and Planetary Sciences, 14: 493-571.

Chapter 4

Determining the controls on rheomorphism of a Mesoproterozoic lava-like ignimbrite in the subaqueously emplaced, intra-caldera, high-silica Kathleen Ignimbrite, west Musgrave Province, central Australia

C.C. Medlin[1], S.M. Jowitt[1] and R.A.F. Cas[1]

[1]School of Geosciences, Monash University, Clayton, Victoria, 3800, Australia

Keywords: fluorine, geothermometry, Mesoproterozoic, rheomorphic ignimbrite, rhyolite, viscosity, west Musgrave Province

Abstract

The 1071 ± 5 Ma Kathleen Ignimbrite eruption sequence of the Mesoproterozoic west Musgrave Province of central Australia is a rare example of a thick intra-caldera rheomorphic ignimbrite emplaced in a shallow-water environment. These ignimbrites is an evolved, high-silica, A-type, metaluminous (to slightly peraluminous) rhyolite that is significantly enriched in the rare earth elements (REE; up 794 ppm) and F (≤0.8 wt%) compared to crustal values. This study focuses on the rheomorphic nature of the deposit and assesses the factors that controlled the extremely high-grade welding conditions attained during and after emplacement. Despite the ignimbrite's subaqueous emplacement, the <50 m thick basal facies contains folded and deformed lava-like flow banding and laminations, with a basal contact with an underlying shallow-water turbidite succession characterised by pervasive hyaloclastite and peperite development.

This study uses petrological and textural observations, whole-rock geochemistry and geothermometry data to determine the viscosity of the deposit during eruption. The results indicate that the ignimbrite was erupted at lower temperatures and lower viscosities than similar rheomorphic ignimbrites, potentially related to the elevated fluorine concentrations present in the magma and possibly the presence of water. However, the modelling undertaken during this study indicates that removing all of the F and H_2O from the magma that formed the Kathleen Ignimbrite would not have prevented rheomorphism. The data presented here also indicate that the Kathleen Ignimbrite would have behaved rheomorphically at higher strain rates and over shorter deformation timescales than have been recorded for other similar lava-like rheomorphic ignimbrites. This, combined with existing knowledge of the physical and chemical factors responsible for rheomorphism, indicates there is no single specific factor that caused the Kathleen Ignimbrite to behave rheomorphically, but rather the rheomorphic nature of the deposit was caused by a combination of factors working in unison

to affect the rheology and viscosity of the ignimbrite. This resulted in extremely high-grade welding and lava-like rheomorphism, despite the initial subaqueous emplacement of the ignimbrite, and the lower temperatures and unfavourable chemistry (e.g., high SiO_2, lower H_2O and lower alkalis) of this ignimbrite compared to the majority of other rheomorphic ignimbrites (e.g., the higher-temperature metaluminous Snake River-type and peralkaline Gran Canaria rheomorphic ignimbrites).

4.1 Introduction

Lava-like rheomorphic ignimbrites form when extreme degrees of welding results in an ignimbrite deposit flowing like a lava after initial deposition as a particulate pyroclastic flow deposit (Branney *et al*., 2004). These high-grade end-members fall within a welding continuum from non-welded tuffs to agglutinated fountain-fed lavas (Branney and Kokelaar, 1992) and are well documented from the geological record (e.g., Sumner and Branney, 2002; Andrews and Branney, 2011; Chapter 2). The conditions that facilitate rheomorphism in ignimbrites have been discussed and summarised in various studies (e.g., Wolff and Wright, 1981; Branney *et al*., 1992; Andrews and Branney, 2011); in some cases specific factors may have been responsible for rheomorphism (e.g., shear heating; Robert *et al*., 2013; load pressure on a slope; Kobberger and Schmincke, 1999) whereas in other cases a combination of factors may have contributed to the development of rheomorphism (e.g., Schmincke and Swanson, 1967; Leat and Schmincke, 1993; Sommer *et al*., 2013).

This study focuses on the factors that contributed to rheomorphism within the rhyolitic, rheomorphic, lava-like Mesoproterozoic Kathleen Ignimbrite (KI) (Formation) of central Australia. The KI was emplaced in a subaqueous environment (Chapter 2) at lower temperatures than the majority of other rheomorphic ignimbrites, but provides evidence of very high degrees of welding during the development of lava-like rheomorphic textures. In addition, the KI is preserved as a caldera-fill ignimbrite, providing another example and further understanding of a favourable environment where rheomorphism can develop. This study focuses on the relative importance of the factors that contributed to rheomorphic behaviour of the KI, including the geochemistry of the magma, magmatic crystallisation temperatures, viscosity, and strain, furthering our understanding of the factors that contribute to and control rheomorphism in ignimbrites.

4.1.1 Regional geology

The 1.60–1.15 Ga Mesoproterozoic Musgrave Province (Fig. 4.1a) of central Australia is an ESE–WSW-trending 800 km long and 350 km wide belt of high-grade amphibolite to granulite facies metamorphic rocks that is bound by mid-Neoproterozoic to Mesozoic sedimentary basins and lies at the convergence of the Proterozoic amalgamation of the North, West and South Australian Cratons (Fig. 4.1b; Wade *et al*., 2008;). A series of bimodal felsic and basaltic volcanics, granitic and mafic-ultramafic layered and massive intrusions and variably deformed and low-grade metamorphosed sedimentary rocks were either intruded into, or were extruded and deposited onto the Musgrave Province of Western Australia (Glikson *et al*. 1996; Smithies *et al*., 2013). The volcanic rocks in this area include very thick, large volume rhyolite units that have been interpreted as ignimbrites (Daniels, 1974; Howard *et al*., 2011; Werner *et al*., 2012), including the initially subaqueously-emplaced, intra-caldera, lava-like rheomorphic to eutaxitically welded 1071 ± 5 Ma Kathleen Ignimbrite. These rhyolite units are part of the Bentley Supergroup and formed between 1085 and 1040 Ma during a failed, intra-continental, rifting event that formed the Bentley Basin and its smaller Talbot Sub-basin (Evins *et al*., 2010; Smithies *et al*., 2013). This rifting is associated with a >30 Ma felsic magmatic event that included the formation of the Warakurna Large Igneous Province (Wingate *et al*., 2004; Smithies *et al*., 2013).

The Talbot Sub-basin contains the southward dipping and younging bimodal volcanic-sedimentary Pussy Cat Group (Daniels, 1974). The lower portion of the Pussy Cat Group is exposed in the Whitby Range, which forms the focus of this study. This range is structurally subdivided into five main domains by dominant NNW–SSE striking faults (Fig. 4.2), namely a deformed and sheared western domain (A), a low-relief middle domain (B), a well-preserved and relatively undeformed eastern domain (C), a fault-offset northeast domain (D), and a faulted and displaced southeast domain (E). The study area (shown as a red box in Fig. 4.1a; Fig. 4.2.) consists of a previously unnamed basal, felsic, volcaniclastic-sedimentary formation, here informally named the Cleghorne Formation (CF), which is underlain by effusive rhyolite lavas and ignimbrites of the Mount Palgrave Group. This in turn is overlain by the felsic volcanic KI and, by the stratigraphically higher mafic volcano-sedimentary Glyde Formation (Fig. 4.2). A suite of sub-volcanic porphyritic rhyolites, here named the Rowland Suite (RS), form voluminous intrusions within the volcano-sedimentary succession of the lower Pussy Cat Group (Fig. 4.2). Further detailed descriptions of the all the units in this area are provided by Howard *et al*. (2011) and in Chapters 1 and 2. In Chapter 3 it was established that this suite of intrusions is co-magmatic and coeval with the KI, with the magmas that formed both units originating from a common stratified magma chamber; the KI represents the evolved aphyric melt-rich end-member, whereas the RS represents the slightly more primitive crystal-rich cumulate end-member of a magmatic differentiation continuum.

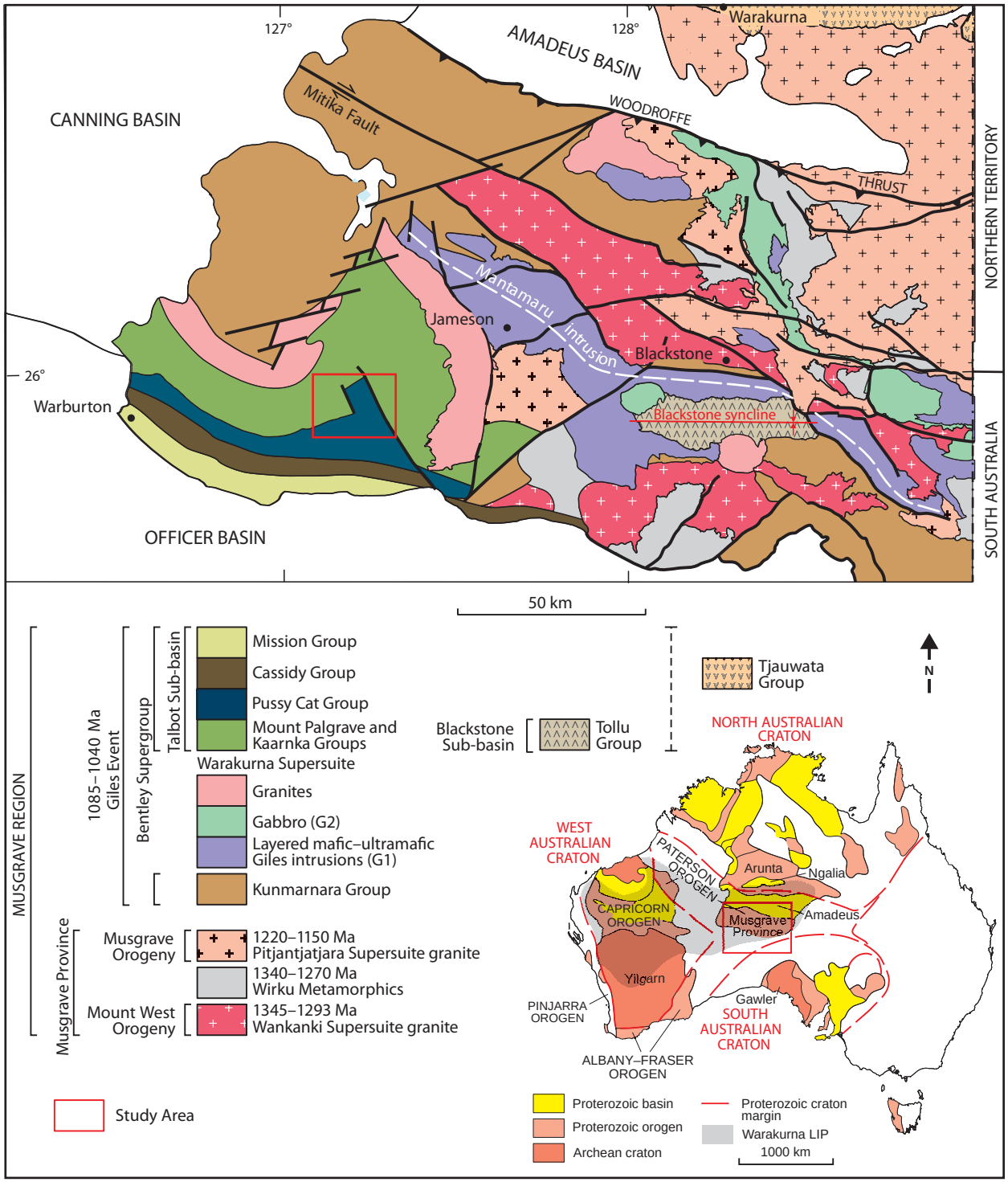

Figure 4.1: a) Location of the west Musgrave Province and surrounding regional geology (adapted from Glikson *et al*., 1996; Edgoose *et al*., 2004; Howard *et al*., 2011; Smithies *et al*., 2013). b) Location of the Musgrave Province in terms of the tectonic framework of Proterozoic Australia, and the extent of the Warakurna LIP (adapted from Myers *et al*., 1996; Smithies *et al*., 2013). Location of study area highlighted in red, and expanded on in Fig. 4.2.

In the study area, the KI has a maximum preserved stratigraphic thickness of ≤650 m, the accumulated thickness of the CF is ~100 m, and the stratiform rhyolites of the RS that underlie the KI have a maximum thickness of ≤250 m (Fig. 4.3). The CF, RS and KI package (Fig. 4.3) dips at 20°–30° to the south-southeast and outcrops over a minimum strike length of ~22 km, before disappearing under Quaternary sands.

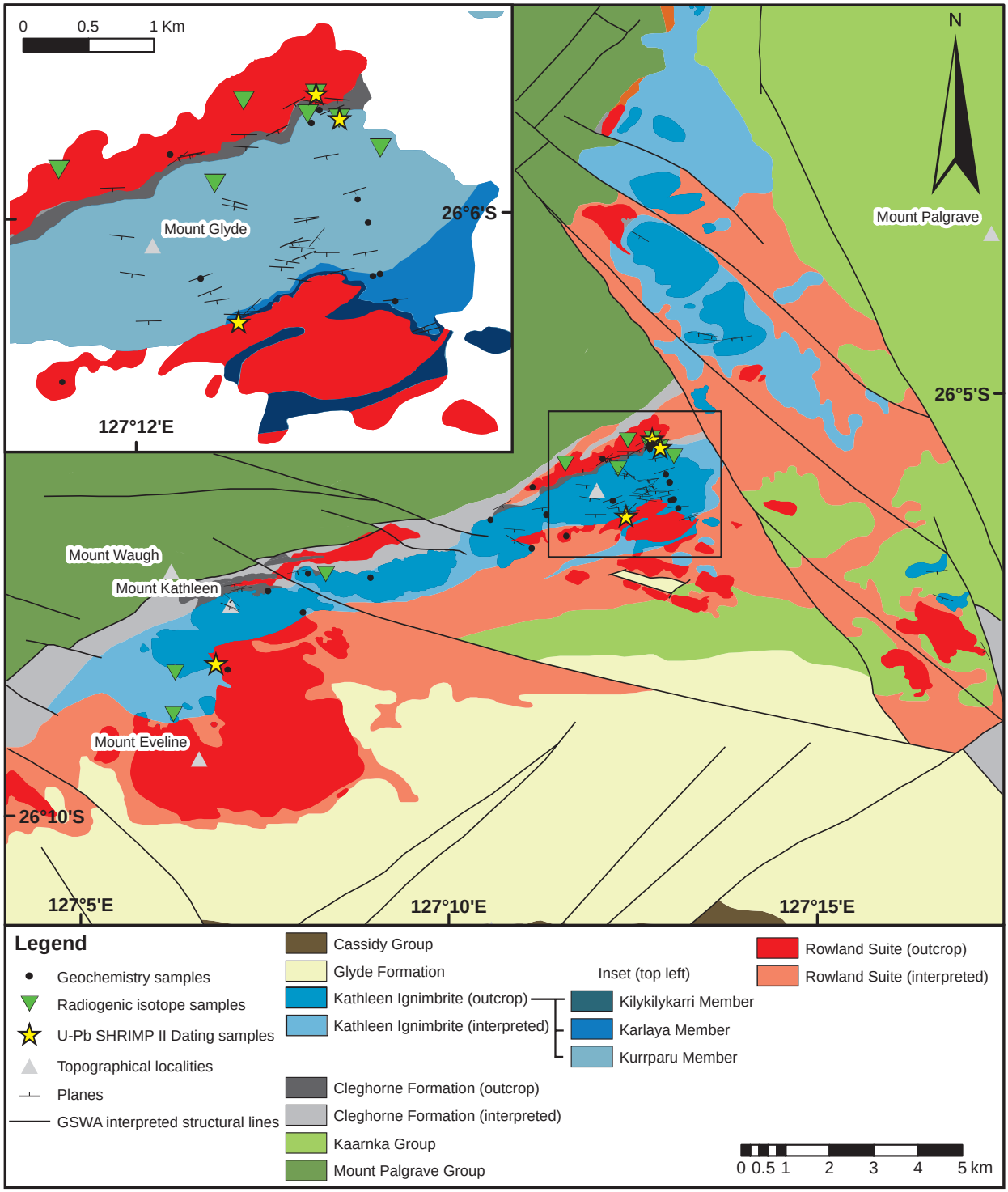

Figure 4.2: Geological map of the study area. Dark colours indicate exposures, whereas lighter shades of the same colour indicates interpreted bedrock. Geochemical sample locations are indicated by yellow stars. Structural sections A, B, C, D and E are indicated on the map (adapted from Werner *et al*., 2012).

4.2 The Kathleen Ignimbrite (KI)

The KI (Formation) was generated by a very large, caldera-forming rhyolitic explosive eruption at ca. 1070 Ma and comprises a large part of a ~1 km thick well-preserved volcanic–sedimentary succession that covers an area of ~40 km^2. The formation consists of the ≤500 m thick intra-caldera welded Kurrparu Member that contains well-defined fiamme and eutaxitic textures and a well-developed, ≤50 m thick, rheomorphic

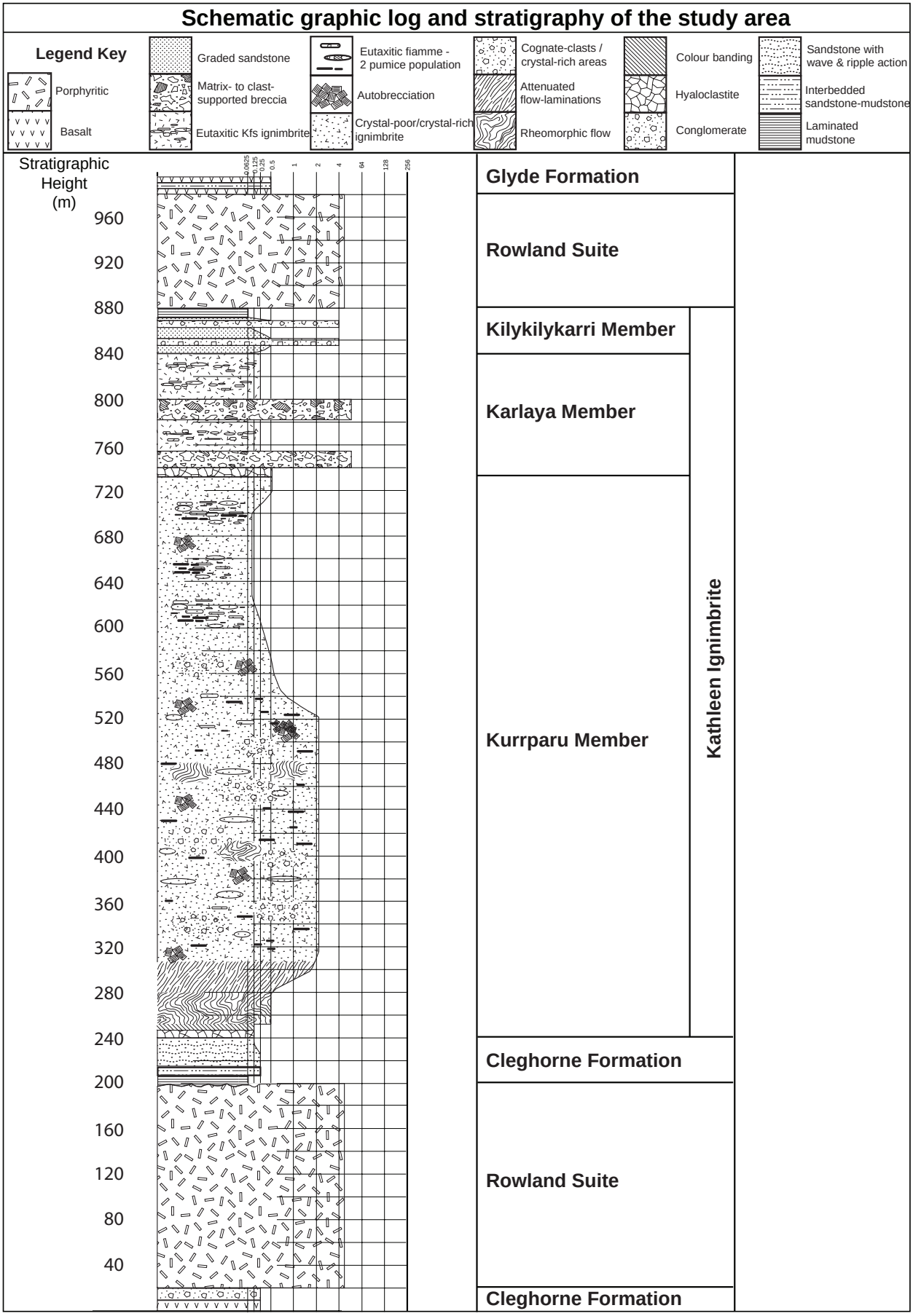

Figure 4.3: Schematic graphic log of the ~1 km volcanic-sedimentary succession that hosts the KI. Observations predominantly from the eastern section (C; Fig. 4.2), as this section offers the best exposure, least deformation, and most continuous outcrop. This log is representative of the whole KI, with similar facies and textures were observed in the other sections. The true vertical thickness is plotted on the left hand column, calculated using an average dip for the entire succession of 25°.

lava-like basal facies, the non-welded, ≤100 m thick, ignimbritic Karlaya Member, and the ≤50 m thick, upper shallow-water turbiditic volcaniclastic Kilykilykarri Member. The basal Kurrparu Member is underlain by shallow-water storm shelf-type turbiditic sediments of the Cleghorne Formation. The base of the KI is marked by extensive peperite and hyaloclastite along the basal contact (Fig. 4.4a), providing evidence of initial subaqueous emplacement (Chapter 2). Although the KI (Formation) consists of variably welded ignimbrites and reworked and resedimented volcaniclastic deposits, this paper focuses exclusively on the ignimbrites. In addition, ignimbrites within both the Kurrparu and Karlaya members are collectively referred to as the Kathleen Ignimbrite (KI) from this point on; both members formed during a fairly continuous eruptive event that created the Kathleen Caldera.

4.2.1 Lithofacies architecture of the Kathleen Ignimbrite

The base of the KI is a ≤50 m thick crystal-poor (<5%) closely-spaced laminar flow- and colour-banded rhyolite, with a basal zone of jigsaw fit to clast-rotated fragments of flow- and colour-banded rhyolite clasts (Fig. 4.4a) at the contact with the underlying sedimentary rocks. The flow banding records lava-like flow conditions and is planar at the base, with the laminations becoming folded further upwards, ranging from gentle (Fig. 4.4b) to ptygmatic (Fig. 4.4c). The flow bands have pervasive lineations and gas-driven shear partings (Fig. 4.4d), with associated vugs and vein-like features that are indicative of vapour-phase crystallisation (Fig. 4.4e). Gradational upward attenuation of the flow bands and partings, together with an increase in the crystal contact, marks the end of this basal facies, followed by a thick (300–350 m) poorly-sorted, crystal-rich to crystal-poor (25–10%) matrix-supported facies (Fig. 4.4f) with unequivocal vitriclastic textures, such as fragmented crystals, fiamme and cognate clasts. This facies grades into an overlying facies containing two well-developed eutaxitic fiamme populations, crystal-rich (Fig. 4.4g) and aphyric (Fig. 4.4h). These pumice populations are concentrated towards the base of this eutaxitic facies, which grades up into a 100–150 m thick crystal-poor (<5%) facies that contains plastically deformed cuspate and platy glass-shard remnant textures. This in turn has a sharp contact to an overlying thin package of thinly interbedded breccias and crystal-rich to crystal-poor eutaxitic to non-eutaxitic vitriclastic deposits with well preserved shard textures. Deformation in the basal facies is recorded in structures ranging from open symmetrical to recumbent isoclinal folds, refolded folds, and sheath folds (Fig. 4.4i)

4.2.2 Lithofacies interpretation

The features of the KI, including poor sorting, frequently broken crystals, eutaxitic fiamme and remnant glass shard textures in the upper crystal-poor facies, are all consistent with the KI being erupted as an ignimbrite. The gradational contacts between the lower facies imply that the coherent lava-like basal facies is also ignimbritic, and flow banding

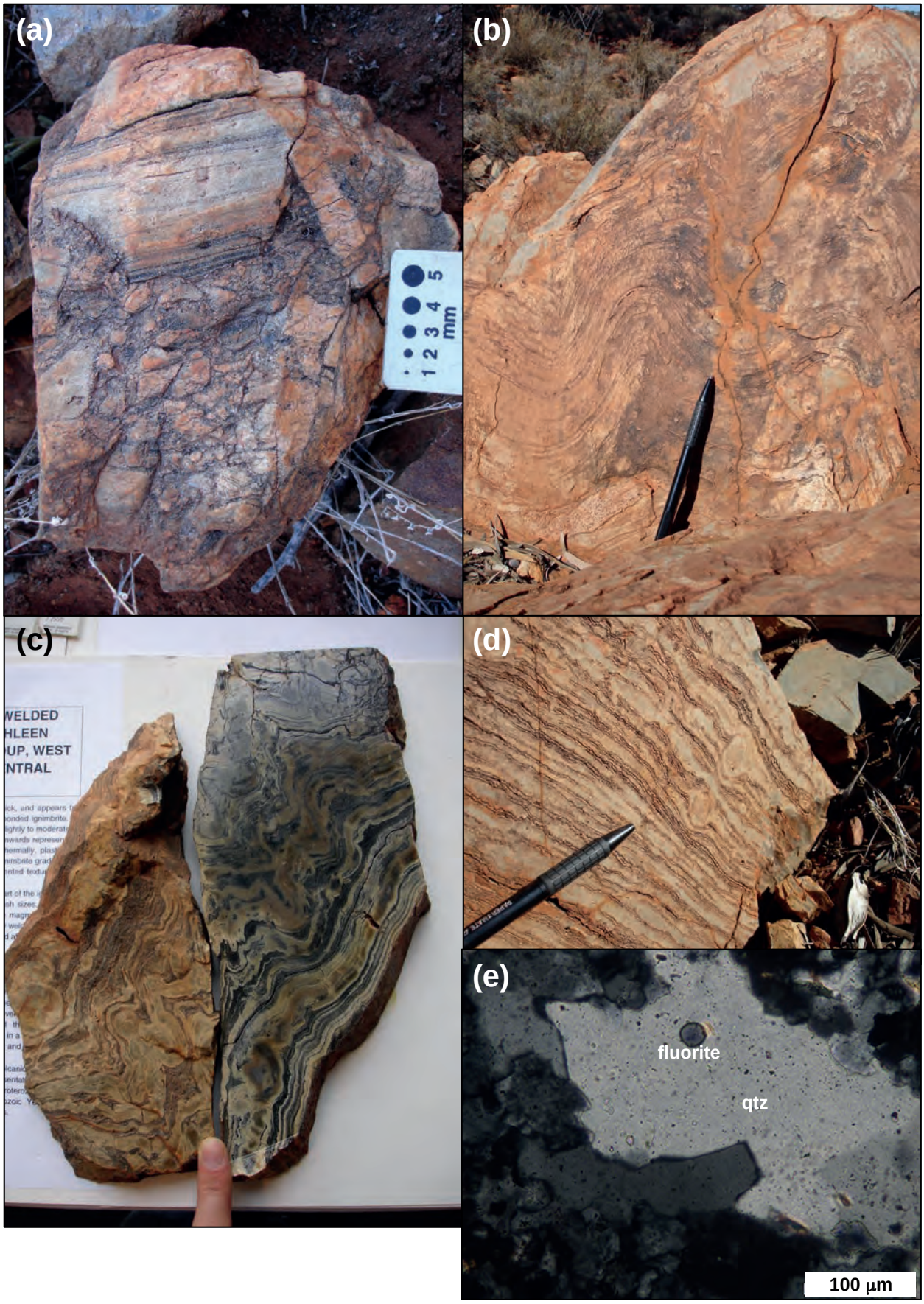

Figure 4.4: Lithofacies architecture of the KI. a) Basal contact facies with jigsaw-fit clasts of flow- and colour-banded rhyolite, interpreted to be hyaloclastite and locally as peperite. b) Gently folded laminations with open symmetrical folds in the basal lava-like rheomorphic facies. c) Ptygmatic folded laminations due to rheomorphic flow (cut and polished slab). d) Pervasive lineations along gas-driven shear partings with rounded spherulite clast development. e) Photomicrograph of vapour phase quartz found within a shear parting with a fluorite fluid inclusion (PPL).

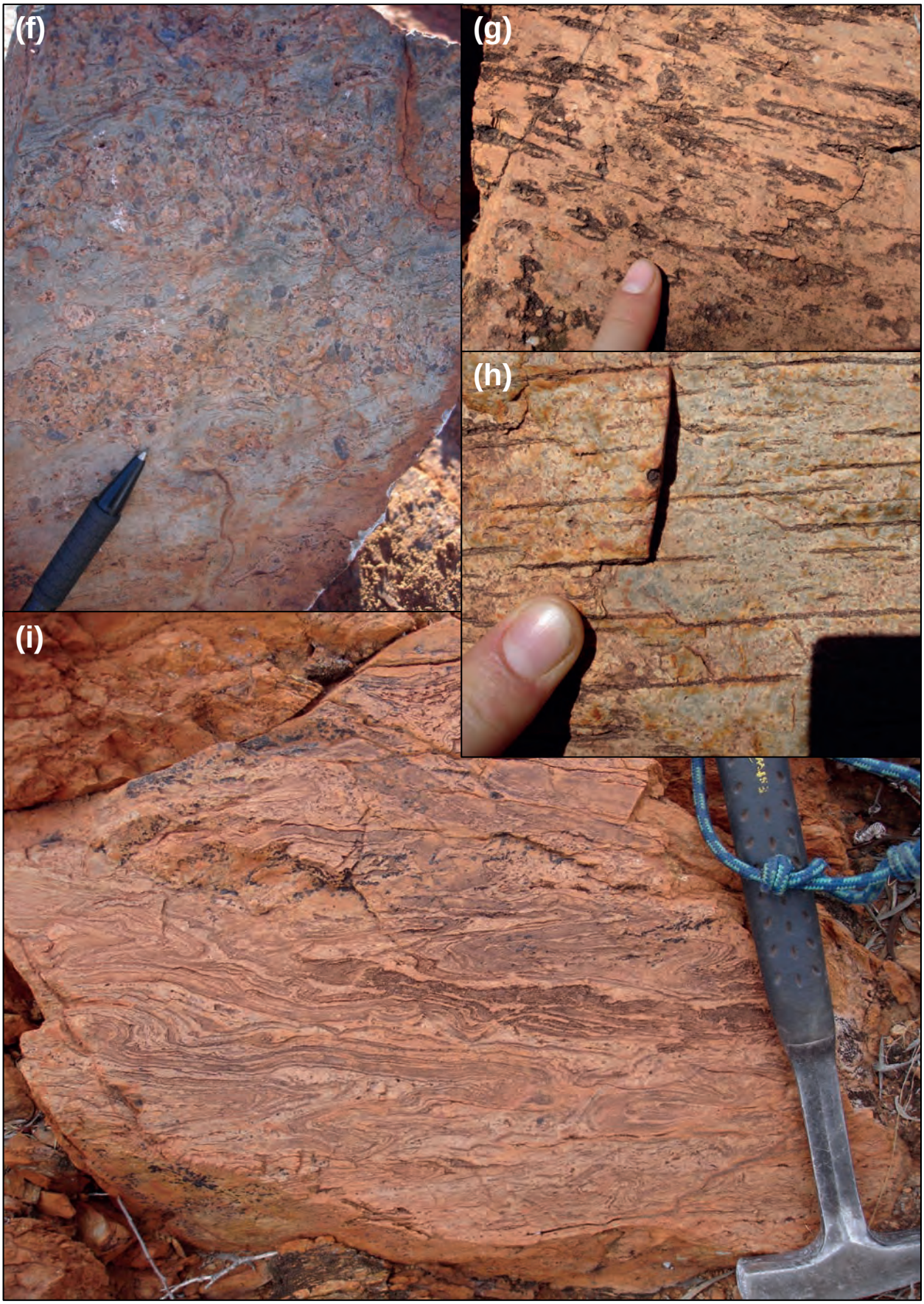

Figure 4.4 (continued): f) Poorly-sorted, crystal-rich to crystal-poor texture of the thick matrix-supported lapilli-tuff facies – *main zone facies*. g) Eutaxitic crystal-rich fiamme. h) Eutaxitic aphyric fiamme. i) Rheomorphism in the KI - intensity of rheomorphic shear and deformation recorded in structures occurring in the basal lava-like facies of the KI, such as isoclinal folds, refolded folds, and sheath folds - this photo is a good indication of the strain recorded in the rheomorphic shear zone.

and folding like this within an ignimbrite must have formed by rheomorphism during extremely high grade welding and secondary flow. The presence of a gradational stack of multiple progressively or incrementally aggraded ignimbritic depositional units that defines a crude stratigraphic layering and vertical variations in welding intensity indicates that there was no time break during the deposition of this ~500 m of stratigraphy. The KI is therefore interpreted to represent a continuously erupted and emplaced ignimbrite succession that cooled to form a single simple cooling unit (Smith, 1960; Riehle *et al*., 2010). In addition, the thickness and extent of the KI is indicative of formation as an intra-caldera ignimbrite deposit (Cas and Wright, 1987), and the fragmentation along the basal contact of the KI with the underlying shallow-water turbiditic sediments is interpreted to be hyaloclastite development that also locally formed peperites (Pichler 1965; Skilling *et al*., 2002; Wohletz, 2002), indicative of initial emplacement in subaqueous conditions. To summarise, the KI is an extremely high-grade welded lava-like rheomorphic ignimbrite, much like the Snake River (SR)-type lava-like rheomorphic Grey's Landing Ignimbrite of Idaho, USA (Andrews and Branney, 2011).

4.3 Methods

Field mapping and sampling were undertaken as part of an on-going regional mapping program with the Geological Survey of Western Australia; samples were collected at regular intervals along traverses with the majority of sampling from the well-preserved and undeformed eastern section of the study area (C; Fig. 4.2). Petrological descriptions are based on hand specimens and representative thin sections.

All geochemical sample preparation was undertaken at the School of Geosciences, Monash University. Samples were cut, crushed, and milled using a diamond saw, ceramic hydraulic press, ceramic jaw-crusher, and tungsten-carbide mill. Whole-rock major element, F, and Cl concentrations were determined by X-Ray Fluorescence (XRF) spectrometry and a Bruker-AXS S4 Pioneer XRF Spectrometer at the Advanced Analytical Centre, James Cook University, Townsville, Australia. Prior to major element analysis ~2 g of each sample was ignited in a muffle furnace at 1000°C to determine loss on ignition (LOI) values before 1 g of ignited sample was fused with 8 g of lithium tetraborate flux in Pt crucibles for 12 minutes at 1100°C to produce homogeneous glass fusion beads for XRF analysis. F and Cl concentrations were determined on pressed pellets formed by mixing milled sample powders with a binding agent and pressing the mixture into aluminium cups. Trace and rare earth element (REE) concentrations were determined using inductively coupled plasma-mass spectrometry (ICP-MS) and a Thermo Finnigan X series II quadrupole instrument at the School of Geosciences, Monash University. Prior to analysis, approximately 50 mg of milled sample powder was digested using a high pressure mixed HF-HNO_3-HCl acid attack and placed on a hot plate at 150°C for

approximately 48 hours. Subsequently the samples were dried down and taken back into solution using 3% HNO_3 for final presentation to the mass spectrometer. Count rates were externally standardised using recommended values for the Sco 1 certified reference material, and drift corrections were applied using In and Bi as internal standards and by repeat analysis of dummy standards. The precision and accuracy for all elements presented in this study is better than 7.5% and repeat analysis of standards indicate negligible contamination during digestion and analysis.

4.4 Results

4.4.1 Geochemistry

All whole-rock compositions were corrected to 100% anhydrous before interpretation and are shown as corrected, with iron concentrations provided as total Fe_2O_3 (data from Chapter 3; Table 4.1 – Appendix B). For reference the RS samples have been included on some diagrams and plots with the KI samples.

All KI samples analysed during this study contain high concentrations of SiO_2 (74.88–78.27 wt%), and have Al_2O_3, CaO, Fe_2O_3, Zn, Hf, Nd and Zr concentrations that negatively correlate with SiO_2, while Sr and U concentrations correlate positively with SiO_2 in Harker diagrams (e.g., Figs. 4.5a and 4.5b). All samples contain high concentrations of fluorine (up to 0.8 wt%; Fig. 4.5c). All samples are classified as rhyolitic on the total alkali (K_2O+Na_2O) vs. SiO_2 TAS diagram of Le Maitre *et al*. (1989, 2002; Fig. 4.6a). Samples from both suites plot along or below the alkaline dividing line of Irvine and Baragar (1971), indicating they are generally subalkaline, and the majority of these samples have aluminium saturation index (ASI, molar ratio of Al_2O_3 to CaO + K_2O + Na_2O or A/CNK; Frost & Frost, 2008, Zen, 1988) values that indicate they are metaluminous (ASI = 0.91–1.09), with a few samples classified as peraluminous (ASI >1.0; Frost *et al.*, 2001). All samples have FeO* (FeO/FeO+MgO; Frost & Frost, 2008) values of 0.86–0.97 with modified alkali-lime index (MALI; Frost and Frost, 2008) values of 6.58–9.25, classifying them as intermediate between alkali-calcic and calc-alkalic. In addition, all samples analysed during this study are classified as A-type and plot within the anorogenic granite field of Whalen *et al*. (1987) or the within-plate regions of tectonic discrimination diagrams of Pearce *et al*. (1984; Fig. 4.6b), and Verma *et al*. (2013).

4.4.2 Mineralogy

A detailed description of the petrography of the KI is provided in Chapters 2 and 3. Although this ignimbrite has undergone pervasive devitrification, there is little evidence for pervasive secondary alteration of the deposit. The principal primary magmatic crystals

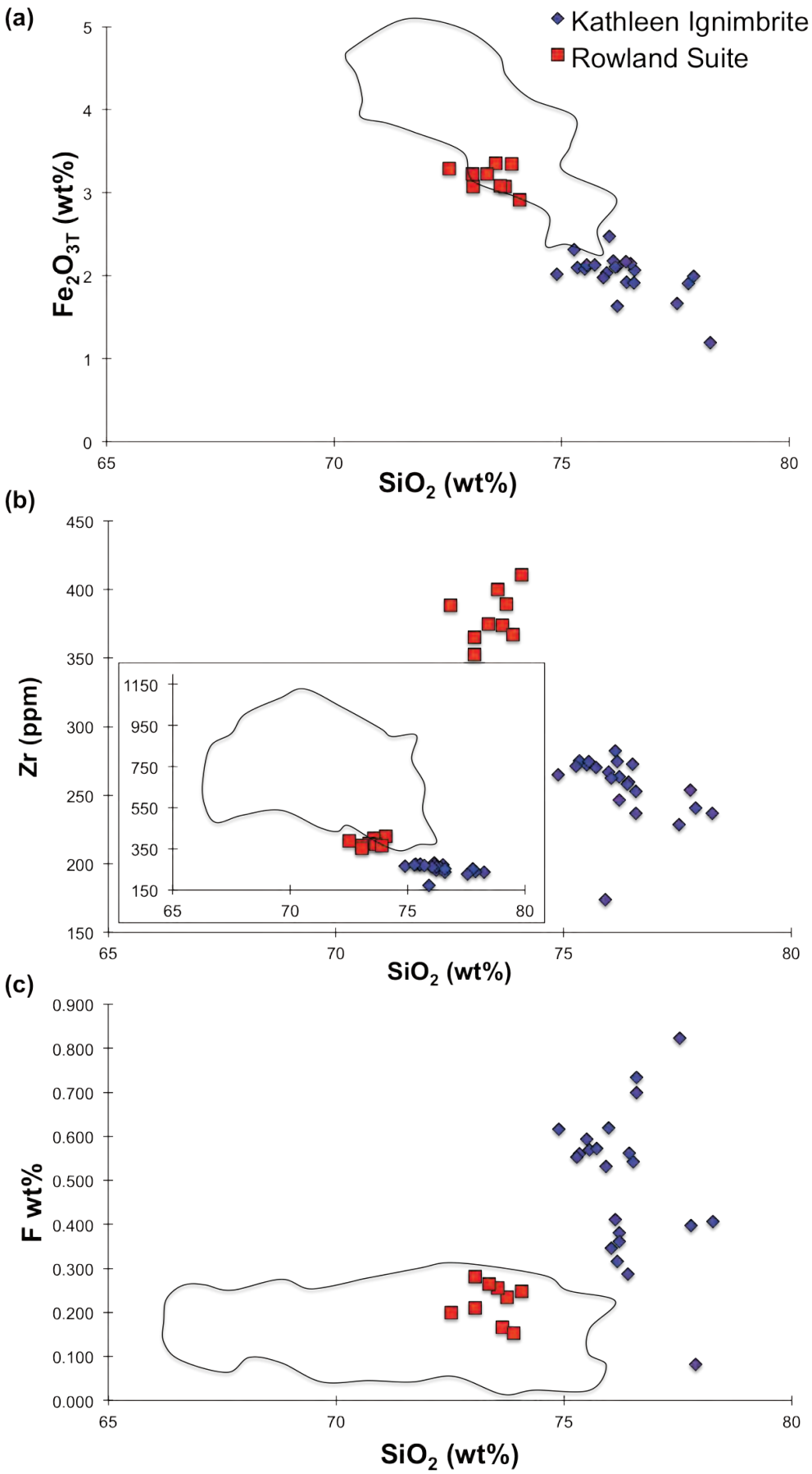

Figure 4.5: Selected Harker plots showing SiO_2 *vs*. a) Fe_2O_3, b) F and c) Zr
These graphs demonstrate the elevated F concentration of the KI compared to other felsic rocks of the west Musgrave Province, the evolved nature of the KI, and provide evidence of zircon saturation in the KI and RS. Black-line field represents the other Talbot Sub-basin rhyolites (Smithies *et al*., 2013).
KI (blue diamonds) RS (red squares)

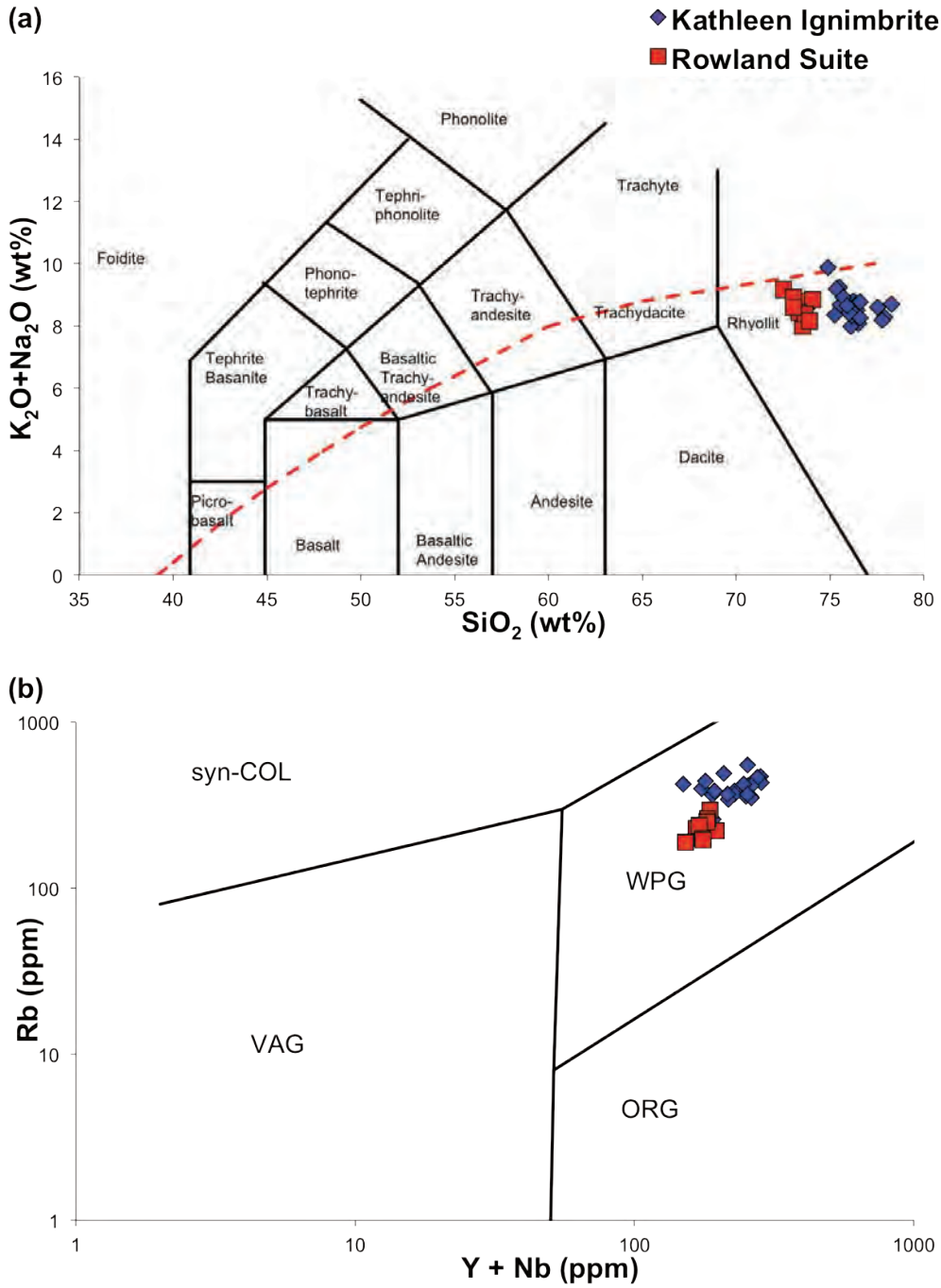

Figure 4.6:
a) TAS diagram after Le Maitre *et al*. (1989; 2002), showing the alkaline dividing line of Irvine and Baragar (1971), with all samples plotting in the rhyolite field.
b) Tectonic discrimination diagram showing that the samples plot in the *within-plate* granite (WPG) field of Pearce *et al*. (1984). ORG – ocean ridge granites; VAG – volcanic-arc granites; syn-COL – syn-collisional granites. Symbols the same as in Fig. 4.5.

(Fig. 4.7a) are bi-pyramidal to embayed volcanic quartz (~30%), mesoperthitic K-feldspar (~25%), plagioclase (~20%), biotite (~10%) and Fe–Ti oxides (~5%), along with accessory fluorite, apatite, titanite, zircon and garnet. Interstitial chlorite and muscovite are present as secondary mineral phases. The matrix is a very fine-grained devitrified microgranular quartz-feldspar mosaic (Fig. 4.7b) that forms ≥60% of the units, with crystals and crystal fragments forming the remaining ≤40%. Purple fluorite is abundant in the KI (Fig. 4.7c), found within the matrix as free crystals or aggregates within the ignimbrite matrix (Fig.

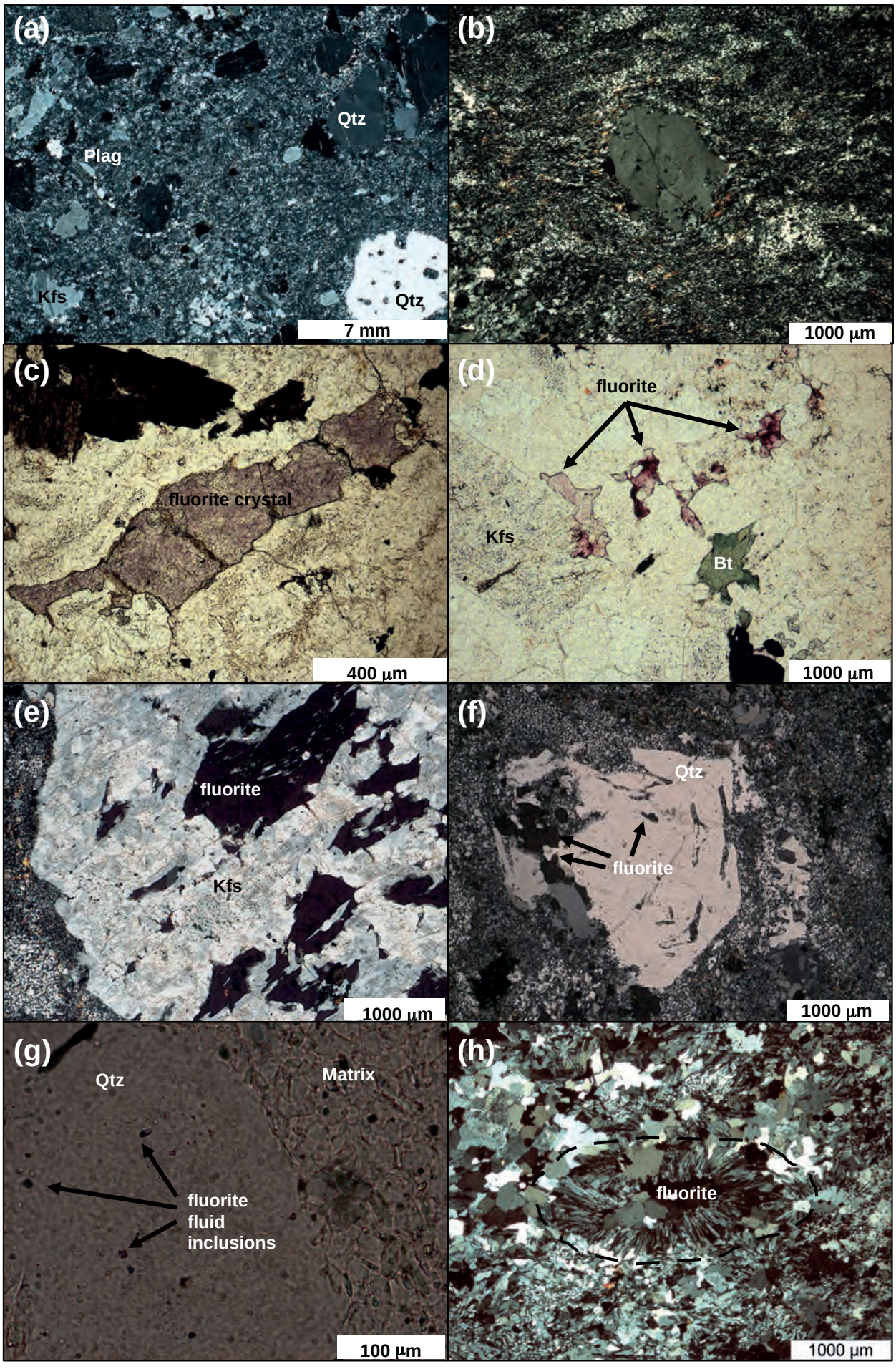
(a)
Qtz
Plag
Kfs
Qtz
7 mm
(b)
1000 µm
(c)
fluorite crystal
400 µm
(d)
fluorite
Kfs
Bt
1000 µm
(e)
fluorite
Kfs
1000 µm
(f)
Qtz
fluorite
1000 µm
(g)
Qtz
Matrix
fluorite
fluid
inclusions
100 µm
(h)
fluorite
1000 µm

Figure 4.7 (opposite page): Photomicrographs of a) typical ignimbrite texture, with a devitrified granophyric quartz-feldspar matrix containing subhedral to fragmental quartz (often embayed and resorbed), K-feldspar and plagioclase phenocrysts (XPL). b) Bi-pyramidal volcanic quartz surrounded by granophyric matrix showing a flow fabric and rotation of the phenocryst due to rheomorphic flow (XPL). c) Typical purple fluorite crystal, abundant throughout the KI. d) Fluorite in the matrix of the KI (PPL). e) Isotropic fluorite inclusions within K-feldspar phenocryst (XPL). F) Fluorite inclusions within a bi-pyramidal volcanic quartz phenocryst (XPL). g) Small fluorite fluid inclusions within a quartz phenocryst (PPL). h) Granophyric devitrified quartz-feldspar groundmass of an aphyric fiamme containing a spherulite with an isotropic fluorite crystal forming the central core, surrounded by radial fibrous quartz crystallites (XPL).

4.7d), as inclusions within feldspar (Fig. 4.7e), quartz (Figs. 4.4e, 4.7f and 4.7g) and as fills in vugs or shear partings between flow bands in the basal lava-like facies. Fluorite is also present within the fine-grained crystal-poor fiamme (Fig. 4.4h), forming cores of spherulites that have radial fibrous quartz crystallite rims.

4.4.3 Geothermometry

The temperature of emplacement of the KI was estimated using zircon saturation thermometry (Watson, 1979; Watson and Harrison, 1983; Hanchar and Watson, 2003), yielding an average temperature of ~830°C (793°C–853°C), that is slightly lower than the average temperature of ~850°C (846°C–875°C) for intrusive porphyritic rhyolites of the RS (Table 4.2 – Appendix C); Fig. 4.8a). Rhyolite-MELTS modelling indicates that the KI has liquidus temperatures that average ~970°C for a pressure of 1 kbar (~3 km depth; Table 4.2 – Appendix C; Gualda *et al*., 2012), indicating that zircon saturation thermometry-derived magmatic crystallisation temperatures are on average 140°C lower than the liquidus temperatures of the magmas that formed the KI.

4.4.4 Viscosity calculations

The viscosity of the KI was determined using the model of Giordano *et al*. (2008), which predicts the non-Arrhenian Newtonian viscosity of silicate melts as a function of temperature and melt composition, including H_2O and F as volatile constituents. Zircon saturation temperatures for individual samples (Table 4.2 – Appendix C; Fig. 4.8a) were used during viscosity calculations, and a range of viscosity values for each sample were determined using three different water contents (0 wt% H_2O, 'LOI value' = wt% H_2O or the measured volatile composition of each KI sample, and 1.0 wt% H_2O) in order to evaluate the effect of changes in water content on viscosity. The effect of F concentrations on viscosity within this magmatic system was also evaluated by calculating several viscosity values: (a) without F, (b) with measured whole-rock F concentrations (see *Section 4.5.4*) for each sample, representing the measured KI composition of each sample, and (c) 5.0 wt% F.

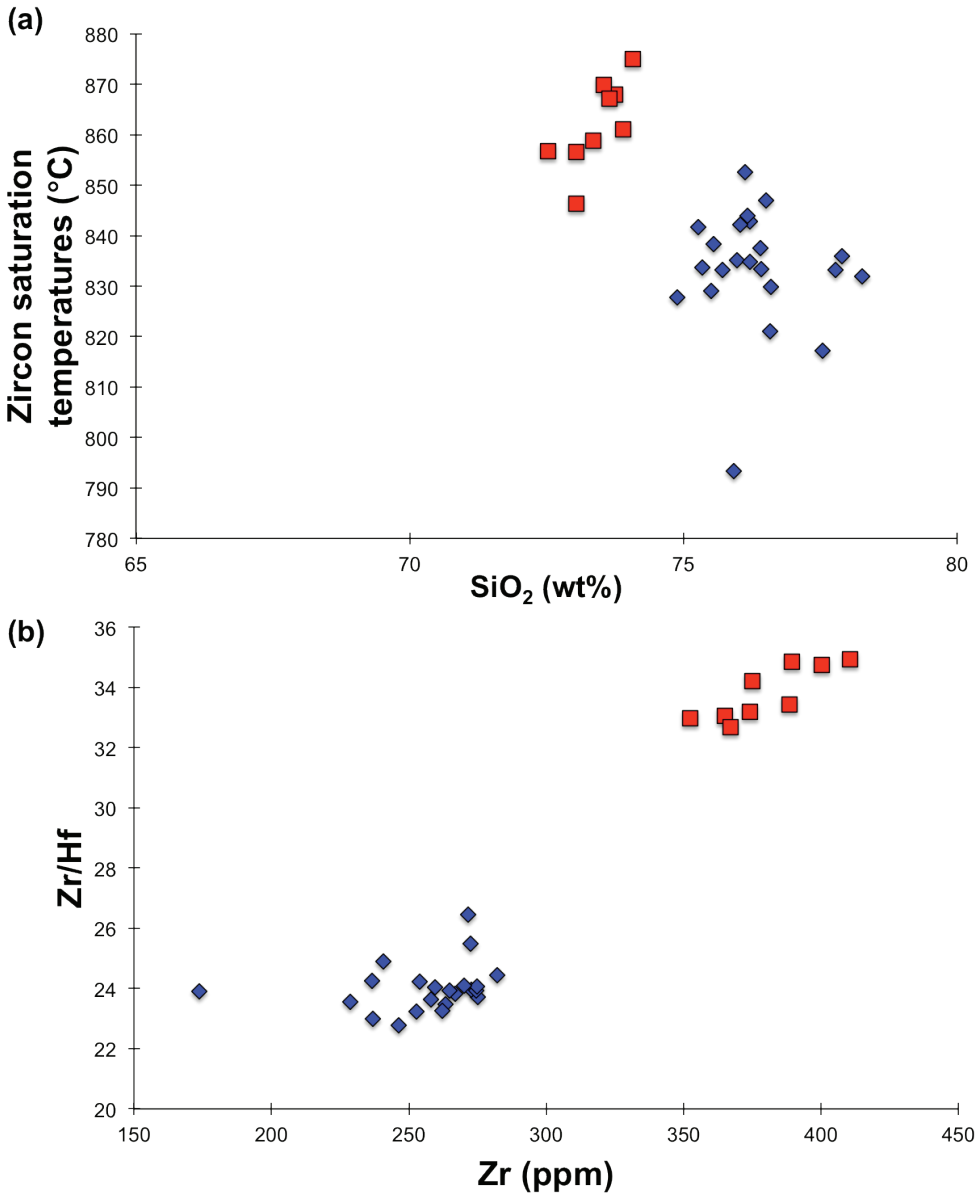

Figure 4.8:
a) Zircon saturation temperatures *vs*. SiO_2 variation
b) Zr/Hf *vs*. Zr variation demonstrating zircon saturation in the KI and RS. The decrease of Zr/Hf ratios with decreasing Zr concentrations is indicative of zircon fractionation. Symbols the same as in Fig. 4.5.

The results (Table 4.2 – Appendix C) returned a tight range of viscosity values from $10^{7.7}$–$10^{8.85}$ Pa.s, with an average viscosity of $10^{8.16}$ Pa.s for all 22 samples based on measured KI sample compositions, using LOI values as an indicator of H_2O content and whole-rock F concentrations (see section 4.1 and 5.3). The viscosity values for anhydrous samples range from $10^{10.19}$–$10^{9.16}$ Pa.s, with an average viscosity of $10^{9.54}$ Pa.s. In comparison, samples assigned a uniform H_2O content of 1.0 wt% and with measured F concentrations have viscosity values of $10^{7.16}$–$10^{7.96}$ Pa.s, with an average viscosity of $10^{7.43}$ Pa.s. Fluorine-free compositions have viscosities of $10^{7.81}$–$10^{8.9}$ Pa.s, with an average viscosity of $10^{8.38}$ Pa.s, while assigning all samples an F content of 5.0 wt% and using LOI values as a proxy for H_2O concentrations yielded viscosities of $10^{6.65}$–$10^{7.41}$ Pa.s.

4.5 Interpretation

4.5.1 Geochemistry

The geochemistry presented here indicates that the KI is a fluorine-enriched (relative to average to crustal values; Bailey, 1977; Hu and Gao, 2008) A-type, alkali-calcic to calc-alkalic, metaluminous (to slightly peraluminous), high-silica rhyolite. The KI has characteristics that are typical of A-type granites or rhyolites (Loiselle & Wones, 1979, Collins *et al.*, 1982, White & Chappell, 1983; Frost *et al*., 2001; Frost and Frost, 2008; 2011) generated during magmatism in within-plate or anorogenic extensional tectonic settings, such as rifts and oceanic basins or at the end of orogenic cycles (Whalen *et al.*, 1987, Eby, 1990, Shellnutt & Zhou, 2007). The KI is the most evolved rhyolite suite in the Talbot Sub-basin stratigraphy (Figs. 4.5a–c) and contains the highest concentrations of F of any of the felsic rocks in the Talbot Sub-basin (Fig. 4.6c; Smithies *et al*., 2013; Chapter 3).

4.5.2 Mineralogy

The presence of fluorite inclusions within unaltered euhedral K-feldspar and quartz macrocrysts (Figs. 4.7e, 4.7f and 4.7g) that are considered to be phenocrysts indicates that fluorite was a primary igneous mineral during emplacement of the KI and reflects F saturation, similar to other rhyolitic systems (e.g., Gawler Range Volcanics (GRV); Agangi *et al*., 2010). Fluorite within fine-grained crystal-poor fiamme also has a primary magmatic origin as the pumice within the KI is representative of the original magmatic components of the melt. The microscopic fluorite within the laterally continuous, stratiform shear-partings and in the matrix, most likely crystallised during or after rheomorphic flow (Wolff and Wright, 1981). The fluorite found in vugs, partings and in the ignimbrite matrix is interpreted as forming through primary vapour phase crystallisation during volcanic degassing, as has been seen and documented in other rheomorphic ignimbrites (e.g., Schmincke and Swanson, 1967; Bonnichsen and Citron, 1982; Andrews and Branney, 2011). In addition, the lack of hydrothermal alteration within the deposit, including an absence of cross-cutting veins or pervasive alteration, is not supportive of a hydrothermal secondary alteration origin for the fluorite in the KI. Additionally the presence of abundant crystals in some facies and few in others indicates eruption temperatures from near liquidus for some magmatic components to sub-liquidus for others (Chapter 2).

4.5.3 Geothermometry

Zircon saturation thermometry provides a minimum estimate of the magmatic temperature if magmas are undersaturated in zircon, and a maximum estimate if they are

saturated (Miller *et al*., 2003). The fact that the Zr/Hf ratios of the KI samples decrease with decreasing Zr concentrations (Fig. 4.8b), and the presence of negative correlations for both Zr and Hf with SiO_2 (Fig. 4.5b), is both indicative of zircon fractionation, suggests that both the KI and the RS were zircon saturated, indicating that the zircon saturation temperatures used here (Table 4.2 – Appendix C; Fig. 4.8a) are indicative of maximum magmatic temperatures of the system immediately prior to eruption, and more representative than the higher liquidus temperatures (Table 4.2 – Appendix C) of this unit (Linnen and Keppler, 2002; Thomas *et al*., 2002; Agangi *et al*., 2012). This in turn means that using Zr saturation temperatures provides an estimate of the lowest possible viscosity of the magma prior to eruption for a given composition. However, it should be noted that the eruption and subsequent deposition temperatures were most likely similar to or lower than the zircon saturation temperatures (i.e. eruption temperature ≤ magmatic temperature) and therefore using zircon saturation temperatures provides an upper limit for the eruption and deposition temperature of the KI.

4.5.4 Viscosity calculations

Water as a volatile component plays a role in depolymerising and reducing the viscosity of a silicate melt (Dingwell and Mysen, 1985; Holtz *et al*., 1999; Giordano *et al*., 2004) and therefore most likely had an important role in controlling the viscosity of the KI. Direct determination of the original water content of the KI was not possible, although the fact that the KI is an anhydrous (<1.0 wt %) high-silica rhyolite means that the magma that formed this deposit contained very little water. Almeev *et al*. (2012) experimentally detemined that similar composition rhyolites within the Snake River Plain contained ≤1.5 wt% H_2O. Andrews (*pers. comm.*) also states that compositions with more than 1.0 wt% H_2O would not be plausible in these types of magmas, therefore 1.0 wt% H_2O is considered to be a maximum possible water content for the KI. In addition, MELTS-based modelling of parental composition magmas could reproduce Talbot Sub-basin compositions with water contents between 0.4 and 0.6 wt% (Smithies *et al*., 2013), and Pankhurst *et al*. (2011) used LOI values as a proxy for the water contents of Mesoproterozoic rhyolites of the GRV, South Australia, similar to that of the water-by-difference method established by Devine *et al*. (1995), and stated that these values are most likely overestimates of the original magmatic water contents due to degassing and devolatisation. The LOI values for the KI range from 0.34–0.71 wt% and therefore a similar approach was adopted here, using the LOI values for each sample as a proxy of the original water contents to provide a 'natural' KI composition for each sample. However to account for possible inaccuracies in the assumption of water content and to investigate the effect of varying water content on this system, viscosity values under the three different water content scenarios were calculated (0 wt% H_2O, 'LOI value' = wt% H_2O, and 1.0 wt% H_2O). This yielded a range of values from an absolute maximum viscosity through an LOI-based 'natural' viscosity to a

minimum at a given maximum possible temperature value (i.e. the magmatic crystallisation temperature defined using Zr saturation thermometry as discussed above).

Fluorine in silicate melts acts as a network modifier, affecting the rheology of the melt, reducing the viscosity and increasing ion diffusivity (Wolff and Wright, 1981; Dingwell *et al*., 1985; Giordano *et al*., 2004). Given that F is an important control on viscosity, the effect that this element would have on the KI magmatic system was determined by varying concentrations of F prior to determining the viscosity of the KI samples. The nominal upper limit of F concentrations within melt inclusions in highly evolved rhyolites and granites is around 5.0 wt% F (Chabiron *et al*., 2001; Giordano *et al*., 2004; Webster *et al*., 2004; Thomas *et al*., 2005). The measured whole-rock fluorine concentrations are at best a minimum estimate of F contents in a magma at the time of eruption and deposition as F is frequently lost during degassing and devolatisation (Noble *et al*., 1967; Holtz *et al*., 1993; Webster and Duffield, 1994; Aiuppa *et al*., 2002). Agangi *et al*. (2012) also indicated that F concentrations from fluid-melt inclusions in the high-silica rhyolites of the GRV of South Australia are higher than measured whole-rock concentrations and that the fluid-melt inclusions are considered more representative of the original magma concentration at the time of eruption. It is therefore reasonable to assume that the magmatic F content in the KI would have been even higher than 0.8 wt% and that the whole-rock F concentrations used represent minimum values.

4.6 Discussion

4.6.1 Rheomorphism and rheomorphic ignimbrites

Normal welding (Freundt, 1998; Quane *et al*., 2009) at sufficiently high enough temperatures combined with low enough yield strengths (i.e. low viscosities) causes viscous pumice and matrix particles to weld immediately through a process known as agglutination; continuation of this welding can cause coalescence and the formation of non-particulate and fluidal viscous lava-like material (Mahood, 1984; Branney and Kokelaar, 1992). This material can then either undergo fairly localised coaxial strain that generates both welded ignimbrites and low-grade rheomorphic ignimbrites (Chapin and Lowell, 1979; Wolff and Wright, 1981; Kobberger and Schmincke, 1999), or laminar shear caused by the passage of overlying particulate sections of the same flow (Branney *et al*., 1992; Branney and Kokelaar, 1992) or pervasive and intense non-coaxial strain in a transient, vertically migrating shear zone, both of which generate high-grade lava-like rheomorphic ignimbrites (Andrews and Branney, 2011; Robert *et al*., 2013).

'Rheomorphism' was originally defined by Rittmann (1958) to explain the secondary mass flowage features seen in welded ignimbrites (i.e. rheoignimbrites), and the definition

was expanded by Wolff and Wright (1981) to encompass any pyroclastic deposit that has undergone secondary flow change due to welding processes described above. Branney *et al*. (1992) further suggested the term rheomorphism be used to describe all viscous flow structures in welded ignimbrites and defined a welding continuum from non-welded tuffs (lowest grade end-members of the continuum) to the development of lava-like rheomorphic ignimbrites (the highest grade end-members), with the onset of rheomorphism coincident with the process of agglutination, continuing up to coalescence and subsequent lava-like flow.

The timing of rheomorphism is controversial, with Wolf and Wright (1981) indicating that rheomorphism occurs after deposition, whereas Branney and Kokelaar (1992; 1994) suggest that rheomorphism can occur both during and after deposition. Regardless of the timing of rheomorphism, the factors that control and favour this process remain the same and are summarised in (Table 4.3). The interdependence of some of these factors means that the most important controls on rheomorphism are the chemistry of the ignimbrite, temperature (magmatic, eruption and deposition), strain (both rate and heating), viscosity of the magma and the presence of a substrate slope, however slight, along which gravity-driven viscous flow caused by overlying load pressure can take place.

Most rheomorphic ignimbrites are peralkaline rhyolites that have unusually low glass viscosities when compared to calc-alkaline rhyolites (Shaw, 1972; Wolff and Wright, 1981; Cas and Wright, 1987). However, recent research has identified rheomorphic anhydrous metaluminous rhyolites with very high eruption temperatures (900°C–1000°C) from the Miocene Snake River Plain volcanic province of central-western USA (Honjo *et al*., 1992; Andrews and Branney, 2005; 2011; Andrews *et al*., 2006; 2008) that are associated with Snake-River (SR)-type volcanism (Branney *et al*., 2008) and often record the extreme grades of welding necessary to develop lava-like facies (e.g., Grey's Landing ignimbrite; Andrews and Branney, 2011). The lava-like rheomorphic KI is another example of an extremely high-grade anhydrous metaluminous rhyolitic ignimbrite similar to that of the Grey's Landing deposit, although it has significantly higher fluorine concentrations (up to 0.8 wt%) than typical SR-type rheomorphic ignimbrites (0.02–0.37 wt%; Ekren *et al*., 1984; Ellis, 2009); the F concentrations within the KI are more similar to Cenozoic topaz rhyolites from the western USA and Mexico that are thought to be the extrusive equivalents of rapakivi granites (Christiansen *et al*., 2007).

4.6.2 Subaqueous pyroclastic flows and welding-rheomorphism

Sparks *et al*. (1980) indicated that a subaqueous environment could actually be more favourable to welding than many subaerial environments as steam is soluble in

rhyolitic glass, reducing glass viscosity at moderate water depths, and as heat loss in the deposit through interaction with water is minimal as long as the pyroclastic flow has a density greater than water. It is not clear at this point what effect the initial shallow-water subaqueous emplacement of the KI may have had on the welding and rheomorphism in the deposit, although a logical assumption would be that contact with a wet substrate, and possible initial deposition in shallow-water subaqueous conditions, would have caused mixing of the pyroclastic flow with water, resulting in cooling and welding retardation in the deposit. This is dependent on the timing of rheomorphism and emplacement and whether welding and rheomorphism took place after or before the emplacement of the pyroclastic flow in a subaqueous environment. The preferred model in this study is that welding and subsequent rheomorphism took place during deposition and emplacement, but before the flow entered the water, resulting in a significantly denser and much less permeable ignimbrite that incorporated very little water upon contact (Sparks *et al*., 1980; Mcleod *et al*., 1999), thus offsetting any cooling effect associated with the conversion of water into steam or by conductive heat loss. At least the base of the KI was deposited in water; this area of the KI also contains the most significant and extreme (i.e. lava-like) development of rheomorphism. The possible resorption of external water into magma or glass through volatile resorption and gas retention (Sparks *et al*., 1999), a process that in turn lowers viscosity and enhances welding, during subaqueous emplacement of an ignimbrite (Sparks, 1980) or emplacement over wet ground (McBirney, 1968), could also have significiantly facilitated or aided rheomorphism during emplacement of the KI. However, it is difficult to quantitatively assess whether or not the interpreted palaeoenvironment and initial subaqueous emplacement of the KI, which differs from that of all other known lava-like rheomorphic ignimbrites, was a distinct factor in the development of rheomorphism in this unit.

4.6.3 Rheomorphism in the Kathleen Ignimbrite

Recent work by Robert *et al*. (2013) and Cordonnier *et al*. (2012a) on the brittle–viscous domains for silicate melts indicates that the boundaries for such domains in these types of magmas can be defined using their relaxation state or Deborah number (De), defined as the dimensionless ratio of relaxation (τ_{rel}) and deformation (τ_{def}). Maxwell (1866) defined the theoretical structural relaxation time scale as $\tau_{rel} = \eta/G_{\infty}$, which is the inverse of the strain rate, with a Deborah number of 10^0 being linked to the brittle–ductile transition, although in reality a De = 10^{-3} marks the onset of non-Newtonian behaviour and a De = 10^{-2} indicates the onset of brittle behaviour in a crystal-free silicate melt (Webb and Dingwell, 1990; Dingwell, 1996; Cordonnier *et al*., 2012a; 2012b). Robert *et al*. (2013) took this further and plotted Deborah number values against dimensionless temperatures (i.e. the ratio of deposition temperature (T_{dep}) over the glass transition temperature (T_g)) and used the fluid-solid behaviour of silicic magmas to define boundaries where rheomorphism is

Table 4.3: Summary of all factors that control rheomorphism in ignimbrites.

Rheomorphism-controlling factors	Linked factors	Constraints/comments	Presence/role in the Kathleen Ignimbrite	References
Magmatic or eruption temperature	Viscosity, deposition temperature, chemistry	Needs to be high, above 650-750°C for rhyolites, below this and they behave in a brittle manner. Most are >850°C (900 - 1050°C). Higher temperature=lower viscosity.	Eruption temperatures ≤~830°C. Liquidus temperatures of ~970°C	Ekren *et al*., 1984; Branney *et al*., 1992; Bachmann et al., 2000; Robert *et al*. 2013
Deposition temperature	Eruption style, transport processes, chemistry, environment, viscosity, strain rate, deposit thickness	Needs to high in order for rheomorphism (i.e. welding, agglutination and coalescence) to occur and not quenching	Difficult to constrain the deposition temperature accurately in rheomorphic ignimbrites or assess the cooling rate as we have not witnessed such an event.	Ekren *et al*., 1984; Branney *et al*., 1992; Bachmann *et al*., 2000
Cooling rate	Heat loss, environment, strain heating, temperature, deposit thickness	Deposit needs to cool slowly with minimal heat loss to achieve an optimal strain rate, too fast and it will behave in a brittle manner	Little evidence for brittle deformation apart from the quench fragmented contact facies	Branney *et al*., 1992; Branney and Kokelaar, 1994; Robert *et al*. 2013
Viscosity	Temperature (magmatic eruption and deposition), chemistry, H_2O and other volatile content, porosity	H_2O lowers viscosity. Low viscosity values are critical (see discussion in text)	As calculated, see discussion in text.	Shaw, 1972; Wolf and Wright 1981; Dingwell, 1996; Giordano *et al*., 2008;
Chemistry (magma composition)	Viscosity	Peralkaline chemistry favoured, where abundant alkalis lower particle viscosities through silicate polymerisation disruption (Higher Na and Fe relative to Si and Al); lower H_2O content relative to F and Cl	No, metaluminous to slightly peraluminous, similar to SR-type rheomorphic ignimbrites	Schmincke and Swanson, 1967; Macdonald and Bailey, 1973; Bailey and Macdonald, 1975; Wolff and Wright, 1981; Mahood, 1984
Slope		Needs to be a slope	Yes, inferred caldera type and associated volcanotectonic subsidence	Chapin and Lowell, 1979; Wolf and Wright, 1981
Glass transition temperature (Tg)	Temperature, chemistry, H_2O content	Temperature needs to be above Tg for glassy particles to deform viscously and allow welding.	Yes, otherwise rheomorphism would not be present	Freundt 1998; 1999; Russell *et al*. 2004; Giordano et al., 2005
Effective eruption style	Deposition temperature, heat loss	Eruptions of high mass-flux (high eruption discharge rate), low-velocity, boil-over type eruptions with continuously collapsing eruption columns (low-columns), pyroclastic fountaining from fissure vents	Inferred intra-caldera deposit type requires this type of eruption style	Ekren *et al*., 1984; Branney *et al*., 1992; Bachmann et al., 2000
Volatiles	Viscosity, chemistry	High residual H2O, F in pyroclasts at time of deposition. Higher volatile contents decrease the viscosity of a melt.	Yes, high F content	Shaw, 1972; Henry *et al*., 1988; Duffield and Dalrymple, 1990; Branney and Kokelaar 1992; Stevenson *et al*., 1998
Heat loss	Eruption style, depositional environment, deposit thickness	Needs to be insulated, ponding, thickness (although rheomorphism occurs in both extra and intracaldera settings, but a thicker deposit will retain more heat, cool slower), sustained PCF, rapid deposition	Ponding and thickness in an intra-caldera setting = Yes. Initial subaqueous emplacement = No.	Branney *et al*., 1992; Branney and Kokelaar, 1994
Crystal content	Temperature (magmatic and eruption), chemistry, viscosity	Crystal-poor indicates eruption near liquidus temperature	Yes, basal lava-like facies <5%	Branney *et al*., 1992

Rheomorphism-controlling factors	Linked factors	Constraints/comments	Presence/role in the Kathleen Ignimbrite	References
Late-stage vesiculation (liberation of volatiles)	Volatiles, viscosity	Porosity. Trapped volatiles lower viscosity and enhance rheomorphism. SR-type less vesicular, Peralkaline-type are pervasively vesicular.	Yes, vesiculation confined mostly to sheared partings along flow bands where vapour-phase fluorite has crystallised	Andrews and Branney, 2011
Welding to a non-particulate flow	Temperature, chemistry, volatiles, eruption style	Highest grade of welding, agglutination and coalescence of pyroclasts to form coherent liquid, fluidal pyroclasts	Yes, petrographic evidence	Wolf and Wright, 1981; Branney and Kokelaar, 1992; Branney *et al*., 1992; Quane and Russell, 2005
Rapid deposition	Eruption style, depositional environment, cooling rate	Minimal ingestion of atmospheric air or water into the density current during transport	Inferred intracaldera deposit type requires rapid deposition	Branney and Kokelaar, 1992
Pyroclasts	Deposition temperature, chemistry, volatiles, eruption style, viscosity	Sufficiently fluidal and able to deform. Little opportunity for cooling and quenching.	Yes, petrographic evidence	Mahood, 1984; Henry and Wolf, 1992; Branney *et al*., 2002; 2004; Capaccioni and Cuccoli, 2005; Sumner *et al*., 2005; Andrews and Branney, 2011
Strain heating	Deposition temperature, strain rate and strain duration	Only effective above a critical strain rate. Higher for hotter deposition temperatures.	Not sure if this has played a role?	Robert *et al*., 2013
Depositional environment	Temperature (magmatic eruption and deposition), volatile content, cooling rate, heat loss	Preferably the deposit or PCF needs to be insulated, thick, ponded, wet substrate/subaqueous environment may enhance welding (? - see text for discussion)	Thick deposit, intra-caldera setting, wet substrate and possible initial subaqueous emplacement.	Sparks *et al*., 1980
Strain rate	Temperature (magmatic eruption and deposition), cooling rate, heat loss, viscosity	Needs to be low and the deposition temperature needs to be high	Similar to Grey's Landing	Andrews and Branney, 2011; Robert *et al*., 2013
Deposit thickness	Eruption style, depositional environment, heat loss, cooling rate, deposition temperature	Thick deposits will assist rheomorphism, although rheomorphism can occur in both thick intracaldera and thin extra-caldera ignimbrites	>500 m Thick intracaldera deposit	Henry and Wolf, 1992

possible (i.e. a field where viscous or ductile deformation occurs) and not possible (i.e. a field where brittle deformation takes place).

Figure 4.9 has been recreated from Cordonnier *et al*. (2012a; 2012b) and Figure 4.10 has been recreated from Robert *et al*. (2013). In Figure 4.10, strain rate (τ_{def}) is plotted against apparent viscosity (η_{app}), to determine whether rheomorphism would be possible at various deformation strain rates and time scales, by varying both the water and F contents of the KI samples during viscosity calculations as discussed above (Table 4.2 – Appendix C). It should also be noted that new fields of rheomorphic and non-rheomorphic behaviour is suggested for the Robert *et al*. (2013) figure by correlation with the viscous behaviour fields defined by Cordonnier *et al*. (2012a; 2012b), a relationship that is corroborated by the similar location of the data on both diagrams.

The fact that the Grey's Landing lava-like rheomorphic ignimbrite is very similar to the KI in terms of textures, thickness, chemistry and deformation means that the same deformation strain rates ($\varepsilon_{def} = \varepsilon/t_{res}$; observed strain ($\varepsilon$) / shear zone residence time (t_{res})) and deformation timescales ($\tau_{def} = 1/\varepsilon_{def}$) as used by Robert *et al*. (2013) for their study of the Grey's Landing ignimbrite. Calculations used in this study show both low (0.2 hours) and high (2 hours) shear zone residence times ($t_{res} = h_{sz}/v_{sz}$; Andrews and Branney, 2011) and a shear zone vertical migration velocity ($v_{sz} = h_{dep}/t_{er}$; 1–10; Andrews and Branney, 2011) that is based on a conservative observed strain of 100 (Andrews *et al*., 2008; Andrews and Branney, 2011; Chapter 2), an eruption duration (t_{er}) of tens of hours (5–50; Self, 2006), a lava-like rheomorphic facies thickness (h_{dep}) of 50 m (Chapter 2) and a shear zone thickness (h_{sz}) of 2 m (Andrews and Branney, 2011; Chapter 2). This gives deformation time scales (τ_{def}) of 7.2–72 s and deformation strain rates (ε_{def}) of 1.4×10^{-2} –1.4×10^{-3} s^{-1} over which rheomorphism can take place, both of which are dependent on variations in relaxation timescales ($\tau_{rel} = \eta_{app}/G_{\infty}$; apparent viscosity ($\eta_{app}$)/unrelaxed elastic shear modulus (~10^{10} Pa; Dingwell and Webb, 1989; Whittington *et al*., 2012) as demonstrated by Robert *et al*. (2013).

The results in Table 4.2 – Appendix C and Figures 4.9 and 4.10 indicate that even at a very low shear zone residence time (t_{res}) of 12 minutes, which corresponds to a deformation time scale of 7.2 seconds, all the 'natural' KI samples (LOI = H_2O content; F = whole-rock concentration) would behave rheomorphically (Figs. 4.9a and 4.10a). Reducing the magma water content to anhydrous (i.e. 0 wt% H_2O) does not prevent rheomorphic behaviour as the samples still plot in the field of possible rheomorphism (Figs. 4.9a and 10a). In addition, the complete removal of F and H_2O from the KI sample compositions (effectively creating the most viscous sample compositions possible) still does not prevent rheomorphism (Figs. 4.9b and 4.10b). Increasing water contents to a maximum of 1.0 wt% H_2O and F contents to a theoretical maximum (i.e. 5.0 wt%) would,

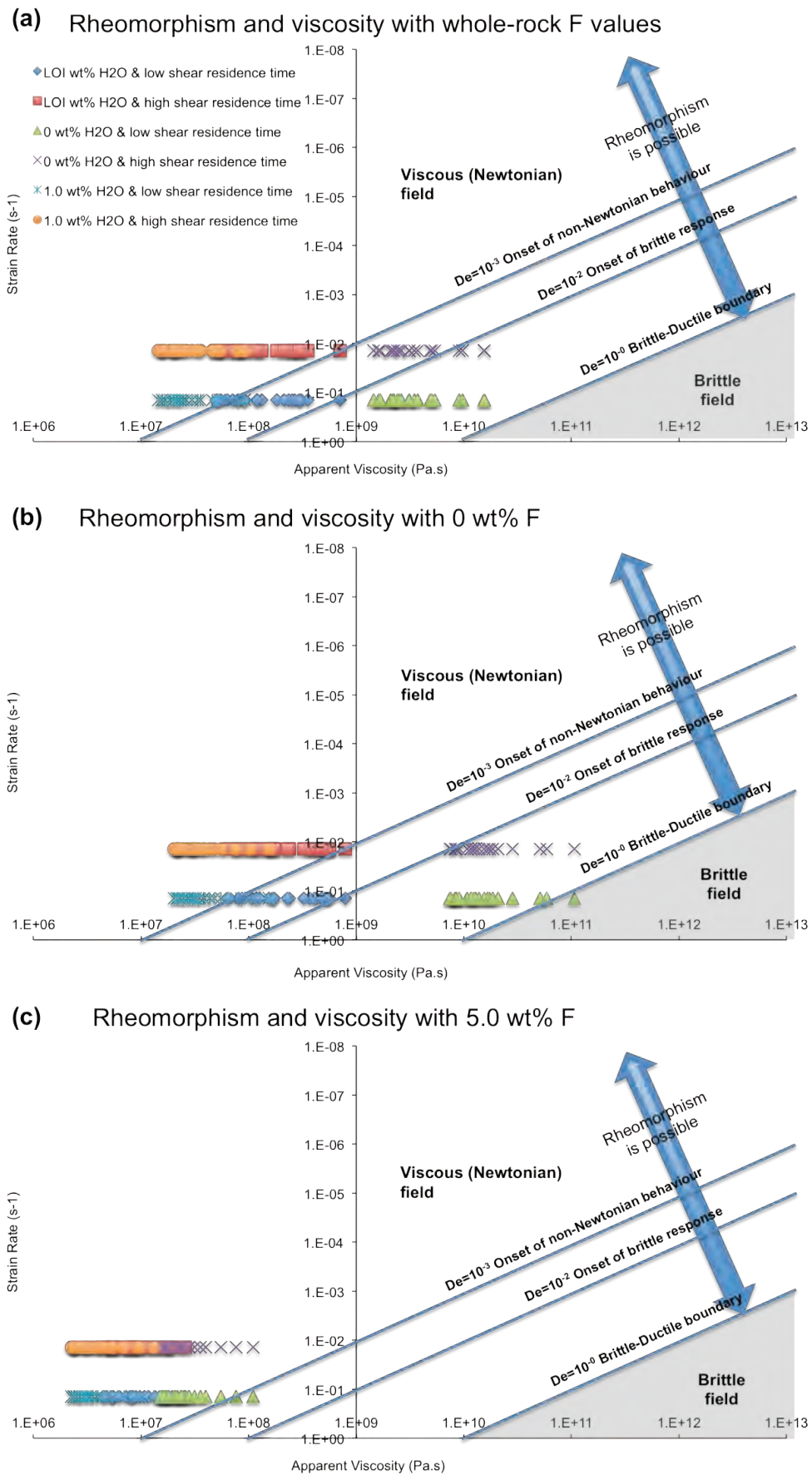

Figure 4.9: Strain rate against viscosity adapted from Cordonnier *et al*. (2012a; 2012b). This diagram effectively shows theoretical fields where a material will deform in a ductile (Newtonian) manner and behave viscously as opposed to brittle deformation (non-Newtonian behaviour; grey shaded field). a) Viscosity calculations using whole-rock F values. b) Viscosity calculations after removing F from the samples. c) Viscosity calculations with a nominally high F value of 5.0 wt%.

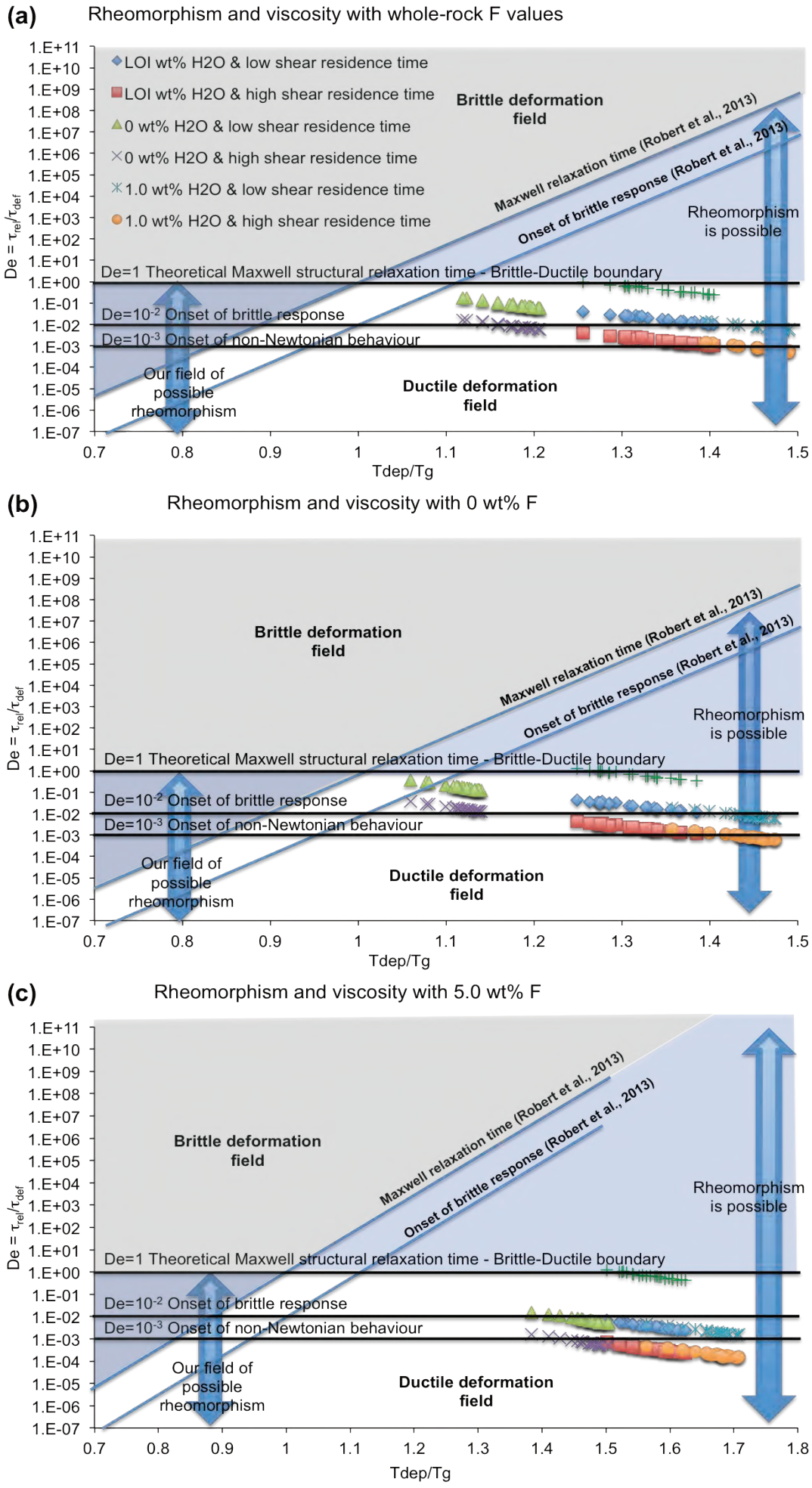
(a)
Rheomorphism and viscosity with whole-rock F values
LOI wt% H2O & low shear residence time
LOI wt% H2O & high shear residence time
0 wt% H2O & low shear residence time
0 wt% H2O & high shear residence time
1.0 wt% H2O & low shear residence time
1.0 wt% H2O & high shear residence time
Brittle deformation field
Maxwell relaxation time (Robert et al., 2013)
Onset of brittle response (Robert et al., 2013)
Rheomorphism is possible
De=1 Theoretical Maxwell structural relaxation time - Brittle-Ductile boundary
De=10-2 Onset of brittle response
De=10-3 Onset of non-Newtonian behaviour
Our field of possible rheomorphism
Ductile deformation field
De = τrel/τdef
Tdep/Tg
(b)
Rheomorphism and viscosity with 0 wt% F
(c)
Rheomorphism and viscosity with 5.0 wt% F

Figure 4.10 (opposite page): Deborah number (De = ratio of relaxation time scale (τ_{rel}) over deformation time scale (τ_{def})) against dimensionless temperature (i.e. the ratio of deposition temperature (T_{dep}) over glass transition temperature (T_g) adapted from Robert *et al*. (2013). This diagram has been used to show fields where rheomorphism is theoretically possible and where brittle deformation (shaded grey field) will occur.
Note the difference (highlighted in shaded blue) between the fields of brittle deformation defined by Robert *et al*. (2013) and my fields, adapted from Cordonnier *et al*. (2012a; 2012b).
a) Viscosity calculations using whole-rock F values. b) Viscosity calculations after removing F from the samples. c) Viscosity calculations with a nominally high F value of 5.0 wt%.

as expected, significantly reduce viscosity and promote viscous behaviour over brittle deformation, allowing rheomorphism to occur at much higher strain rates and significantly shorter deformation timescales and shear zone residence times (Figs. 4.9c and 4.10c). The volatile resorption and gas retention welding regimes suggested by Sparks *et al*. (1999), both of which enhance the potential and reduce the time needed for welding in thick intra-caldera and/or subasqueously emplaced ignimbrites, is confirmed by the latter modelling, where the addition of H_2O to the samples significantly promotes rheomorphism. This may have occurred when the pyroclastic flows that formed the KI initially entered the water or were emplaced over a wet substrate, and can explain why the base of the KI is highly rheomorphic (i.e. lava-like). In addition, F increases the water solubility of magmas (Manning, 1981; Dingwell *et al*., 1985; Giordano *et al*., 2004; 2008), and the high concentration of F in the KI may have further enhanced the amount of external water that was absorbed by the KI magmas or volcanic glass within the KI.

Finally, Fig. 4.10a clearly demonstrates that the natural KI samples were rheomorphic at even the highest possible geologically reasonable strain rate (3.33 s^{-1}), with a a deformation time scale (τ_{def}) of 0.3 seconds as opposed to 7.2 seconds (at $\varepsilon_{def} = 1.4 \times 10^{-2}$) and a shear zone residence time (t_{res}) of 30 seconds, compared to the 12 minutes used by Robert *et al*. (2013) for the Grey's Landing lava-like rheomorphic ignimbrite. This demonstrates that the KI would most likely have behaved rheomorphically even under geologically reasonable conditions that acted to prevent rheomorphism.

4.6.4 Assessment of the main controls on rheomorphism within the Kathleen Ignimbrite and comparison to other rheomorphic rhyolites

As previously mentioned in *Section 4.6.1*, all of the factors that aid rheomorphism (Table 4.3) can be summarised into five main factors: chemistry, temperature (magmatic, eruption and deposition), viscosity, strain (both rate and heating) and slope. Here, these factors are assessed and discussed in terms of favouring or acting against the rheomorphism of the KI.

4.6.4.1. Slope

The fact that all rheomorphic ignimbrites are load-pressure, gravity driven flows

means that topographic slope is an important control on rheomorphism. Downslope gravity-induced flow caused by an overlying load is needed to produce non-coaxial strain in an otherwise non-rheomorphic deposit. The intra-caldera KI was most likely associated with either downsag- or trapdoor-style caldera collapse (Lipman, 2000; Chapter 2), which providing a suitable gradient for gravity-driven rheomorphic flow driven by the load pressure of the overlying thick intra-caldera KI deposit.

4.6.4.2. Chemistry

Most rheomorphic ignimbrites, such as those on Gran Canaria, Canary Islands (e.g., Schmincke and Swanson, 1967; Leat and Schmincke, 1993; Kobberger and Schmincke, 1999; Sumner and Branney, 2002), are strongly peralkaline and have unusually low glass viscosities compared to calc-alkaline rhyolites (Shaw, 1972; Wolff and Wright, 1981; Mahood, 1984; Cas and Wright, 1987). Rare calc-alkaline rheomorphic ignimbrites do occur (e.g., Bad Step and Oxendale Tuffs, Lake District, England, Branney *et al*., 1992; Branney and Kokelaar, 1994; Etive rhyolites of Glencoe, Scotland, Moore and Kokelaar, 1998; Pagosa Peak Dacite, San Juan volcanic field, Colorado, USA, Bachmann *et al*., 2000), and recent research has identified rheomorphic characteristics in anhydrous metaluminous rhyolitic ignimbrites of the Snake River Plain, Idaho, USA (e.g., Andrews and Branney, 2005; 2011; Andrews *et al*., 2008). The rheomorphic KI is geochemically similar to these SR-type rheomorphic ignimbrites, but contains higher concentrations of F.

Rheomorphism is more prevalent in peralkaline ignimbrites as these magmas contain abundant alkalis that lower particle viscosities through disruption of silicate polymerisation, a process that aids rheomorphism (Schmincke and Swanson, 1967; Macdonald and Bailey, 1973; Bailey and Macdonald, 1975; Mahood, 1984; Andrews and Branney, 2011). This means that the chemistry of the KI could be a potentially rheomorphism-limiting factor, but, as suggested by Andrews *et al*. (2011), the higher temperatures of these ignimbrites offsets this unfavourable chemistry, although it should be noted that the KI was erupted at a far lower temperature (~830°C) that ignimbrites of the SRP (>900°C).

The presence of F in elevated concentrations in ignimbrite deposits is often associated with hydrothermal vein-type mineralisation (e.g., Dill, 2010) and indicative of secondary processes, not related to the primary rock type or magma. Fluorine-rich topaz rhyolites, their equivalent A-type granites, and many evolved high-silica rhyolites (e.g., rhyolite lavas of the GRV, Australia) contain fluorite as a characteristic primary accessory phase (Burt *et al*., 1982; Collins *et al*., 1982; Christiansen *et al*., 1983; 1984; Whalen *et al*., 1987; Duffield and Dalrymple, 1990; Taylor and Fallick, 1997; Sallet *et al*., 2000; Pankhurst *et al*., 2011; Agangi *et al*., 2012). The fluorite in these rocks is commonly

believed to precipitate during late-stage magmatic and/or magmatic-hydrothermal vapour phase crystallisation (Huspeni *et al*., 1984; Congdon and Nash, 1988; 1993; Johnston and Chappell, 1992; Price *et al*., 1992; Webster and Duffield, 1994; Sallet *et al*., 2000). In the KI, I am able to provide strong supporting evidence that the fluorite and fluorine concentration is of a primary magmatic origin. Sparks *et al*. (1999) showed that the escape of primary magmatic gases from an ignimbrite inhibits welding, indicating that gases (i.e. volatiles) need to be trapped or resorbed for a period of time in an ignimbrite to facilitate rheomorphism, especially for intra-caldera ignimbrites like the KI. In time these gases/ volatiles are released in the form of vapour (fluid) phases that ascend through degassing volcanic deposits. This vapour phase can precipitate minerals such as fluorite in porous features such as parallel laminations, vugs or partings (post-rheomorphism) during post-eruption and- depositional degassing, leading to the misidentification of these minerals as secondary hydrothermal phases whereas in fact this vapour phase still represents the original magmatic volatile component of the magma and therefore these precipitates should be viewed as primary magmatic components (Christiansen *et al*., 1986). Agangi *et al*. (2010) demonstrated that F-rich magmas can also produce distinctive trace element-rich late-stage magmatic volatile-rich fluid phases that preferentially crystallise REE-, Y-, HFSE-, Rb- and F-bearing accessory minerals late in the history of the magma within degassing features of a volcanic deposit. This phenomenon may explain some of the apparent hydrothermal characteristics of the fluorite in the KI, such as the crystallisation of fluorite in vein-like features, even though this fluorite is still a primary magmatic constituent of the original magma. Another piece of evidence which supports a primary magmatic origin for the fluorine in the KI is that it has the highest concentration of fluorine of any of the lithological units within the Talbot Sub-basin (Fig. 4.5c) and is also the most evolved unit in the province. In evolved high-silica rhyolite systems fluorine is highly incompatible, remaining in the melt phase, and therefore it is normal for it be to closely associated with the final, most differentiated and evolved end-members of such a system (Christiansen *et al*., 1983). If fluorine and subsequent fluorite precipitation was a late-stage secondary feature related to post-lithification hydrothermal alteration then it would most likely be present in a number of units in the area, rather than being restricted entirely to the rhyolitic units (i.e. it is not found in bounding porous sediments) and being preferentially concentrated in the KI compared to the coeval and comagmatic Rowland suite.

Numerous studies have examined the behaviour, origin and influence of fluorine in rhyolites (e.g., Bailey, 1977; Dingwell *et al*., 1985; Dingwell, 1988; Lange, 1994; Stix *et al*., 1995; Agangi *et al*., 2010; McPhie *et al*., 2011), including research into the effect of F on viscosity reduction and the eruption style and effusivity of these rhyolites (e.g., Kirstein *et al*., 2001; Ellis, 2009; Pankhurst *et al*., 2011). The fact that the F within the KI is magmatic and is present at high concentrations (up to 0.8 wt%), compared to crustal values (Bailey, 1977; Hu and Gao, 2008) and the knowledge of the effect of F on these magmatic systems

suggests that elevated concentrations of F may have caused or strongly contributed to the rheomorphic behaviour in the KI. However, as indicated by the viscosity calculations presented in this study (Table 4.2 – Appendix C; Figs. 4.9 and 4.10) the removal of F from the system would not have prevented rheomorphism of the KI.

4.6.4.3 Temperature

Peralkaline rheomorphic ignimbrites have eruption temperatures of 700°C–900°C (Schmincke, 1974; Leat and Schmincke, 1993; Kobberger and Schmincke, 1999; Sumner and Branney, 2002) although anhydrous metaluminous SR-type rheomorphic ignimbrites have much higher eruption temperatures (900°C–1000°C; Honjo *et al*., 1992; Andrews and Branney, 2005; 2011; Andrews *et al*., 2006; 2008), with magmatic temperatures ≥850°C (Cathey and Nash, 2004; Andrews and Branney, 2011). The KI has magmatic temperatures of ~830°C, with eruption temperatures ≤830°C, lower than the SR-type rheomorphic ignimbrites and meaning that these lower temperatures could have limited rheomorphism within the KI. Experimental data for rhyolitic systems under anhydrous conditions indicate minimum welding temperatures between 900°C and 1000°C (Grunder *et al*., 2005; Sommer *et al*., 2013), although these temperatures can be significantly lowered to ~600°C by increasing the concentrations of H_2O in metaluminous melts (Quane and Russell, 2005). Even though the KI temperatures are somewhat cooler than the metaluminous SR-type rheomorphic ignimbrites, they are still above this minimum welding temperature and therefore were high enough to facilitate the development of significant rheomorphism.

4.6.4.4 Strain heating and strain rates

Very little work has been undertaken on the structural kinematics (e.g., Andrews and Branney, 2011) and recognising the effect of strain heating (e.g., Robert *et al*., 2013) in rheomorphic ignimbrites, even though strain plays an important role in controlling rheomorphism. Typically, strain in most non-rheomorphic, welded ignimbrites is coaxial and localised as a result of the compaction-load of overlying material. However, extremely welded, high-grade rheomorphic end-members that develop lava-like facies are associated with non-coaxial and pervasive strain that developed in transient vertically-migrating shear zones (Robert *et al*., 2013), meaning that the structural kinematics of these deposits can determine the role of strain in rheomorphism of these units. Robert *et al*. (2013) demonstrated that deformation of an ignimbrite causes strain heating that increases the temperature of a deposit, further lowering the viscosity of the deposit and promoting rheomorphism. They argue that lava-like textural facies do not require high pre-eruption temperatures or high-volatile contents that reduce viscosity, but instead that strain heating within a narrow window of strain rates can be just as effective in reducing

viscosity. The curvilinear rheomorphic folds and the development of isoclinal folds, sheath folds, and refolded folds and pervasive flow banding and laminations within the KI (Figs. 4.4b, 4.4c, 4.4d, and 4.4i; Chapter 2) are similar to the deformation and strain recorded in the Grey's Landing rheomorphic ignimbrite, which has documented strains of 10–1000 as estimated using stretched vesicles (Andrews *et al*., 2008; Andrews and Branney, 2011; Robert *et al*., 2013). Given this, a similar amount of strain for the KI (i.e. 100) was used during deformation calculations. However, the modelling presented here indicates that high strain rates (3.33 s^{-1}), conservative total strain values (up to 100), and very short deformation times scales (0.3 s) and shear zone residence times (30 s) could still have led to rheomorphism of the KI, effectively negating the need for strain heating to aid and contribute to the rheomorphism of this unit.

4.6.4.5 Viscosity

Viscosity is essentially the most important factor in controlling rheomorphism, and is closely linked and is co-dependent on all of the other rheomorphic factors discussed above. If the bulk viscosity of an ignimbrite deposit is too high, the deposit will not behave in a ductile manner, and the lower the viscosity, the easier it is to achieve rheomorphism in an ignimbrite.

Key factors that affect the viscosity of a magma are magmatic temperature, magma chemistry, dissolved volatile content (concentration of H_2O, F, Cl, CO_2, etc.), the presence of crystals, bubbles or other solids (crystallinity) and pressure (Dingwell and Mysen, 1985; Bottinga *et al*., 1995; Dingwell, 1996; Giordano *et al*., 2008). Low viscosities allow welded pyroclastic flows to deform plastically (i.e. behave rheomorphically; Wolff and Wright, 1981; Henry and Wolff, 1992). Factors that reduce viscosity in rheomorphic ignimbrites include high eruption temperature, strongly peralkaline chemistry (high alkali contents) and high contents of dissolved gases such as water vapour or halogens (Branney and Kokelaar, 1992; 2002). Dissolved gases (e.g.,H_2O and F), high alkali contents, and high emplacement temperatures can all combine to maintain a low viscosity of an agglutinate and help facilitate ignimbrite rheomorphism (Branney and Kokelaar, 2002). Small variations in the concentration of dissolved volatiles such as H_2O and F in a magma can generate large, non-linear variations in magma viscosity (Dingwell *et al*., 1985; Dingwell, 1996; Giordano *et al*., 2008; Agangi *et al*., 2012), meaning that these need to be considered during viscosity calculations.

Very few calculated or measured apparent viscosity values have been reported in the literature for rheomorphic ignimbrites, meaning that there are relatively few data to compare to the average calculated viscosity of the KI (~$10^{8.16}$ Pa.s; $10^{7.7}$–$10^{8.85}$ Pa.s; Table 4.2 – Appendix C). Calculated viscosities of peralkaline rheomorphic ignimbrites have

published for the Acampamento Velho Formation, Rio Grande do Sul, Brazil, ($10^{6.95}$–$10^{8.45}$ Pa.s; Sommer *et al*., 2013) and the TL Ignimbrite, Gran Canaria ($10^{3.1}$–$10^{7.0}$ Pa.s; Sumner and Branney, 2002). The calc-alkaline Pagosa Peak Dacite, a rheomorphic ignimbrite within the San Juan volcanic field, has calculated viscosity values of $10^{5.2}$–$10^{6.0}$ Pa.s (Bachmann *et al*., 2000). In addition, the majority of dacitic and rhyolitic magmas with low water contents and temperatures between 700°C and 1000°C (i.e. peraluminous to metaluminous) have viscosities of $10^{8.5}$–10^{13} Pa.s (McBirney and Murase, 1984; Stevenson *et al*., 1998; Kirstein *et al*., 2001), whereas calc-alkaline rhyolitic melts containing 2 wt% H_2O have viscosities of $10^{4.0}$–$10^{8.0}$ Pa.s (Dingwell and Hess, 1998; Kirstein *et al*., 2001), and Mesoproterozoic A-type rhyolitic lavas from the GRV, Australia, which have elevated halogen contents, from the GRV, Australia, yielded viscosities of $<10^{3.5}$ Pa.s (Pankhurst *et al*., 2011).

Robert *et al*. (2013) measured apparent viscosity (avg. $10^{10.6}$ Pa.s; ranging from $10^{9.67}$–$10^{11.82}$ Pa.s) instead of calculating viscosity for the metaluminous SR-type Grey's Landing rheomorphic ignimbrite. This effectively accounts for solids, such as crystal abundances, which can affect viscosity, whereas the calculated viscosity measurements from Giordano *et al*. (2008) used here, do not. The crystal content in the basal lava-like rheomorphic facies of the KI is less than 5 wt%, and the overall the crystal content of the KI is 15–25 wt% (taking all units and facies into account), which is similar to that of the Grey's Landing Ignimbrite. There is also no significant difference in viscosity or temperature between KI facies with varying crystal contents indicating that the effect of crystal content on the samples is negligible and the calculated viscosities are comparable with the viscosity measurements of Robert *et al*. (2013).

The results of this study indicate that the KI had lower viscosities (by two orders of magnitude) than the somewhat analogous Grey's Landing lava-like rheomorphic ignimbrite, by two orders of magnitude, although these viscosities are still higher than most peralkaline rheomorphic ignimbrites, possibly due to higher silica and lower alkali and H_2O contents. Even though the KI has somewhat unfavourable chemistry and was erupted at lower temperatures than the majority of other rheomorphic ignimbrites, the low viscosity of this unit favoured rheomorphism and, as stated earlier, is one of the most, if not the most, important control on rheomorphism.

4.6.4.6 Final assessment of the cause of rheomorphism in the Kathleen Ignimbrite

A logical initial assumption is that the high concentration of magmatic fluorine present in the KI was the major control on the low viscosity of this unit and therefore the main control on the development of rheomorphism in the KI. The modelling presented here shows that this is clearly not the case; the same applies for the presence of water,

both in the magma and externally, although it is still unclear whether external water favours welding (e.g., Sparks *et al*., 1999). The presence of fluorine and water in the magma undoubtedly favoured the rheomorphic behaviour of the KI, although these two factors were not the only controls on the rheomorphism of the unit. The lower temperature of the KI compared to the SR-type rheomorphic ignimbrites and the slightly unfavourable chemistry (e.g., high SiO_2, lower H_2O and lower alkalis) of this unit compared with peralkaline rheomorphic ignimbrites that contain abundant alkalis, both acted to limit but did not prevent rheomorphism. This is clearly shown by the calculated viscosities for this unit, based on the chemistry and temperature of the KI, which are lower than those documented for the higher temperature SR-type lava-like Grey's Landing rheomorphic ignimbrite. It is most likely this lower viscosity, together with a combination of all the other rheomorphism-aiding factors such as the presence of a slope ultimately resulted in the rheomorphic nature of the KI, rather than any one dominating factor such as high F concentrations.

4.7 Conclusions

The Kathleen Ignimbrite (Formation) provides an excellent natural laboratory to assess the relative importance of the various factors that controlled rheomorphism within this rheomorphic ignimbrite. Although these factors are somewhat interdependent, the five main controls are the chemistry of the magma, temperature (magmatic, eruption and deposition), strain (both rate and heating), viscosity and the presence of a slope (a given for all rheomorphic ignimbrites in order to facilitate gravity-driven flow deformation). Although the KI is chemically similar to the fairly well-documented metaluminous, high-silica, SR-type lava-like rheomorphic ignimbrites of the western USA, it has lower magmatic crystallisation temperatures (~830C), lower eruption and deposition temperatures, and lower viscosity values ($10^{8.16}$ Pa.s) than these SR-type ignimbrites. In addition, although the elevated F concentrations within the KI are not present in SR-type ignimbrites, the modelling of F-free KI compositions undertaken during this study indicates that the viscosity lowering effect of this element was not the main control on rheomorphism of the KI. In addition, the presence of water during initial emplacement of the KI may or may not have enhanced welding and rheomorphism, although the water-free modelling undertaken during this study demonstrates that water-free (and both water and F-free) KI magmas most likely would have still behaved rheomorphically.

Modelling of conditions that were highly unfavourable for rheomorphism, such as much higher strain rates (3.33 s^{-1} and based on a conservative total strain up to 100) than those recorded during the emplacement of other lava-like rheomorphic ignimbrites and very short deformation timescales (0.3 s) and shear zone residence times (30 s), still indicated that the KI would most likely have undergone rheomorphism, effectively negating the need for strain heating to aid and contribute to rheomorphism of this

unit. This demonstrates that the rheomorphism in the KI resulted through a unique combination of various rheomorphism-controlling factors. These produced sufficiently low enough viscosities to result in the extremely high-degrees of welding, deformation and subsequent textures displayed in KI, making this an ideal case study of a lava-like rheomorphic ignimbrite preserved in the rock record.

4.8 Acknowledgements

I acknowledge the Geological Survey of Western Australia (GSWA) for funding and logistical support and the Monash Volcanology Research Group (MonVolc) for research collaboration and additional funding. The Ngaanyatjarra Council and their people are also thanked for the privilege of working in their shire and providing a unique opportunity to work on these rocks. I would also like to thank various GSWA field assistants, laboratory staff at Monash University, Kelly Russell, Graham Andrews and Genevieve Robert for discussions that helped improve this manuscript.

4.9 References

Agangi, A., Kamenetsky, V.S. and McPhie, J., 2010. The role of fluorine in the concentration and transport of lithophile trace elements in felsic magmas: insights from the Gawler Range Volcanics, South Australia. Chemical Geology, 273(3): 314-325.

Agangi, A., Kamenetsky, V.S. and McPhie, J., 2012. Evolution and emplacement of high fluorine rhyolites in the Mesoproterozoic Gawler silicic large igneous province, South Australia. Precambrian Research, 208-211: 124-144.

Aiuppa, A., Federico, C., Paonita, A., Pecoraino, G. and Valenza, M., 2002. S, Cl and F degassing as an indicator of volcanic dynamics: the 2001 eruption of Mount Etna. Geophysical research letters, 29(11): 54-51-54-54.

Almeev, R.R., Bolte, T., Nash, B.P., Holtz, F., Erdmann, M. and Cathey, H.E., 2012. High-temperature, low-H2O Silicic Magmas of the Yellowstone Hotspot: an Experimental Study of Rhyolite from the Bruneau–Jarbidge Eruptive Center, Central Snake River Plain, USA. Journal of Petrology, 53(9): 1837-1866.

Andrews, G.D.M., Branney, M.J., Bonnichsen, B., Ellis, B.S., Barry, T. and McCurry, M.O., 2006. Snake River (SR)-type. Eos, Transactions, American Geophysical Union, 87(Fall Meeting Suppl.).

Andrews, G.D.M. and Branney, M.J., 2005. Folds, fabrics, and kinematic criteria in rheomorphic ignimbrites of the Snake River plain, Idaho; insights into emplacement and flow. GSA Field Guide, 6: 311-327.

Andrews, G.D.M. and Branney, M.J., 2011. Emplacement and rheomorphic deformation of a large, lava-like rhyolitic ignimbrite; Grey's Landing, southern Idaho. Geological Society of America Bulletin, 123(3-4): 725-743.

Andrews, G.D.M., Branney, M.J., Bonnichsen, B. and McCurry, M., 2008. Rhyolitic ignimbrites in the Rogerson Graben, southern Snake River Plain volcanic province; volcanic stratigraphy, eruption history and basin evolution. Bulletin of Volcanology, 70(3): 269-291.

Bachmann, O., Dungan, M. and Lipman, P., 2000. Voluminous lava-like precursor to a major ash-flow tuff: low-column pyroclastic eruption of the Pagosa Peak Dacite, San Juan volcanic field, Colorado. Journal of Volcanology and Geothermal Research, 98(1): 153-171.

Bailey, D. and Macdonald, R., 1975. Fluorine and chlorine in peralkaline liquids and the need for magma generation in an open system. Mineral. Mag, 40(312): 405-414.

Bailey, J.C., 1977. Fluorine in granitic rocks and melts: A review. Chemical Geology, 19(1,Äì4): 1-42.

Bonnichsen, B. and Citron, G.P., 1982. The Cougar Point Tuff, southwestern Idaho and vicinity. Bulletin - Idaho Bureau of Mines and Geology, 26: 255-281.

Bottinga, Y., Richet, P. and Sipp, A., 1995. Viscosity regimes of homogeneous silicate melts. American Mineralogist, 80(3): 305-318.

Branney, M.J., Barry, T. and Godchaux, M., 2004. Sheathfolds in rheomorphic ignimbrites. Bulletin of Volcanology, 66(6): 485-491.

Branney, M.J., Bonnichsen, B., Andrews, G.D.M., Ellis, B., Barry, T.L. and McCurry, M., 2008. 'Snake River (SR)-type' volcanism at the Yellowstone hotspot track; distinctive products from unusual, high-temperature silicic super-eruptions. Bulletin of Volcanology, 70(3): 293-314.

Branney, M.J. and Kokelaar, B.P., 2002. Pyroclastic density currents and the sedimentation of ignimbrites. Geological Society Publishing House, Bath, United Kingdom, 143 pp.

Branney, M.J., Kokelaar, B.P. and McConnell, B.J., 1992. The Bad Step Tuff; a lava-like rheomorphic ignimbrite in a calc-alkaline piecemeal caldera, English Lake District. Bulletin of Volcanology, 54(3): 187-199.

Branney, M.J. and Kokelaar, P., 1992. A reappraisal of ignimbrite emplacement: progressive aggradation and changes from particulate to non-particulate flow during emplacement of high-grade ignimbrite. Bulletin of Volcanology, 54(6): 504-520.

Branney, M.J. and Kokelaar, P., 1994. Volcanotectonic faulting, soft-state deformation, and rheomorphism of tuffs during development of a piecemeal caldera, English Lake District. Geological Society of America Bulletin, 106(4): 507-530.

Burt, D.M., Sheridan, M.F., Bikun, J.V. and Christiansen, E.H., 1982. Topaz rhyolites; distribution, origin, and significance for exploration. Economic Geology and the Bulletin of the Society of Economic Geologists, 77(8): 1818-1836.

Cas, R.A.F. and Wright, J.V., 1987. Volcanic successions: modern and ancient. A geological approach to processes, products and successions. Allen & Unwin, London, UK,

528 pp.

Cas, R.A.F. and Wright, J.V., 1991. Subaqueous pyroclastic flows and ignimbrites: an assessment. Bulletin of Volcanology, 53(5): 357-380.

Capaccioni, B. and Cuccoli, F., 2005. Spatter and welded air fall deposits generated by fire-fountaining eruptions: cooling of pyroclasts during transport and deposition. Journal of volcanology and geothermal research, 145(3): 263-280.

Cathey, H.E. and Nash, B.P., 2004. The Cougar Point Tuff: implications for thermochemical zonation and longevity of high-temperature, large-volume silicic magmas of the Miocene Yellowstone hotspot. Journal of Petrology, 45(1): 27-58.

Chabiron, A., Alyoshin, A.P., Cuney, M., Deloule, E., Golubev, V.N., Velitchkin, V.I. and Poty, B., 2001. Geochemistry of the rhyolitic magmas from the Streltsovka caldera (Transbaikalia, Russia): a melt inclusion study. Chemical Geology, 175(3): 273-290.

Chapin, C.E. and Lowell, G.R., 1979. Primary and secondary flow structures in ash-flow tuffs of the Gribbles Run paleovalley, central Colorado. Special Paper - Geological Society of America(180): 137-154.

Christiansen, E.H., Bikun, J.V., Sheridan, M.F. and Burt, D.M., 1984. Geochemical evolution of topaz rhyolites from the Thomas Range and Spor Mountain, Utah. American Mineralogist, 69(3-4): 223-236.

Christiansen, E.H., Burt, D.M., Sheridan, M.F. and Wilson, R.T., 1983. The petrogenesis of topaz rhyolites from the Western United States. Contributions to Mineralogy and Petrology, 83(1-2): 16-30.

Christiansen, E.H., Haapala, I. and Hart, G.L., 2007. Are Cenozoic topaz rhyolites the erupted equivalents of Proterozoic rapakivi granites? Examples from the Western United States and Finland. Lithos, 97(1-2): 219-246.

Christiansen, E.H. and McCurry, M., 2008. Contrasting origins of Cenozoic silicic volcanic rocks from the western Cordillera of the United States. Bulletin of Volcanology, 70(3): 251-267.

Christiansen, E.H., Sheridan, M.F. and Burt, D.M., 1986. The geology and geochemistry of Cenozoic topaz rhyolites from the Western United States. Geological Society of America (GSA), Boulder, CO, United States, 82 pp.

Collins, W.J., Beams, S.D., White, A.J.R. and Chappell, B.W., 1982. Nature and origin of A-type granites with particular reference to southeastern Australia. Contributions to Mineralogy and Petrology, 80(2): 189-200.

Congdon, R.D. and Nash, W., 1988. High-fluorine rhyolite: an eruptive pegmatite magma at the Honeycomb Hills, Utah. Geology, 16(11): 1018-1021.

Cordonnier, B., Caricchi, L., Pistone, M., Castro, J., Hess, K.-U., Gottschaller, S., Manga, M., Dingwell, D. and Burlini, L., 2012a. The viscous-brittle transition of crystal-bearing silicic melt: Direct observation of magma rupture and healing. Geology, 40(7): 611-614.

Cordonnier, B., Schmalholz, S., Hess, K.U. and Dingwell, D., 2012b. Viscous heating in silicate melts: An experimental and numerical comparison. Journal of Geophysical Research: Solid Earth (1978–2012), 117(B2).

Daniels, J.L., 1974. The geology of the Blackstone region, Western Australia. Bulletin - Geological Survey of Western Australia, 123: 257.

Devine, J.D., Gardner, J.E., Brack, H.P., Layne, G.D. and Rutherford, M.J., 1995. Comparison of microanalytical methods for estimating H2O contents of silicic volcanic glasses. American Mineralogist, 80(3): 319-328.

Dill, H.G., 2010. The “chessboard” classification scheme of mineral deposits: mineralogy and geology from aluminum to zirconium. Earth-Science Reviews, 100(1): 1-420.

Dingwell, D.B., 1988. The structures and properties of fluorine-rich magmas; a review of experimental studies. Special Volume - Canadian Institute of Mining and Metallurgy, 39: 1-12.

Dingwell, D.B., 1996. Volcanic Dilemma--Flow or Blow? Science, 273(5278): 1054-1055.

Dingwell, D.B. and Hess, K., 1998. Melt viscosities in the system Na-Fe-Si-OF-Cl: Contrasting effects of F and Cl in alkaline melts. American Mineralogist, 83: 1016-1021.

Dingwell, D.B. and Mysen, B.O., 1985. Effects of water and fluorine on the viscosity of albite melt at high pressure: a preliminary investigation. Earth and Planetary Science Letters, 74(2): 266-274.

Dingwell, D.B., Scarfe, C.M. and Cronin, D.J., 1985. The effect of fluorine on viscosities in the system Na2O-Al2O3-SiO2: implications for phonolites, trachytes and rhyolites. American Mineralogist(1-2): 80-87.

Dingwell, D.B. and Webb, S.L., 1989. Structural relaxation in silicate melts and non-Newtonian melt rheology in geologic processes. Physics and Chemistry of Minerals, 16(5): 508-516.

Duffield, W.A. and Dalrymple, G.B., 1990. The Taylor Creek Rhyolite of New Mexico: a rapidly emplaced field of lava domes and flows. Bulletin of Volcanology, 52(6): 475-487.

Eby, G.N., 1990. The A-type granitoids; a review of their occurrence and chemical characteristics and speculations on their petrogenesis. Lithos, 26(1-2): 115-134.

Edgoose, C.J., Scrimgeour, I.R. and Close, D.F., 2004. Geology of the Musgrave Block, Northern Territory. Northern Territory Geological Survey, Report 15.

Ekren, E.B., McIntyre, D.H. and Bennett, E.H., 1984. High-temperature, large-volume, lavalike ash-flow tuffs without calderas in southwestern Idaho. U. S. Geological Survey, Reston, VA, United States, 76 pp.

Ellis, B.S., 2009. Rhyolitic explosive eruptions of the central Snake River Plain, Idaho: investigations of the lower Cassia Mountains succession and surrounding areas. PhD Thesis, University of Leicester.

Evins, P.M., Smithies, R.H., Howard, H.M., Kirkland, C.L., Wingate, M.T.D. and Bodorkos,

S., 2010. Devil in the detail; the 1150-1000 Ma magmatic and structural evolution of the Ngaanyatjarra Rift, west Musgrave Province, central Australia. Precambrian Research, 183(3): 572-588.

Freundt, A., 1998. The formation of high-grade ignimbrites, I: Experiments on high- and low-concentration transport systems containing sticky particles. Bulletin of Volcanology, 59(6): 414-435.

Frost, B.R., Barnes, C.G., Collins, W.J., Arculus, R.J., Ellis, D.J. and Frost, C.D., 2001. A geochemical classification for granitic rocks. Journal of Petrology, 42(11): 2033-2048.

Frost, B.R. and Frost, C.D., 2008. A geochemical classification for feldspathic igneous rocks. Journal of Petrology, 49(11): 1955-1969.

Frost, C.D. and Frost, R., 2011. On ferroran (A-type) granitoids; their compositional variability and modes of origin. Journal of Petrology, 52(1): 39-53.

Giordano, D., Romano, C., Dingwell, D., Poe, B. and Behrens, H., 2004. The combined effects of water and fluorine on the viscosity of silicic magmas. Geochimica et Cosmochimica Acta, 68(24): 5159-5168.

Giordano, D., Russell, J.K. and Dingwell, D.B., 2008. Viscosity of magmatic liquids; a model. Earth and Planetary Science Letters, 271(1-4): 123-134.

Glikson, A.Y., Stewart, A.J., Ballhaus, C.G., Clarke, G.L., Feeken, E.H.J., Leven, J.H., Sheraton, J.W. and Sun, S.S., 1996. Geology of the western Musgrave Block, central Australia, with particular reference to the mafic-ultramafic Giles Complex. Bulletin - Australian Geological Survey Organisation, 239.

Grunder, A.L., Laporte, D. and Druitt, T.H., 2005. Experimental and textural investigation of welding: effects of compaction, sintering, and vapor-phase crystallization in the rhyolitic Rattlesnake Tuff. Journal of volcanology and geothermal research, 142(1): 89-104.

Gualda, G.A., Ghiorso, M.S., Lemons, R.V. and Carley, T.L., 2012. Rhyolite-MELTS: a modified calibration of MELTS optimized for silica-rich, fluid-bearing magmatic systems. Journal of Petrology, 53(5): 875-890.

Hanchar, J.M. and Watson, E.B., 2003. Zircon saturation thermometry. Reviews in mineralogy and geochemistry, 53(1): 89-112.

Henry, C.D., Price, J.G., Rubin, J.N., Parker, D.F., Wolff, J.A., Self, S., Franklin, R. and Barker, D.S., 1988. Widespread, lavalike silicic volcanic rocks of Trans-Pecos Texas. Geology (Boulder), 16(6): 509-512.

Henry, C.D. and Wolff, J.A., 1992. Distinguishing strongly rheomorphic tuffs from extensive silicic lavas. Bulletin of Volcanology, 54(3): 171-186.

Holtz, F., Dingwell, D.B. and Behrens, H., 1993. Effects of F, B2O3 and P2O5 on the solubility of water in haplogranite melts compared to natural silicate melts. Contributions to Mineralogy and Petrology, 113(4): 492-501.

Holtz, F., Roux, J., Ohlhorst, S., Behrens, H. and Schulze, F., 1999. The effects of silica and

water on the viscosity of hydrous quartzofeldspathic melts. American Mineralogist, 84: 27-36.

Honjo, N., Bonnichsen, B., Leeman, W.P. and Stormer Jr, J.C., 1992. Mineralogy and geothermometry of high-temperature rhyolites from the central and western Snake River Plain. Bulletin of Volcanology, 54(3): 220-237.

Howard, H.M., Werner, M., Smithies, R.H., Evins, P.M., Kirkland, C.L., Kelsey, D.E., Hand, M., Collins, A.S., Pirajno, F., Wingate, M.T.D., Maier, W.D. and Raimondo, T., 2011. The geology of the west Musgrave Province and the Bentley Supergroup -- a field guide. Record - Geological Survey of Western Australia, Perth, Australia, 2011/14: 125.

Hu, Z. and Gao, S., 2008. Upper crustal abundances of trace elements: a revision and update. Chemical Geology, 253(3): 205-221.

Huspeni, J.R., Kesler, S.E., Ruiz, J., Tuta, Z., Sutter, J.F. and Jones, L.M., 1984. Petrology and geochemistry of rhyolites associated with tin mineralization in northern Mexico. Economic Geology, 79(1): 87-105.

Irvine, T.N. and Baragar, W.R.A., 1971. A guide to the chemical classification of the common volcanic rocks. Canadian Journal of Earth Sciences = Journal Canadien des Sciences de la Terre, 8(5): 523-548.

Johnston, C. and Chappell, B., 1992. Topaz-bearing rocks from Mount Gibson, North Queensland, Australia. American Mineralogist, 77(3-4): 303-313.

Kirkland, C.L., Smithies, R.H., Woodhouse, A.J., Howard, H.M., Wingate, M.T.D., Belousova, E.A., Cliff, J., Murphy, R. and Spaggiari, C.V., 2013. Constraints and deception in the isotopic record; the crustal evolution of the west Musgrave Province, central Australia. Gondwana Research, 23: 759-781.

Kirstein, L.A., Hawkesworth, C.J. and Garland, F.G., 2001. Felsic lavas or rheomorphic ignimbrites; is there a chemical distinction? Contributions to Mineralogy and Petrology, 142(3): 309-322.

Kobberger, G. and Schmincke, H.U., 1999. Deposition of rheomorphic ignimbrite D (Mogan Formation), Gran Canaria, Canary Islands, Spain. Bulletin of Volcanology, 60(6): 465-485.

Lange, R.A., 1994. The effect of H2O, CO2 and F on the density and viscosity of silicate melts. Reviews in Mineralogy and Geochemistry, 30(1): 331-369.

Le Maitre, R.W., Bateman, P., Dudek, A., Keller, J., Lameyre, J., Le Bas, M.J., Sabine, P.A., Schmid, R., Sorensen, H., Streckeisen, A., Woolley, A.R. and Zanettin, B., 1989. A classification of igneous rocks and glossary of terms. Blackwell Sci. Publ., Oxford, United Kingdom, 193 pp.

Le Maitre, R.W., Streckeisen, A., Zanettin, B., Le Bas, M.J., Bonin, B., Bateman, P., Bellieni, G., Dudek, A., Efremova, S., Keller, J., Lameyre, J., Sabine, P.A., Schmid, R., Sorensen, H. and Woolley, A.R., 2002. Igneous rocks; a classification and glossary of terms; recommendations of the International Union of Geological

Sciences Subcommission on the Systematics of Igneous Rocks. Cambridge University Press, Cambridge, United Kingdom, 236 pp.

Leat, P.T. and Schmincke, H.-U., 1993. Large-scale rheomorphic shear deformation in Miocene peralkaline ignimbrite E, Gran Canaria. Bulletin of Volcanology, 55(3): 155-165.

Linnen, R.L. and Keppler, H., 2002. Melt composition control of Zr/Hf fractionation in magmatic processes. Geochimica et Cosmochimica Acta, 66(18): 3293-3301.

Lipman, P.W., 2000. Calderas. In: H. Sigurdsson (Editor), Encyclopedia of Volcanoes. Academic Press, San Francisco.

Loiselle, M.C. and Wones, D.R., 1979. Characteristics and origin of anorogenic granites. Abstracts with Programs - Geological Society of America, 11(7): 468.

Macdonald, R. and Bailey, D.K., 1973. Chemistry of Igneous Rocks: The Chemistry of the Peralkaline Oversaturated Obsidians. US Government Printing Office.

Mahood, G.A., 1984. Pyroclastic rocks and calderas associated with strongly peralkaline magmatism. Journal of Geophysical Research, 89(B10): 8540-8552.

Manning, D., 1981. The effect of fluorine on liquidus phase relationships in the system Qz-Ab-Or with excess water at 1 kb. Contributions to Mineralogy and Petrology, 76(2): 206-215.

Maxwell, J.C., 1866. On the dynamical theory of gases. Philosophical Transactions of the Royal Society of London: 49-88.

McBirney, A.R., 1968. Second additional theory of origin of fiamme in ignimbrites. Nature (London), 217(5132): 938.

McBirney, A.R. and Murase, T., 1984. Rheological properties of magmas. Annual Review of Earth and Planetary Sciences, 12: 337.

Mcleod, P., Carey, S. and Sparks, R.S.J., 1999. Behaviour of particle-laden flows into the ocean: experimental simulation and geological implications. Sedimentology, 46(3): 523-536.

McPhie, J., Kamenetsky, V., Allen, S., Ehrig, K., Agangi, A. and Bath, A., 2011. The fluorine link between a supergiant ore deposit and a silicic large igneous province. Geology, 39(11): 1003-1006.

Miller, C.F., McDowell, S.M. and Mapes, R.W., 2003. Hot and cold granites? Implications of zircon saturation temperatures and preservation of inheritance. Geology, 31(6): 529-532.

Moore, I. and Kokelaar, P., 1998. Tectonically controlled piecemeal caldera collapse: A case study of Glencoe volcano, Scotland. Geological Society of America Bulletin, 110(11): 1448-1466.

Myers, J.S., Shaw, R.D. and Tyler, I.M., 1996. Tectonic evolution of Proterozoic Australia. Tectonics, 15(6): 1431-1446.

Nash, W., 1993. Fluorine iron biotite from the Honeycomb Hills rhyolite, Utah; the halogen record of decompression in a silicic magma. American Mineralogist, 78(9-10):

1031-1040.

Noble, D.C., Smith, V.C. and Peck, L.C., 1967. Loss of halogens from crystallized and glassy silicic volcanic rocks. Geochimica et Cosmochimica Acta, 31(2): 215-223.

Pankhurst, M., Schaefer, B., Betts, P., Phillips, N. and Hand, M., 2011. A Mesoproterozoic continental flood rhyolite province, the Gawler Ranges, Australia: the end member example of the Large Igneous Province clan. Solid Earth, 2(1): 25-33.

Pearce, J.A., Harris, N.B.W. and Tindle, A.G., 1984. Trace element discrimination diagrams for the tectonic interpretation of granitic rocks. Journal of Petrology, 25(4): 956-983.

Pichler, H., 1965. Acid hyaloclastites. Bulletin of Volcanology, 28: 293-310.

Price, J.G., Castor, S.B. and Miller, D.M., 1992. Highly radioactive topaz rhyolites of the Toano Range, northeastern Nevada. American Mineralogist;(United States), 77.

Quane, S.L. and Russell, J.K., 2005. Ranking welding intensity in pyroclastic deposits. Bulletin of Volcanology, 67(2): 129-143.

Quane, S.L., Russell, J.K. and Friedlander, E.A., 2009. Time scales of compaction in volcanic systems. Geology, 37(5): 471-474.

Riehle, J.R., Miller, T.F. and Paquereau-Lebti, P., 2010. Compaction profiles of ash-flow tuffs; modeling versus reality. Journal of Volcanology and Geothermal Research, 195(2-4): 106-120.

Rittmann, A., 1958. Cenni sulle colate di ignimbriti. Boll. Acad. Gioenia, serie IV, 4: 525-533.

Robert, G., Andrews, G.D., Ye, J. and Whittington, A.G., 2013. Rheological controls on the emplacement of extremely high-grade ignimbrites. Geology, 41(9): 1031-1034.

Russell, J.K., Giordano, D. and Dingwell, D., 2004. High-temperature limits on viscosity of non-Arrhenian silicate melts. American Mineralogist, 88(8-9): 1390-1394.

Sallet, R., Moritz, R. and Fontignie, D., 2000. Fluorite 87Sr/86Sr and REE constraints on fluid–melt relations, crystallization time span and bulk D(Sr) of evolved high-silica granites. Tabuleiro granites, Santa Catarina, Brazil. Chemical Geology, 164(1): 81-92.

Schmincke, H.-U. and Swanson, D.A., 1967. Laminar viscous flowage structures in ash-flow tuffs from Gran Canaria, Canary islands. Journal of Geology, 75(6): 641-664.

Schmincke, H.-U., 1974. Volcanological aspects of peralkaline silicic welded ash-flow tuffs. Bulletin Volcanologique, 38(2): 594-636.

Schmincke, H.-U. and Swanson, D.A., 1967. Laminar viscous flowage structures in ash-flow tuffs from Gran Canaria, Canary islands. Journal of Geology, 75(6): 641-664.

Self, S., 2006. The effects and consequences of very large explosive volcanic eruptions. Philosophical Transactions of the Royal Society A: Mathematical, Physical and Engineering Sciences, 364(1845): 2073-2097.

Shaw, H., 1972. Viscosities of magmatic silicate liquids; an empirical method of prediction. American Journal of Science, 272(9): 870-893.

Shellnutt, J.G. and Zhou, M.-F., 2007. Permian peralkaline, peraluminous and

metaluminous A-type granites in the Panxi district, SW China; their relationship to the Emeishan mantle plume. Chemical Geology, 243(3-4): 286-316.

Skilling, I., White, J. and McPhie, J., 2002. Peperite: a review of magma–sediment mingling. Journal of Volcanology and Geothermal Research, 114(1): 1-17.

Smith, R.L., 1960. Zones and zonal variations in welded ash flows. U. S. Geological Survey Professional Paper: 149-159.

Smithies, R.H., Howard, H.M., Kirkland, C.L., Werner, M., Medlin, C.C., Wingate, M.T.D. and Cliff, J.B., 2013. Geochemical evolution of rhyolites of the Talbot Sub-basin and associated felsic units of the Warakurna Supersuite, Geological Survey of Western Australia, Perth, Australia, 118: 74.

Sommer, C.A., Lima, E.F., Machado, A., Rossetti, L.d.M.M. and Pierosan, R., 2013. Recognition and characterisation of high-grade ignimbrites from the Neoproterozoic rhyolitic volcanism in southernmost Brazil. Journal of South American Earth Sciences, 47(0): 152-165.

Sparks, R.S.J., Sigurdsson, H. and Carey, S.N., 1980. The entrance of pyroclastic flows into the sea; II, Theoretical considerations on subaqueous emplacement and welding. Journal of Volcanology and Geothermal Research, 7(1-2): 97-105.

Sparks, R.S.J., Tait, S.R. and Yanev, Y., 1999. Dense welding caused by volatile resorption. Journal of the Geological Society of London, 156, Part 2: 217-225.

Stevenson, R., Bagdassarov, N., Dingwell, D. and Romano, C., 1998. The influence of trace amounts of water on the viscosity of rhyolites. Bulletin of volcanology, 60(2): 89-97.

Stix, J., Layne, G.D. and Spell, T.L., 1995. The behavior of light lithophile and halogen elements in felsic magma; geochemistry of the post-caldera Valles Rhyolites, Jemez Mountains Volcanic Field, New Mexico. Journal of Volcanology and Geothermal Research, 67(1-3): 61-77.

Sumner, J., Blake, S., Matela, R. and Wolff, J., 2005. Spatter. Journal of Volcanology and Geothermal Research, 142(1): 49-65.

Sumner, J.M. and Branney, M.J., 2002. The emplacement history of a remarkable heterogeneous, chemically zoned, rheomorphic and locally lava-like ignimbrite; "TL" on Gran Canaria. Journal of Volcanology and Geothermal Research, 115(1-2): 109-138.

Taylor, R.P. and Fallick, A.E., 1997. The evolution of fluorine-rich felsic magmas; source dichotomy, magmatic convergence and the origins of topaz granite. Terra Nova, 9(3): 105-108.

Thomas, J., Bodnar, R., Shimizu, N. and Sinha, A., 2002. Determination of zircon/melt trace element partition coefficients from SIMS analysis of melt inclusions in zircon. Geochimica et Cosmochimica Acta, 66(16): 2887-2901.

Thomas, J.B., Watson, E.B., Spear, F.S., Shemella, P.T., Nayak, S.K. and Lanzirotti, A., 2010. TitaniQ under pressure: the effect of pressure and temperature on the

solubility of Ti in quartz. Contributions to Mineralogy and Petrology, 160(5): 743-759.

Thomas, R., Foerster, H.-J., Rickers, K. and Webster, J.D., 2005. Formation of extremely F-rich hydrous melt fractions and hydrothermal fluids during differentiation of highly evolved tin-granite magmas; a melt-fluid-inclusion study. Contributions to Mineralogy and Petrology, 148(5): 582-601.

Wade, B.P., Kelsey, D.E., Hand, M. and Barovich, K.M., 2008. The Musgrave Province; stitching north, west and south Australia. Precambrian Research, 166(1-4): 370-386.

Watson, E.B., 1979. Zircon saturation in felsic liquids: experimental results and applications to trace element geochemistry. Contributions to Mineralogy and Petrology, 70(4): 407-419.

Watson, E.B. and Harrison, T.M., 1983. Zircon saturation revisited; temperature and composition effects in a variety of crustal magma types. Earth and Planetary Science Letters, 64(2): 295-304.

Webb, S.L. and Dingwell, D.B., 1990. Non-Newtonian rheology of igneous melts at high stresses and strain rates: Experimental results for rhyolite, andesite, basalt, and nephelinite. Journal of Geophysical Research: Solid Earth (1978–2012), 95(B10): 15695-15701.

Webster, J., Thomas, R., Förster, H.-J., Seltmann, R. and Tappen, C., 2004. Geochemical evolution of halogen-enriched granite magmas and mineralizing fluids of the Zinnwald tin-tungsten mining district, Erzgebirge, Germany. Mineralium Deposita, 39(4): 452-472.

Webster, J.D. and Duffield, W.A., 1994. Extreme halogen abundances in tin-rich magma of the Taylor Creek Rhyolite, New Mexico. Economic Geology and the Bulletin of the Society of Economic Geologists, 89(4): 840-850.

Werner, M., Howard, H.M. and Smithies, R.H., 2012. Mount Eveline, WA Sheet 4345 1:100 000 Geological Series. Geological Survey of Western Australia, Perth, Australia.

Whalen, J.B., Currie, K.L. and Chappell, B.W., 1987. A-type granites; geochemical characteristics, discrimination and petrogenesis. Contributions to Mineralogy and Petrology, 95(4): 407-419.

White, A.J.R. and Chappell, B.W., 1983. Granitoid types and their distribution in the Lachlan fold belt, southeastern Australia. Memoir - Geological Society of America, 159: 21-34.

Whittington, A.G., Richet, P. and Polian, A., 2012. Water and the compressibility of silicate glasses: A Brillouin spectroscopic study. American Mineralogist, 97(2-3): 455-467.

Wingate, M.T.D., Pirajno, F. and Morris, P.A., 2004. Warakurna large igneous province: A new Mesoproterozoic large igneous province in west-central Australia. Geology, 32(2): 105-108.

Wolff, J.A. and Wright, J.V., 1981. Rheomorphism of welded tuffs. Journal of Volcanology

and Geothermal Research, 10(1-3): 13-34.

Wohletz, K., 2002. Water/magma interaction: some theory and experiments on peperite formation. Journal of volcanology and geothermal research, 114(1): 19-35.

Zen, E.A., 1988. Phase relations of peraluminous granitic rocks and their petrogenetic implications. Annual Review of Earth and Planetary Sciences, 16: 21-51.

Chapter 5

Rare Earth Element (REE) mineralisation within highly fractionated rhyolites: the equivalent of low-grade porphyry deposits in the REE world?

Chris C. Medlin[1], Simon M. Jowitt[1], Ray A.F. Cas[1]

[1]School of Geosciences, Monash University, Melbourne, VIC, 3800, Australia

Keywords: REE, high-silica rhyolites, fractionation, mineral deposit

Abstract

Rare earth elements (REE) are crucial in transforming modern industry, technology and medicine, with the demand for these elements increasing significantly over the past few years and the current supply restricted to a only few well-known mineral deposits. This has created a supply-demand gap in the REE market, driving a focus on finding new sources of these sought-after elements. The primary fractionation processes involved in the petrogenesis of highly fractionated, high-silica rhyolites causes the magmas that form these units to become preferentially enriched in the REE, especially in the more valuable heavy REE. This, combined with the presence of enrichments in other important by- and co-product metals (e.g., Y, Nb, Ta, Be, Li, F, Sn, Rb, Th, and U) means these rhyolites should be considered as potential sources of these critical metals. In addition, these rhyolites are often large volume and outcrop at the Earth's surface, making them ideally suited for more economical bulk open pit extraction. This suggests that these high-silica REE-enriched rhyolites should be considered potential REE analogues of bulk-tonnage, low-grade porphyry Cu deposits, meaning these rhyolites are a potential new source of the REE and are worthy of further research and mineral exploration.

5.1 Introduction

The global demand for the rare earth elements (REE) has increased significantly during recent decades, as these elements have crucial uses in modern technology (e.g., computers, magnets, lasers, screens), alloys, batteries, glass, petroleum refining and catalysts (Haxel *et al*., 2005; Maestro and Huguenin, 1995). This has driven exploration for both traditional sources of the REE (e.g., carbonatites, including the world's largest REE resource at Bayan Obo, Inner Mongolia, China and important REE mineralisation at Mountain Pass, California, USA; Drew *et al*., 1990; Olson *et al*., 1954) and the identification of other "unconventional" sources of the REE. Although carbonatite-hosted REE deposits have dominated the supply of these elements for the past 50 years (Haxel *et al*., 2005;

Weng *et al*., 2013), these deposits are high grade (e.g., ~5–6 wt% REE_2O_3 – Bayan Obo; ~9 wt% REE_2O_3 – Mountain Pass; McLennan and Taylor, 2013), but with the exception of Bayan Obo they are generally small tonnage (e.g., Mountain Pass, with 16.7 Mt of resources, Mt. Weld, with 23.9 Mt of resources; Weng *et al*., 2013). More importantly, these carbonatites have REE assemblages that are dominated by the low price light REE (LREE) and contain only small amounts of the equally critical, but rarer and therefore more valuable heavy REE (HREE). This study focusses on a new potential source of the REE (and more importantly HREE): highly fractionated high-silica rhyolites. These rhyolites are exemplified by the Round Top Mountain rhyolite in Texas, USA, a deposit that contains 1.03 Bt of ore resource at a total REE (TREE) grade of ~305 ppm (+ 220 ppm Y; Hulse *et al*., 2013; Pingitore *et al*., 2014). A number of other REE- and HREE-enriched but under-explored rhyolites are also known, including the Kathleen Ignimbrite of the west Musgrave Province of central Australia. These rhyolites may be the REE equivalents of low grade porphyry-Cu deposits, enabling large-scale extraction of the REE from bulk tonnage but low grade mineral deposits. These magmas form through extended fractionation (e.g., Chapter 3), a process that concentrates the REE in the melt fraction of a magmatic system, with these melts then going on to form highly fractionated REE-enriched rhyolites (Chakhmouradian and Zaitsev, 2012). In addition, these highly fractionated rhyolites are often preferentially enriched in the HREE relative to the LREE as a result of either extreme fractionation (Miller and Mittlefehldt, 1982) or by late-stage magmatic upgrading and potential vapour phase crystallisation (Price *et al*., 1990; Agangi *et al*., 2010). It should be noted that the global mining industry often uses a slightly different classification than the IUPAC (2005) classification of the REE, with Pm, Sm, Eu, Gd and Y (not strictly a REE) included with the HREE (Weng *et al*., 2013); as such, and given the mineral exploration focus of this paper, Y is omitted from the TREE concentrations and report it separately (where possible) and define the following in this study: LREE (La, Ce, Pr, Nd) and HREE (Sm, Eu, Gd, Tb, Dy, Ho, Er, Tm, Yb, Lu). The higher demand for, and higher prices of the HREE relative to the LREE, means these rhyolites should be considered highly prospective future sources of the REE; in addition, these rhyolites are often enriched in other critical elements such as Y, Mo, Nb, Ta, Be, Li, Cs, F, Sn, Rb, Th and U, making them even more attractive exploration targets (Castor and Hedrick, 2006; Chakhmouradian and Wall, 2012; Hatch, 2012). This chapter provides an overview of these rhyolites, outlines potential problems associated with the extraction and processing of these deposits, and comments on a potential “mineralogical barrier” for REE mineralisation within these rhyolites.

5.2 Highly fractionated high-silica REE rhyolites

Highly fractionated rhyolites generally contain >70 wt% SiO_2 and are typically enriched in the REE and lithophile elements relative to crustal abundances (Wedepohl, 1995). They occur as rheomorphically welded or lava-like ignimbrites (e.g., the Kathleen Ignimbrite; Chapter 3), lavas, domes, and intrusions in bimodal volcanic provinces that are often related to voluminous magmatic events (Pankhurst *et al*., 2011a). These rhyolites form from high-temperature anhydrous magmas that have typical A-type geochemical characteristics, have been identified in a number of places (e.g., Fig. 5.1), and are known to have formed at differing times during the geological record. Examples include the Mesoproterozoic Gawler Range Volcanic (GRV) Province of South Australia (Agangi *et al*., 2012; Pankhurst *et al*., 2011b), the Mesoproterozoic west Musgrave Province of Western Australia (Chapter 2; Chapter 3), the Miocene Snake River Plain (SRP) of Idaho, USA (Branney *et al*., 2008; Ekren *et al*., 1984), within the Cenozoic of the western USA (Christiansen *et al*., 1983; 1986), in the Yukon Territory of Canada (Sinclair, 1986), in Mexico (Huspeni *et al*., 1984), in eastern Russia and Mongolia (Kovalenko and Kovalenko, 1984) and in southern Finland (Haapala, 1997). The formation of these rhyolites remains somewhat controversial, with three main models for the generation of the magmas that formed them: (a) extreme fractional crystallisation of a basaltic magma (e.g., McCurry *et al*., 2008; Turner *et al*., 1992a; Chapter 3), (b) fractional crystallisation of silicic magmas generated during small degree of partial melting of hybridised gabbro–diorite intrusive complexes in the crust (e.g., Christiansen *et al*., 2007; Turner *et al*., 1992b), and (c) partial melting of older continental crust by heat derived from underplated mantle-derived magmas and subsequent fractional crystallisation (e.g., Anderson and Morrison, 2005; Creaser *et al*., 1991; Frindt *et al*., 2004; Haapala and Rämö, 1992; Patino Douce, 1997). Regardless of the model, the petrogenesis of all of these evolved rhyolites involved significant fractionation that led to an overall increase in REE abundance and an eventual change in REE compatibility. Fractionation of LREE-bearing minerals such as allanite and monazite means that these elements become compatible, whereas the HREE remain highly incompatible, causing enrichment of the HREE relative to the LREE and leading to the generation of HREE-enriched (and potentially economic) parts of these magmatic systems.

5.3 Mineral hosts for the REE in highly fractionated rhyolites

The compatibility or incompatibility of a trace element is dependent on a number of factors and varies for different magmatic systems. The large-ion lithophile elements (LILE), namely K, Rb, Cs, Sr, and Ba, and high field strength elements (HFSE), such as Zr, Nb, Hf, the REE, Y, Th, U, Pb and Ta, are generally incompatible in magmatic systems, meaning they remain trapped in melt phases during fractionation and as such are preferentially concentrated in mineral phases formed during late-stage crystallisation. However, the

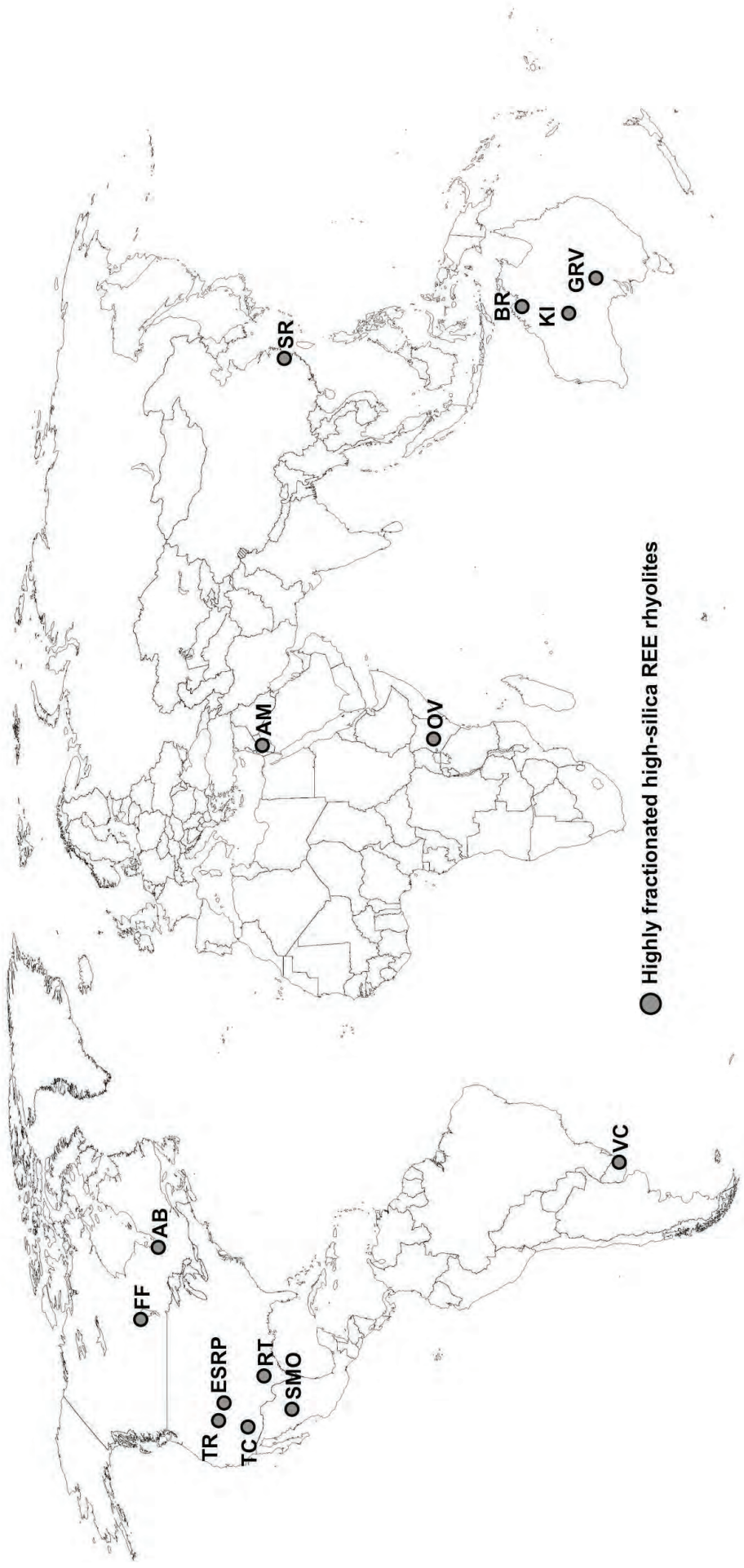

Figure 5.1: World map showing the localities of the highly fractionated high-silica REE rhyolite deposits discussed in the text. FF = Flin Flon, AB = Abitibi, TR = Topaz rhyolites, ESRP = Eastern Snake River Plain, TC = Taylor Creek, RT = Round Top, SMO, Sierra Madre Occidental, VC = Valle Chico, AM = Amram Massif, OV = Olkaria Volcanics, SR = Sangshu rhyolites, BR = Brockman rhyolites, KI = Kathleen Ignimbrite, GRV = Gawler Range Volcanics.

behaviour of these elements can and will vary during fractionation, especially during the extended fractionation needed to generate highly fractionated high-silica rhyolites. These rhyolites are the most evolved end-members of magmatic suites and represent the last melt phases to crystallise, meaning they typically contain high concentrations of incompatible elements such as the REE.

The lanthanide REE (La, Ce, Pr, Nd, Pm, Sm, Eu, Gd, Tb, Dy, Ho, Er, Tm, Yb, Lu) are specifically arranged from lightest to heaviest, corresponding to the lower ionic radius from La (highly incompatible) to Lu (slightly incompatible). The larger LREE readily and easily fractionate into minerals with large co-ordination polyhedra while minerals with small co-ordination polyhedra tend to favour the smaller HREE. Minerals with intermediate-size polyhedra do not show any particular preference for the LREE or HREE, but favour the middle REE (Jaireth *et al*., 2014). Although the LREE are more incompatible than the HREE in the majority of igneous melts (with the exception of Eu), this is not the case for highly fractionated rhyolites, where the onset of the fractionation of LREE-enriched phases (e.g., allanite, chevkinite, bastnaesite, monazite, etc.) causes these elements to become compatible (Agangi *et al*., 2010; Christiansen *et al*., 1986; Eby, 1990; Exley, 1980; MacDonald and Belkin, 2002; Mahood and Hildreth, 1983; Mariano, 1989; Michael, 1988; Miller and Mittlefehldt, 1982; Ni *et al*., 1995), whereas the HREE remain incompatible during this fractionation. Extended fractionation and final crystallisation then leads to the formation of distinct HREE-enriched phases (e.g., xenotime, Y-bearing fluorite, zircon etc.) and a change in REE patterns from typical rhyolite LREE-enriched patterns to HREE-enriched and slightly LREE-depleted patterns (e.g., Fig. 5.2).

The major REE and Y-bearing ore minerals are bastnäsite, monazite, xenotime, Y-bearing fluorite (also known as yttrofluorite, yttrocerite and cerfluorite; Pingitore *et al*., 2014) and allanite (Mariano, 1989). Bastnäsite (a readily processed REE carbonate) and monazite are the dominant REE ore minerals in the Bayan Obo deposit, and these ore minerals together with allanite account for most of the world's REE production (Mariano, 1989). A much more comprehensive list of the common REE-bearing minerals is provided in Hoatson *et al*. (2011).

5.4 Round Top – A HREE rhyolite REE resource

The most important of the known and prospective rhyolitic REE deposits is the Round Top Mountain rhyolite deposit (Texas, USA; Fig. 5.1), one of five Sierra Blanca rhyolite laccoliths in the Trans-Pecos area of Texas and the only rhyolite-hosted REE deposit with a NI43-101 compliant resource (Hulse *et al*., 2013). The deposit is currently owned by Texas Rare Earth Resources Corporation (Weng *et al*., 2013), and is hosted by a quartz-saturated peralkaline rhyolite intrusion that is significantly enriched in the HREE compared to the LREE. The deposit is a bulk tonnage (~1034 Mt) low-grade

(~305 ppm TREE + 220 ppm Y) but HREE-enriched (e.g., 57 ppm Yb; LREE/HREE = 0.81) REE deposit that is also associated with significant beryllium skarn mineralisation that will provide significant by-product credits, with further enrichment in Nb, Ta, Li, F, Sn, Rb, Th and U (Pingitore *et al*., 2014). The accessory minerals that host the REE are disseminated throughout the rhyolite and include LREE-enriched bastnasite and HREE-enriched cerfluorite, yttrofluorite and yttrocerite, all of which are extractable by a simple acid leach process.

5.5 The Kathleen Ignimbrite – a case example of HREE-enrichment associated with extended fractionation

The Mesoproterozoic 1071 ± 5 Ma Kathleen Ignimbrite (KI) of the west Musgrave Province of Western Australia (Fig. 5.1) formed during a large, caldera-forming felsic supereruption at ca. 1071 Ma and is hosted by a ~1 km thick well-preserved volcanic–sedimentary succession that covers an area of ~40 km^2. The KI (≤ 650 m) contains the ≤500 m thick intra-caldera, welded, rhyolitic Kurrparu Member, displaying well-defined fiamme and eutaxitic textures and a well-developed rheomorphic lava-like basal facies, and the thinner ≤100 m thick, rhyolitic interbedded ignimbrite and breccia dominated Karlaya Member. It is both under- and overlain by shallow-water turbiditic sediments, as well as being associated with large-volume coeval and comagmatic, subvolcanic rhyolite intrusions of the Rowland Suite (RS). Detailed descriptions of the field relationships, physical volcanology and palaeoenvironmental setting of these units are provided in Chapter 2.

The geochemistry, geochronology and petrogenesis of the KI and RS are discussed in Chapter 3, but are briefly summarised here. The rhyolitic ignimbrites (KI) and associated intrusive rhyolites (RS) are broadly geochemically similar to Miocene rhyolites from the Snake River Plain (SRP; Branney *et al*., 2008), USA, but contain higher concentrations of F (KI = ~0.50 wt%; up to 0.82 wt%) than SRP-type rhyolites (0.02–0.37 wt%; Ekren *et al*., 1984; Ellis, 2009), and in fact are more like the F-enriched (>0.2 wt%; Christiansen *et al*., 1986) topaz rhyolites of the western USA that are thought to be the extrusive equivalents of rapakivi granites (Christiansen *et al*., 2007). The KI and RS are evolved, A-type, metaluminous (to slightly peraluminous) high-silica rhyolites with elevated REE concentrations (e.g., 794 ppm TREE + 200 ppm Y and with 23 ppm Yb) relative to crustal abundances (Sun and McDonough, 1989; Wedepohl, 1995). These rhyolites formed during a failed intra-plate rifting event (Evins *et al*., 2010) related to the 1085–1040 Ma Giles Event (Glikson *et al*., 1996), which is associated with a >30 Ma period of felsic magmatism. This magmatism generated the silicic component of a likely large igneous province (LIP) in the west Musgrave Province that is temporally and spatially associated with the shorter duration emplacement Warakurna LIP (Smithies *et al*., 2014; Wingate *et al*., 2004).

The development of HREE enrichments relative to the LREE within highly felsic systems is outlined above and is well demonstrated in the KI and the associated RS. On-going extended fractionation from the more primitive RS to the more evolved KI preferentially increased HREE concentrations (Fig. 5.2a), whereas LREE concentrations decreased as a result of the fractionation of LREE-bearing minerals. This process also occurs in other highly evolved or differentiated felsic systems (e.g., Bacon *et al*., 1981; Christiansen *et al*., 1984; 1986; McCurry *et al*., 2008; Miller and Mittlefehldt, 1982; Webster *et al*., 1996).

The KI forms a prominent topographic feature, known as the Whitby Range, and is roughly 6.4 km^3 in volume, calculated from an outcrop area of 18.3 km^2 and an average thickness of 350 m; this, when combined with a typical rhyolite density of 2.52 g/cm^3 yields a minimum tonnage of ~2.54 Bt. This is a minimum estimate of the volume and tonnage of the deposit, which in reality would be significantly higher if faulted offsets of the KI are included; the original intracaldera volume of the KI is calculated to have been ~190 km^3 (Chapter 2). The average TREE grade of the deposit is ~580 ppm (Standard Deviation (SD) of 107 ppm; LREE/HREE = 3.24), with one sample having a TREE grade of 794 ppm (LREE/HREE = 5.09) and a few samples being preferentially HREE enriched up to ≥20% of the TREE budget. Therefore, although the KI is larger than Round Top, it is also lower grade and has lower HREE concentrations (Fig. 5.2b). However, there are probably sections within the KI (and the other rhyolites detailed below) that are preferentially HREE-enriched, and detailed sampling and analysis should be able to pinpoint these areas for mineral exploration. The REE mineralisation most likely occurs in the accessory minerals fluorite, apatite, titanite, allanite and zircon, and the KI is also enriched in U and Th, representing potential by-products at average concentrations of ~13 and ~70 ppm, respectively.

5.6 Other global occurrences of high-silica REE-enriched rhyolites

There are a number of global occurrences (Fig. 5.1) of large-volume high-silica rhyolites that are REE enriched, some of which are HREE-enriched (Fig. 5.3). Very few of these have been actively explored, meaning that the REE concentrations presented here are most likely a minimum, and further examination and exploration of these rhyolites would most likely identify areas that are preferentially HREE-enriched. This study provides an overview of some of these occurrences and summarise their REE potential in Table 5.1, with tonnages calculated using an assumed dry rock density of 2.52 g/cm^3 for all rhyolites.

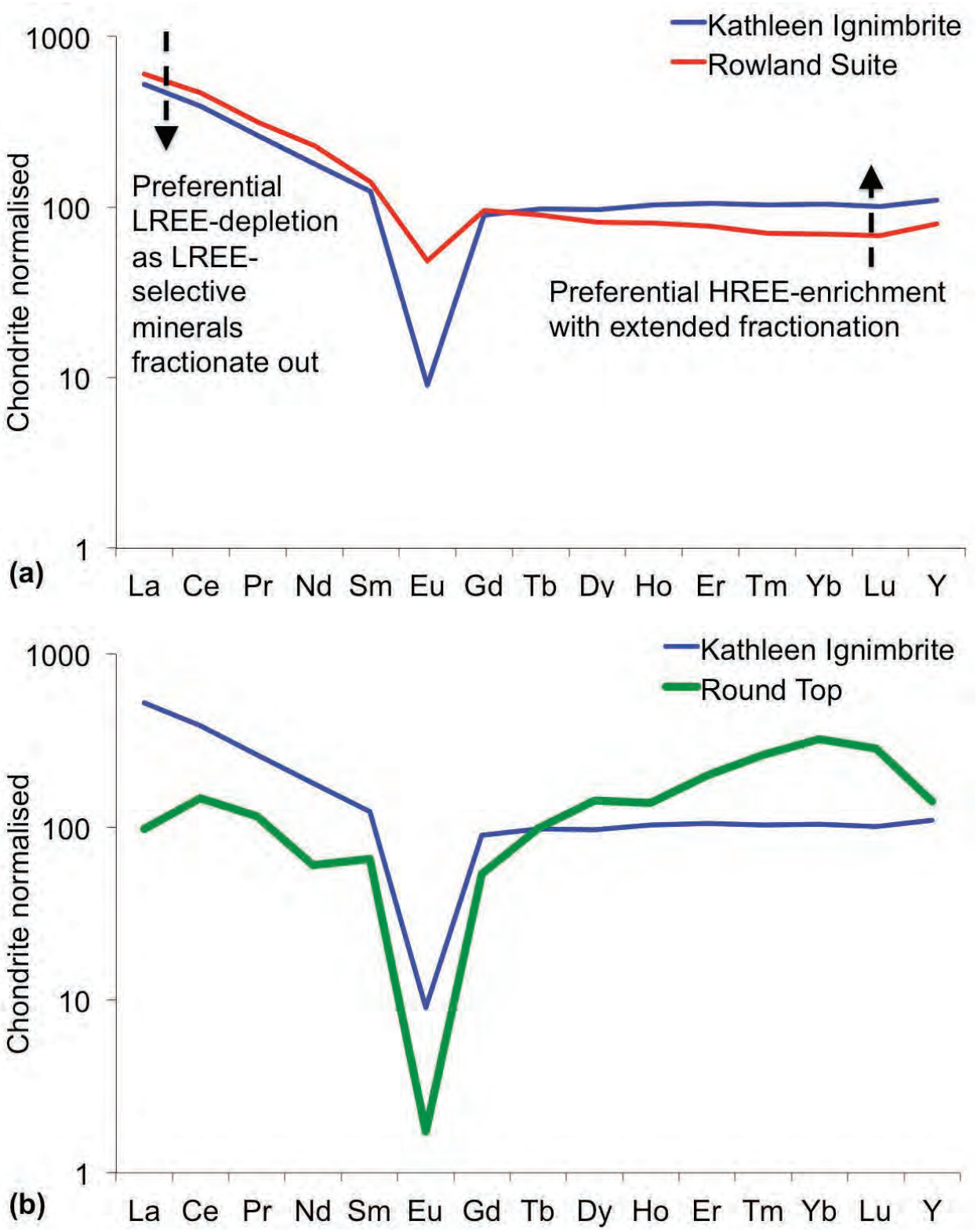

Figure 5.2: REE variation diagrams, chondrite normalised using Sun and McDonough (1989). a) REE variation diagram for the cogenetic KI and RS rhyolites showing the enrichment of the HREE relative to the LREE with extended fractionation from the slightly more primitive RS to the more evolved KI. b) REE variation diagram of the KI and Round Top deposits demonstrating the extreme HREE-enrichment in the Round Top rhyolite.

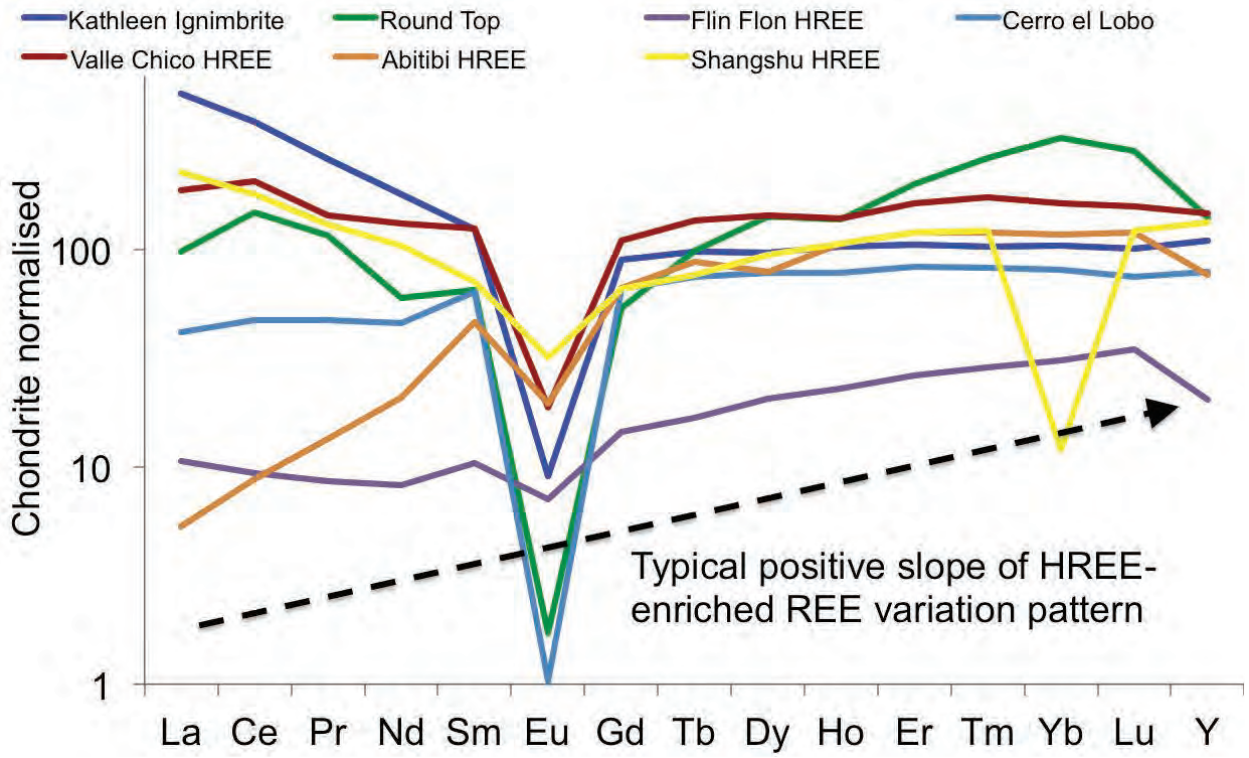

Figure 5.3: REE variation diagram of a few of the high-silica REE rhyolite occurrences worldwide showing variable HREE-enrichment and LREE-depletion in these types of rhyolites and the typical positive slope indicating HREE-enrichment on this type of diagram.

5.6.1 Topaz rhyolites of the western USA

Christiansen *et al*. (1986) presented a comprehensive overview of topaz rhyolites of the western USA and determined that these rhyolites are enriched in incompatible elements, have high REE concentrations, are typically HREE-enriched with flat chondrite-normalised REE variation diagram patterns relative to average rhyolites that have negative slopes on REE variation diagrams, and generally have high F concentrations. These topaz rhyolites include rhyolite lavas and tuffs from the Thomas Range in Utah that contain up to 283 ppm TREE (missing Pr, Gd, Dy, Ho, Er, Tm, + 75 ppm Y, and with 10 ppm Yb), up to 0.54 wt% F, and have more evolved sections that are HREE-enriched and somewhat LREE-depleted (LREE/HREE = 4.92). The volume estimates of Christiansen *et al*. (1984) and Turley and Nash (1980) yield an overall tonnage of ~19.84 Bt for the Thomas Range using the same rhyolite density as used for the KI. In comparison, the Spor Mountain rhyolites in Utah contain REE concentrations up to 291 ppm TREE (missing Pr, Gd, Dy, Ho, Er, Tm; + 135 ppm Y; 16 ppm Yb), have a LREE/HREE ratio of 6.25 and have F concentrations up to 1 wt% (Burt *et al*., 1982; Christiansen *et al*., 1984; 2007). The nearby Honeycomb Hills rhyolite domes contains up to 1.2 wt% F and up to 305 ppm TREE (missing Pr, Gd, Dy, Ho, Er, Tm; + 156 ppm Y; 32 ppm Yb; LREE/HREE = 4.22) with a combined tonnage of 60–198 Mt. Other examples of topaz rhyolites that are HREE-enriched and LREE-depleted are the Mineral Mountains of western Utah, numerous fluorine-rich rhyolite lava flows in the adjacent Wah Wah Mountains of Utah (Thompson,

Table 5.1: Details of some global REE rhyolite deposits, including volumes and/or tonnages, grades and other metal concentrations.

Deposit	Location	Deposit Type (Weng *et al.*, 2013)	Associated Mineralisation	Volume (km3)	Tonnage	TREE concentration (ppm)	TREE Status	Y (ppm)	Yb (ppm)	F (wt%)	LREE/HREE Ratio	References
Bayan Obo	Inner Mongolia, China	CAR	Fe, Nb		1460 Mt	~5-6% REO						Castor & Hedrick 2006; Drew *et al.*, 1990
Mountain Pass	California, USA	CAR			16.7 Mt	~8-9% REO						Olson *et al.*, 1954
Mt Weld	Australia	CAR			14.9 Mt	~10% REO						Weng *et a*l., 2013
Kathleen Ignimbrite	west Musgrave Province, Western Australia	G&R	U, Th	~6.4	2.54 Bt	794	Complete	200	23	0.82	3.24	Chapter 3
Round Top	Sierra Blanca Peaks, Texas	G&R	Li, Be, F, Zn, Rb, Y, Zr, Nb, Sn, Ta, Th	~4	1.03 Bt	305	Complete	220	57	1.3	0.81	Rubin *et al.*, 1987; Price *et al.*, 1990; Rubin 1990; McAnulty 1980
Thomas Range	west-central Utah	G&R			19.84 Bt	283	Missing Pr, Gd, Dy, Ho, Er, Tm	75	10	0.54	4.92	Christiansen *et al.*, 1984
Spor Mountain	west-central Utah	G&R	F, Be			291	Missing Pr, Gd, Dy, Ho, Er, Tm	135	16	1	6.25	Lindsey, 1977
Honeycomb Hills	west-central Utah	G&R	Be, Li, Cs, Rb	0.15-0.5	60-198 Mt	305	Missing Pr, Gd, Dy, Ho, Er, Tm	156	32	1.2	4.22	Congdon and Nash, 1988; 1991; Christiansen, 1986
Mineral Mountains	western Utah	G&R					Not reported					Thompson, 2002
Wah Wah, Needle Range and White Rock Mountains	SW Utah and Nevada	G&R	Mo, U				Not reported					Christiansen *et al.*, 1986; Keith *et al.*, 1986
Blackfoot volcanic field	SE Utah	G&R	Y, Th, U				Mostly incomplete	150	15	0.58	3.56	Christiansen *et al.*, 1986; Ford, 2005
Sierra Madre Occidental	northern Mexico	G&R	Sn, Hg, Sb, F	>3.9 x 10^5		459	Missing Pr, Nd, Gd, Dy, Ho, Er, Tm, Y		18	0.31	2.49	Huspeni *et al.*, 1984; Bryan *et al.*, 2008
Cerro el Lobo	Mexican tin rhyolite belt	G&R	Sn, F	0.1	39 Mt	146	Complete	124	14		0.79	Burt and Aguillon, 1988; Webster *et al.*, 1996
Cerro el Pajaro	Mexican tin rhyolite belt	G&R	Sn, F	1.2	476 Mt		Not reported					Webster *et al.*, 1997
Valle Chico	SE Uruguay	G&R				1000	Complete	230	28		1.57	Kirstin *et al.*, 2000; Lustrino *et al.*, 2005

Deposit	Location	Deposit Type (Weng *et al.*, 2013)	Associated Mineralisation	Volume (km3)	Tonnage	TREE concentration (ppm)	TREE Status	Y (ppm)	Yb (ppm)	F (wt%)	LREE/HREE Ratio	References
Abitibi Belt	Ontario–Quebec, Canada	VMS	Cu, Zn, Pb, Au, Ag			390	Complete	115	20	<0.2	0.18	Barrie *et al.*, 1993; Gaboury and Pearson, 2008
Shangshu Formation	south China	G&R				821	Complete	259	22		2.12	Li *et al.*, 2008; Wang and Li, 2003
Brockman	Halls creek Orogen, Western Australia	G&R	Nb			1736	Missing Pr, Gd, Dy, Er, Tm	575	42	1.48	0.11	Taylor *et al.*, 1995; Blake *et al.*, 1999; Ramsden *et al.*, 1993
Brockman Nb Tuff	Halls creek Orogen, Western Australia	G&R	Nb			517	Missing Pr, Gd, Dy, Er, Tm	1661	175	1.48	0.55	Taylor *et al.*, 1995; Blake *et al.*, 1999; Ramsden *et al.*, 1994
Taylor Creek	New Mexico, USA	G&R		0.58	230 Mt	215	Missing Pr, Dy, Ho, Er	128	17	3.9	3.45	Duffield and Ruiz, 1992; Duffield and Dalrymple, 1990; Webster and Duffield, 1991; 1994
Flin Flon	Manitoba-Saskatchewan, Canada	VMS	Sn, Zn, Cu, Au, Ag		62.4 Mt	122	Complete	61	8		0.55	Syme and Bailes, 1993; Syme, 1998; Syme *et al.*, 2000
Lower GRV	Gawler Range Volcanics, South Australia	G&R		>150		472	Complete	102	14	1.3	1.05	Agangi *et al.*, 2012; Allen *et al.*, 2008; McPhie *et al.*, 2011
Upper GRV	Gawler Range Volcanics, South Australia	G&R		>1000			Not reported					Agangi *et al.*, 2012; Allen *et al.*, 2008; McPhie *et al.*, 2012
Amram Massif	southern Israel	G&R		~4.5 (1% of 450 total)	~1.8 Bt	536	Complete	104	10		3.62	Mushkin *et al.*, 2003
SRP (REE data from ESRP)	Idaho, USA	G&R				488	Missing Pr, Gd, Dy, Ho, Er, Tm, Y		20	0.37	6.17	Ford, 2005
Olkaria Volcanic Complex (Naivasha rhyolites)	Kenya	G&R	Th, U, Y	13-15	5.2 Bt	780	Missing Pr; Dy; Ho; Er	296	35	0.95	4.61	Macdonald *et al.*, 1987; 2008; Marshall *et al.*, 2009

2002), and in the Needle Range and White Rock Mountains of SW Utah and Nevada, both of which are associated with the Pine Grove porphyry Mo deposit and numerous smaller U deposits and prospects (Christiansen *et al*., 1986; Keith *et al*., 1986). Topaz-bearing rhyolite lava domes also occur in the Blackfoot volcanic field on the edge of the eastern Snake River Plain of SE Utah. These rhyolites have high F content (0.35–0.58 wt%) and contain high concentrations of Y (>150 ppm; Christiansen *et al*., 1986; Ford, 2005), Th (27–60 ppm) and U (>15 ppm), with up to 15 ppm Yb (albeit without complete REE analyses).

5.6.2 Sierra Madre Occidental rhyolites

The voluminous high-silica rhyolites (flows, domes and ignimbrites) of the Sierra Madre Occidental (SMO) volcanic province of northern Mexico, which covers an area >500,000 km^2 (Bryan and Ernst, 2008) and has a estimated volume >3.9 x 10^5 km^3 (Bryan *et al*., 2008), are REE-enriched in a similar fashion to the KI and the Round Top deposit (up to 459 ppm TREE; missing Pr, Nd, Gd, Dy, Ho, Er, Tm, Y; 18 ppm Yb; Huspeni *et al*., 1984). The SMO reportedly contains >1000 small Sn mines and prospects (Foshag and Fries, 1942; Lee Moreno, 1972; Webster *et al*., 1996). Other rhyolites in the region are genetically associated with Hg, Sb, and fluorite deposits (Tuta *et al*., 1988). The extensive Mexican tin rhyolite belt forms part of the SMO and hosts a small volume, highly evolved tin rhyolite dome complex, Cerro el Lobo (Mexico), which contains up to 146 ppm TREE (+ 124 ppm Y; 14 ppm Yb) but is extremely HREE-enriched in terms of LREE/HREE ratios (LREE/HREE = 0.79; Webster *et al*., 1996) and has a tonnage of ~39 Mt calculated using the same density used for the KI tonnage calculation.

5.6.3 Valle Chico rhyolites

The volcanic section of the Cretaceous Valle Chico Igneous complex of SE Uruguay hosts highly evolved silica-saturated rhyolites that are HREE-enriched (230 ppm Y; 28 ppm Yb; LREE/HREE = 1.57). More primitive samples contain high REE concentrations but have higher LREE/HREE ratios, again showing the influence of fractionation (up to 1000 ppm; LREE/HREE = 4.52; Lustrino *et al*., 2005). This complex is linked with the formation of the ~800 000 km^3 Paraná–Etendeka Large Igneous Province and the first stages of the South Atlantic Ocean rifting, suggesting that more highly fractionated and HREE-enriched rhyolites may be present within silicic portions of this LIP (Kirstein *et al*., 2000; Lustrino *et al*., 2005).

5.6.4 Abitibi Belt rhyolites

REE-enriched high-silica rhyolites are present within the Abitibi Belt of Ontario and

Quebec, Canada; these rhyolites host >50% of the Cu-Zn-Pb-Au-Ag VMS deposits in this area and are characterised by high HFSE and HREE concentrations (up to 390 ppm TREE; + 115 ppm Y; 20 ppm Yb), with some extremely low LREE/HREE ratios (0.18) and low F concentrations (<0.2 wt%; Barrie *et al*., 1993; Gaboury and Pearson, 2008).

5.6.5 The Shangshu rhyolites

The Shangshu Formation rhyolites of northern Zhejiang Province, south China, are a 1786 m thick bimodal volcanic sequence that contains an upper ~1000 m of felsic rocks formed during intraplate magmatism associated with the rifting and break-up of Rodinia (Li *et al*., 2008; Wang and Li, 2003). This province contains high-silica rhyolites that are significantly enriched in the REE (up to 821 ppm TREE; + 259 ppm Y; 22 ppm Yb) and have low LREE/HREE ratios (2.12).

5.6.6 Brockman

The Brockman volcanics in the Halls Creek Mobile Zone (NW Australia) contain a rare-metal deposit hosted by a fluorite-bearing (up to 1.48 wt% F) rhyolitic volcaniclastic unit called the Niobium Tuff. Although these rhyolites (excluding the Niobium Tuff) are not as HREE enriched as some of the other rhyolites discussed above (LREE/HREE = 11), they exemplify the potential for these types of units to contain significant concentrations of a wide range of critical elements. They contain anomalously high concentrations of the REE (up to 1736 ppm TREE without Pr, Gd, Dy, Er, and Tm; + 575 ppm Y; 42 ppm Yb) and the Niobium Tuff is Nb-enriched (up to 3176 ppm) and extremely HREE-enriched (e.g., 1661 ppm Y; 175 ppm Yb; 517 ppm TREE; LREE/HREE = 0.55; Taylor *et al*., 1995a; 1995b).

5.6.7 Other HREE-enriched rhyolites

Several other HREE-enriched rhyolites have been documented in various areas; these rhyolites are not as significantly enriched in the HREE or TREE as the examples documented above, but may contain areas or regions that are enriched and are worthy of further investigation. The large volume (>55 km^3) variably F-enriched (0.15–3.9 wt%) Taylor Creek Rhyolite of New Mexico, USA, consists of a complex of lava domes and flows that contain evolved areas which are HREE-enriched, including one particular rhyolite unit (RDM) that contains 215 ppm TREE (with Pr, Dy, Ho, and Er data missing; + 128 ppm Y; 17 ppm Yb; LREE/HREE = 3.45) and has a tonnage of 230 Mt (Duffield and Ruiz, 1992; Duffield and Dalrymple, 1990; Webster and Duffield, 1991; 1994). The Flin Flon Belt of Manitoba and Saskatchewan in Canada also hosts some high-silica ore-bearing rhyolites that are stratigraphically associated with Zn-Cu-Au-Ag VMS deposits (Syme, 1998; Syme

and Bailes, 1993; Syme *et al*., 2000). These rhyolites are HREE-enriched compared to the LREE (avg. LREE/HREE = 1.95, with one sample 0.55) and have flat REE patterns, but have generally low TREE (up to 122 ppm TREE).

5.7 Regions containing large volume LREE-enriched rhyolites

Large volumes (e.g., the >150 km^3 lower Gawler Range Volcanics [GRV] and the >1000 km^3 upper GRV) of high-silica extrusive rhyolite lavas and ignimbrites occur in the GRV of South Australia and form part of a silicic LIP (SLIP; Agangi *et al*., 2012; Allen *et al*., 2008; McPhie *et al*., 2011). These provinces have areal extents of >0.1 Mkm^3, and extrusive magmatic volumes >0.25 Mkm^3, and >80% of the GRV is dacitic-rhyolitic in composition (Bryan, 2007). Agangi *et al*. (2010) demonstrated that the high REE, Y, HFSE, Rb and F concentrations within the GRV are the result of the precipitation of accessory minerals such as zircon, REE-F-carbonate, Ti oxide, apatite and titanite. The high fluorine concentrations (≤1.3 wt%) within the melts that formed these magmas meant that the REE behaved incompatibly during magmatic crystallisation and were preferentially enriched in volatile-rich late-stage magmatic fluids that deposited REE-bearing minerals in vesicles, micromiaroles and interstices within GRV rhyolites, thus enriching these rhyolites in the REE (up to 472 ppm TREE; + 102 ppm Y; 14 ppm Yb). Although the GRV units are LREE- rather than HREE-enriched, the processes that led to these enrichments provide key insights into the formation of REE enriched rhyolites both here and elsewhere (e.g., Agangi *et al*., 2012) and the massive volume of the GRV means that this area may well contain rhyolites that are TREE or HREE enriched.

Some high-silica rhyolite samples from the alkaline magmatic Amram Massif of southern Israel that formed during extended fractionation are REE-enriched (up to 536 ppm TREE; + 104 ppm Y; 10 ppm Yb; LREE/HREE = 3.62) but are generally LREE- rather than HREE-enriched (Mushkin *et al*., 2003). The volume of A-type rocks within the Amram Massif is ~450 km^3, meaning that if only 1% of this volume was REE-enriched, this might represent some 1.78 Bt at concentrations >500 ppm TREE.

Large volumes of SRP-type high-silica rhyolites also occur in Idaho, USA, where they are present as ignimbrites and lavas within the Snake River Plain (SRP). They are generally LREE-enriched and have fairly low fluorine concentrations as previously mentioned, although the total REE concentrations and LREE/HREE distributions of these rhyolites are still unknown due to mostly incomplete REE data. Ellis *et al*. (2013) commented that that no LREE accommodating minerals, such as allanite, chevkinite or monazite, have been documented in the central SRP rhyolites, and therefore no LREE-depletion or subsequent HREE-enrichment is observed within these rhyolites. However, McCurry *et al*. (2008) found that very evolved rhyolites (>70% SiO_2) from the Eastern SRP have the reverse of the typical LREE-enriched patterns found elsewhere within the SRP;

these samples have unusually low LREE/HREE ratios that correlate with the appearance of chevkinite at Cedar Butte and East Butte, suggesting that some of these rhyolites may be HREE enriched. The eastern SRP rhyolites appear to have high REE concentrations (up to 488 ppm TREE; missing Pr, Gd, Dy, Ho, Er, Tm, Y; 20 ppm Yb; Ford, 2005).

5.7.1 Kenyan high-silica rhyolites

High-silica and F-enriched (avg. 0.64 wt%) peralkaline comendite rhyolites of East African Rift Valley of Kenya form part of the Greater Olkaria Volcanic Complex (previously referred to as the Naivasha complex) that contains 13–15 km^3 of erupted rhyolites (Macdonald *et al*., 2008; Marshall *et al*., 2009). These rhyolites contain extremely high REE concentrations (up to 780 ppm TREE but missing Pr, Dy, Ho and Er; + 296 ppm Y; 35 ppm Yb) and are variably HREE-enriched (LREE/HREE = 4.61; Macdonald *et al*., 1987). These rhyolites represent some ~5.2 Bt of REE-enriched material that is also Th and U enriched (up to 124 and 25 ppm, respectively), calculated using the same density assumed for the KI. The potential of this area is exemplified by some samples presented by Marshall *et al*., (2009) that contain even higher concentrations of some individual elements (e.g., Y up to 507 ppm; Nb up to 1022 ppm).

5.8 REE ore deposit potential and grade-tonnage comparisons

Many of the rhyolites discussed above are missing the full set of REE concentrations, primarily as in the past these elements were not always routinely analysed; as such, this study utilises Yb in various plots. The use of Yb is two fold, one as a proxy for HREE concentrations as the concentration of this element was determined for the vast majority of the rhyolites discussed here, and two as a proxy for TREE concentrations, as Yb concentrations are also proportional to TREE concentrations. This allows us to compare these rhyolites to each another and to other known REE ore deposits. To demonstrate relative HREE-enrichment, the NI43-101 certified Round Top deposit will be used as the type example of a rhyolitic REE deposit. Rhyolites with higher REE concentrations than Round Top and LREE/HREE ratios <1 (i.e. enriched in the HREE) should be considered the most prospective of these high-silica rhyolites, although as discussed above the vast majority of these rhyolites are worthy of further investigation. Figure 5.4a shows that the majority of the high-silica rhyolites are slightly LREE-enriched (LREE/HREE ratios >1) and have high REE concentrations that may mean that these could be prospective for LREE-dominated mineralisation. However, these rhyolites are probably less economically viable than the HREE-enriched rhyolites, primarily as a function of the relative value of the HREE versus the LREE. In addition, the majority of these rhyolites are not fully characterised, and therefore the majority of these occurrences have TREE and HREE concentrations that are erroneously low. Finally, these figures do not include Y, which, as stated earlier, is routinely incorporated in the mining industry and reported in TREE concentrations.

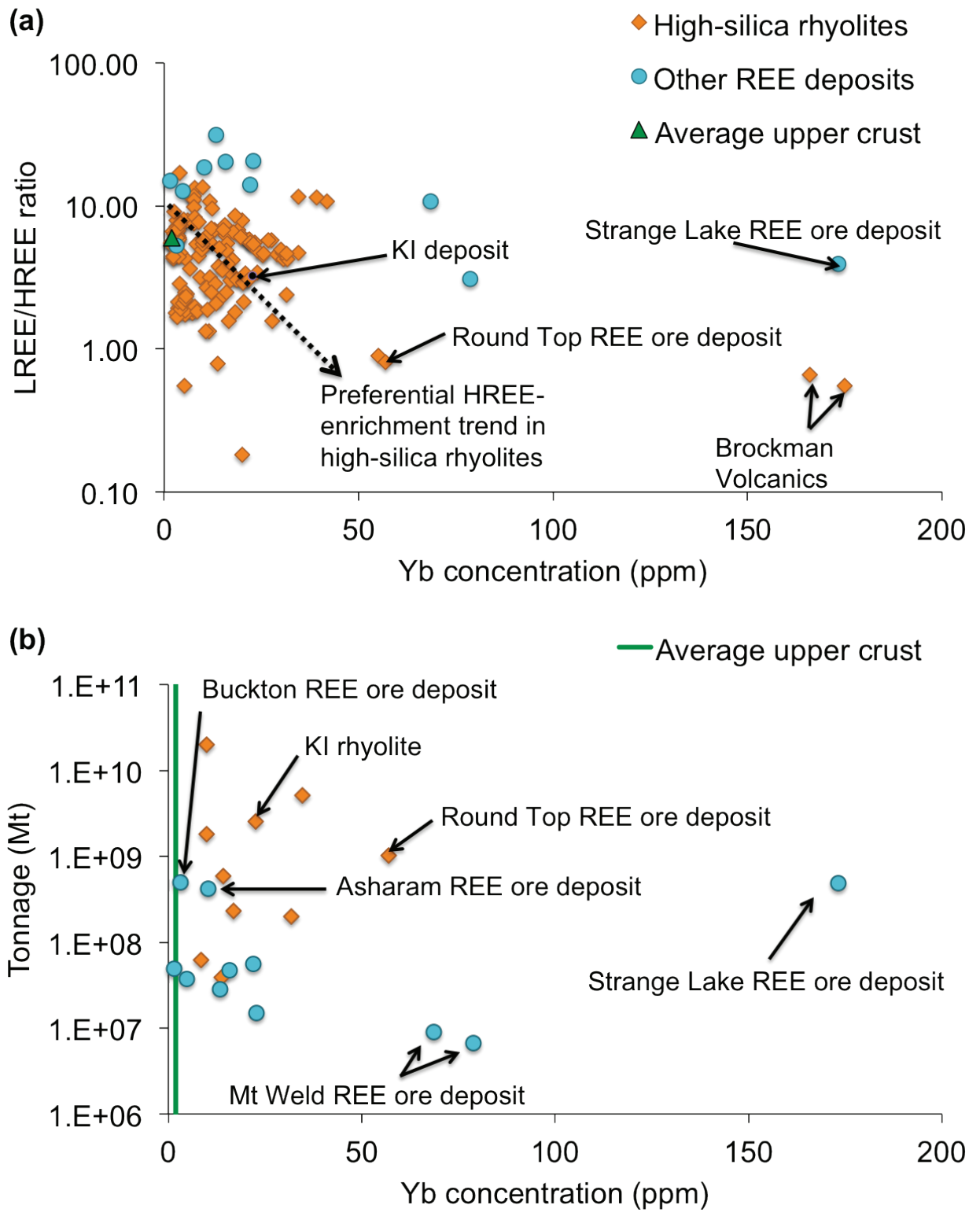

Figure 5.4: a) Plot demonstrating the HREE-enrichment of high-silica rhyolites compared to some known REE ore deposits, from Weng *et al*. (2013), using the LREE/HREE ratio. b) REE concentration–tonnage plot showing some high-silica rhyolites and a few REE ore deposits, for which tonnages are known (from Weng *et al*. 2013), demonstrating the bulk tonnage nature of high-silica rhyolite deposits compared to the other known REE ore deposits. Yb concentration is used as a proxy for both TREE concentration and indicator of HREE-enrichment due to incomplete REE sets in the high-silica rhyolites.

The approximate TREE concentrations and tonnages of the high-silica rhyolites discussed above are shown in Fig. 5.4b; this figure indicates that a significant number of high-silica rhyolites are HREE-enriched and their overall tonnages are often greater than other types of REE deposits. This suggests that if effective mineral processing approaches can be outlined (as has been done at Round Top), these rhyolites may represent future low-grade, but high-volume or bulk-tonnage sources of the REE and other critical elements, especially the HREE.

5.9 Mineralogical barriers and considerations for recovery in REE deposits

Skinner (1976) formalised the 'mineralogical barrier' concept for geochemically scarce metals (Fig. 5.5), indicating the importance of mineralogy to mineral processing and the economic recovery of metals. In this concept there is a point when energy costs make extraction of a given metal from a given mineral or minerals prohibitively expensive (for example Ni from olivine), an extremely important consideration in terms of discussing the economic potential of low-grade REE resources. Efficient extraction from a potentially economic REE resource is strongly dependent on the REE mineralogy of the deposit (Castor and Hedrick, 2006; Jordens *et al*., 2013), and this could be a significant constraint on the viability of REE extraction from the high-silica rhyolites outlined above. In addition, the vast majority of demand for the REE is as single high-purity pure REE products, meaning that the wide range of REE substitutions within various minerals, even within a single deposit, could create difficulties in processing, concentration and extraction. REE extraction and processing is often a deposit-specific challenge, with solutions having to be tailored to each deposit, adding to the complexity and variability of REE recovery as opposed to more conventional mining operations involving sulphide or oxide mineralisation (e.g., Cu, Ni, Au, Ag, PGE, etc.; Weng *et al*., 2013). Minerals that are easily broken down, such as bastnäsite, or minerals that are easy to concentrate because of their coarse grain size, different density, or other attributes, are more desirable than those that are difficult to dissociate, such as allanite or monazite. The latter also contains high concentrations of Th, meaning that any monazite that is left in mining or processing waste may be considered a potentially hazardous radioactive waste product (Castor and Hedrick, 2006). However, one positive consideration is that coarse-grained zones within highly evolved rhyolites are often preferentially HREE- and REE-enriched; these textures often occur in porphyritic rhyolites and slow-cooled rhyolite intrusions, including both the KI and the RS. In comparison, finer-grained rhyolites with faster cooling rates and finer crystalline textures, such as lavas, would have a more even distribution of REE, which could be either deleterious or advantageous for processing depending on the mineralogy present (e.g., Round Top).

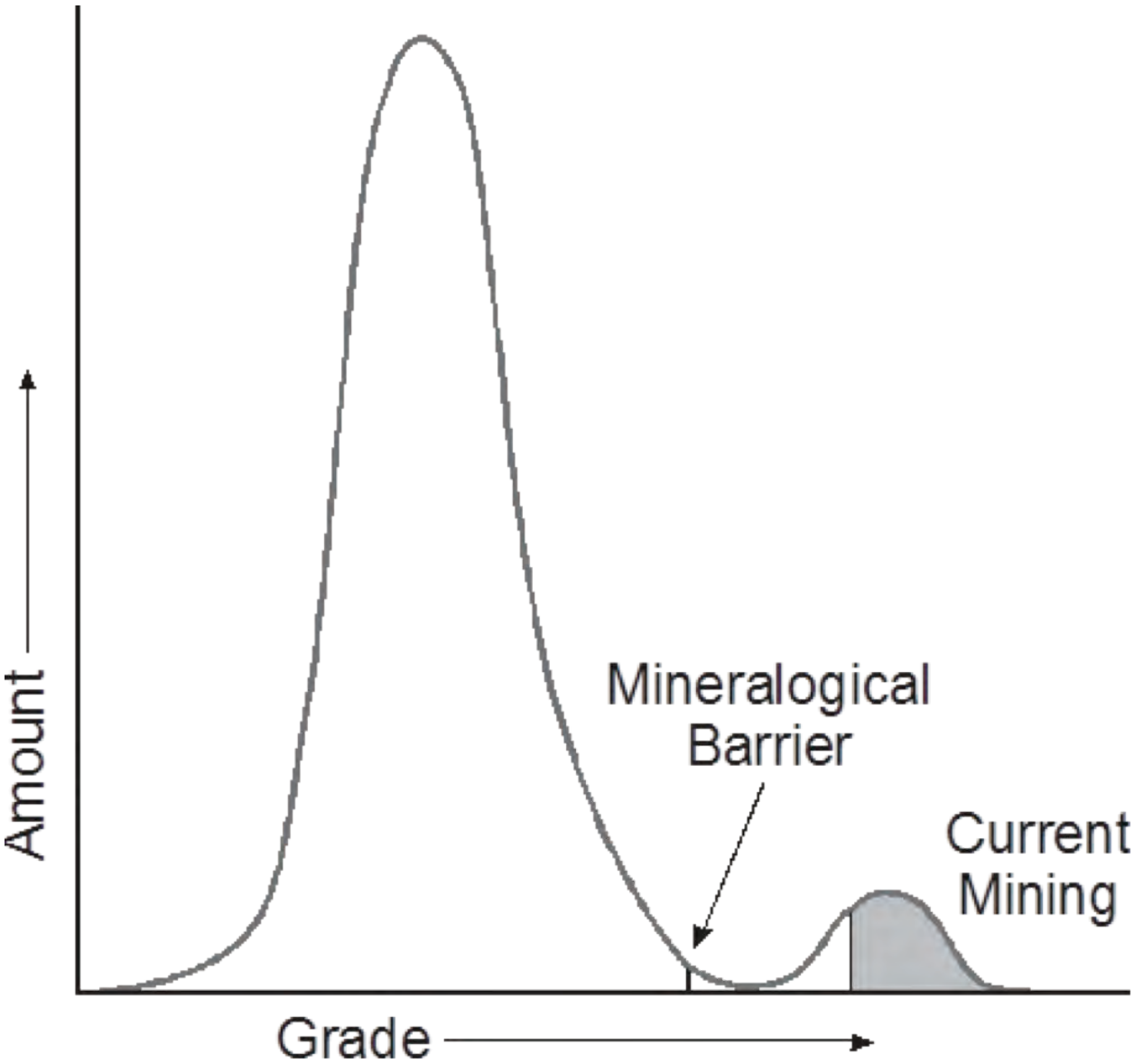

Figure 5.5: The "mineralogical barrier" diagram. A conceptual view of grade versus contained metal for geochemically scarce metals, current mining and the 'mineralogical barrier' (redrawn from Skinner, 1976). This graph demonstrates that deposits containing low grades of a particular resource are strongly cost dependent on the extraction and recovery of ore, which increases exponentially with lower grades.

Many of the issues outlined in the paragraph above in terms of processing of rhyolitic REE mineralisation may not be applicable to these rhyolites. For example, the Round Top deposit returned a recovery percentage in excess of 70% REE (TREE+Y; Hulse *et al*., 2013) during metallurgical feasibility studies. These studies investigated viable REE processing, extraction and recovery methods in this particular type of REE mineral deposit. These included crushing, dispersion and attrition, gravity, magnetic separation, flotation, acid bakes and leaching, liquid separation, chemical treatments and selective removal of U, Th and the REE. The most effective methods appear to be crushing and a simple heap leaching process, primarily as the Y-bearing fluorite, bastnäsite, xenotime and monazite minerals that host the REE in the Round Top deposit (and potentially in other highly evolved rhyolites) are soluble in dilute sulphuric acid at room temperature. Further solvent extraction by conventional and commercial Chinese-designed metal

separation technology is able to remove impurities, recover, concentrate and produce individual HREE single-elements products and a mixed LREE product (Pingitore *et al*., 2014). Accessory metal by-products such as U, Th, Fe and Al could also either be sold or disposed of by environmentally acceptable methods. Similar readily soluble REE-F-carbonate host minerals occur in other high-silica REE-enriched rhyolites (e.g., Agangi *et al*., 2010), indicating that as this metallurgical process is considered to be viable for the Round Top deposit there is no reason why a similar extraction and recovery process cannot be applied to other high-silica REE-enriched rhyolite deposits, such as the KI, where similar soluble minerals are likely to host the HREE.

5.10 The need for late stage magmatic-vapour phase crystallisation?

Price *et al*. (1990) suggested that late stage magmatic-hydrothermal vapour phase crystallisation affected the Round Top rhyolite deposit and that this process may have caused some of the extreme HREE-enrichments present within this rhyolite. In addition, London *et al*. (1988) demonstrated that the HREE are more soluble in a vapour phase than the LREE, and therefore this process could be responsible for sufficient enrichment and concentration of HREE to upgrade a rhyolite to economic concentrations of the HREE. It is unclear whether this process means that the Round Top deposit is fairly unique compared to the other high-silica REE-enriched rhyolites (as reflected by the HREE concentrations within this deposit; Fig. 5.4), or whether this process may have affected some or the majority of high silica rhyolites.

This quandary is exemplified by the presence of fluorite and gas-rich shear partings within the KI (Chapter 2; Chapter 4), which indicate that vapour phase crystallisation also occurred within this deposit, potentially leading to the HREE enrichments in this unit (Fig. 5.4b). Vapour phase crystallisation within the KI is primary magmatic and is related to the original KI magma rather than being a very late-stage secondary hydrothermal alteration process. It is therefore possible that the same upgrading process described by Price *et al*., (1990) and demonstrated by London *et al*. (1988), may also have taken place in the KI, increasing the enrichment of the HREE that was already present as a result of the primary extended fractionation process described above. This process of vapour phase HREE-enrichment relative to the LREE also occurs in the small volume (0.1 km^3) Sn- and F-mineralised Cerro el Lobo topaz rhyolite dome complex of the Mexican Tin rhyolite belt (Webster *et al*., 1996; Webster and Rebbert, 1998). This deposit is not significantly REE-enriched, but the extensive nature of the Mexican tin rhyolite belt means further exploration in this area is warranted to determine whether this region hosts HREE-enriched rhyolites.

Another important factor in the formation of high-silica rhyolites with high REE concentrations and preferential HREE enrichments (e.g., Round Top, Brockman, Spor Mountain; Honeycomb Hills) is the presence of high fluorine concentrations (1.3, 1.48,

1.25 and 0.61 wt% F, respectively). This link has been previously proposed (e.g., Agangi *et al*., 2010; Keppler, 1993; McPhie *et al*., 2011), and it is known that incompatible elements, such as the REE, have increased solubilities in melts containing F, with mineralisation intimately associated with such F-bearing fluids (e.g., Eppinger and Closs, 1990; Keppler, 1993). In addition, topaz rhyolites by definition are enriched in F (Burt *et al*., 1982; Christiansen *et al*., 1986), further demonstrating the link between REE-enrichment and high F concentrations. This may also be responsible for the lack of HREE- and REE-enriched rhyolites within the SRP, as the magmas in this area generally have low F contents compared to other areas discussed here.

Regardless of whether rhyolite hosted REE-deposits are specifically HREE-enriched through viable primary enrichment processes or secondary upgrading processes, these deposits are generally REE-enriched to a certain degree and remain viable prospects for REE exploration, primarily as a result of their extensive volumes (Fig. 5.4a) and their high HREE concentrations (Fig. 5.4b).

5.11 Exploration for high-silica rhyolite-hosted HREE deposits

High-silica rhyolites with A-type geochemical affinities tend to form in extensional tectonic environments with sustained high heat flow (Bonin, 2007; Dall'Agnol *et al*., 2012; Whalen *et al*., 1987). The HREE- and REE- enriched rhyolites discussed here represent the most evolved suites or units within an area (e.g., the KI; Chapter 3), favouring a model whereby REE- and HREE-enrichment is related to extended fractionation. In addition, the correlation between high-F contents and REE-enrichment and/or mineralisation (e.g., Christiansen *et al*., 1984) indicates that a possible exploration model involving extensional environments, rhyolitic volcanism (often a bimodal association), and the presence of highly differentiated and evolved suites with elevated F concentrations may be a useful approach for rhyolite-hosted REE mineralisation. Areas that host voluminous felsic suites, such as SLIPs, would be good targets, primarily as SLIP-forming events produce large volume rhyolitic volcanism. The rhyolitic products of SLIPS are more likely to contain high-F units (e.g., Pankhurst *et al*., 2011; Agangi *et al*., 2012), which in turn are also more likely to be REE- and HREE-enriched, and in addition may have undergone vapour phase magmatic HREE upgrading.

5.11.1 Implications for mineral exploration

5.11.1.1 Positive aspects

The fact that these rhyolites have potential for bulk tonnage extraction means that they ideally need to be located in surface or near-surface environments to facilitate

surface mining operations. The bulk of these deposits contain unreactive and insoluble feldspar and quartz gangue material that would aid recovery by acid leaching. Some of these rhyolites can be quite extensive deposits, with some lavas and ignimbrites formed during voluminous super-eruptions (i.e. >1000 km^3 of extruded material, if all preserved), which increases the prospectivity of these rhyolites to be large bulk tonnage sources of low grade REE. These rhyolites are also mineralogically homogenous, aiding mineral processing (e.g., Round Top and KI).

These high-silica rhyolites often host significant potential by-product mineralisation, including the association between topaz rhyolites and belts of fluorite and silver–base metal, tungsten and Climax- and Henderson-type topaz-rich porphyry Mo-W mineralisation (Burt *et al*., 1982). Large Be deposits (as bertrandite), small deposits of U and F, and sub-economic occurrences of red beryl, Li, Cs, and Sn are also directly related to topaz rhyolites, including the Be (Li–F–U) mineralised cogenetic tuff that underlies underlying the Spor Mountain rhyolite (Christiansen *et al*., 2007) and Be mineralisation in tuffs associated with the Honeycomb Hills (Christiansen *et al*., 1986). The KI is associated with a Giles event aged tourmaline breccia in the upper Mount Palgrave Group of the West Musgrave Province of central Australia (Howard *et al*., 2011), and high-silica rhyolites within the GRV are associated with hydrothermal breccias that host the world's largest hydrothermal ore deposit, Olympic Dam, a supergiant Fe oxide Cu-U-Au-Ag ore deposit (~9 x 10^9 t) that is also enriched in REE and F (McPhie *et al*., 2011). Finally, the Round Top deposit is associated with Be mineralised skarn deposits that occur along the base of the rhyolite laccolith (Price *et al*., 1990). The rhyolites in the Sierra Madre Occidental region are also genetically associated with Hg, Sb and fluorite deposits (Tuta *et al*., 1988), and rhyolites in the Abitibi Belt are also associated with volcanic rocks that host both VMS mineralisation and important Ni-Cu-PGE sulphide deposits (Barrie *et al*., 1993). All of this associated mineralisation either represents important by-products of potential REE mineralisation, or indicates that REE mineralisation may be an important by-product of other types of mineralisation and should be considered during exploration for these other commodities.

5.11.1.2 Negative aspects

Weng *et al*. (2013) give a thorough review of the environmental aspects and challenges that are involved in efficient extraction and processing of REE mining. This includes the significant use of chemicals and associated liquid wastes treatment and management, presence of high Th and U concentrations in REE ores and concentrates as well as the radioactive nature of some of the refining wastes, corrosive fluorine-bearing gases and other emissions, and the occupational and public health risks associated with these various concerns. Furthermore the intensive processing of REE ores and the

individual element extraction or refining involved is a major concern for REE mining, making it expensive, highly variable and difficult, with little published literature on the full lifecycle of REE mining as compared to other mining operations (e.g., porphyry Cu deposits), making this type of mining fairly new and unchartered territory. These negative implications need to be seriously considered when assessing the economic potential of the high-silica REE-enriched rhyolite deposits discussed here, even though they may be preferentially enriched in the favourable and more valuable HREE. However, one potential advantage of this type of mineralisation is that the REE may be more readily extractable than from other types of REE deposit, as has been discussed for Round Top above and may also apply to other rhyolites, such as the KI.

5.12 Limitations and future work

Until now, these highly fractionated rhyolite deposits, have not been significantly considered for their REE potential and much of the data in the literature and presented here is incomplete (e.g., missing key elements) or lacking important grade estimate criteria (e.g., volumes, tonnages, measured densities, etc.), and very little is known about these potentially highly prospective units. Much more detailed sampling and geochemistry is needed on all of these and other rhyolites before the true REE potential of these highly fractionated rhyolites is realised.

5.13 Conclusions

Highly fractionated REE-enriched rhyolites have the potential to be the bulk-tonnage, low-grade porphyry Cu deposits of the REE world. The fact that the magmatic processes that form these rhyolites naturally lead to HREE enrichments during extended fractionation, and the generally favourable host mineralogy of deposits such as Round Top, means that these rhyolites may be an important future source of the REE and especially the HREE. It is possible that late stage magmatic processes, such as vapour phase crystallisation, may be required to further significantly enrich these deposits in the HREE in order to upgrade them to potential economic ore bodies and that high fluorine contents are necessary for REE enrichment. Further work needs to be undertaken to determine whether these are necessary additional processes or whether the primary extended fractionation process that dominates the petrogenesis of these highly fractionated high-silica REE rhyolites is sufficient to produce potentially economic HREE and REE mineralisation.

5.14 Acknowledgements

The Ngaanyatjarra Council and their people are thanked for the privilege of working in their shire and providing a unique opportunity to work on these rocks. I acknowledge

the Geological Survey of Western Australia (GSWA) for funding and logistical support and the Monash Volcanology Research Group (MonVolc) for research collaboration and additional funding. I also would like to thank various GSWA field assistants, laboratory staff at Monash University and Gavin Mudd for providing some figures.

5.15 References

Agangi, A., Kamenetsky, V. S., and McPhie, J., 2010. The role of fluorine in the concentration and transport of lithophile trace elements in felsic magmas: insights from the Gawler Range Volcanics, South Australia: Chemical Geology, 273: 314-325.

Agangi, A., Kamenetsky, V. S., and McPhie, J., 2012. Evolution and emplacement of high fluorine rhyolites in the Mesoproterozoic Gawler silicic large igneous province, South Australia: Precambrian Research, 208-211: 124-144.

Allen, S. R., McPhie, J., Ferris, G., and Simpson, C., 2008. Evolution and architecture of a large felsic Igneous Province in western Laurentia: The 1.6 Ga Gawler Range Volcanics, South Australia: Journal of Volcanology and Geothermal Research, 172: 132-147.

Anderson, J. L., and Morrison, J., 2005. Ilmenite, magnetite, and peraluminous Mesoproterozoic anorogenic granites of Laurentia and Baltica: Lithos, 80: 45-60.

Bacon, C. R., Macdonald, R., Smith, R. L., and Baedecker, P. A., 1981. Pleistocene high-silica rhyolites of the Coso Volcanic Field, Inyo County, California: Journal of Geophysical Research: Solid Earth (1978–2012), 86: 10223-10241.

Barrie, C. T., Ludden, J. N., and Green, T. H., 1993. Geochemistry of volcanic rocks associated with Cu-Zn and Ni-Cu deposits in the Abitibi subprovince: Economic Geology, 88: 1341-1358.

Bonin, B., 2007. A-type granites and related rocks: evolution of a concept, problems and prospects: Lithos, 97: 1-29.

Branney, M. J., Bonnichsen, B., Andrews, G. D. M., Ellis, B., Barry, T. L., and McCurry, M., 2008. 'Snake River (SR)-type' volcanism at the Yellowstone hotspot track; distinctive products from unusual, high-temperature silicic super-eruptions: Bulletin of Volcanology, 70: 293-314.

Bryan, S., 2007. Silicic large igneous provinces: Episodes, 30: 20-31.

Burt, D. M., Sheridan, M. F., Bikun, J. V., and Christiansen, E. H., 1982. Topaz rhyolites; distribution, origin, and significance for exploration: Economic Geology and the Bulletin of the Society of Economic Geologists, 77: 1818-1836.

Castor, S. B., and Hedrick, J. B., 2006. Rare earth elements: Industrial Minerals volume, 7th edition: Society for Mining, Metallurgy, and Exploration, Littleton, Colorado: 769-792.

Chakhmouradian, A. R., and Wall, F., 2012. Rare earth elements: Minerals, mines,

magnets (and more): Elements, 8: 333-340.

Chakhmouradian, A. R., and Zaitsev, A. N., 2012. Rare earth mineralization in igneous rocks: Sources and processes: Elements, 8: 347-353.

Christiansen, E. H., Bikun, J. V., Sheridan, M. F., and Burt, D. M., 1984. Geochemical evolution of topaz rhyolites from the Thomas Range and Spor Mountain, Utah: American Mineralogist, 69: 223-236.

Christiansen, E. H., Burt, D. M., Sheridan, M. F., and Wilson, R. T., 1983. The petrogenesis of topaz rhyolites from the Western United States: Contributions to Mineralogy and Petrology, 83: 16-30.

Christiansen, E. H., Haapala, I., and Hart, G. L., 2007. Are Cenozoic topaz rhyolites the erupted equivalents of Proterozoic rapakivi granites? Examples from the Western United States and Finland: Lithos, 97: 219-246.

Christiansen, E. H., Sheridan, M. F., and Burt, D. M., 1986. The geology and geochemistry of Cenozoic topaz rhyolites from the Western United States, Geological Society of America (GSA), Boulder, CO, United States, 82 p.

Creaser, R. A., Price, R. C., and Wormald, R. J., 1991. A-type granites revisited; assessment of a residual-source model: Geology (Boulder), 19: 163-166.

Dall'Agnol, R., Frost, C. D., and Rämö, O. T., 2012. IGCP Project 510 “A-type Granites and Related Rocks through Time”: Project vita, results, and contribution to granite research: Lithos, 151: 1-16.

Drew, L. J., Qingrun, M., and Weijun, S., 1990. The Bayan Obo iron-rare-earth-niobium deposits, Inner Mongolia, China: Lithos, 26: 43-65.

Duffield, W. A., and Ruiz, J., 1992. Compositional gradients in large reservoirs of silicic magma as evidenced by ignimbrites versus Taylor Creek Rhyolite lava domes: Contributions to Mineralogy and Petrology, 110: 192-210.

Duffield, W. A., and Dalrymple, G. B., 1990. The Taylor Creek Rhyolite of New Mexico: a rapidly emplaced field of lava domes and flows: Bulletin of Volcanology, 52: 475-487.

Eby, G. N., 1990. The A-type granitoids; a review of their occurrence and chemical characteristics and speculations on their petrogenesis: Lithos, 26: 115-134.

Ekren, E. B., McIntyre, D. H., and Bennett, E. H., 1984. High-temperature, large-volume, lavalike ash-flow tuffs without calderas in southwestern Idaho, U. S. Geological Survey, Reston, VA, United States, 76 pp.

Ellis, B. S., Wolff, J. V., Boroughs, S., Mark, D., Starkel, W., and Bonnichsen, B., 2013. Rhyolitic volcanism of the central Snake River Plain: a review: Bulletin of Volcanology, 75: 1-19.

Ellis, B. S., 2009. Rhyolitic explosive eruptions of the central Snake River Plain, Idaho: investigations of the lower Cassia Mountains succession and surrounding areas: Unpub. PhD thesis, University of Leicester.

Eppinger, R. G., and Closs, L. G., 1990. Variation of trace elements and rare earth

elements in fluorite; a possible tool for exploration: Economic Geology, 85: 1896-1907.

Evins, P. M., Smithies, R. H., Howard, H. M., Kirkland, C. L., Wingate, M. T. D., and Bodorkos, S., 2010. Devil in the detail; the 1150-1000 Ma magmatic and structural evolution of the Ngaanyatjarra Rift, west Musgrave Province, central Australia: Precambrian Research, 183: 572-588.

Exley, R., 1980. Microprobe studies of REE-rich accessory minerals: implications for Skye granite petrogenesis and REE mobility in hydrothermal systems: Earth and Planetary Science Letters, 48: 97-110.

Ford, M. T., 2005. The petrogenesis of Quaternary rhyolite domes in the bimodal Blackfoot volcanic field, southeastern Idaho, Idaho State University.

Foshag, W. F., and Fries, C., 1942. Tin deposits of the Republic of Mexico: U. S. Geological Survey Bulletin, 935-C: 99-176.

Frindt, S., Trumbull, R. B., and Romer, R. L., 2004. Petrogenesis of the Gross Spitzkoppe topaz granite, central western Namibia; a geochemical and Nd-Sr-Pb isotope study: Chemical Geology, 206: 43-71.

Gaboury, D., and Pearson, V., 2008. Rhyolite geochemical signatures and association with volcanogenic massive sulfide deposits: examples from the Abitibi Belt, Canada: Economic Geology, 103: 1531-1562.

Glikson, A. Y., Stewart, A. J., Ballhaus, C. G., Clarke, G. L., Feeken, E. H. J., Leven, J. H., Sheraton, J. W., and Sun, S. S., 1996. Geology of the western Musgrave Block, central Australia, with particular reference to the mafic-ultramafic Giles Complex: Bulletin - Australian Geological Survey Organisation, 239 pp.

Haapala, I., 1997. Magmatic and postmagmatic processes in tin-mineralized granites; topaz-bearing leucogranite in the Eurajoki Rapakivi granite stock, Finland: Journal of Petrology, 38: 1645-1659.

Haapala, I., and Rämö, O. T., 1992. Tectonic setting and origin of the Proterozoic rapakivi granites of southeastern Fennoscandia: Special Paper - Geological Society of America, 272: 165-171.

Hatch, G. P., 2012. Dynamics in the global market for rare earths: Elements, 8: 341-346.

Haxel, G. B., Hedrick, J. B., and Orris, G. J., 2005. Rare Earth Elements: Critical Resources for High Technology: U.S.G.S Fact Sheet 087-02.

Hoatson, D. M., Jaireth, S., and Miezitis, Y., 2011. The major rare-earth-element deposits of Australia: geological setting, exploration, and resources: Canberra, Geoscience Australia.

Howard, H. M., Werner, M., Smithies, R. H., Evins, P. M., Kirkland, C. L., Kelsey, D. E., Hand, M., Collins, A. S., Pirajno, F., Wingate, M. T. D., Maier, W. D., and Raimondo, T., 2011. The geology of the west Musgrave Province and the Bentley Supergroup -- a field guide: Record - Geological Survey of Western Australia, Perth, Australia, 2011/14: 125 pp.

Hulse, D. E., Newton, M.C., and Malhotra, D., 2013. NI 43-10 Preliminary economic assessment Round Top project Sierra Blanca, Texas, Gustavason Associates.

Huspeni, J. R., Kesler, S. E., Ruiz, J., Tuta, Z., Sutter, J. F., and Jones, L. M., 1984. Petrology and geochemistry of rhyolites associated with tin mineralization in northern Mexico: Economic Geology, 79: 87-105.

IUPAC, 2005. Nomenclature of inorganic chemistry: IUPAC recommendations 2005, *in* Connelly, N. G., ed., International Union of Pure and Applied Chemistry (IUPAC) Royal Society of Chemistry.

Jaireth, S., Hoatson, D. M., and Miezitis, Y., 2014. Geological Setting and Resources of the Major Rare-Earth-Element Deposits in Australia: Ore Geology Reviews.

Jordens, A., Cheng, Y. P., and Waters, K. E., 2013. A review of the beneficiation of rare earth element bearing minerals: Minerals Engineering, 41: 97-114.

Keith, J. D., Shanks, W. C., III, Archibald, D. A., and Farrar, E., 1986. Volcanic and intrusive history of the Pine Grove porphyry molybdenum system, southwestern Utah: Economic Geology and the Bulletin of the Society of Economic Geologists, 81: 553-577.

Keppler, H., 1993. Influence of fluorine on the enrichment of high field strength trace elements in granitic rocks: Contributions to Mineralogy and Petrology, 114: 479-488.

Kirstein, L. A., Peate, D. W., Hawkesworth, C. J., Turner, S. P., Harris, C., and Mantovani, M. S., 2000. Early Cretaceous basaltic and rhyolitic magmatism in southern Uruguay associated with the opening of the South Atlantic: Journal of Petrology, 41: 1413-1438.

Kovalenko, V. I., and Kovalenko, N. I., 1984. Problems of the origin, ore-bearing and evolution of rare-metal granitoids: Physics of the Earth and Planetary Interiors, 35: 51-62.

Lee Moreno, J. L., 1972. Geological and Geochemical Exploration Characteristics of Mexican Tin Deposits in Rhyolitic Rocks: Unpub. PhD thesis.

Li, X.-H., Li, W.-X., Li, Z.-X., and Liu, Y., 2008. 850–790 Ma bimodal volcanic and intrusive rocks in northern Zhejiang, South China: a major episode of continental rift magmatism during the breakup of Rodinia: Lithos, 102: 341-357.

London, D., Hervig, R. L., and VI, G. B. M., 1988. Melt-vapor solubilities and elemental partitioning in peraluminous granite-pegmatite systems: experimental results with Macusani glass at 200 MPa: Contributions to Mineralogy and Petrology, 99: 360-373.

Lustrino, M., Melluso, L., Brotzu, P., Gomes, C. B., Morbidelli, L., Muzio, R., Ruberti, E., and Tassinari, C. C., 2005. Petrogenesis of the early Cretaceous Valle Chico igneous complex (SE Uruguay): relationships with Paraná–Etendeka magmatism: Lithos, 82: 407-434.

MacDonald, R., and Belkin, H., 2002. Compositional variation in minerals of the chevkinite

group: Mineralogical Magazine, 66: 1075-1098.

Macdonald, R., Belkin, H., Fitton, J., Rogers, N., Nejbert, K., Tindle, A., and Marshall, A., 2008. The roles of fractional crystallization, magma mixing, crystal mush remobilization and volatile–melt interactions in the genesis of a young basalt–peralkaline rhyolite suite, the Greater Olkaria Volcanic Complex, Kenya rift valley: Journal of Petrology, 49: 1515-1547.

Macdonald, R., Davies, G. R., Bliss, C. M., Leat, P. T., Bailey, D. K., and Smith, R. L., 1987. Geochemistry of High-silica Peralkaline Rhyolites, Naivasha, Kenya Rift Valley: Journal of Petrology, 28: 979-1008.

Maestro, P., and Huguenin, D., 1995. Industrial applications of rare earths: which way for the end of the century: Journal of Alloys and Compounds, 225: 520-528.

Mahood, G., and Hildreth, W., 1983. Large partition coefficients for trace elements in high-silica rhyolites: Geochimica et Cosmochimica Acta, 47: 11-30.

Mariano, A. N., 1989. Economic geology of rare earth elements: Reviews in Mineralogy, 21: 309-337.

Marshall, A., Macdonald, R., Rogers, N., Fitton, J., Tindle, A., Nejbert, K., and Hinton, R., 2009. Fractionation of peralkaline silicic magmas: The greater olkaria volcanic complex, Kenya Rift Valley: Journal of Petrology, 50: 323-359.

McCurry, M., Hayden, K. P., Morse, L. H., and Mertzman, S., 2008. Genesis of post-hotspot, A-type rhyolite of the eastern Snake River Plain volcanic field by extreme fractional crystallization of olivine tholeiite: Bulletin of Volcanology, 70: 361-383.

McLennan, S. M., and Taylor, S. R., 2013. Geology, Geochemistry, and Natural Abundances of the Rare Earth Elements, *in* Atwood, D. A., ed., The rare earth elements: fundamentals and applications, John Wiley & Sons.

McPhie, J., Kamenetsky, V., Allen, S., Ehrig, K., Agangi, A., and Bath, A., 2011. The fluorine link between a supergiant ore deposit and a silicic large igneous province: Geology, 39: 1003-1006.

Michael, P. J., 1988. Partition coefficients for rare earth elements in mafic minerals of high silica rhyolites: The importance of accessory mineral inclusions: Geochimica et Cosmochimica Acta, 52: 275-282.

Miller, C. F., and Mittlefehldt, D. W., 1982. Depletion of light rare-earth elements in felsic magmas: Geology (Boulder), 10: 129-133.

Mushkin, A., Navon, O., Halicz, L., Hartmann, G., and Stein, M., 2003. The petrogenesis of A-type magmas from the Amram Massif, southern Israel: Journal of Petrology, 44: 815-832.

Ni, Y., Hughes, J. M., and Mariano, A. N., 1995. Crystal chemistry of the monazite and xenotime structures: American Mineralogist, 80: 21-26.

Olson, J. C., Shawe, D., Pray, L., and Sharp, W., 1954. Rare-earth mineral deposits of the Mountain Pass district, San Bernardino county, California: Science, 119: 325-326.

Pankhurst, M., Schaefer, B., and Betts, P., 2011a. Geodynamics of rapid voluminous felsic magmatism through time: Lithos, 123: 92-101.

Pankhurst, M., Schaefer, B., Betts, P., Phillips, N., and Hand, M., 2011b. A Mesoproterozoic continental flood rhyolite province, the Gawler Ranges, Australia: the end member example of the Large Igneous Province clan: Solid Earth, 2: 25-33.

Patino Douce, A. E., 1997. Generation of metaluminous A-type granites by low-pressure melting of calc-alkaline granitoids: Geology (Boulder), 25: 743-746.

Pingitore, N., Clague, J., and Gorski, D., 2014. Round Top Mountain rhyolite (Texas, USA), a massive, unique Y-bearing-fluorite-hosted heavy rare earth element (HREE) deposit: Journal of Rare Earths, 32: 90-96.

Price, J. G., Rubin, J. N., Henry, C. D., Pinkston, T. L., Tweedy, S. W., and Koppenaal, D. W., 1990. Rare-metal enriched peraluminous rhyolites in a continental arc, Sierra Blanca area, Trans-Pecos Texas; chemical modification by vapor-phase crystallization: Ore-bearing granite systems; petrogenesis and mineralizing processes. Geol Soc Am Spec Pap, 246: 103-120.

Sinclair, W., 1986. Early Tertiary topaz rhyolites and associated mineral deposits in the northern Canadian Cordillera; products of anorogenic magmatism: Program with abstracts—Geological Association of Canada. Mineralogical Association of Canada Annual Meeting, 1986: 127-128.

Skinner, B. J., 1976. Second iron age ahead: Am. Sci.;(United States), 64 pp.

Smithies, R. H., Kirkland, C. L., Korhonen, F. J., Aitken, A. R. A., Howard, H. M., Maier, W. D., Wingate, M. T. D., Quentin de Gromard, R. and Gessner, K., 2014. The Mesoproterozoic thermal eveolution of the Musgrave Province in central Australia - plume vs. the geological record. Gondwana Research.

Sun, S. S., and McDonough, W. F., 1989. Chemical and isotopic systematics of oceanic basalts; implications for mantle composition and processes: Geological Society Special Publications, 42: 313-345.

Syme, E., 1998. Ore-associated and barren rhyolites in the central Flin Flon belt: case study of the Flin Flon mine sequence, OF98-9: Winnipeg, Manitoba Energy and Mines, Geological Services.

Syme, E., and Bailes, A., 1993. Stratigraphic and tectonic setting of early Proterozoic volcanogenic massive sulfide deposits, Flin Flon, Manitoba: Economic Geology, 88: 566-589.

Syme, E., Lucas, S., Bailes, A., and Stern, R., 2000. Contrasting arc and MORB-like assemblages in the Paleoproterozoic Flin Flon Belt, Manitoba, and the role of intra-arc extension in localizing volcanic-hosted massive sulphide deposits: Canadian Journal of Earth Sciences, 36: 1767-1788.

Taylor, W., Esslemont, G., and Sun, S.-S., 1995a. Geology of the volcanic-hosted Brockman rare-metals deposit, Halls Creek Mobile Zone, northwest Australia. II. Geochemistry and petrogenesis of the Brockman volcanics: Mineralogy and Petrology, 52: 231-255.

Taylor, W., Page, R., Esslemont, G., Rock, N., and Chalmers, D., 1995b. Geology of the volcanic-hosted Brockman rare-metals deposit, Halls Creek Mobile Zone, northwest Australia. I. Volcanic environment, geochronology and petrography of the Brockman volcanics: Mineralogy and Petrology, 52: 209-230.

Thompson, T. J., 2002. A model for the origin of red beryl in topaz rhyolite, Wah Wah Mountains, Utah, USA: Unpub. M.S. thesis, Brigham Young University, 99 pp.

Turley, C., and Nash, W., 1980. Petrology of late Tertiary and Quaternary volcanism in western Juab and Millard Counties, Utah: Studies in Late Cenozoic Volcanism in West-Central Utah: Utah Geological and Mineral Survey Special Studies, 52: 1-33.

Turner, S., Foden, J., and Morrison, R., 1992a. Derivation of some A-type magmas by fractionation of basaltic magma: an example from the Padthaway Ridge, South Australia: Lithos, 28: 151-179.

Turner, S., Sandiford, M., and Foden, J., 1992b. Some geodynamic and compositional constraints on" postorogenic" magmatism: Geology, 20: 931-934.

Tuta, Z. H., Sutter, J. F., Kesler, S. E., and Ruiz, J., 1988. Geochronology of mercury, tin, and fluorite mineralization in northern Mexico: Economic Geology, 83: 1931-1942.

Wang, J., and Li, Z.-X., 2003. History of Neoproterozoic rift basins in South China: implications for Rodinia break-up: Precambrian Research, 122: 141-158.

Webster, J. D., Burt, D. M., and Aguillon, R., 1996. Volatile and lithophile trace-element geochemistry of Mexican tin rhyolite magmas deduced from melt inclusions: Geochimica et Cosmochimica Acta, 60: 3267-3283.

Webster, J. D., and Duffield, W. A., 1991. Volatiles and lithophile elements in Taylor Creek Rhyolite; constraints from glass inclusion analysis: American Mineralogist, 76: 1628-1645.

Webster, J. D., and Duffield, W. A., 1994. Extreme halogen abundances in tin-rich magma of the Taylor Creek Rhyolite, New Mexico: Economic Geology and the Bulletin of the Society of Economic Geologists, 89: 840-850.

Webster, J. D., and Rebbert, C. R., 1998. Experimental investigation of H_2O and Cl^- solubilities in F-enriched silicate liquids; implications for volatile saturation of topaz rhyolite magmas: Contributions to Mineralogy and Petrology, 132: 198-207.

Wedepohl, K. H., 1995. The composition of the continental crust: Geochimica et cosmochimica Acta, 59: 1217-1232.

Weng, Z., Jowitt, S., Mudd, G., and Haque, N., 2013. Assessing rare earth element mineral deposit types and links to environmental impacts: Applied Earth Science (Trans. Inst. Min. Metall. B), 122: 83-96.

Whalen, J. B., Currie, K. L., and Chappell, B. W., 1987. A-type granites; geochemical characteristics, discrimination and petrogenesis: Contributions to Mineralogy and Petrology, 95: 407-419.

Wingate, M. T. D., Pirajno, F., and Morris, P. A., 2004. Warakurna large igneous province: A new Mesoproterozoic large igneous province in west-central Australia: Geology, 32: 105-108.

Chapter 6

Conclusion and Discussion

6.1 Introduction

This chapter provides an overview of the thesis, and demonstrates that the aims outlined in the introduction have been addressed by summarising the main results and conclusions from the previous research chapters. The new knowledge gained from this research feeds into a discussion on the significance of the research in general and on the broader tectonic setting of the west Musgrave Province and evolution of Proterozoic Australia. Lastly, suggestions for future research in the west Musgrave Province, and on the topic of highly evolved, intensely welded rheomorphic ignimbrites, are given.

The research presented and discussed in this thesis aimed to address the following:

- Whether the KI sequence represents an explosive caldera-forming eruption sequence that was deposited within an intra-caldera setting.
- The palaeoenvironmental depositional setting of the volcanic-succession through an analysis of the sediments that host the sequence.
- The type of eruption, transportation and emplacement model for the KI sequence.
- The petrogenesis of the KI and its associated magmas.
- Constraints on the age of eruption and timing of events in the volcanic-sedimentary succession.
- Potential links is (if any) between the KI and associated voluminous intruding porphyritic rhyolites.
- The contentious issue of subaqueous pyroclastic flows.
- The nature of rheomorphism in extremely welded ignimbrites, the controls of rheomorphism, and the factors that caused the KI to behave rheomorphically.
- Whether the KI has any potential economic interest.
- Whether this research can be used to improve our broader tectonic understanding of the Musgrave region and in doing so contribute to a better understanding of the palaeotectonic setting, evolution and formation of Proterozoic Australia.

6.2 Conclusions

6.2.1 Chapter 2

This chapter examined the physical volcanology of a Mesoproterozoic, ~1 km thick, rhyolitic, ignimbrite-dominated volcanic-sedimentary succession in the west Musgrave Province of central Australia that contains the Kathleen Ignimbrite (KI). This succession

represents the basal part of the Pussy Cat Group (PCG) that was deposited in the Talbot Sub-basin, the main preserved depositional basin of the Bentley Supergroup. The main findings are summarised below:

- The KI is a ≤640 m thick rhyolitic, eruption fill-sequence that formed during a very large, explosive, caldera-forming eruption of magnitude VEI 7 or greater and is split into the Kurrparu, Karlaya and Kilykilykarri members. It is dominated by the ≤500 m thick, intra-caldera, lava-like rheomorphic to normally welded Kurrparu Member. This member represents a simple, single cooling unit with multiple facies that range from intensely high-grade lava-like rheomorphic to normal eutaxitic welding conditions. The KI conformably overlies shallow-water (<50 m), volcaniclastic-sedimentary, turbidite *marine shelf-type* or *large lake-type* sediments of the upper Cleghorne Formation (CF).
- The initial emplacement of the KI and possibly the initial eruption of the Kathleen Caldera were within this shallow-water subaqueous palaeoenvironment. The upper parts of the thick intra-caldera Kurrparu Member were subaerially exposed as a result of shoreline displacement/regression, and the overlying Kilykilykarri Member records shoreline transgression and the inundation of the caldera during the transgression of a shallow-water palaeoenvironment.
- The coeval porphyritic rhyolite Rowland Suite (RS) intrusion underlying the KI may represent late-stage resurgent activity in the magma chamber below the Kathleen Caldera.
- The formation and emplacement of such a highly welded (i.e. lava-like rheomorphic) pyroclastic flow in subaqueous conditions is highly unusual, making the KI a rare example of a subaqueous pyroclastic flow deposit that records a hot state of emplacement and rheomorphism within an initially subaqueous depositional environment and an intra-caldera setting.
- The KI eruption was a high-temperature, felsic, explosive, caldera-forming boil-over type eruption that was characterised by a sustained, low, continuously collapsing, ignimbrite-forming, eruption column and the deposition of a thick, high-temperature, low-viscosity, progressively or incrementally aggrading pyroclastic flow.
- The eruption involved at least two types of magmas, as evidenced by the presence of crystal rich and aphyric pumice populations, the presence of two crystal-poor basal facies, the mixed crystal-rich and -poor *main facies zone*, the upper crystal-poor facies of the Kurrparu Member, the eutaxitic two pumice-bearing crystal-rich ignimbrite facies of the Karlaya Member and lastly the underlying crystal-rich RS intrusion. These facies define a crude vertical stratification within the KI and are interpreted to be cogenetic, with both derived from a stratified common magma chamber or reservoir where the aphyric magma was present as either a melt-rich cap or a hot silicic recharge magma, and the crystal-rich magma was present as

cumulate material within the chamber.

- The intra-caldera setting provided an ideal environment for a thick, heat-retaining intra-caldera ignimbrite deposit to pond and to develop basal non-particulate flow that enabled the development of lava-like rheomorphism. This was facilitated by the formation of a continuously subsiding, sloping (trapdoor?) volcano-tectonic depression and the progressive or incremental aggradation of pyroclastic flow material.
- The Kathleen Caldera has a minimum diameter of ~22 km and an estimated intra-caldera volume of ~190 km^3 and provides unequivocal evidence for at least one very large caldera-forming eruption at ca. 1070 Ma in the west Musgrave Province. This caldera is possibly part of a once even larger, nested caldera complex, indicating the high-likelihood of a supereruption or supervolcano within the active Ngaanyatjarra Rift zone. This, coupled with evidence for more widespread and long-lived (>30 Ma) felsic magmatism during the formation and deposition of the bimodal Bentley Supergroup within the Talbot Sub-basin, supports the presence of a large silicic igneous volcanic province in the west Musgrave Province, potentially similar to the Yellowstone Caldera Complex and Snake River Plain volcanic province of central-western USA.
- The KI shares similar palaeoenvironmental settings to the non-rheomorphic Ordovician intra-caldera Lower Rhyolitic Tuff, Garth Tuff, Capel Curig and rheomorphic, but extra-caldera, Pitts Head Tuff formations, North Wales, UK, as well as the Mineral King Monarch Tuff, Sierra Nevada, USA. Lastly it shares many of the characteristics of other lava-like, rheomorphic ignimbrites such as the intra-caldera Bad-Step Tuff Formation, English Lake District, UK, and the extra-caldera Grey's Landing ignimbrite, southern Idaho, USA and Pitts Head Tuff, North Wales, UK.

6.2.2 Chapter 3

This chapter assessed the isotope and major and trace element geochemistry, and geochronology of the PCG rhyolites (i.e. the KI and RS), to determine the petrogenesis of this Mesoproterozoic rhyolitic suite. The main findings of this research are summarised below:

- These units are highly evolved A-type, metaluminous (to weakly peraluminous) rhyolites that have *within-plate* geochemical affiliations and are rare earth element (REE)- and F-enriched (relative to average crustal abundances). They formed as a result of extreme fractional crystallisation of a basaltic magma.
- The ca. 1070 Ma KI and RS magmas are interpreted to be coeval and cogenetic, linked through fractional crystallisation with little crustal contamination. They most likely originated from a deep-seated, common, large-volume magma reservoir

(21–14 km depth) below the Talbot Sub-basin before rising into a shallow (10–3 km depth) stratified magma chamber directly below the Kathleen caldera.

- The RS represents a more primitive, crystal-rich cumulate end-member of the system, whereas the KI represents a more evolved, high-silica, crystal-poor, melt-rich end-member of the cogenetic PCG rhyolites, albeit an end-member that contains RS-like crystal-rich regions. Furthermore, the evidence for the involvement of at least two types of magmas (one crystal-rich, the other aphyric) in the KI eruption, as discussed above, suggests that the crystal-rich regions of the KI represent more cumulate-rich sections of a pre-eruption crystal mush within the Kathleen magma chamber, whereas aphyric regions represent either a melt-rich cap above the pre-eruptive mush and/or a hot (near liquidus temperature) buoyant aphyric silicic recharge magma that originated from the deeper Talbot Sub-basin magma reservoir.
- The pre-emplacement and pre-eruption petrogenesis of the PCG rhyolites involved a minimum of two stages of K-feldspar dominated fractionation, with initial fractionation and formation of the partly crystallised RS magma followed by further fractionation that formed an evolved REE- and melt-rich KI composition cap. Polybaric fractionation of a primitive basaltic magma firstly formed the light REE (LREE)-enriched RS magmas and the more evolved heavy REE (HREE)-enriched KI magmas. The RS magmas initially formed in the mid-crustal Talbot Sub-basin magma reservoir (a proposed common source for all felsic magmatism during this >30 Ma period), before ascending to an upper-crustal magma chamber where further fractionation formed the KI magmas.
- The radiogenic isotope composition of PCG rhyolites provides evidence of a significant juvenile mantle contribution during much of the felsic magmatism associated with the 1085–1040 Ma Giles Event, and is consistent with the known magmatic history of the west Musgrave Province.

6.2.3 Chapter 4

One of the most striking features of the KI is the presence of lava-like textures that are particularly evidence within the basal 50 m of the eruption sequence. These are features that record rheomorphic flow and provide evidence for extremely high degrees of welding within the deposit. This chapter focuses on an assessment of the relative importance of the various factors that controlled rheomorphism within this rheomorphic ignimbrite, combining the physical volcanological features discussed in Chapter 2 with the geochemistry discussed in Chapter 3:

- All of the factors controlling rheomorphism are somewhat interdependent, and can be summarised as five main controls, these being the chemistry of the magma, temperatures (magmatic, eruption and deposition), strain (both rate and heating),

viscosity and an inferred slope, which would help to facilitate gravity-driven flow deformation.

- The KI is chemically similar to the well-documented metaluminous, high-silica Snake River (SR)-type lava-like rheomorphic ignimbrites of the central-western USA. However, it contains higher concentrations of F, has lower magmatic crystallisation (~830°C), eruption and deposition temperatures, and was lower viscosity ($10^{8.16}$ Pa.s) than these SR-type ignimbrites.
- The modelling of F-free KI compositions that behave rheomorphically, indicate that the lowering of viscosity by the presence of this element within the magma was not the main control on rheomorphism of the KI.
- The presence of water during initial emplacement of the KI may or may not have enhanced welding and rheomorphism, although the water-free modelling undertaken during this study demonstrates that water-free (and both water and F-free) KI magmas most likely would still have behaved rheomorphically.
- Modelling of factors that were considered to be highly unfavourable for rheomorphism, such as much higher strain rates (3.33 s^{-1} and based on a conservative total strain up to 100) than those recorded during the emplacement of other lava-like rheomorphic ignimbrites and very short deformation timescales (0.3 s) and shear zone residence times (30 s) still indicate that the KI would most likely have behaved rheomorphically, effectively negating the need for strain heating as a driver for the rheomorphism of this unit during eruption and emplacement.
- The rheomorphism of the KI was the result of a unique combination of various rheomorphism-related factors, rather than as a consequence of one single control (e.g., high F or high H_2O, etc.). This combination produced sufficiently low viscosities to form the extremely high-degrees of welding, deformation and subsequent lava-like textures recorded within the KI.

6.2.4 Chapter 5

This chapter focused on the petrogenetic magmatic process (described and demonstrated in Chapter 3) during the formation of highly evolved felsic systems, including the PCG rhyolites, which results in the development of HREE enrichments. The main findings of this study are summarised below:

- The petrogenesis of the magmas that formed these highly evolved rhyolites involved an initial enrichment in the REE. Further extreme fractionation, causes the LREE to become compatible, and led to saturation of the magma in LREE-rich, but HREE-poor minerals (e.g., allanite, monazite, chevkinite, etc.). This generates LREE-depleted and HREE-enriched residual magmas.
- Very few REE mineral deposits are HREE-enriched. This, coupled with a significant recent increase in demand for the HREE, has meant that these elements have

become highly valuable.

- Preliminary assessments on the Round Top rhyolite deposit of Texas, a NI43-101 compliant REE resource, suggests that highly fractionated, high-silica rhyolites are potentially viable bulk tonnage, low grade but HREE-enriched REE deposits that formed through the petrogenetic processes documented in the PCG during this study. This means that these and other rhyolites may be an important future source of the REE, and especially the more valuable HREE.
- Late stage magmatic processes, such as vapour phase crystallisation, and F-enrichment, as documented within the PCG and especially within the KI, may be key in the development of significantly enriched or upgraded sections of these rhyolites that are preferentially enriched in the HREE and other potential by-products (e.g., U, Th, Nb, etc.), making these enriched sections highly prospective for future mineral exploration.
- More detailed sampling needs to be undertaken both within the west Musgrave Province and globally to determine whether vapour phase- and/or F-enrichment is necessary to generate potentially economic REE and HREE concentrations or whether the extended fractionation that dominates the petrogenesis of these highly fractionated high-silica REE-enriched rhyolites is sufficient to produce potentially economic HREE and REE mineralisation in these unconventional but highly prospective HREE-enriched rhyolites.
- This chapter outlines an exploration model involving an extensional, intra-plate environment, F-rich, high-silica A-type rhyolites and the identification of the most evolved units within these suites.
- Highly fractionated REE-enriched rhyolites such as the KI, could thus be considered potential bulk tonnage, low grade REE ore deposits, similar to low grade porphyry Cu base metal deposits.

6.3 Discussion

6.3.1 Significance of the Kathleen Ignimbrite for the tectonics of the west Musgrave Province

Calderas form during regional tectonism, and are frequently located along regionally important fault zones or within the active axes of rift zones. Both are active before and after the caldera cycle and most likely control the emplacement of caldera forming magmas, as well as the location, structure, and development of caldera systems within a rift zone (Rytuba, 1994; Spinks *et al*., 2005). The Taupo Volcanic Zone (TVZ), New Zealand, is an example of how rift architecture influences the characteristics of magma generation and emplacement and the type of volcanism observed at the surface. This is exemplified by the research of Spinks *et al*. (2005), which showed that large volume rhyolitic calderas

are most likely to occur in areas with the highest extension or tensile conditions, and that intra-rift calderas have rectilinear margins with multiple collapse structures, whereas extra-rift calderas tend to be sub-circular monogenetic collapse structures associated with one major ignimbrite (Fig. 6.1).

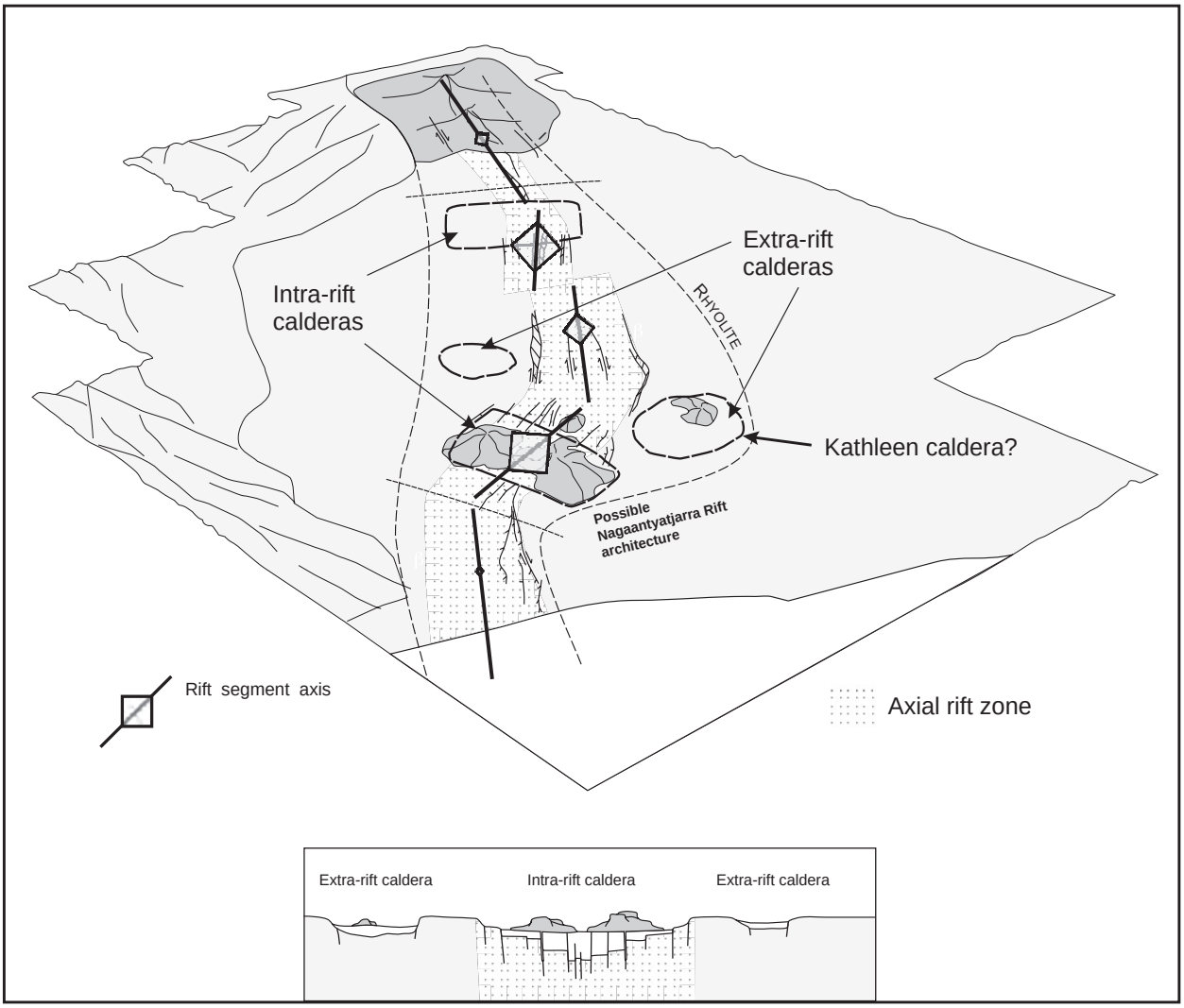

Figure 6.1: Schematic representation of the possible Ngaanyatjarra Rift (based on the modern Taupo Volcanic Zone, [TVZ]), demonstrating the intra- and extra-rift caldera settings and suggested position of the Kathleen caldera (adapted from Spinks *et al*., 2005)

A regional-scale extensional environment with active rifting and faulting in the failed intra-plate Ngaanyatjarra Rift, is proposed for the west Musgrave Province at 1085–1040 Ma (Evins *et al*., 2010). This is coeval with the generation of the KI and RS magmas and the caldera-forming Kathleen eruption. A-type magmas, such as those that formed the KI and RS, often occur in intra-plate extensional environments associated with active rifting (e.g., Whalen *et al*., 1987; Mushkin *et al*., 2003; Anderson and Morrison, 2005; Dall'Agnol *et al*., 2012), suggesting that the RS and KI and the associated large volume rhyolitic caldera might also reflect a similar tectonic environment. It is speculated that the Kathleen caldera represents an extra-rift caldera setting (i.e. just outside the active Ngaanyatjarra rift axis), as there is no evidence for multiple collapse structures associated

with the Kathleen caldera and the intra-caldera fill is dominated by one major ignimbrite, the Kurrparu Member. This implies there should be even larger volume intra-rift caldera structures with multiple collapse structures along the active Ngaanyatjarra rift axis within the Talbot Sub-basin.

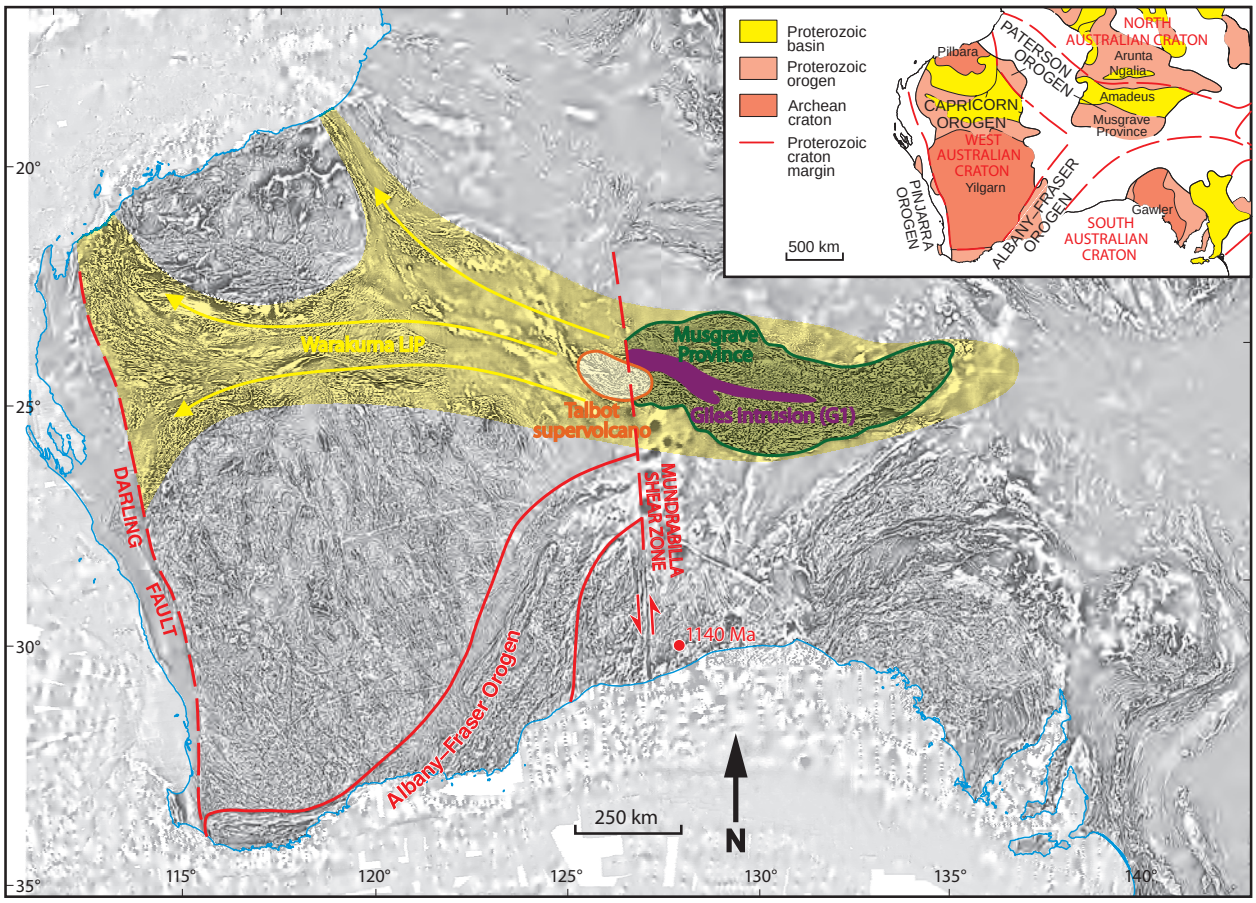

Figure 6.2: The extent of the Warakurna LIP and the Mundrabilla Shear Zone (MSZ). The MSZ represents a prominent south-north trending, continent-scale basement structural lineament (Aitken *et al*., 2012), which intersects the west Musgrave Province and was active at the time of the 1085–1040 Ma Giles Event (adapted from Smithies *et al*., 2014).

In support of this speculative hypothesis, it is proposed that a prominent south-north trending, continent-scale basement structural lineament, known as the Mundrabilla Shear Zone (MSZ; Fig. 6.2), which intersects the west Musgrave Province, was an active rift-forming fault during the 1085–1040 Ma Giles Event (Aitken *et al*., 2013). Movement along the MSZ could have triggered a catastrophic disruption of the long-term regional Musgrave thermal anomaly below the province (Chapter 1; Smithies *et al*., 2014), creating the anomalously high temperature heat source that drove the Giles Event and associated magmatism. Such regional tectonic instability coincides well with the extensional intra-plate setting of the Ngaanyatjarra Rift and could have expressed itself on the surface, with the formation of caldera structures and large volume eruptions, such as the KI and Kathleen caldera. It is quite likely that the active Ngaanyatjarra rift axis was coincident with the MSZ at some point during their evolution. The MSZ manifests itself as a surface expression defined by Permian-aged sedimentary rocks infilling a linear graben, 10–20 km

to the east of the KI, and intersects the middle of one of two proposed caldera structures (Fig. 6.3; Smithies *et al*., 2013) within the Kaarnka Group. It is suggested that the active Ngaanyatjarra rift axis runs through the centre of the Kaarnka Group, with the proposed Kaarnka caldera cluster representing intra-rift calderas within the rift zone along the MSZ. The extensive ignimbrites of the Kaarnka and Mount Palgrave groups, originally defining the proposed Palgrave cauldron of Daniels (Chapter 1; Daniels, 1974), are in fact most likely the products of these intra-rift calderas.

Large igneous provinces (LIP; Bryan and Ernst, 2008; Bryan and Ferrari, 2013) are magmatic provinces that form during (<50 Ma), large volume (>0.1 Mkm^3), laterally extensive (>0.1 Mkm^2) igneous events within an intra-plate tectonic setting or geochemical affinity thereof, and involve short pulses (1–5 Ma) of magmatism during which a dominant portion (>75%) of the total igneous volume is emplaced; these events represent periods of extreme crustal growth via direct mantle input (Pankhurst *et al*., 2011). Characteristics of LIPs include a dominant mafic component, but they can also have significant ultramafic and silicic components (Bryan and Ernst, 2008). Often the silicic component of a LIP is overlooked, due to poor preservation or sampling bias towards the mafic component, but these can play a large role in the evolution of a LIP and their associated rifts (Bryan *et al*., 2002). When the silicic component of these LIPs exceeds the minimum areal and volumetric constraints of a LIP, it is termed a silicic LIP (SLIP; Bryan *et al*., 2002). Two types of SLIPs are described: an intra-plate style and a back-arc environment style, with both driven by anomalous thermal and mass transfer into the crust by hot asthenospheric mantle upwellings, often accompanied by lithospheric extension (Bryan *et al*., 2002; Pankhurst *et al*., 2011). SLIPs are characterised by bimodal volcanism, elevated concentrations of F and extensive rhyolite ignimbrites, lavas and intrusions (Pankhurst *et al*., 2011). The >30 Ma period of wholly mantle derived felsic magmatism and volcanism in the Talbot Sub-basin, during the Giles Event, demonstrated here by the PCG rhyolites, is consistent with that of SLIP formation described above. However, the volume of preserved felsic material within the Talbot Sub-basin (~22 000 km^3), even with a possible original basin extent of >50 000 km^2 (Smithies *et al*., 2014), is still below the volume required for a true SLIP. The Giles Event does however, include the already known 1078–1073 Ma 1.5 Mkm^2 Warakurna LIP (Wingate et al., 2004) and the mafic-ultramafic Giles intrusions in the Musgrave Province, which are coeval with this period of magmatism and cogenetic with the parental mafic magmas of felsic magmatism (Smithies *et al*., 2014). It is therefore suggested that the felsic magmatism in Talbot Sub-basin, represented here in this study by the PCG rhyolites, be considered the silicic component of a likely LIP in the west Musgrave Province associated with the Giles Event, or alternatively that the Warakurna LIP needs to be redefined as a longer lived event (of Giles Event duration), with these its silicic members (Smithies *et al*., 2013; 2014).

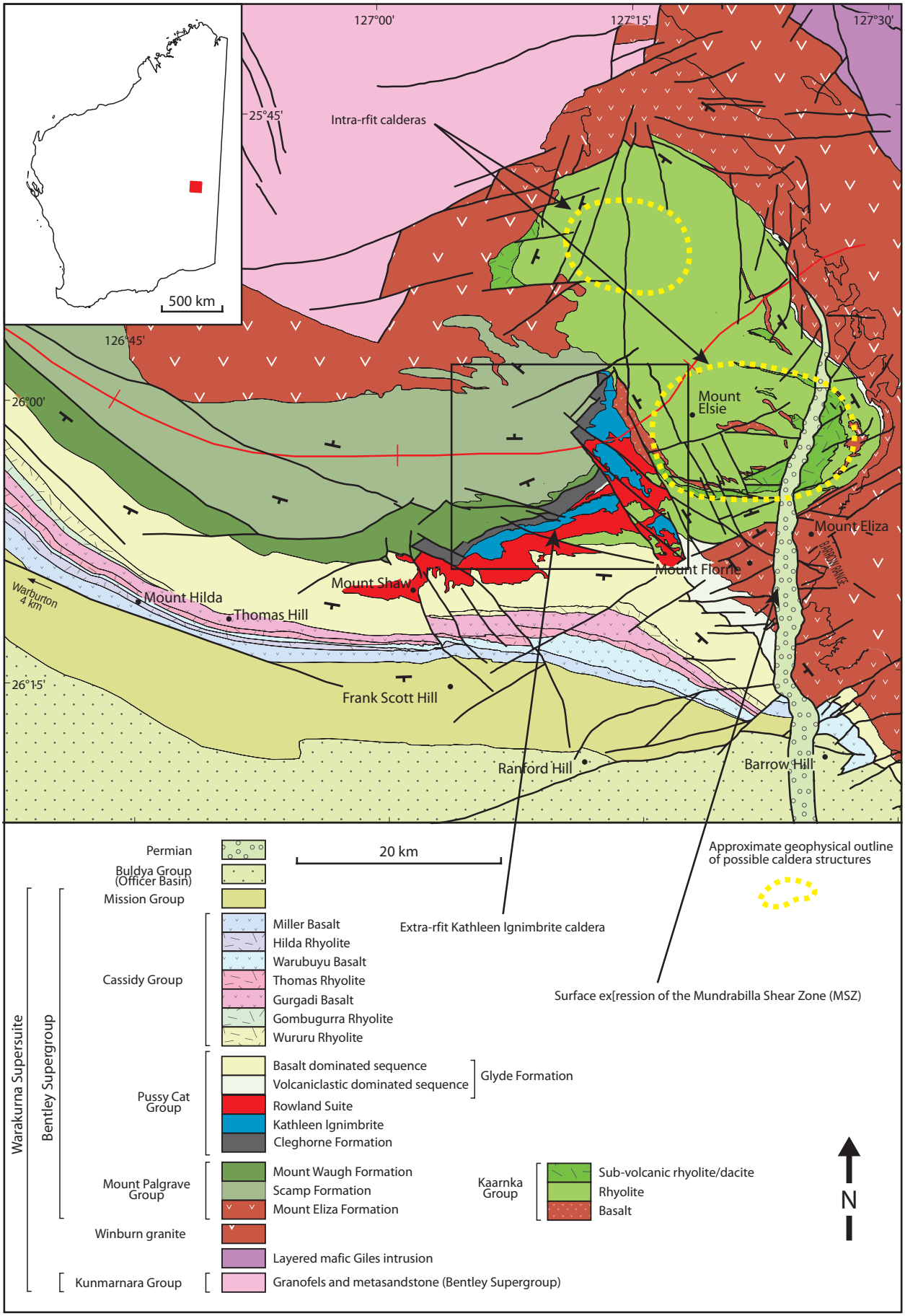

Figure 6.3: Proposed caldera structures within the Kaarnka Group of the west Musgrave Province, lying on the intersection of the Ngaanyatjarra Rift axis and the MSZ (represented here by the Permian aged graben seen cutting through the possible caldera structure in the Kaarnka Group). The Kathleen Ignimbrite succession and Kathleen caldera lie to the west of these structures within a proposed extra-rift setting, whereas the Kaarnka Caldera structures lie within a possible intra-rift zone (adapted from Smithies *et al.*, 2013).

In further support of Smithies *et al*. (2014) proposal of a supervolcano and supereruption within the Talbot Sub-basin, these systems, in addition to large upper crustal magma chambers, require even larger-volume mid-crustal magma reservoirs that need to be maintained in a partially molten state (Bachmann and Bergantz, 2008). Direct input from the mantle, in the form of mantle-derived basaltic melts during periods of high magmatic flux are considered critical components to providing the heat sources to facilitate this (de Silva, 2008; Miller and Wark, 2008). As discussed above these conditions were present during the Giles Event and together with the presence of a known caldera demonstrated by this study lend further weight to this proposal.

6.3.2 Broader implications of this research

Some of the new findings outlined in this research have broader implications for our understanding of the physical volcanology of ignimbrites and intra-caldera settings, the rheomorphism of ignimbrites, the petrogenesis of A-type magmas, and economic potential of new types of HREE deposits, including those highlighted in the following paragraphs.

This study provides the oldest documented case of an intra-caldera, lava-like rheomorphic ignimbrite, and the first documented case of the development of lava-like rheomorphism and such extreme grades of welding during the initial emplacement of an intra-caldera ignimbrite into a subaqueous environment (Chapter 2). Lava-like rheomorphism has primarily been documented in extra-caldera outflow settings (e.g., Ekren *et al*., 1984; Andrews and Branney, 2011) but only in a few intra-caldera settings (e.g., Branney *et al*., 1992). Thus the KI is a natural laboratory for further understanding processes that can occur within intra-caldera settings (Chapters 2 and 4).

The extreme rheomorphism demonstrated in KI deposit (Chapter 4), coupled with the unusual initial subaqueous emplacement of the ignimbrite (Chapter 1), the lower magmatic, eruption and deposition temperatures, and the lower viscosity compared with otherwise similar SR-type rheomorphic ignimbrites has provided new insight into interpretations of rheomorphism in such rhyolites. Additionally this research has suggested newly revised fields (Chapter 4) that define conditions under which rheomorphism is possible in rheomorphic ignimbrites that differ slightly to those fields presented by Robert *et al*. (2013).

Large-volume crystal-rich ignimbrites such as the Cerro Galan Ignimbrite, Andes (Cas *et al*., 2011; Folkes *et al*., 2011), the Ora Ignimbrite, Italy (Willcock *et al*., 2013), and the KI of central Australia (Chapter 2) all lack a preceding basal Plinian fallout deposit beneath the ignimbrite deposits. This has important implications for the style of eruption

associated with these types of ignimbrites, and indicates that caldera and eruption column collapse were near simultaneous events, that the eruption was continuous with a constant high mass flux, and that eruption columns associated with these types of caldera-forming eruptions are low, unstable, and continuously collapsing without the development of high, buoyant Plinian-style eruption columns (Cas *et al*., 2011). This also implies that cooling of the pyroclasts was very limited, ensuring rapid heat transfer to pyroclastic flow deposits, an important factor in the development of rheomorphism (Chapter 4). The lack of a buoyant eruption column could suggest that the magmas were not initially volatile rich, and only became sufficiently volatile saturated to initiate an explosive eruption when they had reached an advanced stage of crystallisation.

The physical volcanology (Chapter 2 and 4), the interpreted palaeoenvironment (Chapter 2), geochemistry (Chapter 3) and petrogenesis (Chapter 3) of the KI suggests that the rhyolitic ignimbrites of the PCG, together with related rhyolitic volcanics of the Talbot Sub-basin within the west Musgrave Province, be considered as a new type locality for SR-type volcanism (Branney *et al*., 2008) outside of the Snake River Plain, central-western USA.

The petrogenesis of A-type rhyolites (e.g., Dall'Agnol *et al*., 2012) is still controversial, with three main models suggested: (a) extreme fractional crystallisation of a basaltic magma (e.g., Turner *et al*., 1992a; McCurry *et al*., 2008), (b) fractional crystallisation of silicic magmas generated during small degree of partial melting of hybridised gabbro–diorite intrusive complexes in the crust (e.g., Turner *et al*., 1992b; Christiansen *et al*., 2007), and (c) partial melting of older continental crust by heat derived from underplated mantle-derived magmas and subsequent fractional crystallisation (e.g., Creaser *et al*., 1991; Haapala and Rämö, 1992; Patino Douce, 1997; Frindt *et al*., 2004; Anderson and Morrison, 2005). The petrogenesis of the cogenetic KI and RS magmas (Chapter 3) by extreme fractional crystallisation of a basaltic magma adds an additional case study and example of model (a).

Christiansen *et al*. (2007) used geochemistry to suggest that the Cenozoic topaz rhyolites of the central USA are extrusive equivalents of ancient Proterozoic rapakivi-textured granites, meaning that the petrogenesis and setting of recent topaz rhyolites may be used to better understand their more ancient counterparts. Topaz rhyolites form during periods of regional extension, lithospheric thinning, and high heat flow (Christiansen *et al*., 2007). The geochemical similarity of the KI to these topaz rhyolites (Chapter 3; Christiansen *et al*., 1986; 2007) and the same tectonic conditions during the Giles Event (Smithies *et al*., 2014), suggests a similar link between the KI and topaz rhyolites, with both shown to share a similar possible petrogenesis (as demonstrated in Chapter 3), although this was not the preferred model later suggested by Christiansen *et al*. (2007).

However, this still shows that the processes and setting that formed the younger topaz rhyolites may also have occurred during the Mesoproterozoic and led to the formation of the KI, vindicating the link suggested by Christiansen *et al*. (2007) for similar petrogenetic processes and tectonic settings operating in ancient terranes. Furthermore, the presence of the rapakivi-textured Winburn granite that originates from the same Talbot Sub-basin magma reservoir as the KI and emplaced during Giles Event (Smithies *et al*., 2013), adds further support to this link.

6.4 Suggested future work

6.4.1. In the west Musgrave Province

The fact that calderas tend not to occur in isolation but often occur as nested caldera complexes or as intra- and extra-rift calderas within an active rift zone (Lipman, 2000; Spinks *et al*., 2005) suggests that the Kathleen caldera is likely to be associated with other hitherto unidentified calderas within the Talbot Sub-basin of the west Musgrave Province. Further work should be devoted to identifying more calderas through detailed field mapping and detailed facies analysis as carried out in this study, and to test geophysically identified caldera structures in the Kaarnka Group (Smithies *et al*., 2013). In addition, the extensive ignimbrites of the Kaarnka and Mount Palgrave groups (Smithies *et al*., 2013) should be characterised, and correlated if possible. These should be compared in terms of their physical and geochemical characteristics with those of the KI to assess similarities or differences. Identification of intra- and extra-caldera outflow ignimbrites in these groups would help establish possible caldera sources, allow for better volume estimates for the erupted pyroclastics, and could potentially provide definitive proof for the existence of supereruptions (>450 km^3 erupted magma or >1000 km^3 erupted pyroclastic material; Sparks *et al*., 2005; Self, 2006) proposed by Smithies *et al*. (2014) for the Talbot Sub-basin.

Many of the rhyolites within the Talbot Sub-basin have been mapped as lavas or alternatively as rheomorphic ignimbrites (Howard *et al*., 2011; Werner *et al*., 2012; Smithies *et al*., 2013). The extreme difficulty of distinguishing between lava-like rheomorphic ignimbrites and true silicic lavas (e.g., Henry and Wolff, 1992; Manley, 1995; Kirstein *et al*., 2001) means that it is possible that units with these characteristics in the west Musgrave Province may have been incorrectly mapped, as the obliteration of any primary vitriclastic features means that even after a detailed assessment of the physical volcanology it may not be possible to determine the exact origin of these units. One suggestion is that many of the ignimbrites and lavas within the Talbot Sub-basin be revisited to reassess their interpretations, especially within the extensive lavas of the Scamp Group.

6.4.2 Rheomorphism and rheomorphic ignimbrites

In terms of research into rheomorphism and rheomorphic ignimbrites, in order to better understand the processes that occur in these intensely welded ignimbrites and controls of rheomorphism, additional work, in the form of individual case studies (e.g., this study; Robert *et al*., 2013), should be carried out with a particular focus on lava-like rheomorphic ignimbrites. These high-grade end-members of the welding continuum (Branney and Kokelaar, 1992) would allow for rigorous testing of hypotheses, as they tend to exhibit the most diverse range of welding intensities, from non-welded/partially-welded through to the highest degree of welding with the development of lava-like facies.

The difficulty in distinguishing flow banded lava-like rheomorphic ignimbrites and true silicic lavas, primarily as a result of the obliteration of vitriclastic features, is an ongoing issue (e.g., Henry and Wolff, 1992; Andrews and Branney, 2011), with some studies looking at alternative ways to characterise and identify the origin of such deposits (e.g., Kirstein *et al*., 2001). To determine if a distinction can be made at a microscopic scale, it is proposed a detailed strain analysis be carried out, making use of a fabric analyser, to compare strain in a flow-banded lava to that of a flow-banded rheomorphic ignimbrite.

The role of water during welding and the formation of rheomorphic ignimbrites also needs to better constrained, as this may either greatly aid rheomorphism through resorption and lowering of volcanic glass viscosity (Sparks *et al*., 1999), or impede welding as a result of heat transfer and mixing upon contact (Trofimovs *et al*., 2006; 2008). The results of such research could contribute significantly to the debate surrounding subaqueous pyroclastic flows (e.g., Cas and Wright, 1991; Kokelaar and Busby, 1992).

6.4.3 Highly fractionated high-silica rhyolites as a source for REE

As highlighted in Chapter 5, these rhyolites are generally under-recognised in terms of REE concentrations. The research presented here suggests that these rhyolites should be considered prospective REE and HREE deposits, primarily as a result of the enrichment processes occurred during their petrogenesis. This means that more work should be undertaken on these rhyolites, both within the west Musgrave Province and elsewhere, focusing on those associated with elevated concentrations of fluorine. It is also suggested that further work be carried out in silicic large igneous provinces that also contain large volumes of these rhyolites, including the identification of highly evolved suites that are also potentially REE and HREE enriched.

6.5 References

Aitken, A.R., Smithies, R.H., Dentith, M.C., Joly, A., Evans, S. and Howard, H.M., 2013. Magmatism-dominated intracontinental rifting in the Mesoproterozoic: The Ngaanyatjarra Rift, central Australia. Gondwana Research, 24(3): 886-901.

Anderson, J.L. and Morrison, J., 2005. Ilmenite, magnetite, and peraluminous Mesoproterozoic anorogenic granites of Laurentia and Baltica. Lithos, 80(1-4): 45-60.

Andrews, G.D.M. and Branney, M.J., 2011. Emplacement and rheomorphic deformation of a large, lava-like rhyolitic ignimbrite; Grey's Landing, southern Idaho. Geological Society of America Bulletin, 123(3-4): 725-743.

Bachmann, O. and Bergantz, G., 2008. The magma reservoirs that feed supereruptions. Elements, 4(1): 17-21.

Branney, M.J., Kokelaar, B.P. and McConnell, B.J., 1992. The Bad Step Tuff; a lava-like rheomorphic ignimbrite in a calc-alkaline piecemeal caldera, English Lake District. Bulletin of Volcanology, 54(3): 187-199.

Branney, M.J. and Kokelaar, P., 1992. A reappraisal of ignimbrite emplacement: progressive aggradation and changes from particulate to non-particulate flow during emplacement of high-grade ignimbrite. Bulletin of Volcanology, 54(6): 504-520.

Branney, M.J., Bonnichsen, B., Andrews, G.D.M., Ellis, B., Barry, T.L. and McCurry, M., 2008. 'Snake River (SR)-type' volcanism at the Yellowstone hotspot track; distinctive products from unusual, high-temperature silicic super-eruptions. Bulletin of Volcanology, 70(3): 293-314.

Bryan, S.E, 2007. Silicic large igneous provinces. Episodes, 30(1): 20-31.

Bryan, S.E. and Ernst, R.E., 2008. Revised definition of large igneous provinces (LIPs). Earth-Science Reviews, 86(1-4): 175-202.

Bryan, S.E. and Ferrari, L., 2013. Large igneous provinces and silicic large igneous provinces; progress in our understanding over the last 25 years. Geological Society of America Bulletin, Pre-Issue Publication.

Bryan, S.E., Riley, T.R., Jerram, D.A., Stephens, C.J. and Leat, P.T., 2002. Silicic volcanism; an undervalued component of large igneous provinces and volcanic rifted margins. Special Paper - Geological Society of America, 362: 97-118.

Cas, R.A.F., Wright, H.M., Folkes, C.B., Lesti, C., Porreca, M., Giordano, G. and Viramonte, J.G., 2011. The flow dynamics of an extremely large volume pyroclastic flow, the 2.08-Ma Cerro Galán Ignimbrite, NW Argentina, and comparison with other flow types. Bulletin of volcanology, 73(10): 1583-1609.

Cas, R.A.F. and Wright, J.V., 1991. Subaqueous pyroclastic flows and ignimbrites: an assessment. Bulletin of Volcanology, 53(5): 357-380.

Christiansen, E.H., Haapala, I. and Hart, G.L., 2007. Are Cenozoic topaz rhyolites the

erupted equivalents of Proterozoic rapakivi granites? Examples from the Western United States and Finland. Lithos, 97(1-2): 219-246.

Christiansen, E.H., Sheridan, M.F. and Burt, D.M., 1986. The geology and geochemistry of Cenozoic topaz rhyolites from the Western United States. Geological Society of America (GSA), Boulder, CO, United States, 82 pp.

Creaser, R.A., Price, R.C. and Wormald, R.J., 1991. A-type granites revisited; assessment of a residual-source model. Geology (Boulder), 19(2): 163-166.

Dall'Agnol, R., Frost, C.D. and Rämö, O.T., 2012. IGCP Project 510 “A-type Granites and Related Rocks through Time”: Project vita, results, and contribution to granite research. Lithos, 151(0): 1-16.

Daniels, J.L., 1974. The geology of the Blackstone region, Western Australia. Bulletin - Geological Survey of Western Australia, 123: 257.

de Silva, S.L., 2008. Arc magmatism, calderas, and supervolcanoes. Geology (Boulder), 36(8): 671-672.

Ekren, E.B., McIntyre, D.H. and Bennett, E.H., 1984. High-temperature, large-volume, lavalike ash-flow tuffs without calderas in southwestern Idaho. U. S. Geological Survey, Reston, VA, United States, 76 pp.

Evins, P.M., Smithies, R.H., Howard, H.M., Kirkland, C.L., Wingate, M.T.D. and Bodorkos, S., 2010. Devil in the detail; the 1150-1000 Ma magmatic and structural evolution of the Ngaanyatjarra Rift, west Musgrave Province, central Australia. Precambrian Research, 183(3): 572-588.

Folkes, C.B., Wright, H.M., Cas, R.A., de Silva, S.L., Lesti, C. and Viramonte, J.G., 2011. A re-appraisal of the stratigraphy and volcanology of the Cerro Galán volcanic system, NW Argentina. Bulletin of volcanology, 73(10): 1427-1454.

Frindt, S., Trumbull, R.B. and Romer, R.L., 2004. Petrogenesis of the Gross Spitzkoppe topaz granite, central western Namibia; a geochemical and Nd-Sr-Pb isotope study. Chemical Geology, 206(1-2): 43-71.

Haapala, I. and Rämö, O.T., 1992. Tectonic setting and origin of the Proterozoic rapakivi granites of southeastern Fennoscandia. Special Paper - Geological Society of America, 272: 165-171.

Henry, C.D. and Wolff, J.A., 1992. Distinguishing strongly rheomorphic tuffs from extensive silicic lavas. Bulletin of Volcanology, 54(3): 171-186.

Howard, H.M., Werner, M., Smithies, R.H., Evins, P.M., Kirkland, C.L., Kelsey, D.E., Hand, M., Collins, A.S., Pirajno, F., Wingate, M.T.D., Maier, W.D. and Raimondo, T., 2011. The geology of the west Musgrave Province and the Bentley Supergroup -- a field guide. Record - Geological Survey of Western Australia, Perth, Australia, 2011/14: 125 pp.

Kirstein, L.A., Hawkesworth, C.J. and Garland, F.G., 2001. Felsic lavas or rheomorphic ignimbrites; is there a chemical distinction? Contributions to Mineralogy and Petrology, 142(3): 309-322.

Kokelaar, P. and Busby, C., 1992. Subaqueous explosive eruption and welding of pyroclastic deposits. Science, 257(5067): 196-201.

Lipman, P.W., 2000. Calderas. In: H. Sigurdsson (Editor), Encyclopedia of Volcanoes. Academic Press, San Francisco.

Manley, C.R., 1995. How voluminous rhyolite lavas mimic rheomorphic ignimbrites; eruptive style, emplacement conditions, and formation of tuff-like textures. Geology (Boulder), 23(4): 349-352.

McCurry, M., Hayden, K.P., Morse, L.H. and Mertzman, S., 2008. Genesis of post-hotspot, A-type rhyolite of the eastern Snake River Plain volcanic field by extreme fractional crystallization of olivine tholeiite. Bulletin of Volcanology, 70(3): 361-383.

Miller, C.F. and Wark, D.A., 2008. Supervolcanoes and their explosive supereruptions. Elements, 4(1): 11-15.

Mushkin, A., Navon, O., Halicz, L., Hartmann, G. and Stein, M., 2003. The petrogenesis of A-type magmas from the Amram Massif, southern Israel. Journal of Petrology, 44(5): 815-832.

Pankhurst, M., Schaefer, B. and Betts, P., 2011. Geodynamics of rapid voluminous felsic magmatism through time. Lithos, 123(1): 92-101.

Patino Douce, A.E., 1997. Generation of metaluminous A-type granites by low-pressure melting of calc-alkaline granitoids. Geology (Boulder), 25(8): 743-746.

Robert, G., Andrews, G.D., Ye, J. and Whittington, A.G., 2013. Rheological controls on the emplacement of extremely high-grade ignimbrites. Geology, 41(9): 1031-1034.

Rytuba, J.J., 1994. Evolution of volcanic and tectonic features in caldera settings and their importance in localization of ore deposits. Economic Geology, 89(8): 1687-1696.

Self, S., 2006. The effects and consequences of very large explosive volcanic eruptions. Philosophical Transactions of the Royal Society A: Mathematical, Physical and Engineering Sciences, 364(1845): 2073-2097.

Smithies, R., Kirkland, C., Korhonen, F., Aitken, A., Howard, H., Maier, W., Wingate, M., Quentin de Gromard, R. and Gessner, K., 2014. The Mesoproterozoic thermal evolution of the Musgrave Province in central Australia–plume vs. the geological record. Gondwana Research.

Smithies, R.H., Howard, H.M., Kirkland, C.L., Werner, M., Medlin, C.C., Wingate, M.T.D. and Cliff, J.B., 2013. Geochemical evolution of rhyolites of the Talbot Sub-basin and associated felsic units of the Warakurna Supersuite. Report - Geological Survey of Western Australia. Perth, Australia, 118: 74 pp.

Sparks, R.S.J., Self, S., Grattan, J.P., Oppenheimer, C., Pyle, D.M. and Rymer, H., 2005. Super-eruptions: global effects and future threats, London, UK.

Sparks, R.S.J., Tait, S.R. and Yanev, Y., 1999. Dense welding caused by volatile resorption. Journal of the Geological Society of London, 156, Part 2: 217-225.

Spinks, K.D., Acocella, V., Cole, J.W. and Bassett, K.N., 2005. Structural control of volcanism and caldera development in the transtensional Taupo Volcanic Zone,

New Zealand. Journal of Volcanology and Geothermal Research, 144(1): 7-22.

Trofimovs, J., Amy, L., Boudon, G., Deplus, C., Doyle, E., Fournier, N., Hart, M.B., Komorowski, J.C., Le Friant, A., Lock, E.J., Pudsey, C., Ryan, G., Sparks, R.S.J. and Talling, P.J., 2006. Submarine pyroclastic deposits formed at the Soufriere Hills Volcano, Montserrat (1995-2003); what happens when pyroclastic flows enter the ocean? Geology (Boulder), 34(7): 549-552.

Trofimovs, J.R., Sparks, S.J. and Talling, P.J., 2008. Anatomy of a submarine pyroclastic flow and associated turbidity current; July 2003 dome collapse, Soufriere Hills Volcano, Montserrat, West Indies. Sedimentology, 55(3): 617-634.

Turner, S., Foden, J. and Morrison, R., 1992a. Derivation of some A-type magmas by fractionation of basaltic magma: an example from the Padthaway Ridge, South Australia. Lithos, 28(2): 151-179.

Turner, S., Sandiford, M. and Foden, J., 1992b. Some geodynamic and compositional constraints on" postorogenic" magmatism. Geology, 20(10): 931-934.

Werner, M., Howard, H.M. and Smithies, R.H., 2012. Mount Eveline, WA Sheet 4345 1:100 000 Geological Series. Geological Survey of Western Australia.

Whalen, J.B., Currie, K.L. and Chappell, B.W., 1987. A-type granites; geochemical characteristics, discrimination and petrogenesis. Contributions to Mineralogy and Petrology, 95(4): 407-419.

Willcock, M.A.W., Cas, R.A.F., Giordano, G. and Morelli, C., 2013. The eruption, pyroclastic flow behaviour, and caldera in-filling processes of the extremely large volume (1290 km^3), intra- to extra-caldera, Permian Ora (ignimbrite) Formation, southern Alps, Italy. Journal of Volcanology and Geothermal Research, 265: 102-126.

Wingate, M.T.D., Pirajno, F. and Morris, P.A., 2004. Warakurna large igneous province: A new Mesoproterozoic large igneous province in west-central Australia. Geology, 32(2): 105-108.

Appendices

Appendix A

Regional Geology

A.1 The Musgrave region and west Musgrave Province

This section will provide a concise introduction on the Musgrave region of central Australia (Fig. 1.3), with specific focus on the 1.60–1.15 Ga west Musgrave Province (Fig. 1.4), the Western Australia part of the larger Mesoproterozoic Musgrave Province that straddles the borders between the Northern Territory, South Australia and Western Australia (Wade *et al*., 2008; Smithies *et al*., 2009).

The Musgrave Province is defined as a WNW-ESE orientated belt of high-grade metamorphic rocks, bounded by the mid-Neoproterozoic–mid-Palaeozoic Amadeus Basin to the north, the mid-Neoproterozoic–early-Palaeozoic Officer Basin to the south, the Paleozoic–Mesozoic Canning Basin to the west, and the Permian–Mesozoic Eromanga Basin to the east (Fig. 1.3; Wade *et al*., 2008; Smithies *et al*., 2009). In broad terms, the Musgrave Province consists of high-grade metamorphic rocks (amphibolite to granulite facies), with voluminous volcanic and lesser sedimentary rocks (Conor, 1987; Scrimgeour *et al*., 1999; Wade *et al*., 2006; Smithies *et al*., 2014) that are intruded by a number of younger granitoids, mafic-ultramafic layered and massive intrusions, and mafic and felsic dykes (Wade *et al*., 2006). The Musgrave Province as a whole has a clearly identifiable geophysical signature, expressed as a series of west-east trending aeromagnetic anomalies up to 800 km long and 350 km wide lying at the convergence of three Proterozoic structural trends formed by the amalgamation of the North, West and South Australian Cratons (Fig. 1.5; Wade *et al*., 2008; Smithies *et al*., 2009; Howard *et al*., 2011).

A.1.1 Major structural domains of the Musgrave Province

The Musgrave Province has been previously separated into different structural and metamorphic zones by major west- and west-northwest trending faults last activated during the 620–530 Ma Petermann Orogeny (Smithies *et al*., 2009). There are two main metamorphic domains within the Musgrave Province, the granulite facies Fregon Zone to the south and the amphibolite facies Mulga Park Zone in the north (Fig. 1.3; Collerson *et al*., 1972; Maboko, 1988; Edgoose *et al*., 1993; Major and Conor, 1993; Camacho *et al*., 1997), separated by the south-dipping Woodroffe Thrust which strikes roughly east-west throughout the length of the province (Wade *et al*., 2008). Geochemical and geochronological similarities between the two zones indicate similar tectonic histories (Camacho and Fanning, 1995). The eastern part of the Fregon Zone shows a north-south change in metamorphism, from high-pressure (10–14 kbar; Scrimgeour and Close, 1999) metamorphism occurring during the Petermann Orogen, to low-pressure, high temperature metamorphism during the Mesoproterozoic

(Clarke *et al*., 1995b). The west Musgrave Province (Fig. 1.4) is restricted to the Fregon Zone and can be further subdivided into the Walpa Pulka Zone, Tjuni Purlka Zone, and the Mamutjarra Zone, based on changes in the age and distribution of various rock types, and furthermore on the style and intensity of the deformation (Smithies *et al*., 2009; 2010).

A.1.2 Basement to the Musgrave Province

The extent and tectonic setting of the basement to the Province is poorly understood. The earliest basement components of the Musgrave Province include a ca. 1950 Ma mantle derived mafic to intermediate component (Kirkland *et al*., 2013), with further juvenile mantle input at a 1650–1550 Ma convergent margin (Wade *et al*., 2008; Kirkland *et al*., 2013; Smithies *et al*., 2014). The rocks that were either formed or deposited ca. 1600–1540 Ma (later metamorphosed during the 1220–1150 Ma Musgrave Orogeny), include the Musgravian Gneiss, also termed the Olia Gneiss in the Mulga Park Domain, and the Birksgate Complex in the Fregon Domain (Major and Conor, 1993; Edgoose *et al*., 2004), ranging from amphibolite facies to granulite facies respectively (Collerson *et al*., 1972; Maboko, 1988; Edgoose *et al*., 1993; Major and Conor, 1993; Camacho *et al*., 1997; Wade *et al*., 2008). In both domains the Musgravian Gneiss is dominantly felsic in composition, with interlayered subordinate mafic units and rare metapelite with local mafic and felsic interlayering (Wade *et al*., 2008). This succession of magmatic, volcanic and lesser metasediments may represent a magmatic arc environment with major juvenile crustal additions of intercalated felsic and mafic gneiss, followed by the closure of the ocean separating the North Australian Craton and the South Australian Craton at ca. 1.54 Ga (Major and Conor, 1993; Glikson *et al*., 1996; Scrimgeour *et al*., 1999; Edgoose *et al*., 2004; Wade *et al*., 2006; 2008).

According to Howard *et al*. (2011) there is no clear evidence for exposed crust that formed before ca. 1400 Ma in the west Musgrave Province, except for very poorly preserved and isolated Papulankutja Supersuite granites that intruded during a ca. 1410 Ma event; (Smithies *et al*., 2014). Most of the exposed basement is composed of supracrustal packages of banded gneiss preserved as rafts within granites, whose protoliths were emplaced between ca. 1340 and 1270 Ma (Evins *et al*., 2011), and are named the Wirku Metamorphics (Smithies *et al*., 2009; Howard *et al*., 2011). The interpreted sedimentary and lesser volcaniclastic and volcanic origin of the protoliths to the Wirku Metamorphics were deposited in the Ramarama Basin (Evins *et al*., 2011) and represent a supracrustal depositional component of the 1345–1293 Ma Mount West Orogeny (Howard *et al*., 2011). The protoliths to the gneisses, which form the dominant oldest components of the Musgrave Province, are supracrustal rocks dominated by volcanic, volcaniclastic and clastic material, deposited at ca. 1550 Ma (Gray, 1971; 1978; Gray and Compston, 1978; Maboko *et al*., 1991; Major and Conor, 1993; Camacho and Fanning, 1995; Edgoose *et al*., 2004).

A.2 Tectonic evolution of the Musgrave Region and west Musgrave Province

According to Aitken and Betts (2009), the Musgrave Province records a large part of the Australian continent's evolution, with continental growth in the early Mesoproterozoic (ca. 1600 Ma; Gray, 1978; Camacho and Fanning, 1995; Wade *et al*., 2006), Rodinia assembly in the mid to late Mesoproterozoic (ca. 1.30–1.1 Ga; Maboko *et al*., 1992; Glikson *et al*., 1995; Camacho *et al*., 1997; Edgoose *et al*., 2004; Wade *et al*., 2008), Rodinia break-up in the mid-Neoproterozoic (ca. 800 Ma; Zhao and McCulloch, 1993; Wade *et al*., 2008) and Gondwana assembly in the late Neoproterozoic to early Cambrian (ca. 600–500 Ma; Maboko *et al*., 1991; Camacho and McDougal, 2000; Wade *et al*., 2005). Therefore understanding the tectonic setting of the Musgrave Province has important implications for both current and future work on the reconstructions of the early Australian continent.

The Musgrave Province has recorded a number of deformational events in its history and these have been summarised in detail by Wade *et al*. (2008). The major events include the ca. 1345–1293 Ma Mount West Orogeny, which is represented by metagranitic rocks from the Wankanki Supersuite, with crystallization ages from 1326–1312 Ma (White *et al*., 1999; Kirkland *et al*., 2008; Howard *et al*., 2011). This may have formed in a possible continental arc tectonic setting that may reflect the final stage of Proterozoic amalgamation of central Australia through final subduction and lateral accretion. This occurred before the onset of the Musgrave Orogeny, with a collisional event that produced northeast-trending folds (Giles *et al*., 2004; Betts and Giles, 2006; Smithies *et al*., 2009; 2010; 2011; Evins *et al*., 2011; Kirkland *et al*., 2013). During this period, it has been proposed by several authors (Clark *et al*., 2000; Bodorkos and Clark, 2004; Cawood and Korsch, 2008; Kirkland *et al*., 2011) that the Albany-Fraser Orogen, to the southwest of the Musgrave Province, involved the convergence, collision, and suturing of the West Australian Craton with the southern Mawson Craton. This occurred along either a north- or south-dipping subduction zone between ca. 1345–1290 Ma, which coincides with the Mount West Orogeny and thus links the two orogens (Howard *et al*., 2011). The granites of the Wankanki Supersuite are metaluminous, calcic to calcic-alkaline granodiorites and monzogranites compositionally similar to modern continental arc granites (Smithies *et al*., 2011).

Howard *et al*. (2011) interprets large-scale northwest-southeast compression, followed by crustal thinning, somewhere between the end of the Mount West Orogeny and the beginning of the Musgrave Orogeny, but suggests that even this may be an oversimplification of pre-Musgrave Orogeny events in the area.

The 1220–1150 Ma Musgrave Orogeny affected the whole Musgrave Province and

involved intense mylonitic deformation, with widespread amphibolite- to granulite-facies metamorphism and the generation of large amounts of syn- and post-tectonic, rapakivi-textured, orthopyroxene-bearing, anhydrous, alkali-calcic, Pitjantjatjara Supersuite granites, in a suggested intraplate setting (Edgoose *et al*., 2004; Wade *et al*., 2008; Howard *et al*., 2011; Smithies *et al*., 2011). This event represents an unusually long period of ultra-high temperature metamorphism (Kelsey *et al*., 2009; 2010) and continuous lower crustal thinning in an extensional intracontinental setting developed within a suture zone between three older cratonic blocks (Smithies *et al*., 2010; 2014; Howard *et al*., 2011). This gave rise to a unique, plate tectonic, regional low-pressure "melt trap" below the Musgrave Province, due to a relatively thinner continental crust than that of the surrounding north, west, and south Australian cratons, allowing it to act as an asthenospheric heat-trapping sink for a long period of time (Smithies *et al*., 2010; 2011; 2014; Howard *et al*., 2011). By the end of the Musgrave Orogeny, the Musgrave Province had undergone a 100 Ma period of ultra-high-temperature metamorphism, in either an intracontinental or distal backarc environment (Kirkland *et al*., 2013; Smithies *et al*., 2011).

Following the Musgrave Orogeny was the 1085–1040 Ma Giles Event, which coincides with the assembly of Rodinia (Cawood, 2005). This event has been interpreted to be the result of a deep mantle plume (Zhao and McCulloch, 1993; Wingate *et al*., 2004; Morris and Pirajno, 2005; Godel *et al*., 2011; Pirajno and Hoatson, 2012). However, a more complex intra-plate geodynamic setting has been suggested for the event due to almost continuous (>30 Ma) continental mafic magmatism and felsic magmatism (Smithies *et al*., 2011, 2014). The heat responsible for this magmatism involved conductive heat (including a large radiogenic component), residual heat from under- and intra-plating of mantle-derived melts during the Musgrave Orogeny, and advective heat resulting from a continuation of this process during the Giles Event (Smithies *et al*., 2010, 2011; 2013; Kirkland *et al*., 2013). Movement along the then active Mundrabilla Shear Zone (Fig. 6.2), a prominent south-north trending, continent-scale, basement structural lineament that intersects the west Musgrave Province (Aitken *et al*., 2012), could have provided a trigger mechanism for catastrophically disrupting the long-term regional Musgrave thermal anomaly (still present after the Musgrave Orogeny), by juxtaposing lithosphere of contrasting thermal and physical properties, causing major asthenospheric upwellings of source heat for the Giles Event (Smithies *et al*., 2014). The Alcurra Dolerite (Suite) that cross-cuts and dissects most of the Musgrave Province may represent the feeder dykes to these Giles intrusions (Zhao and McCulloch, 1993; Zhao *et al*., 1994; Glikson *et al*., 1996; Scrimgeour *et al*., 1999; Wade *et al*., 2008).

The next event was intrusion of the ca. 820 Ma Amata Dolerite dykes (Zhao *et al*., 1994; Glikson *et al*., 1996; Wade *et al*., 2008), which are believed to be plume-related mafic intrusions linked to the initial Adelaide Rift Complex (Preiss, 2000). This represents

the break-up of Proterozoic Australia (Direen and Crawford, 2003) and the initiation of the Centralian Superbasin, covering most of central and southern Australia during the late Proterozoic (Maboko, 1988; Zhao and McCulloch, 1993; Zhao *et al*., 1994; Walter *et al*., 1995; Wade *et al*., 2006).

Following this is the ca. 580–530 Ma intracratonic Petermann Orogeny, defined by movements along the tectonic boundaries of the Musgrave Province and expressed locally in strongly deformed rocks throughout the Musgrave Province, with emphasis on rocks from the Bentley Supergroup and Warakurna Supersuite (Camacho, 1997; Edgoose *et al*., 2004; Howard *et al*., 2011). During this orogeny, granulites and high-grade gneisses were thrust northwards and over or interleaved with rocks of the bounding Neoproterozoic basins (Camacho, 1997; Edgoose *et al*., 2004) in a process likely involving intracontinental channel flow (Raimondo *et al*., 2009; 2010), with significant vertical displacements (Howard *et al*., 2011). During this orogeny an intraplate transpressional event resulted in the exhumation of the northern Musgrave Province (Zhao *et al*., 1994; Walter *et al*., 1995; Wade *et al*., 2008). The Petermann Orogeny coincides with the global Pan-African Event, during the assembly of Gondwana (Cawood and Buchan, 2007).

The last main tectonic event to affect central Australia is the ca. 450–300 Ma Alice Springs Orogeny (Collins and Teyssier, 1989; Haines *et al*., 2001), a major intraplate orogenic event, but there is no firm evidence that this affected the Musgrave Province (Howard *et al*., 2011).

A.3 The Giles Event

Mafic to felsic magmas were emplaced into and erupted onto the Musgrave Province during the 1085–1040 Ma Giles Event (Howard *et al*., 2011; Smithies *et al*., 2014). These include variably deformed mafic-ultramafic layered and massive intrusions, voluminous bimodal volcanics, granitic intrusions, massive gabbros mixed and intermingled with the granites, felsic and mafic dykes and a supracrustal rift-related succession (Glikson *et al*., 1995; 1996; Sun *et al*., 1996; Close *et al*., 2003; Edgoose *et al*., 2004; Wade *et al*., 2008; Howard *et al*., 2011). All igneous rocks that are related to this event have been assigned to the Warakurna Supersuite, which outcrops across ~1.5 million km^2 of central and western Australia, part of which forms the 1078–1073 Ma Warakurna Large Igneous Province (LIP; Fig. 1.5; Wingate *et al*., 2004; Morris and Pirajno, 2005; Howard *et al*., 2011).

The mafic-ultramafic layered and massive intrusions, known collectively as the ‘Giles intrusions’, are restricted to the Fregon Domain (Glikson *et al*., 1995; 1996; Sun *et al*., 1996; White *et al*., 2002; Wade *et al*., 2008). The Giles intrusions vary in

composition from gabronorite to peridote and anorthosites (Goode, 1970; Moore, 1970; Daniels, 1974; Glikson *et al*., 1996). The first occurring mafic units associated with the Giles Event, termed “G1”, are broadly troctolitic, peridotitic, or gabbroic in composition, and attain a maximum cumulative stratigraphic thickness of 10 km, with the possibility of originally being 170 km long and 25 km wide. They have emplacement ages of between ca. 1078–1075 Ma (Howard *et al*., 2011). After the G1 event there was the emplacement of massive, unlayered gabbros and leucogranites, termed “G2” (ca. 1078 and 1074 Ma) which form features focused along syn-magmatic shear zones, and display mixing and mingling textures with one another (Howard *et al*., 2011). The G2 intrusions are interpreted as being younger than the G1 layered intrusions, through temporal field relationships (Howard *et al*., 2011). The narrow period of G2 intrusion is accompanied by evidence for both northwest-trending folding and shearing (Howard *et al*., 2007; Howard *et al*., 2011), confirming suggestions by Clark *et al* (1995a) that substantial deformation occurred in the Musgrave Province during the Giles Event.

The granitic intrusions and felsic dykes associated with the Giles Event are found to occur across the Musgrave Province, while the bimodal volcanic rocks of the Warakurna Supersuite are restricted to the Fregon Domain, and form the main components of the Bentley Supergroup (Daniels, 1974). The supra-crustal rift-related succession that is related to the Giles Event is confined to the Mulga Park Domain (Glikson *et al*., 1996; Sun *et al*., 1996; Close *et al*., 2003; Edgoose *et al*., 2004; Wade *et al*., 2008; Howard *et al*., 2011).

A.3.1 The Ngaanyatjarra Rift

The structural expression of the Giles Event is the long-lived failed intracontinental Ngaanyatjarra Rift, which formed the Bentley Basin (Evins *et al*., 2010) into which the Bentley Supergoup (Daniels, 1974) is deposited. The development of the Ngaanyatjarra Rift can be broken down into four major stages, an early rifting stage, which produced the Kunmarnara and Tjauwata groups (see Bentley Supergroup below), followed by voluminous mafic intrusion with the up to 8–10 km thick (cumulative), 170 km long and 25 km wide Giles Intrusions. This was followed by formation of the extensive, but short-lived (ca. 1078–1073 Ma) Warakurna LIP, represented by dykes and sills of the Alcurra Dolerite (Suite) with equivalents intruding across large parts of central and Western Australia (Wingate *et al*., 2004), and finally ending with the bimodal volcanism component of the Warakurna Supersuite (Evins *et al*., 2010; Smithies *et al*., 2014).

A.3.2 The Bentley Supergroup

The Bentley Supergroup, which hosts all the bimodal volcanic rocks of the

Warakurna Supersuite and Ngaanyatjarra Rift-related successions, is preserved only in the 'upper-crustal' west Musgrave Province, and is made up of felsic and mafic volcanics, volcaniclastic rocks, and interlayered sedimentary rocks (Smithies *et al*., 2009; 2014). The volcanic rocks associated with the Bentley Supergroup have been suggested to be comagmatic with the layered mafic-ultramafic Giles intrusions and coeval granites (Compston and Nesbitt, 1967; Daniels, 1974; Glikson *et al*., 1995; 1996).

The outcrop extent of the Bentley Supergoup defines the preserved extent of the Bentley Basin, which can be subdivided into the three sub-basins, the Talbot, Blackstone and Finlayson Sub-basins (Fig. 1.6; Howard *et al*., 2011; Smithies *et al*., 2014). An episode of syn- to post-depositional folding deformed the rocks of the Blackstone Sub-Basin, resulting in a synclinal fold axis roughly parallel to the axis of the basin, known as the Blackstone syncline (Howard *et al*., 2011). The Talbot Sub-basin, comprising a series of thick and regionally continuous layers of rhyolitic ignimbrites, rheomorphic ignimbrites and lava flows, interlayered with basaltic lava flows and siliciclastic rocks, has several spatially closely associated, semi-connected, and fault bounded depositional domains. Each of these is characterised by a specific stratigraphy, structural style, and diagenetic-metamorphic history, with overlap in the timing of volcanism and sedimentation in each depositional area. This indicates structurally compartmentalised syn-depositional tectonics, with caldera subsidence, subvolcanic doming and possible compressional deformation taking place during the Giles Event (Howard *et al*., 2011; Smithies *et al*., 2014).

The stratigraphy of the Bentley Supergroup is comprised of the basal northeastern Tjauwata Group (Bloods Range, Northern Territory) and the southeastern to central Kunmarnara Group, which is composed of basal sandstones, pebbly sandstones, and conglomerates of the MacDougall Formation, the Mummawarrawarra basalts, and minor felsic volcanics (Howard *et al*., 2011). There is a correlatable fault-bounded volcanic succession, known as the Skirmish Hill volcanic association (Daniels, 1974) in the southeast corner of the west Musgraves, comprising rhyolitic-dacitic volcanic and volcaniclastic rocks, interlayered with andesitic volcanic rocks (Howard *et al*., 2011). Minimum depositional ages for the Kunmarnara Group are constrained by 1090 Ma granites (Edgoose *et al*., 2004) and the initial 1078 Ma Giles intrusions (Howard *et al*., 2011).

The Kunmarnara Group is unconformably overlain by the Blackstone Sub-basin, to the south of the Blackstone Community, which comprises felsic and mafic volcanic units, which include the centrally-restricted ca. 1071–1073 Ma Tollu Group, comprised of the felsic lavas of the Smoke Hill Volcanics, and basic to intermediate lavas of the ca. 1068 Ma Hogarth Formation (Howard *et al*., 2011). Coeval with the Tollu Group, but

located in the Mulga Park Domain, is the rift-related supra-crustal succession, which forms the Tjauwata Group, consisting of the basal Smoke Hill Felsic Volcanic (ca. 1075 Ma) and the upper Wankari Volcanics (ca. 1.04 Ga) unit (Sun *et al*., 1996; Close *et al*., 2003).

To the west of the Jamieson Community is the Talbot Sub-Basin, which is largely undeformed, except locally close to shears and faults, with most of the rocks typically preserved at greenschist facies (Smithies *et al*., 2013). This basin contains the largest exposure of rocks of the Bentley Supergroup. The stratigraphic base of this group is represented by the effusive and ignimbritic rocks of the Mount Palgrave Group, a west- to southwest-younging succession of dacitic to rhyolitic volcanic and pyroclastic rocks, with minor intercalations of basalt and sedimentary rocks (Howard *et al*., 2011). The eastern margin of the Palgrave area is intruded by the syn-volcanic Winburn granite, a suite of monzogranitic to alkali-feldspar granites and quartz alkali feldspar syenites, which removed the base of the thick volcanic succession that makes up the group (Smithies *et al*., 2013; 2014). The northwestern part of the Talbot Sub-basin consists of the Scamp rhyolite, an area of extrusive volcanic lavas and granites, occupying an oval-shaped region ~75 km long and ~40 km wide (Howard *et al*., 2011). These felsic rocks belong to the Mount Palgrave Group due to age and geochemical similarities (Smithies *et al*., 2013). The Mount Palgrave Group as a whole reflects a series of voluminous, highly-evolved, rhyolitic magmas and lesser tholeiitic mafic magmas, with high-energy, violent eruptions (Smithies *et al*., 2013).

The Mount Palgrave Group is overlain by the Kaarnka Group, representing a discrete north-northwest trending oval-shaped basin, up to 27 km wide and 46 km long, thought to represent a caldera cluster (Daniels, 1974; Smithies *et al*., 2013). This group is characterised by massive to flow-banded rhyolite with intercalations of ignimbrite and lesser amounts of siliciclastic sedimentary rocks and minor basalt (Smithies *et al*., 2013).

In the southern part of the Talbot Sub-Basin, the Mount Palgrave and Kaarnka groups are directly overlain (apparently conformably) by the Pussy Cat Group, which is in turn overlain by the Cassidy Group, which comformably underlies the Mission Group. These are south-dipping and south-younging volcanic-sedimentary successions that form a stratigraphically continuous, bow-shaped, southeast to east-trending outcrop, attaining a cumulative thickness of several kilometres (Howard *et al*., 2011). The basal two groups comprise bimodal volcanic and lesser sedimentary rocks (Smithies *et al*., 2013). Units within the Cassidy Group are considered to be the result of single voluminous supereruptions (erupted volumes >450 km^3; Sparks *et al*., 2005; Self, 2006; Smithies *et al*., 2014). The Mission Group is the youngest preserved stratigraphic interval of the Bentley Supergroup and comprises a lower sedimentary part and upper basaltic part, with no felsic volcanism (Smithies *et al*., 2013). This group is conformably to unconformably

overlain by the Townsend Quartzite, with the thickest preserved continuous stratigraphic column of the Bentley Supergroup in the Talbot Sub-basin measuring ~12 km (Smithies *et al*., 2013).

Daniels (1974) originally interpreted the Palgrave, Scamp and Skirmish Hill areas as discreet fault-bounded cauldrons (an eroded caldera complex; Fig. 1.7), however, Howard *et al*. (2011) suggest that these areas rather be seen as large volcano-tectonic depressions with possible localised syn-magmatic faulting and/or caldera formational features. Smithies *et al*. (2013) do not currently recognise the Scamp caldera, but recognise the Palgrave cauldron (now termed the Kaarnka caldera cluster; Fig. 6.3), with a modification of the original postulated extent.

A.4 References

Aitken, A.R.A. and Betts, P.G., 2009. Constraints on the Proterozoic supercontinent cycle from the structural evolution of the south-central Musgrave Province, central Australia. Precambrian Research, 168(3-4): 284-300.

Aitken, A.R.A., Smithies, R.H., Dentith, M.C., Joly, A., Evans, S. and Howard, H.M., 2012. Magmatism-dominated intracontinental rifting in the Mesoproterozoic: The Ngaanyatjarra Rift, central Australia. Gondwana Research.

Betts, P.G. and Giles, D., 2006. The 1800-1100 Ma tectonic evolution of Australia. Precambrian Research, 144(1-2): 92-125.

Bodorkos, S. and Clark, D.J., 2004. Evolution of a crustal-scale transpressive shear zone in the Albany-Fraser Orogen, SW Australia: 2. Tectonic history of the Coramup Gneiss and a kinematic framework for Mesoproterozoic collision of the West Australian and Mawson cratons. Journal of Metamorphic Geology, 22(8): 713-731.

Camacho, A., 1997. An isotopic study of deep-crustal orogenic processes, Musgrave Block, central Australia. Ph.D. Thesis, Australian National University, Canberra.

Camacho, A., Compston, W., McCulloch, M. and McDoucall, I., 1997. Timing and exhumation of eclogite facies shear zones, Musgrave Block, central Australia. Journal of Metamorphic Geology, 15(6): 735-751.

Camacho, A. and Fanning, C.M., 1995. Some isotopic constraints on the evolution of the granulite and upper amphibolite facies terranes in the eastern Musgrave Block, central Australia. Precambrian Research, 71(1-4): 155-181.

Camacho, A. and McDougal, I., 2000. Intracratonic, strike-slip partitioned transpression and the formation and exhumation of eclogite facies rocks: An example from the Musgrave Block, central Australia. Tectonics, 19(5): 978-996.

Cawood, P.A., 2005. Terra Australis Orogen; Rodinia breakup and development of the Pacific and Iapetus margins of Gondwana during the Neoproterozoic and Paleozoic. Earth-Science Reviews, 69(3-4): 249-279.

Cawood, P.A. and Buchan, C., 2007. Linking accretionary orogenesis with supercontinent assembly. Earth-Science Reviews, 82(3-4): 217-256.

Cawood, P.A. and Korsch, R.J., 2008. Assembling Australia: Proterozoic building of a continent. Precambrian Research, 166(1-4): 1-35.

Clark, D.J., Hensen, B.J. and Kinny, P.D., 2000. Geochronological constraints for a two-stage history of the Albany-Fraser Orogen, Western Australia. Precambrian Research, 102(3-4): 155-183.

Clarke, G.L., Buick, I.S., Glikson, A.Y. and Stewart, A.J., 1995a. Structural and pressure-temperature evolution of host rocks of the Giles Complex, western Musgrave Block, central Australia: evidence for multiple high-pressure events. AGSO Journal of Australian Geology & Geophysics, 16(1-2): 127-146.

Clarke, G.L., Sun, S.S. and White, R.W., 1995b. Grenville-age belts and associated older terranes in Australia and Antarctica. AGSO Journal of Australian Geology & Geophysics, 16(1-2): 25-39.

Close, D.F., Edgoose, C.J. and Scrimgeour, I.R., 2003. Hull and Bloods Range Special, Northern Territory. 1:100000 Geological Map Series Explanatory Notes, Northern Territory Geological Survey, Darwin.

Collerson, K.D., Oliver, R.L. and Rutland, R.W.R., 1972. An example of structural and metamorphic relationships in the Musgrave Orogenic Belt, central Australia. Journal of the Geological Society of Australia, 18: 379-393.

Collins, W.J. and Teyssier, C., 1989. Crustal scale ductile fault systems in the Arunta Inlier, central Australia. Tectonophysics, 158(1-4): 49-58,60,63-66.

Compston, W. and Nesbitt, R.W., 1967. Isotopic age of the Tollu volcanics, W. A. Journal of the Geological Society of Australia, 14, Part 2: 235-238.

Conor, C.H.H., 1987. The geology of the Eateringinna 1:100000 sheet area eastern Musgrave Block, South Australia. M.Sc Thesis, University of Adelaide, Adelaide.

Daniels, J.L., 1974. The geology of the Blackstone region, Western Australia. Bulletin - Geological Survey of Western Australia, 123: 257.

Direen, N.G. and Crawford, A.J., 2003. Fossil seaward-dipping reflector sequences preserved in southeastern Australia: A 600 Ma volcanic passive margin in eastern Gondwanaland. Journal of the Geological Society, 160(6): 985-990.

Edgoose, C.J., Camacho, A., Wakelin-King, G.W. and Simons, B., 1993. Kulgera, N.T. 1:250000 Geological Series Explanatory Notes SG53-5, Northern Territory Geological Survey.

Edgoose, C.J., Scrimgeour, I.R. and Close, D.F., 2004. Geology of the Musgrave Block, Northern Territory. Northern Territory Geological Survey, Report 15.

Evins, P.M., Smithies, R.H., Howard, H.M., Kirkland, C.L., Wingate, M.T.D. and Bodorkos, S., 2010. Devil in the detail; the 1150-1000 Ma magmatic and structural evolution of the Ngaanyatjarra Rift, west Musgrave Province, central Australia. Precambrian Research, 183(3): 572-588.

Giles, D., Betts, P.G. and Lister, G.S., 2004. 1.8-1.5-Ga links between the North and South Australian Cratons and the Early-Middle Proterozoic configuration of Australia. Tectonophysics, 380(1-2): 27-41.

Glikson, A.Y., Ballhaus, C.G., Clarke, G.L., Sheraton, J.W., Stewart, A.J. and Sun, S.S., 1995. Geological framework and crustal evolution of the Giles mafic- ultramafic complex and environs, western Musgrave Block, central Australia. AGSO Journal of Australian Geology & Geophysics, 16(1-2): 41-67.

Glikson, A.Y., Stewart, A.J., Ballhaus, C.G., Clarke, G.L., Feeken, E.H.J., Leven, J.H., Sheraton, J.W. and Sun, S.S., 1996. Geology of the western Musgrave Block, central Australia, with particular reference to the mafic-ultramafic Giles Complex. Bulletin - Australian Geological Survey Organisation, 239.

Godel, B., Seat, Z., Maier, W.D. and Barnes, S.-J., 2011. The Nebo-Babel Ni-Cu-PGE sulfide deposit (West Musgrave Block, Australia): Pt. 2. Constraints on parental magma and processes, with implications for mineral exploration. Economic Geology, 106(4): 557-584.

Goode, A.D.T., 1970. The petrology and structure of the Kalka and Ewarara layered basic intrusions, Giles Complex, central Australia. Ph.D Thesis, University of Adelaide, Adelaide.

Gray, C.M., 1971. Strontium isotope studies on granites. Ph.D. Thesis, Australian National University, Canberra.

Gray, C.M., 1978. Geochronology of granulite-facies gneisses in the western Musgrave Block, central Australia. J. Geol. Soc. Aust., 25: 403-414.

Gray, C.M. and Compston, W., 1978. A rubidium-strontium chronology of the metamorphism and prehistory of central Australian granulites. Geochimica et Cosmochimica Acta, 42(11): 1735-1747.

Haines, P.W., Hand, M. and Sandiford, M., 2001. Palaeozoic synorogenic sedimentation in central and northern Australia; a review of distribution and timing with implications for the evolution of intracontinental orogens. Australian Journal of Earth Sciences, 48(6): 911-928.

Howard, H.M., Smithies, R.H. and Pirajno, F., 2007. Geochemical and Nd isotopic signatures of mafic dykes in the western Musgrave Complex. Geological Survey of Western Australia Annual Review, Perth, Australia, 2005-06: 64-71.

Howard, H.M., Werner, M., Smithies, R.H., Evins, P.M., Kirkland, C.L., Kelsey, D.E., Hand, M., Collins, A.S., Pirajno, F., Wingate, M.T.D., Maier, W.D. and Raimondo, T., 2011. The geology of the west Musgrave Province and the Bentley Supergroup -- a field guide. Record - Geological Survey of Western Australia, Perth, Australia, 2011/14: 125.

Kelsey, D.E, Hand, M., Smithies, R.H., Evins, P., Clark, C. and Kirkland, C.L, 2009. High-temperature, high geothermal gradient metamorphism in the Musgrave Province, central Australia; potential constraints on tectonic setting, Kangaroo Island 2009,

Biennial Conference of the Specialist Group for Geochemistry, Mineralogy and Petrology, November 2009. Geological Society of Australia Abstracts, pp. 28.

Kelsey, D.E., Smithies, R.H., Hand, M., Evins, P.M., Clark, C. and Kirkland, C.L., 2010. What is the tectonic setting of long-lived Grenvillian-aged ultrahigh temperature, high geothermal gradient metamorphism in the Musgrave Province, central Australia, Geological Society of America, Abstracts with Programs, Denver Colorado, 42:5.

Kirkland, C.L., Smithies, R.H., Woodhouse, A.J., Howard, H.M., Wingate, M.T.D., Belousova, E.A., Cliff, J., Murphy, R. and Spaggiari, C.V., 2013. Constraints and deception in the isotopic record; the crustal evolution of the west Musgrave Province, central Australia. Gondwana Research, 23: 759-781.

Kirkland, C.L., Spaggiari, C.V., Pawley, M.J., Wingate, M.T.D., Smithies, R.H., Howard, H.M., Tyler, I.M., Belousova, E.A. and Poujol, M., 2011. On the edge: U-Pb, Lu-Hf, and Sm-Nd data suggests reworking of the Yilgarn craton margin during formation of the Albany-Fraser Orogen. Precambrian Research, 187(3-4): 223-247.

Kirkland, C.L., Wingate, M.T.D. and Bodorkos, S., 2008. 183496: orthogneiss, Mount West. Geochronology Record 747: Geological Survey of Western Australia, Perth, Australia, 5.

Maboko, M.A.H., 1988. Metamorphic and Geochronological Evolution in the Musgrave Ranges, Central Australia. Ph.D. Thesis, Australian National University, Canberra.

Maboko, M.A.H., McDougall, I., Zeitler, P.K. and Williams, I.S., 1992. Geochronological evidence for ~530-550 Ma juxtaposition of two Proterozoic metamorphic terranes in the Musgrave Ranges, central Australia. Australian Journal of Earth Sciences, 39(4): 457-471.

Maboko, M.A.H., Williams, I.S. and Compston, W., 1991. Zircon U-Pb chronometry of the pressure and temperature history of granulites in the Musgrave Ranges, central Australia. Journal of Geology, 99(5): 675-697.

Major, R.B. and Conor, C.H.H., 1993. The Musgrave Block. In: Parker, A.J. (Ed.), The Geology of South Australia. The Precambrian. Geol. Surv. South. Aust. Bull., 1: pp. 156-167.

Moore, A., 1970. The Geology of the Gosse Pile Ultramafic intrusion and of the surrounding granulites, Tomkinson Ranges, central Australia. Ph.D. Thesis, University of Adelaide, Adelaide.

Morris, P.A. and Pirajno, F., 2005. Mesoproterozoic sill complexes in the Bangemall Supergroup, Western Australia; geology, geochemistry, and mineralization potential, Geological Survey of Western Australia, Perth, West. Aust., Australia, 99: 75.

Pirajno, F. and Hoatson, D.M., 2012. A review of Australia's Large Igneous Provinces and associated mineral systems: Implications for mantle dynamics through geological time. Ore Geology Reviews, 48: 2-54.

Preiss, W.V., 2000. The Adelaide Geosyncline of South Australia and its significance in

Neoproterozoic continental reconstruction. Precambrian Research, 100(1-3): 21-63.

Raimondo, T., Collins, A.S., Hand, M., Walker-Hallam, A., Smithies, R.H., Evins, P.M. and Howard, H.M., 2009. Ediacaran intracontinental channel flow. Geology, 37(4): 291-294.

Raimondo, T., Collins, A.S., Hand, M., Walker-Hallam, A., Smithies, R.H., Evins, P.M. and Howard, H.M., 2010. The anatomy of a deep intracontinental orogen. Tectonics, 29(4).

Scrimgeour, I. and Close, D., 1999. Regional high-pressure metamorphism during intracratonic deformation: The Petermann Orogeny, central Australia. Journal of Metamorphic Geology, 17(5): 557-572.

Scrimgeour, I.R., Close, D.F. and Edgoose, C.J., 1999. Petermann Ranges, N.T. 1:250000 Geological Series Explanatory Notes SG52-7, Department of Mines and Energy, Northern Territory Geological Survey.

Self, S., 2006. The effects and consequences of very large explosive volcanic eruptions. Philosophical Transactions of the Royal Society A: Mathematical, Physical and Engineering Sciences, 364(1845): 2073-2097.

Smithies, R.H., Howard, H.M., Evins, P.M., Kirkland, C.L., Bordorkos, S. and Wingate, M.T.D., 2009. The west Musgrave Complex - new geological insights from recent mapping, geochronology, and geochemical studies. Record - Geological Survey of Western Australia, Perth, Australia, 2008/19: 20.

Smithies, R.H., Howard, H.M., Evins, P.M., Kirkland, C.L., Kelsey, D.E., Hand, M., Wingate, M.T.D., Collins, A.S. and Belousova, E., 2011. High-temperature granite magmatism, crust-mantle interaction and the Mesoproterozoic intracontinental evolution of the Musgrave Province, central Australia. Journal of Petrology, 52(5): 931-958.

Smithies, R.H., Howard, H.M., Evins, P.M., Kirkland, C.L., Kelsey, D.E., Hand, M., Wingate, M.T.D., Collins, A.S., Belousova, E.A. and Allchurch, S., 2010. Geochemistry, geochronology and petrogenesis of Mesoproterozoic felsic rocks in the west Musgrave Province, Central Australia, and implications for the Mesoproterozoic tectonic evolution of the region. Record - Geological Survey of Western Australia, Perth, Australia, 106: 82.

Smithies, R.H., Howard, H.M., Kirkland, C.L., Werner, M., Medlin, C.C., Wingate, M.T.D. and Cliff, J.B., 2013. Geochemical evolution of rhyolites of the Talbot Sub-basin and associated felsic units of the Warakurna Supersuite, Geological Survey of Western Australia, Perth, Australia, 118: 74.

Smithies, R., Kirkland, C., Korhonen, F., Aitken, A., Howard, H., Maier, W., Wingate, M., Quentin de Gromard, R. and Gessner, K., 2014. The Mesoproterozoic thermal evolution of the Musgrave Province in central Australia–plume vs. the geological record. Gondwana Research.

Sparks, R.S.J., Self, S., Grattan, J.P., Oppenheimer, C., Pyle, D.M. and Rymer, H., 2005. Super-eruptions: global effects and future threats, London, UK.

Sun, S.S., Sheraton, J.W., Glikson, A.Y. and Stewart, A.J., 1996. A major magmatic event during 1050-1080 Ma in central Australia, and emplacement age for the Giles Complex. AGSO Research Newsletter, 24: 13-15.

Wade, B.P., Barovich, K.M., Hand, M., Scrimgeour, I.R. and Close, D.F., 2006. Evidence for early Mesoproterozoic arc magmatism in the Musgrave Block, central Australia; implications for Proterozoic crustal growth and tectonic reconstructions of Australia. Journal of Geology, 114(1): 43-63.

Wade, B.P., Hand, M. and Barovich, K.M., 2005. Nd isotopic and geochemical constraints on provenance of sedimentary rocks in the eastern Officer Basin, Australia: Implications for the duration of the intracratonic Petermann Orogeny. Journal of the Geological Society, 162(3): 513-530.

Wade, B.P., Kelsey, D.E., Hand, M. and Barovich, K.M., 2008. The Musgrave Province; stitching north, west and south Australia. Precambrian Research, 166(1-4): 370-386.

Walter, M.R., Veevers, J.J., Calver, C.R. and Grey, K., 1995. Neoproterozoic stratigraphy of the Centralian Superbasin, Australia. Precambrian Research, 73(1-4): 173-195.

White, R.W., Clarke, G.L. and Nelson, D.R., 1999. SHRIMP U-Pb zircon dating of Grenville-age events in the western part of the Musgrave Block, central Australia. Journal of Metamorphic Geology, 17(5): 465-481.

White, R.W., Powell, R. and Clarke, G.L., 2002. The interpretation of reaction textures in Fe-rich metapelitic granulites of the Musgrave Block, Central Australia: Constraints from mineral equilibria calculations in the system. Journal of Metamorphic Geology, 20(1): 41-55.

Wingate, M.T.D., Pirajno, F. and Morris, P.A., 2004. Warakurna large igneous province: A new Mesoproterozoic large igneous province in west-central Australia. Geology, 32(2): 105-108.

Zhao, J.-x. and McCulloch, M.T., 1993. Melting of a subduction-modified continental lithospheric mantle: evidence from late Proterozoic mafic dike swarms in central Australia. Geology, 21(5): 463-466.

Zhao, J.-x., McCulloch, M.T. and Korsch, R.J., 1994. Characterisation of a plume-related ~ 800 Ma magmatic event and its implications for basin formation in central-southern Australia. Earth and Planetary Science Letters, 121(3-4): 349-367.

Appendix B

Appendix B - Table 3.1

Table 3.1 and Table 4.1: Whole-rock composition data and selected trace element data for the Kathleen Ignimbrite (KI) and the Rowland Suite (RS). Data is anhydrous corrected.

Sample	**164689**	**195074**	**195077**	**195091**	**195099**	**199221**	**199234**
Latitude	321427	313625	315042	317757	318683	321340	321798
Longitude	7112816	7109892	7109800	7111098	7110458	7112796	7111955
Unit	KI	KI	KI	KI	KI	KI	KI
SiO_2(wt%)	78.27	75.99	74.88	76.43	75.34	76.22	76.22
TiO_2(wt%)	0.17	0.18	0.18	0.19	0.19	0.17	0.21
Al_2O_3(wt%)	10.86	12.03	12.05	11.92	12.25	12.01	12.21
Fe_2O_3(wt%)	1.19	2.03	2.02	1.93	2.09	1.63	2.12
MnO(wt%)	0.01	0.04	0.01	0.02	0.02	0.02	0.01
MgO(wt%)	0.12	0.13	0.12	0.17	0.12	0.48	0.12
CaO(wt%)	0.46	0.71	0.64	0.66	0.57	0.47	0.44
Na_2O(wt%)	0.85	2.81	1.72	3.02	3.16	2.02	2.77
K_2O(wt%)	7.85	5.86	8.17	5.48	6.05	6.77	5.69
P_2O_5(wt%)	bd	0.01	bd	bd	bd	bd	0.01
SO_3(wt%)	bd	bd	bd	bd	bd	bd	bd
F (wt%)	0.41	0.62	0.62	0.56	0.56	0.38	0.36
Cl (wt%)	0.00	0.03	0.02	0.02	0.02	0.00	0.03
LOI	0.63	0.55	0.42	0.49	0.57	0.59	0.36
Totals	99.27	100.64	100.14	100.55	100.15	99.74	100.78
Li (ppm)	9.54	27.17	9.77	21.06	11.48	39.08	9.22
Be (ppm)	7.42	11.69	12.24	11.48	15.19	10.65	8.90
Sc (ppm)	1.10	1.67	1.46	1.56	1.46	0.95	1.61
V (ppm)	0.50	0.55	1.64	0.90	0.30	0.80	1.01
Cr (ppm)	0.26	0.12	0.18	0.02	bd	1.17	3.05
Co (ppm)	107.50	40.29	47.16	45.75	51.29	100.73	146.9
Ni (ppm)	0.58	0.15	0.19	0.11	0.03	0.42	0.68
Cu (ppm)	2.06	1.38	1.73	1.24	3.47	bd	0.70
Zn (ppm)	10.46	40.57	14.28	26.17	26.85	34.53	11.9
Ga (ppm)	18.07	25.68	20.33	25.43	26.92	22.41	22.9
Rb (ppm)	426.57	472.44	553.22	414.49	434.34	400.32	366.2
Sr (ppm)	39.13	26.76	25.08	22.95	21.09	30.60	12.7
Y (ppm)	102.32	199.85	192.48	177.36	200.32	137.49	152.0
Zr (ppm)	236.75	266.79	264.79	259.48	275.06	246.39	263.4
Nb (ppm)	46.62	83.11	61.37	77.93	84.75	36.47	37.8
Mo (ppm)	5.31	10.66	2.04	3.78	1.07	1.76	3.34
Cd (ppm)	0.05	0.07	0.07	0.07	0.07	0.05	0.06
Sn (ppm)	22.75	17.28	7.01	22.25	32.32	25.50	18.6
Sb (ppm)	0.42	0.07	0.12	0.08	0.18	0.38	0.13
Cs (ppm)	0.83	1.22	0.78	1.11	0.67	1.40	0.54
Ba (ppm)	601.88	46.80	129.33	41.81	85.96	344.13	103.7
La (ppm)	87.10	140.00	112.10	133.54	138.70	82.46	151.3
Ce (ppm)	141.81	253.67	217.38	252.27	262.37	157.60	317.1
Pr (ppm)	17.39	28.11	22.86	26.33	27.22	17.19	30.6
Nd (ppm)	61.66	93.99	77.05	88.23	91.81	58.59	100.8
Sm (ppm)	14.62	21.38	18.42	19.57	20.96	14.28	20.5
Eu (ppm)	0.37	0.47	0.41	0.44	0.47	0.33	0.55
Gd (ppm)	13.25	21.08	19.03	18.84	21.01	14.68	19.0
Tb (ppm)	2.50	4.14	3.90	3.68	4.24	3.13	3.66
Dy (ppm)	16.06	28.01	26.76	24.70	28.84	21.75	24.1
Ho (ppm)	3.67	6.61	6.40	5.84	6.82	5.23	5.62
Er (ppm)	10.97	19.88	19.26	17.53	20.36	16.06	16.9
Tm (ppm)	1.71	2.99	2.91	2.67	3.05	2.49	2.61
Yb (ppm)	12.11	20.10	19.65	18.05	20.27	16.98	17.8
Lu (ppm)	1.79	2.90	2.82	2.62	2.92	2.47	2.60
Hf (ppm)	10.29	11.20	11.07	10.79	11.60	10.82	11.2
Ta (ppm)	0.35	1.49	0.97	2.56	4.38	0.31	0.28
Hg (ppm)	2.69	1.58	1.31	1.57	1.87	1.45	3.25
Tl (ppm)	1.46	1.05	1.08	1.04	0.89	1.24	0.72
Pb (ppm)	23.37	22.36	12.39	12.25	14.53	11.81	14.7
Th (ppm)	72.25	72.58	72.87	70.51	75.33	73.25	80.5
U (ppm)	13.42	13.64	13.51	13.87	13.13	12.64	14.8

Sample	164689	195074	195077	195091	195099	199221	199234
Latitude	321427	313625	315042	317757	318683	321340	321798
Longitude	7112816	7109892	7109800	7111098	7110458	7112796	7111955
Unit	Kl	Kl	Kl	Kl	Kl	Kl	Kl
SiO_2(wt%)	78.27	75.99	74.88	76.43	75.34	76.22	76.22
TiO_2(wt%)	0.17	0.18	0.18	0.19	0.19	0.17	0.21
Al_2O_3(wt%)	10.86	12.03	12.05	11.92	12.25	12.01	12.21
Fe_2O_3(wt%)	1.19	2.03	2.02	1.93	2.09	1.63	2.12
MnO(wt%)	0.01	0.04	0.01	0.02	0.02	0.02	0.01
MgO(wt%)	0.12	0.13	0.12	0.17	0.12	0.48	0.12
CaO(wt%)	0.46	0.71	0.64	0.66	0.57	0.47	0.44
Na_2O(wt%)	0.85	2.81	1.72	3.02	3.16	2.02	2.77
K_2O(wt%)	7.85	5.86	8.17	5.48	6.05	6.77	5.69
P_2O_5(wt%)	bd	0.01	bd	bd	bd	bd	0.01
SO_3(wt%)	bd	bd	bd	bd	bd	bd	bd
F (wt%)	0.41	0.62	0.62	0.56	0.56	0.38	0.36
Cl (wt%)	0.00	0.03	0.02	0.02	0.02	0.00	0.03
LOI	0.63	0.55	0.42	0.49	0.57	0.59	0.36
Totals	99.27	100.64	100.14	100.55	100.15	99.74	100.78
Li (ppm)	9.54	27.17	9.77	21.06	11.48	39.08	9.22
Be (ppm)	7.42	11.69	12.24	11.48	15.19	10.65	8.90
Sc (ppm)	1.10	1.67	1.46	1.56	1.46	0.95	1.61
V (ppm)	0.50	0.55	1.64	0.90	0.30	0.80	1.01
Cr (ppm)	0.26	0.12	0.18	0.02	bd	1.17	3.05
Co (ppm)	107.50	40.29	47.16	45.75	51.29	100.73	146.9
Ni (ppm)	0.58	0.15	0.19	0.11	0.03	0.42	0.68
Cu (ppm)	2.06	1.38	1.73	1.24	3.47	bd	0.70
Zn (ppm)	10.46	40.57	14.28	26.17	26.85	34.53	11.9
Ga (ppm)	18.07	25.68	20.33	25.43	26.92	22.41	22.9
Rb (ppm)	426.57	472.44	553.22	414.49	434.34	400.32	366.2
Sr (ppm)	39.13	26.76	25.08	22.95	21.09	30.60	12.7
Y (ppm)	102.32	199.85	192.48	177.36	200.32	137.49	152.0
Zr (ppm)	236.75	266.79	264.79	259.48	275.06	246.39	263.4
Nb (ppm)	46.62	83.11	61.37	77.93	84.75	36.47	37.8
Mo (ppm)	5.31	10.66	2.04	3.78	1.07	1.76	3.34
Cd (ppm)	0.05	0.07	0.07	0.07	0.07	0.05	0.06
Sn (ppm)	22.75	17.28	7.01	22.25	32.32	25.50	18.6
Sb (ppm)	0.42	0.07	0.12	0.08	0.18	0.38	0.13
Cs (ppm)	0.83	1.22	0.78	1.11	0.67	1.40	0.54
Ba (ppm)	601.88	46.80	129.33	41.81	85.96	344.13	103.7
La (ppm)	87.10	140.00	112.10	133.54	138.70	82.46	151.3
Ce (ppm)	141.81	253.67	217.38	252.27	262.37	157.60	317.1
Pr (ppm)	17.39	28.11	22.86	26.33	27.22	17.19	30.6
Nd (ppm)	61.66	93.99	77.05	88.23	91.81	58.59	100.8
Sm (ppm)	14.62	21.38	18.42	19.57	20.96	14.28	20.5
Eu (ppm)	0.37	0.47	0.41	0.44	0.47	0.33	0.55
Gd (ppm)	13.25	21.08	19.03	18.84	21.01	14.68	19.0
Tb (ppm)	2.50	4.14	3.90	3.68	4.24	3.13	3.66
Dy (ppm)	16.06	28.01	26.76	24.70	28.84	21.75	24.1
Ho (ppm)	3.67	6.61	6.40	5.84	6.82	5.23	5.62
Er (ppm)	10.97	19.88	19.26	17.53	20.36	16.06	16.9
Tm (ppm)	1.71	2.99	2.91	2.67	3.05	2.49	2.61
Yb (ppm)	12.11	20.10	19.65	18.05	20.27	16.98	17.8
Lu (ppm)	1.79	2.90	2.82	2.62	2.92	2.47	2.60
Hf (ppm)	10.29	11.20	11.07	10.79	11.60	10.82	11.2
Ta (ppm)	0.35	1.49	0.97	2.56	4.38	0.31	0.28
Hg (ppm)	2.69	1.58	1.31	1.57	1.87	1.45	3.25
Tl (ppm)	1.46	1.05	1.08	1.04	0.89	1.24	0.72
Pb (ppm)	23.37	22.36	12.39	12.25	14.53	11.81	14.7
Th (ppm)	72.25	72.58	72.87	70.51	75.33	73.25	80.5
U (ppm)	13.42	13.64	13.51	13.87	13.13	12.64	14.8

Sample	199250	199251	199253	199254	195020	195076	195100
Latitude	322003	312716	310608	310570	320520	314019	319011
Longitude	7111358	7109496	7107641	7106703	7111531	7109865	7111218
Unit	Kl	Kl	Kl	Kl	Kl	Kl	Kl
SiO_2(wt%)	76.59	75.92	76.59	77.54	75.50	76.51	77.90
TiO_2(wt%)	0.18	0.18	0.17	0.18	0.20	0.18	0.18
Al_2O_3(wt%)	11.47	12.28	11.76	10.59	11.91	11.80	11.11
Fe_2O_3(wt%)	1.91	1.98	2.06	1.66	2.08	2.15	1.99
MnO(wt%)	0.03	0.03	0.02	0.02	0.01	0.05	0.01
MgO(wt%)	0.12	0.13	0.12	0.12	0.12	0.35	0.15
CaO(wt%)	0.69	0.67	0.79	1.05	0.71	0.64	0.16
Na_2O(wt%)	2.40	3.73	3.03	0.53	2.81	2.19	2.36
K_2O(wt%)	6.38	4.94	5.24	8.09	6.43	5.90	5.92
P_2O_5(wt%)	0.01	0.01	0.01	0.01	0.01	0.01	0.01
SO_3(wt%)	bd	0.01	bd	0.02	bd	0.01	bd
F (wt%)	0.70	0.53	0.73	0.82	0.59	0.54	0.08
Cl (wt%)	0.02	0.02	0.03	0.02	0.02	0.00	0.03
LOI	0.46	0.52	0.63	0.67	0.47	0.70	0.35
Totals	100.67	100.41	100.78	100.84	100.12	100.64	100.60
Li (ppm)	4.05	18.0	22.4	9.97	5.25	56.2	27.3
Be (ppm)	12.2	9.10	12.1	14.2	11.8	11.4	13.6
Sc (ppm)	1.32	0.97	1.42	1.23	1.87	1.59	1.52
V (ppm)	0.58	0.27	0.85	1.59	2.10	0.76	1.63
Cr (ppm)	bd	0.02	bd	0.53	0.54	bd	0.35
Co (ppm)	52.0	28.8	45.8	51.4	50.4	42.7	52.8
Ni (ppm)	0.16	bd	0.14	0.34	0.46	0.23	0.23
Cu (ppm)	16.3	1.05	1.21	3.04	61.1	9.72	1.06
Zn (ppm)	174.6	16.0	24.1	14.9	53.6	25.4	31.1
Ga (ppm)	20.8	17.4	25.8	18.9	22.2	27.5	23.6
Rb (ppm)	388.0	260.8	359.1	494.9	357.6	469.1	416.8
Sr (ppm)	15.8	20.9	42.7	60.4	17.2	36.2	15.2
Y (ppm)	169.1	146.0	187.3	165.8	171.4	196.7	199.2
Zr (ppm)	236.6	173.8	252.7	228.7	272.3	272.6	240.7
Nb (ppm)	59.0	45.1	73.2	42.4	79.7	78.3	63.2
Mo (ppm)	0.44	3.19	5.63	0.72	3.31	3.58	0.59
Cd (ppm)	0.09	0.05	0.07	0.06	0.08	0.07	0.07
Sn (ppm)	40.1	14.7	26.7	12.8	33.0	28.5	51.6
Sb (ppm)	0.21	0.05	0.17	0.18	0.16	0.13	0.18
Cs (ppm)	0.54	0.71	1.38	2.74	0.34	1.61	0.85
Ba (ppm)	125.7	28.3	113.3	165.2	244.7	127.1	74.7
La (ppm)	110.8	93.9	150.4	124.6	134.2	123.5	191.8
Ce (ppm)	203.9	171.7	273.8	229.7	255.1	243.8	321.3
Pr (ppm)	23.2	19.3	27.7	23.9	27.2	25.7	35.6
Nd (ppm)	78.4	65.1	91.1	79.2	91.3	86.2	115.2
Sm (ppm)	18.3	15.2	20.2	17.7	20.1	20.0	22.0
Eu (ppm)	0.45	0.32	0.43	0.39	0.72	0.43	0.52
Gd (ppm)	18.2	15.1	19.9	17.4	19.5	19.9	20.7
Tb (ppm)	3.62	3.02	3.91	3.41	3.74	4.01	3.89
Dy (ppm)	23.9	20.3	26.4	23.0	24.7	27.2	26.7
Ho (ppm)	5.48	4.81	6.27	5.45	5.77	6.47	6.59
Er (ppm)	15.8	14.3	18.9	16.4	17.2	19.5	20.9
Tm (ppm)	2.30	2.16	2.85	2.49	2.57	2.95	3.29
Yb (ppm)	15.2	14.5	19.3	16.8	17.2	19.7	22.6
Lu (ppm)	2.16	2.09	2.77	2.43	2.48	2.84	3.28
Hf (ppm)	9.76	7.27	10.9	9.71	10.7	11.4	9.67
Ta (ppm)	3.21	0.84	2.92	1.34	2.62	1.48	2.53
Hg (ppm)	1.36	0.88	1.56	1.43	2.38	1.49	1.75
Tl (ppm)	0.79	0.59	1.03	1.54	0.69	1.25	0.84
Pb (ppm)	269.4	8.6	28.6	15.3	21.3	8.45	14.5
Th (ppm)	62.4	52.6	71.5	62.6	66.4	73.3	61.3
U (ppm)	11.2	9.3	13.3	11.9	11.2	14.4	11.4

Sample	199238	195001	195019	195031	195058	195064	205319
Latitude	321891	321398	319463	320807	311532	311802	318710
Longitude	7111564	7112944	7110737	7111201	7107868	7107718	7111843
Unit	Kl	Rs	Rs	Rs	Rs	Rs	Rs
SiO_2(wt%)	76.04	72.52	73.75	74.08	73.55	73.36	73.65
TiO_2(wt%)	0.19	0.39	0.37	0.36	0.42	0.39	0.36
Al_2O_3(wt%)	11.67	12.90	12.52	12.38	12.48	12.44	12.69
Fe_2O_3(wt%)	2.47	3.29	3.08	2.92	3.36	3.22	3.08
MnO(wt%)	0.06	0.04	0.05	0.04	0.08	0.05	0.06
MgO(wt%)	0.56	0.27	0.29	0.35	0.37	0.35	0.35
CaO(wt%)	0.37	1.10	0.84	0.69	1.42	1.43	1.10
Na_2O(wt%)	2.25	3.77	3.11	3.06	2.89	2.73	2.83
K_2O(wt%)	6.15	5.40	5.70	5.80	5.10	5.69	5.55
P_2O_5(wt%)	0.01	0.05	0.04	0.04	0.05	0.05	0.04
SO_3(wt%)	bd	0.01	bd	bd	0.01	0.01	bd
F (wt%)	0.35	0.20	0.23	0.25	0.26	0.27	0.17
Cl (wt%)	0.00	0.03	0.03	0.02	0.02	0.03	0.03
LOI	0.71	0.78	0.62	0.64	1.16	0.80	0.77
Totals	99.64	100.11	100.53	100.48	100.43	100.10	100.49
Li (ppm)	45.47	22.15	18.38	16.7	28.4	16.8	18.2
Be (ppm)	5.97	6.09	5.96	6.63	5.09	5.68	5.78
Sc (ppm)	1.47	3.98	4.20	4.24	4.38	4.36	3.44
V (ppm)	8.85	9.50	8.52	8.61	10.0	9.65	7.59
Cr (ppm)	1.08	6.83	6.74	6.53	8.63	9.20	6.78
Co (ppm)	147.1	49.9	39.7	56.8	42.3	45.6	68.2
Ni (ppm)	5.67	1.70	1.92	1.79	1.84	1.99	1.69
Cu (ppm)	19.52	8.14	51.8	2.41	9.57	7.39	4.80
Zn (ppm)	213.4	41.8	92.6	48.5	65.7	59.4	51.7
Ga (ppm)	26.17	23.05	22.68	22.8	23.1	23.2	23.1
Rb (ppm)	445.6	222.8	230.1	296.7	264.9	251.4	239.3
Sr (ppm)	17.4	36.1	45.7	36.8	81.8	82.9	62.6
Y (ppm)	141.6	130.9	120.6	123.0	119.2	121.4	130.3
Zr (ppm)	262.3	388.5	389.4	410.6	400.1	374.9	373.9
Nb (ppm)	38.1	65.0	45.4	63.2	63.9	60.2	40.5
Mo (ppm)	1.05	1.17	6.01	1.96	4.25	5.13	2.18
Cd (ppm)	0.06	0.12	0.11	0.11	0.13	0.12	0.09
Sn (ppm)	58.6	7.94	20.7	13.9	14.3	15.2	10.2
Sb (ppm)	0.21	0.22	0.17	0.14	0.38	0.15	0.19
Cs (ppm)	1.65	1.27	0.65	0.78	0.99	0.64	1.04
Ba (ppm)	176.2	895.6	793.3	707.5	808.4	886.9	998.1
La (ppm)	86.7	147.7	140.7	150.4	135.0	139.9	148.8
Ce (ppm)	164.0	301.3	270.8	292.2	260.3	271.1	308.8
Pr (ppm)	18.0	31.3	28.9	30.6	28.1	29.0	31.1
Nd (ppm)	63.4	112.4	101.2	106.2	99.9	102.4	111.0
Sm (ppm)	15.4	22.8	20.2	20.8	20.3	20.6	22.4
Eu (ppm)	0.52	3.00	2.51	2.49	2.64	2.65	2.97
Gd (ppm)	15.8	21.0	18.6	19.0	18.7	19.0	20.5
Tb (ppm)	3.26	3.57	3.15	3.21	3.17	3.22	3.52
Dy (ppm)	21.7	21.8	19.4	19.7	19.5	19.8	21.6
Ho (ppm)	5.08	4.83	4.28	4.35	4.32	4.39	4.77
Er (ppm)	14.9	13.5	12.0	12.2	12.1	12.2	13.3
Tm (ppm)	2.21	1.90	1.70	1.73	1.72	1.74	1.88
Yb (ppm)	14.6	12.5	11.1	11.3	11.2	11.4	12.2
Lu (ppm)	2.14	1.84	1.62	1.64	1.64	1.66	1.79
Hf (ppm)	11.3	11.6	11.2	11.8	11.5	11.0	11.3
Ta (ppm)	0.30	2.90	0.98	2.44	3.58	1.55	0.53
Hg (ppm)	3.35	1.61	2.35	2.04	1.56	2.11	1.95
Tl (ppm)	1.05	0.67	0.62	0.79	0.74	0.66	0.62
Pb (ppm)	12.3	16.9	17.7	12.2	25.1	21.8	19.6
Th (ppm)	75.1	44.9	45.6	46.2	44.2	45.5	46.3
U (ppm)	18.2	4.94	5.53	5.72	6.05	6.21	5.10

Sample	205320	205321	205323
Latitude	319435	320285	320848
Longitude	7112363	7112479	7112891
Unit	Rs	Rs	Rs
SiO_2(wt%)	73.05	73.04	73.89
TiO_2(wt%)	0.38	0.41	0.39
Al_2O_3(wt%)	12.81	12.57	12.34
Fe_2O_3(wt%)	3.08	3.23	3.35
MnO(wt%)	0.05	0.06	0.07
MgO(wt%)	0.25	0.33	0.28
CaO(wt%)	1.13	1.45	1.17
Na_2O(wt%)	3.17	3.53	3.19
K_2O(wt%)	5.75	5.07	4.99
P_2O_5(wt%)	0.04	0.05	0.05
SO_3(wt%)	bd	bd	bd
F (wt%)	0.21	0.28	0.15
Cl (wt%)	0.03	0.03	0.03
LOI	0.82	0.76	0.61
Totals	100.65	100.62	99.96
Li (ppm)	18.1	21.1	22.6
Be (ppm)	5.21	5.50	5.95
Sc (ppm)	3.48	3.39	3.43
V (ppm)	7.80	4.93	7.58
Cr (ppm)	8.47	7.26	6.88
Co (ppm)	76.1	68.1	57.3
Ni (ppm)	1.59	1.73	1.77
Cu (ppm)	31.22	6.57	7.28
Zn (ppm)	76.0	146.9	109.8
Ga (ppm)	22.3	21.9	22.7
Rb (ppm)	200.5	190.3	196.8
Sr (ppm)	75.0	61.4	64.7
Y (ppm)	123.4	122.8	127.7
Zr (ppm)	365.0	352.4	367.0
Nb (ppm)	51.5	29.6	48.4
Mo (ppm)	2.16	1.66	0.96
Cd (ppm)	0.13	0.14	0.09
Sn (ppm)	10.1	6.91	10.4
Sb (ppm)	0.22	0.22	0.26
Cs (ppm)	0.88	1.04	1.44
Ba (ppm)	1106.3	800.2	947.2
La (ppm)	141.2	136.1	139.2
Ce (ppm)	286.0	283.5	294.0
Pr (ppm)	30.1	29.4	29.8
Nd (ppm)	108.1	105.8	107.5
Sm (ppm)	21.9	21.7	21.9
Eu (ppm)	3.03	2.93	2.90
Gd (ppm)	20.1	20.0	20.2
Tb (ppm)	3.40	3.44	3.48
Dy (ppm)	20.7	21.1	21.4
Ho (ppm)	4.56	4.68	4.77
Er (ppm)	12.7	13.0	13.3
Tm (ppm)	1.79	1.82	1.88
Yb (ppm)	11.8	11.9	12.3
Lu (ppm)	1.73	1.73	1.80
Hf (ppm)	11.0	10.7	11.2
Ta (ppm)	2.38	0.33	1.28
Hg (ppm)	2.47	0.98	1.22
Tl (ppm)	0.60	0.61	0.62
Pb (ppm)	34.8	26.2	23.9
Th (ppm)	43.4	42.9	45.0
U (ppm)	4.83	6.20	4.70

Sample	AGV 1-1	AGV 1-2	AGV 1-3	AGV 1-1	AGV 1-2	AGV-1 Rac
Unit	Standard	Standard	Standard	Standard	Standard	Standard
Li (ppm)	9.94	10.4	10.2	10.4	10.5	12
Be (ppm)	1.99	2.13	2.30	1.97	2.08	2.1
Sc (ppm)	12.9	11.7	11.3	13.1	11.6	12.2
V (ppm)	138.6	132.1	129.4	136.9	132.6	121
Cr (ppm)	11.5	10.9	11.0	11.9	11.6	10.1
Co (ppm)	16.4	15.8	15.7	16.2	15.6	15.3
Ni (ppm)	16.4	15.7	15.6	17.3	15.2	16
Cu (ppm)	69.5	65.4	64.2	55.5	53.2	60
Zn (ppm)	95.9	92.5	91.5	85.4	82.0	88
Ga (ppm)	20.6	19.8	19.5	20.3	19.9	20
Rb (ppm)	70.9	66.9	66.3	69.4	68.0	68
Sr (ppm)	726.3	700.7	695.4	659.9	661.0	660
Y (ppm)	21.3	20.7	20.6	21.2	20.8	20
Zr (ppm)	232.4	229.5	228.2	234.6	229.0	225
Nb (ppm)	14.4	14.3	14.4	14.5	14.4	14.5
Mo (ppm)	1.95	1.95	1.96	2.13	2.04	2.1
Cd (ppm)	83.5	76.8	79.3	86.6	85.7	69
Sn (ppm)	5.06	5.20	5.21	6.39	6.31	4.5
Sb (ppm)	4.77	4.88	4.82	4.84	4.79	4.3
Cs (ppm)	1.30	1.26	1.25	1.30	1.27	1.25
Ba (ppm)	1251.2	1223.6	1215.9	1240.1	1229.6	1200
La (ppm)	42.8	42.4	42.2	43.1	42.1	39
Ce (ppm)	71.7	71.3	70.8	71.8	70.7	70
Pr (ppm)	8.68	8.66	8.64	8.71	8.67	8
Nd (ppm)	32.3	32.3	32.3	32.5	32.2	32
Sm (ppm)	6.17	6.24	6.26	6.22	6.24	5.9
Eu (ppm)	1.71	1.71	1.71	1.70	1.72	1.55
Gd (ppm)	5.18	5.19	5.13	5.11	5.21	4.7
Tb (ppm)	0.73	0.73	0.73	0.72	0.72	0.7
Dy (ppm)	3.92	3.92	3.95	3.90	3.93	3.8
Ho (ppm)	0.77	0.78	0.78	0.77	0.79	0.7
Er (ppm)	1.97	2.01	2.01	2.00	2.01	1.9
Tm (ppm)	0.26	0.27	0.27	0.26	0.27	0.275
Yb (ppm)	1.70	1.74	1.72	1.70	1.74	1.75
Lu (ppm)	0.25	0.26	0.26	0.25	0.26	0.27
Hf (ppm)	5.03	5.19	5.23	5.12	5.22	5.17
Ta (ppm)	0.87	0.91	0.92	0.88	0.90	0.9
Hg (ppm)	0.00	0.02	0.03	0.01	0.02	0.02
Tl (ppm)	0.29	0.28	0.29	0.31	0.30	0.34
Pb (ppm)	38.0	38.4	38.5	38.4	38.4	37
Th (ppm)	6.35	6.63	6.72	6.27	6.54	6.5
U (ppm)	1.87	1.99	2.00	1.93	2.01	1.9

Appendix B - Table 3.2

Table 3.2: SIMS (SHRIMP II) U-Th-Pb geochronology data for samples from the Kathleen Ignimbrite and the Rowland Suite. Grain.spot is the grain identification and the number of analysis on that grain. f204% is the percentage of non-radiogenic ^{206}Pb, based on the measurement of ^{204}Pb. * refers to common Pb corrected data (based on measured ^{204}Pb). Disc. % is the age discordance. Additional details for all samples are available online at <http://www.dmp.wa.gov.au/geochron>.

Grain .spot	^{238}U (ppm)	^{232}Th (ppm)	$^{232}Th/^{238}U$	f^{204} (%)	$^{238}U/^{206}Pb$	±1s	$^{207}Pb/^{206}Pb$	±1s
195031-1.1	676	602	0.92	0.032	5.521	0.077	0.0757	0.0004
195031-2.1	32	20	0.65	-0.193	5.718	0.146	0.0771	0.0020
195031-3.1	121	108	0.92	0.044	5.663	0.096	0.0747	0.0009
195031-4.1	131	101	0.80	0.000	5.691	0.094	0.0761	0.0008
195031-5.1	108	118	1.12	0.146	5.534	0.097	0.0754	0.0010
195031-6.1	154	175	1.18	-0.125	5.505	0.089	0.0756	0.0008
195031-7.1	1373	1039	0.78	0.020	5.507	0.075	0.0756	0.0003
195031-7.2	345	285	0.85	0.013	5.426	0.079	0.0753	0.0005
195031-8.1	2828	2959	1.08	0.007	5.204	0.070	0.0751	0.0002
195031-8.2	133	114	0.88	0.153	5.824	0.097	0.0776	0.0009
195031-9.1	60	58	0.99	0.160	5.615	0.111	0.0744	0.0012
195031-10.1	1231	1568	1.32	0.008	5.505	0.075	0.0750	0.0003
195031-11.1	3092	2510	0.84	0.014	5.300	0.071	0.0753	0.0008
195031-12.1	1448	1671	1.19	0.009	5.466	0.074	0.0753	0.0002
195031-13.1	125	95	0.79	-0.037	5.440	0.091	0.0756	0.0008
195031-14.1	150	98	0.67	0.088	5.494	0.089	0.0748	0.0007
195031-14.2	146	94	0.67	0.130	5.541	0.090	0.0749	0.0008

$^{238}U/^{206}Pb^*$	±1s	$^{207}Pb^*/^{206}Pb^*$	±1s	$^{238}U/^{206}Pb^*$ Date (Ma)	±1s	$^{207}Pb^*/^{206}Pb^*$ Date (Ma)	±1s	Disc. (%)
5.523	0.077	0.0754	0.0004	1073	14	1080	11	0.7
5.707	0.147	0.0787	0.0025	1041	25	1164	64	10.6
5.666	0.096	0.0743	0.0010	1048	17	1049	27	0.1
5.691	0.094	0.0761	0.0008	1044	16	1099	22	5.0
5.542	0.097	0.0742	0.0012	1069	17	1047	32	-2.1
5.498	0.089	0.0767	0.0009	1077	16	1112	25	3.2
5.508	0.075	0.0755	0.0003	1075	14	1081	7	0.5
5.427	0.079	0.0752	0.0005	1090	15	1075	14	-1.5
5.204	0.070	0.0751	0.0002	1133	14	1070	5	-5.9
5.833	0.097	0.0763	0.0011	1020	16	1104	28	7.6
5.624	0.112	0.0730	0.0016	1055	20	1015	43	-4.0
5.506	0.075	0.0749	0.0003	1076	14	1067	8	-0.9
5.300	0.071	0.0752	0.0008	1114	14	1075	22	-3.7
5.466	0.074	0.0752	0.0002	1083	14	1075	7	-0.7
5.438	0.091	0.0759	0.0009	1088	17	1092	23	0.4
5.499	0.089	0.0741	0.0009	1077	16	1043	23	-3.2
5.549	0.090	0.0738	0.0010	1068	16	1036	26	-3.1

Grain .spot	^{238}U (ppm)	^{232}Th (ppm)	$^{232}Th/^{238}U$	f^{204} (%)	$^{238}U/^{206}Pb$	±1s	$^{207}Pb/^{206}Pb$	±1s
195001-1.1	137	110	0.83	-0.085	5.690	0.097	0.0762	0.0037
195001-1.2	124	160	1.33	2.858	5.459	0.092	0.1077	0.0012
195001-2.1	80	53	0.68	0.127	5.612	0.104	0.0756	0.0042
195001-4.1	95	68	0.74	-0.054	5.634	0.101	0.0771	0.0010
195001-5.1	102	84	0.85	0.317	5.659	0.098	0.0780	0.0009
195001-5.2	164	204	1.28	0.091	5.540	0.089	0.0759	0.0008
195001-7.1	148	172	1.20	0.032	5.690	0.092	0.0758	0.0008
195001-8.1	175	127	0.75	0.083	5.534	0.088	0.0757	0.0028
195001-9.1	14	11	0.82	0.327	5.468	0.186	0.0748	0.0025
195001-10.1	99	69	0.72	0.164	5.604	0.100	0.0755	0.0010
195001-11.1	163	107	0.68	0.155	5.528	0.089	0.0764	0.0008
195001-12.1	176	167	0.98	0.463	5.603	0.088	0.0782	0.0007
195001-13.1	117	86	0.76	-0.131	5.590	0.096	0.0765	0.0009
195001-14.1	208	148	0.74	0.116	5.487	0.085	0.0751	0.0007
195001-15.1	154	121	0.81	0.031	5.623	0.091	0.0758	0.0008
195001-3.1	271	226	0.86	0.095	5.631	0.085	0.0762	0.0006
195001-6.1	117	100	0.88	-0.136	5.659	0.098	0.0747	0.0009

Grain .spot	^{238}U (ppm)	^{232}Th (ppm)	$^{232}Th/^{238}U$	f^{204} (%)	$^{238}U/^{206}Pb$	±1s	$^{207}Pb/^{206}Pb$	±1s
195031-1.1	676	602	0.92	0.032	5.521	0.077	0.0757	0.0004
195031-2.1	32	20	0.65	-0.193	5.718	0.146	0.0771	0.0020
195031-3.1	121	108	0.92	0.044	5.663	0.096	0.0747	0.0009
195031-4.1	131	101	0.80	0.000	5.691	0.094	0.0761	0.0008
195031-5.1	108	118	1.12	0.146	5.534	0.097	0.0754	0.0010
195031-6.1	154	175	1.18	-0.125	5.505	0.089	0.0756	0.0008
195031-7.1	1373	1039	0.78	0.020	5.507	0.075	0.0756	0.0003
195031-7.2	345	285	0.85	0.013	5.426	0.079	0.0753	0.0005
195031-8.1	2828	2959	1.08	0.007	5.204	0.070	0.0751	0.0002
195031-8.2	133	114	0.88	0.153	5.824	0.097	0.0776	0.0009
195031-9.1	60	58	0.99	0.160	5.615	0.111	0.0744	0.0012
195031-10.1	1231	1568	1.32	0.008	5.505	0.075	0.0750	0.0003
195031-11.1	3092	2510	0.84	0.014	5.300	0.071	0.0753	0.0008
195031-12.1	1448	1671	1.19	0.009	5.466	0.074	0.0753	0.0002
195031-13.1	125	95	0.79	-0.037	5.440	0.091	0.0756	0.0008
195031-14.1	150	98	0.67	0.088	5.494	0.089	0.0748	0.0007
195031-14.2	146	94	0.67	0.130	5.541	0.090	0.0749	0.0008

$^{238}U/^{206}Pb^*$	±1s	$^{207}Pb^*/^{206}Pb^*$	±1s	$^{238}U/^{206}Pb^*$ Date (Ma)	±1s	$^{207}Pb^*/^{206}Pb^*$ Date (Ma)	±1s	Disc. (%)
5.523	0.077	0.0754	0.0004	1073	14	1080	11	0.7
5.707	0.147	0.0787	0.0025	1041	25	1164	64	10.6
5.666	0.096	0.0743	0.0010	1048	17	1049	27	0.1
5.691	0.094	0.0761	0.0008	1044	16	1099	22	5.0
5.542	0.097	0.0742	0.0012	1069	17	1047	32	-2.1
5.498	0.089	0.0767	0.0009	1077	16	1112	25	3.2
5.508	0.075	0.0755	0.0003	1075	14	1081	7	0.5
5.427	0.079	0.0752	0.0005	1090	15	1075	14	-1.5
5.204	0.070	0.0751	0.0002	1133	14	1070	5	-5.9
5.833	0.097	0.0763	0.0011	1020	16	1104	28	7.6
5.624	0.112	0.0730	0.0016	1055	20	1015	43	-4.0
5.506	0.075	0.0749	0.0003	1076	14	1067	8	-0.9
5.300	0.071	0.0752	0.0008	1114	14	1075	22	-3.7
5.466	0.074	0.0752	0.0002	1083	14	1075	7	-0.7
5.438	0.091	0.0759	0.0009	1088	17	1092	23	0.4
5.499	0.089	0.0741	0.0009	1077	16	1043	23	-3.2
5.549	0.090	0.0738	0.0010	1068	16	1036	26	-3.1

Grain .spot	^{238}U (ppm)	^{232}Th (ppm)	$^{232}Th/^{238}U$	f^{204} (%)	$^{238}U/^{206}Pb$	±1s	$^{207}Pb/^{206}Pb$	±1s
195001-1.1	137	110	0.83	-0.085	5.690	0.097	0.0762	0.0037
195001-1.2	124	160	1.33	2.858	5.459	0.092	0.1077	0.0012
195001-2.1	80	53	0.68	0.127	5.612	0.104	0.0756	0.0042
195001-4.1	95	68	0.74	-0.054	5.634	0.101	0.0771	0.0010
195001-5.1	102	84	0.85	0.317	5.659	0.098	0.0780	0.0009
195001-5.2	164	204	1.28	0.091	5.540	0.089	0.0759	0.0008
195001-7.1	148	172	1.20	0.032	5.690	0.092	0.0758	0.0008
195001-8.1	175	127	0.75	0.083	5.534	0.088	0.0757	0.0028
195001-9.1	14	11	0.82	0.327	5.468	0.186	0.0748	0.0025
195001-10.1	99	69	0.72	0.164	5.604	0.100	0.0755	0.0010
195001-11.1	163	107	0.68	0.155	5.528	0.089	0.0764	0.0008
195001-12.1	176	167	0.98	0.463	5.603	0.088	0.0782	0.0007
195001-13.1	117	86	0.76	-0.131	5.590	0.096	0.0765	0.0009
195001-14.1	208	148	0.74	0.116	5.487	0.085	0.0751	0.0007
195001-15.1	154	121	0.81	0.031	5.623	0.091	0.0758	0.0008
195001-3.1	271	226	0.86	0.095	5.631	0.085	0.0762	0.0006
195001-6.1	117	100	0.88	-0.136	5.659	0.098	0.0747	0.0009

Grain .spot	^{238}U (ppm)	^{232}Th (ppm)	$^{232}Th/^{238}U$	f^{204} (%)	$^{238}U/^{206}Pb$	±1s	$^{207}Pb/^{206}Pb$	±1s
195723-1.1	220	177	0.83	0.400	5.557	0.053	0.0774	0.0006
195723-2.1	182	156	0.89	0.258	5.558	0.056	0.0779	0.0007
195723-3.1	143	117	0.84	0.337	5.437	0.060	0.0797	0.0008
195723-4.1	174	141	0.83	0.425	5.555	0.057	0.0793	0.0007
195723-5.1	204	272	1.38	0.399	5.463	0.054	0.0777	0.0006
195723-6.1	176	135	0.79	0.494	5.513	0.057	0.0802	0.0007
195723-7.1	487	306	0.65	0.227	5.555	0.044	0.0768	0.0004
195723-8.1	326	335	1.06	0.316	5.630	0.049	0.0776	0.0005
195723-9.1	835	780	0.96	0.092	5.520	0.041	0.0756	0.0003
195723-10.1	303	221	0.76	0.175	5.504	0.049	0.0765	0.0005
195723-11.1	209	144	0.71	0.251	5.513	0.054	0.0788	0.0006
195723-12.1	221	156	0.73	0.352	5.513	0.053	0.0787	0.0006
195723-13.1	186	188	1.05	0.685	5.467	0.056	0.0779	0.0007
195723-14.1	1679	1464	0.90	0.046	5.424	0.038	0.0753	0.0002
195723-15.1	228	201	0.91	0.235	5.536	0.053	0.0779	0.0006
195723-16.1	138	112	0.83	0.542	5.542	0.062	0.0798	0.0008

$^{238}U/^{206}Pb^*$	±1s	$^{207}Pb^*/^{206}Pb^*$	±1s	$^{238}U/^{206}Pb^*$ Date (Ma)	±1s	$^{207}Pb^*/^{206}Pb^*$ Date (Ma)	±1s	Disc. (%)
5.579	0.060	0.0741	0.0009	1063	13	1044	25	-1.8
5.573	0.063	0.0757	0.0010	1064	13	1088	25	2.2
5.455	0.066	0.0769	0.0011	1085	14	1118	29	3.0
5.579	0.064	0.0757	0.0011	1063	13	1088	29	2.3
5.485	0.061	0.0743	0.0010	1080	13	1050	26	-2.8
5.540	0.064	0.0760	0.0011	1070	13	1095	30	2.3
5.568	0.053	0.0749	0.0005	1065	11	1066	15	0.1
5.648	0.056	0.0749	0.0007	1051	11	1066	19	1.5
5.525	0.049	0.0748	0.0004	1072	10	1064	10	-0.8
5.514	0.056	0.0750	0.0007	1074	12	1070	18	-0.5
5.527	0.061	0.0767	0.0009	1072	13	1113	22	3.6
5.532	0.060	0.0757	0.0009	1071	13	1087	24	1.5
5.505	0.063	0.0722	0.0013	1076	13	991	36	-8.6
5.427	0.046	0.0749	0.0002	1090	10	1066	6	-2.3
5.549	0.060	0.0760	0.0008	1068	13	1094	21	2.4
5.573	0.069	0.0752	0.0013	1064	14	1074	36	1.0

Appendix B - Table 3.3

Table 3.3: Whole-rock Rb-Sr and Sm-Nd isotope data for selected samples from the Kathleen Ignimbrite (KI) and Rowland Suite (Rs). Age T = 1070 Ma, USGS = United States Geological Survey Standards.

Sample	Unit	Rb (ppm)	Sr (ppm)	$^{87}Rb/^{86}Sr$	$^{87}Sr/^{86}Sr$	Sm (ppm)	Nd (ppm)
195076	KI	438.0	37.00	35.89	1.199146	18.38	82.64
199222	KI	359.8	43.19	24.95	1.069975	20.35	98.79
199228	KI	416.6	16.00	84.06	1.896636	20.61	101.36
199253	KI	349.7	44.51	23.50	1.055500	19.01	89.90
199254	KI	456.5	63.03	21.63	1.036846	16.75	78.31
205322	KI	395.5	20.80	59.58	1.558788	20.27	97.54
195001	RS	220.9	37.84	17.30	0.955825	21.75	113.72
205320	RS	202.0	77.51	7.620	0.818615	20.73	107.63
205323	RS	212.0	69.93	8.880	0.835418	21.22	110.50
BCR-2	USGS std.	46.54	338.19	0.398	0.705001	6.47	28.30
BCR-2	USGS std.				0.704954		
BCR-2	USGS std.						
BHVO-2	USGS std.						

Sample	$^{147}Sm/^{144}Nd$	$^{143}Nd/^{144}Nd$	εNd(0)	$^{87}Sr/^{86}Sr(T)$	$^{143}Nd/^{144}Nd(T)$	εNd(T)	(T_{DM}^{2}) Ga
195076	0.1343	0.512232	-7.92	0.64962	0.511289	0.6	1.66
199222	0.1244	0.512182	-8.90	0.68793	0.511309	1.0	1.57
199228	0.1228	0.512152	-9.48	0.60966	0.511290	0.6	1.60
199253	0.1277	0.512178	-8.97	0.69577	0.511282	0.5	1.61
199254	0.1291	0.512206	-8.43	0.70573	0.511299	0.8	1.58
205322	0.1255	0.512178	-8.97	0.64664	0.511297	0.8	1.59
195001	0.1155	0.512108	-10.34	0.69096	0.511297	0.8	1.59
205320	0.1163	0.512110	-10.30	0.70195	0.511293	0.7	1.59
205323	0.1160	0.512104	-10.42	0.69947	0.511290	0.6	1.60
BCR-2	0.1381	0.512634	-0.08				
BCR-2		0.512648	0.20				
BCR-2		0.512653	0.29				
BHVO-2		0.513013	7.32				

Appendix B - Table 3.4

Table 3.4: In-situ zircon Lu-Hf isotope data for selected samples from the Pussy Cat Group rhyolites. Age T = 1070 Ma.

Unit	Analysis no.	$^{176}Lu/^{177}Hf$	2se	$^{176}Hf/^{177}Hf_{(i)}$	2se	εHf	Age(T) Ga	$^{176}Hf/^{177}Hf(T)$	εHf(T)	(T_{DM}^2) Ga
KI	195723_010	0.001240	0.000007	0.282303	0.000047	-16.6	1.070	0.282278	6.2	1.51
KI	195723_011	0.000885	0.000003	0.282322	0.000043	-15.9	1.070	0.282304	7.1	1.45
KI	195723_012	0.001066	0.000014	0.282305	0.000051	-16.5	1.070	0.282284	6.4	1.50
KI	195723_016	0.000931	0.000005	0.282287	0.000058	-17.2	1.070	0.282268	5.9	1.53
KI	195723_022	0.000789	0.000008	0.282251	0.000044	-18.4	1.070	0.282235	4.7	1.61
KI	195723_023	0.000956	0.000004	0.282268	0.000050	-17.8	1.070	0.282249	5.2	1.58
KI	195723_030	0.001132	0.000042	0.282271	0.000054	-17.7	1.070	0.282248	5.2	1.58
KI	195723_035	0.001131	0.000009	0.282249	0.000044	-18.5	1.070	0.282226	4.4	1.63
KI	195723_036	0.000905	0.000002	0.282242	0.000044	-18.7	1.070	0.282224	4.3	1.63
KI	195723_037	0.001026	0.000004	0.282248	0.000047	-18.5	1.070	0.282227	4.4	1.63
KI	195723_041	0.000684	0.000015	0.282285	0.000047	-17.2	1.070	0.282271	6.0	1.53
KI	195723_047	0.000807	0.000003	0.282221	0.000046	-19.5	1.070	0.282205	3.6	1.68
KI	195723_055	0.001607	0.000020	0.282324	0.000053	-15.8	1.070	0.282292	6.7	1.48
KI	195723_061	0.003590	0.000130	0.282338	0.000054	-15.3	1.070	0.282266	5.8	1.54
KI	195723_065	0.000831	0.000003	0.282274	0.000050	-17.6	1.070	0.282257	5.5	1.56
KI	195723_067	0.001245	0.000013	0.282249	0.000045	-18.5	1.070	0.282224	4.3	1.63
KI	195723_068	0.001372	0.000024	0.282303	0.000044	-16.6	1.070	0.282275	6.1	1.52
KI	195723_069	0.000858	0.000015	0.282269	0.000048	-17.8	1.070	0.282252	5.3	1.57
KI	195723_070	0.000948	0.000010	0.282301	0.000059	-16.7	1.070	0.282282	6.3	1.50
KI	195723_074	0.000987	0.000003	0.282266	0.000047	-17.9	1.070	0.282246	5.1	1.58
KI	195723_075	0.000963	0.000011	0.282272	0.000047	-17.7	1.070	0.282253	5.3	1.57
KI	199228_001	0.001401	0.000011	0.282325	0.000053	-15.8	1.070	0.282297	6.9	1.47
KI	199228_002	0.001890	0.000049	0.282337	0.000059	-15.4	1.070	0.282299	7.0	1.47
KI	199228_006	0.001250	0.000027	0.282285	0.000060	-17.2	1.070	0.282260	5.6	1.55
KI	199228_008	0.003436	0.000090	0.282320	0.000061	-16.0	1.070	0.282251	5.2	1.57
KI	199228_009	0.001089	0.000022	0.282277	0.000054	-17.5	1.070	0.282255	5.4	1.56
KI	199228_010	0.000875	0.000014	0.282272	0.000051	-17.7	1.070	0.282254	5.4	1.57
KI	199228_018	0.001188	0.000017	0.282292	0.000077	-17.0	1.070	0.282268	5.9	1.53
KI	199228_019	0.003470	0.000140	0.282365	0.000068	-14.4	1.070	0.282295	6.8	1.48
KI	199228_020	0.000914	0.000005	0.282253	0.000056	-18.4	1.070	0.282235	4.7	1.61
KI	199228_021	0.001690	0.000032	0.282290	0.000060	-17.0	1.070	0.282256	5.4	1.56
KI	199228_022	0.002409	0.000042	0.282364	0.000059	-14.4	1.070	0.282315	7.5	1.43
KI	199228_023	0.001088	0.000027	0.282313	0.000055	-16.2	1.070	0.282291	6.7	1.48
KI	199228_024	0.001998	0.000032	0.282281	0.000057	-17.4	1.070	0.282241	4.9	1.60
KI	199228_026	0.000942	0.000016	0.282253	0.000054	-18.4	1.070	0.282234	4.7	1.61
KI	199228_028	0.000745	0.000006	0.282267	0.000041	-17.9	1.070	0.282252	5.3	1.57
KI	199228_029	0.001424	0.000006	0.282301	0.000053	-16.7	1.070	0.282272	6.0	1.53
KI	199228_030	0.001047	0.000028	0.282242	0.000051	-18.7	1.070	0.282221	4.2	1.64
KI	199228_036	0.001011	0.000008	0.282263	0.000053	-18.0	1.070	0.282243	5.0	1.59
KI	199228_041	0.001668	0.000007	0.282281	0.000054	-17.4	1.070	0.282247	5.1	1.58
KI	199228_044	0.001395	0.000024	0.282270	0.000051	-17.8	1.070	0.282242	4.9	1.59
KI	199228_047	0.001591	0.000019	0.282309	0.000050	-16.4	1.070	0.282277	6.2	1.52
KI	195076_001	0.001299	0.000014	0.282321	0.000070	-15.9	1.070	0.282295	6.8	1.48
KI	195076_002	0.003065	0.000003	0.282353	0.000046	-14.8	1.070	0.282291	6.7	1.48
KI	195076_003	0.002365	0.000019	0.282324	0.000052	-15.8	1.070	0.282276	6.2	1.52
KI	195076_004	0.001324	0.000007	0.282290	0.000049	-17.0	1.070	0.282263	5.7	1.55
KI	195076_013	0.005199	0.000070	0.282391	0.000054	-13.5	1.070	0.282286	6.5	1.49
KI	195076_017	0.001101	0.000036	0.282271	0.000051	-17.7	1.070	0.282249	5.2	1.58
KI	195076_018	0.001629	0.000011	0.282303	0.000059	-16.6	1.070	0.282270	5.9	1.53
KI	195076_024	0.001361	0.000006	0.282236	0.000053	-19.0	1.070	0.282209	3.7	1.67
KI	195076_029	0.001858	0.000062	0.282269	0.000053	-17.8	1.070	0.282232	4.6	1.62
KI	195076_037	0.000891	0.000017	0.282297	0.000054	-16.8	1.070	0.282279	6.2	1.51
KI	195076_016	0.002580	0.000005	0.282294	0.000046	-16.9	1.070	0.282242	4.9	1.59
KI	195076_021	0.001423	0.000015	0.282299	0.000047	-16.7	1.070	0.282270	5.9	1.53
KI	195076_026	0.001394	0.000008	0.282331	0.000056	-15.6	1.070	0.282303	7.1	1.46
KI	195076_027	0.003052	0.000030	0.282291	0.000048	-17.0	1.070	0.282229	4.5	1.62
KI	195076_033	0.002499	0.000061	0.282281	0.000059	-17.4	1.070	0.282231	4.5	1.62
KI	195076_041	0.003297	0.000029	0.282302	0.000049	-16.6	1.070	0.282236	4.7	1.61
KI	195076_042	0.002677	0.000031	0.282300	0.000045	-16.7	1.070	0.282246	5.1	1.58
KI	195076_036	0.003038	0.000029	0.282324	0.000058	-15.8	1.070	0.282263	5.7	1.55

Unit	Analysis no.	$^{176}Lu/^{177}Hf$	2se	$^{176}Hf/^{177}Hf_{(i)}$	2se	εHf	Age(T) Ga	$^{176}Hf/^{177}Hf(T)$	εHf(T)	(T_{DM}^{2}) Ga
RS	195001_002	0.001314	4.6E-05	0.28231	5.6E-05	-16.3	1.070	0.282284	6.4	1.50
RS	195001_006	0.001443	6.2E-05	0.282293	6.4E-05	-16.9	1.070	0.282264	5.7	1.54
RS	195001_008	0.001427	0.00002	0.282305	6.4E-05	-16.5	1.070	0.282276	6.1	1.52
RS	195001_009	0.004323	2.5E-05	0.282341	7.9E-05	-15.2	1.070	0.282254	5.4	1.57
RS	195001_010	0.00542	6.1E-05	0.282385	7.2E-05	-13.7	1.070	0.282276	6.1	1.52
RS	195001_011	0.000743	1.4E-05	0.282269	5.4E-05	-17.8	1.070	0.282254	5.4	1.57
RS	195001_014	0.001028	8.8E-06	0.28225	6.3E-05	-18.5	1.070	0.282229	4.5	1.62
RS	195001_017	0.001268	4.2E-05	0.282303	6.2E-05	-16.6	1.070	0.282277	6.2	1.51
RS	195001_018	0.004602	3.6E-05	0.282419	6.8E-05	-12.5	1.070	0.282326	7.9	1.41
RS	195001_019	0.000719	6.9E-06	0.282313	5.9E-05	-16.2	1.070	0.282299	6.9	1.47
RS	195001_020	0.00129	3.6E-06	0.282277	6.6E-05	-17.5	1.070	0.282251	5.3	1.57
RS	195001_021	0.0018	1.7E-05	0.282261	4.9E-05	-18.1	1.070	0.282225	4.3	1.63
RS	195001_027	0.002191	7.5E-06	0.282242	5.2E-05	-18.7	1.070	0.282198	3.4	1.69
RS	195001_015	0.000697	1.7E-06	0.282313	5.1E-05	-16.2	1.070	0.282299	7.0	1.47
RS	195001_033	0.001033	0.00002	0.282321	5.8E-05	-15.9	1.070	0.282300	7.0	1.46
RS	195001_036	0.00318	0.00011	0.282373	6.9E-05	-14.1	1.070	0.282309	7.3	1.44
RS	195001_037	0.000829	1.7E-05	0.28229	6.1E-05	-17.0	1.070	0.282273	6.0	1.52
RS	195001_039	0.000727	1.8E-05	0.282305	4.7E-05	-16.5	1.070	0.282290	6.6	1.49
RS	195001_040	0.000926	1.9E-05	0.282267	5.4E-05	-17.9	1.070	0.282248	5.2	1.58
RS	195001_043	0.000932	3.8E-06	0.282227	0.00006	-19.3	1.070	0.282208	3.7	1.67
RS	195001_047	0.000867	8.4E-07	0.282256	5.1E-05	-18.2	1.070	0.282239	4.8	1.60
RS	195001_051	0.001121	3.6E-05	0.282273	6.7E-05	-17.6	1.070	0.282250	5.2	1.57
RS	195001_041	0.0007	1.9E-06	0.28227	0.00005	-17.8	1.070	0.282256	5.4	1.56
RS	195001_045	0.001051	0.00002	0.282309	6.3E-05	-16.4	1.070	0.282288	6.6	1.49
RS	199253_001	0.000545	4.4E-06	0.282293	7.7E-05	-16.9	1.070	0.282282	6.4	1.50
RS	199253_003	0.003125	2.4E-05	0.282282	6.4E-05	-17.3	1.070	0.282219	4.1	1.64
RS	199253_006	0.004115	3.3E-05	0.282318	0.00006	-16.1	1.070	0.282235	4.7	1.61
RS	199253_007	0.000986	1.5E-05	0.282291	6.3E-05	-17.0	1.070	0.282271	6.0	1.53
RS	199253_008	0.00075	3.4E-06	0.282229	5.1E-05	-19.2	1.070	0.282214	3.9	1.66
RS	199253_009	0.001647	1.5E-05	0.282283	6.8E-05	-17.3	1.070	0.282250	5.2	1.58
RS	199253_014	0.002376	1.2E-05	0.282308	5.8E-05	-16.4	1.070	0.282260	5.6	1.55
RS	199253_015	0.002449	1.4E-05	0.282302	6.9E-05	-16.6	1.070	0.282253	5.3	1.57
RS	199253_017	0.002781	5.7E-06	0.282318	5.8E-05	-16.1	1.070	0.282262	5.6	1.55
RS	199253_020	0.004125	2.5E-05	0.28228	6.4E-05	-17.4	1.070	0.282197	3.3	1.69
RS	199253_023	0.002405	2.5E-05	0.282281	0.00007	-17.4	1.070	0.282233	4.6	1.61
RS	199253_028	0.000841	8E-06	0.282316	6.8E-05	-16.1	1.070	0.282299	7.0	1.47
RS	199253_029	0.001073	7E-06	0.28225	5.1E-05	-18.5	1.070	0.282228	4.5	1.62
RS	199253_030	0.00355	0.00013	0.282326	6.3E-05	-15.8	1.070	0.282254	5.4	1.57
RS	199253_032	0.003501	1.7E-05	0.282271	6.4E-05	-17.7	1.070	0.282200	3.5	1.69
RS	199253_033	0.003124	4.8E-06	0.282288	5.6E-05	-17.1	1.070	0.282225	4.3	1.63
RS	199253_002	0.005553	2.4E-05	0.282299	6.4E-05	-16.7	1.070	0.282187	3.0	1.72
RS	199253_019	0.003726	4.2E-06	0.282324	0.00007	-15.8	1.070	0.282249	5.2	1.58
RS	199253_021	0.003338	8.9E-06	0.28231	5.4E-05	-16.3	1.070	0.282243	5.0	1.59
RS	199253_024	0.0032	4.8E-05	0.282369	6.1E-05	-14.3	1.070	0.282305	7.1	1.45
RS	205322_001	0.000945	0.00003	0.282291	7.6E-05	-17.0	1.070	0.282272	6.0	1.53
RS	205322_002	0.004392	3.4E-05	0.282348	7.1E-05	-15.0	1.070	0.282259	5.6	1.55
RS	205322_003	0.000897	1.7E-05	0.282264	6.4E-05	-18.0	1.070	0.282246	5.1	1.58
RS	205322_004	0.004262	1.9E-05	0.282307	0.00007	-16.4	1.070	0.282221	4.2	1.64
RS	205322_005	0.00079	5.4E-06	0.282306	6.5E-05	-16.5	1.070	0.282290	6.6	1.49
RS	205322_006	0.002095	7.1E-05	0.28233	6.5E-05	-15.6	1.070	0.282288	6.6	1.49
RS	205322_007	0.003862	0.00008	0.282397	8.2E-05	-13.3	1.070	0.282319	7.7	1.42
RS	205322_009	0.00472	2.9E-05	0.282342	6.4E-05	-15.2	1.070	0.282247	5.1	1.58
RS	205322_017	0.000989	8.6E-06	0.282262	6.3E-05	-18.0	1.070	0.282242	4.9	1.59
RS	205322_019	0.000725	1.5E-06	0.282281	5.8E-05	-17.4	1.070	0.282266	5.8	1.54
RS	205322_020	0.00111	0.00003	0.282252	0.00006	-18.4	1.070	0.282230	4.5	1.62
RS	205322_022	0.000788	2E-06	0.282231	5.3E-05	-19.1	1.070	0.282215	4.0	1.65
RS	205322_025	0.00093	1.8E-05	0.282267	5.9E-05	-17.9	1.070	0.282248	5.2	1.58
RS	205322_026	0.000915	1.4E-05	0.282246	5.5E-05	-18.6	1.070	0.282228	4.4	1.62
RS	205322_032	0.001299	2.3E-05	0.282317	6.2E-05	-16.1	1.070	0.282291	6.7	1.48
RS	205322_033	0.001927	2.9E-05	0.282274	6.8E-05	-17.6	1.070	0.282235	4.7	1.61

Unit	Analysis no.	$^{176}Lu/^{177}Hf$	2se	$^{176}Hf/^{177}Hf_{(i)}$	2se	εHf	Age(T) Ga	$^{176}Hf/^{177}Hf(T)$	εHf(T)	(T_{DM}^{2}) Ga
RS	205322_035	0.000928	1.9E-06	0.282281	4.6E-05	-17.4	1.070	0.282262	5.7	1.55
RS	205322_039	0.001467	5.8E-06	0.282305	5.8E-05	-16.5	1.070	0.282275	6.1	1.52
RS	205322_041	0.001633	9.8E-06	0.282291	5.2E-05	-17.0	1.070	0.282258	5.5	1.56
RS	205322_015	0.003561	4.7E-05	0.282271	0.00007	-17.7	1.070	0.282199	3.4	1.69
RS	205322_029	0.00082	1.4E-06	0.2822	6.5E-05	-20.2	1.070	0.282183	2.9	1.72
RS	205322_024	0.003072	1.9E-05	0.282306	6.6E-05	-16.5	1.070	0.282244	5.0	1.59
RS	205322_027	0.001527	1.6E-05	0.282229	7.2E-05	-19.2	1.070	0.282198	3.4	1.69
RS	205322_031	0.000797	1.8E-05	0.282234	6.3E-05	-19.0	1.070	0.282218	4.1	1.65
RS	199254_001	0.003111	9.9E-06	0.282262	6.3E-05	-18.0	1.070	0.282199	3.4	1.69
RS	199254_008	0.000876	1.1E-05	0.282221	5.6E-05	-19.5	1.070	0.282203	3.6	1.68
RS	199254_010	0.00257	5.9E-05	0.282236	6.1E-05	-19.0	1.070	0.282184	2.9	1.72
RS	199254_013	0.003312	0.00002	0.28226	6.2E-05	-18.1	1.070	0.282193	3.2	1.70
RS	199254_017	0.005838	7.1E-05	0.282303	7.1E-05	-16.6	1.070	0.282185	2.9	1.72
RS	199254_018	0.003079	4.6E-05	0.282253	8.7E-05	-18.4	1.070	0.282191	3.1	1.71
RS	199254_020	0.002779	8.2E-06	0.282238	5.9E-05	-18.9	1.070	0.282182	2.8	1.73
RS	199254_021	0.003744	0.00004	0.282265	0.00007	-17.9	1.070	0.282190	3.1	1.71
RS	199254_022	0.001857	0.00005	0.282225	6.5E-05	-19.3	1.070	0.282188	3.0	1.71
RS	199254_023	0.000701	3.9E-06	0.282216	5.6E-05	-19.7	1.070	0.282202	3.5	1.68
RS	199254_028	0.003816	0.00005	0.282303	6.7E-05	-16.6	1.070	0.282226	4.4	1.63
RS	199254_030	0.003021	1.7E-05	0.282246	5.4E-05	-18.6	1.070	0.282185	2.9	1.72
RS	199254_032	0.003667	7E-06	0.28224	5.7E-05	-18.8	1.070	0.282166	2.2	1.76
RS	199254_035	0.001548	2.1E-05	0.282267	5.8E-05	-17.9	1.070	0.282236	4.7	1.61
RS	199254_036	0.000897	6.9E-06	0.282272	5.8E-05	-17.7	1.070	0.282254	5.4	1.57
RS	199254_037	0.001256	2.1E-05	0.282205	5.6E-05	-20.1	1.070	0.282180	2.7	1.73
RS	199254_039	0.003579	2.8E-05	0.282346	6.8E-05	-15.1	1.070	0.282274	6.1	1.52
RS	199254_040	0.00516	0.00026	0.28235	8.2E-05	-14.9	1.070	0.282246	5.1	1.58
RS	199254_042	0.002339	0.00005	0.282285	7.7E-05	-17.2	1.070	0.282238	4.8	1.60
RS	199254_045	0.003143	5.2E-05	0.28229	6.1E-05	-17.0	1.070	0.282227	4.4	1.63
RS	199254_047	0.003107	2.1E-05	0.282272	6.3E-05	-17.7	1.070	0.282209	3.8	1.67
RS	199254_003	0.001932	1.3E-05	0.282328	5.6E-05	-15.7	1.070	0.282289	6.6	1.49
RS	199222-004	0.000883	2.9E-05	0.2823	0.00011	-16.7	1.070	0.282282	6.4	1.50
RS	199222-003	0.000923	3.7E-05	0.282257	5.2E-05	-18.2	1.070	0.282238	4.8	1.60
RS	199222-006	0.001121	2.2E-05	0.282236	6.7E-05	-19.0	1.070	0.282213	3.9	1.66
RS	199222-007	0.007559	5.4E-05	0.282457	7.7E-05	-11.1	1.070	0.282305	7.2	1.45
RS	199222-008	0.001212	4.3E-06	0.282229	5.9E-05	-19.2	1.070	0.282205	3.6	1.68
RS	199222-009	0.000758	1.6E-06	0.282217	7.3E-05	-19.6	1.070	0.282202	3.5	1.68
RS	199222-014	0.00348	8.9E-06	0.282269	6.8E-05	-17.8	1.070	0.282199	3.4	1.69
RS	199222-015	0.000683	5E-06	0.282199	6.9E-05	-20.3	1.070	0.282185	2.9	1.72
RS	199222-016	0.001099	2.4E-05	0.282274	6.6E-05	-17.6	1.070	0.282252	5.3	1.57
RS	199222-017	0.002366	2.2E-05	0.28228	8.4E-05	-17.4	1.070	0.282232	4.6	1.61
RS	199222-018	0.000925	3.4E-06	0.282258	5.5E-05	-18.2	1.070	0.282239	4.8	1.60
RS	199222-019	0.000654	1.1E-05	0.282229	6.8E-05	-19.2	1.070	0.282216	4.0	1.65
RS	199222-024	0.001319	2.1E-05	0.282248	5.9E-05	-18.5	1.070	0.282221	4.2	1.64
RS	199222-027	0.001087	9.4E-06	0.282296	5.5E-05	-16.8	1.070	0.282274	6.1	1.52
RS	199222-029	0.001498	3.3E-05	0.282274	6.2E-05	-17.6	1.070	0.282244	5.0	1.59
RS	199222-030	0.001076	9.3E-06	0.282349	7.6E-05	-15.0	1.070	0.282327	8.0	1.40
RS	199222-037	0.001256	3.6E-05	0.282307	9.1E-05	-16.4	1.070	0.282282	6.3	1.50
RS	199222-038	0.001189	1.5E-05	0.282265	5.7E-05	-17.9	1.070	0.282241	4.9	1.60
RS	199222-039	0.000849	3.9E-06	0.282297	6.5E-05	-16.8	1.070	0.282280	6.3	1.51
RS	199222-044	0.002107	6.5E-05	0.28235	7.7E-05	-14.9	1.070	0.282308	7.3	1.45
RS	199222-047	0.002164	0.00006	0.282246	6.8E-05	-18.6	1.070	0.282202	3.5	1.68
RS	199222_050	0.000947	1.4E-06	0.282257	0.00006	-18.2	1.070	0.282238	4.8	1.60
RS	199222_055	0.000967	1.9E-05	0.282287	6.7E-05	-17.2	1.070	0.282268	5.8	1.54
RS	199222_057	0.001112	4.2E-06	0.282356	6.7E-05	-14.7	1.070	0.282334	8.2	1.39
RS	199222_059	0.00118	2.5E-05	0.282278	5.9E-05	-17.5	1.070	0.282254	5.4	1.57
RS	199222_001	0.001198	9.6E-06	0.282293	6.9E-05	-16.9	1.070	0.282269	5.9	1.53

Appendix C

Table 4.2.: Viscosity and temperature calculations for the KI

Sample	Zircon Saturation Temp (°C)	Viscosity log (pa.s) 0wt% H_2O	Viscosity log (pa.s) LOI = H_2O	Viscosity log (pa.s) 1.0wt% H_2O	Glass Transition (Tg) K 0wt% H_2O	Glass Transition (Tg) C 0wt% H_2O	Glass Transition (Tg) K LOI = H_2O	Glass Transition (Tg) °C LOI = H_2O	Glass Transition (Tg) K 1.0wt% H_2O	Glass Transition (Tg) °C 1.0wt% H_2O	Melt Fragility (m) 0wt% H_2O	Melt Fragility (m) LOI = H_2O	Melt Fragility (m) 1.0wt% H2O	Liquidus Temp (rhyolite-MELTS) @ QFM, 1kbar	Liquidus Temp (rhyolite-MELTS) @QFM, 100bar	Diff btw Zircon Sat Temp
164689	831.87	10.19	8.47	7.9	1013.6	740.45	905.5	632.35	866	592.85	22.52	20.38	19.72	1032.23	987.5	200.36
195074	835.08	9.32	7.96	7.31	972.1	698.95	882.8	609.65	836.3	563.15	22.84	20.95	20.11	939.84	924.22	104.76
195077	827.83	9.4	8.26	7.73	969.2	696.05	896	622.85	832.8	559.65	22.66	21.1	19.44	965.82	962.89	137.99
195091	833.38	9.42	8.12	7.36	976	702.85	892.3	619.15	837.9	564.75	22.86	21.08	20.09	961.91	930.66	128.53
195099	833.70	9.21	7.8	7.2	965.3	692.15	871.8	598.65	827.4	554.25	22.84	20.85	20.04	951.95	937.5	118.25
199221	834.73	9.69	8.08	7.47	992.9	719.75	890.3	617.15	846.8	573.65	23.14	20.98	20.2	956.84	936.53	122.11
199234	842.83	9.54	8.4	7.34	992.2	719.05	920	646.85	844.8	571.65	23.19	21.62	20.22	991.21	946.29	148.38
199250	821.02	9.57	8.37	7.55	971.3	698.15	895.2	622.05	838	564.85	22.52	20.92	19.89	966.21	921.68	145.19
199251	793.27	9.96	8.49	7.73	968.2	695.05	880	606.85	829.3	556.15	22.95	21.06	20.13	967.97	954.3	174.70
199253	829.87	9.35	7.9	7.39	968.2	695.05	873.3	600.15	836.8	563.65	22.69	20.72	20.07	951.95	920.5	122.08
199254	817.23	9.99	8.43	7.96	988.9	715.75	891.1	617.95	858.8	585.65	22.29	20.37	19.82	993.36	949.41	176.13
195020	829.04	9.32	8.08	7.3	966.1	692.95	886.1	612.95	829.5	556.35	22.75	21.03	19.99	950.78	935.94	121.74
195076	846.91	9.38	7.74	7.33	987.2	714.05	878.3	605.15	848.6	575.45	23.1	20.85	20.32	968.36	924.61	121.45
195100	835.95	10.19	8.85	7.66	1020.1	746.95	938.8	665.65	856.6	583.45	23.22	21.49	19.97	1068.55	1022.46	232.60
199222	852.65	9.34	7.9	7.22	991.8	718.65	897.3	624.15	848.3	575.15	23.47	21.43	20.53	978.71	951.56	126.06
199224	843.88	9.49	8.33	7.27	991.3	718.15	918	644.85	842.4	569.25	23.34	21.73	20.3	986.72	946.09	142.84
199228	838.37	9.16	7.85	7.16	967.6	694.45	881	607.85	830.8	557.65	23.03	21.16	20.23	951.37	937.31	113.00
199232	837.58	9.7	8.55	7.42	995.9	722.75	924.3	651.15	844.7	571.55	23.15	21.6	20.11	1000.59	955.47	163.01
199249	833.20	9.21	7.96	7.2	964.5	691.35	882.6	609.45	827.1	553.95	22.83	21.06	20.04	961.13	947.07	127.93
199252	833.27	9.73	8.47	7.53	992.1	718.95	912.2	639.05	846.1	572.95	22.8	21.11	19.91	1028.71	983.4	195.44
205322	841.62	9.22	7.71	7.2	975.1	701.95	875.2	602.05	838.1	564.95	23.31	21.17	20.49	936.13	931.34	94.51
199238	842.21	9.49	7.7	7.3	989.9	716.75	872.8	599.65	843.5	570.35	23.39	20.92	20.39	980.27	965.82	138.06
164689_F_Free	831.87	10.77	8.63	8.02	1045.1	771.95	916.5	643.35	874.6	601.45	23.17	20.6	19.88			
195074_F_Free	835.08	10.09	8.22	7.48	1016.2	743.05	901.2	628.05	848.7	575.55	23.81	21.33	20.36			
195077_F_Free	827.83	10.19	8.57	7.54	1013.6	740.45	916.9	643.75	845.2	572.05	23.64	21.53	20.19			
195091_F_Free	833.38	10.14	8.38	7.51	1016.7	743.55	910.2	637.05	849.2	576.05	23.76	21.45	20.32			
195099_F_Free	833.70	9.92	8.03	7.34	1006.1	732.95	888	614.85	838.7	565.55	23.74	21.19	20.27			
199221_F_Free	834.73	10.22	8.24	7.58	1022.4	749.25	901.1	627.95	854.6	581.45	23.79	21.21	20.36			
199234_F_Free	842.83	10.03	8.61	7.43	1020.1	746.95	934	660.85	852.1	578.95	23.81	21.92	20.37			
199250_F_Free	821.02	10.45	8.71	7.74	1020	746.85	917.9	644.75	852	578.85	23.58	21.39	20.17			
199251_F_Free	793.27	10.71	8.74	7.88	1007	733.85	896.4	623.25	840	566.85	23.82	21.4	20.34			
199253_F_Free	829.87	10.24	8.19	7.58	1018.5	745.35	893.9	620.75	851.2	578.05	23.8	21.14	20.36			

Sample	Zircon Saturation Temp (°C)	Viscosity log (pa.s) 0wt% H_2O	Viscosity log (pa.s) LOI = H_2O	Viscosity log (pa.s) 1.0wt% H_2O	Glass Transition (Tg) K 0wt% H_2O	Glass Transition (Tg) C 0wt% H_2O	Glass Transition (Tg) K LOI = H_2O	Glass Transition (Tg) °C LOI = H_2O	Glass Transition (Tg) K 1.0wt% H_2O	Glass Transition (Tg) °C 1.0wt% H_2O	Melt Fragility (m) 0wt% H_2O	Melt Fragility (m) LOI = H_2O	Melt Fragility (m) 1.0wt% H2O	Liquidus Temp (rhyolite-MELTS) @ QFM, 1kbar	Liquidus Temp (rhyolite-MELTS) @QFM, 100bar	Diff btw Zircon Sat Temp
199254_F_Free	817.23	11.03	8.75	8.19	1044.6	771.45	913	639.85	875.3	602.15	23.46	20.79	20.14			
195020_F_Free	829.04	10.07	8.36	7.45	1008.9	735.75	905	631.85	841.4	568.25	23.7	21.43	20.23			
195076_F_Free	846.91	10.07	7.94	7.48	1026.6	753.45	892.6	619.45	859.4	586.25	23.97	21.14	20.54			
195100_F_Free	835.95	10.32	8.9	7.68	1027.1	753.95	942.4	669.25	858.4	585.25	23.37	21.56	20			
199222_F_Free	852.65	9.88	8.07	7.33	1023.1	749.95	909.4	636.25	856.7	583.55	24.16	21.69	20.7			
199224_F_Free	843.88	9.93	8.51	7.36	1016.2	743.05	929.9	656.75	848.9	575.75	23.89	21.98	20.43			
199228_F_Free	838.37	9.87	8.1	7.31	1008.8	735.65	898.8	625.65	842.2	569.05	23.95	21.53	20.46			
199232_F_Free	837.58	10.11	8.73	7.5	1018.6	745.45	936.2	663.05	850.5	577.35	23.65	21.85	20.22			
199249_F_Free	833.20	9.92	8.23	7.35	1005.8	732.65	901	627.85	838.5	565.35	23.75	21.45	20.27			
199252_F_Free	833.27	10.27	8.68	7.64	1022.3	749.15	926.5	653.35	854.2	581.05	23.46	21.41	20.07			
205322_F_Free	841.62	9.93	7.91	7.34	1015.6	742.45	889.7	616.55	849.2	576.05	24.22	21.48	20.72			
199238_F_Free	842.21	9.96	7.81	7.39	1016.9	743.75	881.3	608.15	850.6	577.45	24	21.09	20.53			
164689_5.0%_F	831.87	7.88	7.29	6.98	863.1	589.95	818	544.85	794.2	521.05	19.57	18.78	18.43			
195074_5.0%_F	835.08	7.34	6.86	6.5	837.4	564.25	799.8	526.65	771.1	497.95	20.04	19.32	18.86			
195077_5.0%_F	827.83	7.4	7.03	6.55	834	560.85	804.9	531.75	767.4	494.25	19.87	19.3	18.7			
195091_5.0%_F	833.38	7.38	6.95	6.53	837.9	564.75	804.2	531.05	771.5	498.35	20	19.34	18.82			
195099_5.0%_F	833.70	7.21	6.72	6.38	827.3	554.15	788.4	515.25	761.3	488.15	19.94	19.19	18.76			
199221_5.0%_F	834.73	7.44	6.92	6.59	843.4	570.25	802.7	529.55	776.9	503.75	20.04	19.27	18.87			
199234_5.0%_F	842.83	7.31	6.99	6.46	841.2	568.05	816.2	543.05	774.4	501.25	20.05	19.55	18.87			
199250_5.0%_F	821.02	7.6	7.19	6.73	840.7	567.55	808.9	535.75	773.8	500.65	19.85	19.24	18.68			
199251_5.0%_F	793.27	7.74	7.25	6.84	828.7	555.55	793.2	520.05	762.7	489.55	20.02	19.32	18.83			
199253_5.0%_F	829.87	7.45	6.9	6.59	839.8	566.65	797.4	524.25	773.5	500.35	20.04	19.24	18.86			
199254_5.0%_F	817.23	8.04	7.41	7.12	863.7	590.55	817.4	544.25	795.9	522.75	19.82	19	18.68			
195020_5.0%_F	829.04	7.32	6.91	6.48	830.1	556.95	797.8	524.65	764	490.85	19.91	19.28	18.73			
195076_5.0%_F	846.91	7.34	6.74	6.5	848.1	574.95	800.9	527.75	782	508.85	20.21	19.34	19.04			
195100_5.0%_F	835.95	7.55	7.24		847.5	574.35	822.7	549.55			19.7	19.21				
199222_5.0%_F	852.65	7.2	6.74	6.38	845.6	572.45	808.7	535.55	780	506.85	20.38	19.66	19.2			
199224_5.0%_F	843.88	7.23	6.92	6.4	837.9	564.75	812.9	539.75	771.6	498.45	20.11	19.61	18.93			
199228_5.0%_F	838.37	7.18	6.74	6.35	830.9	557.75	795.9	522.75	765.3	492.15	20.14	19.45	18.95			
199232_5.0%_F	837.58	7.37	7.07		839.6	566.45	816.1	542.95			19.91	19.44				
199249_5.0%_F	833.20	7.22	6.8	6.38	827.3	554.15	794.5	521.35	761.2	488.05	19.95	19.3	18.76			
199252_5.0%_F	833.27	7.5	7.13	6.64	843.1	569.95	813.8	540.65	775.8	502.65	19.76	19.19	18.59			
205322_5.0%_F	841.62	7.21	6.67	6.38	837.9	564.75	795.3	522.15	772.6	499.45	20.39	19.57	19.21			
199238_5.0%_F	842.21	7.26	6.65	6.43	839.3	566.15	791.6	518.45	774	500.85	20.21	19.31	19.03			

Appendix D

Table Appendix D.: PhD field samples, locations and brief notes

Sample	Easting (X)	Northing (Y)	Section	Lithology	Unit	Facies	TS	TS Type	Geochem	Geochron	Hf Isotope	Rb-Sr Isotope	Sm-Nd Isotope	Comments
195001	321398	7112944	Eastern	Porphyritic rhyolite	RS	Lower PCG	2	std	Yes	Yes	Yes	Yes	Yes	Underlies KI
195002	321550	7112890	Eastern	Laminated mudstone	CF									
195003	321550	7112890	Eastern	Porphyritic rhyolite	RS	Lower PCG								Contact with CF. Very weathered sample
195004	321550	7112890	Eastern	Porphyritic rhyolite	RS	Lower PCG								Contact with CF. Very weathered sample
195005	321532	7112900	Eastern	Porphyritic rhyolite	RS	Lower PCG								Contact with CF. Crystal rich/crystal poor on contact.
195006	321466	7112874	Eastern	Sediment	CF	Laminated Mudstone	3	std	Yes					Laminated mudstone
195007	321533	7112905	Eastern	Porphyritic rhyolite	RS	Lower PCG								Inclusion of Cleghorne Fm. Sediment in porphyritic rhyolite
195008	321436	7112861	Eastern	Porphyritic rhyolite	RS	Lower PCG								Contact with CF
195009	320332	7112436	Eastern	Interbedded sst-mudstone	CF									Graded. Similar to Kilykilykarri. Coarse beds scour down. Fine beds - planar contacts & cross-bedding. Upward fining
195010	321007	7112629	Eastern	Sediment	CF									Very fine-grained micaceous sample
195011	320981	7112600	Eastern	Sst	CF									Lots of hbl needles. Massive sst
195012	320850	7112526	Eastern	Rhyolitic ignimbrite	KI	Flow-laminated								Colour-banded?
195013	320850	7112526	Eastern	Rhyolitic ignimbrite	KI	Flow-laminated								Colour-banded?
195014	320850	7112526	Eastern	Rhyolitic ignimbrite	KI	Flow-laminated								Gradation btw flow-laminated to colour-banded?
195015	320850	7112526	Eastern	Rhyolitic ignimbrite	KI	Flow-laminated								Transition?
195016	320928	7112415	Eastern	Rhyolitic ignimbrite	KI	Main Zone								3 samples. 1x coarse-grained pumice. 1x Matrix. 1x textural slab of main zone texture.
195017	320951	7112180	Eastern	Rhyolitic ignimbrite	KI	Main Zone								Contains dark, micaceous, fine-grained clast.
195018	320807	7111896	Eastern	Rhyolitic ignimbrite	KI	Main Zone								2 pumice pop. Fresh sample of typical main zone
195019	319463	7110737	Eastern	Porphyritic rhyolite	RS	Upper PCG	2	std	Yes					Isolated outcrop above KI
195020	320520	7111531	Eastern	Rhyolitic ignimbrite	KI	Kurrparu Eutaxitic	2	std	Yes					2 pumice pop
195021	321337	7112881	Eastern	Laminated mudstone	CF									Weathered
195022	320865	7112641	Eastern	Porphyritic rhyolite	RS	Lower PCG								Contact with CF. Apophyses
195023	320865	7112641	Eastern	Sediment	CF									Contact with RS. Apophyses
195024	321424	7112827	Eastern	Rhyolitic ignimbrite	KI	Flow-laminated								3 samples. 2x hand samples. 1x textural slab of flow-laminated texture.
195025	320918	7111311	Eastern	Rhyolitic ignimbrite	KI	Kurrparu Eutaxitic								No fiamme?
195026	320918	7111311	Eastern	Rhyolitic ignimbrite	KI	Karlaya								Contact btw KI and new flow unit?
195027	320790	7111247	Eastern	Rhyolitic ignimbrite	KI	Karlaya								Eutaxitic K-feldspar ign. Check location and facies
195028	320782	7111245	Eastern	Rhyolitic ignimbrite	KI	Karlaya								Eutaxitic K-feldspar ign. 2 samples. 1x hand sample. 1x textural slab.
195029	320803	7111240	Eastern	Rhyolitic ignimbrite	KI	Karlaya								K-feldspar ign. No fiamme present. Poorly sorted. Check facies and location.
195030	320772	7111227	Eastern	Rhyolitic ignimbrite	KI	Karlaya								K-feldspar ign. No fiamme present. Abundant k-feldspar.
195031	320807	7111201	Eastern	Porphyritic rhyolite	RS	Upper PCG	2	std	Yes	Yes				Stratiform with the turbidites. Frag or coherent?

Sample	Easting (X)	Northing (Y)	Section	Lithology	Unit	Facies	TS	TS Type	Geochem	Geochron	Hf Isotope	Rb-Sr Isotope	Sm-Nd Isotope	Comments
195032	321281	7111518	Eastern	Volcaniclastics	KI	Kilykliykarri								Volcaniclastic turbidite. 3 samples. 1x finely laminated interval. 1x graded beds. 1x textural slab of turbidite
195033	321454	7111629	Eastern	Rhyolitic ignimbrite	KI	Karlaya								Autoclastic breccia. Check location and facies. Very good pictures of quench fragmentation
195035	309868	7106662	Western	Rhyolitic ignimbrite	KI									Contact with Mt Eveline. See chill margin
195036	309853	7106692	Western	Rhyolitic ignimbrite	KI									Check location and facies?
195037	309751	7106727	Western	Rhyolitic ignimbrite	KI									Check location and facies? 2 samples. Spherulites
195038	310551	7106689	Western	Rhyolitic ignimbrite	KI									Check location and facies? Fabric, pitted, clasts?
195039	321404	7111589	Western	Rhyolitic ignimbrite	KI									Eutaxitic. Fine-grained pop. Check location and facies?
195040	310882	7106898	Western	Volcaniclastics	KI									Matrix-supported breccia. Check location and facies?
195041	311366	7108012	Western	Volcaniclastics	KI									Matrix-supported breccia. Check location and facies? Very small black lithic clasts
195042	321268	7111798	Eastern	Rhyolitic ignimbrite	KI	Karlaya								Eutaxitic K-feldspar ign. 2 samples.
195043	321286	7111754	Eastern	Rhyolitic ignimbrite	KI	Main Zone								See both coarse and fine-grained sections in 2 TS. Compare 195042 & 195043 to the main zone.
195044	321231	7111812	Eastern	Rhyolitic ignimbrite	KI	Karlaya								Eutaxitic K-feldspar ign.
195045	321415	7111631	Eastern	Volcaniclastics	KI	Karlaya								Matrix-supported breccia. Check facies and location?
195046	321444	7111632	Eastern	Rhyolitic ignimbrite	KI	Main Zone								Contact with Karlaya matrix-supported breccia facies (195033)
195047	321391	7111909	Eastern	Rhyolitic ignimbrite	KI									Eutaxitic. Fine-grained pop. Check facies and location?
195048	321641	7111539	Eastern	Volcaniclastics	KI	Karlaya								Conglomerate. Rounded clasts. Check facies and location?
195049	321646	7111520	Eastern	Volcaniclastics	KI	Karlaya								Clast to matrix-supported breccia. Angular to sub-angular clasts. Check facies and location?
195050	322258	7111118	Eastern	Volcaniclastics	KI	Kilykliykarri								Volcaniclastic turbidite. Sample of laminated unit
195051	322232	7111142	Eastern	Porphyritic rhyolite	RS	Upper PCG								Shows layering. Coherent or fragmental?
195052	322229	7111150	Eastern	Volcaniclastics	KI	Kilykliykarri								Volcaniclastic turbidite. 4 samples. 1x very fine-grained. 1x clast supported. 1x pebble conglomerate. 1x tuff
195053	322197	7111158	Eastern	Volcaniclastics	KI	Kilykliykarri								Volcaniclastic turbidite. Above K-feldspar ign, shows alternating coarse and fine grained intervals
195054	322203	7111169	Eastern	Rhyolitic ignimbrite	KI	Karlaya								Eutaxitic K-feldspar ign. Check facies and location?
195055	312135	7109505	Western	Rhyolitic ignimbrite	KI	Hyaloclastite								Contact with CF
195056	311814	7109026	Western	Rhyolitic ignimbrite	KI	Kurrparu Eutaxitic								Fine-grained pop?
195057	311767	7108727	Western	Rhyolitic ignimbrite	KI	Kurrparu Eutaxitic								2 pumice pop
195058	311532	7107868	Western	Porphyritic rhyolite	RS	Upper PCG	2	std	Yes	Yes				Mt Eveline - contact with KI
195059	311335	7106906	Western	Sediment	CF	Clastic dyke								
195060	311335	7106906	Western	Rhyolitic ignimbrite	KI									On the contact with a large clastic dyke
195061	311335	7106906	Western	Rhyolitic ignimbrite	KI									Contains porphyritic rhyolite clast
195062	311428	7107007	Western	Sediment	CF	Clastic dyke								Contains rounded clasts - conglomerate? Or is this Karlaya matrix-supported breccia facies?
195063	311399	7107020	Western	Rhyolitic ignimbrite	KI	Kurrparu Eutaxitic								Fine-grained pop?

Sample	Easting (X)	Northing (Y)	Section	Lithology	Unit	Facies	TS	TS Type	Geochem	Geochron	Hf Isotope	Rb-Sr Isotope	Sm-Nd Isotope	Comments
195064	311802	7107718	Western	Porphyritic rhyolite	RS	Upper PCG	2	std	Yes					Mt Eveline - Centre
195065	310680	7107557	Western	Rhyolitic ignimbrite	KI									Eutaxitic. Pitted. Check facies and location?
195066	310699	7107637	Western	Sediment	CF	Clastic dyke								
195067	310743	7107680	Western	Rhyolitic ignimbrite	KI	Kurrparu Eutaxitic								Fine-grained pop?
195068	313392	7109888	Middle	Rhyolitic ignimbrite	KI	Flow-laminated								Transition? Schleren
195069	313432	7109903	Middle	Sediment	CF	Clastic dyke								
195070	313432	7109903	Middle	Sediment	CF	Clastic dyke								
195071	313421	7109924	Middle	Sediment	CF	Clastic dyke								
195072	313529	7109936	Middle	Rhyolitic ignimbrite	KI	Flow-laminated								Contains porphyritic rhyolite clast
195073	313580	7109956	Middle	Rhyolitic ignimbrite	KI	Flow-laminated								Transition. Lots of fine grained fiamme
195074	313625	7109892	Middle	Rhyolitic ignimbrite	KI	Kurrparu Eutaxitic	2	std	Yes					Fine-grained pop 1
195075	313274	7110064	Middle	Porphyritic rhyolite	RS									Contact with CF. Very crystal-rich (50%)
195076	314019	7109865	Middle	Rhyolitic ignimbrite	KI	Flow-laminated	2	std	Yes		Yes	Yes	Yes	Transition
195077	315042	7109800	Middle	Rhyolitic ignimbrite	KI	Flow-laminated	2	std	Yes					
195078	313602	7109820	Middle	Dolerite										Dyke cutting through the KI
195079	310378	7108602	Western	Rhyolitic ignimbrite	KI	Kurrparu Eutaxitic								
195080	310496	7108367	Western	Rhyolitic ignimbrite	KI	Kurrparu Eutaxitic								Fine-grained pop? Sheared sample
195081	310502	7108244	Western	Rhyolitic ignimbrite	KI	Kurrparu Eutaxitic								Schleren
195082	310448	7108063	Western	Rhyolitic ignimbrite	KI	Kurrparu Eutaxitic								Pitted. See small fine-grained fiamme
195083	310450	7107874	Western	Rhyolitic ignimbrite	KI	Kurrparu Eutaxitic								Pitted. Should be same as 195082
195084	312126	7109464	Western	Rhyolitic ignimbrite	KI	Kurrparu Eutaxitic								Fine-grained pop? Good sample of fine-grained fiamme pop
195085	312204	7109328	Western	Rhyolitic ignimbrite	KI	Flow-laminated								Transition?
195086	312329	7109173	Western	Rhyolitic ignimbrite	KI									Check location and facies
195087	312421	7108974	Western	Rhyolitic ignimbrite	KI									Eutaxitic. Fine-grained pop?
195088	312479	7108862	Western	Rhyolitic ignimbrite	KI	Kurrparu Eutaxitic								Schleren
195089	312573	7108656	Western	Rhyolitic ignimbrite	KI	Kurrparu Eutaxitic								Check location and facies
195090	312708	7108513	Western	Rhyolitic ignimbrite	KI									Check location and facies
195091	317757	7111098	Middle	Rhyolitic ignimbrite	KI	Flow-laminated	2	std	Yes					
195092	318009	7111406	Middle	Sediment	CF	Turbidite								Graded sst? Upward fining
195093	317874	7111241	Middle	Rhyolitic ignimbrite	KI	Flow-laminated								
195094	318032	7111136	Middle	Rhyolitic ignimbrite	KI	Flow-laminated								Transition?
195095	318148	7111039	Middle	Rhyolitic ignimbrite	KI	Kurrparu Eutaxitic								Fine-grained pop?
195096	318276	7110856		Rhyolitic ignimbrite	KI	Kurrparu Eutaxitic								Lithophysae

Sample	Easting (X)	Northing (Y)	Section	Lithology	Unit	Facies	TS	TS Type	Geochem	Geochron	Hf Isotope	Rb-Sr Isotope	Sm-Nd Isotope	Comments
195097	318295	7110607		Rhyolitic ignimbrite	KI	Flow-laminated								Transition? Lots of fine grained fiamme, but also flow-laminated in places.
195098	318505	7110495		Rhyolitic ignimbrite	KI	Kurrparu Eutaxitic								Pitted
195099	318683	7110458		Rhyolitic ignimbrite	KI	Kurrparu Eutaxitic	2	std	Yes					Transition
195100	319011	7111218	Eastern	Rhyolitic ignimbrite	KI	Main Zone	2	std	Yes					Autobreccia in the Main Zone.
199201	320115	7111022	Eastern	Rhyolitic ignimbrite	KI									Pitted. Might be Karlaya?? Matrix-supported breccia?
199202	320130	7111013	Eastern	Volcaniclastics	KI	Karlaya								Matrix-supported breccia? Difficult to assign this to a facies
199203	320119	7111195	Eastern	Rhyolitic ignimbrite	KI	Kurrparu Eutaxitic								Fine-grained pop? Schleren. Little phenocrysts, lack of feldspar.
199204	320056	7111370	Eastern	Rhyolitic ignimbrite	KI	Kurrparu Eutaxitic								2 pumice pop. Has k-feldspar. Also has lots of fluorite.
199205	319994	7111552	Eastern	Rhyolitic ignimbrite	KI	Kurrparu Eutaxitic								2 pumice pop? Can't see if it has coarse-grained fiamme?
199206	319970	7111654	Eastern	Rhyolitic ignimbrite	KI	Main Zone								Autoclastic breccia?
199207	319917	7111840	Eastern	Rhyolitic ignimbrite	KI	Main Zone								Transition. See flow-laminations (rafted blocks?), porphyritic rhyolite clasts, 2 pumice pop.
199208	319815	7111962	Eastern	Rhyolitic ignimbrite	KI	Flow-laminated								Transition. Lots of porphyritic rhyolite clasts
199209	319724	7112088	Eastern	Rhyolitic ignimbrite	KI	Flow-laminated								Columnar jointing outcrop
199210	319725	7112115	Eastern	Sediment	CF	Sst								Lots of hbl needles
199211	319620	7112077	Eastern	Rhyolitic ignimbrite	KI	Flow-laminated								On the contact. Colour-banded
199212	323059	7114903	N KI ext	Rhyolitic ignimbrite	KI									Autoclastic breccia? Check location and facies? A new PCF above main zone, correlatable with Mt Glyde?
199213	323050	7114908	N KI ext	Rhyolitic ignimbrite	KI									Schleren. Check location and facies? A new PCF above main zone, correlatable with Mt Glyde?
199214	322530	7113830	E KI	Rhyolitic ignimbrite	KI	Main Zone								Check location and facies
199215	322540	7113730	E KI	Rhyolitic ignimbrite	KI	Main Zone								Check location and facies
199216	322658	7113654	E KI	Rhyolitic ignimbrite	KI	Kurrparu Eutaxitic								Transition? Check location and facies. See Mario Werner sample
199217	321497	7112811	Eastern	Rhyolitic ignimbrite	KI	Hyaloclastite								Contact
199218	321497	7112811	Eastern	Sediment	CF	Clastic dyke								Contact. Micaceous clastic dyke sample
199219	321395	7112808	Eastern	Rhyolitic ignimbrite	KI	Flow-laminated								Contact. Also see hyaloclastite. Colour-banded
199220	321395	7112808	Eastern	Sediment	CF	Clastic dyke								Contact. Micaceous clastic dyke sample with lithic fragments
199221	321340	7112796	Eastern	Rhyolitic ignimbrite	KI	Flow-laminated	1	std	Yes					
199222	321339	7112788	Eastern	Rhyolitic ignimbrite	KI	Main Zone	1	std	Yes		Yes	Yes	Yes	
199223	321346	7112785	Eastern	Rhyolitic ignimbrite	KI	Main Zone	1	std						
199224	321365	7112718	Eastern	Rhyolitic ignimbrite	KI	Main Zone	2	std+1XL	Yes					Good fiamme, eutaxitic texture.
199225	321413	7112653	Eastern	Rhyolitic ignimbrite	KI	Main Zone	2	std+1XL						
199226	321428	7112558	Eastern	Rhyolitic ignimbrite	KI	Main Zone	1	std						
199227	321480	7112454	Eastern	Rhyolitic ignimbrite	KI	Main Zone	1	std						

Sample	Easting (X)	Northing (Y)	Section	Lithology	Unit	Facies	TS	TS Type	Geochem	Geochron	Hf Isotope	Rb-Sr Isotope	Sm-Nd Isotope	Comments
199228	321893	7112529	Eastern	Rhyolitic ignimbrite	KI	Main Zone	4	std+1XL	Yes		Yes	Yes	Yes	Autobreccia in Main Zone
199229	321532	7112376	Eastern	Rhyolitic ignimbrite	KI	Main Zone	1	std						
199230	321618	7112296	Eastern	Rhyolitic ignimbrite	KI		1	std						Cant Assign
199231	321686	7112208	Eastern	Rhyolitic ignimbrite	KI	Main Zone	1	std						Transition. Cant Assign
199232	321722	7112134	Eastern	Rhyolitic ignimbrite	KI	Kurrparu Eutaxitic	4	std	Yes					2 pumice pop
199233	321792	7112046	Eastern	Rhyolitic ignimbrite	KI	Kurrparu Eutaxitic	2	std						Transition
199234	321798	7111955	Eastern	Rhyolitic ignimbrite	KI	Kurrparu Eutaxitic	1	std	Yes					Fine-grained pop 1
199235	321774	7111838	Eastern	Rhyolitic ignimbrite	KI	Kurrparu Eutaxitic	1	std						Fine-grained pop 2
199236	321779	7111717	Eastern	Rhyolitic ignimbrite	KI	Kurrparu Eutaxitic	1	std						Fine-grained pop 2
199237	321870	7111635	Eastern	Rhyolitic ignimbrite	KI	Kurrparu Eutaxitic	1	std						Pitted
199238	321891	7111564	Eastern	Volcaniclastics	KI	Karlaya	1	std	Yes					Matrix-supported breccia
199239	321896	7111561	Eastern	Rhyolitic ignimbrite	KI	Karlaya	1	std						Autoclastic breccia?
199240	321914	7111529	Eastern	Volcaniclastics	KI	Karlaya	2	std						Matrix-supported breccia. Shards
199241	321907	7111519	Eastern	Volcaniclastics	KI	Karlaya	1	std						Matrix-supported breccia. Very similar to 199238
199242	321927	7111469	Eastern	Rhyolitic ignimbrite	KI	Karlaya	1	std						Autoclastic breccia? Vein quartz, hydrothermal alteration?
199243	321901	7111567	Eastern	Volcaniclastics	KI	Karlaya	3	std						Matrix-supported breccia. Very similar to 199238
199244	321939	7111418	Eastern	Rhyolitic ignimbrite	KI	Karlaya	2	std						Eutaxitic ignimbrite. First new ignimbrite flow above KI
199245	321985	7111377	Eastern	Rhyolitic ignimbrite	KI	Karlaya	1	std						Non-welded ignimbrite. Part of the same flow as 199244. Lacks K-feldspar
199246	322000	7111307	Eastern	Rhyolitic ignimbrite	KI	Karlaya	1	std						Non-welded ignimbrite. Same as 199245. Lacks K-Feldspar.
199247	322018	7111298	Eastern	Volcaniclastics	KI	Karlaya	1	std						K-feldpar ignimbrite. New flow above 199244 (second flow above KI?)
199248	322140	7111253	Eastern	Rhyolitic ignimbrite	KI	Karlaya	1	std						Non-welded ignimbrite. Is it the same as 199246?
199249	321835	7111546	Eastern	Rhyolitic ignimbrite	KI		1	std	Yes					Eutaxitic. 2 pumice pop? Check location and facies
199250	322004	7111358	Eastern	Rhyolitic ignimbrite	KI	Karlaya	1	std	Yes					Eutaxitic ignimbrite Check if similar to 199250? Check location and facies
199251	312716	7109496	Western	Rhyolitic ignimbrite	KI	Flow-laminated	3	std	Yes					Check location and facies
199252	313503	7109012	Western	Rhyolitic ignimbrite	KI		2	std	Yes					
199253	310609	7107641	Western	Rhyolitic ignimbrite	KI	Main Zone	2	std	Yes		Yes	Yes	Yes	
199254	310570	7106703	Western	Rhyolitic ignimbrite	KI		1	std	Yes		Yes	Yes	Yes	Eutaxitic. Pitted. Lowest epsilon Hf - diff PCF to the Kurrparu. Karlaya?
199282	328433	7109259		Ignimbrite			3	std	Yes					Southern KI ext
199283	328430	7109358		Porphyritic rhyolite			2	std	Yes					Southern KI ext porpyhritic rhyolite
199284	327976	7109296		Ignimbrite			3	std	Yes					Southern KI ext
199285	327968	7109309												
199286	327772	7109760												
199287	327491	7109991		Porphyritic rhyolite	RS		1	std	Yes					Southern KI ext porpyhritic rhyolite

Sample	Easting (X)	Northing (Y)	Section	Lithology	Unit	Facies	TS	TS Type	Geochem	Geochron	Hf Isotope	Rb-Sr Isotope	Sm-Nd Isotope	Comments
199288	328050	7110265		Ignimbrite	KI		2	std	Yes					Southern KI ext
199289	327848	7109904		Ignimbrite	KI		2	std	Yes					Southern KI ext
199290	333684	7106583												
199291	333882	7106542												
199292	334068	7106507												
199293	334248	7106543												
199294	334537	7106545												
199295	332808	7105996												
199296	332262	7105931												
199297	332308	7105946												
199298	332481	7105811												
199299	333466	7104959												
199300	333463	7104967												
205313	342050	7110848												
205314	342730	7110907												
205315	335501	7111720												
205316	335997	7112137												
205317	335934	7121807												
205318	312276	7109669		Porphyritic rhyolite	RS		1	std	Yes					
205319	318710	7111843		Porphyritic rhyolite	RS		2	std	Yes					
205320	319435	7112363		Porphyritic rhyolite	RS		1	std	Yes			Yes	Yes	
205321	320285	7112479		Porphyritic rhyolite	RS		1	std	Yes					
205322	320627	7112257		Rhyolitic ignimbrite	KI	Main Zone	1	std	Yes		Yes	Yes	Yes	
205323	320848	7112891		Porphyritic rhyolite	RS		1	std	Yes			Yes	Yes	
205324	323734	7114537		Porphyritic rhyolite	RS		1	std	Yes					Porpyhritic rhyolite opp the north KI ext
205325	321838	7116624												
205326	334872	7111678												
205327	330270	7118600												
205328	334015	7106665												
205329	334002	7106650												
205330	334002	7106650												
205331	333962	7106647												
205333	334327	7106843												

Sample	Easting (X)	Northing (Y)	Section	Lithology	Unit	Facies	TS	TS Type	Geochem	Geochron	Hf Isotope	Rb-Sr Isotope	Sm-Nd Isotope	Comments
205334	334565	7106662												
205335	334542	7106600												
205336	334885	7106630												
205337	334929	7106620												
205338	335002	7106571		Ignimbrite	Kaarnka		3	std	Yes					Handpump Ign
205339	335097	7106593												
205340	335182	7106553												
205341	335176	7106324												
205342	334711	7106378												
205343	336431	7112081												
205360	341576	7123878		Porphyritic rhyolite	Palgrave		2	std	Yes					Base of succession N of main road
205367	341353	7122343		Ignimbrite	Palgrave		4	std	Yes					Ign in succession N of main road
205372	334697	7106376		Lava	Kaarnka		2	std	Yes					Handpump lava
205374	340141	7121968		Ignimbrite	Palgrave		2	std	Yes					Ign near base camp with large fiamme
205375	340175	7121979		Porphyritic rhyolite	Palgrave		1	std	Yes					Porpyhritic rhyolite near base camp
205380	337287	7112799		Lava	Kaarnka		4	std	Yes					Succession west of N-S track
164689	321428	7112816	Eastern	Rhyolitic Ignimbrite	KI	Flow-laminated	4	std	Yes					Colour-banded
195723	321577	7112756	Eastern	Rhyolitic Ignimbrite	KI	Main Zone	2	std	Yes	Yes	Yes			

This Report outlines the physical volcanology, palaeoenvironment and geochemistry of the Kathleen Ignimbrite in the Talbot sub-basin of the Musgrave region, central Australia. The ignimbrite was emplaced in a shallow-water marine shelf-type or large lake-type palaeodepositional environment and forms part of a thick bimodal volcanic-sedimentary succession. It is an intra-caldera fill-sequence that resulted from a very large explosive caldera-forming eruption during the Mesoproterozoic evolution of the west Musgrave Province. The Report highlights the high volumes of juvenile mantle-derived felsic magma and supports the presence of possible supervolcanoes in central Australia during the Mesoproterozoic.

Further details of geological products and maps produced by the Geological Survey of Western Australia are available from:

Information Centre
Department of Mines and Petroleum
100 Plain Street
EAST PERTH WA 6004
Phone: (08) 9222 3459 Fax: (08) 9222 3444

www.dmp.wa.gov.au/GSWApublications

MEDLIN

THE VOLCANOLOGY, PETROGENESIS, AND ECONOMIC POTENTIAL OF THE MESOPROTEROZOIC SHALLOW-WATER, INTRA-CALDERA, LAVA-LIKE RHEOMORPHIC KATHLEEN IGNIMBRITE, WEST MUSGRAVE PROVINCE, CENTRAL AUSTRALIA

REPORT 171